

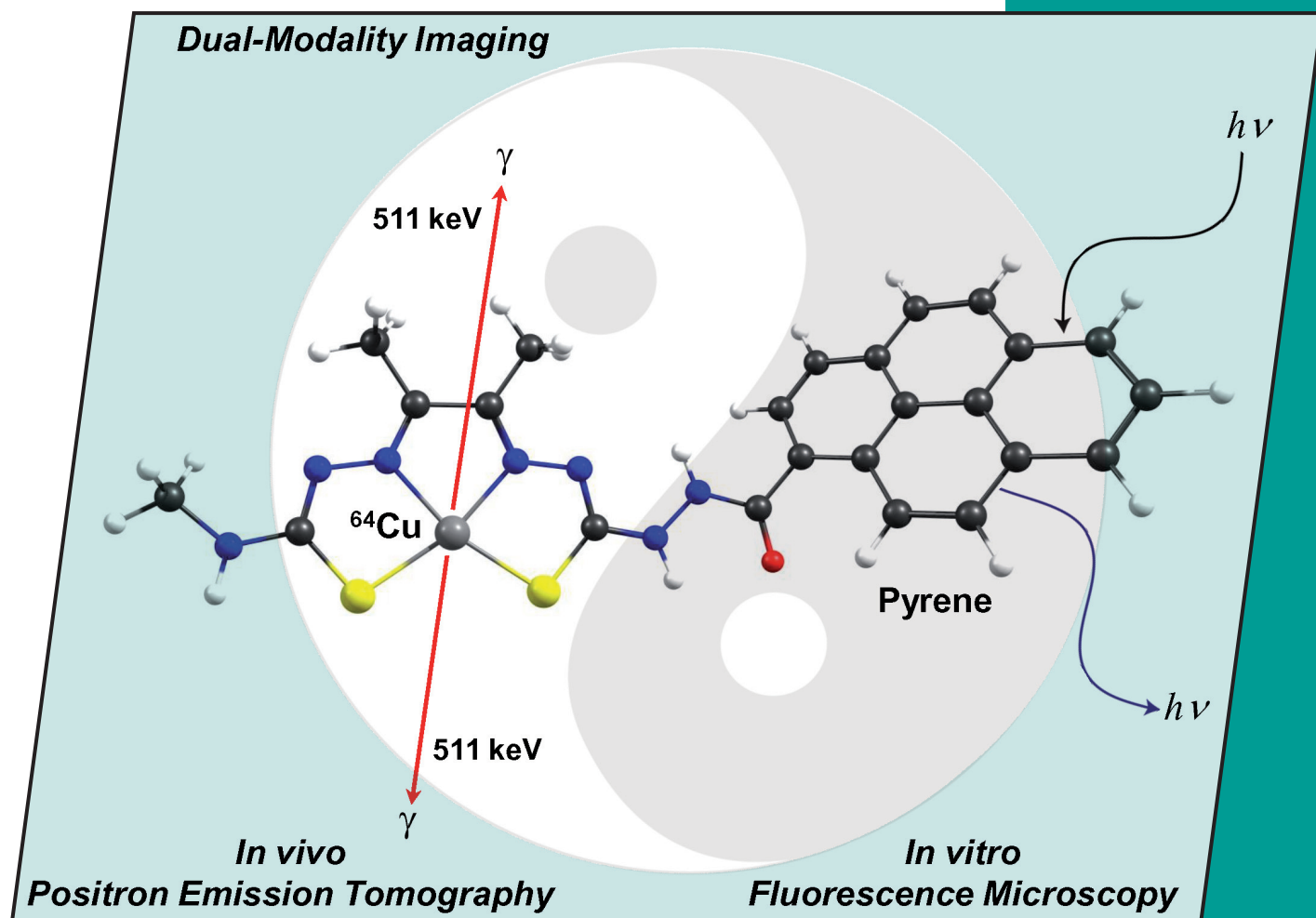
1/2010

1st January Issue

**EurJIC**  
European Journal of  
Inorganic Chemistry

[01]

Eur. J. Inorg. Chem. 2010, 1–184

**Cover Picture**

Jason P. Holland, Josephine M. Peach *et al.*  
Copper Complexes as Dual-Modality Imaging Agents

**Microreview**

Teodor Todorov and David B. Mitzi  
Direct Liquid Coating of Chalcopyrite Light-Absorbing Layers

 **WILEY-VCH**

www.eurjic.org

A Journal of



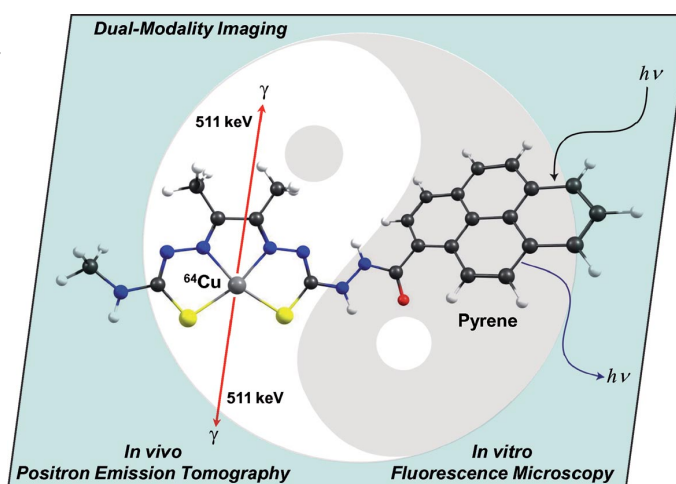


EurJIC is co-owned by 11 societies of ChemPubSoc Europe, a union of European chemical societies for the purpose of publishing high-quality science. All owners merged their national journals to form two leading chemistry journals, the *European Journal of Inorganic Chemistry* and the *European Journal of Organic Chemistry*. Three further members of ChemPubSoc Europe (Austria, Czech Republic and Sweden) are Associates of the two journals.

Other ChemPubSoc Europe journals are *Chemistry – A European Journal*, *ChemBioChem*, *ChemPhysChem*, *ChemMedChem*, *ChemSusChem* and *ChemCatChem*.

## COVER PICTURE

The cover picture shows the structure of a pyrene-functionalised bis(thiosemicarbazonato)copper complex that has been designed as a first-generation dual-modality agent for combination with in vivo positron emission tomography and in vitro fluorescence microscopy. Details of the synthesis as well as characterisation of the electronic properties by using spectroelectrochemistry, fluorescence emission spectroscopy and density functional calculations are reported in the article by J. P. Holland, J. M. Peach et al. on p. 48ff.





**Karen Hindson**  
Editor, EurJIC

## The Topical Importance of Inorganic Chemistry

The organisation for the United Nations Climate Conference is in the news as I write this editorial. The major ecological challenge involved in reducing global warming underlines the significance of chemistry in radical solutions to international problems. For once the heavily overworked term “paradigm shift” is apt. New sources of energy that do not contribute to a global climate catastrophe and that are as suitable for the developing world as for developed countries are urgently required. Two interrelated aspects of research will be equally essential to create the energy supply of the future: there is a need for innovative interdisciplinary research and high-quality research into the basic chemistry of promising systems. The importance of inorganic chemists in the teams cannot be emphasized enough. Without the basic knowledge of the chemistry of, for instance, the appropriate oxides or light-harvesting complexes, and the properties of inorganic semiconductors and the effects of nanostructure and morphology on these properties, to mention but a few of the topical research directions in inorganic chemistry in this field, the progress would be too small and too slow to improve the situation within the limited time frame required.

EurJIC presents you with excellent research in inorganic chemistry in the widest sense. Amongst the most accessed articles in November 2009 on the topic of inorganic materials for energy applications, for instance, are Microreviews by Gabriele Centi on the role of the nanostructure of electrode materials on their performance and Dmitry Bavykin

on titanate nanostructures including their prospective energy applications (see Table 1). These Microreviews also appeared in the top twenty list of Most Accessed Articles in 2009, together with another from 2008 by Shunichi Fukuzumi on hydrogen storage. Not only current articles have relevance to this topic: a full paper published in 1999 by Abdelkrim Chemseddine on nanostructured titania is still attracting enough attention of readers to be included in the list, as is a Microreview from 2001 on the synthesis of nanoscopic metal particles by Helmut Bönemann. Those articles are evidence of a great history in this field, but what of the coming year? In this issue EurJIC brings you a Microreview by David Mitzi on light-absorbing layers for photovoltaic devices. In our family of journals owned by ChemPubSoc Europe, the union of societies in Europe created to combine their publishing activities (see <http://www.chempubsoc.eu>), a young journal, *ChemSusChem*, is the best choice for the papers with a strong interdisciplinary aspect on this subject.

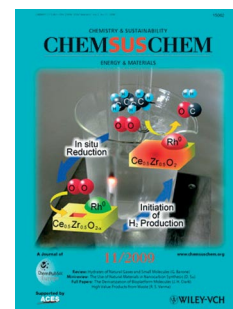


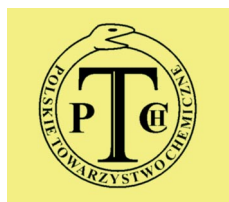
Table 1. A selection of EurJIC's most accessed articles from the period November 2008–November 2009 in the field of materials for energy applications.

| Year | Authors                        | Title  | Page |
|------|--------------------------------|--|------|
| 1999 | A. Chemseddine*<br>T. Moritz   | Nanostructuring Titania: Control over Nanocrystal Structure, Size, Shape, and Organisation             | 235  |
| 2001 | H. Bönemann*<br>R. M. Richards | Nanoscope Metal Particles – Synthetic Methods and Potential Applications                               | 2455 |
| 2008 | S. Fukuzumi                    | Bioinspired Energy Conversion Systems for Hydrogen Production and Storage                              | 1351 |
| 2009 | G. Centi*<br>S. Perathoner     | The Role of Nanostructure in Improving the Performance of Electrodes for Energy Storage and Conversion | 3851 |
|      | D. V. Bavykin*<br>F. C. Walsh  | Elongated Titanate Nanostructures and Their Applications   | 977  |

\* Correspondence author

The topic of energy was picked at random. The diversity of inorganic chemistry covered in EurJIC can be shown by a mention of other topics that you can find under the button “Most Accessed” on the homepage (<http://www.eurjic.org>): chirality in polyoxometalates and in metal-organic frameworks; other MOF research from thermally robust compounds to post-synthetic modification and photoluminescent frameworks; carbene complexes and their applications; magnetism; mixed valency; and anticancer drug design. Short lists of the most accessed Microreviews and the other article categories (Full Papers and Short Communications) are shown in Table 2 and Table 3, respectively. EurJIC thus satisfies the owner societies’ vision that all aspects of inorganic chemistry are covered in their specialist journal for Inorganic Chemistry.

One more of these societies who make up ChemPubSoc Europe has joined the group of societies that co-own EurJIC and its twin journal EurJOC. To become a co-owner, a society has to amalgamate a national journal with these two specialist journals. The Polskie Towarzystwo Chemiczne (PTC, the Polish Chemical Society) took this step at the end of 2009. It is my pleasure to welcome the society among the group that receive full royalties for their journals EurJIC and EurJOC. Three other ChemPubSoc Europe members are unable to merge a journal, but as members



are Associates and also receive royalties, though half the amount that they would receive as full co-owners. The logos of all fourteen societies can be found both electronically and in print at the beginning of the table of contents of every issue. ChemPubSoc Europe itself is expanding to include “Supporting Societies”, societies that are not founding members and who join as co-owners of the latest addition of the society-owned European family of journals, *ChemCatChem*. The first Supporting Society is the Slovenská chemická spoločnosť (SCHS, the Slovak Chemical Society).

SLOVENSKÁ CHEMICKÁ SPOLOČNOSŤ  
SLOVAK CHEMICAL SOCIETY



The policy of the Societies is implemented in EurJIC through an Editorial Board and an International Advisory Board. The advice and peer review work of the members of these Boards is invaluable and I wish here to thank them most sincerely for their commitment to the journal and to the excellence in Inorganic Chemistry publishing in general. In particular, I wish to thank the retiring members of the International Advisory Board, Prof. Barbara Milani (Trieste, Italy) and Professor Thanos Salifoglou (Thessaloniki, Greece) for their help throughout their terms of office. EurJIC wishes them both continuing success in their careers. To strengthen the International Advisory Board in

Table 2. Highly Accessed Microreviews from 2009.

| Authors                    | Title   | Page |
|----------------------------|---|------|
| Arjan W. Kleij             | Nonsymmetrical Salen Ligands and Their Complexes: Synthesis and Applications              | 193  |
| Pedro Tartaj               | Superparamagnetic Composites: Magnetism with No Memory                                    | 333  |
| Clifford P. Kubiak, et al. | Mixed Valency at the Nearly Delocalized Limit: Fundamentals and Forecast                  | 585  |
| Michel Pfeffer, et al.     | Cycloruthenated Compounds – Synthesis and Applications                                    | 817  |
| Jan Reedijk                | Platinum Anticancer Coordination Compounds: Study of DNA Binding Inspires New Drug Design | 1303 |

Table 3. Highly Accessed Short Communications and Full Papers in 2009.

| Authors                               | Title  | Page |
|---------------------------------------|--|------|
| Stuart R. Batten, Yao-Yu Wang, et al. | Topological Diversification in Metal–Organic Frameworks: Secondary Ligand and Metal Effects [Full Paper] | 147  |
| Sui Wing Or, et al.                   | Hydrothermal Synthesis of Three-Dimensional Hierarchical CuO Butterfly-Like Architecture [Full Paper]    | 168  |
| Christopher W. Bielawski, et al.      | Synthesis and Study of 5,5'-Bibenzimidazolylienes and Their Bimetallic Complexes [Full Paper]            | 1729 |
| Rina Tannenbaum, et al.               | Synthesis and Structure Characterization of Copper Terephthalate Metal–Organic Frameworks [Full Paper]   | 2338 |
| Peng Cheng, et al.                    | A Chiral Metal–Organic Framework Based on Heptanuclear Zinc Cores [Short Communication]                  | 2559 |

the fields of molecular magnetism and in bioinorganic chemistry, I welcome two new members, Spyros Perlepes (Patras, Greece) and Lucia Banci (Florence, Italy). Both are well known to the journal and I look forward to working with them in a closer capacity.

**E**urJIC has had a very successful year. The journal has attracted more readers to its articles, judging by the number of downloads, and the Impact Factor increased to 2.694. Our cluster issues on N-Heterocyclic Carbene Complexes and on Polyoxometales were so well received that we are planning to bring you more such issues that focus on a topical subject in Inorganic Chemistry in the future.

**T**he importance of Inorganic Chemistry for the challenges of globally sustainable life makes the job of Editor of an Inorganic Chemistry journal an exciting one. This sub-discipline has an influential prospect within stimulating collab-



Professor Lucia Banci



Professor Spyros Perlepes

New members of the International Advisory Board

orations. I look forward to 2010 and your papers that address the pressing problems and improve all aspects of human endeavour. In this sense EurJIC wishes all our authors and readers motivating developments for their research in 2010. Happy New Year!

Dr. Karen J. Hindson  
Editor

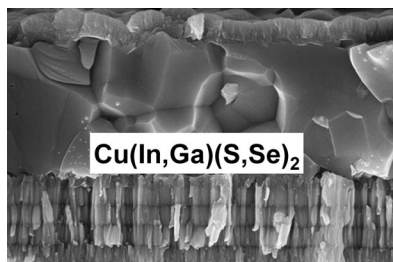
## MICROREVIEW

### Solution-Processed Chalcopyrites

T. Todorov, D. B. Mitzi\* ..... 17–28

Direct Liquid Coating of Chalcopyrite Light-Absorbing Layers for Photovoltaic Devices

**Keywords:** Energy conversion / Photovoltaic materials / Thin films / Chalcopyrite / Solution processing

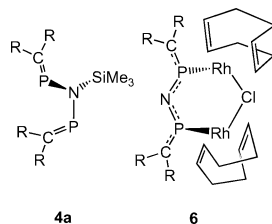


High-throughput deposition techniques available from coating and printing industries can be adapted for photovoltaic manufacturing, replacing costly vacuum processing. Recent advances in direct liquid-coating techniques for chalcopyrite thin films have achieved high device efficiencies. Transfer of these techniques to large-volume and low-cost production is in progress.

## SHORT COMMUNICATIONS

### Imidobis(phosphaalkene) Complexes

R. M. Bîrzo, D. Bugnariu, R. G. Gimeno, A. Riecke, C. Daniliuc, P. G. Jones, L. Könczöl, Z. Benkő, L. Nyulászi, R. Bartsch, W.-W. du Mont\* ..... 29–33



The  $[(i\text{PrMe}_2\text{Si})_2\text{C}=\text{P}]_2\text{NSiMe}_3$  (**4a**) is an excellent precursor for binuclear  $\text{Au}^{\text{I}}$  and  $\text{Rh}^{\text{I}}$  complexes of the  $P,P'$ -coordinated imidobis(phosphaalkene) anion  $[(i\text{PrMe}_2\text{Si})_2\text{C}=\text{P}]_2\text{N}^-$ , the first case of elusive  $P=C$ -unsaturated congeners of the “classic” bis(phosphanil)amide ligands.



Access to Metal Complexes of the Elusive Imidobis(phosphaalkene) Anion by N–Si Bond Cleavage of a *N*-Silylimino-Bridged Bis(phosphaalkene)

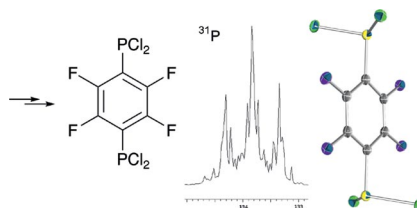
**Keywords:** Bis(phosphaalkenes) / PNP ligands /  $\pi$ -conjugation / Gold / Rhodium / DFT calculations

### Perfluorophosphanes

A. Orthaber, F. Belaj, J. H. Albring, R. Pietschnig\* ..... 34–37



2,3,5,6-Tetrafluoro-*p*-phenylenebis(phosphanes) – Preparation and Structure of an Electron-Poor P–R<sub>F</sub>–P Linker

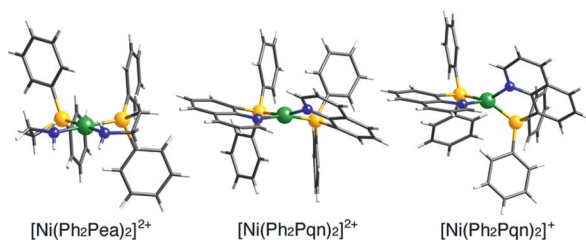


1,4-Bis[bis(diethylamino)phosphanyl]-2,3,5,6-tetrafluorobenzene and 1,4-bis(dichlorophosphanyl)-2,3,5,6-tetrafluorobenzene have been synthesized in good yields and structurally characterized, now opening the way to the synthesis of low-coordinated bis(phosphanes) linked by an electron-deficient aryl moiety.

**Keywords:** Phosphorus / Phosphanes / Fluorinated ligands / Electron-deficient compounds

## FULL PAPERS

### Hemilabile Phosphane Ligands



The coordination geometry of nickel(II) complexes with (2-aminoethyl)phosphanes, *cis*-(*P,P*)-[Ni(RR'Pea)<sub>2</sub>](BF<sub>4</sub>)<sub>2</sub> (RR' = Ph<sub>2</sub> or MePh) is square planar in the solid state and in solution, whereas the corresponding

complexes with 8-quinolylphosphanes, *cis*-(*P,P*)-[Ni(RR'Pqn)<sub>2</sub>](BF<sub>4</sub>)<sub>2</sub>, exhibit a tetrahedral distortion in their coordination planes, which results in weaker ligand-field strengths for RR'Pqn than for RR'Pea.

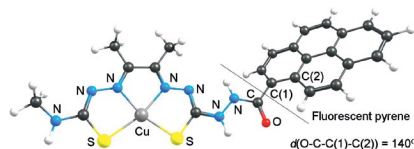
A. Hashimoto, H. Yamaguchi, T. Suzuki,\*  
K. Kashiwabara, M. Kojima,  
H. D. Takagi\* ..... 39–47

Preparation, Crystal Structures, and Spectroscopic and Redox Properties of Nickel(II) Complexes Containing Phosphane–(Amine or Quinoline)-Type Hybrid Ligands and a Nickel(I) Complex Bearing 8-(Diphenylphosphanyl)quinoline

**Keywords:** N,P ligands / Nickel / Phosphane ligands / Ligand effects

### Dual-Modality Imaging

Pyrene-functionalised copper and zinc complexes of bis(thiosemicarbazonato) ligands have been characterised as potential dual-modality imaging agents for in vitro fluorescence microscopy and in vivo positron emission tomography.



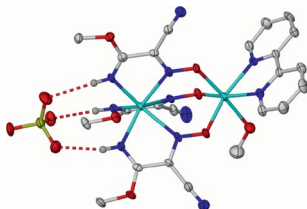
J. P. Holland,\* V. Fisher, J. A. Hickin,  
J. M. Peach\* ..... 48–58

Pyrene-Functionalised Copper Complexes as Potential Dual-Modality Imaging Agents

**Keywords:** Copper / Imaging agents / Coordination chemistry / Density functional calculations

### In-situ Ligand Synthesis

The addition of an alcohol to dicyanonitrosomethanide results in derivative ligands, which have been utilised in the formation of a series of discrete complexes and 1D and 2D coordination polymers. The coordination modes of the ligands often show novel features and the magnetic properties of the resultant products were investigated.



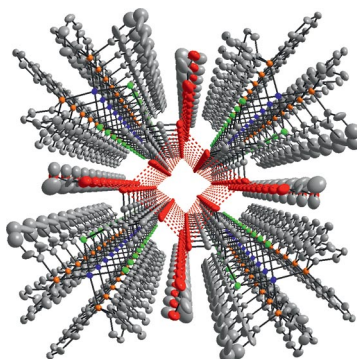
A. S. R. Chesman, D. R. Turner,  
B. Moubaraki, K. S. Murray,  
G. B. Deacon, S. R. Batten\* ..... 59–73

Nucleophilic Addition of Water and Alcohols to Dicyanonitrosomethanide: Ligands with Diverse Bonding Modes in Magnetically Coupled d-Block Complexes

**Keywords:** Self-assembly / Magnetic properties / Transition metals / Coordination modes / In situ synthesis

### Selenium Chemistry

A straightforward synthetic protocol for the preparation of diselenolato metal(II) complexes with various phosphanes is reported. The complexation properties of 2,2-bis(hydroxymethyl)-1,3-diselenolato dianions to group-10 metals were investigated focussing on the structural diversity in the solid-state arrangement due to hydrogen-bonding networks.



T. Niksch, H. Görls, M. Friedrich,  
R. Oilunkaniemi, R. Laitinen,  
W. Weigand\* ..... 74–94

Synthesis and Characterisation of 2,2-Bis-(hydroxymethyl)-1,3-diselenolato Metal(II) Complexes Bearing Various Phosphanes

**Keywords:** Steric demand / Selenolato ligands / Phosphane ligands / Hydrogen bonds / X-ray diffraction

# CONTENTS

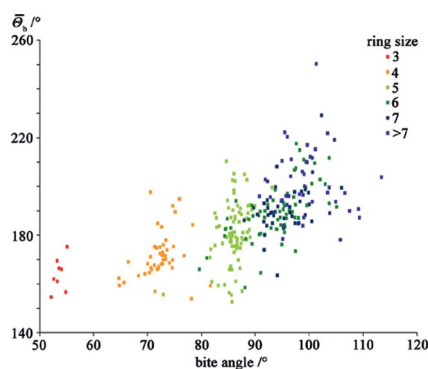
## Steric Demand

T. Nicksch, H. Görls,  
W. Weigand\* ..... 95–105



The Extension of the Solid-Angle Concept to Bidentate Ligands

**Keywords:** Phosphane ligands / Selenolato ligands / Steric demand / Solid-angle concept / Steric hindrance / X-ray diffraction



In search for a new steric parameter that expresses the steric requirements of bidentate ligands, the generalised equivalent cone angle  $\bar{\theta}_b$  was developed. A detailed evaluation of the Cambridge Structural Database and the analysis of more than 900 molecular structures proved  $\bar{\theta}_b$  to be an expedient tool for expressing the steric demand of bidentate ligands.

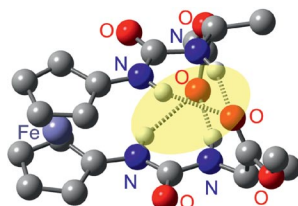
## Bioorganometallic Chemistry

J. Lapić, S. Djaković, M. Cetina,  
K. Heinze,\* V. Rapić\* ..... 106–114



$C_2$ -Symmetric Ferrocene-Bis(ureido)peptides: Synthesis, Conformation and Solid-State Structure

**Keywords:** Conformation analysis / Density functional calculations / Hydrogen bonds / Metallocenes / Peptides



Formal NH insertion in peptidic bioconjugates of ferrocene-1,1'-dicarboxylic acid results in ferrocene-bis(ureido)peptides. Conformational analyses were performed by IR, NMR and CD spectroscopy and augmented by DFT calculations. A stable intramolecular hydrogen-bond pattern with double bifurcated intramolecular hydrogen bonds is revealed.

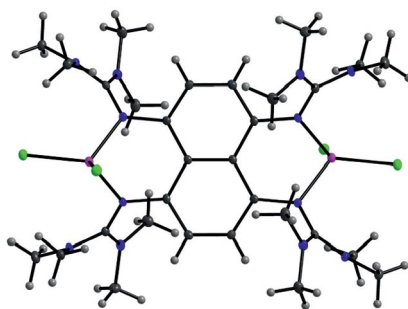
## Binuclear Metal Complexes

V. Vitske, C. König, O. Hübner, E. Kaifer,  
H.-J. Himmel\* ..... 115–126



Syntheses of the First Coordination Compounds of the New Strong Molecular Electron Donor and Double Proton Sponge 1,4,5,8-Tetrakis(tetramethylguanidino)naphthalene

**Keywords:** Electron donor ligands / Cobalt / Aluminum / N ligands



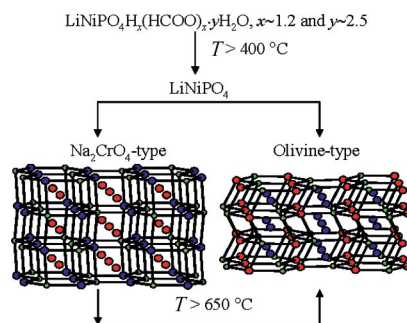
Binuclear coordination compounds with an unusual geometry can be synthesised with the new superbasic tetraguanidino ligand 1,4,5,8-tetrakis(tetramethylguanidino)naphthalene. The consequences on magnetic exchange is analysed for the example of a binuclear  $\text{Co}^{\text{II}}$  complex.

## Metastable Li–Ni Composites

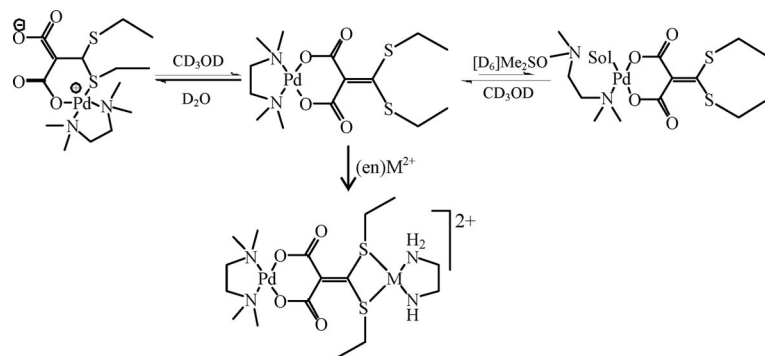
V. Koleva,\* R. Stoyanova,  
E. Zhecheva ..... 127–131

Formation of Metastable  $\text{Na}_2\text{CrO}_4$ -Type  $\text{LiNiPO}_4$  from a Phosphate-Formate Precursor

**Keywords:** Lithium / Nickel / Organic-inorganic hybrid composites / Metastable compounds / X-ray diffraction



Metastable modification of  $\text{LiNiPO}_4$  with a  $\text{Na}_2\text{CrO}_4$ -type structure was obtained at ambient pressure from a mixed  $\text{LiNi}$ -phosphate-formate precursor. Above  $650^\circ\text{C}$ , the metastable modification is transformed into olivine-type  $\text{LiNiPO}_4$ .



Stepwise syntheses of monometallic palladium(II) and bimetallic palladium(II)/platinum(II) complexes containing a series of potential tetradentate (*O,O',S,S'*) ligands were carried out. Pd<sup>II</sup> favored the *O,O'*-chelate whereas Pt<sup>II</sup> favored the

*S,S'*-chelate in the solid state. Notably different solution behavior due to the steric hindrance between the palladium square plane and the ylidene moiety were observed.

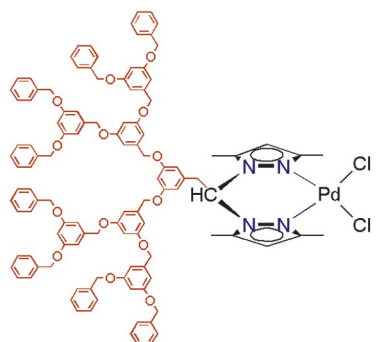
## Palladium(II)/Platinum(II) Complexes

T. H. Noh, Y.-A. Lee,  
O.-S. Jung\* ..... 132–140

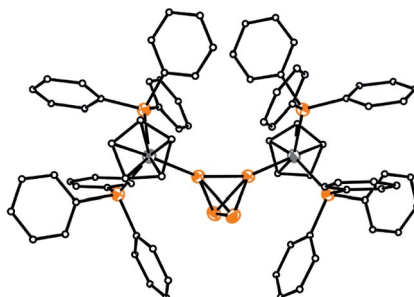
Solvent Effects on Coordination Chemistry – Stepwise Synthesis and Structural Properties of Monometallic Palladium(II) Complexes and Bimetallic Palladium(II)/Platinum(II) Complexes

**Keywords:** Bimetallic complexes / Coordination modes / Crystal engineering / NMR spectroscopy / Palladium

Discrete and dendritic (scorpionato)Pd<sup>II</sup> complexes have been synthesized and evaluated as catalyst precursors in the Heck reaction. The active catalytic species formed from these precursors are apparently not coordinated to the bis(pyrazolyl)methane ligands.



The monometallic complex [CpOs(PPh<sub>3</sub>)<sub>2</sub>-( $\eta^1$ -P<sub>4</sub>)]OTf, in which the tetrahedral white phosphorus P<sub>4</sub> molecule is  $\eta^1$  bound to the CpOs(PPh<sub>3</sub>)<sub>2</sub> metal fragment, and the heterobimetallic [{CpRu(PPh<sub>3</sub>)<sub>2</sub>}{CpOs(PPh<sub>3</sub>)<sub>2</sub>}( $\mu$ , $\eta^{1:1}$ -P<sub>4</sub>)](OTf)<sub>2</sub> compound (see graphic), in which the tetrahedral P<sub>4</sub> tethers two different metal fragments via two phosphorus atoms, have been synthesized and characterized.



A. Sánchez-Méndez, E. de Jesús,\*  
J. C. Flores,\* P. Gómez-Sal ..... 141–151

Fréchet-Type Pallado-Dendrimers Containing Bis(pyrazolyl)methane Ligands

**Keywords:** Dendrimers / N ligands / Palladium / Heck reaction / Pyrazolyl ligands

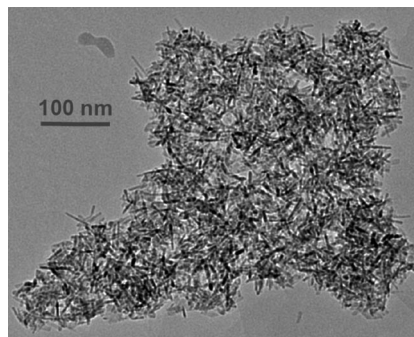
## Osmium Tetraphosphorus Complexes

M. Caporali, M. Di Vaira, M. Peruzzini,\*  
S. Seniori Costantini, P. Stoppioni,\*  
F. Zanobini ..... 152–158

Synthesis, Characterization and Hydrolysis of Osmium Tetraphosphorus Complexes

**Keywords:** Phosphorus / Coordination / Hydrolysis / Cyclopentadienyl ligands / Osmium

UZAR-S1 has been obtained by exfoliation of the layered precursor microporous titanasilicate JDF-L1. The dispersion of this material in commercial polysulfone results in an improved H<sub>2</sub>-selective mixed matrix membrane.



## Microporous Titanosilicates

C. Rubio, C. Casado, P. Gorgojo, F. Etayo,  
S. Uriel, C. Téllez,  
J. Coronas\* ..... 159–163

Exfoliated Titanosilicate Material UZAR-S1 Obtained from JDF-L1

**Keywords:** Intercalations / Layered compounds / Membranes / Organic–inorganic hybrid composites / Zeolite analogues

# CONTENTS

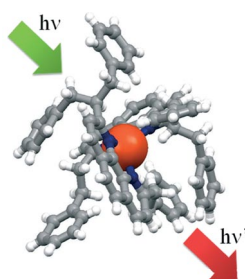
## Luminescent Copper(I) Complexes

G. Accorsi, N. Armaroli,\* C. Duhayon,  
A. Saquet, B. Delavaux-Nicot,\* R. Welter,  
O. Moudam, M. Holler,  
J.-F. Nierengarten\* ..... 164–173



Synthesis and Photophysical Properties of Copper(I) Complexes Obtained from 1,10-Phenanthroline Ligands with Increasingly Bulky 2,9-Substituents

**Keywords:** Luminescence / Copper / Electrochemistry / Electronic structure / Phenanthroline



The electronic properties of a series of bis(2,9-disubstituted 1,10-phenanthroline) copper(I) complexes are discussed as a function of stereoelectronic effects and/or internal exciplex quenching when oxygen-containing functional groups attached to the phenanthroline ligands.

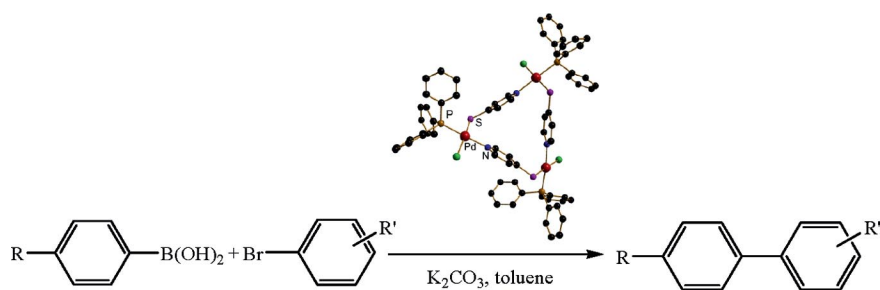
## Neutral Pd Metallocycle as Precatalyst

H. Wang, R. Zhong, X.-Q. Guo,  
X.-Y. Feng, X.-F. Hou\* ..... 174–178



Neutral Trinuclear Palladium(II) Metallocycles with Mixed Phosphane/Pyridine-4-thiolato Ligands and Their Catalytic Tests in Suzuki–Miyaura Coupling Reactions

**Keywords:** Palladium / Metallocycles / Pyridinethiolate / Phosphanes / Catalytic tests / Suzuki–Miyaura cross-coupling reactions



Three neutral trinuclear palladium(II) complexes with mixed phosphane and pyridine-4-thiolato ligands were self-assembled from the corresponding metal fragments  $[R_3PPdCl_2]_2$  with lithium pyr-

idine-4-thiolate (PySLi). A preliminary study on the Suzuki–Miyaura coupling shows that the novel trinuclear  $Pd^{II}$  complexes with a PyS bridge are more active precatalysts than  $[R_3PPdCl_2]_2$  complexes.

\* Author to whom correspondence should be addressed.



Supporting information on the WWW (see article for access details).

If not otherwise indicated in the article, papers in issue 36 were published online on December 8, 2009



On these pages, we feature a selection of the excellent work that has recently been published in our sister journals. If you are reading these pages on a

computer, click on any of the items to read the full article. Otherwise please see the DOIs for easy online access through Wiley InterScience.

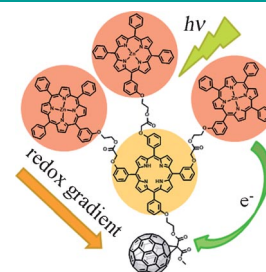


### Dendritic Molecules

S. Schlundt, G. Kuzmanich, F. Spänig, G. de Miguel Rojas, C. Kovacs, M. A. Garcia-Garibay,\* D. M. Guldi,\* A. Hirsch\*

#### Dendritic Porphyrin–Fullerene Conjugates: Efficient Light-Harvesting and Charge-Transfer Events

**Artificial photosynthesis at work:** A dendritic porphyrin–fullerene hybrid capable of light harvesting and photoinduced electron transfer was synthesized and photophysically probed (see scheme). Highly viscous environments were applied and a charge-separated state with lifetimes of up to 460 ns was observed.



*Chem. Eur. J.*  
DOI: 10.1002/chem.200902161

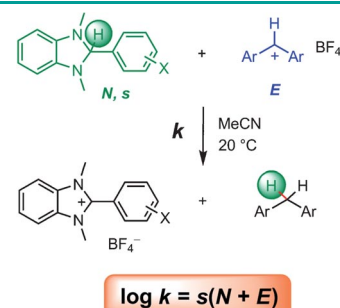


### Hydride Abstraction

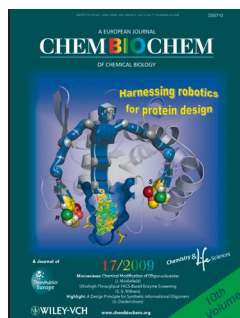
D. Richter, Y. Tan, A. Antipova, X.-Q. Zhu,\* H. Mayr\*

#### Kinetics of Hydride Abstractions from 2-Arylbenzimidazolines

**Strong neutral hydride donors:** The kinetics of hydride abstractions from 2-arylbenzimidazolines by benzhydrylium ions were determined and analyzed according to the linear free energy relationship  $\log k = s(N+E)$ . The nucleophilicity parameters  $N$  show that 2-arylbenzimidazolines are among the most reactive neutral hydride donors which have so far been parameterized, comparable to dihydropyridines.



*Chem. Asian J.*  
DOI: 10.1002/asia.200900322

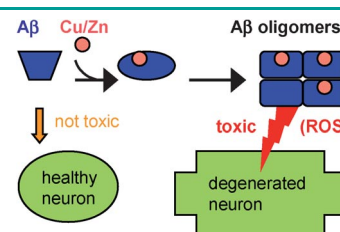


### Protein Aggregation

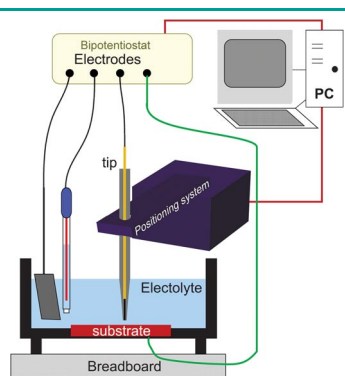
P. Faller\*

#### Copper and Zinc Binding to Amyloid- $\beta$ : Coordination, Dynamics, Aggregation, Reactivity and Metal-Ion Transfer

**The metal side of Alzheimer's disease:** Cu and Zn ions have been shown to be involved in two key steps of Alzheimer's disease (AD): aggregation of the peptide amyloid- $\beta$  (A $\beta$ ) and production of reactive oxygen species. Cu/Zn–A $\beta$  complexes are observed in AD, but not under healthy conditions. Thus, the understanding of how these metal ions interact with A $\beta$  has become an important issue for AD.



*ChemBioChem*  
DOI: 10.1002/cbic.200900321



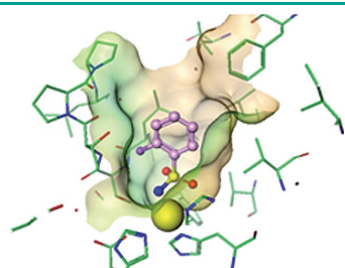
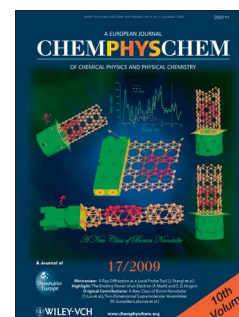
*ChemPhysChem*  
DOI: 10.1002/cphc.200900506

## Electrochemistry

M. Keddad, N. Portail, D. Trinh, V. Vivier\*

### Progress in Scanning Electrochemical Microscopy by Coupling with Electrochemical Impedance and Quartz Crystal Microbalance

**Powerful electrochemical couplings:** The combination of scanning electrochemical microscopy (see picture) with electrochemical impedance spectroscopy and electrochemical quartz crystal microbalance studies provides interesting insights into various systems. The basic aspects and potential applications of such combined studies are described, and the unique advantages—with additional information being obtained from each coupling—are discussed.



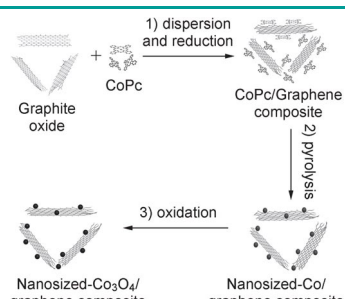
*ChemMedChem*  
DOI: 10.1002/cmdc.200900386

## Drug Design

A. D. Scott,\* C. Phillips, A. Alex, M. Flocco, A. Bent, A. Randall, R. O'Brien, L. Damian, L. H. Jones

### Thermodynamic Optimisation in Drug Discovery: A Case Study using Carbonic Anhydrase Inhibitors

**A systematic thermodynamic analysis** of benzene sulfonamide derivatives binding to carbonic anhydrase revealed a unique change in enthalpy for one of the compounds investigated. Subsequent X-ray analysis showed a different binding mode for this compound and further optimization led to a high-affinity, enthalpy-driven compound, emphasizing the importance of thermodynamic profiling.



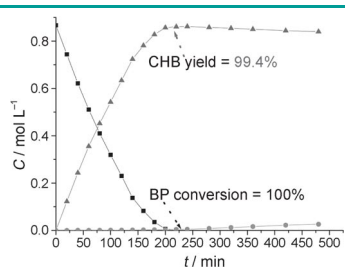
*ChemSusChem*  
DOI: 10.1002/cssc.200900106

## Lithium-Ion Batteries

S. Yang, G. Cui, S. Pang, Q. Cao, U. Kolb, X. Feng,\* J. Maier, K. Müllen\*

### Fabrication of Cobalt and Cobalt Oxide/Graphene Composites: Towards High-Performance Anode Materials for Lithium Ion Batteries

**Pave a way to high-performance anode materials:** Organic metal/graphene composites are fabricated through an in situ assembly of disc-shaped phthalocyanine molecules with graphene sheets during the chemical reduction of graphene oxide, which enables a homogenous dispersion of Co and Co<sub>3</sub>O<sub>4</sub> nanoparticles in the sheets after simple pyrolysis and oxidation. The resulting Co<sub>3</sub>O<sub>4</sub>/graphene composites exhibit remarkable lithium storage performance.



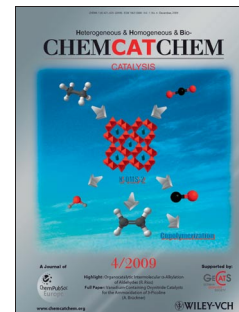
*ChemCatChem*  
DOI: 10.1002/cctc.200900141

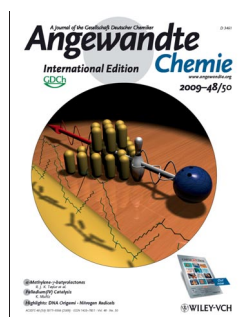
## Catalytic Hydrogenation

L. Lu,\* Z. Rong, W. Du, S. Ma, S. Hu

### Selective Hydrogenation of Single Benzene Ring in Biphenyl Catalyzed by Skeletal Ni

**The nickel lining on a Raney day:** Highly selective catalytic hydrogenation of biphenyl (BP) to cyclohexylbenzene (CHB) was achieved by using skeletal Ni prepared from rapidly quenched Ni–Al alloys ribbons, affording 100 % conversion and 99.4 % selectivity in a one-pot reaction.



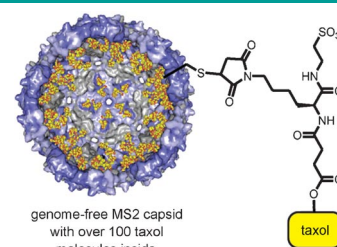


### Drug Delivery

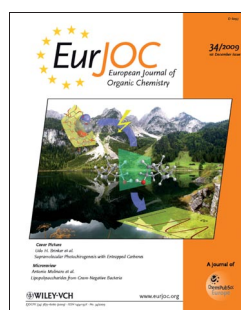
W. Wu, S. C. Hsiao, Z. M. Carrico, M. B. Francis\*

#### Genome-Free Viral Capsids as Multivalent Carriers for Taxol Delivery

**Delivery by Trojan horse:** A water-soluble derivative of the chemotherapeutic agent taxol was synthesized with bioconjugation functionality and attached to capsids of the bacteriophage MS2 (see picture). The modified capsids retained their form and released taxol when incubated with MCF-7 cells. The resulting cell-viability levels were similar to those observed upon treatment with free taxol in solution.



*Angew. Chem. Int. Ed.*  
DOI: 10.1002/anie.200902426

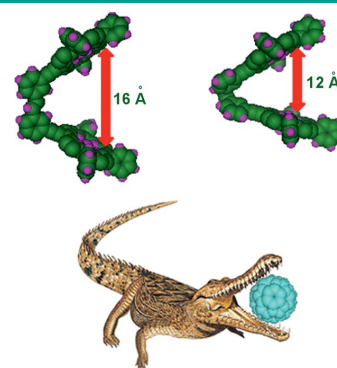


### Porphyrin Jaws

M. Fathalla, J. Jayawickramarajah\*

#### Configurational Isomers of a Stilbene-Linked Bis(porphyrin) Tweezer: Synthesis and Fullerene-Binding Studies

A new stilbene-tethered bis(porphyrin) tweezer has been synthesized that exists as two configurational isomers. UV/Vis, fluorescence, and MALDI-TOF studies have demonstrated that the *Z* isomer exhibits a significantly larger affinity towards fullerenes. The photoisomerization of the high-affinity (*Z*) isomer to the low-affinity (*E*) configuration is also discussed.



*Eur. J. Org. Chem.*  
DOI: 10.1002/ejoc.200901002

**Top Chemistry Global Visibility**

Please visit:  
[www.chempubsoc.eu](http://www.chempubsoc.eu)

ChemPubSoc Europe

Logos of various chemical societies and journals are displayed, including KNCV, GDCh, PT, CAS, GOH, MCE, Société Chimique de France, WILEY-VCH, and others.

# Direct Liquid Coating of Chalcopyrite Light-Absorbing Layers for Photovoltaic Devices

Teodor Todorov<sup>[a]</sup> and David B. Mitzi<sup>\*[a]</sup>

**Keywords:** Energy conversion / Photovoltaic materials / Thin films / Chalcopyrite / Solution processing

Liquid deposition approaches for chalcopyrite films used in thin-film photovoltaic devices are reviewed. Most of the targeted materials are based on Cu-In or Cu-In-Ga sulfides and selenides (i.e., CIS or CIGS, respectively), although recently related alternative materials based on abundant and non-toxic elements such as the kesterite  $\text{Cu}_2\text{ZnSnS}_4$  have been actively investigated. By direct liquid coating we refer collectively to a variety of techniques characterized by distributing a liquid or a paste to the surface of a substrate, followed by necessary thermal/chemical treatments to achieve the desired phase. The deposition media used are solutions or particle (usually submicrometer size) suspensions of metal oxide, organic and inorganic compounds, including metal chalcogenide species. The deposition techniques used are mainly printing and spin-coating, although any standard process such as

spraying, dip-coating or slit casting can be applied. In contrast to other widely investigated liquid-coating methods such as chemical bath and electrodeposition, in which relatively slower solid film growth occurs during the actual deposition step, the techniques discussed in this Microreview are mainly sequential, featuring rapid formation of a precursor film with well-defined metal stoichiometry. The precursor film is then transformed by a thermal treatment, generally in a chalcogen-containing atmosphere, to the final crystalline layer. This approach permits the use of low-cost and high-throughput equipment and the deployment of large-scale production facilities with lower capital investment. Although many of the methods discussed are under laboratory development, there are already industrial start-ups employing these promising methods for future large-scale photovoltaic production.

## 1. Introduction

The dependence of modern society on fossil fuels raises serious environmental and economic concerns. While there

is a general understanding that the use of renewable energy sources can provide the basis for sustainable economic development, satisfying the vast energetic consumption of human civilization (about  $4 \times 10^{20}$  J/year<sup>[1]</sup>) requires unprecedented upscale of as many alternative energy technologies as possible. Solar radiation is one of the cleanest energy sources of almost unlimited potential, delivering in an hour approximately the energy equivalent of the world's annual

[a] IBM T. J. Watson Research Center,  
P.O. Box 218, Yorktown Heights, NY 10598, USA  
E-mails: tktodoro@us.ibm.com, dmitzi@us.ibm.com



David Mitzi received a B.S.E. in Electrical Engineering from Princeton University in 1985 and a Ph.D. in Applied Physics from Stanford University in 1990. In 1990, he joined the IBM T. J. Watson Research Center where he initiated a program examining crystal structure-property relationships and low-cost thin-film deposition techniques for a variety of electronic materials. Currently, he manages the Photovoltaic Science and Technology group at IBM, with a focus on developing solution-processed high-performance inorganic semiconductors for thin-film PV devices. He holds a number of patents and has authored or co-authored more than 140 papers and book chapters.



Teodor Todorov studied Chemical Engineering and Environmental Protection at the Institute of Chemical Technology of Sofia and received his PhD in Materials and Molecular Chemistry at the Jaume-I University of Castellon, Spain in 2008. His thesis work focused on chemical approaches for depositing thin-film photovoltaic absorbers and was carried out partially at the Hahn–Meitner Institute (Helmholtz Zentrum – Berlin), the Institute of Energy Conversion (University of Delaware – USA) and the Institut de Recherche et Développement sur l'Énergie Photovoltaïque (Paris). In 2008 he joined the IBM T. J. Watson Research Center to further pursue the development of solution-processed solar cells.

consumption<sup>[2]</sup> and, in a year, twice the combined capacity of all other renewable and non-renewable reserves on Earth, including uranium.<sup>[3]</sup> The main obstacle that has to be faced in order to make solar energy widely available is the development of low-cost, high-throughput and reliable photovoltaic (PV) production methods.

Numerous promising solar-cell concepts, ranging from single-crystal silicon, through thin-film technologies to purely organic devices, have been developed during the last decades and are being researched intensely by a growing number of scientific teams and companies. Although for the present state of the art, the large-scale implementation of each of these technologies is still a tradeoff between cost, efficiency and reliability, their potential should not be underestimated. Thin-film chalcopyrite PV technology [primarily based on Cu(In,Ga)Se<sub>2</sub> or CuInSe<sub>2-x</sub>S<sub>x</sub> – i.e., CIGS or CIS] has attracted particular interest in terms of future large-scale production, potentially offering high efficiency (19.9% on laboratory-scale devices)<sup>[4]</sup> and stability comparable to that of crystalline silicon.<sup>[5]</sup> Thin-film processing also has huge potential for cost reduction because of low materials consumption and high-throughput processing, especially if monolithic series interconnection over large-area substrates can be implemented. Given these advantages, the current review will address recent developments in the chemistry and deposition of thin-film chalcopyrite-based PV devices, with a particular focus on low-cost liquid-based deposition approaches for the chalcopyrite absorber layer.

## 2. Thin-Film PV Device Structure

While there are a large variety of device structures, processes and materials used in the fabrication of chalcopyrite devices, the main features of these solar cells are similar (Figure 1). The substrate-based structure includes five principal layers, which for high performance devices are:

•**Substrate** – Soda-lime glass, the most commonly used substrate material, offers low-cost, substantial stability in aggressive environments at high temperatures (up to 550 °C), as well as an adequate microscopically smooth surface for the deposition of all active layers. The beneficial effect of sodium doping of the absorber was serendipitously discovered because of the use of soda-lime glass,<sup>[6,7]</sup> which typically contains 14.5% sodium by weight.<sup>[8]</sup> Alternative substrates such as flexible organic and metallic foils have also attracted significant research interest because of their suitability for roll-to roll processes. In these cases, alternative Na-sources are now generally employed.<sup>[9–11]</sup>

•**Back contact** – Sputtered molybdenum is attractive for this layer for both cell and module fabrication because of its relatively low resistivity (0.2–0.3 Ω/□<sup>[6]</sup>), sufficient chemical inertness, high melting point and mechanical hardness, which allows mechanical scribing of the subsequent layers for series interconnection without damaging the bottom contact. In addition, the thin interlayer of molybdenum chalcogenide (e.g., MoSe<sub>2</sub>) that typically forms during the

deposition and thermal processing of the chalcopyrite layer provides an adequate ohmic contact for the *p*-type absorber. Alternative metals such as W, Ta, Nb, Cr, V, have been used as well for the back contact, with good device results being reported in some cases.<sup>[12]</sup>

•**Light-absorbing layer** – The *p*-type chalcopyrite layer, typically Cu(In,Ga)Se<sub>2</sub> (CIGS) or CuInSe<sub>2-x</sub>S<sub>x</sub> (CIS), provides the focus of this review. The combination of a suitable band gap (1–1.5 eV), a very high absorption coefficient (above 10<sup>4</sup>) due to the direct nature of this gap, tolerance to trace impurities and sufficiently passive (with respect to electronic properties) grain boundaries make these materials an excellent choice for photovoltaic absorbers.

•**Buffer** – *n*-Type CdS or alternative Cd-free materials such as In<sub>2</sub>S<sub>3</sub> and ZnS, in some cases with oxide or hydroxide inclusions,<sup>[13–18]</sup> are generally used for the buffer layer. Chemical bath deposition approaches currently result in the highest performance devices. While the reasons for this are beyond the scope of this Microreview article, it is generally accepted that favorable altering of the absorber surface is taking place apparently by Cd indiffusion,<sup>[19]</sup> approximately 10 nm within the absorber.<sup>[20]</sup> The mentioned buffer materials have been selected because of their higher band gaps, allowing substantial light transmission to the absorber layer over the solar spectral range.

•**Transparent conductive oxide (TCO)** – Al-doped ZnO or Indium-Tin Oxide (ITO) are the most common materials used for the TCO layer. For high-performance devices, the TCO layer must exhibit both high transmission (>80% in the visible spectral range) and low resistivity (<20 Ω/□).<sup>[21,22]</sup> In order to prevent leakage current due to defects in the previous layers, the TCO is often preceded by a thinner nominally insulating ZnO layer.<sup>[23]</sup>

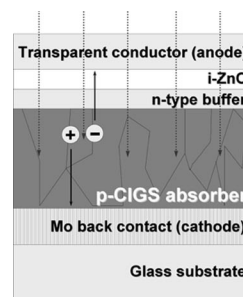


Figure 1. General structure of a high-performance chalcopyrite (e.g., CIGS) device.

## 3. Chalcopyrite-Based Absorber Materials and Devices

Chalcopyrites successfully employed as absorber layers in solar cells are typically ternary compounds or their alloys, A<sup>I</sup>B<sup>III</sup>X<sup>VI</sup><sub>2</sub> (A = Cu, Ag; B = Al, Ga, In, Tl and X = S, Se). The structures are similar to their isoelectronic II–VI binary analogues (zincblende ZnS for example),<sup>[23,24]</sup> from which the chalcopyrite structure can be derived by replacing the single-type cation with two types of cations in

an alternating order – one of lower (A) and one of higher (B) valence. Further substitution of the trivalent cation has also yielded successful devices, as for the indium-free kesterite-type  $\text{Cu}_2\text{ZnSnS}_4$ .<sup>[25]</sup> The unequal strength of the A–X and B–X bonds in chalcopyrites leads to tetragonal distortion, i.e. the lattice constant  $a$  is not exactly half of  $c$  (i.e.  $c/2a \neq 1$ ).<sup>[26,27]</sup>

The history of chalcopyrite thin-film PV technology starts with the synthesis of  $\text{CuInSe}_2$  (CIS) by Hahn et al. in 1953.<sup>[28]</sup> The direct band gap of this material is 1.01 eV, slightly lower than the optimal value for solar energy conversion (1.1–1.5 eV).<sup>[29]</sup> The band gap energies of chalcopyrites are often related to the  $a$ -axis lattice constant or, in a more advanced approximation, to the average lattice constant  $2a/3 + c/6$ .<sup>[30]</sup> A practical example of this dependence is the possibility to tune the band gap by the introduction of isovalent atoms with different size. For instance, the band gap of  $\text{CuInSe}_2$  can be increased either by substituting In atoms with smaller Ga atoms (typically  $\text{Ga/In} + \text{Ga} = 0.3$ )<sup>[4]</sup> or by substituting Se atoms with smaller S atoms.<sup>[31,32]</sup> The ability to tailor the band gap therefore enables tuning the absorption characteristics over the spectral range of interest for the solar spectrum.<sup>[29]</sup> Increase in the band gap can also yield higher open circuit voltage per cell – advantageous for large-area modules because of reduced series resistance losses.

Detailed information on the phase equilibria of Cu–In–(Se, S) (CIS) and related Cu–In–Ga–Se (CIGS) systems can be found elsewhere (e.g. see Stanbery's review<sup>[33]</sup>). One of the undesirable polymorphic modifications of chalcopyrite is the Cu–Au ordering, a nonequilibrium polytype with different cation and identical anion ordering to chalcopyrite.<sup>[34]</sup> The presence of Cu–Au ordering in the film is correlated with worsening of the structural features, i.e. decrease of grain size and increase in density of extended defects within the grain.<sup>[35]</sup> Severely deteriorated solar-cell properties, especially open-circuit voltage, are found in samples containing even a small amount of the Cu–Au ordered phase.<sup>[36,37]</sup> It is important to note that Cu–Au ordering is difficult to distinguish by X-ray diffraction. Raman scattering is widely used for its detection by the presence of a dominant A-1 mode, for instance at about  $290\text{ cm}^{-1}$  for  $\text{CuInS}_2$ .<sup>[37]</sup> The spectral characteristics (especially full width at half maximum, FWHM) of this line prove to be very sensitive to the structural quality of the  $\text{CuInS}_2$  layer. Increased FWHM can be related to an additional peak at  $305\text{ cm}^{-1}$ ,<sup>[38]</sup> which may correspond to a Cu–Au ordered phase. This ordering may also be present in other materials such as  $\text{CuInSe}_2$ .<sup>[39]</sup>

The first chalcopyrite PV device was fabricated in 1974 from single crystal  $\text{CuInSe}_2$  with 12% power conversion efficiency.<sup>[40]</sup> Boeing Corporation developed the first efficient (10%) thin-film devices in the early 1980s using a vacuum-based three-source coevaporation process.<sup>[41]</sup> With some modifications (multistage rather than a two-stage method) it is still the record-performance process used today.<sup>[4]</sup> Evaporation approaches facilitate achieving high efficiencies because of the possibility to control elemental

fluxes during high-temperature reactions. On the one hand, they take advantage of the better crystallization properties of Cu-rich compositions due to the fluxing effect of low melting point Cu–Se phases while, on the other, the process is completed by delivering the more electronically favorable Cu-poor composition. In 1987, Arco Solar increased the device efficiency to 14%.<sup>[42]</sup> The same company under the name Siemens Solar (later Shell Solar and now Avancis) produced the first commercial chalcopyrite photovoltaic module in 1998.<sup>[43]</sup> Today the efficiency frontier has been pushed to 19.9% on single-cell devices by the National Renewable Energy Laboratory,<sup>[4]</sup> while full-sized modules by Showa Shell have reached 13.4%.<sup>[44]</sup>

Because of its inherent band gap of 1.5 eV without additional doping,  $\text{CuInS}_2$  has been one of the most intensely investigated chalcopyrite materials. Another advantage of  $\text{CuInS}_2$  is the lower toxicity of sulfur in comparison with selenium, which makes industrial production environmentally safer. Despite being outperformed in PV devices by some analogous selenide materials, the simple sequential processing developed by Hahn–Meitner Institute (currently Helmholtz Centrum Berlin) has yielded 11.4% efficient devices,<sup>[45]</sup> and has been successfully transferred to industrial production of full-scale modules by Sulfurcell<sup>[46]</sup> with better field performance than amorphous silicon products.<sup>[47]</sup>

Today numerous companies, employing various processes, materials and substrates are involved in intense development work to scale up their pilot facilities to large-scale production. Some use vacuum-based techniques such as sputtering or coevaporation – examples include Wurth Solar, Avancis, Showa Shell, Miosole, HelioVolt, Global Solar, Sulfurcell. At the same time there are already companies that introduce at the industrial level novel low-cost vacuum-free approaches. Institut de Recherche et Développement sur l'Énergie Photovoltaïque (IRDEP) and Solopower use electrodeposition. International Solar Electric Technology (ISET) and Nanosolar employ nanoparticle suspension printing. The number of industrial start-ups is rapidly growing.

## 4. Absorber Layer Deposition Methods

Before focusing on particular deposition methods, it is important to point out common features of most successful chalcopyrite deposition routes. With the exception of some innovative examples, where pre-crystallized monograin powders are directly embedded in the device structure,<sup>[48,49]</sup> the formation routes of all device-quality absorber layer films have met the following conditions:

1) The constituent elements are delivered to the substrate by vacuum or atmospheric pressure techniques. Regardless of the nature of the technique, a high degree of compositional and thickness uniformity must be achieved in order to obtain satisfactory large-area modules and devices. It must be noted that a single defect can shunt a solar cell, while the overall performance of a complete series-connected module, especially its current, is limited by the low-

est-performance device. This fact is of particular relevance for the mass-production of monolithically integrated modules on large substrates, where cells cannot be individually replaced.

2) A high-temperature thermal treatment (400–600 °C) transforms the deposited elements into a crystalline material of the desired phase. Very high efficiency CIS/CIGS devices (>18% power conversion efficiency) with excellent grain structure are generally demonstrated with heat treatment temperatures above the melting point of selected copper-chalcogen binaries (520–530 °C).<sup>[50]</sup>

While the second condition is limiting with respect to the choice of substrate and layer sequence (i.e., the p-n junction quality is deteriorated at temperatures above 250 °C, thereby making it difficult to deposit the CIGS/CIS absorber on top of the buffer layer), the variety of reported material delivery approaches is impressive. Before focusing on non-vacuum deposition, we first review selected processing details of two of the best established and already commercialized vacuum deposition approaches. Many aspects of these proven strategies can be applied to other (e.g., solution-based) deposition methods.

#### 4.1 Vacuum-Based Cu(In,Ga)Se<sub>2</sub> (CIGS) Processing

There are two principal techniques by which highest efficiency full-scale Cu(In,Ga)Se<sub>2</sub> modules are currently produced: coevaporation and sequential processes. The growth of high-quality large-area crystalline materials using vacuum-based approaches is challenging because of the many-element nature and complex phase diagram for this system. In addition, unlike the case of CuInS<sub>2</sub>, final composition must be Cu-poor to avoid undesirable device shunting. Grain growth is inhibited in the Cu-poor regime of the Cu-In-Se phase diagram. While co-evaporation approaches can have a Cu-rich stage followed by an In-rich one, the sequential processes generally use copper-poor precursors from the outset to achieve the proper film stoichiometry.

Record performance Cu(In,Ga)Se<sub>2</sub>-based devices (up to 19.9% power conversion efficiency) are deposited by coevaporation. This process is advantageous for growing excellent quality materials, especially on the small scale, because of the possibility to carefully control elemental fluxes. The Boeing two-stage process starts with Cu-rich (to promote large grains)<sup>[51]</sup> and ends with Cu poor (to achieve proper film stoichiometry) fluxes. The concept was further developed into more advanced three and multistage processes,<sup>[29]</sup> all aiming for improved nucleation and film smoothness. At least during the copper-rich step, the substrate reaches temperatures preferably above 550 °C and excess selenium is evaporated in order to prevent film depletion of this volatile element and provide favorable electronic properties.<sup>[52]</sup> An attractive feature of the co-evaporation method is process flexibility, demonstrated by the high efficiency achieved by multiple groups using this approach. Yet, precise control of compositional uniformity over large areas is challenging because elemental fluxes are sensitive

to very small temperature differences. An industrial in-line co-evaporation process, developed at ZSW, Stuttgart is employed by the company Würth Solar.<sup>[53]</sup>

Sequential processes have proven to be another successful strategy for achieving high-efficiency devices, especially the ones based on thermal treatments of stacked layers of different combinations of metal, chalcogenide and chalcogen precursors. The precursor layers are usually deposited by sputtering or thermal evaporation. The thermal treatment can be performed either in a precisely controlled hydrogen chalcogenide gas atmosphere, as for the method developed at the Institute of Energy Conversion employing metallic precursors,<sup>[54,55]</sup> or by rapid thermal anneal, as for the process developed by Avancis using stacked metal and chalcogen precursors.<sup>[56]</sup> In the latter process, Cu, In and optionally Ga are sputtered, along with a layer containing excess Se. The precursor layers are then heated using rapid thermal processing (10 °C/s), in a Se- or S-containing atmosphere, to temperatures above 450 °C.<sup>[57]</sup>

As already mentioned, an important feature of selenide-based absorbers is the fact that very small amounts of sodium addition (in the range of 0.1 atom-%) are beneficial for device performance.<sup>[6–8]</sup> The effect of sodium addition is manifold. On the one hand, Na<sub>2</sub>(Se)<sub>*n*</sub> phases concentrate at the surface of the growing absorber<sup>[58]</sup> and act as a Se-trapping agent with low melting point, resulting in an excellent grain growth medium. On the other, sodium doping is important for the electronic properties of the absorber. There are many, often controversial, explanations of this effect. Generally, it is thought that Na is concentrated at the grain boundaries, where its effect is mostly manifested in the form of passivation of grain boundary defects (e.g. hole traps). Nevertheless, the influence of intra-granular Na cannot be ruled out completely.<sup>[59]</sup> Sodium incorporation is generally achieved in the absorber layer either unintentionally (diffusion from soda-lime glass substrate) or intentionally via the deposition of Na rich layers either prior to, concurrent with, or after deposition of the CIGS component.<sup>[57,59]</sup> Heat treatment leads to rapid diffusion of the sodium throughout the CIGS layer.

#### 4.2 Vacuum vs. Non-Vacuum Techniques

While non-vacuum deposition techniques are generally promoted as “low-cost,” the existing data on this point is insufficient (or kept company confidential), making it difficult to directly compare production costs of future large-scale vacuum and non-vacuum facilities. It is clear that mature, large-area and series-produced vacuum deposition equipment will yield significantly lower cost per area than today's pilot custom-designed facilities.<sup>[60,61]</sup> In future gigawatt plants, other factors such as yield, efficiency, materials cost, process robustness, energy consumption, safety and environmental spending may have significant impact on end price. Despite this, liquid-coating methods have certain inherent advantages over vacuum-based approaches, which are expected to prove highly competitive in the future:

- *Significantly lower capital cost of the manufacturing equipment.* Due to the absence of vacuum-chambers, load-locks, pumps and heavy-duty power units (for sputtering or evaporation), non-vacuum deposition facilities are expected to be less expensive than vacuum-based approaches.

- *Higher throughput.* Some solution-based deposition techniques, especially in roll-to-roll configuration, can reach deposition rates of up to a thousand meters per minute<sup>[62]</sup> – rates analogous to paper printing. Such substrate speeds cannot be matched by vacuum deposition, which, especially in the case of coevaporation and sputtering typically requires direct substrate exposure to materials sources for substantial time, ranging from several minutes to hours.

- *Compositional uniformity over large area.* The elemental ratio in liquid coating methods is usually predetermined by the composition of the starting solutions or suspensions, in contrast to vacuum deposition from multiple sources, where a small variation in the uniformity of each flux may lead to intolerable stoichiometric or thickness deviations. Precise doping with desired elements, for instance sodium, can be achieved in a highly controlled manner in the precursor liquid.

- *High material utilization.* Although recycling can recover a substantial fraction of the expensive component materials (for instance In and Ga) that do not reach the substrate during vacuum-based deposition, related system shutdown and maintenance may prove expensive. In comparison, most of the liquid coating and printing methods (summarized at the end of this review) can have nearly 100% precursor utilization.

#### 4.3 Non-Vacuum Deposition Methods

A large variety of non-vacuum deposition approaches have been developed and reviewed.<sup>[63,64]</sup> While the direct liquid coating techniques will be discussed in the next section, some of the other key solution-based approaches include:

**Spray-pyrolysis** consists of spraying precursor solution on a heated substrate surface.<sup>[65]</sup> Technically, this technique can be viewed as direct liquid deposition, though it differs in principle from the sequential processes discussed in the following sections. Solvent evaporation occurs upon contact or in close proximity to the substrate surface and solid film growth takes place during the spraying step. High substrate temperature has to be maintained, compensating for the cooling effect of solvent evaporation and precursor decomposition, at the same time maintaining precisely controlled and uniform aerosol flow. Generally, the solutions consist of organometallic compounds or metal salts dissolved in aqueous or organic-based solvents. When complete evaporation of solvents is achieved before the droplets contact the surface (especially in the case of volatile precursors), this method is called **Spray CVD** (chemical vapor deposition).<sup>[66,67]</sup> While the possibility to avoid subsequent high-temperature anneal is advantageous in these spray-growth methods (notably distinguished from spray coating), they

require precise process control and generally longer deposition times than sequential direct liquid coating approaches. In addition, residual aerosols and/or vapors account for lower materials utilization and require enhanced safety and environmental precautions.

Spray pyrolysis and Spray-CVD have been used for the deposition of  $\text{CuInS}_2$ <sup>[65–67]</sup> as well as oxides that were later treated in chalcogen vapor to form  $\text{CuInSe}_2$ .<sup>[68,69]</sup> Power conversion efficiencies of up to 5% have been reported using this approach.<sup>[70]</sup> The main impediment to higher efficiency in devices prepared using these approaches appears to be achieving adequate phase and compositional purity (e.g., inclusion of impurities from the solvent, precursor or atmosphere).<sup>[65]</sup>

**Electrodeposition** has the advantage of being an industrially established process for large-area coating. Materials utilization can be high. Extensive work on chalcopyrite electrodeposition has yielded fundamental understanding of the process and high-performance devices.<sup>[71–75]</sup> Some difficulties appear in co-electrodeposition of several elements, as their redox potentials are generally different, with particular difficulty being described for incorporating well-defined Ga content in CIGS.<sup>[76]</sup> Electrodeposition is already used in the pilot industrial facilities of companies including IRDEP and SoloPower.

## 5. Direct Liquid Coating Methods

The group of techniques we refer to as “direct liquid coating” (Figure 2) includes virtually any method by which a layer of precursor-containing liquid or ink (either true solution or a suspension), is deposited on the surface of a substrate, followed by appropriate thermal/chemical processing to yield the desired phase. The deposition step can be achieved by a variety of low-cost techniques, including spin coating, slit casting, doctor blading, ink-jet printing and spray coating (see section 6 for more detailed discussion). The choice of particular technique is not crucial for the quality of the final film, provided that a uniform liquid layer of desired thickness can be formed. Much more important is the ability of the deposited materials to form a high-quality absorber upon subsequent thermal/chemical treatment.

The drying and intermediate anneals, depending on the nature of the precursor, can be done in air or inert atmosphere. While oxide coatings are often treated in air, in order to eliminate carbon contamination,<sup>[77–79]</sup> air-sensitive samples are handled in inert atmosphere.<sup>[80–82]</sup> The final high temperature heat treatment (350–600 °C) always requires controlled atmosphere, often with the addition of chalcogen vapor or hydrogen chalcogenide. This final anneal can be preceded by reduction treatments (especially when oxygen is present in the film) and is a critical processing step, defining the properties of the absorber. Given the need for solvent evaporation and precursor decomposition, with resulting volume change of the film, each thermal processing step often requires precise optimization in order

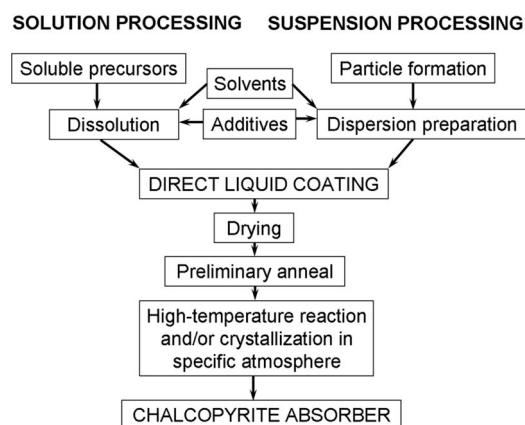


Figure 2. Main processing steps in direct liquid chalcopyrite coating approaches, including both solution-based and suspension-based processes.

to obtain adequate morphology and avoid film delamination, crack and void formation.

Important components of direct liquid coating methods include:

### 5.1 The Ink

We can group the large variety of reported inks (or functional liquids containing the chalcopyrite precursor) into two main groups: solutions and suspensions (Figure 2). While mixed cases may be present, i.e. suspensions containing dissolved components, the presence or absence of solid particles defines the general strategy for solvent and additive selection in order to obtain high-quality layers. In many cases the employed precursors, solvents and additives contain foreign elements, such as carbon, oxygen, and halogens. This must be taken into account during the subsequent processing steps, as incomplete elimination may lead to severely deteriorated electronic properties or at least impeded grain growth. Some of the described methods, especially the ones based on hydrazine solutions,<sup>[80–82]</sup> aim for exclusion of these impurity elements in the preparation step.

Solutions require precise selection of all components (solvents, additives, precursors) and conditions (pH, temperature) in order, not only to achieve complete dissolution, but also to prevent nucleation and growth of large crystals during precursor film formation, which might lead to defects in the final chalcopyrite film. Suspensions also have to be stable and uniform. In most cases, they should include particles smaller than the layer thickness and the formation of aggregates must be avoided. The two most important components of the ink are the solvent and the included precursor.

### 5.2 Solvents

The solvent is one of the key elements of the ink used for deposition. The choice of solvent (for brevity, we will use the term “solvent” also for dispersion media when refer-

ring to suspensions, despite the fact that in these cases a dissolved component may not be present) is important and many factors have to be considered, such as polarity, surface tension, reactivity, toxicity and cost. Solvent volatility should also be taken into account for direct liquid deposition. Solvents, which have very high vapor pressure, may dry too quickly, obstructing the deposition equipment or creating defects in the layer. Solvents with low vapor pressure may require heating during the drying step. While this is a common procedure, in some cases heating of solvents with too low vapor pressure may reduce viscosity and induce surface tension that can cause layer non-uniformity.

Solvents can be water-based or anhydrous. Water has the advantage of being cheap, safe and environmentally friendly, but may introduce substantial oxygen content in the final layer. At the same time, many metallic compounds readily hydrolyze in water. In the cases when this is undesirable, special additives and/or pH control are necessary. Ample choices of organic solvents are available, including alcohols, ketones, amines, alkanes, as well as mixtures of them. Physical and chemical properties can be selected to achieve dissolution of desired materials, including pure chalcogenide compounds.<sup>[80–83]</sup> While organic solvents rarely introduce oxygen contamination, residual carbon upon pyrolysis may remain in the layers, especially when strong coordination with the metal is present.

Hydrazine,  $N_2H_4$ , is another possibility as a solvent.<sup>[80–82]</sup> In many respects, hydrazine is an ideal solvent, since it is strongly reducing and can therefore stabilize the formation of metal chalcogenide anions in solution. It is both small and volatile and also tends not to coordinate strongly.<sup>[84]</sup> Hydrazine is therefore relatively easy to dissociate from the precursor at low temperature and decomposes cleanly into  $N_2$ ,  $NH_3$  and  $H_2$ . The absence of carbon and oxygen in the solvent implies that cleaner film deposition may be possible after the heat treatment (i.e., absence of carbon and oxygen impurities). Hydrazine is, however, also toxic and explosive and should therefore be used only with adequate protective measures in place to avoid contact with either the vapor or the liquid and/or ignition sources.<sup>[85]</sup>

Upon coating, drying and thermal treatments, the layers must preserve their integrity, i.e. cracks and delamination need to be prevented because they may lead to shunt paths. The two most common additives to the solvent, used to address these issues, are:

- *Binders* are synthetic or natural polymers that enhance the integrity of the deposited layer, preventing cracking and delamination. In addition, binders usually increase viscosity, prevent crystallization from solution, surround dispersed particles and help maintain stable suspensions.

- *Surfactants* are ionic and non-ionic surface tension modifiers that improve wetting or dispersion.

In suspension routes binders are often added to the ink in order to improve adhesion between particles and substrate. Solutions often are less susceptible to fragmentation, provided that a critical thickness (or maximum thickness of a crack-free/delamination-free layer) is not exceeded. Unfortunately, because of significant volume contraction upon

drying/anneal, solutions generally yield lower critical thickness, in the range of 100–1000 nm. This may necessitate multiple coatings and treatments for a desired film thickness, which can increase processing costs.

Besides binders and surfactants, other additives to the solution may include complex-forming solubility enhancers, capping agents, dryers, extenders, antioxidants, plasticizers, preservatives, flow and leveling agents.<sup>[86]</sup> It is important to note that despite their beneficial effect on precursor film formation, most additives contain non-volatile organic structures. Their thermolysis is likely to introduce carbon contamination, unless relatively high-temperature oxidizing atmosphere conditions are applied. Because impurities, especially binders and capping agents, decompose at the particle surface, films containing additives often suffer from poor grain growth and deteriorated electronic properties.

### 5.3 Precursor Types

There are several main groups of metal chalcogenide precursors that have been deposited by solution and suspension routes: oxides, metals, salts, metal-organics and chalcogenides (Table 1). In what follows we will discuss some specifics of each of these precursors in the context of several examples.

#### 5.3.1 Methods Employing Oxide Precursor Films

Nanoparticle oxide suspensions have been used for the deposition of very successful devices,<sup>[90–94]</sup> reaching efficiencies of 13.6%.<sup>[91]</sup> In one of the more completely described methods,<sup>[92]</sup> the powders were prepared by precipitation of aqueous metal salt solutions via hydroxide addition, followed by heat treatment of the obtained powders. Suspensions were prepared by ball-milling with the addition of dispersant. The doctor-bladed films were subjected to high temperature reduction at 495 °C in 50% H<sub>2</sub> in argon and then selenized at 425 °C in 5% H<sub>2</sub>Se in nitrogen. Evidently, the annealed oxides used in this approach are highly crystalline and required intense reduction treatments. Gallium oxides are exceptionally difficult to reduce. Ga-incor-

poration and desirable grading was achieved through subsequent in-diffusion of a gallium compound.<sup>[94]</sup>

Solution-based (as opposed to nanoparticle or suspension based) approaches leading to in-situ formation of oxide precursor films have also been developed. Soft chemistry methods, often referred to as “sol-gel” offer an ample choice of solvents and additives and allow the formation of stable solutions that do not segregate upon drying.<sup>[95]</sup> One example of these methods addresses successfully the issue of gallium incorporation by the formation of highly reactive mixed amorphous oxide precursor films.<sup>[78,79]</sup> Metal acetates were dissolved in alcohol containing different ethanolamines. Solutions were spin-coated and subjected to intermediate air-anneal in order to eliminate residual carbon from the organic species. The critical thickness of these films was relatively low (300–400 nm chalcogenide equivalent) and several layers had to be stacked before the final anneal. The temperature of 350–380 °C of this intermediate step was below the crystallization threshold and the obtained oxide films were successfully converted to Cu(In,Ga)Se and Cu(In,Ga)SSe by a single-step treatment with chalcogen vapors in ethanol-saturated nitrogen at 550 °C.

A similar approach has been used for deposition of the indium-free Cu<sub>2</sub>ZnSnS<sub>4</sub>,<sup>[96]</sup> which is an attractive candidate for future large scale production because it contains only earth-abundant elements. A solution of copper and indium acetates and tin chloride in 2-methoxyethanol and monoethanolamine stabilizer was spin-coated, air-annealed at 300 °C and sulfurized with 5% H<sub>2</sub>S.<sup>[97]</sup> Notably, device completion was achieved without vacuum processing (conductive ZnO:Al was deposited by sol-gel spin coating). Despite the low efficiency of 1% achieved by this method, apparently because of small grain size of the absorber and high resistivity of the ZnO:Al, the method is attractive as an integral vacuum-free approach.

#### 5.3.2 Metallic and Metal-Organic Precursors

A principally more straightforward approach resembling vacuum sequential processes and not requiring a reduction step is the deposition of elemental metallic precursors by direct liquid coating methods. Methods employing metal-

Table 1. Precursor materials deposited by direct liquid methods.

| Material       | Advantages  | Disadvantages   | Reported cell efficiency                           |
|----------------|---|---|--|
| Oxides         | allow air anneal to burn out residual carbon from additives   | difficulty to remove oxygen completely from final film  | suspension, 13.6% <sup>[91]</sup>                  |
| Metals         | similarity to standard sequential vacuum processes  | high tendency to alloy and aggregate, possible phase segregation  | suspension, 10% <sup>[90]</sup>                    |
| Salts          | off-the-shelf chemicals and multiple options for choice of salt                                     | difficulty to form high quality layers due to crystallization of precursor layer and impurities from salt | solution, 6.7% <sup>[87]</sup>                     |
| Metal-organics | allow the formation of metallic layers <sup>[88]</sup> or reactive amorphous oxides <sup>[78]</sup> | carbon and/or oxygen contamination in final film; low critical thickness per layer                        | solution, 9% <sup>[88]</sup>                       |
| Chalcogenides  | readily reactive; can be made virtually contamination free  | suspensions: difficult to stabilize without additives/capping agents<br>solutions: solvent toxicity       | suspension, 14% <sup>[89]</sup><br>solution, 12.8% |

containing dispersions have been explored yielding in some cases reasonable grain structure,<sup>[90,98,99]</sup> with reported device power conversion efficiency of 10%.<sup>[90]</sup> One challenge for these approaches is the easy alloying between the metals occurring at temperatures as low as 150 °C,<sup>[100,101]</sup> which may lead to phase segregation in the layers. Additionally, the formation of stable dispersions of these metals is difficult, because indium is a soft metal while gallium and its alloys have low melting point leading to aggregate formation. Ball-milling of metals with selenium has led to a reaction between the elements.<sup>[102]</sup>

Organic solutions of carbon-containing metallic compounds have also been explored. Solutions of acetates, acetylacetonates and alcoxides have been employed for obtaining intermediate metallic film precursors by anneal in reducing atmospheres.<sup>[88]</sup> In the most successful example of this type, copper and indium acetylacetonate precursors were dissolved in monoethanolamine, deposited by spin coating and reduced in N<sub>2</sub> containing carbon monoxide to form copper-indium metallic films that were later selenized, achieving 9% device efficiency.<sup>[88]</sup>

An interesting alternative approach taking advantage of the low melting point of indium and gallium is hot printing of metallic melts into which nanoparticles of other metals may be dispersed.<sup>[103]</sup>

### 5.3.3 Salt Precursors

Solutions of metal salts (e.g., nitrates, sulfates) were also applied as precursors. Salts are attractive because of their high solubility in a wide range of solvents, especially in aqueous media. This is why they are widely used in other low-cost methods such as electrodeposition and spray-pyrolysis. Nevertheless, their application for direct liquid coating is not so straight-forward. Easy crystallization from aqueous solutions may occur, resulting in large segregated grains. This challenge can be addressed by introduction of adequate additives, such as polymeric binders.

In one example of this approach, high viscosity metal nitrate solutions were prepared by the addition of ethylcellulose binder and coated by doctor blading.<sup>[87]</sup> Films were first annealed in air at 250 °C in order to burn out the cellulose binder and then annealed at 560 °C in a tubular reactor with an elemental selenium source at 360 °C. An interlayer of elemental carbon was found between the absorber and the contact, apparently because the ethylcellulose was not burned out completely. Despite this, device efficiency of 6.7% was achieved.

### 5.3.4 Chalcogenide Precursors

Recently reported results on solution processed chalcogenide films<sup>[80–82]</sup> have successfully addressed both the issues of carbon and oxygen contamination by exclusive use of materials free of these elements. Hydrazine was used as a solvent and metals or metal chalcogenides were dissolved at room temperature with addition of extra chalcogen. The additional chalcogen facilitates the disruption of the metal-chalcogenide framework into soluble anionic species separated by small volatile cationic species by a mechanism de-

scribed as dimensional reduction (Figure 3).<sup>[104]</sup> Because of the weak coordination and sufficient volatility, hydrazine species are easily removed through a thermal process, yielding highly pure chalcogenide films with excellent grain morphology (Figure 4).

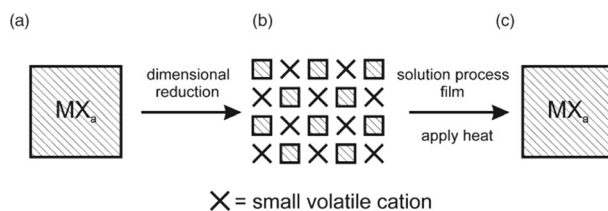


Figure 3. Film formation using a dimensional reduction approach involves three steps: 1) breaking up the insoluble extended inorganic framework (a) into more soluble-isolated anionic species, which are separated by some small and volatile cationic species (b). 2) Solution-processing thin films of the precursor (b). 3) Heating the precursor films such that the cationic species and corresponding excess chalcogen are dissociated, leaving behind the targeted inorganic semiconductor (c). (Reprinted with permission of John Wiley & Sons, Inc. from *Solution Processing of Inorganic Materials*, edited by D. B. Mitzi, 2009; ref.<sup>[104]</sup>).

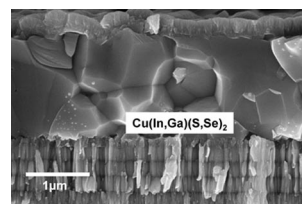


Figure 4. Cross section of a hydrazine solution-processed CIGS film in a device. The fine-grained material on top of the CIGS films is a combination of CdS, ZnO and ITO and the material under the CIGS film is Mo.

Device efficiency of 12.8% has been obtained after anneal at 540 °C for 10 min with  $V_{oc} = 617$  mV,  $J_{sc} = 29$  mA/cm<sup>2</sup> and  $FF = 71\%$  (Figure 5). Given the high toxicity and flammability of hydrazine, different alternative solvents such as ethylenediamine have also been used either alone or in combination with hydrazine to achieve chalcogenide films.<sup>[83]</sup>

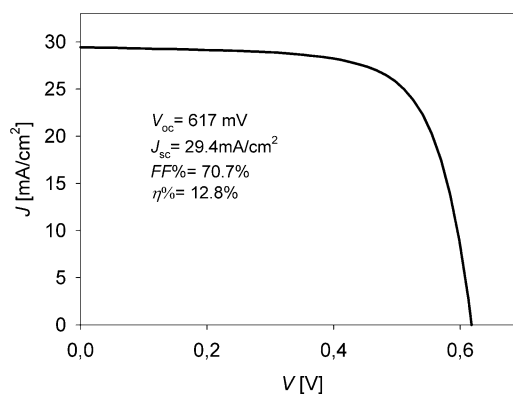


Figure 5. Current-voltage curve for a hydrazine solution processed device under 1.5 AM illumination.

Nanoparticle chalcogenide precursors have been explored in several early works on direct liquid coating for chalcopyrites by screen printing<sup>[105]</sup> and spraying<sup>[106]</sup> reaching efficiencies of 3 and 4.6%, respectively. In these examples large grain formation was found to be challenging and devices suffered from large series resistance. The highest independently confirmed efficiency achieved by a direct liquid coating method (14%),<sup>[89]</sup> was achieved apparently by printing of chalcogenide nanoparticle suspensions by Nanosolar. Despite the scarce information on the specifics of the methods, filed patents contain promising strategies for high-quality absorber deposition. The use of oxygen-free nanoparticles with excess chalcogen (lower melting point) is expected to provide adequate growth media for large-grained materials.<sup>[107]</sup> An interesting variety of additional enhancing approaches such as chalcogen-coated particles,<sup>[108]</sup> thermal and compositional gradients,<sup>[109]</sup> and specially shaped particles<sup>[110]</sup> have also been proposed.

Chalcogenide particle dispersions have also been successfully employed for the deposition of  $\text{Cu}_2\text{ZnSnS}_4$ .<sup>[111]</sup> Quaternary Cu-Zn-Sn-S precursors were formed by reacting metal acetates and chlorides with elemental sulfur in ethylene glycol at 170 °C. Suspended powders were coated on glass substrates and annealed at 550 °C in  $\text{N}_2$  containing elemental sulfur. Binder (polyvinyl alcohol) addition was necessary in order to obtain crack-free films, but this impeded large crystal formation.

## 6. Direct Liquid-Coating Techniques, Suitable for Large-Area Industrial Production

Numerous industries, including newspaper, packaging, photographic and ceramic, employ a variety of high-throughput and exhaustively optimized liquid deposition techniques.<sup>[112]</sup> Most of these can be directly employed for chalcogen deposition and the throughput of any of the roll-to-roll compatible techniques listed below (reaching a deposition speed of 1000 m/min)<sup>[113]</sup> is not likely to be a limiting step in future large-scale photovoltaic production. For example, a single liquid deposition unit operating at a relatively low substrate speed of 30 m/min (1 m substrate width,

80% production yield and 8% module power conversion efficiency) would be capable of carrying out the absorber deposition of a 1 GWp/year production plant – more than a sixth of the global photovoltaic production in 2008.<sup>[114]</sup> Hypothetically, a hundred units operating in the high throughput range of liquid coating techniques (1000 m/min, 3 m web width) would be capable of producing in one year modules with nominal maximum power approaching the Earth's energy consumption.<sup>[2]</sup> Evidently, the rest of the processing steps such as thermal reactions, device completion and encapsulation, would then be limiting the overall throughput.

The variety of liquid deposition techniques can be divided into two main groups: printing and coating. Generally, at least in the past, printing implied ink transfer from one surface to another, such as in flexography, gravure and pad printings, while coating would imply direct ink delivery to the substrate such as in dip, curtain and spray coatings. Today these concepts are merging – for instance ink-jet printing can be regarded as a high-definition spray coating.

While for other liquid deposition industries additives are readily used to tune the ink's parameters, such as stability and viscosity, in many chalcopyrite coating routes it may be preferable to select and/or optimize the deposition technique before resorting to the introduction of undesirable elements such as carbon and oxygen by means of a conditioning additive. Given the ample choice of industrial deposition techniques with different requirements (Table 2), an adequate selection of parameters with regard to ink properties should not present a substantial difficulty.

Another factor that may influence the choice of a technique is the need for patterning. In order to achieve monolithic series interconnection of a module over a single substrate (thus achieving higher output voltage and significantly reduced series resistance losses), patterning of the bottom contact, absorber and front contact is often used.<sup>[115,116]</sup> Reducing the area of the inactive interconnection zones by higher definition patterning increases the useable module area. While the most popular chalcopyrite patterning method today is mechanical scribing, patterning by printing can reduce the number of processing steps.

Table 2. Comparison of different deposition techniques.<sup>[62,112,113,117]</sup>

| Technique        | Pattern dimension / resolution [μm] | Speed rating 1:<1 m/min to 5:>1000 m/min | Ink viscosity 1:<10 cp to 5:>10 <sup>5</sup> cp | Wet thickness [μm] | Roll-to-roll compatible |
|------------------|-------------------------------------|--|---|--------------------|-------------------------|
| Spin coating     | 0                                   | –  | 1–3   | 0–100              | No                      |
| Dip coating      | 0                                   | 1–4                                      | 1–3   | 1–500              | Yes                     |
| Doctor blading   | 1                                   | 1–4                                      | 2–5   | 2–700              | Yes                     |
| Curtain          | 1                                   | 4–5                                      | 1–4   | 5–500              | Yes                     |
| Slide            | 1                                   | 3–5                                      | 1–3   | 25–250             | Yes                     |
| Spraying         | 0                                   | 4  | 1–3   | 1–500              | Yes                     |
| Slit casting     | 1                                   | 3–5                                      | 2–5   | 10–250             | Yes                     |
| Meniscus coating | 1                                   | 3–4                                      | 1–3   | 5–500              | Yes                     |
| Screen printing  | 2/50–100                            | 1–4                                      | 3–5   | 10–500             | Yes                     |
| Ink jet printing | 3/20–50                             | 1–3                                      | 1   | 1–500              | Yes                     |
| Pad printing     | 2                                   | 1–2                                      | 1–2   | 5–250              | Yes                     |
| Flexography      | 2/40                                | 3–5                                      | 1–3   | 5–200              | Yes                     |
| Gravure          | 2/15                                | 3–5                                      | 1–3   | 5–80               | Yes                     |

With respect to patterning, printing techniques can be zero-dimensional (no patterning, such as in dip and spin coating), one-dimensional (line patterning, achievable by, for example, slit casting or meniscus), two-dimensional (any pattern, for instance by flexography, gravure or screen printing) and three-dimensional where either stacked layers can be formed in a single step, such as in advanced curtain and slide coating,<sup>[113]</sup> or the thickness can be varied, such as in prototype ink-jet printing.<sup>[117]</sup> At the present state of the art of chalcopyrite PV processing, where a high temperature step must be implemented before junction formation and parallel lines are used for monolithic series interconnection, either zero or one-dimensional printing (therefore virtually any printing or coating technique) can be employed.

Some of the most widely used liquid deposition techniques and their principal characteristics are (as summarized in Table 2):<sup>[62,112,113,117]</sup>

- *Spin coating* consists of flooding the substrate surface with solution and spinning off the excess, resulting in a uniform layer. Despite the fact that this technique is not applicable for in-line production and ink utilization is generally low, spin coating is one of the most important research techniques for liquid deposition. It has high reproducibility and is suitable over a wide viscosity range, as well as for minimal solution volumes and substrate areas.

- *Doctor blading* distributes the coating solution by moving a blade (often a rod) parallel to the substrate surface or vice versa. Thickness is proportional to the gap between the blade and the substrate. Despite the higher viscosity requirements, this technique has important advantages. Firstly, it can not only be used conveniently at a laboratory scale, as for spin coating, but also in full-scale inline production, making technology transfer more straightforward. Secondly, material utilization can be very high, process control inherently simple and equipment costs minimal.

- *Screen printing* is similar to doctor blading with the difference that a mesh (or screen that can be imprinted with a non- or semi-porous pattern) is inserted between the blade (in this case called “squeegee”) and the substrate. Ink is transferred only through the porous zones of the mesh, resulting in two-dimensional printing. The screen-printing technique is simple and widely used in artist’s workshops and research laboratories, but is also a powerful industrial technique with high material utilization, used for pattern printing on both discrete and roll-to-roll substrates. In the latter case the mesh is shaped as a cylinder and is rolling while the squeegee remains static.

- *Dip coating*, as the name suggests, employs substrate immersion and withdrawal at a constant speed. Usually it is employed when coating of both substrate sides is desired.

- *Meniscus coating* is similar in principle to dip-coating, but circumvents the necessity to coat both substrate sides by providing a meniscus of liquid only to one of the sides. A spinning roller immersed in the ink is usually employed for this purpose.

- *Spray coating* is a technique widely used in all spheres of human life and consists of forming an aerosol and delivering it to the substrate surface. Aerosol formation can

be achieved either by means of pressurized gas or in an “airless” process, for instance by forcing the liquid through a specially designed nozzle. Ultrasonic nozzles can be used for fine and low-velocity aerosols.

- *Pad printing* employs a soft pad that transfers ink from a plate to an object and is best suited for small areas, especially when the surface is not planar.

- *Slit casting* is similar to doctor blading, with the difference that the blade is replaced with a flow-distribution head ending with a slit through which the solution is pumped to the substrate in a highly controlled manner. Multiple slides on a single head can deposit laminar liquid stacks.

- *Curtain* and *slide* coating also employ precisely controlled laminar ink flow. Here the slit is not adjacent to the substrate surface and the ink is either falling to the substrate (curtain) or running down the head surface that is touching the substrate. These techniques are developed by the photographic industry, require very high web speeds (>4 m/s) and can deposit up to 18 layers simultaneously.

- *Gravure printing* employs an engraved metal surface. The ink is introduced in the grooves while the excess is removed by a doctor blade. The recessed image is pressed to the substrate.

- *Flexography* uses a printing cylinder covered with soft material such as silicone rubber that carries the desired pattern. The ink is introduced to an anilox (ceramics engraved with micro indentations) metering cylinder and excess is scraped away by a doctor blade, while the remaining amount is transferred to the substrate by the rubber printing cylinder.

As can be seen from the above summary and Table 2, over the full range of deposition conditions, there is more than one commercial deposition technique that can be readily implemented for direct liquid coating of chalcopyrite absorber layers.

## 7. Conclusions

Recent experience with direct liquid-coating methods for deposition of chalcopyrite absorber layers suggests that these relatively young methods hold promise for achieving future performance comparable to vacuum deposition routes. Some of the important advantages of direct liquid coating include high material utilization, compositional and thickness uniformity and simple technology transfer to extremely high-throughput and relatively low-cost industrial deposition facilities. After addressing specific challenges (for instance the formation of defect-free layers with neither carbon nor oxygen contamination due to enhancing additives), these simple techniques are expected to have significant repercussion on the growth of the photovoltaic industry. The efforts of an increasing number of researchers as well as of the first companies employing direct liquid coating are highly encouraging.

[1] K. Kurokawa, K. Komoto, P. Vleuten, D. Faiman, *Energy from the Desert*, Earthscan, 2007, ISBN 1-84-407363-7.

- [2] O. Morton, *Nature* **2006**, *443*, 19–22.
- [3] A. Simon, *Energy flow charts*, Global Climate and Energy Project, Stanford University, available at <http://gcep.stanford.edu/research/exergycharts.html>.
- [4] I. Repins, M. A. Contreras, B. Egaas, C. DeHart, J. Scharf, C. L. Perkins, B. To, R. Noufi, *Prog. Photovoltaics Res. Appl.* **2008**, *16*, 235–239.
- [5] M. A. Green, K. Emery, Y. Hishikawa, W. Warta, *Prog. Photovoltaics Res. Appl.* **2008**, *16*, 435–440.
- [6] J. Hedstrom, H. Ohlsen, M. Bodegard, A. Kylner, L. Stolt, D. Hariskos, M. Ruckh, H.-W. Schock, *Proc. 23 IEEE Photovoltaic Specialist Conference* **1993**, 364–371.
- [7] J. E. Granata, J. R. Sites, S. Asher, R. Matson, *Proc. 26 IEEE Photovoltaic Specialists Conference* **1997**, 387–390.
- [8] J. J. Cras, C. A. Rowe-Taitt, D. A. Nivens, F. S. Ligler, *Biosens. Bioelectron.* **1999**, *14*, 683–688.
- [9] F. Kessler, D. Rudmann, *Sol. Energy* **2004**, *77*, 685–695.
- [10] F. Kessler, D. Herrmann, M. Powalla, *Thin Solid Films* **2005**, *480–481*, 491–498.
- [11] R. Wuerz, A. Eicke, M. Frankenfeld, F. Kessler, M. Powalla, P. Rogin, O. Yazdani-Assl, *Thin Solid Films* **2009**, *517*, 2415–2418.
- [12] K. Orgassa, H. W. Schock, J. H. Werner, *Thin Solid Films* **2003**, *431–432*, 387–391.
- [13] N. A. Allsop, A. Schoenmann, H.-J. Muffler, M. Bär, M. C. Lux-Steiner, Ch.-H. Fischer, *Prog. Photovoltaics Res. Appl.* **2005**, *13*, 607–616.
- [14] D. Hariskos, S. Spiering, M. Powalla, *Thin Solid Films* **2005**, *480–481*, 99–109.
- [15] Ch. Kaufmann, *Chemical Bath Deposition of Thin Semiconductor Films for Use as Buffer Layers in CuInS<sub>2</sub> Thin Film Solar Cells*, PhD Thesis, Queen's College Oxford, Hilary, **2002**.
- [16] T. Nakada, K. Furumi, A. Kunioka, *IEEE Trans. Electron Devices* **1999**, *46*, 2093–2097.
- [17] M. Bär, A. Ennaoui, J. Klaer, R. Sáez-Araoz, T. Kropp, L. Weinhardt, C. Heske, H.-W. Schock, Ch.-H. Fischer, M. C. Lux-Steiner, *Chem. Phys. Lett.* **2006**, *433*, 71–74.
- [18] T. Todorov, J. Carda, P. Escribano, A. Grimm, J. Klaer, R. Klenk, *Sol. Energy Mater. Sol. Cells* **2008**, *92*, 1274–1278.
- [19] K. Ramanathan, R. Bhattacharya, J. Granata, J. Webb, D. Niles, M. A. Contreras, H. Wiesner, F. Hasoon, R. Noufi, *Proc. of the 26th IEEE Photovoltaic Specialists Conference, Anaheim*, **1997**, pp. 319–322.
- [20] T. Nakada, A. Kunioka, *Appl. Phys. Lett.* **1999**, *74*, 2444–2446.
- [21] U. Malm, M. Edoff, *Prog. Photovoltaics Res. Appl.* **2008**, *16*, 113–121.
- [22] M. W. Denhoff, N. Drolet, *Sol. Energy Mater. Sol. Cells* **2009**, *93*, 1499–1506.
- [23] S. Ishizuka, K. Sakurai, A. Yamada, K. Matsubara, P. Fons, K. Iwata, S. Nakamura, Y. Kimura, T. Baba, H. Nakanishi, T. Kojima, S. Niki, *Sol. Energy Mater. Sol. Cells* **2005**, *87*, 541–548.
- [24] Y. He, *CuInS<sub>2</sub> Thin Films for Photovoltaic: RF Reactive Sputter Deposition and Characterization*, Dissertation, Justus-Liebig-Universität, Gießen, **2003**.
- [25] H. Katagiri, K. Jimbo, W. S. Maw, K. Oishi, M. Yamazaki, H. Araki, A. Takeuchi, *Thin Solid Films* **2009**, *517*, 2455–2460.
- [26] S. H. Wei, L. G. Ferreira, A. Zunger, *Phys. Rev.* **1992**, *45*, 2533–2536.
- [27] S. H. Wei, S. B. Zhang, A. Zunger, *Phys. Rev. B* **1999**, *59*, 2478–2481.
- [28] H. Hahn, G. Frank, W. Klingler, A. Meyer, G. Storer, *Z. Anorg. Allg. Chem.* **1953**, *271*, 153–170.
- [29] W. Shafarman, L. Stolt, in: *Handbook of Photovoltaic Science and Engineering* (Eds.: A. Luque, S. Hegedus), John Wiley & Sons, **2003**.
- [30] I. Kononov, *Thin Solid Films* **2004**, *451–452*, 413–419.
- [31] A. Feltrin, A. Freundlich, *Renewable Energy* **2008**, *33*, 180–185.
- [32] J. Bekker, V. Alberts, A. W. R. Leitch, J. R. Botha, *Thin Solid Films* **2003**, *431–432*, 116–121.
- [33] B. J. Stanbery, *Crit. Rev. Solid State Mater. Sci.* **2002**, *27*, 73–117.
- [34] B. J. Stanbery, S. Kincal, S. Kim, C. H. Chang, S. P. Ahrenkiel, G. Lippold, H. Neumann, T. J. Anderson, O. D. Crisalle, *J. Appl. Phys.* **2002**, *91*, 3598–3604.
- [35] E. Rudigier, B. Barcones, I. Luck, T. Jawhari-Colin, A. Perez-Rodriguez, R. Scheer, *J. Appl. Phys.* **2004**, *95*, 5153–5158.
- [36] E. Rudigier, T. Enzenhofer, R. Scheer, *Thin Solid Films* **2005**, *480–481*, 327–331.
- [37] L. Calvo-Barrio, A. Pérez-Rodríguez, J. Alvarez-García, A. Romano-Rodríguez, B. Barcones, J. R. Morante, K. Siemer, I. Luck, R. Klenk, R. Scheer, *Vacuum* **2001**, *63*, 315–321.
- [38] J. Alvarez-García, J. Marcos-Ruzafa, A. Pérez-Rodríguez, A. Romano-Rodríguez, J. R. Morante, R. Scheer, *Thin Solid Films* **2000**, *361–362*, 208–212.
- [39] B. J. Stanbery, S. Kincal, S. Kim, C. H. Chang, S. P. Ahrenkiel, G. Lippold, H. Neumann, T. J. Anderson, O. D. Crisalle, *J. Appl. Phys.* **2002**, *91*, 3598–3604.
- [40] S. Wagner, J. L. Shay, P. Migliorato, H. M. Kasper, *Appl. Phys. Lett.* **1974**, *25*, 434–435.
- [41] R. A. Mickelsen, W. S. Chen, *Appl. Phys. Lett.* **1980**, *36*, 371–373.
- [42] K. C. Mitchell, E. J. Ermer, D. Pier, *Proc. 20th IEEE Photovoltaic Specialists Conf.*, Las Vegas, **1988**, 1384.
- [43] H. W. Schock, in: *Practical Handbook of Photovoltaics* (Eds: T. Markvart, L. Castañar), Oxford, **2003**, ISBN 1-85-617390-9.
- [44] M. A. Green, K. Emery, Y. Hishikawa, W. Warta, *Prog. Photovoltaics: Res. Appl.* **2009**, *17*, 320–326.
- [45] K. Siemer, J. Klaer, I. Luck, J. Bruns, R. Klenk, D. Braunig, *Sol. Energy Mater. Sol. Cells* **2001**, *67*, 159–166.
- [46] R. Klenk, J. Klaer, R. Scheer, M. Ch. Lux-Steiner, I. Luck, N. Meyer, U. Rühle, *Thin Solid Films* **2005**, *480–481*, 509–514.
- [47] N. Meyer, A. Meeder, D. Schmid, *Thin Solid Films* **2007**, *515*, 5979–5984.
- [48] E. Melikov, D. Meissner, T. Varema, M. Altosaar, M. Kauk, O. Volobujeva, J. Raudoja, K. Timmo, M. Danilson, *Sol. Energy Mater. Sol. Cells* **2009**, *93*, 65–68.
- [49] M. Altosaar, A. Jagomägi, M. Kauk, M. Krunk, J. Krustok, E. Melikov, J. Raudoja, T. Varema, *Thin Solid Films* **2003**, *431–432*, 466–469.
- [50] *Binary Alloy Phase Diagrams* (Eds.: T. B. Massalski, J. L. Murray, L. H. Bennett, H. Baker), American Society for Metals, Materials Park, OH, **1986**.
- [51] R. Klenk, T. Walter, H.-W. Schock, D. Cahen, *Adv. Mater.* **1993**, *5*, 114–119.
- [52] M. A. Contreras, I. Repins, W. K. Metzger, M. Romero, D. Abou-Ras, *Phys. Status Solidi A* **2009**, *206*, 1042–1048.
- [53] M. Powalla, M. Cernjak, J. Eberhardt, F. Kessler, R. Kniese, H. D. Mohring, B. Dimmler, *Sol. Energy Mater. Sol. Cells* **2006**, *90*, 3158–3164.
- [54] U. P. Singh, W. N. Shafarman, R. W. Birkmire, *Sol. Energy Mater. Sol. Cells* **2006**, *90*, 623–630.
- [55] J. Bekker, V. Alberts, A. W. R. Leitch, J. R. Botha, *Thin Solid Films* **2003**, *431–432*, 116–121.
- [56] F. Hergert, R. Hock, A. Weber, M. Purwins, J. Palm, V. Probst, *J. Phys. Chem. Solids* **2005**, *66*, 1903–1907.
- [57] J. Palm, V. Probst, F. H. Karg, *Sol. Energy* **2004**, *77*, 757–765.
- [58] F. Hergert, S. Jost, R. Hock, M. Purwins, J. Palm, *Thin Solid Films* **2006**, *511–512*, 147–152.
- [59] D. Rudmann, *Effects of sodium on growth and properties of Cu(In,Ga)Se<sub>2</sub> thin films and solar cells*, PhD Thesis, Swiss Federal Institute of Technology (ETH), Zürich, **2004**.
- [60] S. Hegedus, *Prog. Photovoltaics Res. Appl.* **2006**, *14*, 393–411.
- [61] M. Keshner, R. Arya, *Study of potential cost reductions resulting from super-large-scale manufacturing of PV modules*, NREL/SR-520-36846, **2004**, available online at [www.nrel.gov/docs/fy05osti/36846.pdf](http://www.nrel.gov/docs/fy05osti/36846.pdf).
- [62] F. C. Krebs, *Sol. Energy Mater. Sol. Cells* **2009**, *39*, 394–412.
- [63] M. Kaelin, D. Rudmann, A. N. Tiwari, *Sol. Energy* **2004**, *77*, 749–756.

- [64] C. J. Hibberd, E. Chassaing, W. Liu, D. B. Mitzi, D. Lincot, A. N. Tiwari, *Prog. Photovolt. Res. Appl.* **2009**, DOI: 10.1002/pip.914.
- [65] I. Oja, M. Nanu, A. Katerski, M. Krunk, A. Mere, J. Raudoja, A. Goossens, *Thin Solid Films* **2005**, 480–481, 82–86.
- [66] J. A. Hollingsworth, K. K. Banger, M. H.-C. Jin, J. D. Harris, J. E. Cowen, E. W. Bohannan, J. A. Switzer, W. E. Buhro, A. F. Hepp, *Thin Solid Films* **2003**, 431–432, 63–67.
- [67] A. F. Hepp, K. K. Banger, M. H.-C. Jin, J. D. Harris, J. S. McNatt, J. E. Dickman, in: *Solution Processing of Inorganic Materials* (Ed.: D. B. Mitzi), John Wiley & Sons, Hoboken, **2009**, p. 157–193.
- [68] S. Weng, M. Cocivera, *J. Appl. Phys.* **1993**, 74, 2046–2052.
- [69] M. Beck, M. Cocivera, *Thin Solid Films* **1996**, 272, 71–82.
- [70] S. Duchemin, J. Bougnot, A. Ghzizal, K. Belghit, *Proc. 9th EPVSEC*, **1989**, 476.
- [71] S. Taunier, J. Sixx-Kurdi, P. P. Grand, A. Chomont, O. Ramdani, L. Parissi, P. Panheleux, N. Naghavi, C. Hubert, M. Ben-Farah, J. P. Fauvarque, J. Connolly, O. Roussel, P. Mogensen, E. Mahé, J. F. Guillemoles, D. Lincot, O. Kerrec, *Thin Solid Films* **2005**, 480–481, 526–531.
- [72] R. N. Bhattacharya, J. F. Hiltner, W. Batchelor, M. A. Contreras, R. N. Noufi, J. R. Sites, *Thin Solid Films* **2000**, 361–362, 396–399.
- [73] O. Ramdani, J. F. Guillemoles, D. Lincot, P. P. Grand, E. Chassaing, O. Kerrec, E. Rzepka, *Thin Solid Films* **2007**, 515, 5909–5912.
- [74] E. Chassaing, O. Ramdani, P.-P. Grand, J.-F. Guillemoles, D. Lincot, *Phys. Status Solidi C* **2008**, 5, 3445–3448.
- [75] O. Roussel, O. Ramdani, E. Chassaing, P.-P. Grand, M. Lamirand, A. Etcheberry, O. Kerrec, J.-F. Guillemoles, D. Lincot, *J. Electrochem. Soc.* **2008**, 155, D141–D147.
- [76] S. Taunier, D. Guimard, D. Lincot, J. Guillemoles, P. Grand, US patent appl. No. 20060151331.
- [77] T. Todorov, E. Cordoncillo, J. F. Sánchez-Royo, J. Carda, P. Escribano, *Chem. Mater.* **2006**, 18, 3145–3150.
- [78] T. Todorov, L. Oliveira, J. Carda, P. Escribano, *Phys. Status Solidi C* **2008**, 5, 3437–3440.
- [79] L. Oliveira, T. Todorov, E. Chassaing, D. Lincot, J. Carda, P. Escribano, *Thin Solid Films* **2009**, 517, 2272–2276.
- [80] D. B. Mitzi, M. Yuan, W. Liu, A. J. Kellock, S. J. Chey, L. Gignac, A. G. Schrott, *Thin Solid Films* **2009**, 517, 2158–2162.
- [81] D. B. Mitzi, *Adv. Mater.* **2009**, 21, 3141–3158.
- [82] D. B. Mitzi, M. Yuan, W. Liu, A. J. Kellock, S. J. Chey, V. Deligne, A. G. Schrott, *Adv. Mater.* **2008**, 20, 3657–3662.
- [83] a) J. A. Nekuda Malik, M. F. A. M. van Hest, A. Miedaner, C. J. Curtis, J. E. Leisch, P. A. Parilla, M. Kaufman, M. Taylor, B. J. Stanbery, R. P. O'Hayre, D. S. Ginley, *J. Mater. Res.* **2009**, 24, 1375–1387; b) C. J. Curtis, A. Miedaner, M. Van Hest, D. S. Ginley, WO2008063190.
- [84] M. Yuan, D. B. Mitzi, *Dalton Trans.* **2009**, 6078–6088.
- [85] E. Sotaniemi, J. Hirvonen, H. Isomäki, J. Takkunen, J. Kaila, *Ann. Clin. Res.* **1971**, 3, 30–33.
- [86] M. R. Robinson, J. K. J. van Duren, C. Leidholm, Pat. Appl. No. US2007/0169813A1.
- [87] M. Kaelin, D. Rudmann, F. Kurdesau, H. Zogg, T. Meyer, A. N. Tiwari, *Thin Solid Films* **2005**, 480–481, 486–490.
- [88] H. Ishihara, S. Nakagawa, N. Mochizuki, M. Ishida, U. S. Pat. 5910336, 1999.
- [89] Nanosolar Inc., PVSEC 17, Tokyo, Japan, **2007**, available at [http://www.nanosolar.com/cache/PVSEC17\\_ns\\_dft.pdf](http://www.nanosolar.com/cache/PVSEC17_ns_dft.pdf).
- [90] B. M. Basol, *Thin Solid Films* **2000**, 361–362, 514–519.
- [91] V. K. Kapur, A. Bansal, P. Le, O. I. Asensio, *Thin Solid Films* **2003**, 431–432, 53–57.
- [92] V. K. Kapur, B. M. Basol, C. R. Leidholm, R. A., Roe, European Pat. Appl. No. EP1870943.
- [93] V. Kapur, R. Kemmerle, A. Bansal, J. Haber, J. Schmitzberger, P. Le, D. Guevarra, T. Stempien, *Proc. 31st IEEE Photovoltaic Specialist Conference*, **2008**, San Diego, CA.
- [94] V. K. Kapur, A. Bansal, P. Le, O. Asensio, N. Shigeoka, *Technical report NREL/SR-520-35574*, available at <http://www.nrel.gov/docs/fy04osti/35574.pdf>.
- [95] J. Brinker, G. Scherrer, *Sol-gel Science* Elsevier Science Academic Press, San Diego, **1989**, ISBN 0-12-134970-5.
- [96] K. Tanaka, N. Moritake, H. Uchiki, *Sol. Energy Mater. Sol. Cells* **2007**, 91, 1199–1201.
- [97] K. Tanaka, M. Oonuki, N. Moritake, H. Uchiki, *Sol. Energy Mater. Sol. Cells* **2009**, 93, 583–587.
- [98] C. Eberspacher, C. Fredric, K. Pauls, J. Serra, *Thin Solid Films* **2001**, 387, 18–22.
- [99] M. Kaelin, D. Rudmann, F. Kurdesau, T. Meyer, H. Zogg, A. N. Tiwari, *Thin Solid Films* **2003**, 431–432, 58–62.
- [100] Ch. von Klopman, J. Djordjevic, R. Scheer, *J. Cryst. Growth* **2006**, 289, 113–120.
- [101] E. Rudigier, J. Djordjevic, C. von Klopman, B. Barcones, A. Perez-Rodriguez, R. Scheer, *J. Phys. Chem. Solids* **2005**, 66, 1954–1960.
- [102] T. Arita, N. Suyama, Y. Kita, S. Kitamura, T. Hibino, H. Takada, K. Omura, N. Ueno, M. Murozono, *Proc. 20th IEEE Photovoltaic Spec. Conf.* **1988**, 1650–1655.
- [103] M. Roscheisen, B. Sager, Pat. Appl. No. WO **2006/073437**.
- [104] D. B. Mitzi, in: *Solution Processing of Inorganic Materials* (Ed.: D. B. Mitzi), John Wiley & Sons, Hoboken, **2009**, p. 77–108.
- [105] F. J. Garcia, M. S. Tomar, *Jpn. J. Appl. Phys. Part 1* **1983**, 22, 535–538.
- [106] D. L. Schulz, C. J. Curtis, R. A. Flitton, H. Wiesner, J. Keane, R. J. Matson, K. M. Jones, P. A. Parilla, R. Noufi, D. S. Ginley, *J. Electron. Mater.* **1998**, 27, 433–437.
- [107] J. K. J. van Duren, B. J. Bollman, M. Roscheisen, B. Sager, Pat. Appl. No. US**2007/0092648**.
- [108] B. M. Sager, D. Yu, M. R. Robinson, Pat. Appl. No. US**2008/0149176**.
- [109] J. K. J. van Duren, M. R. Roscheisen, M. R. Robinson, C. Leidholm, Pat. Appl. No. US **2007/0169811**.
- [110] M. R. Robinson, J. K. J. van Duren, C. Leidholm, Pat. Appl. No. US **2007/0169813**.
- [111] T. Todorov, M. Kita, J. Carda, P. Escribano, *Thin Solid Films* **2009**, 517, 2541–2544.
- [112] A. A. Tracton, *Coating Technology Handbook, Third Edition*, CRC Press, Boca Raton, **2006**.
- [113] D. R. Gamota, P. Brazis, K. Kalyanasundaram, J. Zhang, *Printed Organic And Molecular Electronics*, Kluwer Academic Publishers, **2004**.
- [114] Y. Zhao, *Phys. Status Solidi C* **2009**, 6, 744–747.
- [115] J. Palm, V. Probst, F. H. Karg, *Sol. Energy* **2004**, 77, 757–765.
- [116] M. Powalla, G. Voorwinden, D. Hariskos, P. Jackson, R. Kniese, *Thin Solid Films* **2009**, 517, 2111–2114.
- [117] E. Sachs, M. Cima, J. Cornie, *CIRP Ann.* **1990**, 39, 201–204.

Received: August 25, 2009

Published Online: November 24, 2009

# Access to Metal Complexes of the Elusive Imidobis(phosphaalkene) Anion by N–Si Bond Cleavage of a *N*-Silylimino-Bridged Bis(phosphaalkene)

Roxana M. Bîrzoï,<sup>[a]</sup> Delia Bugnariu,<sup>[a]</sup> Rafael Guerrero Gimeno,<sup>[a]</sup> Antje Riecke,<sup>[a]</sup> Constantin Daniliuc,<sup>[a]</sup> Peter G. Jones,<sup>[a]</sup> László Könczöl,<sup>[b]</sup> Zoltán Benkő,<sup>[b]</sup> László Nyulászi,<sup>[b]</sup> Rainer Bartsch,<sup>[a]</sup> and Wolf-W. du Mont<sup>\*[a]</sup>

**Keywords:** Bis(phosphaalkenes) / PNP ligands / pi-conjugation / Gold / Rhodium / DFT calculations

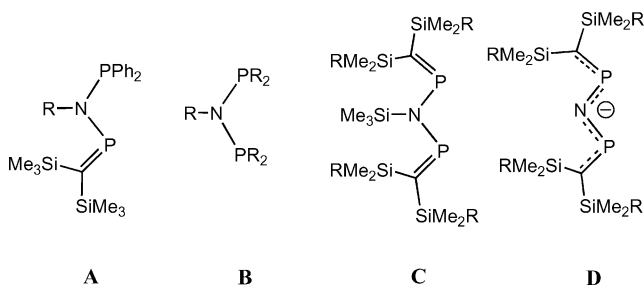
Metalation of the aminophosphaalkene (*i*PrMe<sub>2</sub>Si)<sub>2</sub>C=PN(H)-SiMe<sub>3</sub> (**2**) with lithium diisopropylamide (LDA) in THF solution, followed by the reaction of the lithium salt **3** with the *P*-chlorophosphaalkenes (RMe<sub>2</sub>Si)<sub>2</sub>C=P(Cl) (**1a**, R = Me; **1b**, R = *i*Pr; **1c**, R = Ph), furnishes the first *N*-silylimino-bridged bis(phosphaalkenes) [(*i*PrMe<sub>2</sub>Si)<sub>2</sub>C=P]<sub>2</sub>NSiMe<sub>3</sub> (**4a**) and [(*i*PrMe<sub>2</sub>Si)<sub>2</sub>C=P][(RMe<sub>2</sub>Si)<sub>2</sub>C=P]NSiMe<sub>3</sub> (**4b**, R = Me; **4c**, R = Ph). The N–Si bond cleavage of **4a** under very mild conditions with AuCl(THT) and with [RhCl(COD)]<sub>2</sub> provides binuclear Au<sup>I</sup> and Rh<sup>I</sup> complexes **5**, **6** of the *P,P'*-coordinated imidobis(phosphaalkene) anion [(*i*PrMe<sub>2</sub>Si)<sub>2</sub>C=P]<sub>2</sub>N<sup>−</sup>, the first

case of elusive *P*=C-unsaturated congeners of the “classic” bis(phosphanyl)amide ligands. Solid **4a** exists in a helically distorted S-shaped structure with two inequivalent *P*=C groups, but <sup>31</sup>P-NMR reveals the equivalence of both *P*=C groups in solution at the NMR time scale. The *P*=C and *P*–N bonds distances in **4a** do not indicate significant conjugation within the C=P–N–P=C moieties whereas in complexes **5** and **6** the W-shaped CPNPC heteropentadienide anion exhibits strong 5-center-6- $\pi$  conjugation according to DFT calculations and to the experimental *P*=C and *P*=N bond lengths.

## Introduction

We are currently exploring properties of “hybrid” *P*-phosphanyl-amino-phosphaalkene ligands (Me<sub>3</sub>Si)<sub>2</sub>C=PN-(R)PPh<sub>2</sub> (**A**) with the intention of combining features of catalytically significant, small bite angle iminobisphosphane “PNP” ligands RN(PR<sub>2</sub>)<sub>2</sub> (**B**)<sup>[1]</sup> with those of carbon-bridged bidentate phosphaalkenes such as Yoshifuji’s strongly  $\pi$ -accepting 1,2-diaryl-3,4-diphosphanylidene-cyclobutene ligands.<sup>[2]</sup> The electronegative nitrogen substituent is expected to enhance the  $\pi$ -acceptor properties of the *P*=C bond<sup>[3]</sup> in type **A** and **C** ligands.<sup>[4]</sup>

The recent observation, that bidentate type **A** ligands undergo unusual phosphorus insertion reactions into Pd–Cl and Pt–Cl bonds leading to unique metalla(chloro)ylid chelate complexes,<sup>[4]</sup> gave rise to the expectation that stable iminobis(phosphaalkenes) may also exhibit unusual behaviour as ligands in transition metal chemistry, and *N*-silyl derivatives (**C**) might even be potential precursors of the elusive 2,4-diphospha-3-azapentadienide anion [(Me<sub>3</sub>Si)<sub>2</sub>C=P]<sub>2</sub>N<sup>−</sup> (**D**),<sup>[5]</sup> the *P*=C-unsaturated counterpart of the widely used bis(phosphanyl)amides (R<sub>2</sub>P)<sub>2</sub>N<sup>−</sup>.<sup>[6]</sup>



## Results

[(Me<sub>3</sub>Si)<sub>2</sub>C=P]<sub>2</sub>NSiMe<sub>3</sub>, made from Li[(Me<sub>3</sub>Si)<sub>2</sub>C=PNSiMe<sub>3</sub>] with (Me<sub>3</sub>Si)<sub>2</sub>C=P(Cl), is a thermally unstable oil,<sup>[7]</sup> but bulkier (*i*PrMe<sub>2</sub>Si)<sub>2</sub>C=P groups<sup>[4b]</sup> stabilise type **C** compounds. The reactions of the bulkier aminophosphaalkene **2** with lithium diisopropylamide (LDA) in THF solution [Equation (1)], followed by reactions of the lithium salt **3** with *P*-chlorophosphaalkenes (RMe<sub>2</sub>Si)<sub>2</sub>C=P(Cl) (R = *i*Pr: **1a**; Me: **1b**; Ph: **1c**)<sup>[8–10]</sup> at temperatures below –40 °C furnish solutions of *N*-(trimethylsilyl)imino-bridged bis(phosphaalkenes) **4a–4c**.

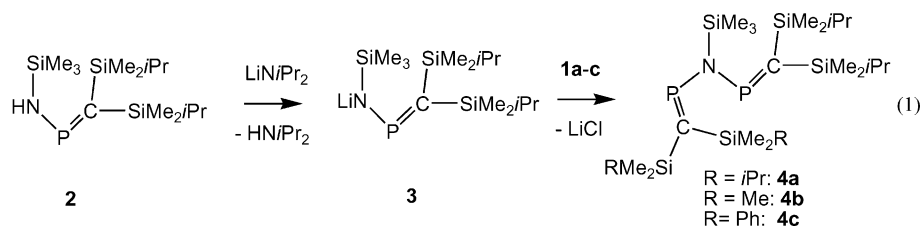
Work-up by recrystallisation gave colorless crystals of **4a**, yellowish crystals of **4b** (both at –20 °C), and a brown oil containing **4c**.

The <sup>31</sup>P NMR spectrum of **4a** exhibits a single resonance whereas the mixed substituted compounds **4b**, **4c** show AM patterns [**4b**:  $\delta$  = <sup>31</sup>P = 365.4 and 361.7 ppm, <sup>2</sup>*J*(P,P) 19.6 Hz; **4c**:  $\delta$  = <sup>31</sup>P = 370.6 and 365.6 ppm, <sup>2</sup>*J*(P,P)

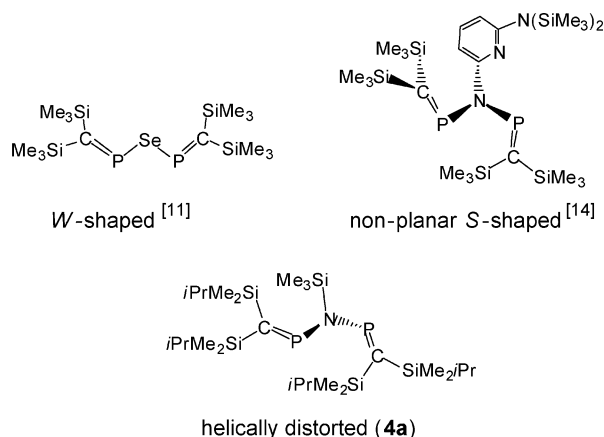
[a] Institut für Anorganische und Analytische Chemie der Technischen Universität Braunschweig, Hagenring 30, 38106 Braunschweig, Germany

[b] Department of Inorganic and Analytical Chemistry, Budapest University of Technology and Economics, Szt Gellert ter 4, 1521 Budapest, Hungary

Supporting information for this article is available on the WWW under <http://dx.doi.org/10.1002/ejic.200900982>.



19.7 Hz]. The NMR equivalence of the two  $^{31}\text{P}$  nuclei of **4a** in solution would be consistent with either a symmetric structure, such as W-shaped  $\{[(\text{Me}_3\text{Si})_2\text{C}=\text{P}]_2\text{N}\}^-$  and  $[(\text{Me}_3\text{Si})_2\text{C}=\text{P}]_2\text{Se}$ ,<sup>[11]</sup> or with a less symmetric ground state conformation<sup>[12–14]</sup> (see Scheme 1), that still allows free rotation of the P–N bonds at the NMR time scale at room temperature in solution. All the B3LYP/6-31+G\* optimized structures of the  $[(\text{R}_3\text{Si})_2\text{C}=\text{P}]_2\text{N}(\text{SiR}_3)$  molecules ( $\text{R}$ : H, Me) were non-planar. For  $\text{R} = \text{H}$  the minima were located within an  $0.9 \text{ kcal mol}^{-1}$  energy range including the S- and W-shaped forms (Scheme 1) – see Supporting Information. The fact that several conformers exist with similar energies on the rotational potential energy surface is indicative of their low energy interconversion. For  $\text{R} = \text{Me}$  only the non-symmetrical S-shaped structure could be optimized, in agreement with the X-ray structure (see below). Similar behaviour was observed in case of the bis(phosphavinyl)ether analogues,<sup>[15]</sup> indicating the effect of steric encumbrance in determining the final structure. The X-ray crystal structure determination of solid **4a** (Figure 1) at low temperature reveals the presence of a helically distorted structure with two inequivalent P=C groups (torsion angles  $\text{C11}–\text{P1}–\text{N}–\text{P2}$  and  $\text{C22}–\text{P2}–\text{N}–\text{P1}$   $-52^\circ$  and  $-45^\circ$ ). The P=C and P–N bonds distances in **4a** do not indicate significant conjugation within the  $\text{C}=\text{P}–\text{N}–\text{P}=\text{C}$  moiety.<sup>[4b,14]</sup>



Scheme 1. Conformations of uncharged heteroatom-bridged bis(phosphaalkenes).

First experiments on the reactivity of **4a** with  $\text{AuCl}(\text{THT})$  and with  $[\text{RhCl}(\text{COD})]_2$  led to the observation of Si–N bond cleavage by chlorotrimethylsilane elimination under very mild conditions furnishing the dinuclear complexes  $\{\text{Au}[(\text{iPrMe}_2\text{Si})_2\text{C}=\text{P}]_2\text{N}\}_2$  (**5**) and  $\text{Rh}_2\text{Cl}\{[(\text{iPrMe}_2\text{Si})_2\text{C}=\text{P}]_2\text{N}\}_2$  (**6**).

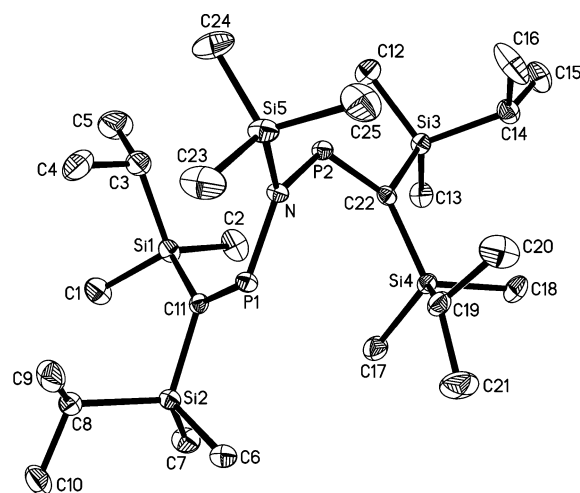
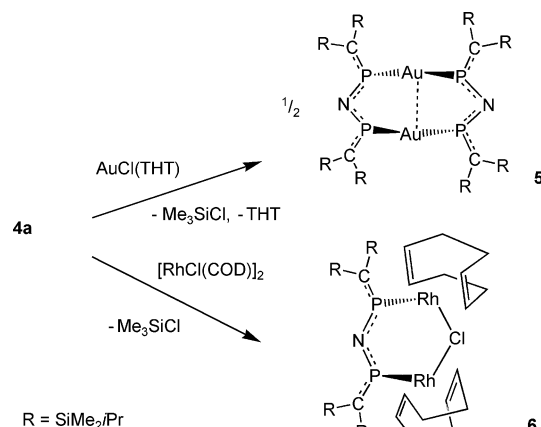


Figure 1. Molecular structure of **4a**. Selected bond lengths [ $\text{\AA}$ ] and angles [ $^\circ$ ]:  $\text{P1}–\text{C11}$  1.6617(17),  $\text{P2}–\text{C22}$  1.6602(18),  $\text{P1}–\text{N}$  1.7226(14),  $\text{P2}–\text{N}$  1.7262(15),  $\text{Si5}–\text{N}$  1.7887(14),  $\text{P1}–\text{N}–\text{P2}$   $130.60(8)$ ,  $\text{P1}–\text{N}–\text{Si5}$   $117.43(8)$ ,  $\text{P2}–\text{N}–\text{Si5}$   $111.92(8)$ . Hydrogen atoms are omitted for clarity. Atoms are drawn as 50% thermal ellipsoids.

$\text{Me}_2\text{Si})_2\text{C}=\text{P}]_2\text{N}\}(\text{COD})_2$  (**6**) that contain, according to X-ray crystal structure determinations, the elusive 2,4-diphospha-3-azapentadienyl anion as a  $P,P'$ -coordinated bidentate ligand (Scheme 2, Figures 2 and 3). Yellow **5** [ $d(\text{Au}–\text{Au}) = 3.02 \text{ \AA}$ ] is related to the insoluble white bis(diphenylphosphanyl)amide gold complex  $[\text{Au}(\text{Ph}_2\text{P})_2\text{N}]_2$  made first by Schmidbaur et al.<sup>[16]</sup> and also regarded as a dimer.



Scheme 2. Reactions of **4a** with  $\text{Au}^{\text{I}}$  and  $\text{Rh}^{\text{I}}$  chloro complexes.

The dinuclear  $\text{Rh}^{\text{I}}$  complex **6** contains as bridging ligands one chloride anion and one sterically crowded  $[(\text{iPrMe}_2\text{Si})_2\text{C}=\text{P}]_2\text{N}^-$  anion, which clearly prevents reac-

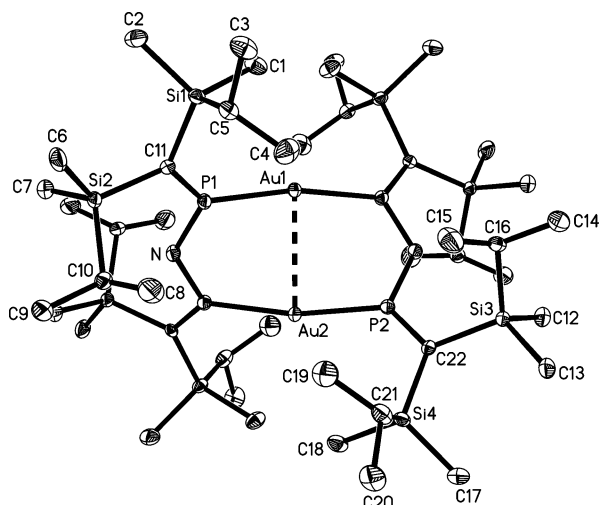


Figure 2. Molecular structure of **5** (the Au–Au vector lies along a twofold axis). Selected bond lengths [Å] and angles [°]: Au1–P1 2.3051(8), Au2–P2 2.2971(8), P1–C11 1.652(3), P2–C2 1.651(3), P1–N 1.616(3), P2–N 1.616(3), P1–N–P2 124.57(13), P1AuP1A 168.58(4), NP1Au1 114.29(8), NP2Au2 114.70(8). Hydrogen atoms are omitted for clarity. Atoms are drawn as 50% thermal ellipsoids.

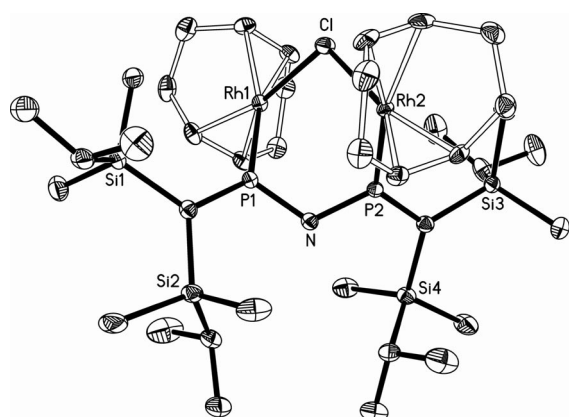
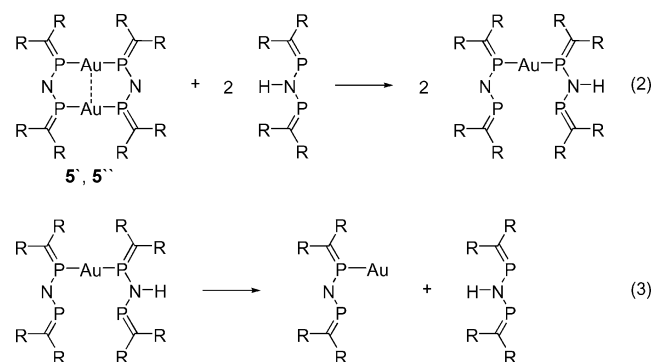


Figure 3. Molecular structure of **6**. Selected bond lengths [Å] and angles [°]: Rh1–P1 2.2891(5), Rh2–P2 2.2781(5), Rh1–Cl 2.4081(5), Rh2–Cl 2.4048(4), P1–C11 1.6599(17), P2–C22 1.6551(17), P1–N 1.6198(14), P2–N 1.6207(15), P1–N–P2 118.94(9), Rh1–Cl–Rh2 112.375(17). Hydrogen atoms are omitted for clarity. Atoms are drawn as 50% thermal ellipsoids.

tions of **6** with another equivalent of **4a**. Each of the COD ligands chelates a Rh atom as in the starting material  $[\text{RhCl}(\text{COD})]_2$ .<sup>[17]</sup> The PN distances in **5** and **6** are about 10 pm shorter than those in the uncharged ligand **4a**. Since the P=C distances are unaffected or even slightly shorter in the complexes, compared with **4a** (see captions of Figures 2 and 3), the large increase of PN bond strength suggests the presence of a highly delocalized heteropentadienide  $6\pi$  system.

DFT calculations on 2,4-diphospha-3-azapentadienes (type **C** and **D** structures)<sup>[18]</sup> reveal that, while the  $[(\text{R}_3\text{Si})_2\text{C}=\text{P}]_2\text{N}(\text{SiR}_3)$  type **C** systems are non-planar even with the small  $\text{R} = \text{H}$  substituent, the corresponding imide anion  $[(\text{R}_3\text{Si})_2\text{C}=\text{P}]_2\text{N}^-$  is perfectly planar in case of  $\text{R} = \text{H}$ . This planarity, together with the short PN distances (see above)

indicates that the delocalisation stabilization for the anion exceeds that of the amine. Indeed, the second order perturbational analysis of the Fock matrix in the NBO basis (which estimates the energy of donor-acceptor interactions between natural orbitals) provides  $37.0 \text{ kcal mol}^{-1}$  stabilization energy between the nitrogen lone pair and each  $\pi(\text{P}=\text{C})^*$  orbital, significantly exceeding the  $19.7 \text{ kcal mol}^{-1}$  stabilization energy for  $[(\text{H}_3\text{Si})_2\text{C}=\text{P}]_2\text{NH}$ .  $[(\text{Me}_3\text{Si})_2\text{C}=\text{P}]_2\text{N}^-$  has an S-shaped and an energetically nearly identical, slightly non-planar W-shaped [still with  $33.0 \text{ kcal mol}^{-1}$   $\text{n} \rightarrow \pi(\text{P}=\text{C})^*$  interaction energy] structure. To elucidate the structure of the complex **5**, Bader analysis and isodesmic reactions were investigated for the model compounds **5'** and **5''** (**5'**,  $\text{R} = \text{H}$ , and **5''**,  $\text{R} = \text{SiH}_3$ , Scheme 3). The topological analysis of the electron density revealed the presence of a bond critical point (CP) between the two gold atoms in **5''**. The electron density at this CP is quite low ( $0.02\text{--}0.03 \text{ e Å}^{-3}$ , see ESI), however, it is comparable to those observed for hydrogen bonded interactions and is slightly larger than the value reported for Au–CN–Ni compounds.<sup>[19]</sup>



Scheme 3. Isodesmic reactions (see text).

The energetic consequences of the auriphilic interaction were estimated using the isodesmic reactions (2) and (3) in Scheme 3. The energy of the reaction (2) is remarkably large ( $27\text{--}30 \text{ kcal mol}^{-1}$  at different levels of theory, see ESI), comparable with the Au–P binding energy ( $30\text{--}34 \text{ kcal mol}^{-1}$ , see ESI), which was determined as the reaction energy of Equation (3). It is important to note that this unusually large interaction energy<sup>[20]</sup> is only partly attributable to the auriphilicity because the extended  $\pi$ -conjugation in the dimeric complex (see the MO representing  $\pi$ -delocalisation in Figure 4) also contributes to the overall stabilization of this reaction.

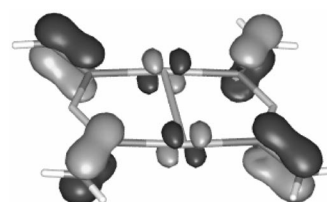


Figure 4. The HOMO-3 of the gold complex **5'**.

## Conclusions

The first stable *N*-(trimethylsilyl)iminobis(phosphaalkene) [(*i*PrMe<sub>2</sub>Si)<sub>2</sub>C=P]<sub>2</sub>NSiMe<sub>3</sub> (**4a**) is an excellent source of the imidobis(phosphaalkene) *P,P'*-metal-coordinated anion [(*i*PrMe<sub>2</sub>Si)<sub>2</sub>C=P]<sub>2</sub>N<sup>−</sup>, the first example of an elusive *P*-unsaturated congener of the classic bis(phosphanyl)-amides (R<sub>2</sub>P)<sub>2</sub>N<sup>−</sup>.<sup>[6,16]</sup> The imidobis(phosphaalkene) anion in binuclear Au<sup>I</sup> and Rh<sup>I</sup> complexes **5** and **6** exhibits strong 5-center-6- $\pi$  conjugation in its W-shaped heteropentadienide CPNPC moiety. N–Si bond cleavage of *N*-(trimethylsilyl)iminobis(phosphaalkenes) under very mild conditions will open the way to an emerging chemistry of PNP complexes with anionic 5-center-6 $\pi$  systems.

## Experimental Section

**General:** All procedures were carried out under standard inert gas techniques in dry solvents.

**2:** A solution prepared from 5.34 g (19.01 mmol) **1a** in 40 mL of dichloromethane, 9 mL (68.8 mmol) triethylamine, and 3.07 g (19.01 mmol) 1,1,1,3,3,3-hexamethyldisilazane was heated for 7 d at 50 °C. After removing the triethylammonium chloride and the formed chlorotrimethylsilane, vacuum distillation at 65 °C (0.5 mbar) furnished 4.94 g (78%) of [(*i*PrMe<sub>2</sub>Si)<sub>2</sub>CPN(H)SiMe<sub>3</sub>] (**2**). C<sub>14</sub>H<sub>36</sub>NPSi<sub>3</sub> (333.67): calcd. C 50.39, H 10.87, N 4.20; found C 49.59, H 10.97, N 4.06.  $\delta$  = <sup>31</sup>P (121.5 MHz; C<sub>6</sub>D<sub>6</sub>) 325.8 ppm.

**4a:** To a solution of **2** (2.20 g, 6.6 mmol) in THF (20 mL) was added LDA (3.5 mL of a 2 M THF/heptane/ethylbenzene solution, 6.6 mmol) at −40 °C. The reaction mixture was warmed to room temperature whilst stirring over 1 h. The <sup>31</sup>P NMR spectrum of the solution indicated quantitative formation of anion **3** [ $\delta$  = <sup>31</sup>P (81 MHz; C<sub>6</sub>D<sub>6</sub>):  $\delta$  = 405.2 ppm]. The formed *i*Pr<sub>2</sub>NH and the solvent were removed in vacuo and the residue was dissolved in 10 mL of THF. The THF solution of **3** was added dropwise to a solution of **1a** (1.85 g, 6.6 mmol) in 10 mL of THF at −40 °C. The solution was warmed to ambient temperature and after 15 min the <sup>31</sup>P NMR spectrum showed the desired product **4a** [ $\delta$  = <sup>31</sup>P (81 MHz; C<sub>6</sub>D<sub>6</sub>):  $\delta$  = 365.1 ppm]. Precipitation of the LiCl by addition of pentane, filtration, and evaporation of the solvent gave **4a** (3.31 g, 87%) as a brown solid. Recrystallisation from hexane at −20 °C gave colorless crystals. C<sub>25</sub>H<sub>61</sub>NP<sub>2</sub>Si<sub>5</sub> (578.13): calcd. C 51.94, H 10.63, N 2.42; found C 50.89, H 10.51, N 2.41.  $\delta$  = <sup>31</sup>P (121.5 MHz; C<sub>6</sub>D<sub>6</sub>) 365.1 ppm. **4b** and **4c** were prepared in a similar way.

**5:** A solution of **4a** (0.170 g, 0.294 mmol) in CH<sub>2</sub>Cl<sub>2</sub> (3 mL) was added dropwise to a stirred solution of Au(THT)Cl (0.095 g, 0.294 mmol) in CH<sub>2</sub>Cl<sub>2</sub> (10 mL). The reaction mixture was allowed to stir at ambient temperature for 1 h. Solvent, tetrahydrothiophene and chlorotrimethylsilane were removed in vacuo and the residue was solved in 3 mL of CH<sub>2</sub>Cl<sub>2</sub> and stored at −20 °C to give yellow crystals (0.096 g, 46%).  $\delta$  = <sup>31</sup>P (162 MHz, CDCl<sub>3</sub>) 252.4 ppm. MS (EI) *m/z* = 1401.8 (M)<sup>+</sup>, 1358.7 [M − *i*Pr]<sup>+</sup>, 1316.7 (M − SiMe-*i*Pr)<sup>+</sup>, 1300.7 (M − SiMe<sub>2</sub>*i*Pr)<sup>+</sup>, 1157.8 [M − PC(SiMe<sub>2</sub>*i*Pr)<sub>2</sub>]<sup>+</sup>.

**6:** A solution of **4a** (1.43 g, 2.48 mmol) in CH<sub>2</sub>Cl<sub>2</sub> (10 mL) was added dropwise to a solution of {RhCODCl}<sub>2</sub> (0.61 g, 1.24 mmol) in CH<sub>2</sub>Cl<sub>2</sub> (10 mL) at ambient temperature and the resulting reaction mixture was subsequently stirred for 12 h. The volume of CH<sub>2</sub>Cl<sub>2</sub> was reduced to 2 mL and the product was precipitated with pentane. Filtration and drying in vacuo afforded **6** (0.78 g, 66%) as a yellow-brown solid. The volume of the filtrate was reduced to

2–3 mL and a few drops of CH<sub>3</sub>CN were added; from this mixture crystals were obtained within 12 h. Yield: 0.78 g, 66%, m.p. 147 °C. C<sub>38</sub>H<sub>68</sub>ClNP<sub>2</sub>Rh<sub>2</sub>Si<sub>4</sub> (954.51): calcd. C 47.82, H 7.18, N 1.47; found C 46.30, H 8.03, N 1.61.  $\delta$  = <sup>31</sup>P (121.5 MHz; C<sub>6</sub>D<sub>6</sub>) 306.2 ppm [typical pattern for an AA'XX'-system, <sup>1</sup>J<sub>P,Rh</sub> = 166.3 Hz, <sup>3</sup>J<sub>P,Rh</sub> = 33.6, <sup>2</sup>J(P,P) = 27.6 Hz].

CCDC-745584 (for **4a**), -745586 (for **5**), and -745587 (for **6**) contain the crystallographic data (excluding structure factors) for this article. These data can be obtained free of charge from The Cambridge Crystallographic Data Centre via [www.ccdc.cam.ac.uk/data\\_request/cif](http://www.ccdc.cam.ac.uk/data_request/cif).

**Supporting Information** (see also the footnote on the first page of this article): Details on the computational studies.

## Acknowledgments

The European Cooperation in the Field of Science and Technology (COST) (CM0802) and the Deutsche Forschungsgemeinschaft (DFG) (MO290/28-1) are acknowledged for financial support.

- [1] a) M. S. Balakrishna, V. Sreenivasa Reddy, S. S. Krishnamurthy, J. F. Nixon, J. C. T. R. Burckett, St. Laurent, *Coord. Chem. Rev.* **1994**, *129*, 1–90; b) A. Carter, S. A. Cohen, N. A. Cooley, A. Murphy, J. Scutt, D. F. Wass, *Chem. Commun.* **2002**, 858–859; c) A. Bollmann, K. Blann, J. T. Dixon, F. M. Hess, E. Klian, H. Maumela, D. S. McGuinness, D. H. Morgan, A. Neveling, S. Otto, M. Overett, A. M. Z. Slavin, P. Wasserscheid, S. Kuhlmann, *J. Am. Chem. Soc.* **2004**, *126*, 14712.
- [2] a) S. Ikeda, F. Ohata, M. Miyoshi, R. Tanaka, T. Minami, F. Ozawa, M. Yoshifuji, *Angew. Chem.* **2000**, *112*, 4686–4687; *Angew. Chem. Int. Ed.* **2000**, *39*, 4512–4513; b) T. Minami, H. Okamoto, S. Ikeda, R. Tanaka, F. Ozawa, M. Yoshifuji, *Angew. Chem.* **2001**, *113*, 4633–4635; *Angew. Chem. Int. Ed.* **2001**, *40*, 4501–4503.
- [3] D. Gudat, E. Niecke, W. Sachs, P. Rademacher, Z. *Anorg. Allg. Chem.* **1987**, *545*, 7–23.
- [4] a) D. Lungu, C. Daniliuc, P. G. Jones, L. Nyulászi, Z. Benko, R. Bartsch, W.-W. du Mont, *Eur. J. Inorg. Chem.* **2009**, 2901–2905; b) R. M. Birzoi, D. Bugnariu, R. Guerrero Gimeno, D. Lungu, V. Zota, C. Daniliuc, P. G. Jones, Z. Benkő, L. Nyulászi, R. Bartsch, W.-W. du Mont, E. Niecke, *Chem. Eur. J.*, DOI: 10.1002/chem.200903166.
- [5] The heavier congeners [(Me<sub>3</sub>Si)<sub>2</sub>C=P]<sub>2</sub>E<sup>−</sup> (E = P, As) are known: a) V. Thelen, D. Schmidt, M. Nieger, E. Niecke, W.-W. Schoeller, *Angew. Chem.* **1996**, *108*, 354; *Angew. Chem. Int. Ed. Engl.* **1996**, *35*, 313–315; b) A. B. Rozhenko, A. Ruban, V. Zota, M. Nieger, W. W. Schoeller, E. Niecke, manuscript to be submitted.
- [6] a) H. Schmidbaur, F. E. Wagner, A. Wohlleben-Hammer, *Chem. Ber.* **1979**, *112*, 496–500; b) J. Ellermann, M. Lietz, Z. *Naturforsch., Teil B* **1980**, *35*, 64–67; c) P. Bhattacharya, J. D. Woollins, *Polyhedron* **1995**, *14*, 3367–3388; d) M. T. Gamer, P. W. Roesky, *Inorg. Chem.* **2005**, *43*, 4903–4906.
- [7] a) V. Zota, Dissertation Univ. of Bonn, **1999**; b) *14th Int. Conf. on Phosphorus Chemistry*, Cincinnati (USA), **1998**, Abstract P270: V. Thelen, M. Nieger, E. Niecke, *Phosphorus Sulfur Silicon Relat. Elem.* **1999**, *147*, 407; c) R. Guerrero Gimeno, Dissertation, Techn. Univ. of Braunschweig, **2008**.
- [8] D. Bugnariu, Dissertation, Techn. Univ. of Braunschweig, **2007**.
- [9] R. Appel, A. Westerhaus, *Angew. Chem.* **1980**, *92*, 578–579; *Angew. Chem. Int. Ed. Engl.* **1980**, *19*, 556–557; R. Appel, J. Peters, A. Westerhaus, *Tetrahedron Lett.* **1981**, *22*, 4957–4960.
- [10] A. Riecke, Diplomarbeit, Techn. Univ. of Braunschweig, **2006**.
- [11] W.-W. du Mont, T. Gust, J. Mahnke, R. M. Birzoi, L. Barra, D. Bugnariu, F. Ruthe, C. Wismach, P. G. Jones, K. Kar-

- aghiosoff, L. Nyulászi, Z. Benkő, *Angew. Chem.* **2007**, *119*, 8836–8839; *Angew. Chem. Int. Ed.* **2007**, *46*, 8682–8685.
- [12] M. J. S. Dewar, M. A. Fox, D. J. Nelson, *J. Organomet. Chem.* **1980**, *185*, 157–181.
- [13] E. Niecke, R. Detsch, M. Nieger, *Chem. Ber.* **1990**, *123*, 797–799.
- [14] C. Volkholz, Dissertation, Univ. of Bonn, **2005**.
- [15] R. M. Birzoi, D. Bugnariu, C. Goers, R. Guerrero Gimeno, T. Gust, A. Riecke, Z. Benkő, L. Könczöl, L. Nyulászi, C. Wismach, P. G. Jones, R. Schmutzler, R. Bartsch, W.-W. du Mont, *Z. Naturforsch., Teil B* **2009**, *64*, 73–82.
- [16] a) H. Schmidbaur, S. Schnatterer, K. C. Dash, A. A. M. Aly, *Z. Naturforsch., Teil B* **1983**, *38*, 62–66; b) R. Usón, A. Laguna, M. Laguna, M. C. Gimeno, P. G. Jones, C. Fittschen, G. M. Sheldrick, *J. Chem. Soc., Chem. Commun.* **1986**, 509–510.
- [17] a) J. A. Ibers, R. G. Snyder, *Acta Crystallogr.* **1962**, *15*, 923–929; b) D. J. A. De Ridder, P. Imhoff, *Acta Crystallogr., Sect. C* **1994**, *50*, 1569–1572.
- [18] For details and references of computations see Supporting Information.
- [19] E. Colacio, F. Lloret, R. Kivekäs, J. Suárez-Varela, M. R. Sundberg, R. Uggla, *Inorg. Chem.* **2003**, *42*, 560.
- [20] P. Pyykkö, *Angew. Chem.* **2004**, *116*, 4512–4557; *Angew. Chem. Int. Ed.* **2004**, *43*, 4412–4456.

Received: October 7, 2009

Published Online: November 25, 2009

## 2,3,5,6-Tetrafluoro-*p*-phenylenebis(phosphanes) – Preparation and Structure of an Electron-Poor P–R<sub>F</sub>–P Linker

Andreas Orthaber,<sup>[a]</sup> Ferdinand Belaj,<sup>[a]</sup> Jörg H. Albering,<sup>[b]</sup> and Rudolf Pietschnig\*<sup>[a]</sup>

**Keywords:** Phosphorus / Phosphanes / Fluorinated ligands / Electron-deficient compounds

A general synthetic access to functional 2,3,5,6-tetrafluoro-*p*-phenylenebis(phosphanes) is presented, which should open the way to linear phosphorus-based conjugated systems incorporating an electron-deficient aryl moiety. 1,4-

Bis[bis(diethylamino)phosphanyl]-2,3,5,6-tetrafluorobenzene and 1,4-bis(dichlorophosphanyl)-2,3,5,6-tetrafluorobenzene have been synthesized in good yields and were characterized by spectroscopic methods and X-ray crystallography.

### Introduction

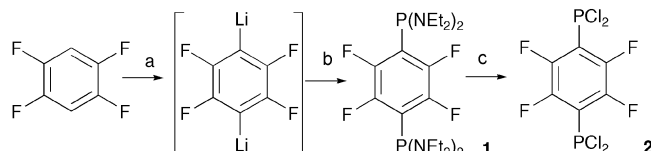
Phosphanes – especially dichlorophosphanes – are important precursors in the synthesis of  $\sigma^2\lambda^3$ -phosphanes. In the last decades general synthetic routes to diphosphenes,<sup>[1]</sup> iminophosphanes,<sup>[2]</sup> phosphaaalkenes<sup>[3,4]</sup> and phospholes<sup>[5]</sup> have been established, which employ dichlorophosphanes as [P<sup>+</sup>] synthons. The parent *p*-phenylenebis(dichlorophosphane) has been prepared in 1962,<sup>[6]</sup> and the 2,3,5,6-tetramethyl-<sup>[7]</sup> and -tetraaryl-substituted<sup>[4]</sup> congeners later on. In 2002, Gates et al. reported the synthesis of a 2,3,5,6-tetramethyl-*p*-phenylenebis(phosphaaalkene) and polymeric derivatives thereof.<sup>[7]</sup> Until now only little is known about electron-deficient bis(phosphaaalkenes),<sup>[8–10]</sup> although many electron-rich low-coordinated phosphanes have been reported in the last decades.<sup>[11–13]</sup> A special focus of experimental and theoretical work was set on push-pull-substituted low-coordinated phosphanes, especially iminophosphanes,<sup>[14,15]</sup> diphosphenes,<sup>[16,17]</sup> and phosphaaalkenes.<sup>[9]</sup> Recently, the twist angle of diphosphenes was studied theoretically, but a detailed explanation highlighting the influence of the electron-accepting groups remains still elusive.<sup>[18,19]</sup> The incorporation of C<sub>6</sub>F<sub>5</sub> groups into phospholes was achieved by Baumgartner and co-workers, and they explained their stabilizing effect on the LUMO level by means of DFT calculations.<sup>[20]</sup>

### Results and Discussion

In the literature the syntheses of fully alkylated or arylated 2,3,5,6-tetrafluoro-*p*-phenylenebis(phosphanes) have

been reported, where the fluorine atoms in higher fluorinated precursors are partially replaced by isolobal PR<sub>2</sub> units.<sup>[21–23]</sup> The latter are, however, not available for further functionalization at the phosphorus atoms, except for the transformation to the corresponding phosphoranes.<sup>[24,25]</sup>

A general route towards the synthesis of dichlorophosphanes includes the reaction of the corresponding R–M (M = Li or MgBr; R = organic substituent) compound with an excess of PCl<sub>3</sub>, if steric protection of R is sufficient to prevent multiple substitution at the phosphorus atom. Recently, we investigated the reaction of 2,3,5,6-F<sub>4</sub>C<sub>6</sub>HLi with PCl<sub>3</sub> and observed the formation of a mixture of multiple-substituted phosphanes [PCl<sub>*n*</sub>(C<sub>6</sub>F<sub>4</sub>H)<sub>3–*n*</sub>] even if a 10-fold excess of PCl<sub>3</sub> was used.<sup>[26]</sup> To circumvent this problem, we treated the “protected” chlorobis(diethylamino)phosphane CIP(NEt<sub>2</sub>)<sub>2</sub> with 2,3,5,6-F<sub>4</sub>C<sub>6</sub>Li<sub>2</sub> at a low temperature. Preparation of the latter dilithio compound is not trivial. On the one hand the temperature must not raise above –50 °C at any time (to prevent the instantaneous formation of highly reactive aryne species), and on the other hand LiCl elimination does not take place at temperatures below –70 °C. Owing to incomplete lithiation, the monosubstituted tetrafluorobenzene derivative is always obtained as a byproduct, but can be removed from the desired product by crystallization (Scheme 1).



Scheme 1. Synthesis of **1** and **2** starting from 2,3,5,6-F<sub>4</sub>C<sub>6</sub>H<sub>2</sub>. Reaction conditions: (a) *n*BuLi/thf, –80 °C; (b) CIP(NEt<sub>2</sub>)<sub>2</sub>, –35 °C; (c) HCl(g)/Et<sub>2</sub>O, 0 °C.

Compound **1** is obtained as a white solid showing a single <sup>31</sup>P NMR resonance at  $\delta$  = 84.9 ppm as well as a single resonance in the <sup>19</sup>F NMR spectrum at  $\delta$  = –141.6 ppm in

[a] University of Graz, Department of Chemistry, Schubertstr. 1, 8010 Graz, Austria  
Fax: +43-316 380 9835  
E-mail: rudolf.pietschnig@uni-graz.at

[b] Graz University of Technology, Institute of Chemistry and Technology of Materials, Stremayrgasse 16, 8010 Graz, Austria

Supporting information for this article is available on the WWW under <http://dx.doi.org/10.1002/ejic.200901042>.

solution, which shows no resolved coupling between  $^{19}\text{F}$  and  $^{31}\text{P}$ . Single crystals of **1** are obtained by crystallization from a cold 1,2-dimethoxyethane (dme)/pentane solution. In the crystal structure, the molecules are arranged around centers of symmetry. The benzene ring shows a significant in-plane deformation with C–C–C angles of only  $112.6(2)^\circ$  at C1 and a mean value of  $123.7(2)^\circ$  at the fluorine-substituted atoms C2 and C3 (Figure 1). Nevertheless, the benzene ring is planar [max. deviation of  $0.005(10)$  Å of the C atoms from the l.s. plane (l.s. = least-squares)], whereas the atoms P1, N1, and N2 are lying  $0.32(1)$ ,  $-0.81(1)$ , and  $-0.15(1)$  Å above/below the l.s. plane through the C atoms, respectively. Consequently, the molecules show significant deviations from  $C_{2h}$  symmetry presumably due to steric and/or electronic interaction of the nitrogen atoms with the central aryl moiety. Examples for the latter are known from the literature.<sup>[27]</sup> The P–C bond is rather long [C1–P1  $1.867(2)$  Å] compared to undistorted P–C bonds. Out of the eight structurally characterized bis[(dialkylamino)aryl]-phosphanes reported so far, also 2,3,5,6- $\text{F}_5\text{C}_6\text{P}(\text{NiPr}_2)_2$  shows an elongated P–C bond [ $1.896(5)$  Å], which is even longer than in **1**.<sup>[28]</sup> Similar to **1**, the only other structurally characterized *P,P'*-bis(dialkylamino)-substituted *p*-phenylenebis(phosphane), i.e. 1,4-bis[(diethylamino)phosphanyl]-2,5-dimethylbenzene,<sup>[29]</sup> shows an out-of-plane angle of the P–C bonds of  $5.2(1)^\circ$ , which is only half of that observed for **1** [ $10.0(1)^\circ$ ]. In addition, the P–C bond [P1–C1  $1.842(1)$  Å] is longer than average, yet shorter than in **1**. Interestingly, **1** is stable under ambient conditions towards moisture and air over weeks.

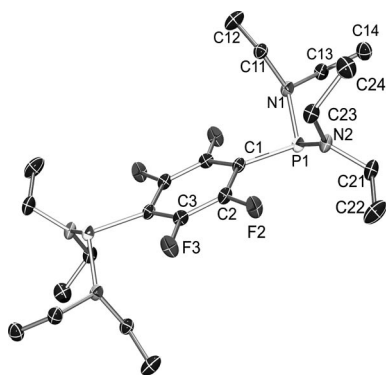


Figure 1. ORTEP drawing of **1**. Thermal ellipsoids are drawn at 50% probability level. Hydrogen atoms are omitted for clarity.

Acidic cleavage with  $\text{HCl}(\text{g})$  of the diethylamino groups requires prolonged reaction times. After complete reaction, the ammonium salt is removed by filtration, and the spectroscopically pure product is obtained after removal of the solvent. The coupling patterns in the NMR spectra of **2** are characterized by higher-order spin systems for which in the simplest case an  $\text{AA}'\text{X}_2\text{X}'_2$  spin system can be expected by assuming unhindered rotation of the phosphane units. The AX and AX' coupling constants have been estimated to 59 and 12 Hz, respectively. Owing to hindered rotation around the P–C bonds at room temperature, the molecule shows in fact a lower symmetry and a more complex spin system.

Crystallization from  $\text{CDCl}_3$  yields crystals of **2** suitable for X-ray diffraction (Figure 2). The central perimeter of **2** is almost planar [max. deviation  $0.003(1)$  Å] and shows significantly smaller deformation than in **1** [C–C–C angle ranging from  $116.4(1)$  to  $122.1(1)^\circ$ ]. The P–C bond length is  $1.843(1)$  Å, which is slightly shorter than **1**. This is attributed to the lower conjugation with the aryl group of the P–Cl bonds compared to the P–N bonds. The central perimeter is bisecting the Cl–P–Cl angle [ $100.86(2)^\circ$ ]. Angles between the l.s. plane and the P–Cl bonds are quite similar [ $49.71(2)$  and  $51.16(2)^\circ$ ]. Each of the molecules has almost  $C_{2h}$  symmetry, and the  $\text{PCl}_2$  groups are thus arranged in an alternating fashion. The structure shows P–Cl distances of  $2.0529(4)$  and  $2.0543(4)$  Å, which is in the normal range for a single bond between these elements. The packing shows short intermolecular contacts  $\text{F1}\cdots\text{C3}$  of  $2.964(1)$  Å, which is  $0.21$  Å shorter than the sum of the van der Waals radii.

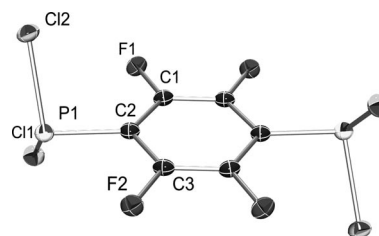


Figure 2. ORTEP drawing of **2**. Ellipsoids are drawn at 50% probability level.

## Conclusions

We report the preparation of a 2,3,5,6-tetrafluoro-*p*-phenylenebis(dichlorophosphane) in good overall yield from cheap starting materials in a straightforward reaction protocol. This molecule is likely to become a key compound in the synthesis of polymeric low-coordinated phosphanes incorporating strongly electron-withdrawing aryl linkers. Further experimental and theoretical work will be needed for a better understanding of the bonding situation and the resulting changes in the electronic properties of perfluorinated arylphosphanes.

## Experimental Section

**General:** Reactions were carried out under argon by using modified Schlenk techniques or in a glovebox. Solvents were degassed and dried by using a PureSolv solvent purification system. *n*BuLi and diethylamine were purchased from Sigma Aldrich and used as received.  $\text{PCl}_3$  (from Sigma Aldrich) was distilled prior to use. 1,2,4,5-tetrafluorobenzene was obtained from ABCR and used as received.  $\text{CIP}(\text{NEt}_2)_2$  was prepared according to a modified procedure by King et al.<sup>[30]</sup> Lithiation of the tetrafluorobenzene was carried out according to a modified procedure by Harper et al.<sup>[31]</sup> NMR spectra were recorded with a Varian Unity Inova 400 and a Bruker Avance 300, operating at  $^1\text{H}$  frequencies of 399.983 MHz and 300.132 MHz, respectively.  $^{19}\text{F}$  NMR spectra for **1** were recorded with a Bruker Avance 500 spectrometer (470.740 MHz for  $^{19}\text{F}$ ). Chemical shifts are given in ppm, referenced externally to

TMS, TMS, H<sub>3</sub>PO<sub>4</sub> (85%), and CF<sub>3</sub>C<sub>6</sub>H<sub>5</sub> for <sup>1</sup>H, <sup>13</sup>C, <sup>31</sup>P, and <sup>19</sup>F, respectively. Mass spectrometry was performed with an Agilent 5975C mass spectrometer equipped with a direct injection unit (DI-EI).

**Preparation of 1:** **CAUTION:** The dilithio intermediate in the preparation of **1** is highly reactive and prone to LiF elimination at temperatures above –50 °C under the formation of very reactive aryne species! To a cooled solution of 1,2,4,5-tetrafluorobenzene (7.61 g, 50.7 mmol) in thf (ca. 50 mL) was added *n*BuLi (hexane solution, 1.6 M, 70 mL, 112 mmol) over a period of 1 h by maintaining the temperature strictly below –75 °C. The suspension was stirred at this temperature for 3 h, until chlorobis(diethylamino)-phosphane (24.23 g, 115 mmol) [dissolved in thf (50 mL)] was slowly added and the mixture warmed to –50 °C and stirred at this temperature for another 3 h. The suspension was allowed to reach room temp. overnight. After filtration, the solvent was removed in vacuo to yield the crude product as a viscous oil. Crystallization from 1,2-dimethoxyethane (dme) at –80 °C yielded a white solid product (15.16 g). Recrystallization from pentane/dme gave crystals suitable for X-ray diffraction. Yield 60% (15.16 g, 30.4 mmol). C<sub>22</sub>H<sub>40</sub>F<sub>4</sub>N<sub>4</sub>P<sub>2</sub> (498.52): calcd. C 53.00, H 8.09; found C 52.65, H 8.45. <sup>1</sup>H NMR (400 MHz, CDCl<sub>3</sub>, 25 °C): δ = 3.05 (m, 8 H, CH<sub>2</sub>), 1.02 (t, <sup>3</sup>J<sub>H,H</sub> = 7.1 Hz, 12 H, CH<sub>3</sub>) ppm. <sup>13</sup>C NMR (75.5 MHz, CDCl<sub>3</sub>, 25 °C): δ = 14.73 (d, <sup>3</sup>J<sub>P,C</sub> = 1.1 Hz, 4 C, CH<sub>2</sub>), 44.17 (d, <sup>2</sup>J<sub>P,C</sub> = 19.1 Hz, 4 C, CH<sub>2</sub>), 121.05 (m, 2 C, C<sub>aryl</sub>-P), 145.40 (dm, <sup>1</sup>J<sub>C,F</sub> = 252.6 Hz, 4 C, C<sub>aryl</sub>-F) ppm. <sup>31</sup>P NMR (121.5 MHz, CDCl<sub>3</sub>, 25 °C): δ = 84.9 (br. m) ppm. <sup>19</sup>F NMR (CDCl<sub>3</sub>, 470.7 MHz, 25 °C): δ = –141.6 (br. m) ppm. M.p. 92 °C (from dme). MS (DI-EI): *m/z* (%) = 426.2 (100) [M – NEt<sub>2</sub>], 104.1 (95) [PNEt], 175.1 (72) [PNEt<sub>2</sub>], 498.4 (35) [M<sup>+</sup>], 355.1 (21) [M – (NEt<sub>2</sub>)<sub>2</sub>].

**Preparation of 2:** Solid **1** (707 mg, 1.4 mmol) was dissolved in diethyl ether (150 mL) and the mixture cooled with an ice bath. Anhydrous HCl(g) was bubbled through the solution for 1 h. After filtration and removal of the solvent, the product was obtained as a white crystalline material. Recrystallization from cold (–10 °C) CDCl<sub>3</sub> afforded crystals suitable for X-ray diffraction. Yield 75% (374 mg, 1.1 mmol). A second crop [10% (49 mg, 0.1 mmol)] was obtained by washing the ammonium salt with diethyl ether (20 mL). C<sub>6</sub>Cl<sub>4</sub>F<sub>4</sub>P<sub>2</sub> (351.82): calcd. C 20.48, H 0.00; found C 20.19, H 0.25. <sup>13</sup>C NMR (75.5 MHz, CDCl<sub>3</sub>, 25 °C): δ = 123.58 (dt, <sup>1</sup>J<sub>P,C</sub> = 84.5, <sup>2</sup>J<sub>C,F</sub> = 16.8 Hz), 146.56 (dm, <sup>1</sup>J<sub>C,F</sub> = 262.2 Hz) ppm. <sup>31</sup>P NMR (121.5 MHz, CDCl<sub>3</sub>, 25 °C): δ = 133.8 (higher-order “tt”, <sup>3</sup>J<sub>P,F</sub> = 59, <sup>4</sup>J<sub>P,F</sub> = 12 Hz) ppm. <sup>19</sup>F NMR (CDCl<sub>3</sub>, 282.4 MHz, 25 °C): δ = –129.4 (higher-order “dd”, <sup>3</sup>J<sub>P,F</sub> = 59.3, <sup>4</sup>J<sub>P,F</sub> = 12.5 Hz) ppm. M.p. 85 °C (from CDCl<sub>3</sub>). MS (DI-EI): *m/z* (%) = 351.8 (100) [M, Cl<sub>4</sub> pattern], 314.9 (61) [M – Cl, Cl<sub>3</sub> pattern], 100.9 (36) [PCl<sub>2</sub>, Cl<sub>2</sub> pattern], 210.9 (33) [M – 4 Cl], 248.9 (6) [M – PCl<sub>2</sub>, Cl<sub>2</sub> pattern].

**X-ray Crystallography:** The structures were solved by direct methods using SHELXS and refined with SHELXL. For **2**, absorption of twinned crystals was treated by using TWINABS correction. Crystal data for **1** (pentane/dme): C<sub>22</sub>H<sub>40</sub>F<sub>4</sub>N<sub>4</sub>P<sub>2</sub>, *M* = 498.52, monoclinic space group *P*2<sub>1</sub>/*c*, *a* = 10.401(3), *b* = 9.786(3), *c* = 13.144(6) Å, β = 102.67(4)°, *V* = 1305.3(8) Å<sup>3</sup>, *Z* = 2, *d<sub>c</sub>* = 1.268 g cm<sup>–3</sup>, μ = 0.212 mm<sup>–1</sup>, *T* = 95 K, *R*1 = 0.0498 for 2184 observed reflections with *I* > 2σ(*I*) and *wR*2 = 0.1239 for all 2835 unique reflections, *GOF* = 1.031. Crystal data for **2** (CDCl<sub>3</sub>): C<sub>6</sub>Cl<sub>4</sub>F<sub>4</sub>P<sub>2</sub>, *M* = 351.80, monoclinic space group *P*2<sub>1</sub>/*c*, *a* = 8.2844(8), *b* = 10.3702(10), *c* = 6.4688(6) Å, β = 90.690(3)°, *V* = 555.70(9) Å<sup>3</sup>, *Z* = 2, *d<sub>c</sub>* = 2.102 Mg/m<sup>3</sup>, μ = 1.370 mm<sup>–1</sup>, *T* = 101(2) K, *R*1 = 0.0209 for all 1877 observed reflections with

*I* > 2σ(*I*) and *wR*2 = 0.0551 for all 2006 unique reflections, *GOF* = 1.087. CCDC-749006 (for **1**) and -749007 (for **2**) contain the supplementary crystallographic data for this paper. These data can be obtained free of charge from The Cambridge Crystallographic Data Centre via [www.ccdc.cam.ac.uk/data\\_request/cif](http://www.ccdc.cam.ac.uk/data_request/cif).

**Supporting Information** (see footnote on the first page of this article): Crystallographic details and selected bond lengths for **1** and **2**.

## Acknowledgments

Financial support by the Austrian Science Fund (FWF) (Grants P18591-B03 and P20575-N19) and the EU-COST Action CM0802 “PhoSciNet” is gratefully acknowledged.

- [1] M. Yoshifuji, I. Shima, N. Inamoto, K. Hirotsu, T. Higuchi, *J. Am. Chem. Soc.* **1981**, *103*, 4587–4589.
- [2] E. Niecke, W. Flick, *Angew. Chem. Int. Ed. Engl.* **1973**, *12*, 585–586.
- [3] S. Shah, J. D. Protasiewicz, *Chem. Commun.* **1998**, 1585–1586.
- [4] S. Shah, T. Concolino, A. L. Rheingold, J. D. Protasiewicz, *Inorg. Chem.* **2000**, *39*, 3860–3867.
- [5] P. J. Fagan, W. A. Nugent, *J. Am. Chem. Soc.* **1988**, *110*, 2310–2312.
- [6] E. M. Evleth, L. D. Freeman, R. I. Wagner, *J. Org. Chem.* **1962**, *27*, 2192–2197.
- [7] V. A. Wright, D. P. Gates, *Angew. Chem. Int. Ed.* **2002**, *41*, 2389–2392.
- [8] M. Yam, C.-W. Tsang, D. P. Gates, *Inorg. Chem.* **2004**, *43*, 3719–3723.
- [9] J. D. Watts, D. J. Watts, M.-J. Huang, *J. Phys. Chem. A* **2009**, *113*, 1886–1891.
- [10] K. B. Dillon, H. P. Goodwin, *J. Organomet. Chem.* **1994**, *469*, 125–128.
- [11] C. Moser, M. Nieger, R. Pietschnig, *Organometallics* **2006**, *25*, 2667–2672.
- [12] R. Pietschnig, E. Niecke, *Organometallics* **1996**, *15*, 891–893.
- [13] R. Pietschnig, E. Niecke, M. Nieger, K. Airola, *J. Organomet. Chem.* **1997**, *529*, 127–133.
- [14] W. W. Schoeller, T. Busch, E. Niecke, *Chem. Ber.* **1990**, *123*, 1653–1654.
- [15] K. Miqueu, J.-M. Sotiropoulos, G. Pfister-Guillouzo, V. L. Rudzevich, H. Gornitzka, V. Lavallo, V. D. Romanenko, *Eur. J. Inorg. Chem.* **2004**, 2289–2300.
- [16] K. B. Dillon, H. P. Goodwin, *J. Organomet. Chem.* **1992**, *429*, 169–171.
- [17] M. Scholz, H. W. Roesky, D. Stalke, K. Keller, F. T. Edelmann, *J. Organomet. Chem.* **1989**, *366*, 73–85.
- [18] T. L. Allen, A. C. Scheiner, Y. Yamaguchi, H. F. Schaefer III, *J. Am. Chem. Soc.* **1986**, *108*, 7579–7588.
- [19] H.-L. Peng, J. L. Payton, J. D. Protasiewicz, M. C. Simpson, *J. Phys. Chem. A* **2009**, *113*, 7054–7063.
- [20] Y. Ren, Y. Dienes, S. Hettel, M. Parvez, B. Hoge, T. Baumgartner, *Organometallics* **2009**, *28*, 734–740.
- [21] S. Sasaki, Y. Tanabe, M. Yoshifuji, *Bull. Chem. Soc. Jpn.* **1999**, *72*, 563–572.
- [22] H. G. Horn, H. J. Lindner, *Chem. Ztg.* **1988**, *112*, 195–200.
- [23] L. I. Goryunov, J. Grobe, V. D. Shteingarts, B. Krebs, A. Lindemann, E.-U. Würthwein, C. Mück-Lichtenfeld, *Chem. Eur. J.* **2000**, *6*, 4612–4622.
- [24] L. I. Goryunov, V. D. Shteingartz, J. Grobe, *Russ. J. Org. Chem.* **2004**, *40*, 757–758.
- [25] R. Weiss, R. May, B. Pomrehn, *Angew. Chem. Int. Ed. Engl.* **1996**, *35*, 1232–1234.
- [26] A. Orthaber, F. Belaj, R. Pietschnig, *J. Organomet. Chem.*, DOI: 10.1016/j.jorganchem.2009.10.025.
- [27] R. Weiss, F. G. Pühlhofer, *J. Am. Chem. Soc.* **2007**, *129*, 547–553.

- [28] P. W. Dyer, J. Fawcett, M. J. Hanton, R. D. W. Kemmitt, R. Padda, N. Singh, *Dalton Trans.* **2003**, 104–113.
- [29] S. D. N. Stephan, S. A. Reiter, S. D. Nogai, H. Schmidbaur, *Z. Naturforsch., Teil B* **2005**, *60*, 511–519.
- [30] R. B. King, P. M. Sundaram, *J. Org. Chem.* **1984**, *49*, 1784–1789.
- [31] R. J. Harper, E. J. Soloski, C. Tamborski, *J. Org. Chem.* **1964**, *29*, 2385–2389.

Received: October 27, 2009

Published Online: November 24, 2009

# Preparation, Crystal Structures, and Spectroscopic and Redox Properties of Nickel(II) Complexes Containing Phosphane–(Amine or Quinoline)-Type Hybrid Ligands and a Nickel(I) Complex Bearing 8-(Diphenylphosphanyl)quinoline

Akira Hashimoto,<sup>[a]</sup> Hiroshi Yamaguchi,<sup>[a]</sup> Takayoshi Suzuki,<sup>\*[b]</sup> Kazuo Kashiwabara,<sup>[a]</sup> Masaaki Kojima,<sup>[b]</sup> and Hideo D. Takagi<sup>\*[a]</sup>

**Keywords:** N,P ligands / Nickel / Phosphane ligands / Ligand effects

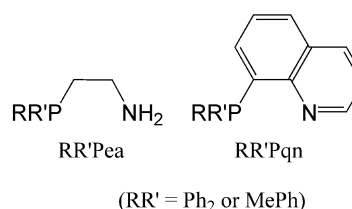
Nickel(II) complexes containing P–N-type bidentate hybrid ligands of 2-aminoethylphosphanes (RR'Pea; RR' = Ph<sub>2</sub> or MePh) or 8-quinolylphosphanes (RR'Pqn), namely [Ni(P–N)<sub>2</sub>](BF<sub>4</sub>)<sub>2</sub> [P–N = Ph<sub>2</sub>Pea (**1**), MePhPea (**2**), Ph<sub>2</sub>Pqn (**3**), or MePhPqn (**4**)] have been prepared, and their structural, spectroscopic, and electrochemical properties determined. The crystal structure analysis indicates that the 2-aminoethylphosphane complexes (**1** and **2**) have a square-planar coordination geometry around the Ni<sup>II</sup> center with a *cis*(*P,P*) configuration, whereas the 8-quinolylphosphane complexes (**3** and **4**) exhibit a severe tetrahedral distortion because of the steric repulsion between the *ortho*-H atoms in the mutually *cis*-positioned quinolyl rings. Complexes **1** and **2** maintain their

diamagnetic square-planar four-coordinate structure on acetonitrile solution, whereas complexes **3** and **4** show paramagnetic behavior. Spectroscopic and electrochemical measurements suggest that the ligand-field strengths of these four P–N-type ligands increase in the order Ph<sub>2</sub>Pqn (**3**) < MePhPqn (**4**) < Ph<sub>2</sub>Pea (**1**) < MePhPea (**2**). The Ph<sub>2</sub>Pqn complex **3** is readily reduced by Zn powder to afford the corresponding nickel(I) complex [Ni(Ph<sub>2</sub>Pqn)<sub>2</sub>](BF<sub>4</sub>) (**5**). The crystal structure of complex **5** reveals that the Ni<sup>I</sup> ion adopts a distorted tetrahedral coordination geometry with slightly longer (≈ 0.05 Å) Ni–P and Ni–N bond lengths than those in the corresponding Ni<sup>II</sup> complex **3**.

## Introduction

Transition-metal complexes containing hybrid-type hemilabile phosphane ligands<sup>[1]</sup> have recently attracted a great deal of interest in applications as wide ranging as effective chemosensors for small molecules,<sup>[2]</sup> homogeneous catalysts for the activation of inert small molecules,<sup>[3]</sup> anticancer agents,<sup>[4]</sup> and so on.<sup>[5]</sup> In order to develop novel functionalities and catalytic and biological activities for these complexes, it is essential to design the electronic differentiations<sup>[1b,1c]</sup> of the donor groups as well as the steric requirements of the hybrid-type ligands. In this respect, we are currently focusing our attention on P–N-type hybrid ligands bearing an amine or pyridine/quinoline donor group and the investigation of their coordination behavior.<sup>[6–11]</sup> Herein we consider nickel(II) complexes having 2-amino-

ethylphosphanes (RR'Pea) or 8-quinolylphosphanes (RR'Pqn) (Scheme 1), which are P–N-type bidentate ligands that form a five-membered chelate ring.



Scheme 1. P–N-type ligands used in this study.

Several transition-metal complexes with (2-aminoethyl)-diphenylphosphane (Ph<sub>2</sub>PCH<sub>2</sub>CH<sub>2</sub>NH<sub>2</sub>; Ph<sub>2</sub>Pea) have been prepared<sup>[12–14]</sup> since the first reports by Issleib and co-workers.<sup>[15]</sup> In contrast, complexes of the analogous P–N-type ligand having an asymmetric phosphorus donor atom, namely (2-aminoethyl)methylphenylphosphane (MePhPCH<sub>2</sub>CH<sub>2</sub>NH<sub>2</sub>; MePhPea), are limited to those of cobalt(III),<sup>[12c]</sup> palladium(II), and platinum(II).<sup>[16]</sup> Moreover, studies on the molecular structures and properties of metal complexes with 8-quinolylphosphanes are also scarce.<sup>[7–9,17,18]</sup> As an example, one of the present authors (T.S.) has reported a novel crystal modification of *cis*(*P,P*)-

[a] Graduate School of Science and Research Center for Materials Science, Nagoya University, Furocho, Chikusa, Nagoya 464-8602, Japan  
Fax: +81-52-789-5473  
E-mail: h.d.takagi@nagoya-u.jp

[b] Department of Chemistry, Faculty of Science, Okayama University, Tsushima-naka 3-1-1, Okayama 700-8530, Japan  
Fax: +81-86-251-7900  
E-mail: suzuki@cc.okayama-u.ac.jp

Supporting information for this article is available on the WWW under <http://dx.doi.org/10.1002/ejic.200900767>.

[Pd(Ph<sub>2</sub>Pqn)<sub>2</sub>Br<sub>2</sub>] (yellow blocks vs. orange prisms) and its chloride and/or tetrafluoroborate salts, which could be related to a tetrahedral distortion of the coordination plane of Pd<sup>II</sup> because of the intramolecular steric interaction between two mutually *cis*-positioned quinolyl groups.<sup>[8]</sup> For the corresponding Ni<sup>II</sup> complexes, including those of the related P–N-type hybrid ligands,<sup>[19]</sup> there are very limited reports on structural determinations and spectroscopic characterization of the complexes. We have previously described the syntheses and structures of [Ni(Me<sub>2</sub>Pea)<sub>2</sub>]Cl<sub>2</sub>, [Ni(Me<sub>2</sub>Pea)<sub>2</sub>][NiCl<sub>4</sub>] (where Me<sub>2</sub>Pea was previously abbreviated as edmp),<sup>[6]</sup> and [Ni(Me<sub>2</sub>Pqn)<sub>2</sub>](BF<sub>4</sub>)<sub>2</sub>.<sup>[7]</sup> Herein we report the syntheses, structural analyses, and spectroscopic and electrochemical properties of the Ni<sup>II</sup> complexes [Ni(P–N)<sub>2</sub>](BF<sub>4</sub>)<sub>2</sub> containing Ph<sub>2</sub>Pea (**1**), MePhPea (**2**), Ph<sub>2</sub>Pqn (**3**), or MePhPqn (**4**) as the P–N ligand (Scheme 1). The corresponding Ni<sup>I</sup> complex, [Ni(Ph<sub>2</sub>Pqn)<sub>2</sub>]BF<sub>4</sub> (**5**), prepared by reduction of complex **3** with Zn powder, is also described.

## Results and Discussion

### Preparation and Crystal Structures of Nickel(II) Complexes

The nickel(II) complexes [Ni(P–N)<sub>2</sub>](BF<sub>4</sub>)<sub>2</sub> (**1–4**) were prepared from Ni(BF<sub>4</sub>)<sub>2</sub>·6H<sub>2</sub>O and a small excess of P–N ligand in methanol or ethanol following a similar method to that used to obtain [Ni(Me<sub>2</sub>Pea or Me<sub>2</sub>Pqn)<sub>2</sub>](BF<sub>4</sub>)<sub>2</sub>.<sup>[6,7]</sup> [Ni(Ph<sub>2</sub>Pea)<sub>2</sub>](BF<sub>4</sub>)<sub>2</sub> (**1**) was obtained analytically pure, and magnetic susceptibility measurements at room temperature indicated that this complex is diamagnetic. The <sup>1</sup>H NMR spectrum of **1** (in CD<sub>3</sub>CN) shows all resonances in the normal diamagnetic region, although the resonances of the 2-aminoethyl moieties (PCH<sub>2</sub>CH<sub>2</sub>NH<sub>2</sub>) are remarkably broad, presumably because of the puckering motion of the chelate ring. The molecular structure of complex **1** was determined by single-crystal X-ray analysis; a perspective view of the divalent Ni<sup>II</sup> complex cation in **1** is given in Figure 1. The coordination geometry around the Ni<sup>II</sup> center was confirmed as four-coordinate square planar with a *cis*(*P,P*) configuration. It is known that the *cis*(*P,P*) isomer is electronically favored when two phosphanyl-donor groups having a strong *trans* influence coordinate to a square-planar metal center, although it sterically disfavored when the phosphanyl-donor groups bear bulky substituents on the P atom.<sup>[6]</sup> The present result indicates that the electronic effect, in other words the *trans* influence, is more important for the Ni<sup>II</sup> complexes, and that the steric interaction between the phenyl substituents may be reduced efficiently by a pair of conformations of two 2-aminoethylphosphane chelate rings (see below).

Complex **2**, which contains MePhPea, was expected to have a similar coordination geometry because the related complex [Ni(Me<sub>2</sub>Pea)<sub>2</sub>](BF<sub>4</sub>)<sub>2</sub> was also obtained as a *cis*(*P,P*) isomer.<sup>[6]</sup> However, complex **2** can form two possible diastereoisomers (*rac* and *meso*) due to the pair of asymmetric P atoms. The crude product isolated from the reaction mixture was found to have the composition Ni-

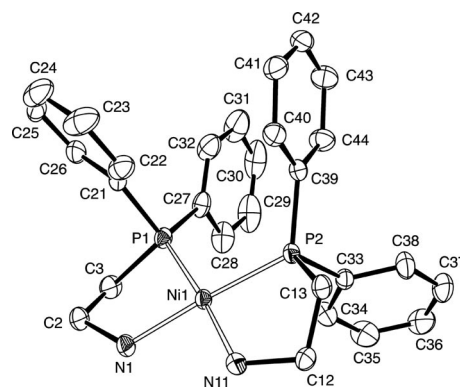


Figure 1. An ORTEP view (50% probability level, hydrogen atoms omitted) of the cationic moiety in [Ni(Ph<sub>2</sub>Pea)<sub>2</sub>](BF<sub>4</sub>)<sub>2</sub> (**1**).

(MePhPea)<sub>2</sub>(BF<sub>4</sub>)<sub>2</sub>, although its <sup>1</sup>H NMR spectrum (in CD<sub>3</sub>CN) was indicative of a mixture of two isomers (Figure S1). These isomers were separated on the basis of their different solubilities in dichloromethane, and the crystal structure of the less soluble product was determined by X-ray analysis. As seen from Figure 2, the analyzed complex is assigned as the *racemic* (*RR/SS*) diastereoisomer (abbreviated as *rac-2*).

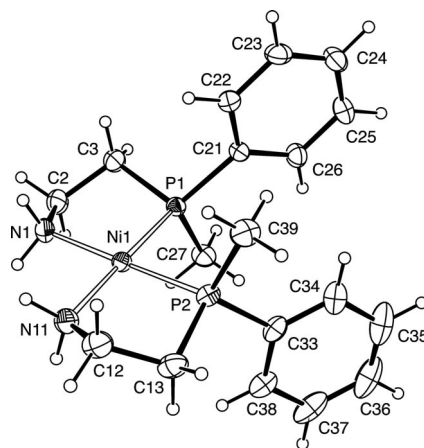


Figure 2. An ORTEP view (50% probability level) of the cationic moiety in *rac*-[Ni(MePhPea)<sub>2</sub>](BF<sub>4</sub>)<sub>2</sub> (*rac-2*). Note that the illustrated complex is assigned as an *SS* stereoisomer; however, this compound crystallized in the centrosymmetric space group *P* $\bar{1}$ .

Complexes **1** and **2** show an ideal planar coordination geometry around the Ni atom. The largest deviation of the constituent atoms from the ideal plane defined by {Ni1,P1,P2,N1,N11} was only 0.023(2) Å (**1** for N11) or 0.131(3) Å (**2** for N11). For both complexes, a pair of conformations of the five-membered 2-aminoethylphosphane chelate rings was determined as  $\delta\delta/\lambda\lambda$  (*racemic*). This conformation, with a pseudo-*C*<sub>2</sub> molecular symmetry, would be the most favorable for reducing the intramolecular steric interactions in the *cis*(*P,P*) isomer, although a different pair of ring conformations was observed in the analogous Me<sub>2</sub>-Pea complexes.<sup>[6]</sup> A weak interaction exists between the metal(II) ion and the chloride in the crystal structures of

$[\text{Ni}(\text{Me}_2\text{Pea})_2]\text{Cl}_2$  and its  $\text{Pd}^{\text{II}}$  and  $\text{Pt}^{\text{II}}$  analogues, and the pair of ring conformations of the  $\text{Me}_2\text{Pea}$  chelates was found to be  $\delta\lambda$  (*meso*), with a pseudo- $C_s$  molecular symmetry. In contrast, the crystal structure of  $[\text{Ni}(\text{Me}_2\text{Pea})_2][\text{NiCl}_4]$  did not exhibit any interaction between the central  $\text{Ni}^{\text{II}}$  ion in the complex and the counter anion, and the chelate ring conformation was found to be  $\delta\delta/\lambda\lambda$  (*racemic*), the same as those of complexes **1** and **2**. Thus, these findings may indicate a relationship between the accessibility of coordination of the fifth ligand and the chelate ring conformation in the  $\text{Ni}^{\text{II}}$  triad complexes.

The  $\text{Ph}_2\text{Pqn}$  complex **3** afforded orange platelet crystals when crystallized from acetonitrile/diethyl ether, but apparently more reddish crystals with a dichloromethane solvate molecule ( $3 \cdot \text{CH}_2\text{Cl}_2$ ) when deposited by vapor diffusion of dichloromethane into an acetonitrile solution. We determined the crystal structures of both **3** and  $3 \cdot \text{CH}_2\text{Cl}_2$  and found that the molecular structures of the complex cations are almost identical. A perspective drawing of the complex cation in **3** is shown in Figure 3 (and that of  $3 \cdot \text{CH}_2\text{Cl}_2$  is in Figure S2). The  $\text{MePhPqn}$  complex  $[\text{Ni}(\text{MePhPqn})_2](\text{BF}_4)_2$  (**4**) was obtained as red platelet crystals, and X-ray structural analysis (Figure 4) confirmed the product to be the *racemic* (*RR/SS*) diastereoisomer. The coordination plane around the  $\text{Ni}^{\text{II}}$  center is distorted toward a tetrahedral geometry in both **3** ( $3 \cdot \text{CH}_2\text{Cl}_2$ ) and **4**. The dihedral angles between the planes defined by  $\{\text{Ni1}, \text{P1}, \text{N1}\}$  and  $\{\text{Ni1}, \text{P2}, \text{N11}\}$  are  $19.7(3)^\circ$ ,  $21.9(3)^\circ$ , and  $27.9(1)^\circ$  for complexes **3**,  $3 \cdot \text{CH}_2\text{Cl}_2$ , and **4**, respectively. This distortion results from the steric hindrance between the *ortho*-H atoms of mutually *cis*-positioned quinolyl groups (Figure 5), and has previously been observed in the crystal structures of  $[\text{Pd}(\text{Me}_2\text{Pqn})_2](\text{BF}_4)_2$ <sup>[7]</sup> and  $[\text{Pd}(\text{Ph}_2\text{Pqn})_2](\text{Cl or Br})_2$ .<sup>[8]</sup> Such a tetrahedral distortion of the coordination plane (around  $20^\circ$ ) forces the phenyl groups on the P atoms to become close enough for appreciable intramolecular stacking interactions (Figure 5, b). However, the crystal structure of the  $\text{MePhPqn}$  complex **4** is *racemic* (*RR/SS*) rather than *meso* (*RS*), the latter of which must be favorable for such an intramolecular stacking interaction. Furthermore, as the  $\text{P1-Ni1-P2}$  angle of the  $\text{Ph}_2\text{Pqn}$  complex [**3**:  $96.76(8)^\circ$ ;  $3 \cdot \text{CH}_2\text{Cl}_2$ :  $96.54(8)^\circ$ ] is much larger than that of the  $\text{MePhPqn}$  complex [**4**:  $93.26(4)^\circ$ ], there is probably no stacking interaction between these phenyl rings.

Table 1 lists selected bond lengths and angles for complexes **1–4**. The Ni–P and Ni–N bond lengths in the 2-aminoethylphosphane complexes **1** and **2** are similar to those in  $[\text{Ni}(\text{Me}_2\text{Pea})_2][\text{NiCl}_4]$  [av. Ni–P:  $2.148(4)$  Å; av. Ni–N:  $1.977(12)$  Å]. We expected that the steric requirement of the phenyl substituent and/or the strong *trans* influence of the phosphanyl donor group might change these bond lengths, but only relatively small differences are observed for the Ni–P and Ni–N bond lengths between all  $[\text{Ni}(\text{P-N})_2]^{2+}$  complexes. On the other hand, the  $\text{P1-Ni1-P2}$  bond angles are indeed affected by the steric requirement of the phosphane substituents {cf. **1**  $98.79(2)^\circ$  > **2**  $94.72(3)^\circ$  >  $[\text{Ni}(\text{Me}_2\text{Pea})_2][\text{NiCl}_4]$   $92.2(1)^\circ$ }. The Ni–P and Ni–N bond lengths in **1** are also similar to those in

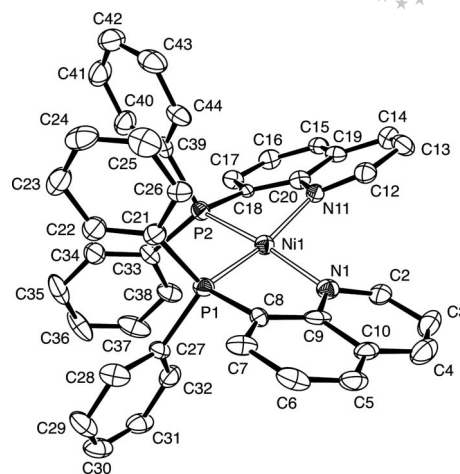


Figure 3. An ORTEP view (50% probability level, hydrogen atoms omitted) of the cationic moiety in  $[\text{Ni}(\text{Ph}_2\text{Pqn})_2](\text{BF}_4)_2$  (**3**).

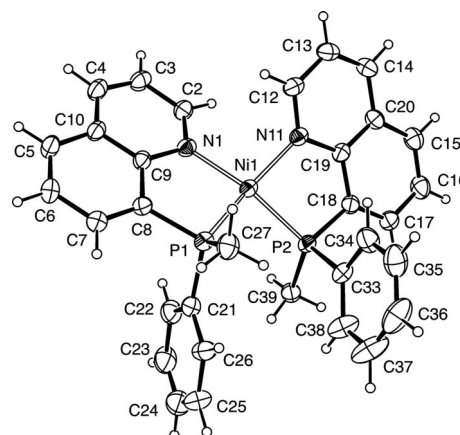


Figure 4. An ORTEP view (50% probability level) of the cationic moiety in  $[\text{Ni}(\text{MePhPqn})_2](\text{BF}_4)_2$  (**4**).

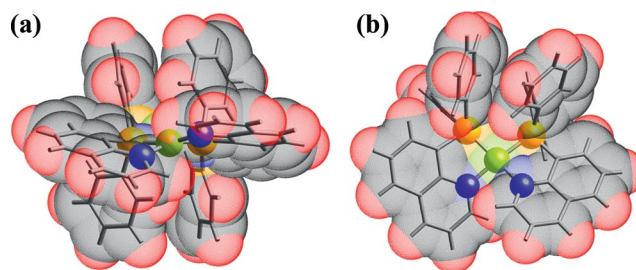


Figure 5. (a) Side and (b) top views of a space-filling model of the cationic moiety in  $[\text{Ni}(\text{Ph}_2\text{Pqn})_2](\text{BF}_4)_2$  (**3**).

$[\text{Ni}(\text{Ph}_2\text{PCH}_2\text{py})_2][\text{NiCl}_4]$  [av. Ni–P:  $2.160(3)$  Å; av. Ni–N:  $1.956(6)$  Å].<sup>[19]</sup> It should also be noted that the Ni–P and Ni–N bond lengths of the 2-aminoethylphosphane and 8-quinolylphosphane complexes (**1** and **2** vs. **3** and **4**) are rather similar, whereas the spectroscopic and electrochemical properties of these complexes exhibit remarkable differences, as discussed below.

Table 1. Selected bond lengths [Å] and angles [°] for complexes **1–4**.

|            | <b>1</b>  | <b>2</b>  | <b>3</b> | <b>3·CH<sub>2</sub>Cl<sub>2</sub></b> | <b>4</b> |
|------------|-----------|-----------|----------|---------------------------------------|----------|
| Ni1–P1     | 2.1584(5) | 2.1526(7) | 2.168(2) | 2.180(2)                              | 2.162(1) |
| Ni1–P2     | 2.1614(5) | 2.1475(8) | 2.177(2) | 2.191(2)                              | 2.151(1) |
| Ni1–N1     | 1.967(2)  | 1.969(2)  | 1.954(6) | 1.969(4)                              | 1.954(3) |
| Ni1–N11    | 1.959(2)  | 1.970(2)  | 1.949(5) | 1.943(4)                              | 1.977(3) |
| P1–Ni1–P2  | 98.79(2)  | 94.72(3)  | 96.76(8) | 96.54(8)                              | 93.26(4) |
| N1–Ni1–N11 | 89.41(6)  | 91.8(1)   | 95.0(2)  | 97.3(2)                               | 99.0(1)  |
| P1–Ni1–N1  | 85.73(5)  | 86.57(7)  | 86.6(2)  | 83.9(2)                               | 87.4(1)  |
| P2–Ni1–N11 | 86.06(5)  | 87.08(8)  | 84.6(2)  | 86.0(2)                               | 86.6(1)  |
| P2–Ni1–N1  | 175.46(5) | 177.07(8) | 168.0(2) | 165.3(2)                              | 162.2(1) |
| P1–Ni1–N11 | 175.08(5) | 175.58(8) | 165.3(2) | 165.2(2)                              | 159.3(1) |

### Spectroscopic Properties and Molecular Structures in Solution

As mentioned above, the <sup>1</sup>H NMR spectra for the 2-aminoethylphosphane complexes (**1** and **2**) in CD<sub>3</sub>CN were typical of diamagnetic complexes. This fact suggested that the square-planar coordination geometry around the Ni<sup>II</sup> center would be retained in solution. The MePhPea complex **2** afforded two diastereoisomers (*rac* and *meso*), which could be separated by fractional recrystallization. The *rac* isomer (*rac*-**2**), the structure of which was confirmed by single-crystal X-ray analysis, showed the P–CH<sub>3</sub> resonance at  $\delta$  = 1.05 ppm as a virtual triplet. This virtual coupling pattern of the P–CH<sub>3</sub> group is normal for square-planar Ni<sup>II</sup> and Pd<sup>II</sup> complexes with a *cis*(*P,P*) configuration.<sup>[6]</sup> The other isomer (*meso*-**2**) gave the corresponding resonance at  $\delta$  = 1.85 ppm (virtual triplet, Figure S1). The relatively large difference in their chemical shifts could result from the ring current effect of the phenyl ring in the mutually *cis*-positioned MePhP donor groups, as seen in Figure 2. Both *rac*-**2** and *meso*-**2** showed rather broad resonances for the 2-aminoethyl moieties (NH<sub>2</sub>CH<sub>2</sub>CH<sub>2</sub>P) at 23 °C, similar to the case of complex **1** (see above). At –16.5 °C, however, each resonance became separated into two broad resonances (Figure S1), thus indicating that there is a fast puckering motion of the five-membered chelate ring at ambient temperature. In addition, it should be noted that no isomerization was observed between *rac*-**2** and *meso*-**2** in CD<sub>3</sub>CN; the relative intensities of the resonances for these two species were independent of temperature (from –16.5 to 40 °C) and unchanged on standing for several days at ambient temperature. Thus, the square-planar coordination of 2-aminoethylphosphanes toward Ni<sup>II</sup> with a *cis*(*P,P*) configuration is robust in acetonitrile solution.

The 8-quinolylphosphane complexes (**3** and **4**) are diamagnetic in the solid state (up to 400 K measured). The <sup>1</sup>H NMR spectrum of the Ph<sub>2</sub>Pqn complex **3** in CD<sub>3</sub>NO<sub>2</sub> shows reasonably sharp resonances for the phenyl and quinolyl protons at  $\delta$  = 7.33–8.90 ppm (Figure S3), thus indicating a diamagnetic nature in solution. The distorted square-planar coordination geometry found in the crystal structure analysis of **3** therefore seems to be maintained in nitromethane solution. However, the <sup>1</sup>H NMR spectrum of **3** in CD<sub>3</sub>CN shows very broad signals in the range  $\delta$  = –20 to 30 ppm (Figure S3). A similar paramagnetic behavior in

CD<sub>3</sub>CN was also observed for the MePhPqn complex **4**. Temperature-dependent <sup>1</sup>H NMR spectra of complex **3** in CD<sub>3</sub>CN (Figure S3) suggest that it exists as an equilibrium mixture of diamagnetic and paramagnetic species. The diamagnetic species must have a distorted square-planar coordination geometry as in CD<sub>3</sub>NO<sub>2</sub>, whereas two possibilities can be considered for the paramagnetic species. One is the existence of an acetonitrile adduct having a five-coordinate square-pyramidal geometry or a six-coordinate octahedral coordination geometry. We attempted to detect such complexes by ESI-TOF mass spectrometry but were unsuccessful. The other possibility for the observed paramagnetism is a much stronger tetrahedral distortion of the Ni<sup>II</sup> coordination geometry. As both diamagnetic and paramagnetic species were detected at lower temperatures, there should be a moderately high-energy transition state, which might be caused by a collision of the phenyl groups arising from the tetrahedral distortion. This explanation seems to be plausible, but we are unsure as to why such a tetrahedral distortion occurs in acetonitrile but not in nitromethane.

The <sup>1</sup>H NMR spectrum of the MePhPqn complex **4** in CD<sub>3</sub>NO<sub>2</sub> (Figure S4) was also indicative of diamagnetism of the solutes, and the temperature-dependent spectral change suggested that they were an equilibrium mixture of two species (*rac*-**4** and *meso*-**4**). Two P–CH<sub>3</sub> resonances from the respective species were observed at  $\delta$  = 1.58 and 2.48 ppm (at 21 °C); this difference in chemical shifts is similar to that of *rac*-**2** and *meso*-**2** (see above) and results from the ring current effect of the mutually *cis*-positioned MePhP donor groups. Thus, the species having a higher-field P–CH<sub>3</sub> resonance would be assigned as *rac*-**4** (Figure 4). The equilibrium fraction of *rac*-**4** (over *meso*-**4**) became larger at higher temperature (*rac*-**4**/*meso*-**4** = 1.7 at 0 °C and 5.5 at 40 °C; Figure S4), which suggests that the 8-quinolylphosphane complexes **3** and **4** are rather labile towards structural change in solution, in contrast to the robustness of 2-aminoethylphosphane complexes **1** and **2**.

The UV/Vis absorption spectra of complexes **1** and **2**<sup>[20]</sup> in acetonitrile are shown in Figure 6. In accordance with the above <sup>1</sup>H NMR study, these spectra are similar in pattern to those in nitromethane and the diffuse-reflectance spectra of the solid samples (Figure S5). Square-planar Ni<sup>II</sup> complexes often exhibit a single, broad unsymmetrical band in the region 20000–25000 cm<sup>–1</sup>, which can be assigned to the superposition of the d–d transition bands; the band en-

ergy corresponds to  $\Delta_{\text{oct}}$  (ligand-field strength) of the ligand to a first approximation.<sup>[21a]</sup> The  $\text{Ph}_2\text{Pea}$  (**1**) and  $\text{MePhPea}$  (**2**) complexes exhibit such an absorption band at 24100 and 25300  $\text{cm}^{-1}$ , respectively, with an intensity,  $\epsilon$ , of around 400  $\text{M}^{-1}\text{cm}^{-1}$  (Figure 6).

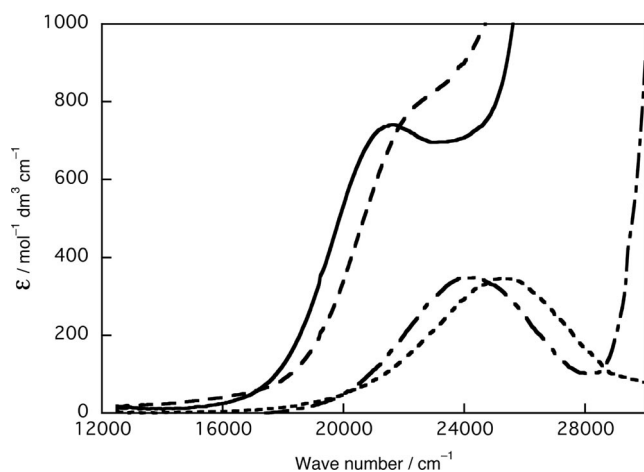


Figure 6. Absorption spectra of 2-aminoethylphosphane complexes **1** (---) and **2** (····) in acetonitrile and those of 8-quinolylphosphane complexes **3** (—) and **4** (— · —) in nitromethane at room temperature.

As seen above, complexes **3** and **4** show a remarkable solvent dependence in their structures in solution. In acetonitrile, complex **3** shows a broad absorption band at 19900  $\text{cm}^{-1}$ , and complex **4** exhibits two broad shoulders at around 20500 and 25500  $\text{cm}^{-1}$  (Figure S6). These spectra are apparently different in pattern from the diffuse-reflectance spectra of the solid samples (Figure S6), although the spectra in nitromethane and the solid diffuse-reflectance spectra are similar in pattern for both complexes. These observations are consistent with the results of the  $^1\text{H}$  NMR measurements above: the distorted square-planar coordination geometry of complexes **3** and **4** is maintained in nitromethane, whereas in acetonitrile they exist as an equilibrium mixture with a paramagnetic species (a five- or six-coordinate acetonitrile adduct or a tetrahedral complex). The  $\text{Ph}_2\text{Pqn}$  (**3**) and  $\text{MePhPqn}$  (**4**) complexes in nitromethane exhibit an absorption band at 21700  $\text{cm}^{-1}$  and a shoulder absorption at around 22000  $\text{cm}^{-1}$  ( $\epsilon \approx 800 \text{ M}^{-1}\text{cm}^{-1}$ ), respectively (Figure 6). These band energies indicate weaker ligand-field strengths of 8-quinolylphosphanes than 2-aminoethylphosphane [ $\Delta_{\text{oct}}$  ( $\text{cm}^{-1}$ ) = 25300 ( $\text{MePhPea}$ ) > 24100 ( $\text{Ph}_2\text{Pea}$ ) >> ca. 22000 ( $\text{MePhPqn}$ ) > 21700 ( $\text{Ph}_2\text{Pqn}$ )].

## Electrochemical Properties

Figure 7 shows cyclic voltammograms of complex **3** in acetonitrile and nitromethane (those for the other complexes are shown in Figure S7). The redox potentials ( $E_{1/2}$  vs.  $\text{Fc}^+/\text{Fc}$ ) and the difference in potential between anodic and cathodic peaks ( $\Delta E_p$ ) are listed in Table 2. These data are indicative of the quasi-reversible one-electron reduction

process of the  $\text{Ni}^{\text{II}}$  complexes, except for  $\text{MePhPea}$  complex **2**,<sup>[20]</sup> which gives an irreversible voltammogram at very low potential, presumably because of immediate decomposition of the reduced product. As seen in Figure 7 (and Table 2), the electrochemical behavior of complex **3** shows a small but clear solvent dependence ( $\Delta E_{1/2} \approx 20 \text{ mV}$  and  $\Delta \Delta E_p \approx 10 \text{ mV}$ ). These differences are likely to be caused by the different molecular structures of the  $\text{Ph}_2\text{Pqn}$  complex in acetonitrile and nitromethane solutions, as described above.

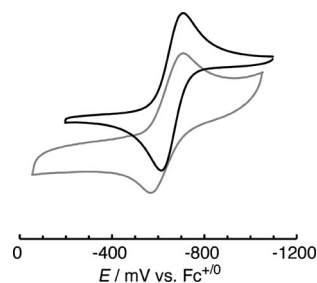


Figure 7. Cyclic voltammograms of  $[\text{Ni}(\text{Ph}_2\text{Pqn})_2](\text{BF}_4)_2$  (**3**) in acetonitrile (black) and nitromethane (gray) at 25 °C. [complex] =  $1.0 \times 10^{-3} \text{ M}$ ,  $I = 0.1 \text{ M}$  ( $\text{TBABF}_4$ ).

Table 2. Redox potential of Ni complexes (in 0.1 M  $\text{TBABF}_4$  solution in acetonitrile or nitromethane at  $298.2 \pm 0.2 \text{ K}$ ).<sup>[a]</sup>

| Complex/solvent                         | Assignment                                    | $E_{1/2}$ [mV] | $\Delta E_p$ [mV] |
|---|---|----------------|-------------------|
| <b>1</b> / $\text{CH}_3\text{CN}$       | $[\text{Ni}(\text{Ph}_2\text{Pea})_2]^{2+/+}$ | −1147          | 87                |
| <b>2</b> / $\text{CH}_3\text{CN}^{[b]}$ | $[\text{Ni}(\text{MePhPea})_2]^{2+/+}$        | −1389          | 59 <sup>[b]</sup> |
| <b>3</b> / $\text{CH}_3\text{CN}$       | $[\text{Ni}(\text{Ph}_2\text{Pqn})_2]^{2+/+}$ | −660           | 98                |
| <b>3</b> / $\text{CH}_3\text{NO}_2$     | $[\text{Ni}(\text{Ph}_2\text{Pqn})_2]^{2+/+}$ | −640           | 109               |
| <b>4</b> / $\text{CH}_3\text{CN}$       | $[\text{Ni}(\text{MePhPqn})_2]^{2+/+}$        | −898           | 98                |

[a] vs.  $\text{Fc}^+/\text{Fc}$ . [b] Irreversible process due to decomposition of the reduced species.

The reduction potentials of these  $\text{Ni}^{\text{II}}$  complexes are largely dependent on the type of phosphane ligands. Thus, substitution of methyl for phenyl on a P donor atom induces an approximately 240 mV negative shift in the redox potential, while 8-quinolylphosphane complexes exhibit less negative (by ca 490 mV) redox potentials than the corresponding 2-aminoethylphosphane complexes. This behavior is consistent with the order of the ligand-field strengths observed by absorption spectroscopy:  $\text{MePhPea}$  (**2**) >  $\text{Ph}_2\text{Pea}$  (**1**) >  $\text{MePhPqn}$  (**4**) >  $\text{Ph}_2\text{Pqn}$  (**3**).

## Preparation and Crystal Structure of Nickel(I) $\text{Ph}_2\text{Pqn}$ Complex

Reduction of  $\text{Ph}_2\text{Pqn}$  complex **3** with Zn powder<sup>[22]</sup> in acetonitrile afforded a dark red solution, from which a dark red precipitate could be isolated on addition of deaerated water. As the cyclic voltammogram of this product (in acetonitrile) was almost identical to that of complex **3**, it was assumed to be the corresponding  $\text{Ni}^{\text{I}}$  complex of  $[\text{Ni}(\text{Ph}_2\text{Pqn})_2]\text{BF}_4$  (**5**). The UV/Vis spectrum of **5** in acetonitrile shows shoulder absorptions at around 11500 and 14500  $\text{cm}^{-1}$  with intensities of around 200  $\text{M}^{-1}\text{cm}^{-1}$  (Figure S8). This spectral pattern is similar to the diffuse-reflectance

spectrum of a solid sample of complex **5**, thus indicating a similar molecular structure of the Ni<sup>I</sup> complex cation in the solid state and in acetonitrile.

The crystal structure of complex **5** was determined by X-ray analysis. The asymmetric unit (triclinic space group  $P\bar{1}$ ,  $Z = 2$ ) contains an  $[\text{Ni}(\text{Ph}_2\text{Pqn})_2]^+$  cation and a  $\text{BF}_4^-$  anion. The structure of the  $[\text{Ni}(\text{Ph}_2\text{Pqn})_2]^+$  moiety is shown in Figure 8. The coordination geometry around the Ni<sup>I</sup> center is distorted tetrahedral; the dihedral angle between the  $\{\text{Ni1}, \text{P1}, \text{N1}\}$  plane and the  $\{\text{Ni1}, \text{P2}, \text{N11}\}$  plane is  $57.6(1)^\circ$ , and that between the least-squares quinolyl rings is  $61.06(9)^\circ$ . The  $\text{P1-Ni1-P2}$  bond angle is  $115.67(4)^\circ$ . If a regular tetrahedral geometry around the Ni center is assumed, a large steric hindrance between the phenyl substituents would be expected. Thus, to reduce such a steric interaction effectively, the coordination geometry is distorted by around  $30^\circ$  toward a *syn* structure.<sup>[23]</sup> A Jahn–Teller effect of the d<sup>9</sup> tetrahedral complex may be another reason for this distortion.<sup>[21b]</sup>

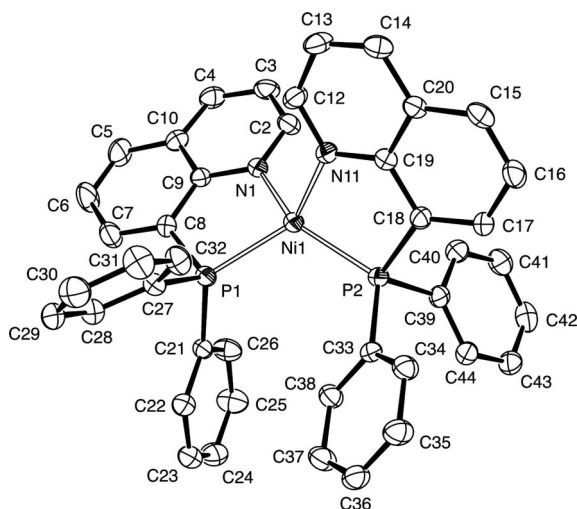


Figure 8. An ORTEP view (30% probability level, hydrogen atoms omitted) of the cation in  $[\text{Ni}(\text{Ph}_2\text{Pqn})_2]\text{BF}_4$  (**5**). Selected bond lengths [Å] and angles [ $^\circ$ ]: Ni1–P1 2.230(1), Ni1–P2 2.224(1), Ni1–N1 2.003(3), Ni1–N11 2.017(3); P1–Ni1–P2 115.67(4), N1–Ni1–N11 96.48(12), P1–Ni1–N1 86.22(9), P2–Ni1–N11 86.19(9), P1–Ni1–N11 134.72(9), P2–Ni1–N1 145.92(9).

The Ni–P and Ni–N bond lengths in complex **5** are 2.224(1)–2.230(1) and 2.003(3)–2.017(3) Å, respectively, around 0.05 Å longer than the corresponding bonds in the Ni<sup>II</sup> complex **3**. This can be explained by the difference in ionic radii between Ni<sup>+</sup> and Ni<sup>2+</sup>.<sup>[24]</sup> The Ni–P bond lengths in  $[\text{Ni}(\text{PMe}_3)_4]\text{BPh}_4$ , where the coordination geometry of Ni<sup>I</sup> is also distorted tetrahedral, are reported to be 2.211(3)–2.221(3) Å.<sup>[25]</sup> The Ni–P bonds in the three-coordinate iminobenzylamide complex  $[\text{Ni}^{\text{I}}(\text{ArN}=\text{CHC}_6\text{H}_4\text{N}-\text{Ar}')(\text{PPh}_3)]$  are 2.210(1) and 2.233(2) Å.<sup>[26]</sup> Several other Ni<sup>I</sup> complexes containing the bidentate phosphane ligand *t*Bu<sub>2</sub>PCH<sub>2</sub>CH<sub>2</sub>P*t*Bu<sub>2</sub> (dtbpe) have been reported by Hilhouse et al., and the Ni<sup>I</sup>–P bond lengths in the chlorido-bridged dimer  $[(\text{dtbpe})\text{Ni}(\mu\text{-Cl})_2]$  are 2.210(1)–

2.216(1) Å.<sup>[27]</sup> Compared with these examples, the present Ni<sup>I</sup>–P bond lengths in complex **5** [av. 2.227(1) Å] seem to be normal for Ni<sup>I</sup> phosphane complexes.

## Conclusions

We have characterized four nickel(II) complexes of the type  $[\text{Ni}(\text{P-N})_2](\text{BF}_4)_2$ , where P–N is a 2-aminoethylphosphane or 8-quinolylphosphane ligand. The coordination geometry of the 2-aminoethylphosphane complexes **1** and **2** is square planar with a *cis*(*P,P*) configuration in the solid state and in acetonitrile solution. It seems that the coordination bonds of Ph<sub>2</sub>Pea and MePhPea to a Ni<sup>II</sup> ion are robust in solution. The diastereoisomers (*rac* and *meso*) of *cis*(*P,P*)- $[\text{Ni}(\text{MePhPea})_2](\text{BF}_4)_2$  (**2**) have been separated by fractional recrystallization and the crystal structure of *rac*-**2** determined by X-ray analysis.

In contrast, the 8-quinolylphosphanes result in distorted square-planar Ni<sup>II</sup> complexes (**3** and **4**) because of the steric repulsion between the *ortho*-H atoms in the mutually *cis*-positioned quinolyl rings. This distortion makes the  $\sigma$ - and  $\pi$ -overlaps between Ni<sup>II</sup> 3d and ligand orbitals ineffective, therefore the ligand-field strengths of the 8-quinolylphosphanes must be weaker in these complexes. In agreement with this conclusion, complexes **3** and **4** exhibit fluxional behavior in solution. The distorted square-planar geometry seems to be maintained in nitromethane as the absorption spectra in nitromethane are similar in pattern to the diffuse-reflectance spectra of the solid samples. Typical diamagnetic <sup>1</sup>H NMR spectra are also observed in CD<sub>3</sub>NO<sub>2</sub>, but the temperature-dependent <sup>1</sup>H NMR spectra of *cis*(*P,P*)- $[\text{Ni}(\text{MePhPqn})_2](\text{BF}_4)_2$  (**4**) indicate that this complex exists as an equilibrium mixture of *rac* and *meso* diastereoisomers. In acetonitrile, however, these complexes show paramagnetic behavior, presumably arising either from the coordination of solvent acetonitrile molecule(s) to form a five- or six-coordinate complex or the stronger tetrahedral distortion of the coordination geometry.

The weaker ligand-field strengths of 8-quinolylphosphanes than 2-aminoethylphosphanes are shown experimentally by the d–d transition energies observed by absorption spectroscopy: Ph<sub>2</sub>Pqn < MePhPqn < Ph<sub>2</sub>Pea < MePhPea. This order is consistent with that of the Ni<sup>III/I</sup> redox potential of the complexes. The most readily reducible Ph<sub>2</sub>Pqn complex (**3**) affords the corresponding nickel(I) complex  $[\text{Ni}(\text{Ph}_2\text{Pqn})_2]\text{BF}_4$  (**5**). The molecular structure of this Ni<sup>I</sup> complex, which contains two bidentate phosphane ligands, is distorted tetrahedral because of the steric repulsion caused by the phenyl substituents and/or a Jahn–Teller effect of the ideally tetrahedral d<sup>9</sup> complex.

## Experimental Section

**Materials and Measurements:** All solvents used during preparation of the phosphanes and their complexes were dried with appropriate drying agents and distilled prior to use. The P–N-type hybrid li-

gands Ph<sub>2</sub>Pea (previously abbreviated as edpp), MePhPea,<sup>[12c]</sup> Ph<sub>2</sub>Pqn,<sup>[28]</sup> and MePhPqn<sup>[17]</sup> were synthesized according to literature methods.

<sup>1</sup>H NMR spectra were acquired on a Varian Mercury 300 spectrometer. Chemical shifts were referenced to the residual <sup>1</sup>H NMR signals of the deuterated solvents and are reported with respect to TMS. The <sup>31</sup>P{<sup>1</sup>H} NMR spectra were obtained on the same spectrometer, using 85% H<sub>3</sub>PO<sub>4</sub> as an external reference for the <sup>31</sup>P NMR chemical shifts. Absorption spectra were recorded with a Jasco V-550 spectrophotometer at room temperature. Diffuse-reflectance spectra of the solid samples were obtained on the same spectrophotometer using an integration sphere (Jasco ISN-470). Cyclic voltammograms were measured at 25.0(2) °C on a BAS-100B/W electrochemical analyzer in acetonitrile or nitromethane solution ([complex] = 1.0 mM, 0.1 M TBABF<sub>4</sub>). A platinum disk (φ 1.8 mm), a platinum wire, and a Ag/AgNO<sub>3</sub> electrode were used as the working, auxiliary, and reference electrodes, respectively. The redox potentials of the samples were calibrated with respect to the redox signal for the ferrocenium/ferrocene couple.

**[Ni(Ph<sub>2</sub>Pea)<sub>2</sub>](BF<sub>4</sub>)<sub>2</sub> (1):** A methanol solution (50 mL) of Ni(BF<sub>4</sub>)<sub>2</sub>·6H<sub>2</sub>O (1.51 g, 4.44 mmol) was added with stirring to a suspension of Ph<sub>2</sub>Pea (2.16 g, 9.42 mmol) in methanol (50 mL). The mixture was refluxed for 30 min and then cooled to 0 °C. The resulting yellow precipitate was collected by filtration, washed with methanol and diethyl ether, and dried in vacuo; yield 1.58 g (51.5%). C<sub>28</sub>H<sub>32</sub>B<sub>2</sub>F<sub>8</sub>N<sub>2</sub>NiP<sub>2</sub> (690.83): calcd. C 48.7, H 4.67, N 4.06; found C 48.4, H 4.53, N 4.33. <sup>1</sup>H NMR (300 MHz, CD<sub>3</sub>CN, 21 °C): δ = 2.58 (br., 2 H, CH<sub>2</sub>), 2.70 (br., 2 H, CH<sub>2</sub>), 3.90 (br., 2 H, NH<sub>2</sub>), 7.33–7.38 (m, 4 H, Ph), 7.48–7.53 (m, 6 H, Ph) ppm. <sup>31</sup>P{<sup>1</sup>H} NMR (152 MHz, CD<sub>3</sub>CN, 21 °C): δ = 49.2 (br) ppm. UV/vis [solvent]: σ<sub>max</sub> (ε<sub>max</sub>/M<sup>-1</sup>cm<sup>-1</sup>) = 24100 (349) [CH<sub>3</sub>CN]; 24500 (575) cm<sup>-1</sup> [CH<sub>3</sub>NO<sub>2</sub>]. Crystals suitable for X-ray analysis were obtained from an acetonitrile solution by vapor diffusion of diethyl ether.

**[Ni(MePhPea)<sub>2</sub>](BF<sub>4</sub>)<sub>2</sub> (2):** Under an argon atmosphere, 1.01 g of (crude) MePhPea was added to an ethanol solution (100 mL) of Ni(BF<sub>4</sub>)<sub>2</sub>·6H<sub>2</sub>O (1.03 g, 3.03 mmol), and the mixture stirred under reflux for 1 h. The resulting yellow solution was concentrated to about 10 mL under reduced pressure, and then cooled to 0 °C to afford the product as a yellow precipitate; yield 0.48 g (28%). C<sub>20</sub>H<sub>34</sub>B<sub>2</sub>F<sub>8</sub>N<sub>2</sub>NiOP<sub>2</sub> (2·EtOH, 612.75): calcd. C 39.3, H 5.61, N 4.59; found C 39.1, H 5.29, N 4.25. <sup>1</sup>H NMR (300 MHz, CD<sub>3</sub>CN, 23 °C): δ = 1.05 (virtual t, Me of *rac*-2), 1.85 (virtual t, Me of *meso*-2), 2.0–2.4 (br., CH<sub>2</sub> of *rac*-2 and *meso*-2), 2.6–3.2 (br., CH<sub>2</sub> of *rac*-2 and *meso*-2), 3.75 (br., NH<sub>2</sub> of *rac*-2 and *meso*-2), 7.13–7.35 (m, Ph of *meso*-2), 7.50–7.85 (m, Ph of *rac*-2) ppm. <sup>31</sup>P{<sup>1</sup>H} NMR (152 MHz, CD<sub>3</sub>CN, 23 °C): δ = 38.3 (*rac*-2) and 39.1 (*meso*-2) ppm. UV/vis [solvent]: σ<sub>max</sub> (ε<sub>max</sub>/M<sup>-1</sup>cm<sup>-1</sup>) = 25300 (347) cm<sup>-1</sup> [CH<sub>3</sub>CN]. This product was found to be a mixture of diastereoisomers (*rac* and *meso*). To obtain suitable crystals for the X-ray diffraction analysis, the crude product was mixed with a minimum amount of dichloromethane and the insoluble precipitate quickly collected by filtration. The resulting yellow product was recrystallized from an acetonitrile solution by vapor diffusion of diethyl ether to give yellow columnar crystals of *rac*-2.

**[Ni(Ph<sub>2</sub>Pqn)<sub>2</sub>](BF<sub>4</sub>)<sub>2</sub> (3):** A methanol solution (50 mL) of Ni(BF<sub>4</sub>)<sub>2</sub>·6H<sub>2</sub>O (830 mg, 2.44 mmol) was added with stirring to a suspension of Ph<sub>2</sub>Pqn (1.76 g, 5.62 mmol) in methanol (50 mL). The mixture was refluxed for 30 min and then cooled to 0 °C. The resulting reddish-brown precipitate was collected by filtration, washed with methanol, thf, and diethyl ether, and dried in vacuo; yield 1.17 g (56.2%). C<sub>43</sub>H<sub>36</sub>B<sub>2</sub>F<sub>8</sub>N<sub>2</sub>NiOP<sub>2</sub> (3·MeOH, 891.01): calcd. C 57.7, H

4.07, N 3.14; found C 57.4, H 3.78, N 3.22. <sup>1</sup>H NMR (300 MHz, CD<sub>3</sub>NO<sub>2</sub>, 21 °C): δ = 7.36 (t, *J* = 7.5 Hz, 4 H, *m*-Ph), 7.57 (t, *J* = 7.5 Hz, 2 H, *p*-Ph), 7.78 (m, 4 H, *o*-Ph), 7.94 (m, 2 H, qn), 8.14 (m, 1 H, qn), 8.42 (d, *J* = 8.1 Hz, 1 H, qn), 8.72 (m, 1 H, qn), 8.88 (d, *J* = 7.5 Hz, 1 H, qn) ppm. <sup>31</sup>P{<sup>1</sup>H} NMR (152 MHz, CD<sub>3</sub>NO<sub>2</sub>, 21 °C): δ = 43.2 (br) ppm. UV/Vis [solvent]: σ<sub>max</sub> (ε<sub>max</sub>/M<sup>-1</sup>cm<sup>-1</sup>) = 12400 (40), 19900 (160), and 26300<sup>sh</sup> (ca. 900) [CH<sub>3</sub>CN]; 21700 (741) cm<sup>-1</sup> [CH<sub>3</sub>NO<sub>2</sub>]. Crystals suitable for X-ray analysis were obtained from an acetonitrile solution by vapor diffusion of diethyl ether (orange platelet crystals of 3) or dichloromethane (red platelet crystals of 3·CH<sub>2</sub>Cl<sub>2</sub>).

**[Ni(MePhPqn)<sub>2</sub>](BF<sub>4</sub>)<sub>2</sub> (4):** A methanol solution (50 mL) of Ni(BF<sub>4</sub>)<sub>2</sub>·6H<sub>2</sub>O (4.1 g, 0.012 mol) was added with stirring to an ethanol solution (100 mL) of (crude) MePhPqn (6.0 g). The mixture was refluxed for 1 h and then cooled to 0 °C. The resulting yellow precipitate was collected by filtration, washed with ethanol and diethyl ether, and dried in vacuo; yield 5.93 g (67%). C<sub>32</sub>H<sub>28</sub>B<sub>2</sub>F<sub>8</sub>N<sub>2</sub>NiP<sub>2</sub> (734.83): calcd. C 52.3, H 3.84, N 3.81; found C 52.0, H 3.83, N 3.75. <sup>1</sup>H NMR (300 MHz, CD<sub>3</sub>NO<sub>2</sub>, 21 °C): δ = 1.58 (s, Me of *rac*-4), 2.48 (s, Me of *meso*-4), 7.19 (t, *J* = 7.5 Hz, qn of *meso*-4), 7.40–7.50 (m, qn of *meso*-4), 7.72 (t, *J* = 7.5 Hz, qn of *rac*-4), 7.80–8.10 (m, qn of *rac*-4 and *meso*-4), 8.44 (d, *J* = 8.1 Hz, qn of *rac*-4), 8.78 (m, qn of *rac*-4), 8.91 (d, *J* = 8.1 Hz, qn of *rac*-4) ppm. <sup>31</sup>P{<sup>1</sup>H} NMR (152 MHz, CD<sub>3</sub>NO<sub>2</sub>, 21 °C): δ = 32.2 (br) ppm. UV/Vis [solvent]: σ<sub>max</sub> (ε<sub>max</sub>/M<sup>-1</sup>cm<sup>-1</sup>) = 12900 (10), 20500<sup>sh</sup> (ca. 300), and 25500<sup>sh</sup> (ca. 800) [CH<sub>3</sub>CN]; 22000<sup>sh</sup> (ca. 750) cm<sup>-1</sup> [CH<sub>3</sub>NO<sub>2</sub>]. Crystals suitable for X-ray analysis were obtained from an acetonitrile solution by vapor diffusion of diethyl ether.

**[Ni(Ph<sub>2</sub>Pqn)<sub>2</sub>](BF<sub>4</sub>)<sub>2</sub> (5):** An acetonitrile solution (20 mL) of 3 (223 mg, 0.260 mmol) was stirred over Zn powder (ca. 1 g) at room temperature for 1 h under argon and then unreacted Zn powder was filtered off. The filtrate was concentrated under reduced pressure, and deaerated water (50 mL) was added to the concentrate. The resulting dark red precipitate was collected by filtration, washed with water and diethyl ether, and dried in vacuo; yield 152 mg (76%). UV/Vis [solvent]: σ<sub>max</sub> (ε<sub>max</sub>/mol<sup>-1</sup>dm<sup>3</sup>cm<sup>-1</sup>) = 11500<sup>sh</sup> (ca. 200) and 14500<sup>sh</sup> (ca. 270) cm<sup>-1</sup> [CH<sub>3</sub>CN]. Crystals suitable for X-ray analysis were obtained by vapor diffusion of diethyl ether into a nitromethane solution.

**Crystallography:** X-ray diffraction data for complexes 1–5 were obtained at –73(2) °C on a Rigaku R-axis rapid imaging plate detector with graphite-monochromated Mo-*K*<sub>α</sub> radiation (λ = 0.71073 Å). A suitable crystal was mounted with a cryoloop and flash-cooled in a cold nitrogen stream. Data were processed by the Process-Auto program package,<sup>[29]</sup> and absorption corrections were applied by the empirical method.<sup>[30]</sup> The structures were solved by either direct methods using SIR92<sup>[31]</sup> or by a heavy-atom method using DIRDIF99-PATY,<sup>[32]</sup> and refined on *F*<sup>2</sup> (with all independent reflections) using the SHELXL97 program.<sup>[33]</sup> All non-H atoms were refined anisotropically, and H atoms were introduced at the positions calculated theoretically and treated with riding models. All calculations were carried out using the CrystalStructure software package.<sup>[34]</sup> Crystal data are collected in Table 3.

CCDC-743141 (for 1), -743142 (for 2), -743143 (for 3), -743144 (for 3·CH<sub>2</sub>Cl<sub>2</sub>), -743145 (for 4), -743146 (for 5) contain the supplementary crystallographic data for this paper. These data can be obtained free of charge from The Cambridge Crystallographic Data Centre via [www.ccdc.cam.ac.uk/data\\_request/cif](http://www.ccdc.cam.ac.uk/data_request/cif).

**Supporting Information** (see also the footnote on the first page of this article): An ORTEP drawing of the cationic moiety in

Table 3. Crystal data for complexes.

| Complex   | 1  | 2  | 3  | 3·CH <sub>2</sub> Cl <sub>2</sub>  | 4  | 5  |
|---|--|--|--|--|--|--|
| Chemical formula  | C <sub>28</sub> H <sub>32</sub> B <sub>2</sub> F <sub>8</sub> ·N <sub>2</sub> NiP <sub>2</sub> | C <sub>18</sub> H <sub>28</sub> B <sub>2</sub> F <sub>8</sub> ·N <sub>2</sub> NiP <sub>2</sub> | C <sub>42</sub> H <sub>32</sub> B <sub>2</sub> F <sub>8</sub> ·N <sub>2</sub> NiP <sub>2</sub> | C <sub>43</sub> H <sub>34</sub> B <sub>2</sub> Cl <sub>2</sub> F <sub>8</sub> ·N <sub>2</sub> NiP <sub>2</sub> | C <sub>32</sub> H <sub>28</sub> B <sub>2</sub> F <sub>8</sub> ·N <sub>2</sub> NiP <sub>2</sub> | C <sub>42</sub> H <sub>32</sub> BF <sub>4</sub> ·N <sub>2</sub> NiP <sub>2</sub> |
| <i>M</i>  | 690.83   | 566.68   | 858.97   | 943.89   | 734.83   | 772.16   |
| Crystal system  | monoclinic   | triclinic  | monoclinic   | orthorhombic   | monoclinic   | triclinic  |
| <i>a</i> [Å]  | 9.3420(3)  | 8.5664(5)  | 14.121(7)  | 15.905(14)   | 9.1097(5)  | 8.837(2)   |
| <i>b</i> [Å]  | 9.2833(4)  | 10.9473(6)   | 15.758(10)   | 17.949(11)   | 20.535(1)  | 11.967(3)  |
| <i>c</i> [Å]  | 35.5768(14)  | 13.8767(8)   | 17.976(7)  | 28.80(2)   | 17.912(1)  | 17.554(4)  |
| $\alpha$ [°]  | 90   | 79.256(2)  | 90   | 90   | 90   | 90.901(5)  |
| $\beta$ [°]   | 94.725(1)  | 79.886(2)  | 94.94(4)   | 90   | 104.597(1)   | 99.519(5)  |
| $\gamma$ [°]  | 90   | 79.508(2)  | 90   | 90   | 90   | 101.362(5)   |
| <i>V</i> [Å <sup>3</sup> ]  | 3074.9(2)  | 1243.56(12)  | 3985(4)  | 8221(11)   | 3242.6(3)  | 1792.8(7)  |
| <i>T</i> [K]  | 200(2)   | 200(2)   | 200(2)   | 200(2)   | 200(2)   | 200(2)   |
| Space group   | <i>P</i> 2 <sub>1</sub> / <i>n</i>   | <i>P</i> $\bar{1}$   | <i>P</i> 2 <sub>1</sub> / <i>c</i>   | <i>Pbca</i>  | <i>P</i> 2 <sub>1</sub> / <i>n</i>   | <i>P</i> $\bar{1}$   |
| <i>Z</i>  | 4  | 2  | 4  | 8  | 4  | 2  |
| <i>D</i> <sub>calc</sub> [Mg m <sup>−3</sup> ]  | 1.492  | 1.497  | 1.432  | 1.525  | 1.505  | 1.430  |
| $\mu$ (Mo- <i>K</i> $\alpha$ ) [mm <sup>−1</sup> ]  | 0.806  | 0.977  | 0.638  | 0.752  | 0.770  | 0.686  |
| <i>R</i> <sub>int</sub>   | 0.0151   | 0.0151   | 0.1127   | 0.2015   | 0.0741   | 0.0719   |
| Number of param./reflections  | 416/6767   | 301/5629   | 515/8795   | 542/9102   | 427/7348   | 470/8039   |
| <i>R</i> 1( <i>F</i> <sup>2</sup> ) [ <i>F</i> <sub>o</sub> <sup>2</sup> > 2σ( <i>F</i> <sub>o</sub> <sup>2</sup> )] <sup>[a]</sup> | 0.0325   | 0.0469   | 0.0886   | 0.0816   | 0.0686   | 0.0605   |
| <i>wR</i> 2( <i>F</i> <sup>2</sup> ) (all data) <sup>[b]</sup>  | 0.0822   | 0.1418   | 0.2218   | 0.0908   | 0.1869   | 0.1751   |

[a]  $R1 = \Sigma ||F_o| - |F_c|| / \Sigma |F_o|$ . [b]  $wR2 = [\Sigma w(F_o^2 - F_c^2)^2 / \Sigma wF_o^2]^{1/2}$ .

[Ni(Ph<sub>2</sub>Pqn)<sub>2</sub>](BF<sub>4</sub>)<sub>2</sub>·CH<sub>2</sub>Cl<sub>2</sub> (3·CH<sub>2</sub>Cl<sub>2</sub>), <sup>1</sup>H NMR spectra, UV/Vis absorption spectra, and cyclic voltammograms of complexes 1–4.

## Acknowledgments

We thank Mr. Keita Ariyoshi and Ms. Yuki Yamane (Okayama University) for <sup>31</sup>P NMR and magnetic measurements, respectively. This work was supported by the Ministry of Education, Culture, Sports, Science, and Technology, Japan, (Grant-in-Aid for Scientific Research; grant numbers 16550055 and 20550064).

- [1] a) C. S. Slone, D. A. Weinberger, C. A. Mirkin, *Prog. Inorg. Chem.* **1999**, 48, 233–350; b) P. Espinet, K. Soullantica, *Coord. Chem. Rev.* **1999**, 193–195, 499–556; c) B. Goldfuss, *J. Organomet. Chem.* **2006**, 691, 4508–4513.
- [2] S. E. Angell, C. W. Rogers, Y. Zhang, M. O. Wolf, W. E. Jones Jr., *Coord. Chem. Rev.* **2006**, 250, 1829–1841.
- [3] a) J. Andrieu, J.-M. Camus, P. Richard, R. Poli, L. Gonsalvi, F. Vizza, M. Peruzzini, *Eur. J. Inorg. Chem.* **2006**, 51–61; b) C. Müller, R. J. Lachicotte, W. D. Jones, *Organometallics* **2002**, 21, 1975–1981.
- [4] a) P. Papathanasiou, G. Salem, P. Waring, A. C. Willis, *J. Chem. Soc., Dalton Trans.* **1997**, 3435–3443; b) A. Habtemariam, B. Watchman, B. S. Potter, R. Palmer, S. Parsons, A. Par-kin, P. Sadler, *J. Chem. Soc., Dalton Trans.* **2001**, 1306–1318.
- [5] a) D. B. Grotjahn, Y. Gong, L. Zakharov, J. A. Golen, A. L. Rheingold, *J. Am. Chem. Soc.* **2006**, 128, 438–453; b) S. Dilsky, W. A. Schenk, *Eur. J. Inorg. Chem.* **2004**, 4859–4870; c) S. Jung, C. D. Brandt, H. Werner, *New J. Chem.* **2001**, 25, 1101–1103.
- [6] T. Suzuki, A. Morikawa, K. Kashiwabara, *Bull. Chem. Soc. Jpn.* **1996**, 69, 2539–2548.
- [7] T. Suzuki, K. Kashiwabara, J. Fujita, *Bull. Chem. Soc. Jpn.* **1995**, 68, 1619–1626.
- [8] T. Suzuki, *Bull. Chem. Soc. Jpn.* **2004**, 77, 1869–1876.
- [9] a) T. Suzuki, T. Kuchiyama, S. Kishi, S. Kaizaki, H. D. Takagi, M. Kato, *Inorg. Chem.* **2003**, 42, 785–795; b) T. Suzuki, T. Kuchiyama, S. Kishi, S. Kaizaki, M. Kato, *Bull. Chem. Soc. Jpn.* **2002**, 75, 2433–2439.
- [10] a) T. Suzuki, K. Fujiwara, H. D. Takagi, K. Kashiwabara, *Dalton Trans.* **2007**, 308–319; b) K. Kashiwabara, A. Morikawa, T. Suzuki, K. Isobe, K. Tatsumi, *J. Chem. Soc., Dalton Trans.* **1997**, 1075–1081; c) T. Suzuki, M. Rude, K. P. Simonsen, M. Morooka, H. Tanaka, S. Ohba, F. Galsøl, J. Fujita, *Bull. Chem. Soc. Jpn.* **1994**, 67, 1013–1023.
- [11] a) T. Suzuki, J. Fujita, *Chem. Lett.* **1992**, 1067–1068; b) T. Suzuki, M. Kita, K. Kashiwabara, J. Fujita, *Bull. Chem. Soc. Jpn.* **1990**, 63, 3434–3442.
- [12] a) I. Kinoshita, Y. Yokota, K. Matsumoto, S. Ooi, K. Kashiwabara, J. Fujita, *Bull. Chem. Soc. Jpn.* **1983**, 56, 1067–1073; b) I. Kinoshita, K. Kashiwabara, J. Fujita, K. Matsumoto, S. Ooi, *Bull. Chem. Soc. Jpn.* **1981**, 54, 2683–2690; c) K. Kashiwabara, I. Kinoshita, T. Ito, J. Fujita, *Bull. Chem. Soc. Jpn.* **1981**, 54, 725–732; d) I. Kinoshita, K. Kashiwabara, J. Fujita, *Bull. Chem. Soc. Jpn.* **1980**, 53, 3715–3716.
- [13] F. Galsøl, M. Kojima, T. Ishii, S. Ohba, Y. Saito, J. Fujita, *Bull. Chem. Soc. Jpn.* **1986**, 59, 1701–1707.
- [14] a) R. Morris, A. Habtemariam, Z. Guo, S. Parsons, P. J. Sadler, *Inorg. Chim. Acta* **2002**, 339, 551–559; b) M. Ito, M. Hirakawa, A. Osaku, T. Ikariya, *Organometallics* **2003**, 22, 4190–4192; c) R. Ares, M. Lopez-Torres, A. Fernandez, D. Vazquez-Garcia, J. M. Vila, L. Naya, J. J. Fernandez, *J. Organomet. Chem.* **2007**, 692, 4197–4208; d) N. Blaquiere, S. Diallo-Garcia, S. I. Gorelsky, D. A. Black, K. Fagnou, *J. Am. Chem. Soc.* **2008**, 130, 14034–14035.
- [15] a) K. Issleib, D. Haferburg, *Z. Naturforsch., Teil B* **1965**, 20, 916–918; b) K. Issleib, H. Oehme, *Chem. Ber.* **1967**, 100, 2685–2693; c) K. Issleib, A. Kipke, V. Hahnfeld, *Z. Anorg. Allg. Chem.* **1978**, 444, 5–20; d) K. Issleib, A. Kipke, *Z. Anorg. Allg. Chem.* **1980**, 464, 176–186.
- [16] J. W. L. Martin, J. A. L. Palmer, S. B. Wild, *Inorg. Chem.* **1984**, 23, 2664–2668.
- [17] a) G. Salem, S. B. Wild, *Inorg. Chem.* **1992**, 31, 581–586; b) D. G. Allen, G. M. McLaughlin, G. B. Robertson, W. L. Steffen, G. Salem, S. B. Wild, *Inorg. Chem.* **1982**, 21, 1007–1014.
- [18] a) W.-H. Sun, Z. Li, H. Hu, B. Wa, H. Yang, N. Zhu, X. Leng, H. Wang, *New J. Chem.* **2002**, 26, 1474–1478; b) P. Wehman, H. M. A. van Donge, A. Hagos, P. C. J. Kamer, P. W. N. W. van Leeuwen, *J. Organomet. Chem.* **1997**, 535, 183–193; c) A. A. Hudali, J. V. Kingston, H. A. Tayim, *Inorg. Chem.* **1979**, 18, 1391–1394; d) T. Tsukuda, C. Nishigata, K. Arai, T. Tsubomura, *Polyhedron* **2009**, 28, 7–12.
- [19] a) J. T. Migue, S. W. Hawbaker, *J. Chem. Crystallogr.* **1997**, 27, 603–608; b) U. E. Z. Schäfer, *Z. Anorg. Allg. Chem.* **1968**, 359, 67–77.

- [20] We used a crude mixture of *rac*-**2** and *meso*-**2** (ca. 2:1) for the spectrophotometric and electrochemical measurements in order to facilitate comparison of the properties with those of an equilibrium mixture of *rac*-**4** and *meso*-**4** in nitromethane (and presumably in acetonitrile, too). It can also be assumed that the spectroscopic and electrochemical properties of these *rac* and *meso* diastereoisomers are not significantly different.
- [21] a) B. N. Figgis, M. A. Hitchman, in: *Ligand Field Theory and Its Applications*, Wiley-VCH, New York, USA, **2000**, p. 211–214; b) B. N. Figgis, M. A. Hitchman, in: *Ligand Field Theory and Its Applications*, Wiley-VCH, New York, USA, **2000**, p. 158–160.
- [22] D. G. Holah, A. N. Hughes, B. C. Hui, C.-T. Kan, *Can. J. Chem.* **1978**, *56*, 2552–2559.
- [23] a) W. Klyne, V. Prelog, *Experientia* **1960**, *16*, 521–523; b) D. Casarini, C. Coluccini, L. Lunazzi, A. Mazzanti, *J. Org. Chem.* **2005**, *70*, 5098–5102.
- [24] There are no data available for the ionic or crystal radius of Ni<sup>I</sup>, but a speculation from the crystal radii of Ni<sup>II</sup>, Ni<sup>III</sup>, and Ni<sup>IV</sup> suggests a larger radius for Ni<sup>I</sup> than for Ni<sup>II</sup> (see: R. D. Shannon, *Acta Crystallogr., Sect. A* **1976**, *32*, 751–767).
- [25] A. Gleizes, M. Dartiguenave, Y. Dartiguenave, J. Galy, H. F. Klein, *J. Am. Chem. Soc.* **1977**, *99*, 1587–1589.
- [26] H.-Y. Wang, X. Meng, G.-X. Jin, *Dalton Trans.* **2006**, 2579–2585.
- [27] a) K. D. Kitiachvili, D. J. Mindiola, G. L. Hillhouse, *J. Am. Chem. Soc.* **2004**, *126*, 10554–10555; b) D. J. Mindiola, R. W. terman, D. M. Jenkins, G. L. Hillhouse, *Inorg. Chim. Acta* **2003**, *345*, 299–308; c) D. J. Mindiola, G. L. Hillhouse, *J. Am. Chem. Soc.* **2001**, *123*, 4623–4624.
- [28] R. D. Feltham, H. G. Metzger, *J. Organomet. Chem.* **1971**, *33*, 347–355.
- [29] Rigaku Co. Ltd., *Process-Auto, Automatic Data Acquisition and Processing Package for Imaging Plate Diffractometer*, Akishima, Tokyo, Japan, **1998**.
- [30] T. Higashi, *ABSCOR, Empirical Absorption Correction based on Fourier Series Approximation*, Rigaku Corporation, Tokyo, Japan, **1995**.
- [31] A. Altomare, G. Cascarano, C. Giacovazzo, A. Guagliardi, M. C. Burla, G. Polidori, M. Camali, *J. Appl. Crystallogr.* **1994**, *27*, 435.
- [32] P. T. Beurskens, G. Admiraal, G. Beruskena, W. P. Bosman, S. Garcia-Granda, R. O. Gould, J. M. M. Smits, C. Smykalla, *PATY, The DIRDIF program system. Technical Report of the Crystallography Laboratory*, University of Nijmegen, The Netherlands, **1992**.
- [33] G. M. Sheldrick, *Acta Crystallogr., Sect. A* **2008**, *64*, 112–122.
- [34] Rigaku and Rigaku/MS, *CrystalStructure ver. 3.6.0. Crystal Structure Analysis Package*, Akishima, Tokyo, Japan and The Woodlands, TX, USA, **2000–2004**.

Received: August 5, 2009

Published Online: November 26, 2009

# Pyrene-Functionalised Copper Complexes as Potential Dual-Modality Imaging Agents

Jason P. Holland,\*<sup>[a,b]</sup> Victoria Fisher,<sup>[a]</sup> Jennie A. Hickin,<sup>[a]</sup> and Josephine M. Peach\*<sup>[a]</sup>

*Dedicated to Prof. Jonathan R. Dilworth on the occasion of his 65th birthday*

**Keywords:** Copper / Imaging agents / Coordination chemistry / Density functional calculations

The syntheses of pyrene-functionalised bis(thiosemicarbazonato)zinc and -copper complexes are reported. In contrast to previously reported bis(thiosemicarbazonato) $\text{Cu}^{2+}$  complexes which are nonfluorescent, the pyrene group remains highly fluorescent. The compounds have been characterised by using a wide range of techniques including reverse-phase HPLC, cyclic voltammetry, NMR, electronic absorption (UV/Vis), infrared and fluorescence emission spectroscopy. Spectroelectrochemistry experiments demonstrated that the  $\text{Cu}^{2+}$  complexes undergo quasi-reversible one-electron reduction

at biologically accessible potentials. Density functional theory calculations were used to probe the electronic structure of the pyrene-functionalised copper complexes and confirmed that the ligand-based fluorescent emission occurs due to the absence of orbital interactions between the pyrene and bis(thiosemicarbazonato)copper groups. These preliminary studies demonstrate that the new copper complexes have potential to be used as dual-modality agents for in vitro cellular fluorescence microscopy and in vivo positron emission tomography experiments.

## Introduction

In the modern clinical environment, in vivo imaging plays a crucial role in the development of new drugs, and in diagnosis and treatment of disease.<sup>[1–5]</sup> Specialist hospitals typically offer a range of medical imaging modalities such as conventional radiography (X-rays), X-ray computed tomography (CT), magnetic resonance imaging (MRI), ultrasound, fluoroscopy, and nuclear tomographic imaging techniques including single-photon emission computerised tomography (SPECT) and positron emission tomography (PET).<sup>[5–8]</sup>

There is a high degree of interest in developing dual-modality agents which can be used in combination with more than one imaging technique. For example,  $\text{Cu}^{2+}$  complexes of bis(thiosemicarbazonato) ligands are under investigation as potential in vivo PET imaging and radiotherapeutic agents,<sup>[9–13]</sup> and the inherent fluorescence emission of the

analogous  $\text{Zn}^{2+}$  complexes has been used to monitor cellular uptake and intracellular localisation in vitro.<sup>[14,15]</sup> The  $^{64}\text{Cu}$ -radiolabelled complex of diacetyl-2,3-bis(4-*N*-methyl-3-thiosemicarbazonato), [ $^{64}\text{Cu}^{\text{II}}$ ATSM], is currently in Phase I clinical trials in the United States of America as an “Investigational New Drug” (IND) for imaging hypoxia in patients with cervical cancer.<sup>[16–22]</sup> However, the paramagnetic nature of these neutral bis(thiosemicarbazonato) $\text{Cu}^{2+}$  complexes inhibits fluorescence emission and prevents investigation of the cellular uptake and intracellular localisation via fluorescence microscopy. Development of fluorescent  $\text{Cu}^{2+}$  complexes would facilitate dual-modality in vitro and in vivo imaging studies.

This article describes the synthesis and characterisation of a range of bis(thiosemicarbazonato)zinc and -copper complexes which have been functionalised with pyrene as a fluorophore. A wide range of techniques has been used to characterise the new complexes including mass spectrometry, NMR, electronic absorption (UV/Vis), fluorescence emission and infrared (IR) spectroscopy, cyclic voltammetry (CV) and spectroelectrochemistry (UV/Vis-SEC). The structure and bonding of the pyrene-functionalised  $\text{Cu}^{2+}$  complexes have also been investigated with density functional theory (DFT).

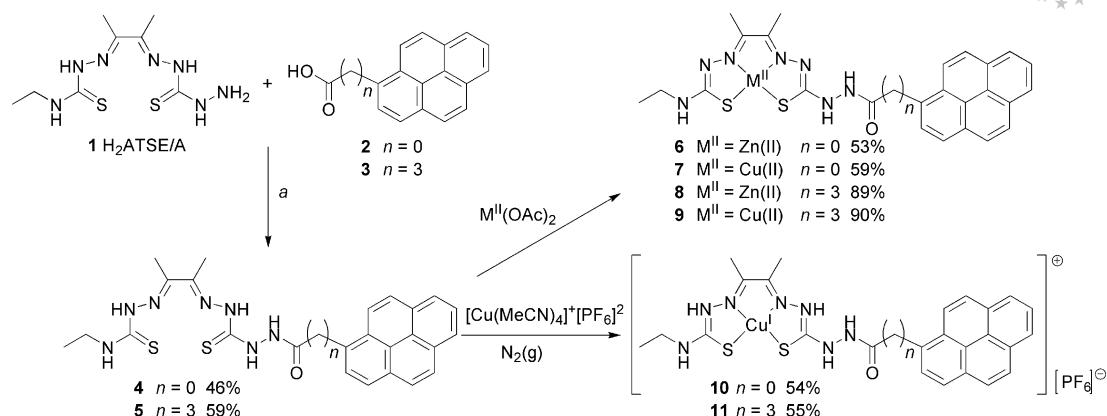
## Results and Discussion

Two different routes have been used to synthesise pyrene-functionalised copper and zinc bis(thiosemicarbazonato)

[a] Department of Chemistry, University of Oxford, Chemistry Research Laboratory, 12 Mansfield Road, OX1 3TA Oxford, United Kingdom  
E-mail: jos.peach@some.ox.ac.uk

[b] Memorial Sloan-Kettering Cancer Center, Department of Radiology, 1275 York Avenue, NY10065 New York, United States of America  
E-mail: hollanj3@mskcc.org  
jasonpholland@gmail.com

Supporting information for this article is available on the WWW under <http://dx.doi.org/10.1002/ejic.200900823>.



Scheme 1. Reaction scheme showing the synthesis of unsymmetrical bis(thiosemicarbazonato)zinc(II), -copper(II) and -copper(I) complexes derived from  $\text{H}_2\text{ATSE/A}$  (**1**) and conjugated to 1-pyrene derivatives.<sup>[12]</sup> (a)  $\text{H}_2\text{ATSE/A}$ , 1-pyrenecarboxylic acid (**2**) or 4-(pyren-1-yl)butyric acid (**3**), 1-hydroxybenzotriazole hydrate (1 equiv.), EDCI (1 equiv.), anhydrous DMF, stirred under nitrogen at room temperature for 24 h.

complexes. The first route used was based on previously reported methods and is shown in Scheme 1. Proligands **4** and **5** were synthesised by coupling either 1-pyrenecarboxylic acid (**2**) or 4-(pyren-1-yl)butyric acid (**3**) with the reactive terminal hydrazinic amine group of  $\text{H}_2\text{ATSE/A}$  (**1**). The synthesis of compound **1** and other derivatives has been reported elsewhere.<sup>[12]</sup> Standard 1-ethyl-3-[3-(dimethylamino)propyl]carbodiimide hydrochloride (EDCI) peptide coupling methods were employed and compounds **4** and **5** were isolated in moderate yield (46% and 59%, respectively). Formation of an amide bond leads to increased chemical stability with respect to hydrolysis in comparison to *N*-glycosylamine and imine bonds which have been used previously as linker groups.<sup>[12,23]</sup>

Compounds **4** and **5** were used to synthesise unsymmetrical  $\text{Zn}^{2+}$  (**6** and **8**),  $\text{Cu}^{2+}$  (**7** and **9**) and  $\text{Cu}^+$  bis(thiosemicarbazonato) complexes (**10** and **11**) by standard procedures (Scheme 1).<sup>[12]</sup> The  $\text{Zn}^{2+}$  and  $\text{Cu}^{2+}$  complexes **6–9** were prepared in moderate to high yields (53–90%) as yellow and brown/red powders, respectively, by reaction of the corresponding proligand with metal(II) diacetate salts in methanol. The isolated yields of complexation reactions with proligand **4** were found to be consistently lower (50% to 60%) than with **5** (approximately 90%). The effect of changing the reaction stoichiometry [by changing the amount of metal(II) acetate], the temperature and time were also investigated for the synthesis of complexes **7**, **8** and **9**. Optimised conditions are reported in the Experimental Section and the Supporting Information. Previously, we found that a slight excess (1.1 equiv.) of metal(II) acetate to ligand gave the highest complexation yields. However, for complex **7** the highest yield was obtained by reaction of **4** with 10 equiv. of  $\text{Cu}(\text{OAc})_2 \cdot \text{H}_2\text{O}$  at room temperature for 24 h.

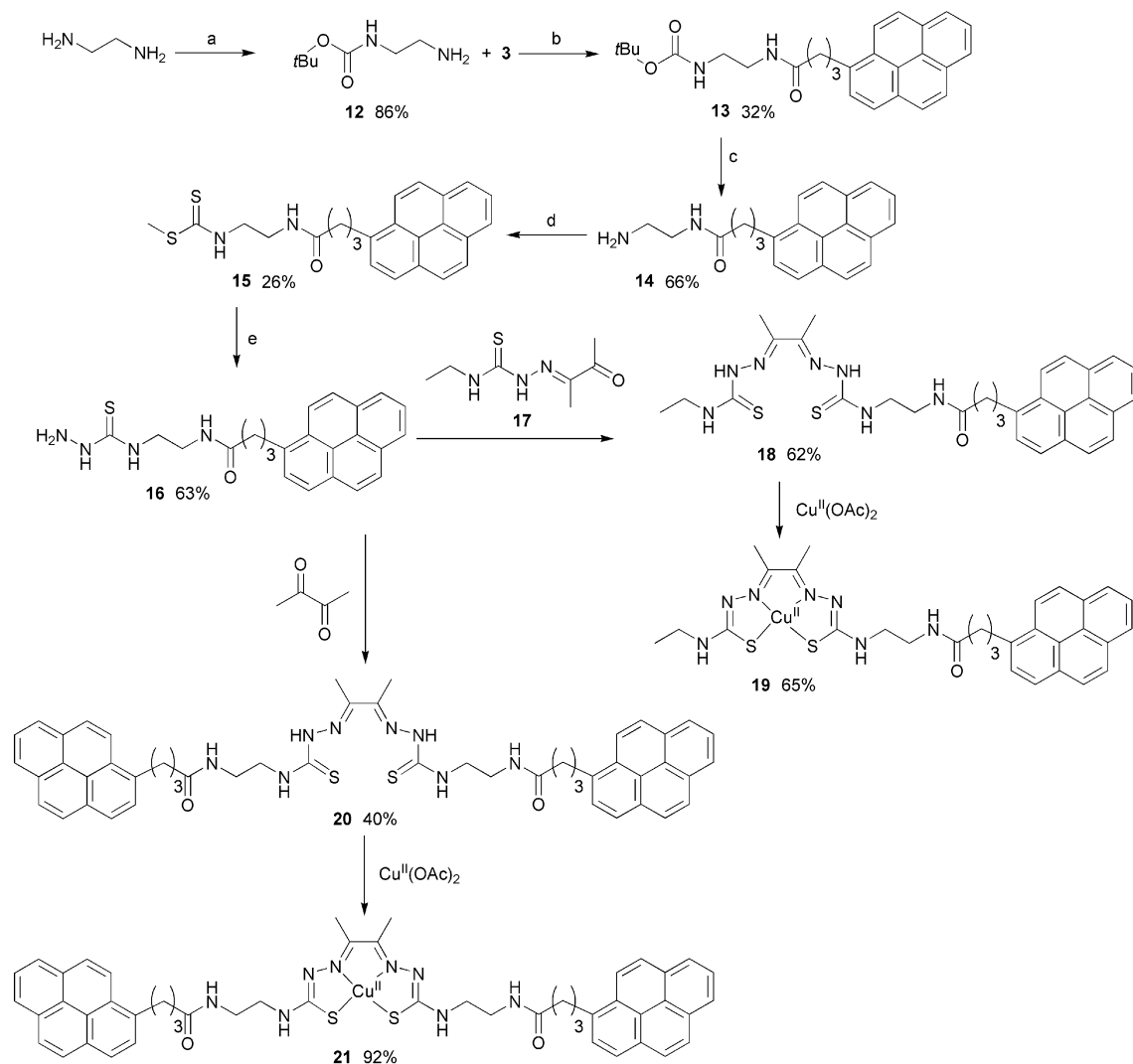
The mono-cationic  $\text{Cu}^+$  complexes **10** and **11** were synthesised under anaerobic conditions (nitrogen atmosphere) by reaction of compounds **4** and **5** with  $[\text{Cu}(\text{MeCN})_4]^+[\text{PF}_6]^-$  in anhydrous dimethylformamide (DMF) at room temperature. Copper(I) complexes of bis(thiosemicarbazonato)

ligands are oxidised rapidly by dioxygen to the corresponding neutral  $\text{Cu}^{2+}$  species and are notoriously difficult to isolate.<sup>[24,25]</sup> Previous studies aimed at probing the mechanism of hypoxia-selectivity of copper bis(thiosemicarbazonato) have reported an X-ray crystal structure of a helical copper(I) dimer<sup>[26]</sup> and identification of numerous reduced species in the solution phase, for example,  $[\text{Cu}^1\text{ATSM}]^-$  and  $[\text{Cu}^1\text{HATSM}]^-$ .<sup>[24,25,27]</sup> The work presented here represents the first structural characterisation of isolated monomeric  $\text{Cu}^+$  bis(thiosemicarbazone) salts by NMR spectroscopy.

The structures and purity of complexes **10** and **11** were confirmed by microanalysis and both  $^1\text{H}$  and  $^{13}\text{C}\{^1\text{H}\}$  NMR spectroscopy. When metal(II) ions (such as  $\text{Cu}^{2+}$  and  $\text{Zn}^{2+}$  ions) are complexed by bis(thiosemicarbazone) proligands, neutral complexes are formed by loss of the two  $\text{C}(\text{S})\text{NHN}=\text{C}$  hydrogen atoms. On complexation with  $[\text{Cu}(\text{MeCN})_4]^+[\text{PF}_6]^-$  monocationic, monomeric species were observed. For example, the  $^1\text{H}$  spectrum of **4** revealed two  $\text{C}(\text{S})\text{NHN}=\text{C}$  peaks at  $\delta = 10.81$  and  $10.83$  ppm. In complex **10** these two peaks remained present but shifted position to  $\delta = 10.71$  and  $12.12$  ppm. These observations confirm that for complexes **10** and **11**, deprotonation of the bis(thiosemicarbazone) ligands does not occur. In contrast to the dark red/brown colour of most bis(thiosemicarbazonato) $\text{Cu}^{2+}$  species, complexes **10** and **11** were found to be light brown in colour.

Despite successful conjugation of the hydrazinic amine group of **1** to a range of biologically relevant molecules, these systems remain less stable with respect to chemical attack at the ligand than complexes with simple aliphatic or aromatic substituents.<sup>[12]</sup> Therefore, symmetrical and unsymmetrical proligands and  $\text{Cu}^{2+}$  complexes in which the 4-(pyren-1-yl)butyric acid fluorophore is conjugated to the bis(thiosemicarbazone) group through an ethylene group were synthesised in accordance with Scheme 2.

Compound **12** was synthesised in 86% yield by the reaction of di-*tert*-butyl dicarbonate with ethylenediamine in chloroform. Once mono-Boc-protected, the primary amine



Scheme 2. Reaction scheme for the synthesis of symmetrical and unsymmetrical Cu<sup>2+</sup> bis(thiosemicarbazonato) complexes conjugated to 4-(pyren-1-yl)butyric acid (**3**) via an ethylenediamine linker group. (a) Di-*tert*-butyl dicarbonate, ethylenediamine, chloroform, 0 °C warming overnight to room temperature. (b) Compound **2**, EDCI, anhydrous DMF, stirred under Ar(g) at room temperature for 24 h. (c) Trifluoroacetic acid (TFA) stirring at room temperature for 1 h. (d) Carbon disulfide, Et<sub>3</sub>N, then MeI, stirring in ethanol at room temperature. (e) Hydrazine hydrate, reflux in ethanol for 2.5 h.

was coupled to **3** by using either standard EDCI coupling or thionyl chloride. Both methods were found to give **13** in approximately 30% yield. The *tert*-butoxycarbonyl (Boc) protecting group was removed by stirring **13** in trifluoroacetic acid (TFA) for 1 h at room temperature to give **14** in 66% yield. The primary amine of **14** was then reacted with carbon disulfide to give **15** which was then converted into the corresponding thiosemicarbazide **16** by reaction with hydrazine hydrate.<sup>[12]</sup> Once **16** was available, the unsymmetrical or symmetrical bis(thiosemicarbazone) proligands **18** and **20** respectively, were synthesised in moderate yields by reaction with either diacetyl-2-(4-*N*-ethyl-3-thiosemicarbazone) (**17**) or 2,3-butanedione, using standard procedures.<sup>[12,28]</sup> Complexation with Cu(OAc)<sub>2</sub>·H<sub>2</sub>O afforded the corresponding neutral Cu<sup>2+</sup> complexes **19** and **21**, in 65% and 92% yield, respectively.

## Electrochemical and Spectroscopic Studies

Bis(thiosemicarbazonato)copper(II) complexes with dimethyl backbone substituents such as [Cu<sup>II</sup>ATSM] are currently under investigation as hypoxia-selective *in vivo* imaging agents. Recent computational,<sup>[27]</sup> spectroelectrochemical,<sup>[24,25]</sup> and *in vitro* kinetic<sup>[29]</sup> studies by our group, in combination with experimental structure–activity relationship studies by Dearling et al.<sup>[30,31]</sup> have shed light on the role of one-electron reduction, reoxidation, protonation and ligand dissociation reactions with respect to the mechanism of hypoxia-selective tumour uptake. Complexes with reduction potentials less than −0.58 V vs. the saturated calomel electrode (SCE) typically show a strong propensity for increased intracellular uptake and trapping under hypoxic conditions.<sup>[30,31]</sup> Therefore, the electrochemistry of the

pyrene-functionalised bis(thiosemicarbazonato)copper complexes was investigated by CV and electronic absorption spectroelectrochemistry (UV/Vis-SEC) experiments.

Figure 1 (top) shows the full potential-sweep width cyclic voltammogram of a  $1.0 \times 10^{-3} \text{ mol dm}^{-3}$  solution of complex **9** in anhydrous, deoxygenated DMF at room temperature. The peaks  $P_1$ – $P_6$  occur at potentials, +0.747, +0.989, –0.155, –0.454, –0.638 and –0.483 V. Peaks  $P_5$  and  $P_6$  correspond to the metal-centred one-electron reduction couple, with half-wave potential,  $E_{1/2}(\text{SCE}) = -0.561 \text{ V}$ , peak current ratio,  $|i_{pa}|/|i_{pc}| = 0.89$ , and a peak-to-peak separation of  $\Delta E_p = 155 \text{ mV}$ . In the same experimental set-up one-electron oxidation of ferrocene displayed a peak-to-peak separation of  $\Delta E_p = 79 \text{ mV}$ . This quasi-reversible reduction process corresponds to the formation of the  $\text{Cu}^+$  anionic species in the solution phase.<sup>[24,25]</sup> Functionalisation with 4-(pyren-1-yl)butyric acid leads to a more facile  $\text{Cu}^{2+}/\text{Cu}^+$  reduction process than observed for  $[\text{Cu}^{\text{II}}\text{ATSM}]$  and this result suggests that complex **9** lies on the periphery of the proposed window for hypoxia-selectivity.<sup>[30,31]</sup>

Peaks  $P_1$  and  $P_2$  correspond to two successive one-electron oxidation processes. By analogy with results reported for the oxidation of  $[\text{Cu}^{\text{II}}\text{ATSM}]$  and related complexes,  $P_1$  is assigned to the irreversible ligand-based oxidation of the bis(thiosemicarbazonato) group and  $P_2$  is assigned to the irreversible ligand-based oxidation of either the pyrene or amide groups.<sup>[24]</sup>

Figure 1 (bottom) shows the change observed in the cyclic voltammogram with varying potential-sweep width. When the two irreversible oxidation processes,  $P_1$  and  $P_2$  are excluded from the scan, the species corresponding to the processes at  $P_3$  and  $P_4$  are absent. After sweeping the potential over the first oxidation wave (corresponding to  $P_1$ ),  $P_3$  is observed but not  $P_4$ . When the sweep width was extended to positive potentials above the peak potential of  $P_2$ , process  $P_4$  was observed. Therefore,  $P_3$  and  $P_4$  can be assigned to separate solution-phase products formed from two distinct, sequential electrochemical-chemical  $E_{\text{irrev}}C_{\text{irrev}}$  processes associated with oxidation of the bis(thiosemicarbazonato) ligand and either the pyrene or amide groups, respectively.

The change in the electronic absorption spectrum of a  $1.0 \times 10^{-3} \text{ mol dm}^{-3}$  solution of complex **9** observed during electrochemical reduction at –1.1525 V, for 620 s to 4.77 % of the initial current in anhydrous, deoxygenated DMF is shown in Figure 2 (top). These UV/Vis-SEC experiments demonstrate that the peaks at 314 and 478 nm, and the shoulder at 525 nm in the visible region, previously assigned to a combination of metal-based  $d \rightarrow d$  and ligand-to-metal charge transfer (LMCT) absorptions by the  $\text{Cu}^{2+}$  bis(thiosemicarbazonato) chromophore, are lost on electrochemical reduction.<sup>[12,24,32]</sup> An increase in absorbance was observed at wavelengths above 565 nm and by the end of the bulk reduction process, a weak peak was observed at 598 nm. The absorbance of the two intense peaks at 328 and 344 nm, assigned to pyrene  $\pi \rightarrow \pi^*$  transitions, remain constant during reduction. These data provide further evidence that the one-electron reduction process observed in

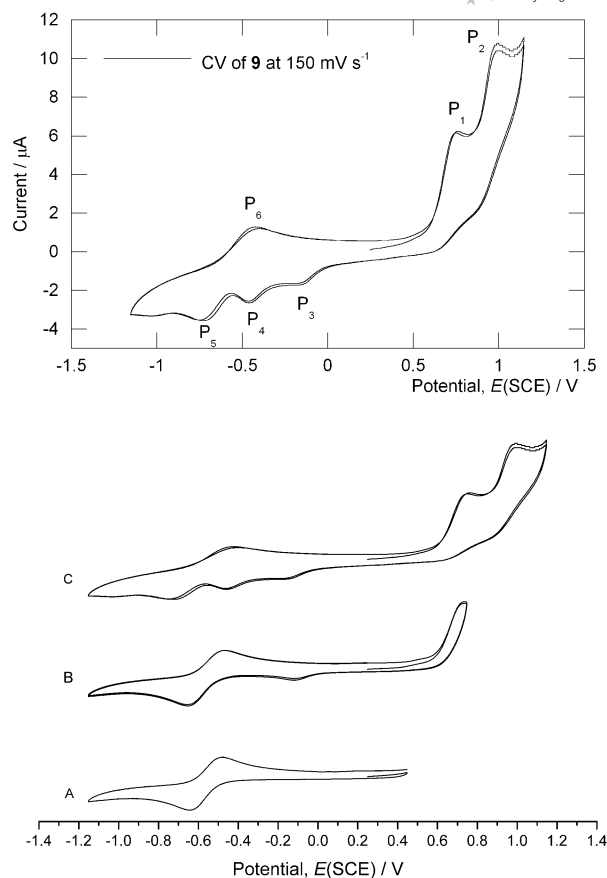


Figure 1. Top: Full potential sweep width cyclic voltammogram of a  $1.0 \times 10^{-3} \text{ mol dm}^{-3}$  solution of complex **9**, recorded by using a platinum disc working electrode at  $150 \text{ mV s}^{-1}$ , in anhydrous, deoxygenated DMF, at 295 K. Peaks  $P_1$ – $P_6$  are discussed in the main text. Bottom: Cyclic voltammograms recorded at  $100 \text{ mV s}^{-1}$  starting at +0.249 V and scanning in a positive direction to high switching potentials of A = +0.448 V, B = +0.748 V and C = +1.148 V. For each experiment the low switching potential of –1.153 V was used. All potentials are reported relative to the SCE.

the cyclic voltammogram is metal-centred and indicate that the orbitals of the pyrene and copper bis(thiosemicarbazonato) groups do not interact (vide infra).

The change observed after switching the potentiostat off (no applied potential) is presented in Figure 2 (bottom). An immediate and constant rate increase in absorbance at 478 nm was observed. After 25 min, the spectrum was the same as that observed of the initial complex **9**. Previous experimental and computational work has established that residual molecular oxygen is capable of rapidly oxidising the copper(I) anion formed on reduction.<sup>[24,25]</sup> Given that the pyrene and bis(thiosemicarbazonato) functional groups remain distinct, it is likely that complex **9** behaves in the same way as  $[\text{Cu}^{\text{II}}\text{ATSM}]$  and related complexes.

In order to assess the potential of the pyrene-functionalised copper complexes to be used as fluorescence imaging agents the emission spectra were recorded in dimethyl sulfoxide (DMSO). Preliminary studies revealed that the copper complexes remained highly fluorescent. For example,

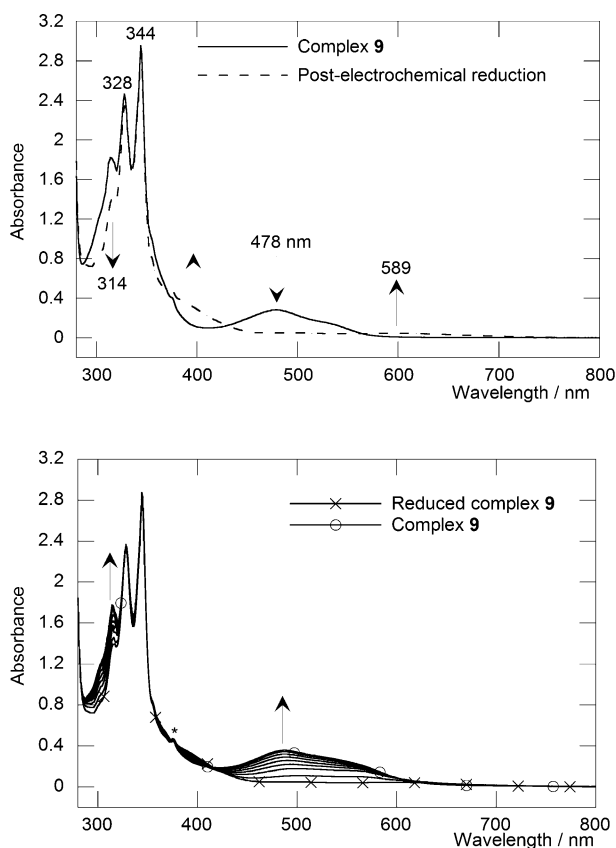


Figure 2. Top: Change in the experimental UV/Vis absorption spectrum recorded during electrochemical reduction of a  $1.0 \times 10^{-3} \text{ mol dm}^{-3}$  solution of complex **9** at  $-1.153 \text{ V}$  (vs. SCE) for 620 s, in anhydrous, deoxygenated DMF at room temperature. Bottom: Change observed in the UV/Vis spectrum post-electrochemical, after switching the potentiostat off (no potential). Residual dioxygen slowly oxidises the electro-generated copper(I) anionic complex to give the neutral complex **9**. An instrumentation artefact was observed at 375 nm as indicated by an asterisk \*. Full analysis of the spectroelectrochemistry of related copper bis(thiosemicarbazonato) complexes has been reported elsewhere.<sup>[24,25]</sup>

for proligand **18** emission peaks were observed at  $\lambda_{\text{em,max.}} = 380 \text{ nm}$  (excitation wavelength,  $\lambda_{\text{ex.}} = 285 \text{ nm}$ ) with an estimated quantum yield of  $\phi_{\text{F}} = 0.28$ .<sup>[33]</sup> For the corresponding  $\text{Cu}^{2+}$  complex **19** an emission peak was observed at  $396 \text{ nm}$  ( $\lambda_{\text{ex.}} = 285 \text{ nm}$ ) with  $\phi_{\text{F}} = 0.28$ . For proligand **20** and complex **21** peak emissions were observed at  $400 \text{ nm}$  ( $\phi_{\text{F}} = 0.27$ ) and  $396 \text{ nm}$  ( $\phi_{\text{F}} = 0.06$ ). In comparison to pyrene ( $\phi_{\text{F}} = 0.30 \pm 0.03$ ) a small decrease in emission quantum yield was observed for both ligands and  $\text{Cu}^{2+}$  complexes **18–21**. However, these results demonstrate that unlike other reported bis(thiosemicarbazonato) $\text{Cu}^{2+}$  complexes, which are nonfluorescent, complexation with paramagnetic  $\text{Cu}^{2+}$  ions does not interfere with either the excitation or emission processes associated with the pyrene group.

In previous studies we have demonstrated facile  $^{64}\text{Cu}$ -radiolabelling of bis(thiosemicarbazones) via either direct metallation or transmetallation from the corresponding  $\text{Zn}^{2+}$  complex.<sup>[12,15,34]</sup> Although radiolabelling experiments

were not conducted in these studies no problems are anticipated. Radiolabelling studies and further in vivo experiments are underway and will be reported elsewhere.

### Density Functional Theory Calculations

The electrochemical and UV/Vis-SEC experiments indicate that in comparison to  $[\text{Cu}^{\text{II}}\text{ATSM}]$ , functionalisation of the bis(thiosemicarbazonato) group with pyrene does not significantly alter the electronic structure of copper complexes **9**, **11**, **19** and **21**. The experiments also suggest that although the absolute energies of the frontier molecular orbitals (FMOs) are raised in comparison to  $[\text{Cu}^{\text{II}}\text{ATSM}]$  (as shown by the less negative one-electron reduction potential), the ordering and orbital mixing remain similar. Therefore, to investigate the electronic structure in more detail, DFT calculations were conducted. In order to restrict the number of potential conformers and facilitate geometry optimisation, calculations were performed by using the modified structure of complex **7** where the terminal ethyl group was replaced by a methyl group. Full computational details are presented in the experimental section and ESI.

The uB3LYP/6-31++G(d,p)-optimised geometry is presented in Figure 3.<sup>[35]</sup> The calculated structure displays a twist between the two planes defined by the  $\text{Cu}^{2+}$  bis(thiosemicarbazonato) (including the amide bond) and the pyrene group with a dihedral angle,  $d(\text{O}-\text{C}-\text{C}(1)-\text{C}(2))$  of  $140^\circ$ . This twist is evident in the electronic structure and prevents the  $\pi\pi^*$  orbitals of pyrene from mixing with the  $\pi\pi^*$  orbitals of the bis(thiosemicarbazonato) $\text{Cu}^{2+}$  group.

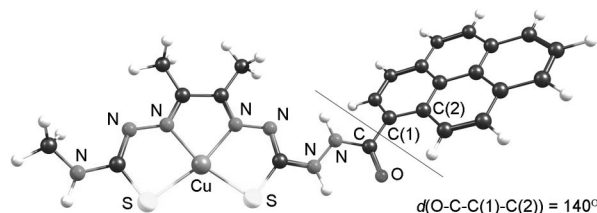


Figure 3. DFT-optimised geometry of the simplified structure of complex **7** showing the structural twist between the plane of the  $\text{Cu}^{2+}$  bis(thiosemicarbazonato) amide group, and the pyrene group. The geometry of the  $\text{Cu}^{2+}$  bis(thiosemicarbazonato) group is consistent with previously reported calculations.<sup>[24,27]</sup>

A molecular orbital (MO) diagram with selected electron density isosurfaces is shown in Figure 4. The MO diagram shows the correlation between MOs of  $[\text{Cu}^{\text{II}}\text{ATSM}]$  and pyrene (in  $D_{2h}$  symmetry) and the MOs of the simplified complex **7**. As suggested by experiment, the electron density associated with the  $\pi$  systems of the bis(thiosemicarbazonato) ligand does not interact with the pyrene group. Furthermore, the lowest unoccupied molecular orbital (LUMO) in the  $\beta$ -spin orbital manifold is a metal–ligand  $\sigma^*$  antibonding orbital consistent with previous DFT studies.<sup>[27]</sup> The LUMO accepts the electron on reduction and confirms the assignment of peaks  $\text{P}_5$  and  $\text{P}_6$  (Figure 1, a) to a  $\text{Cu}^{2+}/\text{Cu}^+$  redox process. The calculated electronic

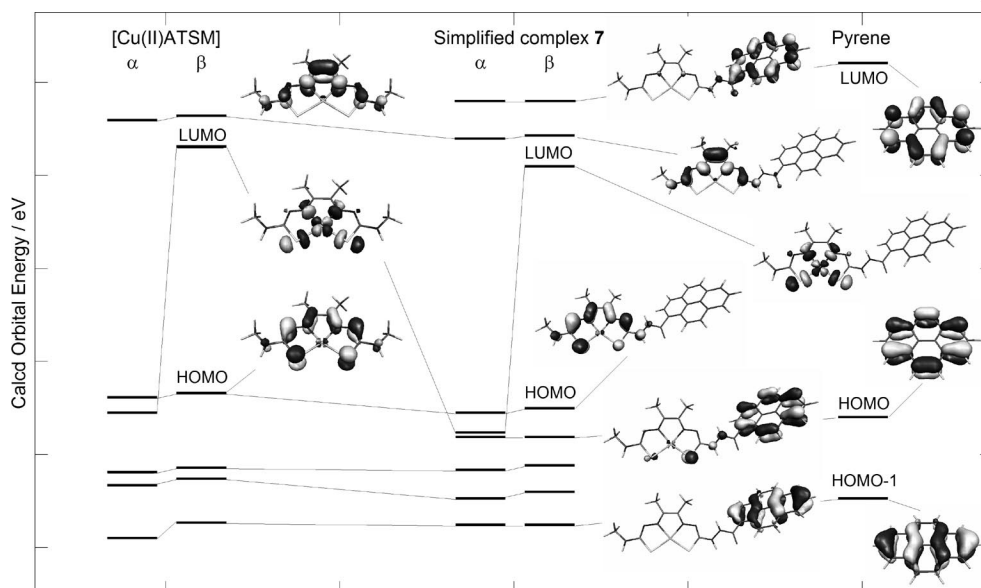


Figure 4. MO diagram showing the correlation between orbitals of  $[\text{Cu}^{\text{II}}\text{ATSM}]$  (left), pyrene in  $D_{2h}$  symmetry (right) and the simplified optimised model complex **7** (centre). All occupied orbitals lie below  $-5.0$  eV and virtual orbitals lie above  $-3.5$  eV. Selected MO isosurfaces (calculated at 96% of the electron density) are shown adjacent to the orbital energy lines. Orbitals with similar spatial distributions are connected by black lines.

structure is also consistent with the UV/Vis-SEC experiments. Only peaks corresponding to absorption by the copper bis(thiosemicarbazonato) chromophore and not the pyrene show change on reduction in the OTTLE cell.

The DFT calculations are consistent with the observed fluorescence emission of the pyrene-functionalised copper complexes. The structural twist and lack of conjugation of the  $\pi$ -orbitals means that communication between the  $\text{Cu}^{2+}$  centre and the emissive excited states produced on excitation of the pyrene group is negated. Hence, the pyrene and  $\text{Cu}^{2+}$  groups absorb light to produce two distinct, non-interacting excited states. The state formed by excitation of the  $\text{Cu}^{2+}$  chromophore decays rapidly via internal conversion and the pyrene-centred excited state is highly emissive.

## Summary and Conclusions

Symmetrical and unsymmetrical pyrene-functionalised  $\text{Cu}^{2+}$  and  $\text{Zn}^{2+}$  bis(thiosemicarbazonato) complexes have been synthesised and characterised using a range of electrochemical, spectroscopic and computational techniques. Fluorescent  $\text{Cu}^{2+}$  complexes have been synthesised and show promise for use as *in vitro* cellular imaging agents for investigating the mechanism of hypoxia-selective uptake and trapping. In addition, cationic  $\text{Cu}^+$  complexes have been synthesised and to the best of our knowledge represent the first structural characterisation of bis(thiosemicarbazone)-copper(I) complexes by  $^1\text{H}$  and  $^{13}\text{C}\{^1\text{H}\}$  NMR spectroscopy. Electrochemistry and spectroelectrochemistry experiments have demonstrated that the  $\text{Cu}^{2+}$  complexes undergo one-electron reduction at potentials close to the range identified as important for the mechanism of hypoxia-selectivity. DFT calculations have been used to probe the nature

of the electronic structure of the pyrene complexes and explain the observed experimental solution-phase spectroscopy. These complexes show potential for use as dual-modality, *in vitro* fluorescence and *in vivo* PET imaging agents. Further studies are underway to evaluate the biological properties of these complexes.

## Experimental Section

**General Details:** All reagents were obtained from commercial sources (Sigma-Aldrich and Lancaster) and unless otherwise stated, were used as received. Reactions involving moisture-sensitive reagents were carried out under nitrogen or argon using standard vacuum-line techniques and glassware was flame-dried and cooled under nitrogen before use. Solvents were dried in accordance with procedures outlined by Grubbs and co-workers.<sup>[36]</sup> Water was purified by an Elix UV-10 system.

Thin-layer chromatography (TLC) was performed on aluminium plates coated with 60  $\text{F}_{254}$  silica. Plates were visualised by using UV light (254 nm), iodine, 1%  $\text{KMnO}_4(\text{aq.})$  or 10% ethanolic phosphomolybdic acid. Flash column chromatography was performed by using either Kieselgel 60 silica or on a Biotage SP4 flash column chromatography platform. Petroleum ether with a boiling range of 40–60  $^{\circ}\text{C}$  was used. Melting points were recorded with a Gallenkamp Hot Stage apparatus and reported values are uncorrected. IR spectra were recorded with Bruker Tensor 27 FTIR spectrometer as either a thin film on NaCl plates (film) or KBr discs (KBr).

Elemental analyses were performed by the microanalysis service of the department at the University of Oxford. Low resolution mass spectrometry (LRMS,  $m/z$ ) was performed with a VG Platform II instrument. High resolution mass spectra were recorded with a Micromass LCT Time of Flight Mass Spectrometer using either positive or negative ion electrospray ( $\text{ESI}^+$  or  $\text{ESI}^-$ , respectively).

Where possible, accurate mass values are reported to four decimal places using tetraoctylammonium bromide (466.5352 Da) as an internal reference.

NMR spectra were recorded with a Varian Mercury VX300 spectrometer, ( $^1\text{H}$  at 300 MHz,  $^{13}\text{C}\{^1\text{H}\}$  at 75.5 MHz), Bruker DPX-400 ( $^1\text{H}$  at 400 MHz,  $^{13}\text{C}\{^1\text{H}\}$  at 100 MHz), AV-400 (400 MHz), AV-500 ( $^1\text{H}$  at 500 MHz,  $^{13}\text{C}\{^1\text{H}\}$  at 125 MHz) and DRX-500 ( $^1\text{H}$  at 500 MHz,  $^{13}\text{C}\{^1\text{H}\}$  at 125 MHz) spectrometers at ambient temperature using the residual solvent signal as an internal reference. Chemical shifts ( $\delta$ ) are reported in parts per million (ppm) and coupling constants ( $J$ ) are reported in Hz.

High-performance liquid chromatography (HPLC) was conducted by using a Gilson HPLC machine equipped with a Hamilton PRP-1 reverse-phase column and UV/Vis detection at 254 nm. Retention times,  $t_{\text{R}}$ /min, are reported for the water/acetonitrile gradient elution method used (% acetonitrile, time): 5%, 0 min; 95%, 15 min; 95%, 25 min; 5%, 27 min; 5%, 30 min.

Electronic absorption spectra were recorded with a Perkin–Elmer Lambda 19 UV/Vis/near-IR spectrometer. Fluorescence emission spectra were recorded with a Perkin–Elmer LS55 luminescence spectrometer and Edinburgh Instruments EPL-375 nm and EPL-405 nm picosecond-pulsed diode lasers. Relative quantum yield measurements were performed on a Perkin–Elmer LS55 luminescence spectrometer following the method of Natrajan et al.<sup>[33]</sup>

Cyclic voltammograms of 1.0 mmol dm<sup>-3</sup> solutions of complex **9** in 5.0 cm<sup>3</sup> of anhydrous dimethylformamide (DMF) with 0.1 mol dm<sup>-3</sup> tetrabutylammonium tetrafluoroborate (TBA-BF<sub>4</sub>) supporting electrolyte, were recorded with a CH Instruments Electrochemical Analyser by using a platinum working electrode, a platinum wire counter/auxiliary electrode and a silver/silver ion reference electrode. Ferrocene was used as an internal reference for which the one-electron redox process occurs at  $E_{1/2} = 0.53$  V (DMF) vs. SCE. Electronic absorption spectroelectrochemistry (UV/Vis-SEC) experiments were performed in anhydrous DMF with 0.1 mol dm<sup>-3</sup> TBA-BF<sub>4</sub> supporting electrolyte, using a custom made, optically transparent thin-layer electrode (OTTLE) cell (path length,  $l = 0.46$  mm). The quartz OTTLE cell was sealed with a Teflon™ cap. The total volume of the OTTLE cell was approximately 4.0 cm<sup>3</sup>. The same auxiliary and reference electrodes as used in the CV experiments were placed in the bulk solution above the optical cavity and a platinum wire mesh (approximately 50-wires per inch, 0.10 mm thickness) located inside the cavity, was used as the working electrode. Comprehensive details on electrode and OTTLE cell preparation have been reported elsewhere.<sup>[24]</sup>

**Density Functional Theory Calculations:** All calculations were conducted by using density functional theory (DFT) as implemented in the Gaussian 03, Revision C.02 suite of ab initio quantum chemistry programs.<sup>[35]</sup> Geometry optimisations and vibrational frequency calculations were performed by using the unrestricted uB3-LYP exchange and correlation functionals and the double- $\zeta$  6-31++G(d,p) basis set for all atoms. Normal SCF and geometry convergence criteria were used and no symmetry constraints were imposed. For all gas-phase calculations, harmonic frequency analysis based on analytical second derivatives was used to characterise the optimised geometries as local minima.

## Syntheses

1-Pyrenecarboxylic acid (**2**) and 4-(pyren-1-yl)butyric acid (**3**) were purchased from Sigma–Aldrich and used as received.

**N-Ethyl-2-{3-[2-(hydrazinylcarbonothioyl)hydrazinylidene]butan-2-ylidene}hydrazinecarbothioamide (H<sub>2</sub>ATSE/A, **1**):** Compound **1** was synthesised in accordance with a procedure described previously.<sup>[12]</sup> Compound **1** was isolated as a white powder (1.83 g, 6.6 mmol, 89%); m.p. >195 °C (dec.). C<sub>8</sub>H<sub>17</sub>N<sub>7</sub>S<sub>2</sub> (275.40): calcd. C 34.9, H 6.2, N 35.6, S 23.3; found C 34.9, H 6.3, N 35.7, S 23.2.  $^1\text{H}$  NMR (300 MHz, [D<sub>6</sub>]DMSO):  $\delta = 1.13$  (t,  $^3J_{\text{HH}} = 7.1$  Hz, 3 H, CH<sub>3</sub>CH<sub>2</sub>NH), 2.18 (two overlapping s, 6 H, CH<sub>3</sub>C=N), 3.59 (m, 2 H, CH<sub>3</sub>CH<sub>2</sub>NH), 4.96 (s, 2 H, NHNH<sub>2</sub>), 8.40 (t,  $^3J_{\text{HH}} = 5.9$  Hz, 1 H, CH<sub>3</sub>CH<sub>2</sub>NH), 9.70 (br. s, 1 H, NHNH<sub>2</sub>), 10.14 (s, 1 H, NHC(=S)NHN=), 10.21 (s, 1 H, NHC(=S)NHN=) ppm.  $^{13}\text{C}\{^1\text{H}\}$  NMR (75.5 MHz, [D<sub>6</sub>]DMSO):  $\delta = 11.6$  (CH<sub>3</sub>C=N), 11.6 (CH<sub>3</sub>C=N), 14.4 (CH<sub>3</sub>CH<sub>2</sub>NH), 38.5 (CH<sub>3</sub>CH<sub>2</sub>NH), 148.4 (C=N), 148.1 (C=N), 175.8 (NH<sub>2</sub>NHC=S), 177.3 (EtNHC=S) ppm. HRMS-ESI<sup>+</sup>: [C<sub>8</sub>H<sub>18</sub>N<sub>7</sub>S<sub>2</sub>]<sup>+</sup>  $m/z$  (%) = (100) [M + H]<sup>+</sup>; calcd. 338.0200; found 338.0191. HPLC:  $t_{\text{R}} = 8.6$  min.

**N-Ethyl-2-[(3E)-3-(2-{2-(pyren-1-ylcarbonyl)hydrazinyl}carbonothioyl)hydrazinylidene]butan-2-ylidene}hydrazinecarbothioamide (**4**):** H<sub>2</sub>ATSE/A (**1**) (50.0 mg, 0.18 mmol), 1-pyrenecarboxylic acid (**2**) (45.0 mg, 0.18 mmol), 1-hydroxybenzotriazole hydrate (28.0 mg, 0.18 mmol) and EDCI (35.0 mg, 0.18 mmol) were dissolved in anhydrous DMF (10 cm<sup>3</sup>) and the solution stirred at room temperature for 24 h under nitrogen. The resulting solution was extracted with EtOAc (3 × 10 cm<sup>3</sup>) and water (3 × 10 cm<sup>3</sup>) and the organic layer was washed with 10% citric acid (20 cm<sup>3</sup>), satd. K<sub>2</sub>CO<sub>3</sub> (aq.) solution (20 cm<sup>3</sup>) and brine (20 cm<sup>3</sup>). The organic layer was dried with anhydrous magnesium sulfate, filtered and concentrated under reduced pressure to give a brown solid. The crude solid was dissolved in DMF (2 cm<sup>3</sup>) and MeOH (8 cm<sup>3</sup>) was added dropwise with stirring until a precipitate formed. The precipitate was left overnight, isolated by filtration, washed with MeOH (10 cm<sup>3</sup>) and Et<sub>2</sub>O (10 cm<sup>3</sup>) then dried in vacuo to give **4** (42.2 mg, 8.4 × 10<sup>-5</sup> mol, 46%), m.p. 205–206 °C. IR (KBr):  $\tilde{\nu}_{\text{max}} = 1671$  (C=O), 1491 (C=N) cm<sup>-1</sup>.  $^1\text{H}$  NMR (400 MHz, [D<sub>6</sub>]DMSO):  $\delta = 1.17$  (t,  $^3J_{\text{HH}} = 7.1$  Hz, 3 H, CH<sub>3</sub>CH<sub>2</sub>NH), 2.33 (two overlapping s, 6 H, 2 × CH<sub>3</sub>C=N), 3.60–3.67 (m, 2 H, CH<sub>3</sub>CH<sub>2</sub>NH), 8.13–8.85 (m, 9 H, Ar), 8.49 (t,  $^3J_{\text{HH}} = 5.9$  Hz, 1 H, CH<sub>3</sub>CH<sub>2</sub>NH), 10.23 (s, 1 H, NH) 10.36 (s, 1 H, NH) 10.81 (s, 1 H, NH) 10.83 (s, 1 H, NH) ppm.  $^{13}\text{C}\{^1\text{H}\}$  NMR (125 MHz, [D<sub>6</sub>]DMSO):  $\delta = 11.8$  (CH<sub>3</sub>C=N), 12.0 (CH<sub>3</sub>C=N), 14.4 (CH<sub>3</sub>CH<sub>2</sub>NH), 38.6 (CH<sub>3</sub>CH<sub>2</sub>NH), 123.6, 123.7, 124.4, 125.0, 125.7, 125.8, 125.9, 126.7, 127.2, 128.2, 127.4, 128.6, 129.6, 130.3, 130.7 and 132.0 (16 × Ar), 148.0 (CH<sub>3</sub>C=N), 150.0 (CH<sub>3</sub>C=N), 167.8 (C=O), 177.5 (C=S), 180.1 (C=S) ppm. LRMS-ESI<sup>+</sup>:  $m/z = 526$  (100) [M + Na]<sup>+</sup>. HRMS-ESI<sup>+</sup>: [C<sub>8</sub>H<sub>18</sub>N<sub>7</sub>S<sub>2</sub>]<sup>+</sup>  $m/z$  (%) = (100) [M + Na]<sup>+</sup> calcd. 526.1454; found 526.1454. UV/Vis:  $\lambda_{\text{max}}$  (DMSO,  $\epsilon/\text{mol}^{-1}\text{dm}^3\text{cm}^{-1}$ ) = 345 (65000) nm. HPLC:  $t_{\text{R}} = 15.7$  min.

**N-Ethyl-2-{3-[2-(2-[4-(pyren-1-yl)butanoyl]hydrazinyl)carbonothioyl)hydrazinylidene]butan-2-ylidene}hydrazinecarbothioamide (**5**):** H<sub>2</sub>ATSE/A (**1**) (190 mg, 0.69 mmol), 4-(pyren-1-yl)butyric acid (**3**) (200 mg, 0.69 mmol), 1-hydroxybenzotriazole hydrate (105.0 mg, 0.69 mmol) and EDCI (132.0 mg, 0.69 mmol) were dissolved in anhydrous DMF (40 cm<sup>3</sup>) and the solution was stirred at room temperature for 24 h. The resulting solution was extracted with EtOAc (3 × 20 cm<sup>3</sup>) and water (3 × cm<sup>3</sup>). The organic layer was washed sequentially with 10% citric acid (aq.) (30 cm<sup>3</sup>), satd. K<sub>2</sub>CO<sub>3</sub> (aq.) (30 cm<sup>3</sup>) and brine (30 cm<sup>3</sup>), dried with anhydrous magnesium sulfate, filtered and concentrated under reduced pressure to give the crude product. The crude solid was then dissolved in DMSO (1 cm<sup>3</sup>) and MeOH was allowed to diffuse in over 48 h at room temperature using the vapour diffusion method to give a pale brown solid. The precipitate was isolated by filtration, washed with MeOH (10 cm<sup>3</sup>) and Et<sub>2</sub>O (10 cm<sup>3</sup>) and dried in vacuo to give **5** as

a light-brown solid (225 mg, 0.41 mmol, 59%); m.p. >195 °C (dec.). IR (KBr):  $\tilde{\nu}_{\max}$  = 1671 (C=O), 1491 (C=N)  $\text{cm}^{-1}$ .  $^1\text{H}$  NMR (400 MHz,  $[\text{D}_6]\text{DMSO}$ ):  $\delta$  = 1.16 (t,  $^3J_{\text{HH}}$  = 7.1 Hz, 3 H,  $\text{CH}_3\text{CH}_2\text{NH}$ ), 2.09–2.13 (m, 2 H,  $\text{C}(3)\text{H}_2$ ), 2.23 (s, 3 H,  $\text{CH}_3\text{C}=\text{N}$ ), 2.26 (s, 3 H,  $\text{CH}_3\text{C}=\text{N}$ ), 2.37 (t,  $^3J_{\text{HH}}$  = 7.0 Hz, 2 H,  $\text{C}(2)\text{H}_2$ ), 3.41 (t,  $^3J_{\text{HH}}$  = 7.4 Hz, 2 H,  $\text{C}(4)\text{H}_2$ ), 3.60–3.61 (m, 2 H,  $\text{CH}_3\text{CH}_2\text{NH}$ ), 7.93–8.47 (m, 10 H,  $\text{Ar}(9\text{H})$  and  $\text{CH}_3\text{CH}_2\text{NH}$ ), 10.00 (s, 1 H,  $\text{NH}$ ), 10.13 (s, 1 H,  $\text{NH}$ ), 10.16 (s, 1 H,  $\text{NH}$ ), 10.62 (s, 1 H,  $\text{NH}$ ) ppm.  $^{13}\text{C}\{^1\text{H}\}$  NMR (125 MHz,  $[\text{D}_6]\text{DMSO}$ ):  $\delta$  = 11.7 ( $\text{CH}_3\text{C}=\text{N}$ ), 11.9 ( $\text{CH}_3\text{C}=\text{N}$ ), 14.4 ( $\text{CH}_3\text{CH}_2\text{NH}$ ), 27.4 ( $\text{C}(3)\text{H}_2$ ), 32.3 ( $\text{C}(4)\text{H}_2$ ), 33.1 ( $\text{C}(2)\text{H}_2$ ), 38.6 ( $\text{CH}_3\text{CH}_2\text{NH}$ ), 123.7, 124.2, 124.3, 124.8, 124.9, 125.0, 126.2, 126.5, 127.2, 127.5, 127.6, 128.2, 129.3, 130.5, 130.9 and 136.7 ( $16\times\text{Ar}$ ), 147.9 ( $\text{CH}_3\text{C}=\text{N}$ ), 149.8 ( $\text{CH}_3\text{C}=\text{N}$ ), 170.9 (C=O), 177.5 (C=S), 180.0 (C=S) ppm. LRMS-(%) ESI:  $m/z$  544 (100)  $[\text{M} - \text{H}]^-$ . HRMS-ESI $^+$ :  $[\text{C}_{28}\text{H}_{30}\text{N}_7\text{OS}_2]^-$   $m/z$  (%) = (100)  $[\text{M} - \text{H}]^-$  calcd. 544.1948; found 544.1970. UV/Vis:  $\lambda_{\max}$  (DMSO,  $\epsilon/\text{mol}^{-1}\text{dm}^3\text{cm}^{-1}$ ) = 345 (70000), 330 (55000) and 315 (30000) nm. HPLC:  $t_{\text{R}}$  = 17.0 min.

**Complex 6:** A solution of zinc diacetate dihydrate  $[\text{Zn}(\text{OAc})_2\cdot 2\text{H}_2\text{O}]$  (22.0 mg, 0.10 mmol) in MeOH (10  $\text{cm}^3$ ) was added to a solution of **4** (50.0 mg, 0.10 mmol) in MeOH (10  $\text{cm}^3$ ) and the reaction mixture was stirred at room temperature for 16 h. The resulting precipitate was isolated by filtration, washed with MeOH (10  $\text{cm}^3$ ) and Et $_2$ O (10  $\text{cm}^3$ ) and dried in vacuo to give complex **6** as a yellow powder (29.9 mg,  $5.3\times 10^{-5}$  mol 53%); m.p. >230 °C. IR (KBr):  $\tilde{\nu}_{\max}$  = 1656 (C=O), 1493 (C=N)  $\text{cm}^{-1}$ .  $^1\text{H}$  NMR (400 MHz,  $[\text{D}_6]\text{DMSO}$ ):  $\delta$  = 1.13 (t,  $^3J_{\text{HH}}$  = 7.0 Hz, 3 H,  $\text{CH}_3\text{CH}_2\text{NH}$ ), 2.26 (s, 3 H,  $\text{CH}_3\text{C}=\text{N}$ ), 2.38 (s, 3 H,  $\text{CH}_3\text{C}=\text{N}$ ), 3.41–3.49 (m, 2 H,  $\text{CH}_3\text{CH}_2\text{NH}$ ), 7.42 (s, 1 H,  $\text{NH}$ ), 8.13–8.82 (m, 9 H,  $\text{Ar}$ ), 9.19 (br. s, 1 H,  $\text{CH}_3\text{CH}_2\text{NH}$ ), 10.49 (s, 1 H,  $\text{NH}$ ) ppm.  $^{13}\text{C}\{^1\text{H}\}$  NMR (125 MHz,  $[\text{D}_6]\text{DMSO}$ ):  $\delta$  = 13.9 ( $\text{CH}_3\text{C}=\text{N}$ ), 14.3 ( $\text{CH}_3\text{C}=\text{N}$ ), 14.7 ( $\text{CH}_3\text{CH}_2\text{NH}$ ), 37.0 ( $\text{CH}_3\text{CH}_2\text{NH}$ ), 123.6, 123.7, 124.5, 125.1, 125.5, 125.7, 125.9, 126.7, 127.2, 128.0, 128.2, 128.5, 130.3, 130.6, 130.7, 131.8 ( $16\times\text{Ar}$ ), 166.0 (C=O), (NB: no quaternary C=S or C=N peaks were observed) ppm. LRMS-(%) ESI:  $m/z$  = 588 (100)  $[\text{M} + \text{Na}]^+$ . HRMS-ESI $^+$ :  $[\text{C}_{25}\text{H}_{23}\text{N}_7\text{NaOS}_2\text{Zn}]^+$   $m/z$  (%) = (100)  $[\text{M} + \text{Na}]^+$  calcd. 588.0589; found 588.0587. UV/Vis:  $\lambda_{\max}$  (DMSO,  $\epsilon/\text{mol}^{-1}\text{dm}^3\text{cm}^{-1}$ ) = 330 (26000), 345 (28000), 440 (12000). HPLC:  $t_{\text{R}}$  = 15.8 min.

**Complex 7:** Copper(II) diacetate monohydrate  $[\text{Cu}(\text{OAc})_2\cdot \text{H}_2\text{O}]$  (119 mg, 0.60 mmol, 10.0 equiv.) was added to a solution of **4** (30.0 mg, 0.060 mmol) in MeOH (20  $\text{cm}^3$ ) and the solution was stirred at room temperature for 24 h. The resulting dark brown precipitate was isolated by filtration, washed with MeOH (10  $\text{cm}^3$ ) and Et $_2$ O (10  $\text{cm}^3$ ) then dried in vacuo to give the complex **7** as a brown powder (19.9 mg,  $3.5\times 10^{-5}$  mol, 59%), m.p. 188–189 °C. IR (KBr):  $\tilde{\nu}_{\max}$  = 1687 (C=O), 1491 (C=N)  $\text{cm}^{-1}$ . LRMS-ESI:  $m/z$  (%) = 587 (100)  $[\text{M} + \text{Na}]^+$ . HRMS-ESI $^+$ :  $[\text{C}_{25}\text{H}_{23}\text{CuN}_7\text{NaOS}_2]^+$   $m/z$  (100)  $[\text{M} + \text{Na}]^+$ ; calcd. 587.0594; found 587.0596. UV/Vis:  $\lambda_{\max}$  (DMSO,  $\epsilon/\text{mol}^{-1}\text{dm}^3\text{cm}^{-1}$ ) = 345 (79000), 331 (72000), 320 (62000), 480 (16000) nm. HPLC:  $t_{\text{R}}$  = 18.0 min.

**Complex 8:** A solution of  $\text{Zn}(\text{OAc})_2\cdot 2\text{H}_2\text{O}$  (18.0 mg, 0.082 mmol, 1.1 equiv.) in MeOH (10  $\text{cm}^3$ ) was added to a solution of **5** (40.0 mg, 0.073 mmol) in MeOH (10  $\text{cm}^3$ ) and the mixture was stirred at 60 °C for 24 h. The resulting precipitate was isolated by filtration, washed with MeOH (5  $\text{cm}^3$ ) and Et $_2$ O (5  $\text{cm}^3$ ) then dried in vacuo to give complex **8** as a yellow powder (39.6 mg,  $6.5\times 10^{-5}$  mol, 89%); m.p. >230 °C. IR (KBr):  $\tilde{\nu}_{\max}$  = 1656 (C=O), 1515 (C=N)  $\text{cm}^{-1}$ .  $^1\text{H}$  NMR (400 MHz,  $[\text{D}_6]\text{DMSO}$ ):  $\delta$  = 1.10 (t,  $^3J_{\text{HH}}$  = 7.1 Hz, 3 H,  $\text{CH}_3\text{CH}_2\text{NH}$ ), 2.07–2.11 (m, 8 H,  $2\times\text{CH}_3\text{C}=\text{N}$  and  $\text{C}(3)\text{H}_2$ ), 2.30 (t,  $^3J_{\text{HH}}$  = 7.0 Hz, 2 H,  $\text{C}(2)\text{H}_2$ ), 3.30–3.45 (m, 4 H,  $\text{C}(4)\text{H}_2$  and  $\text{CH}_3\text{CH}_2\text{NH}$ ), 7.35 (br. s, 1 H,  $\text{NH}$ ),

7.92–8.41 (m, 9 H,  $\text{Ar}$ ), 8.82 (br. s, 1 H,  $\text{CH}_3\text{CH}_2\text{NH}$ ), 9.75 (br. s, 1 H,  $\text{NH}$ ) ppm.  $^{13}\text{C}\{^1\text{H}\}$  NMR (125 MHz,  $[\text{D}_6]\text{DMSO}$ ):  $\delta$  = 13.7 ( $\text{CH}_3\text{C}=\text{N}$ ), 13.9 ( $\text{CH}_3\text{C}=\text{N}$ ), 14.6 ( $\text{CH}_3\text{CH}_2\text{NH}$ ), 27.6 ( $\text{C}(3)\text{H}_2$ ), 32.3 ( $\text{C}(4)\text{H}_2$ ), 33.1 ( $\text{C}(2)\text{H}_2$ ), 37.0 ( $\text{CH}_3\text{CH}_2\text{NH}$ ), 123.6, 124.2, 124.3, 124.8, 124.9, 125.0, 126.1, 126.5, 127.2, 127.5, 127.6, 128.1, 129.3, 130.4, 130.9, 136.6 ( $16\times\text{Ar}$ ), 171.2 (C=O), (NB: no quaternary C=S or C=N peaks were observed) ppm. LRMS-(%) ESI:  $m/z$  (%) = 608 (100)  $[\text{M} + \text{H}]^+$ . HRMS-ESI $^+$ :  $[\text{C}_{28}\text{H}_{30}\text{N}_7\text{OS}_2\text{Zn}]^+$   $m/z$  (%) = (100)  $[\text{M} + \text{H}]^+$ ; calcd. 608.1239; found 608.1235. UV/Vis:  $\lambda_{\max}$  (DMSO,  $\epsilon/\text{mol}^{-1}\text{dm}^3\text{cm}^{-1}$ ) = 347 (70000), 335 (60000), 320 (38000), 442 (25000) nm. HPLC:  $t_{\text{R}}$  = 16.9 min.

**Complex 9:** A solution of  $\text{Cu}(\text{OAc})_2\cdot \text{H}_2\text{O}$  (37.0 mg, 0.185 mmol, 2.0 equiv.) in MeOH (5  $\text{cm}^3$ ) was added to a solution of **5** (50.0 mg, 0.092 mmol) in MeOH (10  $\text{cm}^3$ ) and the mixture was stirred at room temperature for 18 h. The resulting precipitate was isolated by filtration, washed with MeOH (10  $\text{cm}^3$ ) and Et $_2$ O (10  $\text{cm}^3$ ) then dried in vacuo to give complex **9** as a brown powder (50.1 mg,  $8.2\times 10^{-5}$  mol, 90%). m.p. 162–163 °C. IR (KBr):  $\tilde{\nu}_{\max}$  = 1672 (C=O), 1499 (C=N)  $\text{cm}^{-1}$ . LRMS-ESI:  $m/z$  (%) = 629 (100)  $[\text{M} + \text{Na}]^+$ . HRMS-ESI $^+$ :  $[\text{C}_{28}\text{H}_{29}\text{CuN}_7\text{NaOS}_2]^+$   $m/z$  (%) = (100)  $[\text{M} + \text{Na}]^+$ ; calcd. 629.1063; found 629.1062. UV/Vis:  $\lambda_{\max}$  (DMSO,  $\epsilon/\text{mol}^{-1}\text{dm}^3\text{cm}^{-1}$ ) = 345 (50000), 330 (42000), 320 (32000), 478 (6000) nm. HPLC:  $t_{\text{R}}$  = 19.6 min.

**Copper(I) Hexafluorophosphate Coordination Compound 10:** Anhydrous DMF (10  $\text{cm}^3$ ) was added to a Schlenk tube and deoxygenated by freeze-thawing in vacuo. Compound **4** (150 mg, 0.298 mmol) was added and dissolved with stirring. Tetrakis(acetonitrile)copper(I) hexafluorophosphate,  $[\text{Cu}(\text{MeCN})_4]^+[\text{PF}_6]^-$ , was added (111 mg, 0.298 mmol, 1.0 equiv.) and the mixture was stirred at room temperature for 1 h. Then deoxygenated Et $_2$ O (50  $\text{cm}^3$ ) was added until a light brown precipitate formed. The precipitate was left for 15 h and isolated by filtration, washed with deoxygenated Et $_2$ O ( $3\times 20\text{ cm}^3$ ) and dried in vacuo to give complex **10** as a light brown powder (117 mg, 0.164 mmol, 54%).  $\text{C}_{25}\text{H}_{25}\text{CuF}_6\text{N}_7\text{OPS}_2$  (712.15): calcd. C 42.2, H 3.5, N 13.8; found C 42.0, H 3.5, N 13.9.  $^1\text{H}$  NMR (400 MHz,  $[\text{D}_6]\text{DMSO}$ ):  $\delta$  = 1.28 (t,  $^3J_{\text{HH}}$  = 7.0 Hz, 3 H,  $\text{CH}_3\text{CH}_2\text{NH}$ ), 2.24 (s, 3 H,  $\text{CH}_3\text{C}=\text{N}$ ), 2.35 (s, 3 H,  $\text{CH}_3\text{C}=\text{N}$ ), 3.56–3.60 (m, 2 H,  $\text{CH}_3\text{CH}_2\text{NH}$ ), 7.19–8.95 (m, 11 H,  $\text{Ar}(9\text{H})$ ,  $\text{CH}_3\text{CH}_2\text{NH}$  and  $\text{NH}$ ), 9.61 (br. s, 1 H,  $\text{NH}$ ), 10.71 (br. s, 1 H,  $\text{NH}$ ), 12.12 (br. s, 1 H,  $\text{NH}$ ) ppm.  $^{13}\text{C}\{^1\text{H}\}$  NMR (125 MHz,  $[\text{D}_6]\text{DMSO}$ ):  $\delta$  = 13.7 ( $\text{CH}_3\text{CH}_2\text{NH}$ ), 16.5 ( $\text{CH}_3\text{C}=\text{N}$ ), 16.9 ( $\text{CH}_3\text{C}=\text{N}$ ), 37.6 ( $\text{CH}_3\text{CH}_2\text{NH}$ ), 123.4, 124.5, 125.5, 126.0, 126.1, 126.5, 126.6, 126.8, 127.2, 128.7, 123.0, 123.5, 123.7, 129.6, 130.1, 130.7 ( $16\times\text{Ar}$ ), 152.0 ( $\text{CH}_3\text{C}=\text{N}$ ), 152.1 ( $\text{CH}_3\text{C}=\text{N}$ ), 168.5 (C=O), 179.1 (C=S), 180.7 (C=S) ppm.

**Copper(I) Hexafluorophosphate Coordination Compound 11:** A crude sample of  $[\text{Cu}(\text{MeCN})_4]^+[\text{PF}_6]^-$  (1.00 g) was dissolved in MeCN (2  $\text{cm}^3$ ) and filtered to remove a small amount of blue solid (oxidised  $\text{Cu}^{2+}$  complex). Then deoxygenated Et $_2$ O (5  $\text{cm}^3$ ) was added to the filtrate under nitrogen until a white precipitate formed. The precipitate was left at room temperature for 15 h, then filtered under a nitrogen atmosphere, washed with deoxygenated Et $_2$ O (10  $\text{cm}^3$ ) and dried in vacuo to give purified  $[\text{Cu}(\text{MeCN})_4]^+[\text{PF}_6]^-$  as white solid (800 mg, 80%). Anhydrous DMF (10  $\text{cm}^3$ ) was added to a Schlenk tube and deoxygenated by freeze-thawing in vacuo. Compound **5** (150 mg, 0.275 mmol) was added and dissolved with stirring.  $[\text{Cu}(\text{MeCN})_4]^+[\text{PF}_6]^-$  (102 mg, 0.274 mmol, 1.0 equiv.) was added and the mixture was stirred at room temperature for 1 h. Then deoxygenated Et $_2$ O (50  $\text{cm}^3$ ) was added until a light brown precipitate formed. The precipitate was left for 15 h and isolated by filtration, washed with deoxygenated Et $_2$ O ( $3\times 20\text{ cm}^3$ ) and dried in vacuo to give complex **11** as a light brown

powder (114 mg, 0.151 mmol, 55%).  $C_{28}H_{31}CuF_6N_7OPS_2$  (754.23): calcd. C 44.6, H 4.1, Cu 8.4, N 13.0, P 4.1, S 8.5; found C 44.4, H 4.2, Cu 8.3, N 13.1, P 3.9, S 8.2.  $^1H$  NMR (400 MHz,  $[D_6]DMSO$ ):  $\delta$  = 1.22–1.25 (t,  $^3J_{HH}$  = 7.2 Hz, 3 H,  $CH_3CH_2NH$ ), 1.92–2.39 (m, 10 H,  $2 \times CH_3C=N$ ,  $2 \times CH_2$ ), 3.26–3.35 (m, 2 H,  $CH_2$ ), 3.46–3.58 (m, 2 H,  $CH_3CH_2NH$ ), 7.73–8.50 (m, 11 H, *Ar* and  $2 \times NH$ ), 9.38 (br. s, 1 H, *NH*), 11.70 (br. s, 1 H, *NH*), 11.95 (br. s, 1 H, *NH*) ppm.  $^{13}C\{^1H\}$  NMR (125 MHz,  $[D_6]DMSO$ ):  $\delta$  = 13.7 ( $CH_3CH_2NH$ ), 16.4 ( $CH_3C=N$ ), 16.9 ( $CH_3C=N$ ), 26.58 ( $CH_2$ ), 32.0 ( $CH_2$ ), 32.8 ( $CH_2$ ), 37.8 ( $CH_3CH_2NH$ ), 123.3, 123.5, 124.1, 124.3, 124.8, 124.9, 125.0, 126.2, 126.6, 127.3, 127.5, 128.1, 129.3, 130.4, 130.9, 136.0 ( $16 \times Ar$ ), 151.7 ( $CH_3C=N$ ), 152.0 ( $CH_3C=N$ ), 172.1 (C=O), 179.0 (C=S), 179.8 (C=S) ppm.

**tert-Butyl (2-Aminoethyl)carbamate (12):** Di-*tert*-butyl dicarbonate (8.74 g, 40.0 mmol) was dissolved in  $CHCl_3$  (200  $cm^3$ ). This was slowly added over 3 h to an excess of ethylenediamine (28.0  $cm^3$ , 0.428 mol) in  $CHCl_3$  solution (400  $cm^3$ ) at 0 °C. The mixture was warmed to room temperature whilst stirring overnight, during which time a white precipitate formed. The mixture was washed with water (100  $cm^3$ ) and brine ( $5 \times 100$   $cm^3$ ), then the organic phase was dried with anhydrous magnesium sulfate and the solvent removed in vacuo to give **12** as a colourless oil (5.52 g, 34.4 mmol, 86%). IR (film):  $\tilde{\nu}_{max}$  = 3364 (N–H), 2987 (C–H), 1687 (C=O), 1278 (C–O), 1177 (C–O)  $cm^{-1}$ .  $^1H$  NMR (400 MHz,  $[D_6]DMSO$ ):  $\delta$  = 1.37 (s, 9 H,  $C(CH_3)_3$ ), 1.92 (br. s, 2 H,  $NH_2$ ), 2.51 (t,  $^3J_{HH}$  = 6.4 Hz, 2 H,  $CH_2NH$ ), 2.88–2.91 (m, 2 H,  $CH_2NH_2$ ), 6.78 (t,  $^3J_{HH}$  = 5.1 Hz, 1 H, (C=O) $NHCH_2$ ) ppm.  $^{13}C\{^1H\}$  NMR (125 MHz,  $[D_6]DMSO$ ):  $\delta$  = 29.0 ( $C(CH_3)_3$ ), 42.4 ( $CH_2$ ), 44.3 ( $CH_2$ ), 78.1 ( $C(CH_3)_3$ ) 156.6 (C=O) ppm. LRMS-ESI:  $m/z$  (%) = 184 (100)  $[M + Na]^+$ .

**tert-Butyl (2-([4-(Pyren-1-yl)butanoyl]amino)ethyl)carbamate (13):** Compound **13** was synthesised by using two different methods. **Method 1:** Compound **12** (250 mg, 1.56 mmol), 4-(pyren-1-yl)butyric acid (**3**) (450 mg, 1.56 mmol) and EDCI (299 mg, 1.56 mmol) were dissolved in anhydrous DMF (40  $cm^3$ ) and stirred under argon at room temperature for 24 h. The resulting solution was extracted with EtOAc ( $3 \times 20$   $cm^3$ ) and water ( $3 \times 20$   $cm^3$ ) and the organic layer was washed with 10% citric acid (aq.) (30  $cm^3$ ), satd.  $K_2CO_3$ (aq.) (30  $cm^3$ ) and brine (30  $cm^3$ ). The organic layer was then dried with anhydrous magnesium sulfate, filtered, and concentrated in vacuo to give a crude yellow product (0.42 g) which was purified by column chromatography (gradient elution using 80%EtOAc:petroleum ether) to give **13** as a pale yellow solid (215 mg, 0.50 mmol, 32%,  $R_f$  = 0.3 in 80% EtOAc/petroleum ether); m.p. 143–145 °C. IR (KBr):  $\tilde{\nu}_{max}$  = 3351 (N–H), 3041 (*Ar* C–H), 1686 (C=O), 1650 (C=O)  $cm^{-1}$ .  $^1H$  NMR (400 MHz,  $[D_6]DMSO$ ):  $\delta$  = 1.35 (s, 9 H,  $C(CH_3)_3$ ), 2.03–2.05 (m, 2 H,  $C(3)H_2$ ), 2.25–2.27 [m, 2 H,  $C(2)H_2$ ], 3.05 (t,  $^3J_{HH}$  = 5.5 Hz, 2 H,  $CH_2NH$ ), 3.13 (t,  $^3J_{HH}$  = 5.5 Hz, 2 H,  $CH_2NH$ ), 3.32 (t,  $^3J_{HH}$  = 7.5 Hz, 2 H,  $C(4)H_2$ ), 6.84 (br. m, 1 H, *NH*), 7.92–8.42 (m, 10 H, *Ar* and *NH*) ppm.  $^{13}C\{^1H\}$  NMR (125 MHz,  $[D_6]DMSO$ ):  $\delta$  = 28.4 ( $C(3)H_2$ ), 29.0 ( $C(CH_3)_3$ ), 33.1 ( $C(2)H_2$ ), 35.9 ( $C(4)H_2$ ), 40.8 ( $CH_2NH$ ), 41.0 ( $CH_2NH$ ), 78.5 ( $C(CH_3)_3$ ), 124.4–131.7 ( $16 \times Ar$ ), 156.5 (O–C=O), 172.9 ( $NHC=O$ ) ppm. LRMS-(%) ESI:  $m/z$  (%) = 429 (100)  $[M - H]^-$ . HRMS-ESI $^+$ :  $[C_{27}H_{30}N_2NaO_3]^+$   $m/z$  ( $[M + Na]^+$ , 100%) calcd. 453.2149; found 453.2143. HPLC:  $t_R$  = 16.3 min. **Method 2:** Thionyl chloride (38  $\mu L$ , 0.52 mmol) was added dropwise to a stirred suspension of **3** (100 mg, 0.347 mmol) in anhydrous dichloromethane (10  $cm^3$ ) under an atmosphere of argon at 0 °C. The mixture was allowed to stir for 5 min and then pyridine (55 mg, 0.69 mmol) was added dropwise at 0 °C. On addition of pyridine, gas evolved and the cream suspension became a dark orange solution. The solution was allowed to stir for 5 min and then **12** (83 mg,

0.52 mmol) was added portion-wise at 0 °C. The reaction mixture was allowed to stir for 15 h before the solution was washed with 10% citric acid(aq.) (10  $cm^3$ ), satd.  $K_2CO_3$ (aq.) (10  $cm^3$ ) and brine (10  $cm^3$ ). The organic solution was then dried with anhydrous magnesium sulfate and concentrated in vacuo to give a crude yellow solid (100 mg) which was purified by column chromatography (gradient elution 80% EtOAc/petroleum ether) to give **13** as a pale yellow solid (67 mg, 0.16 mmol, 30%). Characterisation data were identical to Method 1 (vide supra).

**N-(2-Aminoethyl)-4-(pyren-1-yl)butanamide (14):** Compound **13** (170 mg, 0.395 mmol), was stirred in trifluoroacetic acid (TFA) (4.0  $cm^3$ ) at room temperature for 1 h. The solution was concentrated in vacuo to approximately 1  $cm^3$  then satd.  $NaHCO_3$ (aq.) was added until a pH 7.0 was reached. The resulting precipitate was collected by filtration, washed with water (20  $cm^3$ ) and  $Et_2O$  (20  $cm^3$ ) then dried in vacuo to give **14** as a cream powder (86 mg, 0.261 mmol, 66%); m.p. 130–132 °C. IR (KBr):  $\tilde{\nu}_{max}$  = 3295–3290 ( $NH_2$ , *NH*), 3037 (*Ar* C–H), 1645 (C=O)  $cm^{-1}$ .  $^1H$  NMR (400 MHz,  $[D_6]DMSO$ ):  $\delta$  = 1.98–2.05 (m, 2 H,  $C(3)H_2$ ), 2.25 (t,  $^3J_{HH}$  = 7.2 Hz, 2 H,  $C(2)H_2$ ), 2.61 (t,  $^3J_{HH}$  = 6.3 Hz, 2 H,  $CH_2N$ ), 3.11 (m, 2 H,  $CH_2N$ ), 3.30–3.32 (m, 2 H,  $C(4)H_2$ ), 7.88–8.39 (m, 9 H, *Ar*) ppm.  $^{13}C\{^1H\}$  NMR (125 MHz,  $[D_6]DMSO$ ):  $\delta$  = 28.3 ( $C(3)H_2$ ), 33.1 ( $C(2)H_2$ ), 35.9 ( $C(4)H_2$ ), 41.3 ( $2 \times CH_2N$ ), 124.3–137.3 ( $16 \times Ar$ ), 173.5 (C=O) ppm. LRMS-ESI:  $m/z$  (%) = 331 (56)  $[M + H]^+$ . HRMS-ESI $^+$ :  $[C_{22}H_{23}N_2O]^+$   $m/z$  (%) = (100)  $[M + H]^+$ ; calcd. 331.1805; found 331.1810.

**Methyl (2-([4-(Pyren-1-yl)butanoyl]amino)ethyl)carbamodithioate (15):** Carbon disulfide ( $CS_2$ ) (45  $\mu L$ , 0.758 mmol) was added dropwise to **14** (250 mg, 0.758 mmol) and  $NEt_3$  (110  $\mu L$ , 0.758 mmol) in EtOH (20  $cm^3$ ). The suspension was stirred at room temperature for 1.5 h before MeI (47  $\mu L$ , 0.758 mmol) was added and stirring continued for a further 2 h. The resulting precipitate was filtered, washed with water (20  $cm^3$ ) and dried in vacuo to give a crude product (160 mg) which was purified by column chromatography (gradient elution 50% EtOAc/petroleum ether) to give **15** as a white solid (83 mg, 0.20 mmol, 26%.  $R_f$  = 0.27 in 50% EtOAc/petroleum ether); m.p. 161–163 °C. IR (KBr):  $\tilde{\nu}_{max}$  = 3330 (N–H), 3206 (N–H), 3036 (*Ar* C–H), 1587 (C=O), 1540 (C–N, SCN), 1435 (*Ar* C–C), 1276 (C–N,  $CH_2NH$ ), 1134 (C=S), 707 (C–S)  $cm^{-1}$ .  $^1H$  NMR (400 MHz,  $[D_6]DMSO$ ):  $\delta$  = 1.98–2.05 (m, 2 H,  $C(3)H_2$ ), 2.25 (t,  $^3J_{HH}$  = 7.2 Hz, 2 H,  $C(2)H_2$ ), 2.50 (s, 3 H,  $SCH_3$ ), 3.29–3.33 (m, 4 H,  $CH_2NH$ ,  $C(4)H_2$ ), 3.61–3.70 (m, 2 H,  $CH_2NH$ ), 7.92–8.39 (m, 10 H, *Ar* and  $NHC=S$ ), 9.88 (t,  $^3J_{HH}$  = 5.0 Hz, 1 H,  $NHC=O$ ) ppm.  $^{13}C\{^1H\}$  NMR (125 MHz,  $[D_6]DMSO$ ):  $\delta$  = 18.2 ( $SCH_3$ ), 28.3 ( $C(3)H_2$ ), 33.1 ( $C(2)H_2$ ), 35.8 ( $C(4)H_2$ ), 37.8 ( $CH_2NH$ ), 47.3 ( $CH_2NH$ ), 124.4–137.4 ( $16 \times Ar$ ), 173.4 (C=O), 198.4 (C=S) ppm. LRMS-ESI:  $m/z$  = 419 (100)  $[M - H]^-$ . HRMS-ESI $^+$ :  $[C_{24}H_{24}N_2NaOS_2]^+$   $m/z$  (%) = (100)  $[M + Na]^+$ ; calcd. 443.1222; found 443.1218.

**N-{2-[(Hydrazinylcarbonothioyl)amino]ethyl}-4-(pyren-1-yl)butanamide (16):** Compound **15** (200 mg, 0.476 mmol) and hydrazine hydrate (32  $\mu L$ , 0.657 mmol) were dissolved in EtOH (10  $cm^3$ ) and heated under reflux for 2.5 h. The solvent was removed under reduced pressure and the residue was dissolved in  $CHCl_3$  (20  $cm^3$ ). The solution was then passed through a plug of silica eluting with  $CHCl_3$  (30  $cm^3$ ) then MeOH (30  $cm^3$ ). The methanolic fraction was concentrated under reduced pressure and the residue was dissolved in  $CHCl_3$  (30  $cm^3$ ) and filtered, then concentrated under reduced pressure until a precipitate formed. The precipitate was dried in vacuo to give **16** as an off-white solid (121 mg, 0.30 mmol, 63%); m.p. 145–147 °C. IR (KBr):  $\tilde{\nu}_{max}$  = 3326 ( $NH_2$ ), 3205 (*NH*), 3036 (*Ar* C–H), 2874 (C–H,  $CH_2N$ ), 1587 (C=O), 1541 (C–N, NCS),

1434 (*Ar* C–C), 1276 (C–N, CH<sub>2</sub>NH), 1134 (C=S) cm<sup>−1</sup>. <sup>1</sup>H NMR (400 MHz, [D<sub>6</sub>]DMSO):  $\delta$  = 1.97–2.05 (m, 2 H, C(3)H<sub>2</sub>), 2.24 (t, <sup>3</sup>J<sub>HH</sub> = 7.5 Hz, 2 H, C(2)H<sub>2</sub>), 3.22–3.27 (m, 2 H, C(4)H<sub>2</sub>), 3.31 (t, <sup>3</sup>J<sub>HH</sub> = 7.5 Hz, 2 H, CH<sub>2</sub>NH), 3.54–3.59 (m, 2 H, CH<sub>2</sub>NH obscured by residual H<sub>2</sub>O, identified in the 2D-COSY NMR spectrum), 4.42 (br. s, 2 H, NH<sub>2</sub>), 7.91–8.39 (m, 11 H, *Ar* and 2 × NHC=S), 8.67 (s, 1 H, NHC=O) ppm. <sup>13</sup>C{<sup>1</sup>H} NMR (125 MHz, [D<sub>6</sub>]DMSO):  $\delta$  = 28.3 (C(3)H<sub>2</sub>), 33.1 (C(2)H<sub>2</sub>), 35.8 (C(4)H<sub>2</sub>), 39.5 (CH<sub>2</sub>NH), 43.6 (CH<sub>2</sub>NH), 124.4–137.4 (16 × *Ar*), 173.2 (C=O), 198.2 (C=S) ppm. LRMS-ESI<sup>−</sup>: *m/z* (%) = 427 (100) [M + Na]<sup>+</sup>. HRMS-ESI<sup>−</sup>: [C<sub>23</sub>H<sub>24</sub>N<sub>4</sub>NaOS]<sup>+</sup> *m/z* (%) = (100) [M + Na]<sup>+</sup>; calcd. 427.1563; found 427.1558.

#### *N*-Ethyl-2-(3-oxobutan-2-ylidene)hydrazinecarbothioamide (17):

Compound **17** was synthesised in accordance with a procedure described previously.<sup>[12]</sup> 2,3-Butadione (1.8 cm<sup>3</sup>, 1.77 g, 20.5 mmol) was added to 4-*N*-ethyl-3-thiosemicarbazide (2.00 g, 16.8 mmol) in 100 cm<sup>3</sup> of aqueous acid. Compound **17** was isolated as a white powder (2.63 g, 14.0 mmol, 84%); m.p. 127–129 °C. C<sub>7</sub>H<sub>13</sub>N<sub>3</sub>OS (187.26): calcd. C 44.9, H 7.0, N 22.4, S 17.1; found C 44.6, H 7.2, N 22.7, S 17.2. <sup>1</sup>H NMR (300 MHz, [D<sub>6</sub>]DMSO):  $\delta$  = 10.57 (s, 1 H, C(=S)NHN=), 8.66 (br. t, 1 H, CH<sub>2</sub>NH), 3.63 (m, <sup>3</sup>J<sub>HH</sub> = 7.1 Hz, 2 H, CH<sub>3</sub>CH<sub>2</sub>NH), 2.42 (s, 3 H, CH<sub>3</sub>C=O), 1.96 (s, 3 H, CH<sub>3</sub>C=N), 1.15 (t, <sup>3</sup>J<sub>HH</sub> = 7.1 Hz, 3 H, CH<sub>3</sub>CH<sub>2</sub>) ppm. <sup>13</sup>C{<sup>1</sup>H} NMR (75.5 MHz, [D<sub>6</sub>]DMSO):  $\delta$  = 10.0 (CH<sub>3</sub>C=N), 14.1 (CH<sub>3</sub>CH<sub>2</sub>), 24.7 (CH<sub>3</sub>C=O), 38.7 (CH<sub>3</sub>CH<sub>2</sub>), 145.5 (C=N), 177.9 (C=S), 197.4 (C=O) ppm. HRMS-ESI<sup>+</sup>: [C<sub>7</sub>H<sub>14</sub>N<sub>3</sub>OS]<sup>+</sup> *m/z* (100) = [M + H]<sup>+</sup>; calcd. 188.0858; found 188.0855.

#### *N*-[7,8-Dimethyl-4,11-dithioxo-3,5,6,9,10,12-hexaazatetradeca-6,8-dien-1-yl]-4-(pyren-1-yl)butanamide (18):

Compound **16** (200 mg, 0.495 mmol) was added to EtOH (20 cm<sup>3</sup>), and the suspension stirred at 50 °C. Compound **17** (92.6 mg, 0.495 mmol) was added portion-wise and the mixture stirred at 50 °C for 1 h. Then concd. HCl (2 drops) was added and the reaction heated under reflux for 6 h. The resulting white precipitate was collected by filtration, washed with EtOH (30 cm<sup>3</sup>) and EtOAc (30 cm<sup>3</sup>) then dried in vacuo to give **18** as a white powder (176 mg, 0.31 mmol, 62%); m.p. 214–216 °C (dec.). C<sub>30</sub>H<sub>35</sub>N<sub>7</sub>OS<sub>2</sub> (573.78): calcd. C 62.8, H 6.15, N 17.1; found C 62.7, H 6.2, N 17.3. IR (KBr):  $\tilde{\nu}_{\max}$  = 3351 (N–H), 3038 (*Ar* C–H), 1641 (C=N), 1528 (C=O), 1428 (*Ar* C–C), 1207 (C–N), 1140 (C=S), 707 (C–S) cm<sup>−1</sup>. <sup>1</sup>H NMR (400 MHz, [D<sub>6</sub>]DMSO):  $\delta$  = 1.13 (t, <sup>3</sup>J<sub>HH</sub> = 7.0 Hz, 3 H, CH<sub>3</sub>CH<sub>2</sub>), 2.01 (tt, <sup>3</sup>J<sub>HH</sub> = 7.0 and 7.0 Hz, 2 H, C(3)H<sub>2</sub>), 2.13 (s, 3 H, CH<sub>3</sub>C=N), 2.23 (s, 3 H, CH<sub>3</sub>C=N), 2.24–2.27 (t, <sup>3</sup>J<sub>HH</sub> = 7.0 Hz, 2 H, C(2)H<sub>2</sub>), 3.23–3.32 (m, 2 H, C(4)H<sub>2</sub>), 3.32–3.41 (m, 2 H, CH<sub>2</sub>NH), 3.56–3.62 (m, 2 H, CH<sub>2</sub>NH), 3.65 (m, 2 H, CH<sub>3</sub>CH<sub>2</sub>NH), 7.86–8.39 (m, 11 H, *Ar* and 2 × NHC=S), 8.54 (m, 1 H, NHC=O), 10.18 (s, 1 H, NHN=CCH<sub>3</sub>), 10.30 (s, 1 H, NHN=C CH<sub>3</sub>) ppm. <sup>13</sup>C{<sup>1</sup>H} NMR (125 MHz, [D<sub>6</sub>]DMSO):  $\delta$  = 12.1 (2 × CH<sub>3</sub>C=N), 15.5 (CH<sub>3</sub>CH<sub>2</sub>NH), 27.4 (C(3)H<sub>2</sub>), 32.2 (C(2)H<sub>2</sub>), 34.9 (C(4)H<sub>2</sub>), 37.7 (CH<sub>3</sub>CH<sub>2</sub>NH), 45.1 (2 × CH<sub>2</sub>NH), 123.1–131.2 (16 × *Ar*), 147.8 (C=N), 148.2 (C=N), 172.8 (C=O), 177.4 (C=S), 178.1 (C=S) ppm. LRMS-ESI<sup>−</sup>: *m/z* (%) = 572 (100) [M – H]<sup>−</sup>. HRMS-ESI<sup>−</sup>: [C<sub>30</sub>H<sub>35</sub>N<sub>7</sub>NaOS<sub>2</sub>]<sup>−</sup> *m/z* ([M + Na]<sup>+</sup>, 100%) calcd. 596.2237; found 596.2234. UV/Vis:  $\lambda_{\max}$  (DMSO,  $\epsilon$ /mol<sup>−1</sup> dm<sup>3</sup> cm<sup>−1</sup>) = 346 (282000), 331 (300000), 278 (26000), 268 (169000) nm. Fl.  $\lambda_{\text{em,max}}$ (DMSO): 419, 398 and 380 (quantum yield,  $\phi_F$  = 0.28 ± 0.03),  $\lambda_{\text{ex}}$  285 nm (270 nm, 300 nm, 375 nm). HPLC: *t\_R* = 15.9 min.

**Copper(II) Complex 19:** A solution of Cu(OAc)<sub>2</sub>·H<sub>2</sub>O (15 mg, 0.075 mmol) in DMSO (2 cm<sup>3</sup>) was added to a solution of **18** (21 mg, 0.037 mmol) in DMSO (2.0 cm<sup>3</sup>), and the mixture was stirred at room temperature for 5 h. Then ice cold H<sub>2</sub>O (20 cm<sup>3</sup>) was added and a precipitate formed over 1 h. The precipitate was

collected by filtration, washed with water (20 cm<sup>3</sup>) and EtOH (20 cm<sup>3</sup>), then dried in vacuo to give complex **19** as a purple solid (15 mg, 2.4 × 10<sup>−5</sup> mol, 65%); m.p. 192–195 °C. C<sub>30</sub>H<sub>33</sub>CuN<sub>7</sub>OS<sub>2</sub>·C<sub>2</sub>H<sub>6</sub>OS (includes one equiv. of DMSO): calcd. C 53.9, H 5.5, N 13.7; found C 53.8, H 5.7, N 13.9. IR (KBr):  $\tilde{\nu}_{\max}$  = 3301 (N–H), 3039 (*Ar* C–H), 1649 (C=O), 1507 (C=N), 1081 (C–N), 709 (C–S) cm<sup>−1</sup>. LRMS-ESI<sup>+</sup>: *m/z* (%) 635 (8) [M]<sup>+</sup>. HRMS-ESI<sup>+</sup>: [C<sub>30</sub>H<sub>33</sub>CuN<sub>7</sub>NaOS<sub>2</sub>]<sup>+</sup> *m/z* ([M + Na]<sup>+</sup>, 100%) calcd. 657.1376; found 657.1366. UV/Vis:  $\lambda_{\max}$  (DMSO,  $\epsilon$ /mol<sup>−1</sup> dm<sup>3</sup> cm<sup>−1</sup>) 477 (13500), 346 (108000), 329 (89600), 279 (19000), 268 (75800) nm. Fl.  $\lambda_{\text{em,max}}$  (DMSO) = 396 nm (quantum yield,  $\phi_F$  = 0.28 ± 0.04),  $\lambda_{\text{ex}}$  300 nm (270 nm, 375 nm). HPLC: *t\_R* = 19.0 min.

#### *N*-[7,8-Dimethyl-16-oxo-19-(pyren-1-yl)-4,11-dithioxo-3,5,6,9,10,12,15-heptaazanonadeca-6,8-dien-1-yl]-4-(pyren-1-yl)butanamide (20):

Compound **16** (100 mg, 0.25 mmol) was suspended in EtOH (5 cm<sup>3</sup>), and 2,3-butadione (0.011 cm<sup>3</sup>, 0.124 mmol) was added followed by the acid catalyst concd. H<sub>2</sub>SO<sub>4</sub> (1 drop). The reaction mixture was stirred at room temperature for 16 h. The resulting white precipitate was collected by filtration then washed with EtOAc (10 cm<sup>3</sup>) and EtOH (10 cm<sup>3</sup>), then dried in vacuo to give **20** as a white solid (43 mg, 5.0 × 10<sup>−5</sup> mol, 40%); m.p. 252–257 °C. C<sub>50</sub>H<sub>50</sub>N<sub>8</sub>O<sub>2</sub>S<sub>2</sub>·C<sub>4</sub>H<sub>8</sub>O<sub>2</sub> (includes one equiv. of EtOAc): calcd. C 68.5, H 6.2, N 11.8; found C 68.4, H 6.2, N 11.9. IR (KBr):  $\tilde{\nu}_{\max}$  = 3329 (N–H), 3205 (N–H), 3036 (*Ar* C–H), 1587 (C=O), 1276 (C–N), 1134 (C=S), 668 (C–S) cm<sup>−1</sup>. <sup>1</sup>H NMR (400 MHz, [D<sub>6</sub>]DMSO):  $\delta$  = 1.98–2.07 (m, 4 H, 2 × C(3)H<sub>2</sub>), 2.26 (t, <sup>3</sup>J<sub>HH</sub> = 7.0 Hz, 4 H, 2 × C(2)H<sub>2</sub>), 2.51 (s, 6 H, 2 × CH<sub>3</sub>C=N), 3.29–3.35 (m, 4 H, 2 × C(4)H<sub>2</sub> obscured by H<sub>2</sub>O), 3.37–3.47 (m, 4 H, 2 × CH<sub>2</sub>NH obscured by H<sub>2</sub>O), 3.67 (m, 4 H, 2 × CH<sub>2</sub>NH), 7.92–8.41 (m, 22 H, 2 × *Ar*(9H), 2 × NHC=S, 2 × NHC=O), 9.89 (br. s, 2 H, 2 × NHN=C) ppm. <sup>13</sup>C{<sup>1</sup>H} NMR (125 MHz, [D<sub>6</sub>]DMSO):  $\delta$  = 18.2 (2 × CH<sub>3</sub>), 28.3 (2 × C(3)H<sub>2</sub>), 33.1 (2 × C(2)H<sub>2</sub>), 35.8 (2 × C(4)H<sub>2</sub>), 37.8 (2 × CH<sub>2</sub>NH), 47.3 (2 × CH<sub>2</sub>NH), 124.4–137.3 (2 × 16 × *Ar*), 148.2 (2 × C=N), 173.3 (2 × C=O), 198.4 (2 × C=S) ppm. LRMS-ESI<sup>−</sup>: *m/z* (%) = 857 (100) [M – H]<sup>−</sup>. HRMS-ESI<sup>−</sup>: [C<sub>50</sub>H<sub>49</sub>N<sub>8</sub>O<sub>2</sub>S<sub>2</sub>]<sup>−</sup> *m/z* (%) = (100) [M – H]<sup>−</sup>, calcd. 857.3425; found 857.3426. UV/Vis:  $\lambda_{\max}$  (DMSO,  $\epsilon$ /mol<sup>−1</sup> dm<sup>3</sup> cm<sup>−1</sup>) = 346 (179000), 329 (144000), 279 (157000), 268 (94000) nm. Fl.  $\lambda_{\text{em,max}}$ (DMSO) = 400 nm (quantum yield,  $\phi_F$  = 0.27 ± 0.03),  $\lambda_{\text{ex}}$  320 nm (355 nm, 375 nm). HPLC: *t\_R* = 20.5 min.

**Copper(II) Complex 21:** A solution of Cu(OAc)<sub>2</sub>·H<sub>2</sub>O (23 mg, 0.116 mmol, 2 equiv.) in DMSO (5.0 cm<sup>3</sup>) was added to a solution of **20** (50.0 mg, 0.058 mmol) in DMSO (5.0 cm<sup>3</sup>), and the mixture was stirred at room temperature for 5 h. An excess of ice cold H<sub>2</sub>O was then added (30 cm<sup>3</sup>) and a purple precipitate formed. The suspension was left to stand for 20 min, then the precipitate was collected by filtration, washed with H<sub>2</sub>O (30 cm<sup>3</sup>) and EtOH (30 cm<sup>3</sup>), then dried in vacuo to give complex **21** as a purple solid (49 mg, 5.3 × 10<sup>−5</sup> mol, 92%); m.p. 212–215 °C. C<sub>50</sub>H<sub>48</sub>CuN<sub>8</sub>O<sub>2</sub>S<sub>2</sub>·C<sub>4</sub>H<sub>12</sub>O<sub>2</sub>S<sub>2</sub> (1076.91; includes two equiv. of DMSO): calcd. C 60.2, H 5.6, N 10.4; found C 60.0, H 5.4, N 10.5. IR (KBr):  $\tilde{\nu}_{\max}$  = 3297 (N–H), 3039 (*Ar* C–H), 1650 (C=O), 1508 (C=N), 1080 (C–N) cm<sup>−1</sup>. LRMS-ESI<sup>−</sup>: *m/z* 920 ([M]<sup>−</sup>, 37%). HRMS-ESI<sup>−</sup>: [C<sub>50</sub>H<sub>48</sub>CuN<sub>8</sub>NaO<sub>2</sub>S<sub>2</sub>]<sup>−</sup> *m/z* (%) = (100) [M + Na]<sup>+</sup>; calcd. 942.2530; found 942.2511. UV/Vis:  $\lambda_{\max}$  (DMSO,  $\epsilon$ /mol<sup>−1</sup> dm<sup>3</sup> cm<sup>−1</sup>) = 483 (12900), 346 (173000), 330 (132000), 279 (193000), 268 (120000) nm. Fl.  $\lambda_{\text{em,max}}$ (DMSO) = 396 nm (quantum yield,  $\phi_F$  = 0.06 ± 0.015),  $\lambda_{\text{ex}}$  320 nm (355 nm, 375 nm). HPLC: *t\_R* = 18.8 min.

**Supporting Information** (see also the footnote on the first page of this article): Details of the optimisation for recrystallisation of compounds **4** and **5** and synthesis of complexes **7–9** are presented.

## Acknowledgments

J. P. H. thanks Merton College and the Engineering and Physical Sciences Research Council (EPSRC) for funding. We thank Prof. Jonathan R. Dilworth and Prof. Jennifer C. Green for helpful discussions. We thank Prof. Stephen Faulkner and his group at the Department of Chemistry, University of Manchester, for preliminary fluorescence emission studies. We are indebted to Dr. Nick Rees, Mr. Colin Sparrow and Mrs. Maria Marshall for technical support. We also thank the Oxford Supercomputing Centre.

- [1] P. Blower, *Dalton Trans.* **2006**, 14, 1705–1711.
- [2] M. J. Adam, D. S. Wilbur, *Chem. Soc. Rev.* **2005**, 34, 153–163.
- [3] C. J. Anderson, M. J. Welch, *Chem. Rev.* **1999**, 99, 2219–2234.
- [4] P. Armstrong, M. Wastie, A. Rockall, *Diagnostic Imaging*, 5th ed., **2004**, Blackwell Publishing Ltd., UK.
- [5] M. Rudin, R. Weissleder, *Nature Rev. Drug Dis.* **2003**, 2, 123–131.
- [6] J. F. A. Mettler, M. J. Guiberteau, *Essentials of Nuclear Medicine Imaging*, 5th ed., **2007**, Elsevier, UK.
- [7] P. V. Prasad, *Magnetic Resonance Imaging: Methods and Biological Applications*, **2006**, Hamana Press, UK.
- [8] J. T. Bushberg, J. A. Seibert, E. W. Leidholdt, J. M. Boone, *The Essential Physics of Medical Imaging*, 2nd ed., **2006**, Lippincott, Williams & Wilkins, UK.
- [9] Y. Fujibayashi, H. Taniuchi, Y. Yonekura, H. Ohtani, J. Konishi, A. Yokoyama, *J. Nucl. Med.* **1997**, 38, 1155–1160.
- [10] A. L. Vavere, J. S. Lewis, *Dalton Trans.* **2007**, 4893–4902.
- [11] A. Obata, S. Kasamatsu, J. S. Lewis, T. Furukawa, S. Takamatsu, J. Toyohara, T. Asai, M. J. Welch, S. G. Adams, H. Saji, Y. Yonekura, Y. Fujibayashi, *Nucl. Med. Biol.* **2005**, 32, 21–28.
- [12] J. P. Holland, F. I. Aigbirhio, H. M. Betts, P. D. Bonnitcha, P. Burke, M. Christlieb, G. C. Churchill, A. R. Cowley, J. R. Dilworth, P. S. Donnelly, J. C. Green, J. M. Peach, S. R. Vasudevan, J. E. Warren, *Inorg. Chem.* **2007**, 46, 465–485.
- [13] J. S. Lewis, R. Laforest, T. L. Buettner, S.-K. Song, Y. Fujibayashi, J. M. Connett, M. J. Welch, *Proc. Natl. Acad. Sci. USA* **2001**, 98, 1206–1211.
- [14] A. R. Cowley, J. Davis, J. R. Dilworth, P. S. Donnelly, R. Dobson, A. Nightingale, J. M. Peach, B. Shore, D. Kerr, L. Seymour, *Chem. Commun.* **2005**, 845–847.
- [15] J. P. Holland, P. J. Barnard, S. R. Bayly, H. M. Betts, G. C. Churchill, J. R. Dilworth, R. Edge, J. C. Green, R. Hueting, *Eur. J. Inorg. Chem.* **2008**, 1985–1993.
- [16] N. Takahashi, Y. Fujibayashi, Y. Yonekura, J. Welch Michael, A. Waki, T. Tsuchida, N. Sadato, K. Sugimoto, H. Itoh, *Ann. Nucl. Med.* **2000**, 14, 323–328.
- [17] K. S. C. Chao, W. R. Bosch, S. Mutic, J. S. Lewis, F. Dehdashti, M. A. Mintun, J. F. Dempsey, C. A. Perez, J. A. Purdy, M. J. Welch, *Int. J. Radiat. Oncol. Biol. Phys.* **2001**, 49, 1171–1182.
- [18] J. A. O'Donoghue, P. Zanzonico, A. Pugachev, B. Wen, P. Smith-Jones, S. Cai, E. Burnazi, R. D. Finn, P. Burgman, S. Ruan, J. S. Lewis, M. J. Welch, C. C. Ling, J. L. Humm, *Int. J. Radiat. Oncol. Biol. Phys.* **2005**, 61, 1493–1502.
- [19] H. Yuan, T. Schroeder, J. E. Bowsher, L. W. Hedlund, T. Wong, M. W. Dewhirst, *J. Nucl. Med.* **2006**, 47, 989–998.
- [20] P. W. Grigsby, R. S. Malyapa, R. Higashikubo, J. K. Schwarz, M. J. Welch, P. C. Huettner, F. Dehdashti, *Mol. Imaging Biol.* **2007**, 9, 278–283.
- [21] F. Dehdashti, W. Grigsby Perry, A. Mintun Mark, S. Lewis Jason, A. Siegel Barry, J. Welch Michael, *Int. J. Radiat. Oncol. Biol. Phys.* **2003**, 55, 1233–1238.
- [22] F. Dehdashti, M. A. Mintun, J. S. Lewis, J. Bradley, R. Govindan, R. Laforest, M. J. Welch, B. A. Siegel, *Eur. J. Nucl. Med. Mol. Imaging* **2003**, 30, 844–850.
- [23] P. D. Bonnitcha, A. L. Vavere, J. S. Lewis, J. R. Dilworth, *J. Med. Chem.* **2008**, 51, 2985–2991.
- [24] J. P. Holland, P. J. Barnard, D. Collison, J. R. Dilworth, R. Edge, J. C. Green, E. J. L. McInnes, *Chem. Eur. J.* **2008**, 14, 5890–5907.
- [25] J. P. Holland, P. J. Barnard, D. Collison, J. R. Dilworth, R. Edge, J. C. Green, J. M. Heslop, E. J. L. McInnes, C. G. Salzmann, A. L. Thompson, *Eur. J. Inorg. Chem.* **2008**, 3549–3560.
- [26] A. R. Cowley, J. R. Dilworth, P. S. Donnelly, E. Labisbal, A. Sousa, *J. Am. Chem. Soc.* **2002**, 124, 5270–5271.
- [27] J. P. Holland, J. C. Green, J. R. Dilworth, *Dalton Trans.* **2006**, 783–794.
- [28] P. J. Blower, T. C. Castle, A. R. Cowley, J. R. Dilworth, P. S. Donnelly, E. Labisbal, F. E. Sowrey, S. J. Teat, M. J. Went, *Dalton Trans.* **2003**, 4416–4425.
- [29] J. P. Holland, J. H. Giansiracusa, S. G. Bell, L.-L. Wong, J. R. Dilworth, *Phys. Med. Biol.* **2009**, 54, 2103–2119.
- [30] J. L. J. Dearling, J. S. Lewis, D. W. McCarthy, M. J. Welch, P. J. Blower, *Chem. Commun.* **1998**, 2531–2532.
- [31] J. L. J. Dearling, J. S. Lewis, G. E. D. Mullen, M. J. Welch, P. J. Blower, *J. Biol. Inorg. Chem.* **2002**, 7, 249–259.
- [32] L. E. Warren, S. M. Horner, W. E. Hatfield, *J. Am. Chem. Soc.* **1972**, 94, 6392–6396.
- [33] L. S. Natrajan, P. L. Timmins, M. Lunn, S. L. Heath, *Inorg. Chem.* **2007**, 46, 10877–10886.
- [34] H. M. Betts, P. J. Barnard, S. R. Bayly, J. R. Dilworth, A. D. Gee, J. P. Holland, *Angew. Chem. Int. Ed.* **2008**, 47, 8416–8419.
- [35] M. J. Frisch, G. W. Trucks, H. B. Schlegel, G. E. Scuseria, M. A. Robb, J. R. Cheeseman, J. A. Montgomery Jr., T. Vreven, K. N. Kudin, J. C. Burant, J. M. Millam, S. S. Iyengar, J. Tomasi, V. Barone, B. Mennucci, M. Cossi, G. Scalmani, N. Rega, G. A. Petersson, H. Nakatsuji, M. Hada, M. Ehara, K. Toyota, R. Fukuda, J. Hasegawa, M. Ishida, T. Nakajima, Y. Honda, O. Kitao, H. Nakai, M. Klene, X. Li, J. E. Knox, H. P. Hratchian, J. B. Cross, V. Bakken, C. Adamo, J. Jaramillo, R. Gomperts, R. E. Stratmann, O. Yazyev, A. J. Austin, R. Cammi, C. Pomelli, J. W. Ochterski, P. Y. Ayala, K. Morokuma, G. A. Voth, P. Salvador, J. J. Dannenberg, V. G. Zakrzewski, S. Dapprich, A. D. Daniels, M. C. Strain, O. Farkas, D. K. Malick, A. D. Rabuck, K. Raghavachari, J. B. Foresman, J. V. Ortiz, Q. A. G. Cui, B. Baboul, S. Clifford, J. Cioslowski, B. B. Stefanov, G. Liu, A. Liashenko, P. Piskorz, I. Komaromi, R. L. Martin, D. J. Fox, T. Keith, M. A. Al-Laham, C. Y. Peng, A. Nanayakkara, M. Challacombe, P. M. W. Gill, B. Johnson, W. Chen, M. W. Wong, C. Gonzalez, J. A. Pople, *Gaussian 03*, Gaussian, Inc., Wallingford CT, **2004**.
- [36] A. B. Pangborn, M. A. Giardello, R. H. Grubbs, R. K. Rosen, F. J. Timmers, *Organometallics* **1996**, 15, 1518.

Received: August 21, 2009

Published Online: October 21, 2009

# Nucleophilic Addition of Water and Alcohols to Dicyanonitrosomethanide: Ligands with Diverse Bonding Modes in Magnetically Coupled d-Block Complexes

Anthony S. R. Chesman,<sup>[a]</sup> David R. Turner,<sup>[a]</sup> Boujemaa Moubaraki,<sup>[a]</sup> Keith S. Murray,<sup>[a]</sup> Glen B. Deacon,<sup>[a]</sup> and Stuart R. Batten<sup>\*[a]</sup>

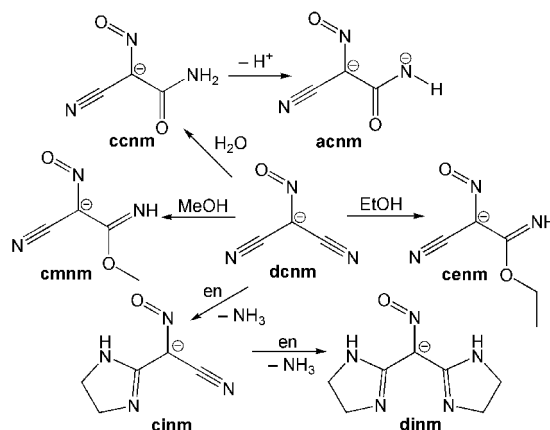
**Keywords:** Self-assembly / Magnetic properties / Transition metals / Coordination modes / In situ synthesis

Ligands resulting from the transition-metal-promoted nucleophilic addition of water or an alcohol to dicyanonitrosomethanide ions (dcnm) have been utilised in the formation of a large series of polynuclear complexes. Addition of water to dcnm results in formation of carbamoylcyanonitrosomethanide (ccnm); deprotonation of this ligand gives amidocarbonyl(cyano)nitrosomethanide (acnm), which has been incorporated into the trinuclear complex  $[\text{Cu}_3(\text{acnm})_2(\text{dmae})_2(\text{H}_2\text{O})_2]$  [dmae = 2-(dimethylamino)ethoxide] (**1**) which shows strong antiferromagnetic coupling with an exchange coupling constant,  $J = -500 \text{ cm}^{-1}$ .  $[\text{Cu}(\text{acnm})(\text{NH}_3)_2]_\infty$  (**2**) marks the first instance of acnm facilitating the formation of a coordination polymer, namely a 1D chain with intramolecular hydrogen bonding. Attempts to synthesise **2** through different reaction conditions instead resulted in the mononuclear  $[\text{Cu}(\text{acnm})-(\text{NH}_3)_2(\text{py})]$  (py = pyridine) (**3**). The addition of ethanol to dcnm results in cyano[imino(ethoxy)methyl]nitrosomethanide (cenm) which features in the mononuclear  $[\text{Cu}(\text{cenm})_2-$

$(\text{H}_2\text{O})_2]$  (**4**) and polymeric  $\{[\text{Cu}(\text{cenm})_2]_2 \cdot \text{H}_2\text{O}\}_\infty$  (**5**). The latter is the first example of the cenm ligand in a coordination polymer and has a highly unusual coordination mode through the nitrile groups and extremely weak antiferromagnetic coupling.  $\{[\text{Mn}_3(\text{ccnm})_2(\text{EtOH})_2(\text{OAc})_4] \cdot 2\text{EtOH}\}_\infty$  (**6**) and  $(\text{Et}_4\text{N})_2-[\text{Cu}(\text{ccnm})_4]$  (**7**) contain previously unobserved coordination modes of the ccnm ligand while the complex  $[\text{Mn}(\text{cmnm})_3-\text{Mn}(\text{bipy})(\text{MeOH})](\text{ClO}_4)$  (**8**) (cmnm = cyano[imino(methoxy)methyl]nitrosomethanide, bipy = 2,2'-bipyridine) displays weak antiferromagnetic coupling between manganese atoms with  $J = -1.44 \text{ cm}^{-1}$ . A change in the solvent systems used in the synthesis of **7** results in the formation of the mononuclear complexes  $[\text{Mn}(\text{bipy})_2(\text{dcnm})_2]$  (**9**) or  $[\text{Mn}(\text{bipy})_2(\text{H}_2\text{O})(\text{dcnm})](\text{dcnm}) \cdot \text{H}_2\text{O}$  (**10**) and  $[\text{Mn}(\text{bipy})_2(\text{dcnm})(\text{H}_2\text{O})](\text{dcnm})$  (**11**). The addition of ethylene glycol monomethyl ether to dcnm gives cyano[imino(2-methoxyethoxy)methyl]nitrosomethanide (cgnm) and the formation of  $[\text{Cu}(\text{cgnm})_2-(\text{H}_2\text{O})_2]$  (**12**).

## Introduction

Pseudohalide ligands such as cyanate,<sup>[1]</sup> dicyanamide,<sup>[2,3]</sup> tricyanomethanide<sup>[4]</sup> and carbamoyldicyanomethanide<sup>[5]</sup> display a propensity to undergo transition-metal-promoted nucleophilic addition. This reaction is also observed with dicyanonitrosomethanide,  $\text{C}(\text{CN})_2(\text{NO})^-$  (dcnm), where the addition of water or methanol to a nitrile group results in the formation of carbamoylcyanonitrosomethanide (ccnm) and cyano[imino(methoxy)methyl]nitrosomethanide (cmnm) ions, respectively (Scheme 1).<sup>[6]</sup> Recently the library of dcnm derivatives has been extended by using amines such as 1,2-diaminoethane as nucleophiles, which may add to both nitrile arms and cyclise to form diimidazolynitrosomethanide (dinm).<sup>[7]</sup> The use of acids may also promote nucleophilic addition but the resulting protonation of the nitroso group to give an oxime results in neutral products with more limited available coordination modes.<sup>[8]</sup>



Scheme 1. Products resulting from nucleophilic addition of alcohols and amines to dcnm.

Despite the apparent divergent nature of these nitroso/cyano ligands they generally form mononuclear complexes and their role in the formation of clusters or coordination polymers is yet to be fully realised. Exceptions to this are salts of dcnm<sup>[9,10]</sup> and dicyanonitromethanide,<sup>[11]</sup>  $\text{C}(\text{CN})_2-$

[a] School of Chemistry, Monash University, Wellington Rd, Clayton, Victoria 3800, Australia  
Fax: +61-3-99054597  
E-mail: stuart.batten@sci.monash.edu.au

(NO<sub>2</sub>)<sup>−</sup>, which crystallise as coordination polymers, and a limited number of polynuclear complexes containing addition derivative ligands.<sup>[12–16]</sup>

More recently ccnm has been included in “lanthanoids”, large polycarbonatolanthanoid clusters in which the ligands act as η<sup>2</sup>-nitroso-bound capping species.<sup>[17]</sup> The related ligand carbamoyldicyanomethanide, known for its participation in numerous hydrogen bond motifs,<sup>[18–22]</sup> has undergone a similar nucleophilic addition of methanol in the formation of a novel network of Fe<sup>III</sup><sub>10</sub> clusters.<sup>[23]</sup> Because the pseudohalide ligands dicyanamide, N(CN)<sub>2</sub><sup>−</sup>, and tricyanomethanide, C(CN)<sub>3</sub><sup>−</sup>, demonstrate versatility in the formation of coordination polymers, which have garnered much attention for their magnetic properties,<sup>[24]</sup> and because the solvothermally synthesised [Cu(cnm)]<sub>∞</sub> network demonstrates ferromagnetic coupling,<sup>[25]</sup> there is a strong impetus to incorporate dcnm-derived ligands in coordination polymers. Related cyanoxime-based complexes have been noted for their cytotoxicity, with their continued development for anti-cancer applications of interest to researchers.<sup>[26]</sup>

While we have reported a metal-free synthesis of the ccnm anion<sup>[17]</sup> the formation of other nucleophilic addition products still relies on the presence of a transition metal. In situ formation has proven to be a reliable and repeatable synthetic approach with this class of ligands and gives access to more exotic ligand derivatives. A reaction of ccnm with a base results in subsequent deprotonation to form the unusual dianionic amidocarbonyl(cyano)nitrosomethanide (acnm) ligand. It has previously been reported only in the complexes (Me<sub>4</sub>N)<sub>2</sub>[Ni(acnm)<sub>2</sub>·2H<sub>2</sub>O] and [(Ph<sub>4</sub>Sb)<sub>2</sub>Ni(acnm)<sub>2</sub>] but was formed from an alternate synthesis, namely the double deprotonation of 2-cyano-2-(hydroxyimino)acetamide by hydroxide.<sup>[27]</sup>

The only evidence of larger alcohols reacting with dcnm is the report of addition of ethanol to form cyano[imino(ethoxy)methyl]nitrosomethanide (cenm).<sup>[28]</sup> This preliminary account hints at the possibility of further derivatisation of the dcnm ligand by alcohols to add targeted functionality.

The first component of this paper details the nucleophilic addition of water or alcohols to dcnm under varying reaction conditions, examining the effects of differing bases, co-ligands and solvent mixtures on the resulting products. The following section shows how these ligands demonstrate a diverse range of coordination modes in their structures, with their incorporation into series of mono- or polynuclear metal complexes and coordination polymers. The magnetic properties of selected complexes are also discussed.

## Results and Discussion

### Synthesis

Details of reactions of dcnm with water or an alcohol in the presence of a transition-metal ion and various co-ligands, together with the resulting products, are shown in Table 1. The transition-metal-promoted nucleophilic addition of water to a nitrile group of dcnm results in the formation of carbamoylcyanonitrosomethanide (ccnm) which may then undergo deprotonation of the carbamoyl group to form amidocarbonyl(cyano)nitrosomethanide (acnm) ions (Scheme 1). Thus the reaction of Na(dcnm), copper perchlorate and 2-(dimethylamino)ethanol (dmeaH) in water results in the formation of blue tabular crystals of the product [Cu<sub>3</sub>(acnm)<sub>2</sub>(dmea)<sub>2</sub>(H<sub>2</sub>O)<sub>2</sub>] [dmea = 2-(dimethylamino)ethoxide] (**1**) in high yield. In the formation of **1**, the excess of dmeaH acts as a base to deprotonate both ccnm and other dmeaH molecules to form the acnm and dmea ions incorporated into **1**. The use of the tertiary amine obviates nucleophilic addition which has been shown to occur preferentially with primary amines in comparison to the addition of alcohols.<sup>[7]</sup>

The acnm ligand also features in the coordination polymer [Cu(acnm)(NH<sub>3</sub>)<sub>2</sub>]<sub>∞</sub> (**2**) which forms a blue crystalline product from reaction of (Me<sub>4</sub>N)(dcnm), copper perchlorate and aqueous ammonia in a water/pyridine solution. The excess of ammonia deprotonates ccnm to form acnm in this case. Attempts to repeat the synthesis of complex **2**

Table 1. Reactions of Na/Me<sub>4</sub>N/Et<sub>4</sub>N dcnm salts with transition-metal salts, nucleophilic solvents and co-ligands.

| Ligand salt               | Metal reagent   | Solvent and/or nucleophile <sup>[a]</sup> | Co-ligand       | Product <sup>[b]</sup>   |           |
|---------------------------|---|---|-----------------|--|-----------|
| Na(dcnm)                  | Cu(ClO <sub>4</sub> ) <sub>2</sub> ·6H <sub>2</sub> O   | H <sub>2</sub> O <sup>[a]</sup>           | dmea            | [Cu <sub>3</sub> ( <i>acnm</i> ) <sub>2</sub> (dmea) <sub>2</sub> (H <sub>2</sub> O) <sub>2</sub> ] <sup>[c]</sup> | <b>1</b>  |
| (Me <sub>4</sub> N)(dcnm) | Cu(ClO <sub>4</sub> ) <sub>2</sub> ·6H <sub>2</sub> O   | py/H <sub>2</sub> O <sup>[a]</sup>        | NH <sub>3</sub> | [Cu( <i>acnm</i> )(NH <sub>3</sub> ) <sub>2</sub> ] <sub>∞</sub> <sup>[c]</sup>                                    | <b>2</b>  |
| (Et <sub>4</sub> N)(ccnm) | Cu(ClO <sub>4</sub> ) <sub>2</sub> ·6H <sub>2</sub> O   | py/H <sub>2</sub> O <sup>[a]</sup>        | NH <sub>3</sub> | [Cu( <i>acnm</i> )(NH <sub>3</sub> ) <sub>2</sub> (py)] <sup>[c]</sup>   | <b>3</b>  |
| (Me <sub>4</sub> N)(dcnm) | Cu(NO <sub>3</sub> ) <sub>2</sub> ·3H <sub>2</sub> O  | EtOH <sup>[a]</sup>                       | –               | {[Cu( <i>cenm</i> ) <sub>2</sub> ] <sub>2</sub> ·H <sub>2</sub> O} <sub>∞</sub>                                    | <b>4</b>  |
| Na(dcnm)                  | Cu(NO <sub>3</sub> ) <sub>2</sub> ·3H <sub>2</sub> O,<br>Gd(NO <sub>3</sub> ) <sub>3</sub> ·6H <sub>2</sub> O | EtOH <sup>[a]</sup>                       | –               | [Cu( <i>cenm</i> ) <sub>2</sub> (H <sub>2</sub> O) <sub>2</sub> ]  | <b>5</b>  |
| Na(dcnm)                  | Mn(OAc) <sub>2</sub> ·4H <sub>2</sub> O   | EtOH/H <sub>2</sub> O <sup>[a]</sup>      | –               | {[Mn <sub>3</sub> ( <i>ccnm</i> ) <sub>2</sub> EtOH <sub>2</sub> (OAc) <sub>4</sub> ·2EtOH] <sub>∞</sub> }         | <b>6</b>  |
| (Et <sub>4</sub> N)(ccnm) | CuCl <sub>2</sub> ·2H <sub>2</sub> O,<br>LaCl <sub>3</sub> ·7H <sub>2</sub> O                                 | MeOH                                      | –               | (Et <sub>4</sub> N) <sub>2</sub> [Cu(ccnm) <sub>4</sub> ]  | <b>7</b>  |
| Na(dcnm)                  | Mn(ClO <sub>4</sub> ) <sub>2</sub> ·6H <sub>2</sub> O   | MeOH <sup>[a]</sup>                       | 2,2'-Bipy       | [Mn( <i>ccnm</i> ) <sub>3</sub> Mn(bipy)(MeOH)](ClO <sub>4</sub> )   | <b>8</b>  |
| (Me <sub>4</sub> N)(dcnm) | Mn(ClO <sub>4</sub> ) <sub>2</sub> ·6H <sub>2</sub> O   | MeOH/H <sub>2</sub> O                     | 2,2'-Bipy       | [Mn(bipy) <sub>2</sub> (dcnm) <sub>2</sub> ]   | <b>9</b>  |
| (Me <sub>4</sub> N)(dcnm) | Mn(ClO <sub>4</sub> ) <sub>2</sub> ·6H <sub>2</sub> O   | MeOH/H <sub>2</sub> O                     | 2,2'-Bipy       | [Mn(bipy) <sub>2</sub> (dcnm)(H <sub>2</sub> O)](dcnm)   | <b>10</b> |
| (Me <sub>4</sub> N)(dcnm) | Mn(ClO <sub>4</sub> ) <sub>2</sub> ·6H <sub>2</sub> O   | MeOH/H <sub>2</sub> O                     | 2,2'-Bipy       | [Mn(bipy) <sub>2</sub> (dcnm)(H <sub>2</sub> O)](dcnm)·H <sub>2</sub> O  | <b>11</b> |
| (Me <sub>4</sub> N)(dcnm) | Cu(ClO <sub>4</sub> ) <sub>2</sub> ·6H <sub>2</sub> O   | 2-methoxyethanol <sup>[a]</sup>           | –               | [Cu( <i>cgnm</i> ) <sub>2</sub> (H <sub>2</sub> O) <sub>2</sub> ]  | <b>12</b> |

[a] Solvent that has acted as nucleophile. [b] Ligands resulting from nucleophilic addition are italicised. [c] Ligand from deprotonation of ccnm.

from  $(\text{Et}_4\text{N})(\text{ccnm})$  rather than  $(\text{Me}_4\text{N})(\text{dcnm})$  resulted in the discrete mononuclear complex  $[\text{Cu}(\text{acnm})(\text{NH}_3)_2(\text{py})]$  (**3**). The formation of a different product may be due to the presence of a different counter-cation or through an alteration of the self assembly process as the preformed ccnm ligand is used as a reactant.

The only prior report of the transition-metal-promoted nucleophilic addition of ethanol to a nitrile group of dcnm to form cyano[imino(ethoxy)methyl]nitrosomethanide (cenm), is a brief mention of the synthesis and structure of  $[\text{Cu}(\text{cenm})_2(\text{H}_2\text{O})_2]$  (**4**).<sup>[28]</sup> The synthetic and crystallographic details, however, are unavailable in this report. In our studies we found that crystals of mononuclear **4** began to form from an ethanolic reaction solution containing copper nitrate and  $(\text{Me}_4\text{N})(\text{dcnm})$  after one month.

In contrast the presence of gadolinium nitrate in an ethanolic reaction solution containing  $\text{Na}(\text{dcnm})$  and copper nitrate resulted in the formation of the 2D sheet coordination polymer  $\{[\text{Cu}(\text{cenm})_2]_2 \cdot \text{H}_2\text{O}\}_\infty$  (**5**), although the lanthanoid metal does not feature in the structure. Without gadolinium nitrate present only crystallisation of **4** is observed. This phenomena of gadolinium influencing the self-assembly of a complex, possibly through pre-coordination of the ligand, without appearing in the final complex has been observed previously.<sup>[29]</sup>

Throughout our studies of ligands forming from the derivatisation of dcnm we have not previously observed formation of the cenm ligand (Scheme 1), despite repeated uses of ethanol as a solvent for crystallisation. It may be that the ethyl substituent has a solubilising effect on the ligand, limiting the ability of complexes containing the ligand to crystallise from solution. Alternatively, the relative rarity of the in situ formation of cenm may be indicative of the effect of the steric bulk of the nucleophile in reducing the rate of reaction. The argument for a lowered reactivity with ethanol is further supported by the formation of  $\{[\text{Mn}^{\text{II}}_3(\text{ccnm})_2(\text{EtOH})_2(\text{OAc})_4] \cdot 2\text{EtOH}\}_\infty$  (**6**), which is synthesised by a reaction of  $\text{Na}(\text{dcnm})$  and manganese(II) acetate in a water/ethanol (1:4) solution. The excess of ethanol is insufficient to yield the ethanol addition product with the water addition product, ccnm, being favoured.

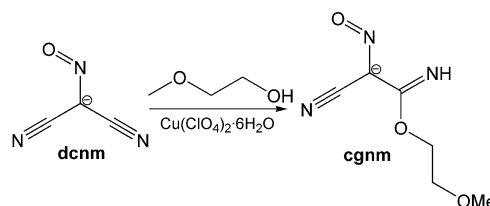
Complex **7**,  $(\text{Et}_4\text{N})_2[\text{Cu}(\text{ccnm})_4]$ , was synthesised by the reaction of preformed ccnm, in the form of the tetraethylammonium salt, and copper chloride in methanol in the presence of lanthanum chloride. A similar reaction solution without lanthanum chloride failed to yield any crystals, again indicating that the lanthanoid plays a role templating product formation.

Reaction of  $\text{Na}(\text{dcnm})$  and manganese perchlorate with the co-ligand 2,2'-bipyridine in methanol leads to the nucleophilic addition of methanol with the formation of cyano[imino(methoxy)methyl]nitrosomethanide (cmnm) in the complex  $[\text{Mn}(\text{cmnm})_3\text{Mn}(\text{bipy})(\text{MeOH})(\text{ClO}_4)]$  (**8**). When this complex is viewed in conjunction with the formation of  $[\text{Mn}^{\text{II}}_2\text{Mn}^{\text{III}}(\text{cmnm})_6](\text{NO}_3)_3$ ,<sup>[12]</sup> which also contains the  $[\text{Mn}^{\text{II}}(\text{cmnm})_3]$  moiety and was not synthesised in the presence of 2,2'-bipyridine, it would suggest that the co-ligand caps one face of the other manganese atom, stopping the

assembly of the trinuclear complex. The crystal structure of **8**·3.4MeOH contains methanol disordered within the lattice but upon isolation of the bulk product the lattice methanol molecules are exchanged for atmospheric moisture (see Exp. Sect.).

The solvent used in the synthesis of **8** plays a major role in the product isolated. A synthesis using only methanol results in complex **8** while the use of a mixed water/methanol solvent system gives a mononuclear complex where unreacted dcnm coordinates to the manganese atom through the oxygen atom of the nitroso group in  $[\text{Mn}(\text{bipy})_2(\text{dcnm})_2]$  (**9**). The use of a purely aqueous reaction solution results in complexes with dcnm as a free anion which participates in hydrogen bonding in the lattice, seen in  $[\text{Mn}(\text{bipy})_2(\text{dcnm})(\text{H}_2\text{O})](\text{dcnm}) \cdot \text{H}_2\text{O}$  (**10**) and  $[\text{Mn}(\text{bipy})_2(\text{dcnm})(\text{H}_2\text{O})](\text{dcnm})$  (**11**). Although this is an unusual result when water is used as a solvent and where ccnm formation can be expected, dcnm has been previously been included into transition-metal complex crystal structures without undergoing nucleophilic addition of the protic solvent.<sup>[30,31]</sup> This may be due to the 2,2'-biyridine in the coordination sphere of the metal centre limiting its ability to promote the nucleophilic addition to the anion.

A reaction of  $(\text{Me}_4\text{N})(\text{dcnm})$  and copper perchlorate in ethylene glycol monomethyl ether results in the addition of the protic solvent to form cyano[imino(2-methoxyethoxy)methyl]nitrosomethanide (cgnm) observed in the discrete complex  $[\text{Cu}(\text{cgnm})_2(\text{H}_2\text{O})_2]$  (**12**) (Scheme 2). The addition of ethylene glycol monomethyl ether to dcnm involves the largest known nucleophile yet added to the dcnm molecule through this reaction route. This product could not be isolated by crystallisation from the reaction solution, but required the complete evaporation of the solvent to yield green tabular crystals. As observed in the formation of cenm, this may be the result of the dangling methoxyethyl group increasing the solubility of the product and prohibiting facile crystallisation.



Scheme 2. Addition of ethylene glycol monomethyl ether to dcnm to form cgnm.

## Crystal Structures and Magnetism

Complex  $[\text{Cu}_3(\text{acnm})_2(\text{dmea})_2(\text{H}_2\text{O})_2]$  (**1**) crystallises from water in the space group  $P\bar{1}$ , with half of the molecule contained within the asymmetric unit. The complex contains two square-pyramidal copper atoms flanking a central square-planar copper atom which lies on an inversion center (Figure 1, a). The coordination spheres of the outer copper atoms contain equatorially chelating acnm and dmea

ligands, and a water molecule in one axial position. This axial coordination is Jahn–Teller distorted with a bond length of 2.308(4) Å, longer than that of the oxygen atom of the dmae ligand that coordinates in an basal position with a bond length of 1.909(4) Å. The outer copper atoms are bridged to the central copper atom through the nitroso groups of the acnm ligand and the oxygen atom of dmae ligand, resulting in  $\mu_2\text{-}\eta^2(\text{N},\text{N}')\text{Cu}:\eta^1(\text{O})\text{Cu}'$  and  $\mu_2\text{-}\eta^2(\text{N},\text{O})\text{Cu}:\eta^1(\text{O})\text{Cu}'$  coordination modes of the respective ligands (Table 2).

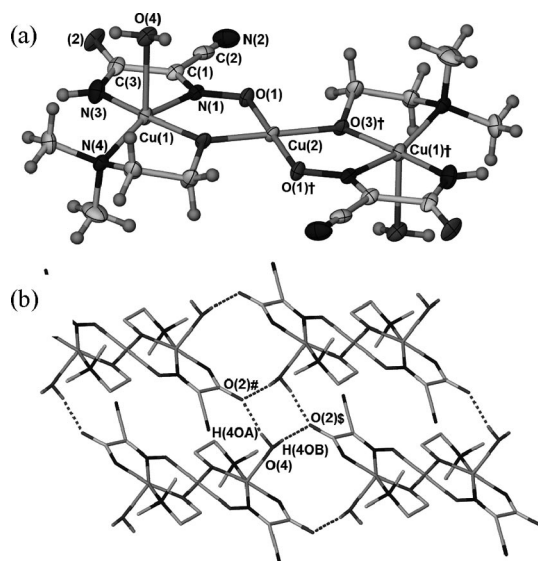


Figure 1. (a) Crystal structure of  $[\text{Cu}_3(\text{acnm})_2(\text{dmae})_2(\text{H}_2\text{O})_2]$  (**1**). Ellipsoids shown at 50% probability. (b) Hydrogen bonding in the crystal structure of **1**. Hydrogen atoms not participating in hydrogen bonding are omitted for clarity. Key hydrogen bond lengths [Å] and angles [°]:  $\text{O}(4)\cdots\text{O}(2)^{\#}$  2.729(6);  $\text{O}(4)\cdots\text{H}(4\text{OA})\cdots\text{O}(2)^{\#}$  164;  $\text{O}(4)\cdots\text{O}(2)^{\S}$  2.760(6);  $\text{O}(4)\cdots\text{H}(4\text{OB})\cdots\text{O}(2)^{\S}$  168. Symmetry elements used:  $\dagger -x, -y, -z$ ;  $\# x-1, y, z$ ;  $\S 1-x, -y, -z-1$ . Hydrogen atoms were refined in restrained positions.

Table 2. Selected bond lengths [Å] and angles [°] of complex **1**.<sup>[a]</sup>

|                                    |           |   |            |
|------------------------------------|-----------|---|------------|
| $\text{Cu}(1)\cdots\text{Cu}(2)$   | 3.3080(7) | $\text{Cu}(1)\cdots\text{Cu}(1)^{\dagger}$              | 6.6160(14) |
| $\text{Cu}(1)\text{--}\text{N}(1)$ | 1.984(5)  | $\text{N}(1)\text{--}\text{Cu}(1)\text{--}\text{N}(3)$  | 81.9(2)    |
| $\text{Cu}(1)\text{--}\text{N}(3)$ | 1.930(6)  | $\text{N}(4)\text{--}\text{Cu}(1)\text{--}\text{O}(3)$  | 86.6(2)    |
| $\text{Cu}(1)\text{--}\text{N}(4)$ | 2.020(5)  | $\text{Cu}(1)\text{--}\text{O}(3)\text{--}\text{Cu}(2)$ | 120.6(2)   |
| $\text{Cu}(1)\text{--}\text{O}(3)$ | 1.909(4)  | $\text{Cu}(1)\text{--}\text{N}(1)\text{--}\text{O}(1)$  | 124.5(4)   |
| $\text{Cu}(1)\text{--}\text{O}(4)$ | 2.308(4)  | $\text{N}(1)\text{--}\text{O}(1)\text{--}\text{Cu}(2)$  | 121.4(5)   |
| $\text{Cu}(2)\text{--}\text{O}(1)$ | 1.971(4)  | $\text{O}(1)\text{--}\text{Cu}(2)\text{--}\text{O}(3)$  | 91.3(2)    |
| $\text{Cu}(2)\text{--}\text{O}(3)$ | 1.900(4)  | $\text{N}(1)\text{--}\text{Cu}(1)\text{--}\text{O}(4)$  | 92.5(2)    |
| $\text{N}(1)\text{--}\text{O}(1)$  | 1.314(6)  | $\text{N}(4)\text{--}\text{Cu}(1)\text{--}\text{O}(4)$  | 105.8(2)   |
| $\text{C}(1)\text{--}\text{N}(1)$  | 1.288(8)  | $\text{O}(1)\text{--}\text{N}(1)\text{--}\text{C}(1)$   | 121.4(5)   |
| $\text{N}(3)\text{--}\text{C}(3)$  | 1.323(9)  | $\text{N}(3)\text{--}\text{C}(3)\text{--}\text{O}(2)$   | 129.9(6)   |
| $\text{O}(2)\text{--}\text{C}(3)$  | 1.246(8)  |   |            |

[a] Symmetry element used:  $\dagger -x, -y, -z$ .

Crystal packing shows that 2D sheets form as each water molecule hydrogen bonds to the oxygen atoms of the amide groups belonging to two adjacent complexes. The oxygen atoms act as bifurcated hydrogen-bond acceptors (Figure 1, b). Interestingly, the nitrile groups do not participate in any hydrogen bonding and are directed into the spaces between the 2D sheets. There are no significant interactions between sheets.

The magnetic properties of **1** are interesting because they allow us to probe the magnetic exchange coupling across the doubly bridged nitroso/alkoxo combination in the linear  $\text{Cu}^{\text{II}}_3$  moieties. A plot of effective magnetic moment, per  $\text{Cu}_3$ , shown in part a of Figure 2, reveals that the  $\mu_{\text{eff}}$  values remain constant, at  $\chi_M T = 0.405 \text{ cm}^3 \text{ mol}^{-1} \text{ K}$  ( $1.8 \mu_B$ ), over the 300 to 4 K range with a small decrease then occurring to reach  $0.38 \text{ cm}^3 \text{ mol}^{-1} \text{ K}$  ( $1.76 \mu_B$ ) at 2 K. The corresponding molar susceptibility data,  $\chi_M$ , is close to Curie-like in its temperature dependence ( $C = 0.4 \text{ cm}^3 \text{ mol}^{-1} \text{ K}$ ;  $\theta = -0.4 \text{ K}$ ). This behaviour is characteristic of an isolated  $S = 1/2$  state being thermally populated, this ground state arising through strong antiferromagnetic coupling between the terminal and central Cu atoms across the double bridges. Alkoxo (oxygen  $\text{sp}^2$ ) bridging and oximato  $[\text{Cu}\text{--}\text{N}(\text{R})\text{O}\text{--}\text{Cu}]$  bridging are known<sup>[32,33]</sup> to provide very effective superexchange pathways, augmented in **1** by the close-to-coplanar equatorial planes of the three Cu centres. Thus the efficient overlap of the  $\text{Cu}(\text{d}_{x^2-y^2})$  “magnetic orbitals” leads to strong, net antiferromagnetic coupling. A good fit was obtained using a  $S = 1/2$  trimer model<sup>[34]</sup> using the parameters  $g = 2.08$ ,  $2J = -1000 \text{ cm}^{-1}$ ,  $N\alpha = 65 \times 10^{-6} \text{ cm}^3 \text{ mol}^{-1}$ . Other trinuclear  $\text{Cu}^{\text{II}}$  compounds reported to show such behaviour include the linear  $[\text{Cu}_3\{\text{C}_2\text{S}_2(\text{NCH}_2\text{CH}_2\text{CH}_2\text{SCH}_2\text{CH}_2\text{OH})_2\}_2](\text{ClO}_4)_2$ <sup>[34]</sup> and the non-linear  $[\text{Cu}_3(\text{Me}_3\text{tacn})_2(\text{dmg})_2\text{Br}](\text{ClO}_4)\cdot\text{MeOH}$  ( $\text{Me}_3\text{tacn} = 1,4,7\text{-trimethyl-1,4,7-triazacyclononane}$ ;  $\text{dmg} = \text{dimethylglyoximate}$ ),<sup>[35]</sup> the latter having similar  $\text{Cu}\text{--}\text{NO}\text{--}\text{Cu}$  pathways to those in **1**.

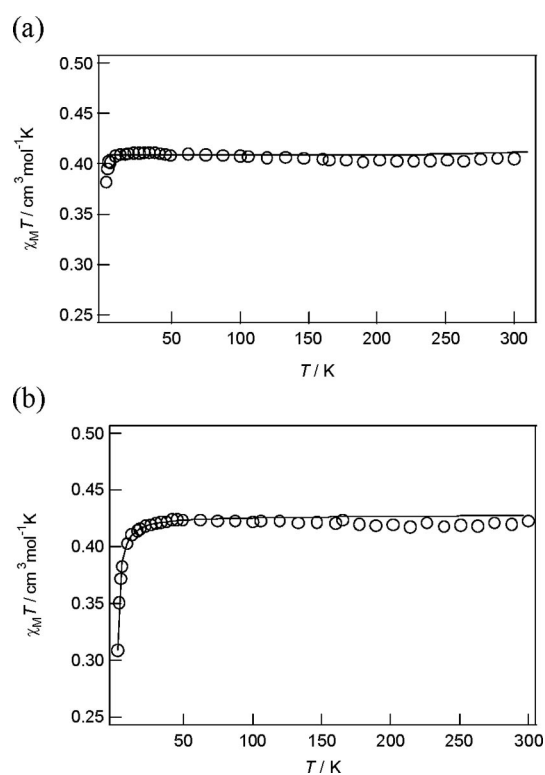


Figure 2. (a) Plot of  $\chi_M T$ , per  $\text{Cu}_3$ , for complex **1**. (b) Plot of  $\chi_M T$ , per Cu, for complex **5**. The solid lines are the calculated plots using the parameters given in the text.

Complex  $[\text{Cu}(\text{acnm})(\text{NH}_3)_2]_\infty$  (**2**) crystallises in the space group  $P2_1/n$  with a single moiety of the repeating unit within the asymmetric unit. The basal positions of each square-pyramidal copper atom are occupied by two *cis* ammonia molecules and one acnm ligand chelating in a similar fashion to those in complex **1**. The coordination sphere is completed by the oxygen atom of a nitroso group from another acnm ligand of an adjacent  $[\text{Cu}(\text{acnm})(\text{NH}_3)_2]$  moiety, facilitating the formation of 1D chains (Figure 3, a). As with complex **1**, the acnm ligand has a  $\mu_2\text{-}\eta^2(\text{N},\text{N}')\text{-Cu}:\eta^1(\text{O})\text{Cu}'$  coordination mode but now with a Jahn–Teller distorted axial bonding mode to a neighbouring copper atom rather than the in plane bridging observed in **1**. The perpendicular bridging mode has previously been reported for this class of ligands only in the  $[\text{Cu}(\text{cmnm})_2]$  coordination polymer.<sup>[25]</sup> Intra-chain hydrogen bonding occurs between a hydrogen atom of a coordinated ammonia ligand and an adjacent oxygen atom of an adjacent nitroso group (Table 3, Figure 3, b).

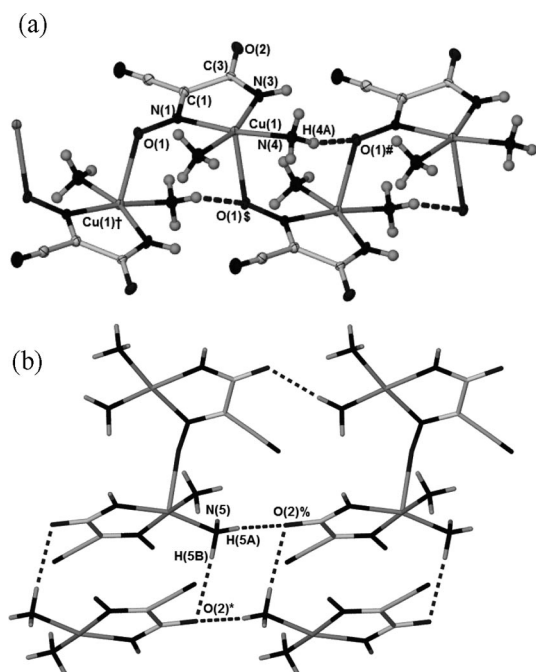


Figure 3. (a) Part of a 1D chain of complex  $[\text{Cu}(\text{acnm})(\text{NH}_3)_2]_\infty$  in the crystal structure of **2**. Ellipsoids shown at 70% probability. Hydrogen bond length and angle:  $\text{N}(4)\cdots\text{O}(1)^\#$  2.967(3) Å;  $\text{N}(4)\text{---}\text{H}(4\text{A})\cdots\text{O}(1)^\#$  162°. Symmetry elements used:  $^\dagger$   $3/2 - x, 1/2 + y, 3/2 - z$ ;  $^\#$   $x, y - 1, z$ ;  $^\S$   $3/2 - x, y - 1/2, 3/2 - z$ . (b) Intermolecular hydrogen bonding between 1D chains in **2** resulting in the formation of a 3D network; portions of four chains displayed. Hydrogen bond lengths [Å] and angles [°]:  $\text{N}(5)\cdots\text{O}(2)^\%$  2.968(3);  $\text{N}(5)\text{---}\text{H}(5\text{A})\cdots\text{O}(2)^\%$  174;  $\text{N}(5)\cdots\text{O}(2)^\ast$  3.166(3);  $\text{N}(5)\text{---}\text{H}(5\text{B})\cdots\text{O}(2)^\ast$  163. Symmetry elements used:  $^\ast$   $2 - x, 2 - y, 2 - z$ ;  $^\%$   $x - 1, y, z$ .

Intermolecular hydrogen bonding results in the formation of a 3D hydrogen-bonded network. The hydrogen atoms of one of the coordinated ammonia ligands form hydrogen bonds to the oxygen atoms of neighbouring carbonyl groups which act as bifurcated hydrogen-bond ac-

Table 3. Selected bond lengths [Å] and angles [°] of complex **2**.<sup>[a]</sup>

|   |           |  |          |
|---|-----------|--|----------|
| $\text{Cu}(1)\cdots\text{Cu}(1)^\dagger$    | 4.4274(7) | $\text{N}(1)\text{---}\text{Cu}(1)\text{---}\text{N}(3)$         | 80.9(1)  |
| $\text{Cu}(1)\text{---}\text{N}(1)$         | 2.051(2)  | $\text{N}(4)\text{---}\text{Cu}(1)\text{---}\text{N}(5)$         | 94.2(1)  |
| $\text{Cu}(1)\text{---}\text{N}(3)$         | 1.950(2)  | $\text{O}(1)\text{---}\text{N}(1)\text{---}\text{Cu}(1)$         | 127.5(2) |
| $\text{Cu}(1)\text{---}\text{N}(4)$         | 2.021(2)  | $\text{Cu}(1)^\dagger\text{---}\text{O}(1)\text{---}\text{N}(1)$ | 117.5(1) |
| $\text{Cu}(1)\text{---}\text{N}(5)$         | 1.950(2)  | $\text{O}(1)\text{---}\text{N}(1)\text{---}\text{C}(1)$          | 120.4(2) |
| $\text{O}(1)\text{---}\text{Cu}(1)^\dagger$ | 2.372(2)  | $\text{N}(3)\text{---}\text{C}(3)\text{---}\text{O}(2)$          | 129.7(2) |
| $\text{N}(1)\text{---}\text{O}(1)$          | 1.301(3)  | $\text{O}(1)^\S\text{---}\text{Cu}(1)\text{---}\text{N}(1)$      | 96.0(1)  |
| $\text{C}(1)\text{---}\text{N}(1)$          | 1.307(3)  | $\text{O}(1)^\S\text{---}\text{Cu}(1)\text{---}\text{N}(3)$      | 100.2(1) |
| $\text{N}(3)\text{---}\text{C}(3)$          | 1.322(3)  | $\text{C}(3)\text{---}\text{O}(2)$                               | 1.253(3) |

[a] Symmetry elements used:  $^\dagger$   $3/2 - x, 1/2 + y, 3/2 - z$ ;  $^\S$   $3/2 - x, y - 1/2, 3/2 - z$ .

ceptors (Figure 3, b). The non-hydrogen-bonding hydrogen atoms of the ammonia ligands are directed into the lattice and do not obviously interact with the nitrile groups.

Complex  $[\text{Cu}(\text{acnm})(\text{NH}_3)_2(\text{py})]$  (**3**) crystallises in the space group  $Pbca$  with the complex containing two *cis* ammonia ligands and one chelating acnm ligand occupying the equatorial positions of the square pyramidal copper atom, similar to the coordination environment of the copper atom in **2**, but now a pyridine molecule coordinates in the Jahn–Teller distorted axial position (Figure 4, a, Table 4). Although complexes **2** and **3** are similar in colour they crystallise in discernibly different morphologies and the purity was established by elemental analyses. The pyridine blocks the coordination site from being bridged by adjacent acnm ligands as in **2**, eliminating the possibility of forming a coordination polymer. Intramolecular hydrogen bonding occurs between the hydrogen atom of a coordinated ammonia ligand and the oxygen of the nitroso group of the acnm ligand to form a five-membered ring (Figure 4, a).

Intermolecular hydrogen bonding results in the formation of a 3D network (Figure 4, b). The oxygen atoms of the carbonyl groups act as trifurcated hydrogen-bond acceptors from the hydrogen atoms of three ammonia ligands. The oxygen atom of the nitroso group is a bifurcated hydrogen-bond acceptor, bonding to the hydrogen atoms of an ammonia ligand (intra) and the amido group (inter) of an acnm ligand.

Due to the delocalisation of charge on pseudohalides and related ligands it can be difficult to accurately assign the bond orders of the ligands. The naming of acnm suggests the second anionic charge is located in the nitrogen atom of the amidocarbonyl group. The alternative is the negative charge being located on the oxygen atom to form an imidate group. Examination of the bond lengths from the crystal structures of **1–3** did not provide a clear determination of bond order. However, the infrared spectra of complexes **1** and **3** indicate the charge is delocalised over the  $\text{CONH}^-$  functional group. Peaks at  $1592\text{ cm}^{-1}$  and  $1580\text{ cm}^{-1}$  for **1** and **3**, respectively, are assigned to  $\nu(\text{CO})$  and are shifted from the higher wavenumbers expected for a carbonyl group.

The mononuclear complex  $[\text{Cu}(\text{cenm})_2(\text{H}_2\text{O})_2]$  (**4**) crystallises in the space group  $P\bar{1}$ , with the asymmetric unit containing one half of the metal complex (Figure 5). As frequently observed with ligands resulting from the nucleo-

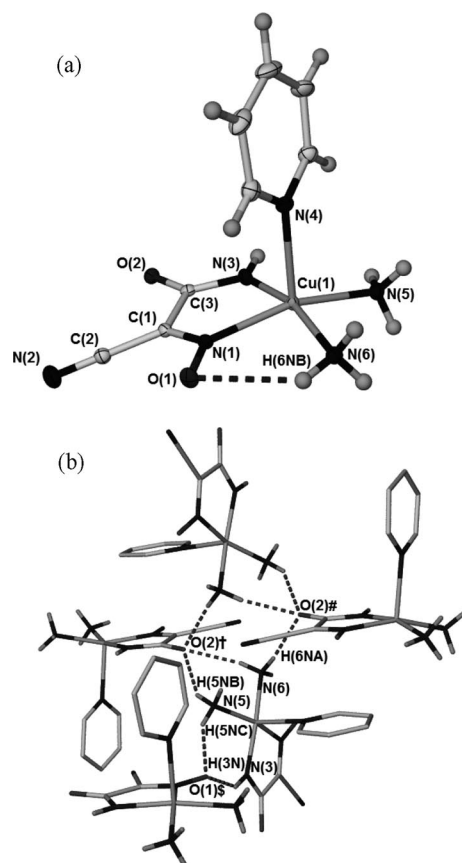


Figure 4. (a) The discrete complex and intramolecular hydrogen bonding in the crystal structure of  $[\text{Cu}(\text{acnm})(\text{NH}_3)_2(\text{py})]$  (**3**). Ellipsoids shown at 50% probability.  $\text{N}(6)\cdots\text{O}(1)$  2.904(2) Å,  $\text{N}(6)\cdots\text{H}(6\text{NB})\cdots\text{O}(1)$  131.2(14). (b) Intermolecular hydrogen bonding in the crystal structure of **3**. Hydrogen atoms of pyridine ligands omitted for clarity. Symmetry elements used:  $^\dagger x, 1/2 - y, 1/2 + z$ ;  $^\# 1 - x, y - 1/2, 1/2 - z$ ;  $^\S x - 1/2, y, 1/2 - z$ .

Table 4. Selected bond and hydrogen bond lengths [Å] and angles [°] in the crystal structure of complex **3**.<sup>[a]</sup>

|  |          |   |          |
|--|----------|---|----------|
| $\text{Cu}(1)\text{--}\text{N}(1)$     | 2.029(1) | $\text{N}(1)\text{--}\text{Cu}(1)\text{--}\text{N}(3)$              | 80.91(4) |
| $\text{Cu}(1)\text{--}\text{N}(3)$     | 1.960(1) | $\text{N}(5)\text{--}\text{Cu}(1)\text{--}\text{N}(6)$              | 94.74(5) |
| $\text{Cu}(1)\text{--}\text{N}(4)$     | 2.253(1) | $\text{N}(3)\text{--}\text{Cu}(1)\text{--}\text{N}(5)$              | 94.96(5) |
| $\text{Cu}(1)\text{--}\text{N}(5)$     | 2.038(1) | $\text{N}(1)\text{--}\text{Cu}(1)\text{--}\text{N}(4)$              | 99.59(4) |
| $\text{Cu}(1)\text{--}\text{N}(6)$     | 2.002(1) | $\text{N}(5)\text{--}\text{Cu}(1)\text{--}\text{N}(4)$              | 99.34(5) |
| $\text{N}(1)\text{--}\text{O}(1)$      | 1.290(1) | $\text{N}(6)\text{--}\text{Cu}(1)\text{--}\text{N}(4)$              | 97.65(4) |
| $\text{N}(1)\text{--}\text{C}(1)$      | 1.313(2) | $\text{O}(1)\text{--}\text{N}(1)\text{--}\text{C}(1)$               | 121.6(1) |
| $\text{N}(3)\text{--}\text{C}(3)$      | 1.307(2) | $\text{N}(3)\text{--}\text{C}(3)\text{--}\text{O}(2)$               | 129.2(1) |
| $\text{C}(3)\text{--}\text{O}(2)$      | 1.264(2) |   |          |
| $\text{N}(3)\cdots\text{O}(1)^\S$      | 2.989(1) | $\text{N}(3)\text{--}\text{H}(3\text{N})\cdots\text{O}(1)^\S$       | 141(1)   |
| $\text{N}(5)\cdots\text{O}(1)^\S$      | 2.956(2) | $\text{N}(5)\text{--}\text{H}(5\text{NC})\cdots\text{O}(1)^\S$      | 149(1)   |
| $\text{N}(5)\cdots\text{O}(2)^\dagger$ | 3.000(2) | $\text{N}(5)\text{--}\text{H}(5\text{NB})\cdots\text{O}(2)^\dagger$ | 148(1)   |
| $\text{N}(6)\cdots\text{O}(2)^\dagger$ | 3.026(2) | $\text{N}(6)\text{--}\text{H}(6\text{NC})\cdots\text{O}(2)^\dagger$ | 160(11)  |
| $\text{N}(6)\cdots\text{O}(2)^\#$      | 2.942(2) | $\text{N}(6)\text{--}\text{H}(6\text{NA})\cdots\text{O}(2)^\#$      | 169(1)   |

[a] Symmetry elements used:  $^\dagger x, 1/2 - y, 1/2 + z$ ;  $^\# -x, y - 1/2, 1/2 - z$ ;  $^\S x - 1/2, y, 1/2 - z$ .

philic addition of alcohol to dcnm, the cenm chelates to the equatorial positions of the metal centre through the nitrogen atoms of the nitroso and imine groups, with water coordinating in the Jahn–Teller distorted axial positions.

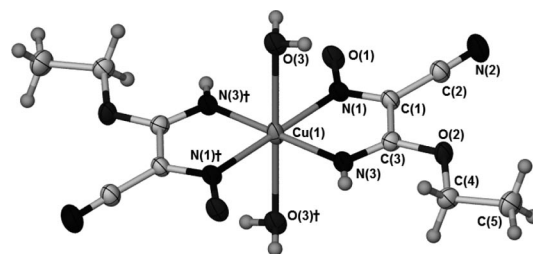


Figure 5. The discrete complex  $[\text{Cu}(\text{cenm})_2(\text{H}_2\text{O})_2]$  (**4**). Symmetry element used:  $^\dagger -x, 2 - y, -z$ . Selected bond lengths:  $\text{Cu}(1)\text{--}\text{N}(1)$  2.0551(14);  $\text{Cu}(1)\text{--}\text{N}(3)$  1.9651(15);  $\text{Cu}(1)\text{--}\text{O}(3)$  2.4942(15);  $\text{N}(1)\text{--}\text{O}(1)$  1.279(2);  $\text{C}(1)\text{--}\text{N}(1)$  1.316(2);  $\text{C}(3)\text{--}\text{N}(3)$  1.270(2);  $\text{C}(3)\text{--}\text{O}(2)$  1.325(2)  $\text{N}(1)\text{--}\text{Cu}(1)\text{--}\text{N}(3)$  80.61(6).

The coordination polymer  $\{[\text{Cu}(\text{cenm})_2]\cdot\text{H}_2\text{O}\}_\infty$  (**5**), crystallises in the space group  $C2/c$ , with the asymmetric unit containing a  $[\text{Cu}(\text{cenm})_2]$  moiety and half a molecule of water. Two cenm ligands chelate equatorially to the central octahedral copper atom, coordinating via the nitrogen atoms of the nitroso group and the imine group. The oxygen atom on the nitroso group of one ligand displays a Jahn–Teller distorted axial bond to a neighbouring  $[\text{Cu}(\text{cenm})_2]$  moiety forming a  $[\text{Cu}(\text{cenm})_2]_2$  unit. This ligand has an out-of-plane  $\mu_2\text{-}\eta^2(\text{N},\text{N}')\text{Cu}:\eta^1(\text{O})\text{Cu}'$  coordination mode, as observed in the coordination polymer  $[\text{Cu}(\text{cmnm})_2]^{[25]}$  and for the acnm ligand of complex **2**. The other unique cenm ligand of the  $[\text{Cu}(\text{cenm})_2]$  moiety has a  $\mu_2\text{-}\eta^2(\text{N},\text{N}')\text{Cu}:\eta^1(\text{N}'')\text{Cu}'$  coordination mode. This cenm ligand chelates to a copper atom and then bridges through the nitrile group to an adjacent  $[\text{Cu}(\text{cenm})_2]_2$  unit into the axial position of the copper atom (Figure 6, a, Table 5). While dcnm has been shown to coordinate through its nitrile groups,<sup>[9–11,13]</sup> it occurs less frequently with derivative ligands resulting from alcohol addition. Here coordination through the nitrile group facilitates the formation of a 2D sheet with a (4,4) topology (Figure 6, b), with copper dimer nodes. The sheets interdigitate, with ethyl groups of each sheet directed into the cavities of an adjoining sheet (and vice versa).

One water molecule resides in each cavity between  $[\text{Cu}(\text{cenm})_2]_2$  units, acting as a hydrogen-bond donor to the oxygen atoms of coordinating nitroso groups and as a hydrogen-bond acceptor from imino groups. This cross-links the sheets into a 3D  $\alpha$ -Po network. Further hydrogen bonding exists between oxygen atoms of the uncoordinated nitroso groups and the imino NH groups (Figure 6, c).

The presence of two crystallographically unique ligands allows a comparison of their different bonding modes and their effects on bond lengths. The ligand with the  $\mu_2\text{-}\eta^2(\text{N},\text{N}')\text{Cu}:\eta^1(\text{O})\text{Cu}'$  coordination mode has a bond length between nitrogen and oxygen atoms of the nitroso group  $[\text{N}(1)\text{--}\text{O}(1)]$  of 1.287(2) Å, marginally longer than the nitroso group of the other cenm ligand  $[\text{N}(4)\text{--}\text{O}(3)]$  which has a bond length of 1.261(2) Å. This difference can be attributed to the electron density being drawn away from the bond to coordinate to the copper atom as it adopts some character of an oximate group. The former bond is also

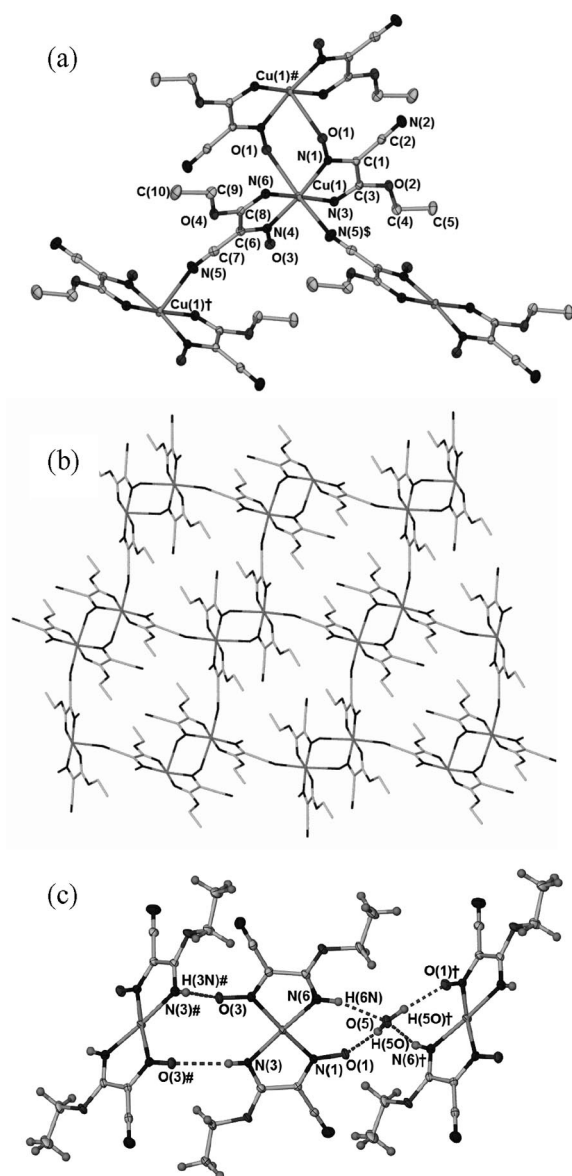


Figure 6. (a) Crystal structure of  $\{[\text{Cu}(\text{cenm})_2]_2 \cdot \text{H}_2\text{O}\}$  (**5**). Ellipsoids at 50% probability, water molecule and hydrogen atoms omitted for clarity. Symmetry elements used:  $^\dagger x, 1-y, z-1/2$ ;  $^\# 3/2-x, 1/2-y, 2-z$ ;  $^\S x, -y, 1/2+z$ . (b) (4,4) Topology of the coordination polymer **5**, hydrogen atoms and water molecule omitted for clarity. (c) Hydrogen bonding within **5**. Key hydrogen bond lengths [Å] and angles [°]:  $\text{N}(6) \cdots \text{O}(5)$  2.867(2);  $\text{N}(6) - \text{H}(6\text{N}) \cdots \text{O}(5)$  161(2);  $\text{O}(5) \cdots \text{O}(1)$  2.727(1);  $\text{O}(5) - \text{H}(5\text{O}) \cdots \text{O}(1)$  160(3);  $\text{N}(3) \cdots \text{O}(3)^\#$  3.070(2);  $\text{N}(3) - \text{H}(3\text{N}) \cdots \text{O}(3)^\#$  177(2). Symmetry elements used:  $^\dagger 2-x, y, 5/2-z$ ;  $^\# 1-x, y, 3/2-z$ .

associated with a shorter C–N(O) bond [1.313(2) Å] than the latter bond as it develops some more C=N character. Interestingly the coordinating nitrile group has no distinguishable change in bond length in comparison to the non-coordinating nitrile group [1.142(2) and 1.140(2) Å respectively]. The infrared spectrum also does not allow for differentiation of the nitrile groups, with only one peak at  $2224\text{ cm}^{-1}$  attributable to a nitrile group, although this is

Table 5. Selected bond lengths [Å] and angles [°] of complex **5**.<sup>[a]</sup>

|  |           |  |            |
|--|-----------|--|------------|
| $\text{Cu}(1) \cdots \text{Cu}(1)^\dagger$ | 7.6427(3) | $\text{Cu}(1) \cdots \text{Cu}(1)^\#$              | 4.3830(4)  |
| $\text{Cu}(1) - \text{N}(1)$               | 2.035(1)  | $\text{N}(1) - \text{Cu}(1) - \text{N}(3)$         | 81.96(6)   |
| $\text{Cu}(1) - \text{N}(3)$               | 1.974(2)  | $\text{N}(4) - \text{Cu}(1) - \text{N}(6)$         | 81.89(6)   |
| $\text{Cu}(1) - \text{N}(4)$               | 2.018(1)  | $\text{N}(1) - \text{Cu}(1) - \text{N}(4)$         | 172.94(5)  |
| $\text{Cu}(1) - \text{N}(6)$               | 1.953(2)  | $\text{N}(6) - \text{Cu}(1) - \text{N}(3)$         | 176.18(6)  |
| $\text{Cu}(1) - \text{O}(1)^\#$            | 2.660(1)  | $\text{N}(1) - \text{Cu}(1) - \text{N}(5)^\S$      | 88.98(6)   |
| $\text{Cu}(1)^\dagger - \text{N}(5)$       | 2.477(2)  | $\text{N}(1) - \text{Cu}(1) - \text{O}(1)^\#$      | 84.85(5)   |
| $\text{N}(1) - \text{O}(1)$                | 1.287(2)  | $\text{N}(3) - \text{Cu}(1) - \text{N}(5)^\S$      | 84.91(6)   |
| $\text{N}(1) - \text{C}(1)$                | 1.313(2)  | $\text{N}(3) - \text{Cu}(1) - \text{O}(1)^\#$      | 98.02(5)   |
| $\text{C}(1) - \text{C}(2)$                | 1.429(2)  | $\text{O}(1)^\# - \text{Cu}(1) - \text{N}(5)^\S$   | 172.72(5)  |
| $\text{C}(2) - \text{N}(2)$                | 1.140(2)  | $\text{O}(1) - \text{N}(1) - \text{Cu}(1)$         | 129.86(10) |
| $\text{N}(3) - \text{C}(3)$                | 1.278(2)  | $\text{C}(7) - \text{N}(5) - \text{Cu}(1)^\dagger$ | 162.57(15) |
| $\text{O}(2) - \text{C}(3)$                | 1.321(2)  | $\text{O}(1) - \text{N}(1) - \text{C}(1)$          | 119.46(13) |
| $\text{N}(4) - \text{O}(3)$                | 1.261(2)  | $\text{O}(3) - \text{N}(4) - \text{C}(6)$          | 121.01(14) |
| $\text{N}(4) - \text{C}(6)$                | 1.336(2)  | $\text{N}(3) - \text{C}(3) - \text{O}(2)$          | 130.65(16) |
| $\text{C}(6) - \text{C}(7)$                | 1.420(2)  | $\text{N}(6) - \text{C}(8) - \text{O}(4)$          | 128.53(16) |
| $\text{C}(7) - \text{N}(5)$                | 1.142(2)  |  |            |
| $\text{N}(6) - \text{C}(8)$                | 1.276(2)  |  |            |
| $\text{O}(4) - \text{C}(8)$                | 1.324(2)  |  |            |

[a] Symmetry elements used:  $^\dagger x, 1-y, z-1/2$ ;  $^\# 3/2-x, 1/2-y, 2-z$ ;  $^\S x, 1-y, 1/2+z$ .

clearly at a higher wavenumber than the corresponding peak in the infrared spectrum of **4** at  $2207\text{ cm}^{-1}$ .

The  $\chi_M T$  data for **5**, per Cu, are plotted as a function of temperature in Figure 2, b.  $\chi_M T$  values remain constant at  $0.41\text{ cm}^3\text{ mol}^{-1}\text{ K}$  ( $1.82\text{ }\mu_B$ ) between 300 and  $\approx 10\text{ K}$ , then decrease to reach  $0.31\text{ cm}^3\text{ mol}^{-1}\text{ K}$  ( $1.57\text{ }\mu_B$ ) at 2 K. The corresponding  $\chi_M$  vs.  $T$  data follow a Curie–Weiss dependence with  $C = 0.42\text{ cm}^3\text{ mol}^{-1}\text{ K}$  and  $\theta = -0.01\text{ K}$  (Figure 2, b). Clearly, any antiferromagnetic coupling within the nitroso-bridged  $\text{Cu}_2$  dinuclear moieties is extremely weak and this is not surprising because bridging is through the  $\text{Cu}(1) - \text{N}(1)\{\text{equatorial}\}\text{O}(1)\{\text{apical}\} - \text{Cu}(1)^\#$  pathways (Figure 6, a) that involve  $\text{Cu}(d_{x^2-y^2}) - \text{O}, \text{N}(p) - \text{Cu}(d_{z^2})$  overlap. The other possible coupling, via  $\text{Cu}(1) - \text{N}(5)^\S(\text{nitrile})$  apical pathways, is negligible. Fitting to a  $S = 1/2$  dimer ( $-2J\mathbf{S}_1 \cdot \mathbf{S}_2$ ) model<sup>[36]</sup> gave best-fit values of  $g = 2.12$ ,  $2J = -1.3\text{ cm}^{-1}$ ,  $N\alpha = 65 \times 10^{-6}\text{ cm}^3\text{ mol}^{-1}$ .

The coordination polymer  $\{[\text{Mn}_3(\text{ccnm})_2(\text{EtOH})_2(\text{OAc})_4] \cdot 2\text{EtOH}\}_\infty$  (**6**) is a 1D chain and the crystals adopt the space group  $P\bar{1}$  (Figure 7, a, Table 6). The repeating unit contains two equivalent seven coordinate manganese atoms and halves of two equivalent six coordinate manganese atoms. The two unique acetate ligands display  $\mu_2\text{-}\eta^2(\text{O}, \text{O}')\text{Mn}-\eta^1(\text{O}')\text{Mn}'$  and  $\mu_2\text{-}\eta^1(\text{O})\text{Mn}:\eta^1(\text{O}')\text{Mn}'$  bridging coordination modes. The  $\mu_3\text{-}\eta^1(\text{O})\text{Mn}:\eta^2(\text{N}, \text{O}')\text{Mn}':\eta^1(\text{O}')\text{Mn}''$  bonding (Figure 7, b) has not previously been observed for the ccnm ligand. The coordination sphere of the seven coordinate manganese atoms contains a bidentate ccnm ligand, two bridging acetate ligands (binding  $\eta^2$  and  $\eta^1$ ), one ethanol and a ccnm ligand from an adjacent unit, bridging via the oxygen atom of the carbamoyl group. The coordination sphere of the six coordinate manganese atoms contain two trans ccnm ligands, which coordinate via the oxygen atoms of the nitroso group, and four acetate ligands (two unique) that display  $\eta^1$  coordination to the metal centre in a trans array.

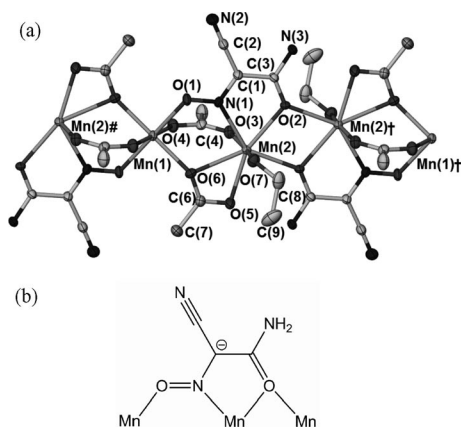


Figure 7. (a) Crystal structure of a portion of the polymeric chain in  $\{[\text{Mn}^{\text{II}}_3(\text{ccnm})_2(\text{EtOH})_2(\text{OAc})_4] \cdot 2\text{EtOH}\}_\infty$  (**6**), non-coordinated ethanol molecules and hydrogen atoms omitted for clarity. Ellipsoids shown at 50% probability. Symmetry element used:  $\dagger 1-x, 1-y, 1-z$ . (b) The  $\mu_3\text{-}\eta^1\text{O}(\text{Mn}):\eta^2\text{N},\text{O}'(\text{Mn}'):\eta^1\text{O}'(\text{Mn}'')$  coordination mode of ccnm.

Table 6. Selected bond lengths [Å] and angles [°] of complex **6**.<sup>[a]</sup>

|                       |           |                            |            |
|-----------------------|-----------|----------------------------|------------|
| Mn(1)···Mn(2)         | 3.7341(9) | Mn(2)···Mn(2) $\dagger$    | 3.7635(14) |
| Mn(1)–O(1)            | 2.168(3)  | O(1)–Mn(1)–O(6)            | 87.5(1)    |
| Mn(1)–O(4)            | 2.193(3)  | O(1)–Mn(1)–O(4)            | 93.0(1)    |
| Mn(1)–O(6)            | 2.130(2)  | O(4)–Mn(1)–O(6)            | 90.8(1)    |
| Mn(2)–N(1)            | 2.330(2)  | O(1)–Mn(1)–O(1) $\#$       | 180.0(1)   |
| Mn(2)–O(2)            | 2.335(3)  | N(1)–Mn(2)–O(2)            | 141.4(1)   |
| Mn(2)–O(3)            | 2.111(3)  | O(6)–Mn(2)–O(5)            | 55.1(1)    |
| Mn(2)–O(5)            | 2.251(3)  | O(3)–Mn(2)–O(7)            | 165.7(1)   |
| Mn(2)–O(6)            | 2.435(3)  | O(2)–Mn(2)–O(7)            | 88.3(1)    |
| Mn(2)–O(7)            | 2.172(3)  | O(5)–Mn(2)–O(3)            | 92.0(1)    |
| Mn(2) $\dagger$ –O(2) | 2.289(2)  | Mn(1)–O(6)–Mn(2)           | 109.6(1)   |
| N(1)–O(1)             | 1.291(4)  | Mn(2)–O(2)–Mn(2) $\dagger$ | 109.0(1)   |
| N(1)–C(1)             | 1.320(4)  | N(1)–O(1)–Mn(1)            | 116.9(2)   |
| O(2)–C(3)             | 1.259(4)  | O(1)–N(1)–Mn(2)            | 126.8(2)   |
| C(3)–N(3)             | 1.322(4)  | O(1)–N(1)–C(1)             | 117.5(3)   |
| C(2)–N(2)             | 1.139(5)  | O(2)–C(3)–N(3)             | 123.5(3)   |

[a] Symmetry elements used:  $\dagger 1-x, 1-y, 1-z$ ;  $\# 1-x, 1-y, -z$ .

Two types of hydrogen bonding are observed along the 1D chain; the oxygen of the coordinating ethanol ligand acts as a hydrogen-bond donor to the ethanol molecule in the lattice. This in turn acts as a hydrogen-bond donor to the oxygen atom of the acetate molecule which bridges between Mn(1) and Mn(2) with a  $\mu_2\text{-}\eta^1\text{-}\eta^1$  coordination mode (Figure 8, a). Intra-chain hydrogen bonding occurs between the amine group of the ccnm ligand and the adjacent bridging acetate ligand which bridges between manganese atoms with a  $\mu_2\text{-}\eta^2\text{-}\eta^1$  coordination mode. The formation of hydrogen-bonded 2D sheets results from the other hydrogen atom of the amine group hydrogen bonding to the nitrile group of a ccnm ligand from a neighbouring chain (Figure 8, b).

Complex  $(\text{Et}_4\text{N})_2[\text{Cu}(\text{ccnm})_4]$  (**7**), crystallises in the space group  $P2_1/n$  with the asymmetric unit containing one unique half of the complex. Two of the ccnm ligands exhibit the usual bidentate chelation via the nitrogen and oxygen atoms of the nitroso and carbamoyl groups, respectively, to

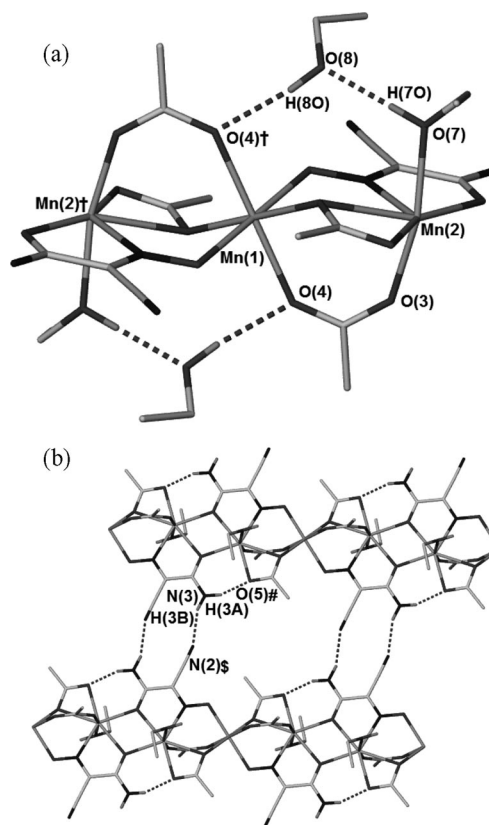


Figure 8. (a) Hydrogen bonding between lattice and coordinated ethanol molecules in **6**. (b) Hydrogen bonding with the amino group acting as the hydrogen-bond donor. Non-hydrogen-bonding hydrogen atoms omitted for clarity. Symmetry elements used:  $\dagger 1-x, 1-y, -z$ ;  $\# 1-x, 1-y, 1-z$ ;  $\S 2-x, 2-y, 1-z$ . Key hydrogen bond lengths [Å] and angles [°]: O(7)···O(8) 2.693(4); O(7)–H(7O)···O(8) 179(6); O(8)···O(4) 2.860(4); O(8)–H(8O)···O(4) 164(4); N(3)···N(2) $\S$  2.993(4); N(3)–H(3B)···N(2) $\S$  159.9; N(3)···O(5) $\#$  2.668(4); N(3)–H(3A)···O(5) $\#$  154.4.

the equatorial positions of the octahedral copper. The other two ccnm ligands coordinate to the Jahn–Teller distorted axial positions of the metal centre through the nitrogen atoms of their nitrile groups. To the best of our knowledge this is the only example of  $\eta^1$  nitrile coordination observed for a derivative of the dcnm ligand (Figure 9, Table 7). This is in contrast to the more normal behaviour of dcnm in a sterically crowded environment around a transition metal, where it often exhibits an  $\eta^1$  coordination through the oxygen atom<sup>[30,31]</sup> or the nitrogen atom<sup>[15,37]</sup> of the nitroso group.

Complex **7** is highly unusual as it is one of the few discrete complexes in which the coordination sphere of the d-block metal is completely filled by dcnm derived ligands and not by additional co-ligands or solvent molecules. Previous examples with relevant ligands included  $[\text{Co}^{\text{III}}(\text{mici})_3]$  (mici = dimethylimidodicarbonimidate),<sup>[38]</sup> where mici is the result of the addition of methanol to both nitrile arms of dca.  $(\text{Et}_4\text{N})_2[\text{Cu}(\text{ccnm})_4]$  is the only discrete complex to have four addition product ligands coordinated to the metal centre, albeit two being bidentate and two unidentate.

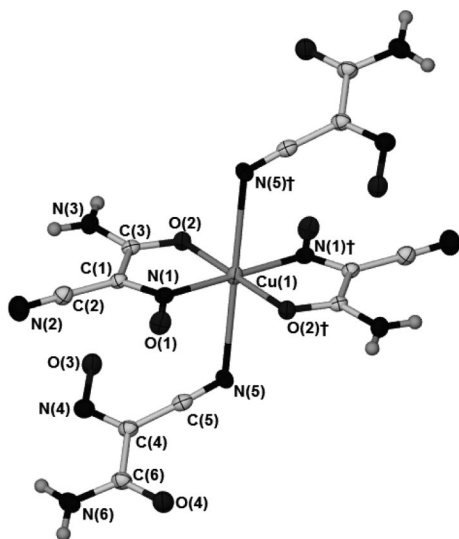


Figure 9. The  $[\text{Cu}(\text{ccnm})_4]^{2-}$  anion in the crystal structure of **7**. Ellipsoids shown at 50% probability. Symmetry element used:  $\dagger 1 - x, -y, -z$ .

Table 7. Selected bond lengths [Å] and angles [°] of complex **7**.<sup>[a]</sup>

|            |          |                              |          |
|------------|----------|------------------------------|----------|
| Cu(1)–N(1) | 1.973(2) | N(1)–Cu(1)–O(2)              | 83.3(1)  |
| Cu(1)–O(2) | 1.955(2) | N(1)–Cu(1)–N(5)              | 82.7(7)  |
| Cu(1)–N(5) | 2.654(2) | O(2)–Cu(1)–N(5)              | 95.9(6)  |
| N(1)–O(1)  | 1.265(2) | N(1)–Cu(1)–O(2) <sup>†</sup> | 96.8(1)  |
| N(1)–C(1)  | 1.328(3) | C(5)–N(5)–Cu(1)              | 119.8(2) |
| N(2)–C(2)  | 1.143(3) | O(1)–N(1)–C(1)               | 121.5(2) |
| O(2)–C(3)  | 1.268(3) | O(2)–C(3)–N(3)               | 121.9(2) |
| N(3)–C(3)  | 1.306(3) | C(1)–C(2)–N(2)               | 178.6(2) |
| N(4)–O(3)  | 1.281(2) | O(3)–N(4)–C(4)               | 117.9(2) |
| N(4)–C(4)  | 1.332(3) | O(4)–C(6)–N(6)               | 123.8(2) |
| N(5)–C(5)  | 1.156(3) | C(4)–C(5)–N(5)               | 175.9(2) |
| O(4)–C(6)  | 1.239(3) |                              |          |
| N(6)–C(6)  | 1.335(3) |                              |          |

[a] Symmetry element used:  $\dagger 1 - x, -y, -z$ .

As with complex **5**, the presence of two crystallographically unique ccnm ligands within the crystal structure of **7** (Figure 10) allows for comparison of different coordination modes and their effect on bond lengths. Although the ligand coordinating through the nitrile group may show a lengthening of the  $\text{C}\equiv\text{N}$  bond [1.156(3) Å] in comparison to the non-coordinating nitrile group [1.143(3) Å], the difference is within  $3\sigma$ , thus prohibiting any definitive distinction between the two. However, the infrared spectra has two  $\nu(\text{CN})$  peaks at  $2218\text{ cm}^{-1}$  and  $2189\text{ cm}^{-1}$  which would correspond to the two different nitrile groups.

Complex  $[\text{Mn}(\text{cmnm})_3\text{Mn}(\text{bipy})(\text{MeOH})](\text{ClO}_4)$  (**8**), crystallises in the space group  $P2_1/m$  and contains the  $[\text{Mn}^{\text{II}}(\text{cmnm})_3]^-$  moiety observed in the  $[\text{Mn}^{\text{III}}\text{Mn}^{\text{II}}_2(\text{cmnm})_6](\text{NO}_3)$  complex.<sup>[12]</sup> It is similar to the  $[\text{Ni}(\text{ccnm})_3]^-$  analogue within  $[\text{Na}(\text{H}_2\text{O})_6][\text{NaNi}_2(\text{ccnm})_6]$ .<sup>[14]</sup> In the metalloligand the octahedral manganese atom is chelated by three cmnm ligands, two of which are crystallographically unique, and is bridged to the other manganese atom via the nitroso group with a  $\mu_2\text{-}\eta^1\text{N}(\text{Mn})\text{:}\eta^1\text{O}(\text{Mn}')$  coordination mode (Figure 11, Table 8). The other manganese atom is also octahedral and has its coordination sphere completed by a

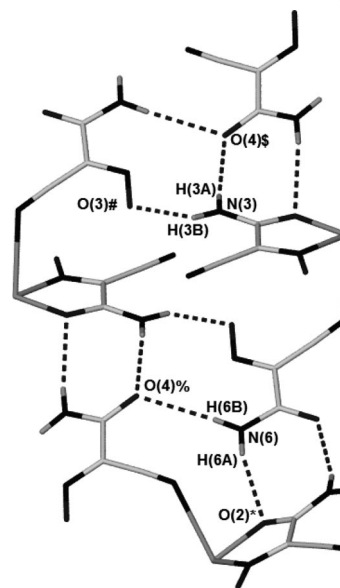


Figure 10. Hydrogen bonding between  $[\text{Cu}(\text{ccnm})_4]^{2-}$  ions, within the crystal structure of **7**, tetraethylammonium counter-cations omitted for clarity. Symmetry elements used:  $\$ x - 1/2, 1/2 - y, z - 1/2$ ;  $\# 1 - x, 1 - y, -z$ ;  $* 1/2 + x, 1/2 - y, 1/2 + z$ ;  $\% 3/2 - x, 1/2 + y, 1/2 - z$ . Key hydrogen bond lengths [Å] and angles [°]: N(3)⋯O(4)<sup>\$</sup> 2.934(2); N(3)–H(3A)⋯O(4)<sup>\$</sup> 151.6; N(3)⋯O(3)<sup>#</sup> 2.777(3); N(3)–H(3B)⋯O(3)<sup>#</sup> 151.5; N(6)⋯O(2)<sup>\*</sup> 3.137(2); N(6)–H(6A)⋯O(2)<sup>\*</sup> 158.8; N(6)⋯O(4)<sup>%</sup> 3.266(3); N(6)–H(6B)⋯O(4)<sup>%</sup> 149.1.

bipy ligand and a methanol molecule, in addition to the three oxygen atoms of the nitroso groups. The configuration of the nitrogen atoms of the imino groups are ideally situated for hydrogen bonding to the perchlorate anion which “docks” into the “back end” of the  $[\text{Mn}(\text{cmnm})_3]^-$  moiety. The crystal structure reveals extensive disorder of methanol solvent contained within the lattice.

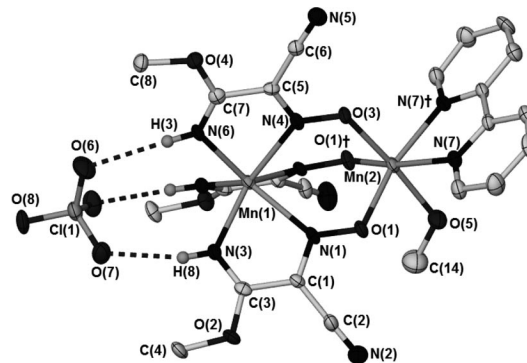


Figure 11. The complex  $[\text{Mn}(\text{cmnm})_3\text{Mn}(\text{bipy})(\text{MeOH})](\text{ClO}_4)$  from within the crystal structure of **8**·3.4MeOH. Non-hydrogen-bonding atoms omitted for clarity, ellipsoids shown at 50% probability. Symmetry element used:  $\dagger x, 1/2 - y, z$ . Hydrogen bond lengths [Å] and angles [°]: N(6)⋯O(6) 3.194(6); N(6)–H(3)⋯O(6) 164(5); N(3)⋯O(7) 3.033(4); N(3)–H(8)⋯O(7) 168(4).

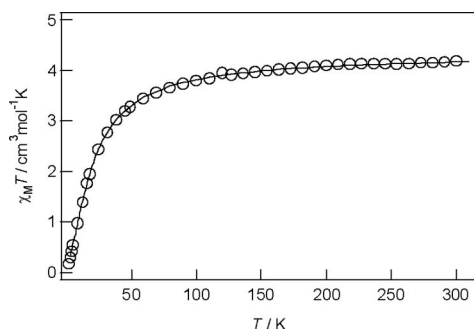
The plot of molar susceptibility,  $\chi_{\text{M}}T$  per Mn, vs. temperature is given for complex **8** in Figure 12. The  $\chi_{\text{M}}T$  values decrease gradually, from  $4.14\text{ cm}^3\text{ mol}^{-1}\text{ K}$  at 300 K ( $5.94\text{ }\mu_{\text{B}}$  per Mn), to ca.  $3.2\text{ cm}^3\text{ mol}^{-1}\text{ K}$  ( $5.06\text{ }\mu_{\text{B}}$ ) at 50 K, reaching  $0.36\text{ cm}^3\text{ mol}^{-1}\text{ K}$  ( $1.7\text{ }\mu_{\text{B}}$ ) at 2 K. The correspond-

Table 8. Selected bond lengths [Å] and angles [°] of complex **8**.<sup>[a]</sup>

|               |            |                              |          |
|---------------|------------|------------------------------|----------|
| Mn(1)···Mn(2) | 3.9152(15) |                              |          |
| Mn(1)–N(1)    | 2.354(3)   | N(1)–Mn(1)–N(3)              | 129.6(1) |
| Mn(1)–N(3)    | 2.212(3)   | N(4)–Mn(1)–N(6)              | 73.3(2)  |
| Mn(1)–N(4)    | 2.294(4)   | N(1)–Mn(1)–N(4)              | 83.6(1)  |
| Mn(1)–N(6)    | 2.194(4)   | N(3)–Mn(1)–N(6)              | 95.0(1)  |
| Mn(2)–O(1)    | 2.125(2)   | N(1)–Mn(1)–N(1) <sup>†</sup> | 84.0(2)  |
| Mn(2)–O(3)    | 2.157(3)   | O(1)–Mn(2)–O(3)              | 92.4(1)  |
| Mn(2)–O(5)    | 2.234(4)   | O(1)–Mn(2)–N(7)              | 93.5(1)  |
| Mn(2)–N(7)    | 2.247(3)   | O(1)–Mn(2)–O(5)              | 84.8(1)  |
| N(1)–O(1)     | 1.315(3)   | N(7)–Mn(2)–N(7) <sup>†</sup> | 72.4(2)  |
| N(1)–C(1)     | 1.309(4)   | Mn(1)–N(1)–O(1)              | 130.8(2) |
| N(3)–C(3)     | 1.267(5)   | Mn(1)–N(4)–O(3)              | 129.5(3) |
| C(3)–O(2)     | 1.342(4)   | N(1)–O(1)–Mn(2)              | 119.8(2) |
| N(4)–O(3)     | 1.299(5)   | O(1)–N(1)–C(1)               | 115.9(3) |
| N(4)–C(5)     | 1.323(6)   | N(3)–C(3)–O(2)               | 129.0(3) |
| N(6)–C(7)     | 1.267(6)   | O(3)–N(4)–C(5)               | 117.2(4) |
| O(4)–C(7)     | 1.335(6)   | N(6)–C(7)–O(4)               | 129.2(5) |

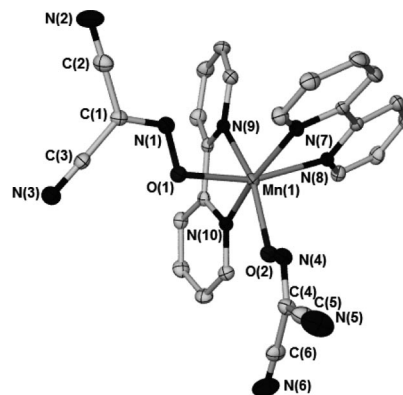
[a] Symmetry element used: <sup>†</sup>  $x, 1/2 - y, z$ .

ing plot of  $\chi_M$  shows a maximum at 10 K indicative of weak antiferromagnetic coupling occurring across the triply bridging Mn–NO–Mn pathways. Fitting to a  $S = 5/2$  Heisenberg  $-2J\mathbf{S}_1\cdot\mathbf{S}_2$  dimer model gave best-fit parameter values of  $g = 1.99$ ,  $J = -1.44 \text{ cm}^{-1}$ . In the many studies reported of triply bridging oximate species, usually heterodinuclear or heterotrinnuclear in character, and often employing pyridinealdoximates<sup>[39]</sup> as bridging groups (analogous to cmnm in **7**), the  $d^5 - d^5$  combination could not be observed for a comparison to be made of  $J$  values. The orbital overlap arguments put forward previously<sup>[33,39,40]</sup> when applied to the  $t_{2g}^3e_g^2 - t_{2g}^3e_g^2$  combination, would predict weak antiferromagnetic coupling, as observed here.

Figure 12. Plot of  $\chi_M T$ , per Mn, for complex **8**. The solid line is the calculated plot using the parameters given in the text.

Complex  $[\text{Mn}(\text{bipy})_2(\text{dcnm})_2]$  (**9**) crystallises from solution in the space group  $P\bar{1}$ . The complex consists of an octahedral manganese atom coordinated by two bidentate bipy ligands and two dcnm ligands with an  $\eta^1$  coordination through the oxygen atom of the nitroso group (Figure 13, Table 9).

Complexes  $[\text{Mn}(\text{bipy})_2(\text{dcnm})(\text{H}_2\text{O})](\text{dcnm})\cdot\text{H}_2\text{O}$  (**10**) and  $[\text{Mn}(\text{bipy})_2(\text{dcnm})(\text{H}_2\text{O})](\text{dcnm})$  (**11**) cocrystallise from the same reaction mixture and contain the same cationic  $[\text{Mn}(\text{bipy})_2(\text{H}_2\text{O})(\text{dcnm})]^+$  complex. The free dcnm counterion in the lattice is disordered over two positions and acts as a hydrogen-bond acceptor to the hydrogen bond

Figure 13. The complex  $[\text{Mn}(\text{bipy})_2(\text{dcnm})_2]$  in the crystal structure of **9**. Ellipsoids shown at 50% probability, hydrogen atoms omitted for clarity.Table 9. Selected bond lengths [Å] for complex **9**.

|             |          |           |          |
|-------------|----------|-----------|----------|
| Mn(1)–O(1)  | 2.159(1) | C(3)–N(3) | 1.142(2) |
| Mn(1)–O(2)  | 2.129(1) | O(2)–N(4) | 1.303(2) |
| Mn(1)–N(7)  | 2.239(1) | N(4)–C(4) | 1.315(2) |
| Mn(1)–N(8)  | 2.267(1) | C(4)–C(5) | 1.431(2) |
| Mn(1)–N(9)  | 2.274(1) | N(1)–O(1) | 1.304(2) |
| Mn(1)–N(10) | 2.289(1) | N(1)–C(1) | 1.317(2) |
| N(1)–O(1)   | 1.304(2) | C(5)–N(5) | 1.144(2) |
| N(1)–C(1)   | 1.317(2) | C(4)–C(6) | 1.435(2) |
| C(1)–C(2)   | 1.428(2) | C(6)–N(6) | 1.140(2) |
| C(2)–N(2)   | 1.141(2) |           |          |

from the water ligands coordinating to the manganese atom (Figure 14, Table 10). Due to the similar colour and morphology of the crystals, manual separation was not possible. Elemental analysis indicates that washing the product with methanol and ether results in the complete removal of lattice water of **10** and the partial removal of water coordinated to the manganese atom.

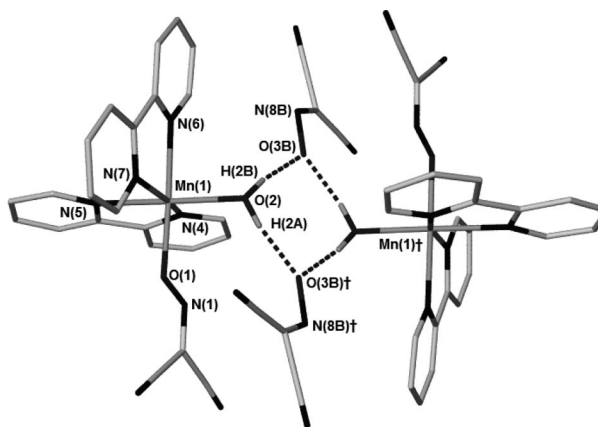
Figure 14. The complex  $[\text{Mn}(\text{bipy})_2(\text{dcnm})(\text{H}_2\text{O})](\text{dcnm})$  in the crystal structure of **11**. Non-hydrogen-bonding hydrogen atoms and one disordered position of the dcnm ligand removed for clarity. Hydrogen bond lengths [Å] and angles [°]: O(2)···O(3B) 2.600(5); O(2)–H(2B)···O(3B) 169(4); O(2)···O(3B)<sup>†</sup> 2.702(6); O(2)–H(2A)···O(3B)<sup>†</sup> 155(4). Symmetry element used: <sup>†</sup>  $2 - x, 1 - y, 2 - z$ . This structure is also representative of complex **10**.

Table 10. Selected bond lengths [Å] for complex **11**. Values also representative of complex **10**.<sup>[a]</sup>

|            |          |                 |          |
|------------|----------|-----------------|----------|
| Mn(1)–O(1) | 2.146(2) | O(1)–Mn(1)–O(2) | 91.9(1)  |
| Mn(1)–O(2) | 2.168(2) | O(1)–Mn(1)–N(4) | 93.7(1)  |
| Mn(1)–N(4) | 2.240(2) | O(1)–Mn(1)–N(6) | 165.0(1) |
| Mn(1)–N(5) | 2.279(2) | O(2)–Mn(1)–N(7) | 95.6(1)  |
| Mn(1)–N(6) | 2.258(2) | O(2)–Mn(1)–N(4) | 95.6(1)  |
| Mn(1)–N(7) | 2.237(2) | O(2)–Mn(1)–N(5) | 170.0(1) |
| O(1)–N(1)  | 1.307(2) | N(1)–O(1)–Mn(1) | 115.1(2) |

[a] Symmetry element used:  $\dagger 2 - x, 1 - y, 2 - z$ .

Complex  $[\text{Cu}(\text{cgnm})_2(\text{H}_2\text{O})_2]$  (**12**), crystallises in the space group  $P\bar{1}$  with half the complex contained within the asymmetric unit (Figure 15, a). Typical of complexes of this type, the Jahn–Teller distorted copper metal centre has its coordination sphere comprised of two trans equatorially  $N,N'$ -chelating cgnm ligands with two aqua ligands in the axial positions. The 2-methoxyethoxy chains of the ligands are directed into the lattice and are not involved in coordination. As with complex **4** an examination of the bond lengths within **12** indicate the cgnm ligand has similar bond orders to those observed in other nucleophilic alcohol addition ligands, with N(1)–O(1) and C(1)–N(1) bond lengths of 1.284(2) and 1.317(2) Å, respectively, supporting the determination of a nitroso, rather than oximate, functional group (Table 11).

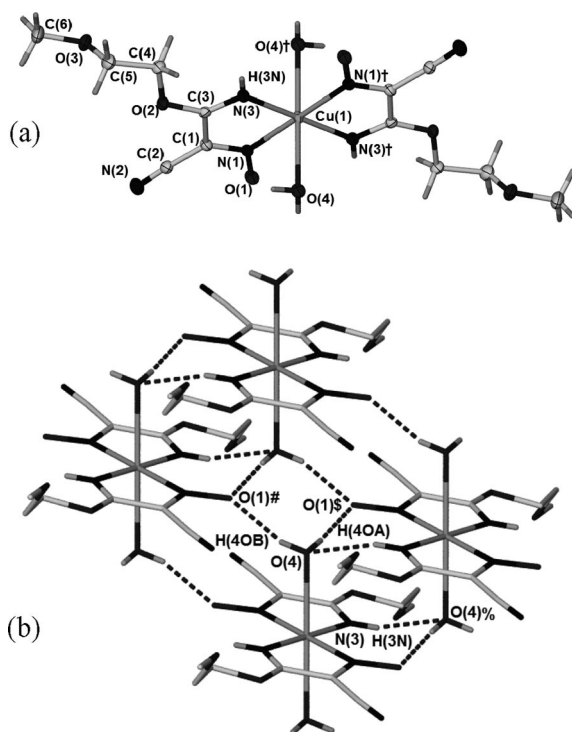


Figure 15. (a) The complex  $[\text{Cu}(\text{cgnm})_2(\text{H}_2\text{O})_2]$  and (b) hydrogen bonding between complex molecules in the crystal structure of **12**. Symmetry elements used:  $\dagger -x, -y, -z$ ;  $\# -x, -y - 1, -z$ ;  $\S 1 + x, y, z$ ;  $\% 1 - x, -y, -z$ . Hydrogen bond lengths [Å] and angles [°]: N(3)⋯O(4)% 2.832(2); N(3)–H(3N)⋯O(4)% 149(2); O(4)⋯O(1) $\S$  2.708(2); O(4)–H(4OA)⋯O(1) $\S$  172(3); O(4)–O(1) $\#$  2.847(2); O(4)–H(4OB)⋯O(1) $\#$  143(2).

Table 11. Selected bond lengths [Å] for complex **12**.<sup>[a]</sup>

|            |          |                           |            |
|------------|----------|---------------------------|------------|
| Cu(1)–N(1) | 2.067(1) | N(1)–Cu(1)–N(3)           | 80.47(5)   |
| Cu(1)–N(3) | 1.959(1) | N(1)–Cu(1)–O(4)           | 81.81(5)   |
| Cu(1)–O(4) | 2.477(2) | N(3)–Cu(1)–O(4)           | 91.88(5)   |
| C(3)–N(3)  | 1.276(2) | N(3)–Cu(1)–N(1) $\dagger$ | 99.53(5)   |
| C(3)–O(2)  | 1.323(2) | O(4)–Cu(1)–N(1) $\dagger$ | 98.19(5)   |
| N(1)–O(1)  | 1.284(2) | N(3)–C(3)–O(2)            | 128.73(14) |
| C(1)–N(1)  | 1.317(2) | Cu(1)–N(1)–C(1)           | 111.61(10) |

[a] Symmetry element used:  $\dagger -x, -y, -z$ .

The hydrogen-bonding network in **12** is the same as that observed in  $[\text{Cu}(\text{cmnm})_2(\text{H}_2\text{O})_2]$ ,<sup>[25]</sup> with the oxygen atom of each nitroso group directed into the lattice acting as a hydrogen-bond acceptor, and with the coordinated water of adjacent complexes acting as the hydrogen-bond donor (Figure 15, b). The imine groups act as hydrogen-bond donors to the oxygen atoms of coordinated waters in adjacent complexes, resulting in the formation of hydrogen-bonded 2D sheets.

## Conclusions

In this paper we report a range of complexes, coordination polymers and new coordination modes of the derivative ligands resulting from the nucleophilic addition of water or alcohol to dcnm. Complexes **1** to **3** contain the dianionic acnm ligand, which results from the deprotonation of ccnm, with bridging modes through the nitroso group. The crystal structure of  $[\text{Cu}(\text{cenm})_2(\text{H}_2\text{O})_2]$  (**4**) is reported in conjunction with the first instance of the ethanol addition ligand cenm being incorporated into a coordination polymer, namely the complex  $\{[\text{Cu}(\text{cenm})_2] \cdot 2\text{H}_2\text{O}\}_\infty$  (**5**). This has a different coordination mode for each unique ligand, one of which unusually shows tridentate coordination. The magnetic properties of **5** are consistent with very weak antiferromagnetic coupling which is in contrast to the magnetic data for the trinuclear species **1** for which strong antiferromagnetic coupling occurs, via the double alkoxo-nitroso bridging, leading to a spin ground state of 1/2. The coordination polymer  $\{[\text{Mn}_3(\text{ccnm})_2\text{EtOH}_2(\text{OAc})_4] \cdot 2\text{EtOH}\}_\infty$  (**6**) contains a ccnm with a previously unobserved  $\mu_2$  bridging mode through the oxygen atom of a carbamoyl group that facilitates the formation of a 1D chain. The discrete complex  $(\text{Et}_4\text{N})_2[\text{Cu}(\text{ccnm})_4]$  (**7**), synthesised from the preformed  $(\text{Et}_4\text{N})(\text{ccnm})$ , has two ligands with an unusual coordination mode, namely solely through the nitrile group, and has various hydrogen-bonding motifs through the carbamoyl and nitroso functional groups.  $[\text{Mn}(\text{cmnm})_3\text{Mn}(\text{bipy})(\text{MeOH})](\text{ClO}_4)$  (**8**) displays weak antiferromagnetic coupling across the three nitroso bridges with a  $J$  value of  $-1.44 \text{ cm}^{-1}$ , a value anticipated from the magnetic exchange observed in triply-bridged oximate compounds. A change in solvent in these  $\text{Mn}^{\text{II}}$ –dcnm reactions resulted in only mononuclear complexes being isolated with no nucleophilic addition to the nitrile groups of dcnm occurring (compounds **9–11**). However, the large alcohol addition ligand cgnm {cyano[imino(2-methoxyethoxy)methyl]nitrosomethanide} in **12** is the result of a copper promoted ad-

dition of ethylene glycol monomethyl ether to dcnm, demonstrating that the nucleophilic addition of alcohols is a general reaction not limited to just small chain alcohols such as methanol or ethanol. More generally, these results demonstrate the existence of a new family of anions that can be obtained through the nucleophilic addition of a range of alcohols to dcnm and other related anions. These anions are remarkably versatile ligands that can show a number of bridging modes between metal centres, and it portends well for their inclusion into higher nuclearity complexes. The heterofunctionalised nature of the ligands derived from nucleophilic addition to dcnm also suggests a future role in the formation of heterometallic complexes. Because oxime groups can bridge manganese atoms in large clusters<sup>[40]</sup> giving single molecule magnets<sup>[41]</sup> and single chain magnets,<sup>[42]</sup> the C–N=O functionality of the present ligand offers scope for building high nuclearity magnetic clusters.

## Experimental Section

**General:** Laboratory reagents and solvents were used as provided commercially. Elemental analyses (C, H, N) were performed by the Campbell Analytical Laboratory, University of Otago, New Zealand. ATR-IR spectra were recorded with a Bruker Equinox 55 series FTIR spectrometer in the range 4000–500 cm<sup>−1</sup> with a resolution of 4 cm<sup>−1</sup>. Ag(dcnm),<sup>[43]</sup> Na(dcnm),<sup>[10]</sup> (Me<sub>4</sub>N)(dcnm)<sup>[37]</sup> and (Et<sub>4</sub>N)(ccnm)<sup>[17]</sup> were prepared according to literature procedures.

**[Cu<sub>3</sub>(acnm)<sub>2</sub>(dmae)<sub>2</sub>(H<sub>2</sub>O)<sub>2</sub>] (1):** Na(dcnm) (30 mg, 256 μmol) and Cu(ClO<sub>4</sub>)<sub>2</sub>·6H<sub>2</sub>O (47 mg, 127 μmol) were dissolved in water (4 mL). 2-(Dimethylamino)ethanol (0.1 mL) was added to the reaction solution. Standing for four days yielded blue tabular crystals of the product which were washed with water, methanol and diethyl ether and air-dried overnight (26 mg, 98%). IR (ATR):  $\tilde{\nu}$  = 3364 (m), 3232 (m, br), 2971 (w), 2881 (w), 2808 (m), 2220 (w), 1592 (s), 1511 (m), 1482 (sh), 1464 (m), 1400 (m), 1260 (m), 1229 (sh), 1147 (m), 1071 (m), 1027 (m), 952 (w), 788 (sh), 744 (w), 660 (w) cm<sup>−1</sup>. C<sub>14</sub>H<sub>26</sub>Cu<sub>3</sub>N<sub>8</sub>O<sub>8</sub> (625.04): calcd. C 26.90, H 4.19, N 17.93; found C 26.73, H 4.18, N 17.82.

**[Cu(acnm)(NH<sub>3</sub>)<sub>2</sub>] (2):** (Me<sub>4</sub>N)(dcnm) (40 mg, 237 μmol) was dissolved in pyridine (4 mL). Cu(ClO<sub>4</sub>)<sub>2</sub>·6H<sub>2</sub>O (44 mg, 119 μmol) dissolved in water (1 mL) and 28% aqueous ammonia (0.5 mL) were added to the reaction solution. Deep blue crystals were isolated after two weeks (5 mg, 20%). C<sub>3</sub>H<sub>7</sub>CuN<sub>5</sub>O<sub>2</sub> (208.67): calcd. C 17.27, H 3.38, N 33.56; found C 17.50, H 3.40, N 33.54.

**[Cu(acnm)(NH<sub>3</sub>)<sub>2</sub>(py)] (3):** (Et<sub>4</sub>N)(ccnm) (71 mg, 293 μmol) dissolved water (0.5 mL) was added to Cu(ClO<sub>4</sub>)<sub>2</sub>·6H<sub>2</sub>O (55 mg, 148 μmol) in water (0.5 mL). Pyridine (5 mL) and 28% aqueous ammonia (0.6 mL) were added to the reaction solution. Deep blue crystals of product formed over two weeks which were washed with pyridine and air-dried (26 mg, 62%). IR (ATR):  $\tilde{\nu}$  = 3337 (s), 3311 (sh), 3223 (s), 3147 (m), 2202 (m), 1635 (w), 1580 (vs), 1571 (sh), 1440 (m), 1398 (m), 1282 (m), 1230 (m), 1215 (m), 1200 (m), 1160 (m), 1035 (w), 1004 (w), 745 (w), 719 (m), 694 (w) cm<sup>−1</sup>. C<sub>8</sub>H<sub>12</sub>Cu<sub>1</sub>N<sub>6</sub>O<sub>2</sub> (287.77): calcd. C 33.39, H 4.20, N 29.20; found C 33.68, H 4.32, N 29.29.

**[Cu(ccnm)<sub>2</sub>(H<sub>2</sub>O)<sub>2</sub>] (4):** (Me<sub>4</sub>N)(dcnm) (50 mg, 297 μmol) and Cu(NO<sub>3</sub>)<sub>2</sub>·3H<sub>2</sub>O (24 mg, 99 μmol) were dissolved in ethanol

(7 mL). Green needle crystals began to form after one month, and after twenty two months the crystals were filtered from the reaction solution, washed with ethanol and diethyl ether and air-dried (17 mg, 45%). IR (ATR):  $\tilde{\nu}$  = 3464 (w, br), 3352 (s), 3266 (w, br), 2995 (w), 2207 (m), 1616 (s), 1414 (m, sh), 1379 (s), 1306 (m, sh), 1146 (s), 1103 (w), 1015 (w), 877 (w), 832 (w), 789 (w), 727 (w), 699 (w) cm<sup>−1</sup>. C<sub>10</sub>H<sub>16</sub>CuN<sub>6</sub>O<sub>6</sub> (379.82): calcd. C 31.62, H 4.25, N 22.13; found C 32.03, H 4.18, N 22.41.

**[{Cu(ccnm)<sub>2</sub>·H<sub>2</sub>O} (5):** Cu(NO<sub>3</sub>)<sub>2</sub>·3H<sub>2</sub>O (23 mg, 95 μmol) and Gd(NO<sub>3</sub>)<sub>3</sub>·6H<sub>2</sub>O (51 mg, 113 μmol) dissolved in ethanol (3 mL) were added to Na(dcnm) (40 mg, 341 μmol) dissolved in ethanol (3 mL). After standing for ten weeks the reaction solution yielded green block crystalline product which was washed with water, ethanol and ether and air-dried overnight (21 mg, 31%). IR (ATR):  $\tilde{\nu}$  = 3168 (m, br), 3005 (w), 2987 (w), 2224 (m), 1618 (s), 1472 (vw), 1433 (s), 1384 (vs), 1360 (m), 1338 (s), 1290 (s), 1248 (sh), 1199 (vw), 1163 (s), 1148 (s), 1109 (s), 1008 (m), 836 (vw), 797 (m), 722 (vw) cm<sup>−1</sup>. C<sub>20</sub>H<sub>20</sub>Cu<sub>2</sub>N<sub>12</sub>O<sub>9</sub> (705.59): calcd. C 34.04, H 3.71, N 23.82; found C 34.03, H 4.02, N 24.06.

**[{Mn<sub>3</sub>(ccnm)<sub>2</sub>(EtOH)<sub>2</sub>(OAc)<sub>4</sub>·2EtOH} (6):** Na(dcnm) (40 mg, 342 μmol) dissolved in ethanol (1 mL) was added to Mn(OAc)<sub>2</sub>·4H<sub>2</sub>O (63 mg, 256 μmol) in an ethanol/water (5:1.5 mL) solution. Small red crystals of **6** formed after three months. Insufficient product could be obtained for further analysis.

**(Et<sub>4</sub>N)<sub>2</sub>[Cu(ccnm)<sub>4</sub>] (7):** (Et<sub>4</sub>N)(ccnm) (71 mg, 293 μmol) in methanol (2 mL) was added to CuCl<sub>2</sub>·2H<sub>2</sub>O (15 mg, 88 μmol) and LaCl<sub>3</sub>·7H<sub>2</sub>O (17 mg, 45 μmol) dissolved in methanol (1 mL). Diethyl ether was slowly diffused into the reaction solution yielding green needle crystals of (Et<sub>4</sub>N)<sub>2</sub>[Cu(ccnm)<sub>4</sub>] in two weeks. The crystals were manually separated from a brown precipitate in a water/methanol solution leading to a slight dissolution of the product, lowering the yield and causing absorption of one molecule of water per copper complex as indicated by elemental analysis (5 mg, 9%). IR (ATR):  $\tilde{\nu}$  = 3314 (vw), 2986 (vw), 2218 (m), 2189 (m), 1665 (m), 1630 (s), 1567 (s), 1486 (m), 1440 (w), 1392 (vs), 1392 (w), 1292 (w), 1250 (s), 1195 (w), 1175 (w), 1095 (s), 1061 (m), 1002 (m), 785 (w), 737 (s), 677 (s) cm<sup>−1</sup>. C<sub>28</sub>H<sub>50</sub>Cu<sub>1</sub>N<sub>14</sub>O<sub>9</sub> (Metal complex plus one absorbed molecule of water) (790.33) calcd. C 42.55, H 6.38, N 24.81; found C 42.96, H 6.42, N 24.51.

**[Mn(ccnm)<sub>3</sub>Mn(bipy)(MeOH)(ClO<sub>4</sub>) (8):** Na(dcnm) (50 mg, 427 μmol) dissolved in methanol (3 mL) was added to Mn(ClO<sub>4</sub>)<sub>2</sub>·6H<sub>2</sub>O (57 mg, 213 μmol) dissolved in methanol (2 mL). 2,2'-Bipyridine (33 mg, 211 μmol) dissolved in methanol (1 mL) was added to the reaction solution. After standing for three weeks the reactions solution yielded red tabular crystals (**8**), which were washed with methanol and diethyl ether and left to air-dry overnight (9 mg, 11%). Exposure to the atmosphere resulted in absorption of one molecule of water per two dinuclear complexes, as indicated by elemental analysis. IR (ATR):  $\tilde{\nu}$  = 3299 (m, br), 2222 (w), 1637 (s), 1598 (w), 1461 (s), 1440 (s), 1431 (s), 1387 (s), 1260 (m), 1196 (m), 1118 (s), 1087 (s), 952 (w), 815 (s), 777 (w), 758 (w), 738 (m), 676 (w), 651 (w), 619 (w) cm<sup>−1</sup>. C<sub>23</sub>H<sub>25</sub>ClMn<sub>2</sub>N<sub>11</sub>O<sub>11.5</sub> (Dinuclear complex plus half a molecule of water) (784.84): calcd. C 35.20, H 3.21, N 19.63; found C 34.74, H 2.88, N 20.12.

**[Mn(bipy)<sub>2</sub>(dcnm)<sub>2</sub>] (9):** (Me<sub>4</sub>N)(dcnm) (50 mg, 297 μmol) in water (2 mL) was added to Mn(ClO<sub>4</sub>)<sub>2</sub>·6H<sub>2</sub>O (25 mg, 69 μmol) in water (2 mL). 2,2'-Bipyridine (15 mg, 96 μmol) in methanol (1 mL) was added to this solution. Over four months crystals of the product formed from the solution, were washed with methanol and left to air-dry (18 mg, 67%). C<sub>26</sub>H<sub>16</sub>MnN<sub>10</sub>O<sub>2</sub> (555.41): calcd. C 56.22, H 2.90, N 25.22; found C 56.34, H 3.01, N 25.43.

**[Mn(bipy)<sub>2</sub>(dcnm)(H<sub>2</sub>O)](dcnm)·H<sub>2</sub>O and (10) [Mn(bipy)<sub>2</sub>(dcnm)-(H<sub>2</sub>O)](dcnm) (11):** (Me<sub>4</sub>N)(dcnm) (50 mg, 297 μmol) in water (2 mL) was added to Mn(ClO<sub>4</sub>)<sub>2</sub>·6H<sub>2</sub>O (25 mg, 69 μmol) in water (4 mL). 2,2'-Bipyridine (15 mg, 96 μmol) was then added as a solid and formed a white suspension. Overnight a crystal of **10** formed from the reaction solution for X-ray crystallography. Ten days later a crystal of **11** was removed from the reaction solution for X-ray crystallography. Both complexes co-crystallised from the reaction solution and their similar colour and morphology prohibited separation. The following day the bulk material was washed with methanol and ether and air-dried (4 mg, 15%). IR (ATR):  $\tilde{\nu}$  = 3248 (vw), 3183 (vw), 3090 (vw), 2220 (m), 1621 (w), 1598 (m), 1576 (w), 1565 (w), 1473 (w), 1437 (s), 1384 (s), 1360 (s), 1316 (w), 1248 (vw), 1168 (s), 1153 (s), 1058 (w), 1014 (m), 758 (m), 735 (m) cm<sup>-1</sup>. Elemental analysis indicates loss of intercalated water of **10** and partial loss of aqua ligands of **10** and **11** upon washing and atmospheric exposure. C<sub>26</sub>H<sub>17</sub>MnN<sub>10</sub>O<sub>2.5</sub> (564.42): calcd. C 55.32, H 3.04, N 24.82; found C 55.20, H 3.12, N 25.02.

**[Cu(cgmm)<sub>2</sub>(H<sub>2</sub>O)<sub>2</sub>] (12):** (Me<sub>4</sub>N)(dcnm) (50 mg, 297 μmol) dissolved in ethylene glycol monomethyl ether (3 mL) was added to Cu(ClO<sub>4</sub>)<sub>2</sub>·6H<sub>2</sub>O (53 mg, 143 μmol) in ethylene glycol monomethyl ether. After standing for two months the reaction solution was allowed to slowly evaporate over two months, yielding olive crystals of **12**, which were washed with ethanol and diethyl ether (42 mg, 66%). IR (ATR):  $\tilde{\nu}$  = 3494 (m, br), 3254 (s, br), 2991 (w), 2945 (w), 2885 (m), 2219 (w), 1628 (s), 1470 (w), 1443 (m), 1412 (s), 1369 (m), 1307 (s), 1244 (w), 1161 (m), 1124 (s), 1098 (w/sh), 1031 (w), 1018 (w), 860 (w), 786 (w) cm<sup>-1</sup>. C<sub>12</sub>H<sub>20</sub>CuN<sub>6</sub>O<sub>8</sub> (439.87): calcd. C 32.77, H 4.58, N 19.11; found C 32.91, H 4.74, N 19.14.

**Crystallographic Details and Data:** Crystals were mounted on fine glass fibres using viscous hydrocarbon oil. Data were collected on a Bruker X8 Apex II CCD (**3**, **4**, **5**, **7**, **9**, **10**, **12**) or Nonius KappaCCD diffractometers (**1**, **2**, **6**, **8**, **3.4MeOH**, **11**), both equipped with graphite-monochromated Mo-K $\alpha$  radiation ( $\lambda$  = 0.71073 Å). Data collection temperatures were maintained at 123 K using open flow N<sub>2</sub> cryostreams. For data collection with a Nonius KappaCCD diffractometer integration was carried out by the program DENZO-SMN and data were corrected for Lorentz-polarisation effects and for absorption using the program SCALEPACK.<sup>[44]</sup> Data integration for data collected with a Bruker X8 Apex II was carried out by the program SAINT and data was correct for Lorentz-polarization effects and for absorption using the Apex program II Suite.<sup>[45]</sup> Solutions were obtained by direct methods or Patterson synthesis using SHELXS-97<sup>[46]</sup> followed by successive refinements using full-matrix least-squares methods against  $F^2$  using SHELXL-97.<sup>[46]</sup> The program X-Seed was used as a graphical SHELX interface.<sup>[47]</sup> Hydrogen atoms attached to carbon atoms were placed in idealised positions and refined against a riding model to the atom to which they are attached. Where possible, hydrogen atoms attached to nitrogen or oxygen atoms were located from the Fourier difference map (see individual crystal data).

CCDC-737442 (for **9**), -737443 (for **4**), -737444 (for **12**), -737445 (for **7**), -737446 (for **8**), -737447 (for **5**), -737448 (for **2**), -737449 (for **6**), -737450 (for **10**), -737451 (for **11**), -737452 (for **1**), -737453 (for **3**) contain the supplementary crystallographic data for this paper. These data can be obtained free of charge from The Cambridge Crystallographic Data Centre via [www.ccdc.cam.ac.uk/data\\_request/cif](http://www.ccdc.cam.ac.uk/data_request/cif).

**[Cu<sub>3</sub>(acnm)<sub>2</sub>(dmae)<sub>2</sub>(H<sub>2</sub>O)<sub>2</sub>] (1):** C<sub>14</sub>H<sub>26</sub>Cu<sub>3</sub>N<sub>8</sub>O<sub>8</sub>,  $M$  = 625.05, blue plate, 0.30 × 0.30 × 0.10 mm<sup>3</sup>, triclinic, space group  $P\bar{1}$  (No. 2),  $a$  = 7.2289(3),  $b$  = 7.5089(3),  $c$  = 10.7812(5) Å,  $\alpha$  = 87.667(2),  $\beta$  = 80.702(2),  $\gamma$  = 88.411(3)°,  $V$  = 576.91(4) Å<sup>3</sup>,  $Z$  = 1,  $D_c$  = 1.799 g/

cm<sup>3</sup>,  $F(000)$  = 317,  $2\theta_{\max}$  = 55.0°, 2926 reflections collected, 2287 unique ( $R_{\text{int}}$  = 0.1010). Final  $GooF$  = 1.022,  $R_1$  = 0.0647,  $wR_2$  = 0.1645,  $R$  indices based on 1687 reflections with  $I > 2\sigma(I)$  (refinement on  $F^2$ ), 165 parameters, 3 restraints.  $\mu$  = 2.797 mm<sup>-1</sup>. Hydrogen atoms attached to nitrogen and oxygen atoms were located from the Fourier difference map and restrained with the DFIX command.

**[Cu(acnm)(NH<sub>3</sub>)<sub>2</sub>] (2):** C<sub>3</sub>H<sub>7</sub>CuN<sub>5</sub>O<sub>2</sub>,  $M$  = 208.68, blue block, 0.30 × 0.20 × 0.20 mm<sup>3</sup>, monoclinic, space group  $P2_1/n$  (No. 14),  $a$  = 8.0740(2),  $b$  = 6.6300(2),  $c$  = 12.7203(4) Å,  $\beta$  = 103.294(1)°,  $V$  = 662.7(2) Å<sup>3</sup>,  $Z$  = 4,  $D_c$  = 2.092 g/cm<sup>3</sup>,  $F(000)$  = 420,  $2\theta_{\max}$  = 55.0°, 3874 reflections collected, 1526 unique ( $R_{\text{int}}$  = 0.0538). Final  $GooF$  = 1.048,  $R_1$  = 0.0307,  $wR_2$  = 0.0753,  $R$  indices based on 1343 reflections with  $I > 2\sigma(I)$  (refinement on  $F^2$ ), 128 parameters, 7 restraints.  $\mu$  = 3.249 mm<sup>-1</sup>. Hydrogen atoms attached to nitrogen atoms were located from the Fourier difference map and restrained with the DFIX command.

**[Cu(acnm)(NH<sub>3</sub>)<sub>2</sub>(py)] (3):** C<sub>8</sub>H<sub>12</sub>CuN<sub>6</sub>O<sub>2</sub>,  $M$  = 287.78, blue block, 0.20 × 0.20 × 0.15 mm<sup>3</sup>, orthorhombic, space group  $Pbca$  (No. 61),  $a$  = 13.1902(3),  $b$  = 13.2981(3),  $c$  = 13.4531(3) Å,  $V$  = 2359.74(9) Å<sup>3</sup>,  $Z$  = 8,  $D_c$  = 1.620 g/cm<sup>3</sup>,  $F(000)$  = 1176,  $2\theta_{\max}$  = 55.0°, 13107 reflections collected, 2696 unique ( $R_{\text{int}}$  = 0.0214). Final  $GooF$  = 1.066,  $R_1$  = 0.0201,  $wR_2$  = 0.0525,  $R$  indices based on 2451 reflections with  $I > 2\sigma(I)$  (refinement on  $F^2$ ), 182 parameters, 7 restraints.  $\mu$  = 1.852 mm<sup>-1</sup>. Hydrogen atoms attached to nitrogen atoms were located from the Fourier difference map and restrained with the DFIX command.

**[Cu(cenm)<sub>2</sub>(H<sub>2</sub>O)<sub>2</sub>] (4):** C<sub>10</sub>H<sub>16</sub>CuN<sub>6</sub>O<sub>6</sub>,  $M$  = 379.83, green needle, 0.20 × 0.10 × 0.04 mm<sup>3</sup>, triclinic, space group  $P\bar{1}$  (No. 2),  $a$  = 5.0402(4),  $b$  = 6.8373(5),  $c$  = 11.8858(8) Å,  $\alpha$  = 75.828(4),  $\beta$  = 85.379(4),  $\gamma$  = 81.262(4)°,  $V$  = 392.12(5) Å<sup>3</sup>,  $Z$  = 1,  $D_c$  = 1.608 g/cm<sup>3</sup>,  $F(000)$  = 195,  $T$  = 200(1) K,  $2\theta_{\max}$  = 55.0°, 4125 reflections collected, 1801 unique ( $R_{\text{int}}$  = 0.0201). Final  $GooF$  = 1.099,  $R_1$  = 0.0277,  $wR_2$  = 0.0613,  $R$  indices based on 1742 reflections with  $I > 2\sigma(I)$  (refinement on  $F^2$ ), 119 parameters, 0 restraints.  $\mu$  = 1.433 mm<sup>-1</sup>.

**{[Cu(cenm)<sub>2</sub>·H<sub>2</sub>O]}<sub>∞</sub> (5):** C<sub>20</sub>H<sub>26</sub>Cu<sub>2</sub>N<sub>12</sub>O<sub>9</sub>,  $M$  = 705.61, Green block, 0.25 × 0.23 × 0.20 mm<sup>3</sup>, monoclinic, space group  $C2/c$  (No. 15),  $a$  = 16.0822(3),  $b$  = 17.8062(4),  $c$  = 12.1685(2) Å,  $\beta$  = 123.9700(10)°,  $V$  = 2889.89(10) Å<sup>3</sup>,  $Z$  = 4,  $D_c$  = 1.622 g/cm<sup>3</sup>,  $F(000)$  = 1440,  $2\theta_{\max}$  = 55.0°, 9860 reflections collected, 3281 unique ( $R_{\text{int}}$  = 0.0231). Final  $GooF$  = 1.056,  $R_1$  = 0.0264,  $wR_2$  = 0.0622,  $R$  indices based on 2933 reflections with  $I > 2\sigma(I)$  (refinement on  $F^2$ ), 209 parameters, 1 restraint. Lp and absorption corrections applied,  $\mu$  = 1.541 mm<sup>-1</sup>. Hydrogen atoms attached to nitrogen and oxygen atoms were located from the Fourier difference map and restrained with the DFIX command.

**{[Mn<sub>3</sub>(cenm)<sub>2</sub>(EtOH)<sub>2</sub>(OAc)<sub>4</sub>·2EtOH]}<sub>∞</sub> (6):** C<sub>22</sub>H<sub>40</sub>Mn<sub>3</sub>N<sub>6</sub>O<sub>16</sub>,  $M$  = 809.42, orange diamond, 0.20 × 0.20 × 0.10 mm<sup>3</sup>, triclinic, space group  $P\bar{1}$  (No. 2),  $a$  = 9.0675(18),  $b$  = 9.5203(19),  $c$  = 11.012(2) Å,  $\alpha$  = 103.961(4),  $\beta$  = 101.049(5),  $\gamma$  = 98.456(6)°,  $V$  = 886.6(3) Å<sup>3</sup>,  $Z$  = 1,  $D_c$  = 1.516 g/cm<sup>3</sup>,  $F(000)$  = 417,  $2\theta_{\max}$  = 55.0°, 8738 reflections collected, 4032 unique ( $R_{\text{int}}$  = 0.1131). Final  $GooF$  = 1.018,  $R_1$  = 0.0564,  $wR_2$  = 0.1272,  $R$  indices based on 2906 reflections with  $I > 2\sigma(I)$  (refinement on  $F^2$ ), 226 parameters, 2 restraints.  $\mu$  = 1.125 mm<sup>-1</sup>. Hydrogen atoms attached to oxygen atoms were located from the Fourier difference map and restrained with the DFIX command.

**(Et<sub>4</sub>N)<sub>2</sub>[Cu(cenm)<sub>4</sub>] (7):** C<sub>28</sub>H<sub>48</sub>CuN<sub>14</sub>O<sub>8</sub>,  $M$  = 772.34, green needle, 0.50 × 0.30 × 0.15 mm<sup>3</sup>, monoclinic, space group  $P2_1/n$  (No. 14),  $a$  = 10.3502(3),  $b$  = 10.1528(3),  $c$  = 16.9498(5) Å,  $\beta$  = 93.916(2)°,  $V$

= 1776.99(9) Å<sup>3</sup>,  $Z = 2$ ,  $D_c = 1.443$  g/cm<sup>3</sup>,  $F(000) = 814$ ,  $2\theta_{\max} = 55.0^\circ$ , 14294 reflections collected, 4077 unique ( $R_{\text{int}} = 0.0289$ ). Final  $\text{Goof} = 1.049$ ,  $R_1 = 0.0512$ ,  $wR_2 = 0.1297$ ,  $R$  indices based on 3466 reflections with  $I > 2\sigma(I)$  (refinement on  $F^2$ ), 236 parameters, 0 restraints.  $\mu = 0.683$  mm<sup>-1</sup>. Hydrogen atoms attached to nitrogen atoms were located from the Fourier difference map and restrained with the DFIX command.

**[Mn(cmmn)<sub>3</sub>Mn(bipy)(MeOH)](ClO<sub>4</sub>)·3.4MeOH (8·3.4MeOH):** C<sub>26.40</sub>H<sub>37.60</sub>ClMn<sub>2</sub>N<sub>11</sub>O<sub>14.40</sub>,  $M = 884.80$ , red block,  $0.20 \times 0.20 \times 0.10$  mm<sup>3</sup>, monoclinic, space group  $P2_1/m$  (No. 11),  $a = 8.8914(2)$ ,  $b = 13.386(4)$ ,  $c = 16.349(5)$  Å,  $\beta = 102.49(1)^\circ$ ,  $V = 1899.9(7)$  Å<sup>3</sup>,  $Z = 2$ ,  $D_c = 1.547$  g/cm<sup>3</sup>,  $F(000) = 910$ ,  $2\theta_{\max} = 55.0^\circ$ , 12001 reflections collected, 4556 unique ( $R_{\text{int}} = 0.1173$ ). Final  $\text{Goof} = 0.974$ ,  $R_1 = 0.0581$ ,  $wR_2 = 0.1251$ ,  $R$  indices based on 2519 reflections with  $I > 2\sigma(I)$  (refinement on  $F^2$ ), 318 parameters, 10 restraints.  $\mu = 0.814$  mm<sup>-1</sup>. Hydrogen atoms attached to nitrogen atoms were located from the Fourier difference map and allowed to refine freely. The alcohol hydrogen atoms of the methanol molecules could not be located in Fourier difference map and were not refined. Carbon to oxygen bond lengths in the disordered methanol molecules were restrained with the DFIX command. The asymmetric unit contains one methanol disordered over two positions with site occupancies refined against each other (37:63). A further partial occupancy methanol (70%) was manually refined in two positions (20:50).

**[Mn(bipy)<sub>2</sub>(dcnm)<sub>2</sub>] (9):** C<sub>26</sub>H<sub>16</sub>MnN<sub>10</sub>O<sub>2</sub>,  $M = 555.43$ , orange prism,  $0.22 \times 0.18 \times 0.15$  mm<sup>3</sup>, triclinic, space group  $P\bar{1}$  (No. 2),  $a = 9.0435(2)$ ,  $b = 10.3753(2)$ ,  $c = 15.1752(3)$  Å,  $\alpha = 79.610(1)$ ,  $\beta = 87.609(1)$ ,  $\gamma = 65.608(1)^\circ$ ,  $V = 1274.67(5)$  Å<sup>3</sup>,  $Z = 2$ ,  $D_c = 1.447$  g/cm<sup>3</sup>,  $F(000) = 566$ ,  $2\theta_{\max} = 55.0^\circ$ , 10585 reflections collected, 5854 unique ( $R_{\text{int}} = 0.0212$ ). Final  $\text{Goof} = 1.028$ ,  $R_1 = 0.0331$ ,  $wR_2 = 0.0764$ ,  $R$  indices based on 5187 reflections with  $I > 2\sigma(I)$  (refinement on  $F^2$ ), 352 parameters, 0 restraints  $\mu = 0.563$  mm<sup>-1</sup>.

**[Mn(bipy)<sub>2</sub>(dcnm)(H<sub>2</sub>O)](dcnm)·H<sub>2</sub>O (10):** C<sub>26</sub>H<sub>20</sub>MnN<sub>10</sub>O<sub>4</sub>,  $M = 591.46$ , orange block,  $0.60 \times 0.50 \times 0.30$  mm<sup>3</sup>, triclinic, space group  $P\bar{1}$  (No. 2),  $a = 9.5202(3)$ ,  $b = 11.8669(4)$ ,  $c = 13.3734(4)$  Å,  $\alpha = 65.043(1)$ ,  $\beta = 89.887(1)$ ,  $\gamma = 79.199(1)^\circ$ ,  $V = 1340.47(7)$  Å<sup>3</sup>,  $Z = 2$ ,  $D_c = 1.465$  g/cm<sup>3</sup>,  $F(000) = 602$ ,  $2\theta_{\max} = 55.0^\circ$ , 9286 reflections collected, 5841 unique ( $R_{\text{int}} = 0.0170$ ). Final  $\text{Goof} = 1.038$ ,  $R_1 = 0.0457$ ,  $wR_2 = 0.1235$ ,  $R$  indices based on 5338 reflections with  $I > 2\sigma(I)$  (refinement on  $F^2$ ), 415 parameters, 12 restraints.  $\mu = 0.546$  mm<sup>-1</sup>. Free dcnm bond lengths restrained by DFIX, and the anion was disordered over two positions. Site occupancies were refined against each other (54:46) although ADP values indicate further disorder. Hydrogen atoms attached to the free water molecule could not be located from the Fourier transform map and were not refined. Hydrogen atoms attached to coordinating water molecule were located from the Fourier difference map and restrained with the DFIX command.

**[Mn(bipy)<sub>2</sub>(dcnm)(H<sub>2</sub>O)](dcnm) (11):** C<sub>26</sub>H<sub>18</sub>MnN<sub>10</sub>O<sub>3</sub>,  $M = 573.44$ , orange block,  $0.60 \times 0.40 \times 0.30$  mm<sup>3</sup>, monoclinic, space group  $P2_1/c$  (No. 14),  $a = 11.0537(2)$ ,  $b = 16.9890(3)$ ,  $c = 14.8872(3)$  Å,  $\beta = 110.210(10)^\circ$ ,  $V = 2623.56(8)$  Å<sup>3</sup>,  $Z = 4$ ,  $D_c = 1.452$  g/cm<sup>3</sup>,  $F(000) = 1172$ ,  $2\theta_{\max} = 55.0^\circ$ , 12937 reflections collected, 6034 unique ( $R_{\text{int}} = 0.0847$ ). Final  $\text{Goof} = 1.061$ ,  $R_1 = 0.0458$ ,  $wR_2 = 0.1062$ ,  $R$  indices based on 4734 reflections with  $I > 2\sigma(I)$  (refinement on  $F^2$ ), 388 parameters, 6 restraints.  $\mu = 0.552$  mm<sup>-1</sup>. Free dcnm bond lengths were restrained by DFIX, and the nitroso groups were disordered over two positions with site occupancies refined against each other (56:44) although ADP values indicate further disorder. Disordered nitrile groups could not be accurately refined separately. Hydrogen atoms attached to the

coordinating water molecule were located from the Fourier difference map and restrained with the DFIX command.

**[Cu(cgmm)<sub>2</sub>(H<sub>2</sub>O)<sub>2</sub>] (12):** C<sub>12</sub>H<sub>20</sub>CuN<sub>6</sub>O<sub>8</sub>,  $M = 439.88$ , green plate,  $0.30 \times 0.30 \times 0.10$  mm<sup>3</sup>, triclinic, space group  $P\bar{1}$  (No. 2),  $a = 4.8634(2)$ ,  $b = 6.9532(2)$ ,  $c = 13.9302(5)$  Å,  $\alpha = 79.564(2)$ ,  $\beta = 87.168(2)$ ,  $\gamma = 80.869(2)^\circ$ ,  $V = 457.30(3)$  Å<sup>3</sup>,  $Z = 1$ ,  $D_c = 1.597$  g/cm<sup>3</sup>,  $F(000) = 227$ ,  $2\theta_{\max} = 55.0^\circ$ , 4810 reflections collected, 2090 unique ( $R_{\text{int}} = 0.0233$ ). Final  $\text{Goof} = 1.041$ ,  $R_1 = 0.0271$ ,  $wR_2 = 0.0651$ ,  $R$  indices based on 2008 reflections with  $I > 2\sigma(I)$  (refinement on  $F^2$ ), 137 parameters, 3 restraints.  $\mu = 1.248$  mm<sup>-1</sup>.

**Magnetic Susceptibility Measurements:** Powder samples of mass ca. 20 mg were accurately weighed and contained in calibrated gel capsules that were held rigidly in the centre of a drinking straw that was fixed to the end of the sample rod, the latter being inserted into the sample chamber of a Quantum Design liquid helium MPMS5 Squid magnetometer. The applied DC field used was 1 Tesla and the instrument was calibrated against the accurately known magnetisation values of a Pd pellet, supplied by Quantum Design, and further checked against the well known Curie–Weiss molar susceptibility data of CuSO<sub>4</sub>·5H<sub>2</sub>O. Diamagnetic corrections for the ligands were obtained using Pascal's tables.

## Acknowledgments

We thank the Australian Research Council for funding to S. R. B. and K. S. M. and for a postdoctoral fellowship (to D. R. T.). A. S. R. C. acknowledges the award of an Australian Postgraduate Award scholarship.

- [1] J. Kohout, M. Hvastijová, J. Gažo, *Coord. Chem. Rev.* **1978**, 27, 141–172.
- [2] a) J. Kožíšek, M. Hvastijová, J. Kohout, *Inorg. Chim. Acta* **1990**, 168, 157–158; b) M.-L. Tong, Y.-M. Wu, Y.-X. Tong, X.-M. Chen, H.-C. Chang, S. Kitagawa, *Eur. J. Inorg. Chem.* **2003**, 2385–2388.
- [3] M. Hvastijová, J. Kohout, H. Köhler, G. Ondrejovič, *Z. Anorg. Allg. Chem.* **1988**, 566, 111–120.
- [4] M. Hvastijová, J. Kohout, R. Skirl, *Collect. Czech. Chem. Commun.* **1993**, 58, 845.
- [5] J. K. Bjernemose, C. J. McKenzie, P. R. Raithby, S. J. Teat, *Dalton Trans.* **2003**, 2639–2640.
- [6] M. Hvastijová, J. Kohout, J. W. Buchler, R. Boča, J. Kožíšek, L. Jäger, *Coord. Chem. Rev.* **1998**, 175, 17–42.
- [7] A. S. R. Chesman, D. R. Turner, G. B. Deacon, S. R. Batten, *Chem. Asian J.* **2009**, 4, 761–769.
- [8] N. Arulsamy, D. Bohle, *J. Org. Chem.* **2000**, 65, 1139–1143.
- [9] Y. M. Chow, D. Britton, *Acta Crystallogr., Sect. B* **1974**, 30, 1117–1118.
- [10] a) N. Arulsamy, D. S. Bohle, B. G. Doletski, *Inorg. Chem.* **1999**, 38, 2709–2715; b) G. Glover, N. Gerasimchuk, R. Biagioni, K. V. Domasevitch, *Inorg. Chem.* **2009**, 48, 2371–2382.
- [11] Y. M. Chow, D. Britton, *Acta Crystallogr., Sect. B* **1974**, 30, 147–151.
- [12] D. J. Price, S. R. Batten, K. J. Berry, B. Moubaraki, K. S. Murray, *Polyhedron* **2003**, 22, 165–176.
- [13] V. Jacob, S. Mann, G. Huttner, O. Walter, L. Zsolnai, E. Kaifer, P. Rutsch, P. Kircher, E. Bill, *Eur. J. Inorg. Chem.* **2001**, 10, 2625–2640.
- [14] N. N. Gerasimchuk, N. K. Dalley, *J. Coord. Chem.* **2004**, 57, 1431–1445.
- [15] K. E. Bessler, L. L. Romualdo, P. d. T. S. Filho, V. M. Deflon, C. Maichle-Mössmer, *Z. Anorg. Allg. Chem.* **2001**, 627, 651–654.
- [16] D. R. Turner, S. R. Batten, *Coordination Chemistry Research Progress* (Eds.: T. W. Carter, K. S. Verley), Nova Science Publishers, Hauppauge, **2008**.

- [17] A. S. R. Chesman, D. R. Turner, B. Moubaraki, K. S. Murray, G. B. Deacon, S. R. Batten, *Chem. Eur. J.* **2009**, *15*, 5203–5207.
- [18] D. R. Turner, S. N. Pek, S. R. Batten, *Chem. Asian J.* **2007**, *2*, 1534–1539.
- [19] D. R. Turner, S. R. Batten, *CrystEngComm* **2008**, *10*, 170–172.
- [20] D. R. Turner, S. N. Pek, S. R. Batten, *New J. Chem.* **2008**, *32*, 719–726.
- [21] D. R. Turner, S. N. Pek, S. R. Batten, *CrystEngComm* **2009**, *11*, 87–93.
- [22] D. R. Turner, R. MacDonald, W. T. Lee, S. R. Batten, *CrystEngComm* **2009**, *11*, 298–305.
- [23] D. R. Turner, S. N. Pek, J. D. Cashion, B. Moubaraki, K. S. Murray, S. R. Batten, *Dalton Trans.* **2008**, 6877–6879.
- [24] S. R. Batten, K. S. Murray, *Coord. Chem. Rev.* **2003**, *246*, 103–130.
- [25] A. S. R. Chesman, D. R. Turner, D. J. Price, B. Moubaraki, K. S. Murray, G. B. Deacon, S. R. Batten, *Chem. Commun.* **2007**, 3541–3543.
- [26] a) N. Gerasimchuk, L. Goeden, P. Durham, C. Barnes, J. F. Cannon, S. Silchenko, I. Hidalgo, *Inorg. Chim. Acta* **2008**, *361*, 1983–2001; b) N. Gerasimchuk, T. Maher, P. Durham, K. V. Domasevitch, J. Wilking, A. Mokhir, *Inorg. Chem.* **2007**, *46*, 7268–7284; c) D. Eddings, C. Barnes, N. Gerasimchuk, P. Durham, K. Domasevich, *Inorg. Chem.* **2004**, *43*, 3894–3909.
- [27] a) T. Y. Sliva, A. M. Duda, T. Glowiak, I. O. Fritsky, V. M. Amirkhanov, A. A. Mokhir, H. Kozlowski, *J. Chem. Soc., Dalton Trans.* **1997**, 273–276; b) A. A. Mokhir, R. Vilaplana, F. Gonzalez-Vilchez, I. O. Fritsky, K. V. Domasevitch, N. M. Dudarenko, *Polyhedron* **1998**, *17*, 2693–2697.
- [28] M. Hvastijová, J. Kohout, J. Kožíšek, L. Jäger, I. Svoboda, Monograph Series of the International Conferences on Coordination Chemistry held periodically at Smolenice in Slovakia, **1997**, *3*, 159–164, Slovak Technical University Press.
- [29] Z. Xu, L. K. Thompson, D. O. Miller, *Chem. Commun.* **2001**, 1170–1171.
- [30] I. Potočník, M. Vavra, L. Jäger, P. Baran, C. Wagner, *Transition Met. Chem.* **2008**, *33*, 1–8.
- [31] M. Dunaj-Jurčo, D. Mikloš, I. Potočník, L. Jäger, *Acta Crystallogr., Sect. C* **1998**, *54*, 1763–1765.
- [32] W. Mazurek, K. J. Berry, K. S. Murray, M. J. O' Connor, M. R. Snow, A. G. Wedd, *Inorg. Chem.* **1982**, *21*, 3071–3080.
- [33] F. Birkelbach, M. Winter, U. Flörke, H.-J. Haupt, C. Butzlaff, M. Lengen, E. Bill, A. X. Trautwein, K. Wiegardt, P. Chaudhuri, *Inorg. Chem.* **1994**, *33*, 3990–4001.
- [34] R. Veit, J. J. Girerd, O. Kahn, F. Roberts, Y. Jeannin, *Inorg. Chem.* **1986**, *25*, 4175–4180.
- [35] P. Chaudhuri, M. Winter, B. P. C. Della Védova, E. Bill, A. Trautwein, S. Gehring, P. Fleischauer, B. Nuber, J. Weiss, *Inorg. Chem.* **1991**, *30*, 2148–2157.
- [36] B. Bleaney, K. D. Bowers, *Proc. R. Soc. London, Sect. A* **1952**, *214*, 451–465.
- [37] D. S. Bohle, B. J. Conklin, C.-H. Hung, *Inorg. Chem.* **1995**, *34*, 2569–2581.
- [38] R. Boča, M. Hvastijová, J. Kožíšek, *J. Chem. Soc., Dalton Trans.* **1995**, 1921–1923.
- [39] S. Ross, T. Weyermüller, E. Bill, K. Wiegardt, P. Chaudhuri, *Inorg. Chem.* **2001**, *40*, 6656–6665.
- [40] P. Chaudhuri, *Coord. Chem. Rev.* **2003**, *243*, 143–190.
- [41] C. J. Milios, W. Wernsdorfer, S. Moggach, S. Parsons, S. P. Perlepes, G. Christou, E. K. Brechin, *J. Am. Chem. Soc.* **2007**, *129*, 2754–2755.
- [42] H.-B. Zu, B.-W. Wang, F. Pan, Z.-M. Wang, S. Gao, *Angew. Chem. Int. Ed.* **2007**, *46*, 7388–7392.
- [43] G. Longo, *Gazz. Chim. Ital.* **1931**, *61*, 575.
- [44] Z. Otwinowski, W. Minor (Eds.), *Methods in Enzymology*, vol. 276 (Eds.: C. W. Carter Jr., R. M. Sweet), p. 99, 307–326, Academic Press, New York, **1997**.
- [45] *ApexII*, v2.1.0, Bruker AXS Ltd., Madison, Wisconsin, **2005**.
- [46] G. M. Sheldrick, *Acta Crystallogr., Sect. A* **2008**, *64*, 112–122.
- [47] L. J. Barbour, *J. Supramol. Chem.* **2001**, *1*, 189–191.

Received: August 10, 2009

Published Online: November 26, 2009

# Synthesis and Characterisation of 2,2-Bis(hydroxymethyl)-1,3-diselenolato Metal(II) Complexes Bearing Various Phosphanes<sup>[‡]</sup>

Tobias Niksch,<sup>[a]</sup> Helmar Görls,<sup>[a]</sup> Manfred Friedrich,<sup>[a]</sup> Raija Oilunkaniemi,<sup>[b]</sup> Risto Laitinen,<sup>[b]</sup> and Wolfgang Weigand<sup>\*[a]</sup>

*Dedicated to Prof. Wolfdieter A. Schenk on the occasion of his 65th birthday*

**Keywords:** Steric demand / Selenolato ligands / Phosphane ligands / Hydrogen bonds / X-ray diffraction

An improved synthesis of 4,4-bis(hydroxymethyl)-1,2-diselenolane and the complexation properties of the corresponding diselenolato dianion to group-10 metals are reported. We describe an efficient and straightforward procedure that bypasses the isolation of the malodorous and air-sensitive diselenol and starts with the diselenide and an appropriate group-10 metal complex bearing phosphane and chlorido ligands. A series of complexes with various mono- and bidentate phosphanes is prepared and characterised by multinuclear NMR spectroscopy, mass spectrometry, and elemental analysis. Furthermore, the structure of most complexes is studied by single-crystal X-ray diffraction to establish their supramolecular arrangement in the solid state. Con-

sequently, several group-10 metal complexes with P–M–P angles (bite angles) in the range from 71–108° are investigated. The use of the sterically demanding bridging phosphane 4,5-bis(diphenylphosphanyl)-9,9-dimethylxanthene, which exhibits a large bite angle yields a mixture of a di- and trinuclear complex. While the platinum-containing complexes are proven to be rather stable, the palladium and nickel analogues tend to decompose. Especially, the nickel complexes were found to be sensitive against oxidation. This circumstance leads to the formation of the so far unknown 1,8-bis(diphenylphosphanyl)naphthalene monooxide, the formation and structure of which could be confirmed from NMR spectroscopic data and single-crystal X-ray diffraction.

## Introduction

Almost a century ago the first metal complexes of organoselenium compounds were reported. In 1911 Fritzmann prepared the first selenoether platinum(II) complexes,<sup>[1a]</sup> and some years later the corresponding palladium(II) analogues.<sup>[1b]</sup> Since that time the chemistry of selenium-containing ligands has developed rapidly. In particular those complexes are of great interest in means of catalytic applications<sup>[2]</sup> and as precursors for electronic devices.<sup>[3]</sup> Beyond this, attention is paid to their biological activities as they are promising antitumor agents.<sup>[4]</sup> A huge variety of selenoether complexes of group-10 metals has been reported during the last decades.<sup>[5]</sup> Though the ligand chemistry of sele-

nols has mainly been concerned with mono-<sup>[6a]</sup> and dinuclear<sup>[6b]</sup> complexes of monodentate selenols. Information of bis(phosphane) platinum-group metal complexes of bidentate organoselenium derivatives is rather sparse and is mainly concerned with Pt<sup>II</sup> complexes of diselenols bearing aromatic fragments in the bridging moieties<sup>[7]</sup> or complexes of diselenocarbonate derivatives<sup>[8]</sup> or diselenolenes.<sup>[9]</sup> Regarding Pd<sup>II</sup><sup>[8a,9d,10]</sup> and Ni<sup>II</sup><sup>[9a,11]</sup> bis(phosphane) complexes with bidentate organoselenium ligands, information is even sparser. Likewise, most of these complexes contain diselenocarbonate<sup>[8a,10a,10b,11d,11e]</sup> or diselenolene<sup>[9a,9d,10c–10g,11c–11e]</sup> derivatives.

More than twenty years ago, Schmidt and Hoffmann have reported the thus far only application of alkylidisenols in complexes of the type [ML<sub>2</sub>(Se,Se'-SeRSe)] (where M = Ni, Pd, Pt; L = phosphane, R = alkyl spacer).<sup>[12]</sup> They also succeeded in the synthesis of the 1,3-diselenolato-2-thiapropane and 1,3-diselenolato-2-selenapropane derivatives, carrying a sulfur or selenium atom in the bridging alkyl group, respectively. This elaborate preparation demanded reduction of the polymeric starting materials in liquid ammonia. Whereas the diselenium analogue of methanedithiol is unknown, Khanna et al. have reported the crystal structure of [Pt(PPh<sub>3</sub>)<sub>2</sub>(CH<sub>2</sub>Se<sub>2</sub>)] that was prepared by the reaction of oligomeric [Pt(PPh<sub>3</sub>)<sub>2</sub>(μ-Se)]<sub>n</sub> with dichlo-

[‡] Determination of the Steric Demand of Bidentate Phosphanes Using X-ray Crystal Structure Data, Part 1. Part 2: T. Niksch, H. Görls, W. Weigand, *Eur. J. Inorg. Chem.* **2010**, 95–105, following paper.

[a] Institut für Anorganische und Analytische Chemie, Friedrich-Schiller-Universität Jena, August-Bebel-Str. 2, 07743 Jena, Germany  
Fax: +49-3641-948102  
E-mail: wolfgang.weigand@uni-jena.de

[b] Department of Chemistry, University of Oulu, P. O. Box 3000, 90041 Oulu, Finland

Supporting information for this article is available on the WWW under <http://dx.doi.org/10.1002/ejic.200900824>.

romethane.<sup>[13]</sup> Applying a similar reaction, Yeo et al. were able to obtain  $[\text{Pt}(\text{PPh}_3)_2(\eta^2\text{-Se}_2\text{C}_2\text{O}_2\text{-Se,Se}')] ]$  by the reaction of  $[\text{Pt}_2(\text{PPh}_3)_4(\mu\text{-Se})_2]$  and oxalyl chloride.<sup>[14]</sup>

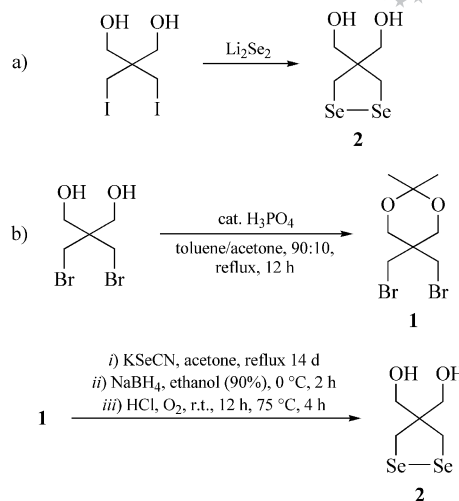
In this work, we report a simple and efficient method for the preparation of the  $[\text{ML}_2\{(\text{SeCH}_2)_2\text{C}(\text{CH}_2\text{OH})_2\}]$  ( $\text{M} = \text{Ni}, \text{Pd}, \text{Pt}$ ;  $\text{L} = \text{mono- or } 1/2\text{-bidentate phosphane}$ ) complexes from the corresponding diselenide and the appropriate precursor  $[\text{MCl}_2\text{L}_2]$ . This straightforward approach circumvents the need to isolate the malodorous and oxygen sensitive diselenols and affords the complexes in good yields in a one-pot reaction. All products were identified and characterised by multinuclear NMR spectroscopy ( $^1\text{H}$ ,  $^{13}\text{C}$ ,  $^{31}\text{P}$ ,  $^{77}\text{Se}$ ,  $^{195}\text{Pt}$  NMR), mass spectrometry and elemental analysis. For further investigations, the compounds were additionally studied by single-crystal X-ray structure analysis, when feasible.

## Results and Discussion

### I. 4,4-Bis(hydroxymethyl)-1,2-diselenolane (2)

It is well known that the diselenolane system tends to polymerise, e.g. the unsubstituted 1,2-diselenolane and the 3-methyl-substituted analogue both form a polymeric gum in the solid state.<sup>[15]</sup> In this work, we utilised 4,4-bis(hydroxymethyl)-1,2-diselenolane (**2**), because it is a stable compound that is easy to handle. It was first reported to be produced in a very poor yield by the reaction of 2,2-bis(iodomethyl)propane-1,3-diol with dilithium diselenide,  $\text{Li}_2\text{Se}_2$  (path **a** in Scheme 1).<sup>[16]</sup> We were able to improve the synthesis by starting from 2,2-bis(bromomethyl)propane-1,3-diol (see path **b** in Scheme 1). Selenium was introduced by using potassium selenocyanate,  $\text{KSeCN}$ , which substitutes the bromine in alkyl bromides to give the corresponding alkyl selenocyanates. The twofold substitution required a long reaction time and harsh reaction conditions. It also proved necessary to protect the hydroxy groups as the ketal **1** to obtain a good conversion. The reaction of **1** with  $\text{KSeCN}$  was carried out in boiling acetone for 14 days, affording the crude diselenocyanated product, which was reduced with sodium borohydride in ethanolic solution. The diselenol was easily oxidised by oxygen followed by acidic deprotection of the hydroxy groups. The overall yield of cyclic diselenide **2** over two steps was 69%.

The  $^1\text{H}$  NMR spectrum of **2** exhibits resonances at  $\delta = 4.76$  ( $\text{OH}$ ), 3.46 ( $\text{CH}_2\text{OH}$ ) and 3.17 ( $\text{CH}_2\text{Se}$ ) ppm, with the last resonance showing typical  $^{77}\text{Se}$  satellites with  $^2J_{\text{H,Se}} = 15.4$  Hz. The coupling to  $^{77}\text{Se}$  is also seen in the  $^{13}\text{C}\{^1\text{H}\}$  NMR spectrum, in which the signal of the methylene group next to the diselenide bridge appears at  $\delta = 35.6$  ppm as a singlet with  $^{77}\text{Se}$  satellites ( $^1J_{\text{C,Se}} = 66.2$  Hz). The coupling constants to  $^1\text{H}$  and  $^{13}\text{C}$  are in good agreement with those reported for alkyl diselenides.<sup>[17]</sup> In addition to that, the presence of selenium in **2** allows its spectroscopic investigation via  $^{77}\text{Se}$  NMR techniques. The selenium atoms of **2** show resonance at  $\delta = 270.0$  ppm that is typical for five-membered cyclic diselenides.<sup>[18]</sup> The strong downfield shift compared to acyclic diselenides<sup>[19]</sup> might be



Scheme 1. Synthesis of 4,4-bis(hydroxymethyl)-1,2-diselenolane (**2**). a) First synthesis of **2** reported from Bergson in 1958.<sup>[16]</sup> b) Improved procedure for the synthesis of **2** via 5,5-bis(bromomethyl)-2,2-dimethyl-1,3-dioxane (**1**).

due to the ring strain, forcing the lone pairs of the selenium atoms in eclipsed conformation.<sup>[20]</sup>

Due to the presence of two hydroxy groups and two selenium atoms in compound **2**, there are some interesting aspects concerning its molecular structure and the supramolecular arrangement in the solid state. On the one hand the hydroxy functions might link molecules and build up a network via hydrogen bonds, while on the other hand non-bonding interactions between the selenium atoms might influence the arrangement of **2** in the solid state. There are several compounds known, showing close intermolecular  $\text{Se}\cdots\text{Se}$  distances,<sup>[21]</sup> that are remarkably shorter than the sum of the van der Waals radii of 4.0 Å.<sup>[22]</sup> For some compounds these chalcogen–chalcogen interactions are most determinant for their arrangement in the solid state, as for instance can be seen in the work of Werz and Gleiter.<sup>[21f–21j]</sup> As shown in Figure 1 short intermolecular  $\text{Se}\cdots\text{Se}$  distances might be characterised as interactions between occupied p(Se) orbitals and empty  $\sigma^*(\text{Se-R}^4)$  orbitals.<sup>[21h,21j,21l,23]</sup>

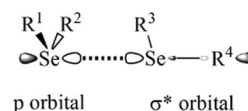


Figure 1. Short intermolecular selenium–selenium distances deriving from interaction of occupied p and unoccupied  $\sigma^*$  orbitals.

The molecular structure of **2** exhibits an interesting interplay of these effects (Figures 2 and 3). Regarding the hydrogen-bonding<sup>[24]</sup> network, only intermolecular hydrogen bonds were present. A closer look reveals that four molecules are connected through four hydrogen bonds building an almost perfect square (Figure 2, middle). Thus the molecules are aligned in a double-chain-like structure. Concerning selenium selenium interactions, we found a huge network of close contacts (Figure 2, right), arranging all selenium atoms in separated layers with a thickness of less than

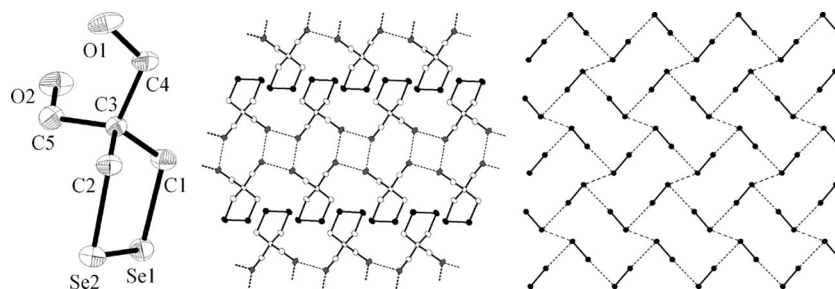


Figure 2. Left: molecular structure of 4,4-bis(hydroxymethyl)-1,2-diselenolane (**2**) in the crystal. Centre: view along the *b*-axis, displaying intermolecular hydrogen-bonding system. Right: Se...Se interactions in the crystal (all other atoms have been omitted). All ellipsoids are drawn at 50% probability level, hydrogen atoms and solvent molecules have been omitted for clarity. Selected bond lengths [Å] and angles [°]: Se1–Se2 2.3743(7), Se1–C1 1.959(5), Se2–C2 1.972(5), O2...O1<sup>i</sup> 2.687 (intrastrand hydrogen bonds), O2...O1<sup>ii</sup> 2.686 (interstrand hydrogen bonds), Se2...Se2<sup>i</sup> 3.358 (dashed lines), Se1...Se2<sup>i</sup> 3.677 (dotted lines); C1–Se1–Se2 91.36(13), C2–Se2–Se1 92.19(13), O1<sup>ii</sup>...O2...O1<sup>i</sup> 88.92 (upper left and lower right corner of the quadrangular hydrogen bridging system), O2...O1<sup>i</sup>...O2<sup>iii</sup> 91.08 (upper right and lower left corner); *i*: *x*, *−y*, *−0.5 + z*; *ii*: *−x*, *y*, *1.5 − z*; *iii*: *−x*, *−y*, *1 − z*.

0.9 Å (based on atom positions). The intermolecular Se...Se distances are 3.36 Å and 3.68 Å and hence significantly shorter than the sum of the van der Waals radii and even shorter than most of the reported selenium–selenium interactions (for some examples see ref.<sup>[21]</sup>). The value of 3.36 Å is even shorter than the interstrand distances in elemental grey selenium, which is reported to be 3.43 Å.<sup>[25]</sup> Figure 3 displays the view along the *c*-axis, clearly showing the separated selenium layers that are connected through hydrogen bonds, building a three-dimensional network.

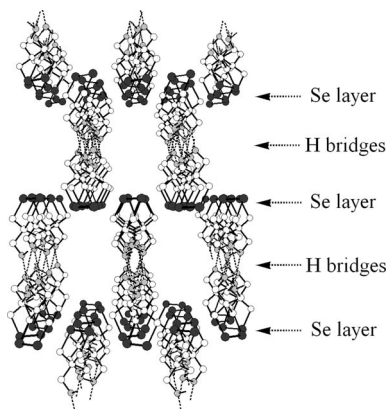


Figure 3. View along the *c*-axis of the crystal structure of **2** showing the three-dimensional supramolecular arrangement due to strong intermolecular Se Se interactions and hydrogen bonds. For the sake of clarity a ball-and-stick model is displayed, while hydrogen atoms and solvent molecules have been omitted.

## II. [PtCl<sub>2</sub>(4-dppdbf)<sub>2</sub>] (**3**), [MCl<sub>2</sub>(dppn)] {M = Ni (**4**), Pd (**5**), Pt (**6**)}, [PdCl<sub>2</sub>(dppn)·PdCl<sub>2</sub>] (**7**) and [PtCl<sub>2</sub>(xantphos)] (**8**)

The phosphanes investigated in this work and their abbreviations are summarised in Figure 4. Important NMR spectroscopic data, coupling constants and P1–M–P2 angles for compounds **2–29** are outlined in Table 1. The main emphasis in this work involves the influence of the bite angle of the phosphane and the spheric crowding at the metal centre.

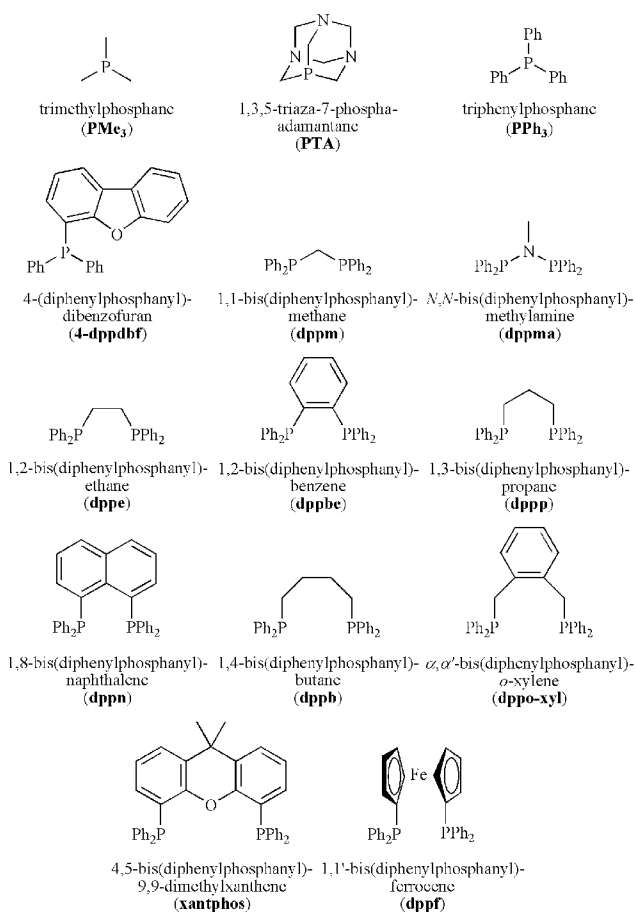


Figure 4. Summary of the investigated mono- and bidentate phosphanes and their systematic names. The abbreviations used in the text are given in parentheses.

The platinum complex *cis*-[PtCl<sub>2</sub>(4-dppdbf)<sub>2</sub>] (**3**) involving the sterically demanding 4-dppdbf, was easily prepared from [PtCl<sub>2</sub>(cod)] in almost a quantitative yield and high selectivity. The <sup>31</sup>P{<sup>1</sup>H} NMR spectrum shows a singlet with typical <sup>195</sup>Pt satellites at δ = 9.7 ppm. The <sup>1</sup>J<sub>Pt</sub> coupling constant of 3742 Hz is consistent with a *cis*-configuration of dichloridodiphosphaneplatinum(II) that has been

Table 1. NMR spectroscopic data, coupling constants and P1–M–P2 angles of compounds **2**–**29**. For the correlation between ring size and  $^{31}\text{P}$  NMR shifts see ref.[26]

| Compound                 | $^{31}\text{P}$ shift /ppm | $^{77}\text{Se}$ shift /ppm <sup>[a]</sup> | $^{195}\text{Pt}$ shift /ppm <sup>[a]</sup> | $^1J_{\text{Pt,P1}}$ /Hz <sup>[b]</sup> | Further coupling constants /Hz                               | P1–M–P2 angle /°                              |
|--------------------------|----------------------------|--|---|---|--|---|
| <b>2</b>                 |                            | 270.0 <sup>[c]</sup>                       |   |   |  |   |
| <b>3</b> <sup>[d]</sup>  | 9.7                        |  |   | 3742                                    |  | 103.36(4)                                     |
| <b>4</b>                 | 39.4                       |  |   |   |  | 91.18(5)                                      |
| <b>5</b>                 | 24.5                       |  |   |   |  | 90.37(5)                                      |
| <b>6</b>                 |                            |  |   |   |  | 86.58(8)                                      |
| <b>7</b> <sup>[d]</sup>  | 5.5                        |  |   | 3312                                    |  | 92.20(7)                                      |
| <b>8</b>                 | 9.8                        |  | –4329.8                                     | 3694                                    |  | 100.87(8)                                     |
| <b>9</b>                 | –26.1                      | –36.0                                      | –4620.0                                     | 2694                                    |  | 94.62(5)                                      |
| <b>10</b>                | –63.5                      | –33.2                                      | –4798.6                                     | 2491                                    |  | 94.98(6)                                      |
| <b>11a/11b</b>           | 22.0                       | 60.0                                       | –4840.9 <sup>[c]</sup>                      | 2897                                    | 47.7 ( $^2J_{\text{P,Se}}$ ), 167.3 ( $^1J_{\text{Pt,Se}}$ ) | 99.13(5), 97.03(8)                            |
| <b>12</b>                | 16.0                       | 66.1                                       | –4848.3 <sup>[c]</sup>                      | 2967                                    | 48.5 ( $^2J_{\text{P,Se}}$ )                                 |   |
| <b>13</b>                | –49.6                      | –20.5                                      | –4655.4 <sup>[c]</sup>                      | 2315                                    | 32.7 ( $^2J_{\text{P,Se}}$ )                                 | 73.05(7)                                      |
| <b>14</b>                | 34.5                       | –47.9                                      | –4364.0                                     | 2442                                    | 33.8 ( $^2J_{\text{P,Se}}$ )                                 | 71.71(4)                                      |
| <b>15</b>                | 47.9                       | –42.6                                      | –4787.3                                     | 2721                                    |  | 85.33(11)                                     |
| <b>16</b>                | 47.9                       | –25.2                                      | –4748.0                                     | 2736                                    | 53.2 ( $^2J_{\text{P,Se}}$ )                                 | 87.81(8)                                      |
| <b>17</b>                | –1.9                       | 12.4                                       | –4758.4                                     | 2652                                    | 45.0 ( $^2J_{\text{P,Se}}$ )                                 | 91.98(8)                                      |
| <b>18</b>                | 8.1                        | 39.7                                       | –4685.9 <sup>[c]</sup>                      | 2573                                    | 40.6 ( $^2J_{\text{P,Se}}$ ), 220.9 ( $^1J_{\text{Pt,Se}}$ ) | 88.36(10)                                     |
| <b>19</b>                | 13.7                       | 27.9                                       | –4816.6                                     | 2783                                    | 45.4 ( $^2J_{\text{P,Se}}$ )                                 | 95.06(8)                                      |
| <b>20</b>                | 1.2                        | 33.2                                       | –4833.6                                     | 2846                                    | 43.8 ( $^2J_{\text{P,Se}}$ )                                 | 101.21(6)                                     |
| <b>21</b> <sup>[e]</sup> | 15.1                       | 64.9                                       | –4891.8                                     | 2886                                    | 39.6 ( $^2J_{\text{P,Se}}$ )                                 | 107.65(5), 100.61(6)/101.69(8) <sup>[f]</sup> |
| <b>24</b>                | 19.8                       | 61.1                                       | –4786.4                                     | 2952                                    | 49.7 ( $^2J_{\text{P,Se}}$ )                                 | 96.99(6)                                      |
| <b>25</b>                | 49.2                       | 8.8  |   |   | 29.6, 50.2 ( $^2J_{\text{P,Se}}$ )                           | 85.84(7), 85.42(7) <sup>[g]</sup>             |
| <b>26</b>                | 13.5                       | 93.0                                       |   |   | 33.7, 40.8 ( $^2J_{\text{P,Se}}$ )                           |   |
| <b>27</b>                | 20.9                       | 134.7                                      |   |   | 48.6 ( $^2J_{\text{P,Se}}$ )                                 | 99.34(6)                                      |
| <b>28</b>                | 59.9                       | 24.9                                       |   |   | 48.7, 54.2 ( $^2J_{\text{P,Se}}$ )                           | 87.58(8)                                      |
| <b>29</b>                | –10.3, 39.4                |  |   |   | 8.9 ( $^2J_{\text{PP}}$ )                                    |   |

[a] If not mentioned otherwise, the shifts derive from HMBC NMR spectra. [b] Coupling constant determined from  $^{31}\text{P}\{^1\text{H}\}$  NMR spectroscopy. [c] Shift deriving from directly measured  $^{77}\text{Se}\{^1\text{H}\}$  or  $^{195}\text{Pt}\{^1\text{H}\}$  NMR spectrum. [d] Due to the poor solubility no  $^{195}\text{Pt}$  resonance could be detected. [e] All NMR spectroscopic data were obtained from solutions of expected **21**, while single-crystal X-ray analysis revealed the composition of complexes **22** and **23**. [f] The first two values were taken from the molecular structure of **22**, the last from that of **23**, respectively. [g] The values belong to two symmetry-independent molecules.

reported to exhibit coupling  $>3000$  Hz.<sup>[27]</sup> The single-crystal X-ray structure of **3** confirmed the formation of *cis*-isomer (Figure 5). Due to the presence of two dibenzofuran moieties, the P1–Pt–P2 angle of  $103.36(4)^\circ$  is ca.  $3.5^\circ$  larger than the corresponding angle in  $[\text{PtCl}_2(\text{PPh}_3)_2]$  [ $99.12(3)^\circ$  and  $99.93(4)^\circ$  for two symmetry-independent molecules<sup>[28]</sup>]. Additionally, intramolecular  $\pi$ – $\pi$  stacking interactions between the two dibenzofuran moieties were seen in **3**. The average distance of the planes of the rings marked with **A** and **B** (see Figure 5) is ca.  $3.22$  Å and the ring centroids are shifted  $1.01$  Å against each other indicating typical face-to-face  $\pi$ – $\pi$  stacking interaction.<sup>[29]</sup>

As chelating phosphane with a bite angle close to  $90^\circ$  and a rigid backbone, dppn<sup>[30]</sup> attracted our attention. While  $[\text{PdCl}_2(\text{dppn})]$  (**5**)<sup>[30a]</sup> and  $[\text{PtCl}_2(\text{dppn})]$  (**6**)<sup>[30a,31]</sup> have been prepared in the past, their nickel analogue  $[\text{NiCl}_2(\text{dppn})]$  (**4**) is not previously known. It could be precipitated as orange solid by stirring equimolar amounts of dppn and  $\text{Ni}^{\text{II}}\text{Cl}_2 \cdot 6\text{H}_2\text{O}$  in ethanol under exclusion of oxygen. Its  $^{31}\text{P}\{^1\text{H}\}$  NMR spectrum shows a resonance at  $\delta = 39.4$  ppm.

Single crystals of **4** suitable for X-ray structure analysis were grown from a concentrated dichloromethane solution. Its molecular structure together with those of isomorphous Pd and Pt complexes **5** and **6** is displayed in Figure 6. All

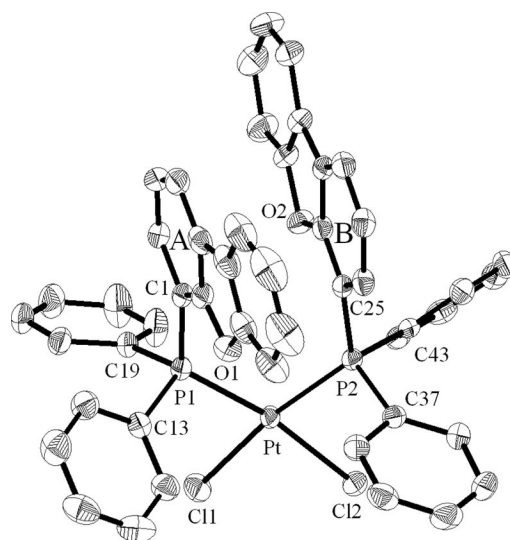


Figure 5. Molecular structure of  $[\text{PtCl}_2(4\text{-dppdbf})_2]$  (**3**) in the crystal. Ellipsoids are drawn at 50% probability level, hydrogen atoms and solvent molecules have been omitted for clarity. Selected bond lengths [Å] and angles [°]: Pt–P1 2.2546(11), Pt–P2 2.2411(10), Pt–Cl1 2.3544(11), Pt–Cl2 2.3627(10); P1–Pt–P2  $103.36(4)$ , Cl1–Pt–Cl2  $87.24(4)$ . The average distance between the planes of the phenyl rings marked **A** and **B** is  $3.22$  Å, while the shift of the two rings is about  $1.01$  Å.

complexes show a twofold axis of rotation through atoms C5, C6 and the corresponding metal atom. The bite angle (P1–M–P1A) of dppn differs only slightly depending on the metal [91.18(5)°, 90.37(5)° and 92.20(7)° for Ni, Pd and Pt, respectively]. The out-of-plane displacement of the two phosphorus atoms, however, increases with the metal atom becoming heavier, as can be seen from the torsion angles (P1–C1...C1A–P1A) that are 33.68°, 34.31° and 35.03° for **4**, **5** and **6**, respectively.

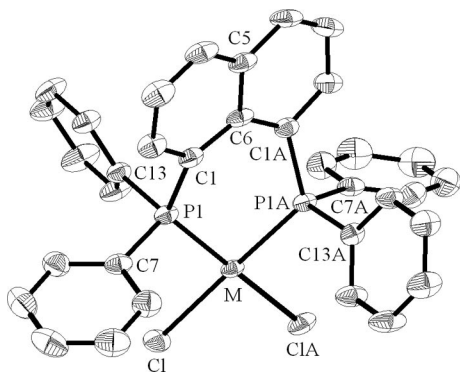


Figure 6. Molecular structure of  $[MCl_2(dppn)]$  [ $M = Ni$  (**4**),  $Pd$  (**5**) and  $Pt$  (**6**)] in the crystal. Ellipsoids are drawn at 50% probability level, hydrogen atoms and solvent molecules have been omitted for clarity. Selected bond lengths [Å] and angles [°] (the first value refers to the Ni, the second to the Pd and the third one to the Pt analogue):  $M-P1$  2.1529(9), 2.2276(10), 2.2195(4),  $M-Cl$  2.2088(9), 2.3651(10), 2.3618(14);  $P1-M-P1A$  91.18(5), 90.37(5), 92.20(7),  $Cl-M-ClA$  91.57(5), 90.33(5), 88.19(7),  $C1-P1-M$  122.15(12), 121.25(13), 119.82(19),  $P1-C1...C1A-P1A$  33.68, 34.31, 35.03.

Surprisingly a small amount of  $[PdCl_2(dppn) \cdot PdCl_2]$  (**7**) was obtained during the preparation of **5**, as verified by single-crystal X-ray structure analysis (see Figure 7). The attempts to separate **7** from **5** by column chromatography or fractional crystallisation were unfortunately not successful, as were attempts to synthesise this compound or its platinum analogue from the appropriate  $[M_2Cl_6]^{2-}$  precursor.<sup>[32]</sup> Instead, compounds **5** or **7** and some amount of precipitated  $MCl_2$  were obtained for palladium and platinum, respectively (see Scheme 2). The small excess of free  $PdCl_2$  forming **7** might be present in the reaction mixture as impurity or it could have been generated from the precursor  $[PdCl_2(NCPh)_2]$ .

$[PtCl_2(xantphos)]$  (**8**) is obtained by reacting 4,5-bis(di-phenylphosphanyl)-9,9-dimethylxanthene (xantphos) that exhibits a large bite angle with an equimolar amount of  $[PtCl_2(cod)]$  in dichloromethane for 12 h. The equivalent phosphorus atoms show a resonance at  $\delta = 9.8$  ppm and a coupling constant of  $^1J_{P,Pt} = 3694$  Hz. The platinum atom is clearly distracted from the main plane of the xanthene moiety (see Figure 8). The angle between the planes through the atoms P1, P2, C2, C12 and P1, P2, Pt, Cl1, Cl2 is about 86.8° and thus shows the platinum atom bound to be almost perpendicular to the xanthene moiety. The platinum atom shows a significantly distorted square-planar coordination with the P1–Pt–P2 angle being enlarged to 100.87(8)°.

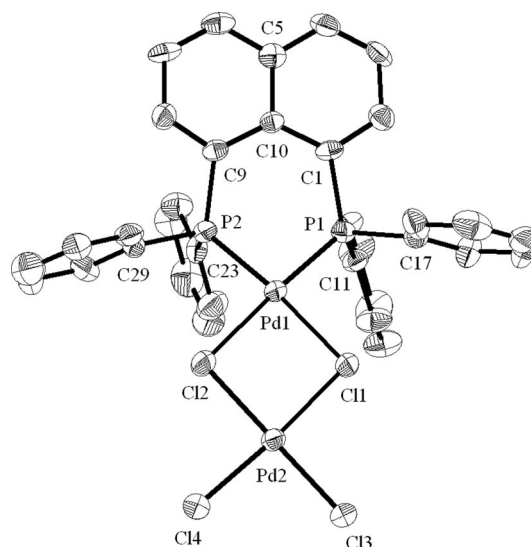
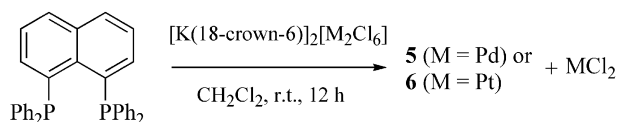


Figure 7. Molecular structure of  $[PdCl_2(dppn) \cdot PdCl_2]$  (**7**) in the crystal. Ellipsoids are drawn at 50% probability level, hydrogen atoms and solvent molecules have been omitted for clarity. Selected bond lengths [Å] and angles [°]:  $Pd1-P1$  2.234(2),  $Pd1-P2$  2.232(2),  $Pd1-Cl1$  2.422(2),  $Pd1-Cl2$  2.400(2),  $Pd2-Cl1$  2.340(2),  $Pd2-Cl2$  2.312(2),  $Pd2-Cl3$  2.295(2),  $Pd2-Cl4$  2.277(2);  $P1-Pd1-P2$  86.58(8),  $Cl1-Pd1-Cl2$  82.49(7),  $Cl1-Pd2-Cl2$  86.20(8),  $Cl3-Pd2-Cl4$  91.23(8),  $P1-C1...C9-P2$  9.89.



Scheme 2. The reaction of dppn with preformed  $[Pd_2Cl_6]^{2-}$  and  $[Pt_2Cl_6]^{2-}$  ions.<sup>[32]</sup>

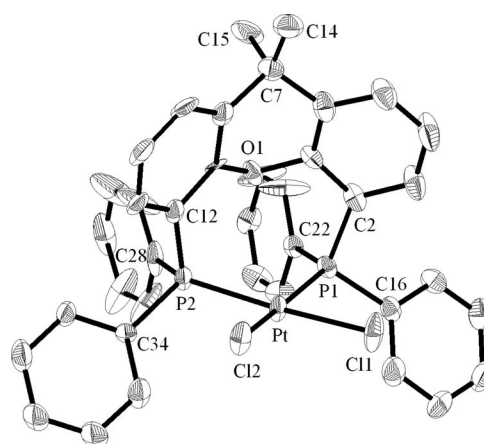


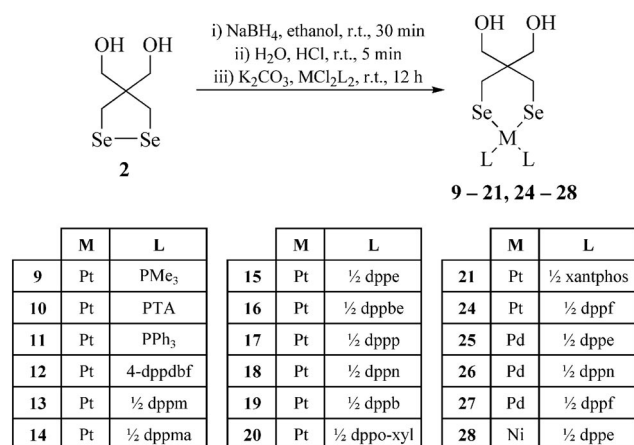
Figure 8. Molecular structure of **8** in the crystal. Ellipsoids are drawn at 50% probability level, hydrogen atoms and solvent molecules have been omitted for clarity. Selected bond lengths [Å] and angles [°]:  $Pt-P1$  2.253(2),  $Pt-P2$  2.264(2),  $Pt-Cl1$  2.354(2),  $Pt-Cl2$  2.348(2);  $P1-Pt-P2$  100.87(8),  $Cl1-Pt-Cl2$  86.83(8),  $P1-Pt-Cl1$  85.71(8),  $P2-Pt-Cl2$  85.17(8); the dihedral angle between the least-squares planes (P1, P2, C2, C12) and (P1, P2, Pt, Cl1, Cl2) is 86.8°.

### III. $[\text{ML}_2\{(\text{SeCH}_2)_2\text{C}(\text{CH}_2\text{OH})_2\}]$ ( $\text{M} = \text{Ni}, \text{Pd}, \text{Pt}$ ; $\text{L} =$ mono- or $\frac{1}{2}$ bidentate phosphane) (9–21 and 24–28)

#### General

Metal(II) phosphane complexes bearing selenolato ligands are generally prepared by the oxidative addition of metal(0) phosphane complex fragments to diselenides (for some examples, see refs.<sup>[7b,7d,33]</sup>), or by substitution of labile ligands at the metal, e.g. halides, by a deprotonated selenol species (as exemplified in ref.<sup>[34]</sup>). As the isolation of malodorous and unstable selenols normally is often inevitable in the second method, the oxidative addition seems to be preferable. The preparation of diselenolato diphosphane  $\text{M}^{\text{II}}$  complexes is, however, a straightforward one-pot synthesis that circumvents the isolation of the bad smelling selenols.

Therefore, the air- and moisture-stable diselenide **2** was placed in a Schlenk vessel and dissolved in ethanol under argon giving a red-coloured solution. The addition of an excess sodium borohydride,  $\text{NaBH}_4$ , resulted in a clear and colourless solution indicating that the diselenide is completely reduced to the corresponding diselenolate dianion. The excess  $\text{NaBH}_4$  was destroyed by the dropwise addition of dilute hydrochloric acid before potassium carbonate,  $\text{K}_2\text{CO}_3$ , was added to deprotonate the diselenol again. The appropriate dichloridodiphosphanemetal(II) complex was added as a suspension in acetone, chloroform, dichloromethane or ethanol. The reaction mixture slowly turned yellow due to the formation of the desired complexes. The reaction proceeds faster in chloroform or dichloromethane suspensions due to the higher solubility of  $[\text{MCl}_2\text{L}_2]$ . Common workup procedures and column chromatography gave complexes **9–28** as yellow to orange air- and moisture-stable solids, which slowly decomposed in chlorinated solvents. The reaction conditions and the summary of the synthesised complexes are shown in Scheme 3.



Scheme 3. Synthesis of complexes **9–21** and **24–28** applying an one-pot procedure starting with **2**. For details see Supporting Information.

The presence of various NMR active nuclei in complexes **9–28** enables manifold NMR investigations, namely the recording of  $^1\text{H}$ ,  $^{13}\text{C}\{^1\text{H}\}$ ,  $^{31}\text{P}\{^1\text{H}\}$ ,  $^{77}\text{Se}$  and  $^{195}\text{Pt}$  NMR

spectra. Indirect methods were performed on the determination of  $^{77}\text{Se}$  and  $^{195}\text{Pt}$  NMR spectra ( $^1\text{H}$   $^{77}\text{Se}$  HMBC and  $^1\text{H}$   $^{195}\text{Pt}$  HMBC NMR, respectively), reducing the accumulation time significantly. The obvious disadvantage of these indirect methods is the loss of information on small coupling constants due to the enlarged half width of the resonances.

#### $[\text{PtL}_2\{(\text{SeCH}_2)_2\text{C}(\text{CH}_2\text{OH})_2\}]$ ( $\text{L} = \text{PMe}_3$ , PTA, $\text{PPh}_3$ , 4-dppdbf) (9–12)

The  $^{31}\text{P}\{^1\text{H}\}$  NMR spectrum of **9** exhibits a single resonance at  $\delta = -26.1$  ppm with the anticipated  $^{195}\text{Pt}$  satellites. The  $^1J_{\text{P,Pt}}$  coupling constant shows a value of 2694 Hz and is expectedly smaller than that in  $[\text{PtCl}_2(\text{PMe}_3)_2]$  ( $^1J_{\text{P,Pt}} = 3481$  Hz) due to the higher *trans* influence of selenium in **9** compared to that of chlorine in  $[\text{PtCl}_2(\text{PMe}_3)_2]$ . The coupling to  $^{77}\text{Se}$  over two bonds was not resolved in the  $^{31}\text{P}\{^1\text{H}\}$  NMR spectroscopy.

The  $^1\text{H}$   $^{77}\text{Se}$  HMBC NMR spectrum exhibited a high order multiplet at  $\delta = -36$  ppm. The indirect HMBC NMR method, however, could not resolve the splittings. Second-order quartet accompanied by  $^{195}\text{Pt}$  satellites were expected for the  $^{77}\text{Se}$  resonance in a similar fashion to that reported by Risto et al.<sup>[34a,34b]</sup> in the  $^{125}\text{Te}$  NMR spectra of the Te-containing *cis*-Pt complexes. We therefore also recorded the direct  $^{77}\text{Se}$  NMR spectrum. Unfortunately, the directly measured  $^{77}\text{Se}$  NMR spectrum also yielded only unresolved multiplets probably due to smaller coupling constants between  $^{77}\text{Se}$  and  $^{31}\text{P}$  compared to those between  $^{125}\text{Te}$  and  $^{31}\text{P}$ . The  $^1\text{H}$   $^{195}\text{Pt}$  HMBC NMR spectrum gave a triplet centred at  $-4620$  ppm with  $^1J_{\text{Pt,P}} = 2706$  Hz in agreement with that obtained from the  $^{31}\text{P}\{^1\text{H}\}$  NMR spectrum.

The spectroscopic data are consistent with the molecular structure of complex **9** that was determined by single-crystal X-ray diffraction (see Figure 9). The platinum atom shows a distorted square-planar coordination with two *cis*-phosphorus and two *cis*-selenium atoms. The P1–Pt–P2 angle is almost  $2^\circ$  smaller than that in *cis*- $[\text{PtCl}_2(\text{PMe}_3)_2]$ ,<sup>[35]</sup> while the Se1–Pt–Se2 angle [ $91.090(17)^\circ$ ] is only slightly larger than  $90^\circ$ . Furthermore, the high *trans* influence of selenium is seen in the relatively long platinum–phosphorus bond lengths of 2.2726(13) Å and 2.2756(13) Å compared to the average of 2.24 Å in  $[\text{PtCl}_2(\text{PMe}_3)_2]$ .<sup>[35]</sup> In the crystal there is a very short contact between a hydroxy group of one molecule and the central platinum atom of another (see Figure 9). The intermolecular oxygen...platinum distance is 3.38 Å, with the oxygen atom located in an apical position above the square-planar coordination plane of platinum. These interactions align the molecules in a chain-like structure along the *b*-axis throughout the crystal as shown in Figure 9.

Complex **10** involves the sterically little demanding phosphane PTA. The most interesting property of complexes bearing this ligand is their improved solubility in protic solvents, especially water.<sup>[36]</sup> This peculiarity requires the purification of **10** to be adjusted, as common aqueous workup procedures cannot be applied. Therefore, **10** was purified by extracting the crude product with chloroform using a

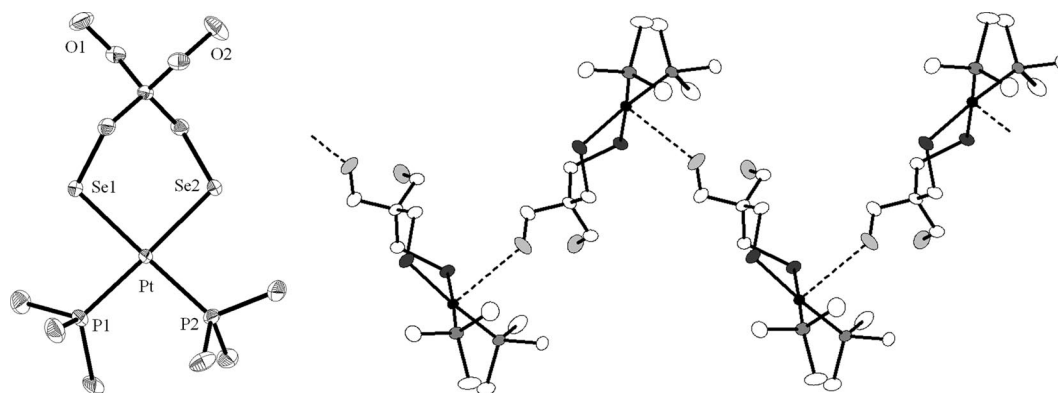


Figure 9. Left: molecular structure of **9** in the crystal. Right: part of a chain of **9** in the crystal, caused by hydrogen bonds between oxygen and platinum atoms. Ellipsoids are drawn at 50% probability level, hydrogen atoms have been omitted for clarity. Selected bond lengths [Å] and angles [°]: Pt–P1 2.2726(13), Pt–P2 2.2756(13), Pt–Se1 2.4708(5), Pt–Se2 2.4576(5), O1...Pt' 3.38; P1–Pt–P2 94.62(5), Se1–Pt–Se2 91.090(17), P1–Pt–Se1 84.96(4), P2–Pt–Se2 87.36(4), O1'<sup>i</sup>...Pt–P1 88.22, O1'<sup>i</sup>...Pt–P2 86.63, O1'<sup>i</sup>...Pt–Se1 89.32, O1'<sup>i</sup>...Pt–Se2 92.27; *i*: 2.5 – *x*, 0.5 + *y*, *z*.

Soxhlet extractor. However, **10** is poorly soluble in chlorinated solvents, so the extraction of 150 mg took about 12 h. Another possibility for the purification seems to be the extraction of the crude product with dmsO, to separate it from inorganic salts. The addition of hexane or methanol precipitated **10** in low purity. Even after several repetitions the product thus obtained did not give satisfying elemental analysis.

The  $^{31}\text{P}\{^1\text{H}\}$  NMR spectrum of **10** displays the expected resonance at  $\delta = -63.5$  ppm ( $^1J_{\text{P,Pt}} = 2491$  Hz) and the  $^{77}\text{Se}$  resonance at  $\delta = -33.2$  ppm. The  $^{195}\text{Pt}\{^1\text{H}\}$  NMR spectrum exhibited a triplet at  $\delta = -4799$  ppm ( $^1J_{\text{Pt,P}} = 2490$  Hz). Suitable crystals for X-ray structure determination were obtained by slow diffusion of methanol into a concentrated dmsO solution of **10** at room temp. during several weeks. The molecular structure of **10** and the packing of the complexes in the crystal are shown in Figure 10. The square-planar coordination sphere around the platinum atom is similar to that in **9** with the P1–Pt–P2 angle being 94.98(6)° and the opposite Se1–Pt–Se2 angle being 90.49(2)°. Both hydroxy groups are involved in the formation of hydrogen bonds, one linking to a nitrogen atom of the PTA ligand of

another complex [ $d(\text{O}\cdots\text{N}) = 2.90$  Å] and the other hydroxy group showing a close contact to the oxygen of solvent dmsO molecule [ $d(\text{O}\cdots\text{O}) = 2.78$  Å]. These interactions arrange **10** in chains along the *b*-axis of the crystal.

The complex **11** that contains triphenylphosphane was easily prepared according to the developed procedure described above. The purification of the crude product by column chromatography using a dichloromethane/ethyl acetate mixture as eluent gave **11** as ethyl acetate solvate. Interestingly, even in solution the solvent molecules are bound through hydrogen bonds to the hydroxy groups of **11**, as deduced from  $^1\text{H}$  and  $^{13}\text{C}\{^1\text{H}\}$  NMR spectra and verified by NOE NMR experiments. However, the use of other eluents (dichloromethane/ethanol, 80:20) gave non-solvated crystals of **11** (assigned **11a**) in analytical purity.

The  $^{31}\text{P}\{^1\text{H}\}$  NMR spectrum of compound **11** showed a resonance at  $\delta = 22.0$  ppm exhibiting  $^{195}\text{Pt}$  and  $^{77}\text{Se}$  satellites. The  $^1J_{\text{P,Pt}}$  coupling constant is 2897 Hz and the  $^2J_{\text{P,Se}}$  is 47.7 Hz. These values are in good agreement with comparable complexes known from literature, but the assignment whether the coupling between  $^{31}\text{P}$  and  $^{77}\text{Se}$  is a matter of *cis*- or *trans*-coupling is ambiguous.<sup>[7b,7d,8e,8f,37]</sup> The  $^{77}\text{Se}$

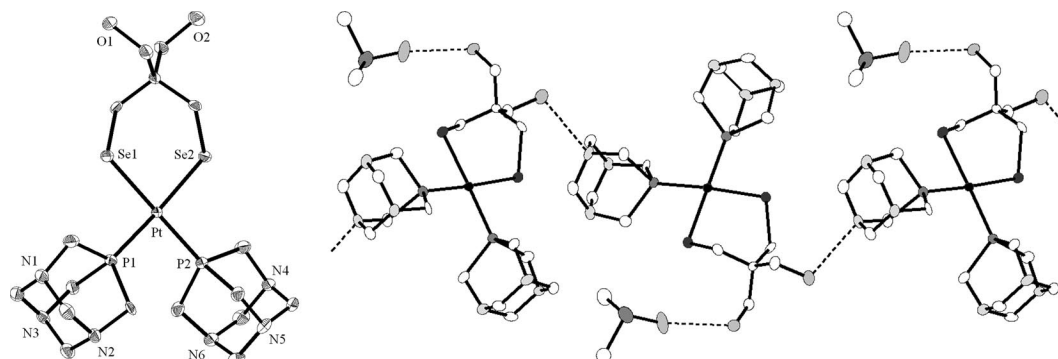


Figure 10. Left: molecular structure of **10** in the crystal. Right: part of the chain of **10** in the crystal, due to intermolecular hydrogen bonds. Ellipsoids are drawn at 50% probability level, hydrogen atoms and non-coordinated solvent molecules have been omitted for clarity. Selected bond lengths [Å] and angles [°]: Pt–P1 2.2663(15), Pt–P2 2.2703(16), Pt–Se1 2.4578(7), Pt–Se2 2.4588(6), O1...OS 2.78 [hydrogen bond to solvent (dmsO)], O2...N3' 2.90; P1–Pt–P2 94.98(6), Se1–Pt–Se2 90.49(2), P1–Pt–Se1 86.25(4), P2–Pt–Se2 88.34(4); *i*: 1 – *x*, –0.5 + *y*, 0.5 – *z*.

nuclei show resonance at  $\delta = 60.0$  ppm and the  $^{195}\text{Pt}\{^1\text{H}\}$  NMR spectrum reveals a triplet with  $^{77}\text{Se}$  satellites at  $\delta = -4841$  ppm ( $^1J_{\text{Pt,P}} = 2897$  Hz;  $^1J_{\text{Pt,Se}} = 167.3$  Hz). The spectroscopic data are in good agreement with values known from literature.<sup>[7b,37a,37b,38]</sup>

The molecular structures of **11a** and **11b** (assigned to the ethyl acetate solvate) revealed some interesting aspects concerning their supramolecular arrangement in the crystal (see Figures 11 and 12, respectively). The bond lengths and angles of **11a** and **11b** are comparable, with the P1–Pt–P2 angle being  $99.13(5)^\circ$  and  $97.03(8)^\circ$ , respectively. The supra-

molecular assemblies of **11a** and **11b** caused by a system of intra- and intermolecular hydrogen bonds are different due to solvent molecules in case of **11b**.

Complex **11a** crystallises in the chiral space group  $P2_12_12_1$ . Due to strong intra- and intermolecular hydrogen bonds between the hydroxy groups [ $d(\text{O1}\cdots\text{O2}) = 2.65$  Å and  $2.77$  Å, respectively] the molecules arrange into a chain-like structure along the  $a$ -axis of the crystal. This alignment can be described as a pseudo-helical arrangement with two molecules in a turn. Even more impressive is the molecular structure of **11b**. It crystallises in the tetragonal

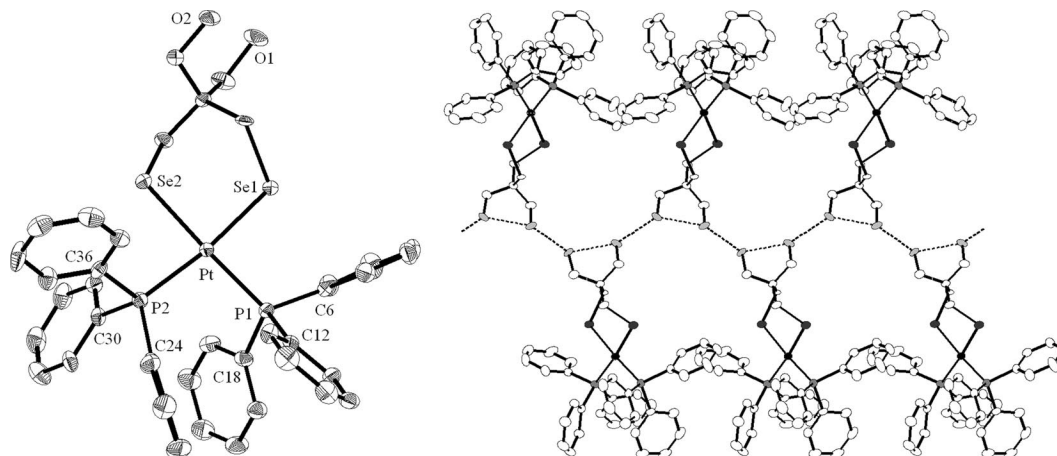


Figure 11. Left: molecular structure of **11a** in the crystal. Right: part of the double chain of **11a** in the crystal, caused by intra- and intermolecular hydrogen bonds. Ellipsoids are drawn at 50% probability level, hydrogen atoms and solvent molecules have been omitted for clarity. Selected bond lengths [Å] and angles  $^\circ$ : Pt–P1 2.2893(14), Pt–P2 2.3032(13), Pt–Se1 2.4551(5), Pt–Se2 2.4647(6), O1 $\cdots$ O2 2.65 (intramolecular), O1 $\cdots$ O2' 2.77 (intermolecular); P1–Pt–P2  $99.13(5)$ , Se1–Pt–Se2  $89.70(2)$ , P1–Pt–Se1  $87.10(4)$ , P2–Pt–Se2  $83.90(4)$ ;  $i$ :  $-0.5 + x, 0.5 - y, -1 - z$ .

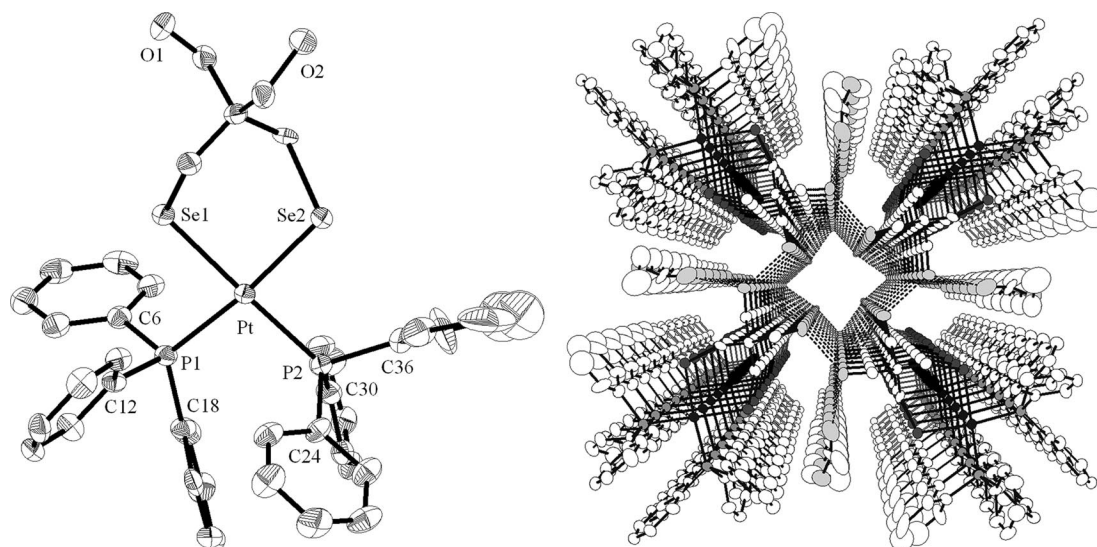


Figure 12. Left: molecular structure of **11b** in the crystal. Right: supramolecular assembly of **11b** caused by intra- and intermolecular hydrogen bonds (view along the  $c$ -axis of the crystal). Ellipsoids are drawn at 50% probability level, hydrogen atoms and non-coordinated solvent molecules have been omitted for clarity. Selected bond lengths [Å] and angles  $^\circ$ : Pt–P1 2.292(2), Pt–P2 2.288(2), Pt–Se1 2.4654(10), Pt–Se2 2.4565(10), O1 $\cdots$ O2 3.25 (intramolecular), O1 $\cdots$ O2' 2.74 (intermolecular), O2 $\cdots$ O1E 2.70 [hydrogen bond to solvent molecule (ethyl acetate)], O1 $\cdots$ O1 $^{ii}$  5.26; P1–Pt–P2  $97.03(8)$ , Se1–Pt–Se2  $90.57(3)$ , P1–Pt–Se1  $83.45(6)$ , P2–Pt–Se2  $88.92(6)$ ; symmetry operations for the tetrameric units (clockwise, starting from the lower left corner):  $i$ :  $1 + y, 1.5 - x, 0.5 - z$ ;  $ii$ :  $2.5 - x, 0.5 - y, z$ ;  $iii$ :  $1.5 - y, -1 + x, 0.5 - z$ .

space group  $P4_2/n$ , in which four molecules form a tetrameric unit through a complex hydrogen-bonding network. The intermolecular oxygen...oxygen distances are 2.74 Å between two hydroxy groups and 2.70 Å between a hydroxy group and an ethyl acetate molecule. The tetramers, accompanied by four ethyl acetate molecules, align along the fourfold axis of rotation (see Figure 12). The stacking of these tetrameric units along the  $c$ -axis results in the formation of a hydrophilic channel throughout the crystal, which is partly filled with dichloromethane molecules. The smallest diameter of the channel determined by two opposite oxygen atoms is about 5.3 Å.

The P–Pt–P angle is expected to be wider in **12** containing the monodentate phosphane 4-dppdbf than in **11** as guessed by an increase of  $^1J_{\text{P,Pt}}$  by 70 Hz to 2967 Hz ( $\delta = 16.0$  ppm). The two-bond coupling to the selenium nuclei is comparable to **11** ( $^2J_{\text{P,Se}} = 48.5$  Hz). The resonances of the  $^{77}\text{Se}$  ( $\delta = 66.1$  ppm) and  $^{195}\text{Pt}$  nuclei ( $\delta = -4848$  ppm) as derived from HMBC NMR spectra are in good agreement with the other compounds. Unfortunately, we were not able

to obtain single crystals suitable for crystal structure determination to verify the structural deductions based on NMR spectroscopy.

**[PtL<sub>2</sub>((SeCH<sub>2</sub>)<sub>2</sub>C(CH<sub>2</sub>OH)<sub>2</sub>)]** ( $L = \frac{1}{2}$  dppm,  $\frac{1}{2}$  dppma,  $\frac{1}{2}$  dppe,  $\frac{1}{2}$  dppbe) (**13–16**)

The influence of the bite angle of bidentate phosphanes on the coordination geometry was explored by utilising bidentate phosphanes of varying bite angles. The magnitude of the bite angle was adjusted by one or more spacer atoms between the two phosphorus atoms. 1,1-Bis(diphenylphosphanyl)methane should reveal a very small bite angle, resulting in a strongly distorted coordination sphere of the central metal atom. The  $^1J_{\text{P,Pt}}$  coupling constant of 2315 Hz in **13** is expectedly smaller than those in **11** and **12**. Analogously, the  $^2J_{\text{P,Se}}$  coupling constant is decreased to 32.7 Hz from ca. 48 Hz found in both **11** and **12**. The molecular structure of **13** shown in Figure 13 verifies that the P1–Pt–P2 angle is only 73.05(7)° and that the opposite Se1–Pt–Se2 angle is clearly widened from the right angle to 93.46(3)°.

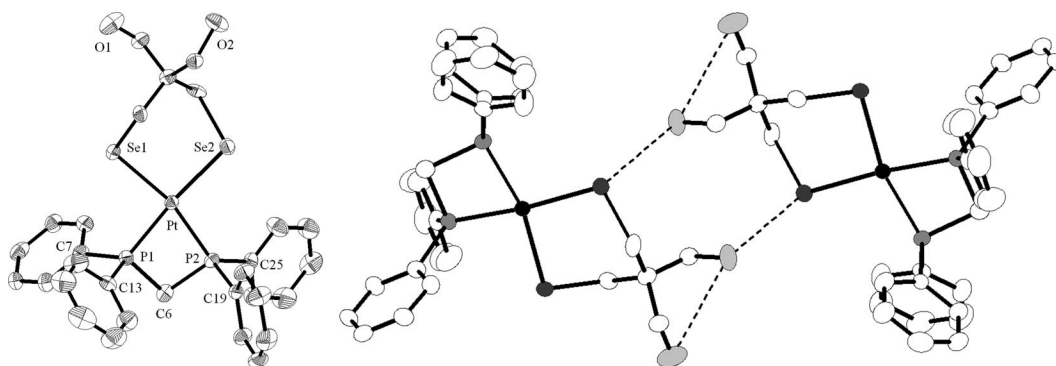


Figure 13. Left: molecular structure of **13** in the crystal. Right: dimeric unit of **13** in the crystal, displaying intramolecular O...O hydrogen bonds and intermolecular O...Se hydrogen bonds. Ellipsoids are drawn at 50% probability level, hydrogen atoms and solvent molecules have been omitted for clarity. Selected bond lengths [Å] and angles [°]: Pt–P1 2.245(2), Pt–P2 2.2713(17), Pt–Se1 2.4422(7), Pt–Se2 2.4537(8), O1...O2 3.30, O2...Se2<sup>i</sup> 3.33; P1–Pt–P2 73.05(7), Se1–Pt–Se2 93.46(3), P1–Pt–Se1 92.41(5), P2–Pt–Se2 101.09(5);  $i: -x, 1 - y, 2 - z$ .

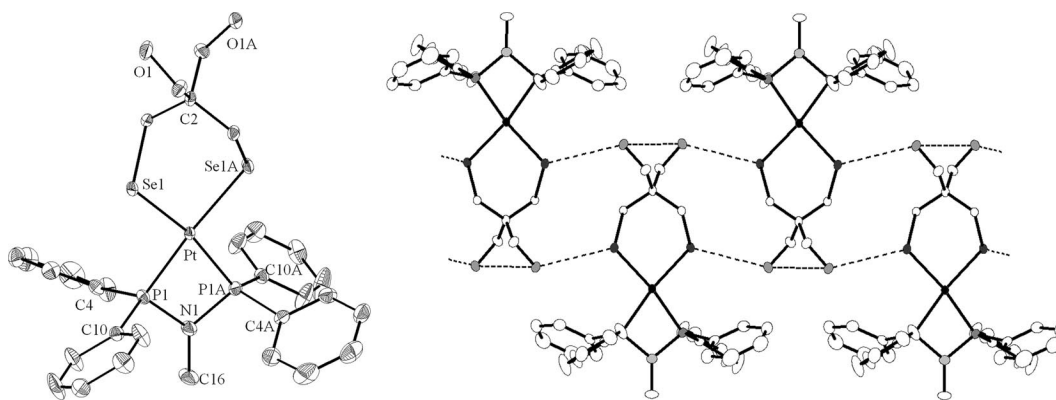


Figure 14. Left: molecular structure of **14** in the crystal. Right: part of the chains of **14** in the crystal, caused by intramolecular O...O hydrogen bonds and intermolecular O...Se hydrogen bonds. Ellipsoids are drawn at 50% probability level, hydrogen atoms have been omitted for clarity. Selected bond lengths [Å] and angles [°]: Pt–P1 2.384(8), Pt–Se1 2.4522(3), P1–N1 1.698(3), N1–C16 1.472(6), O1...O1A 3.17, O1...Se1<sup>i</sup> 3.36; P1–Pt–P1A 71.71(4), Se1–Pt–Se1A 92.480(15), P1–Pt–Se1 98.51(2);  $i: x, 0.5 - y, 0.5 - z$ .

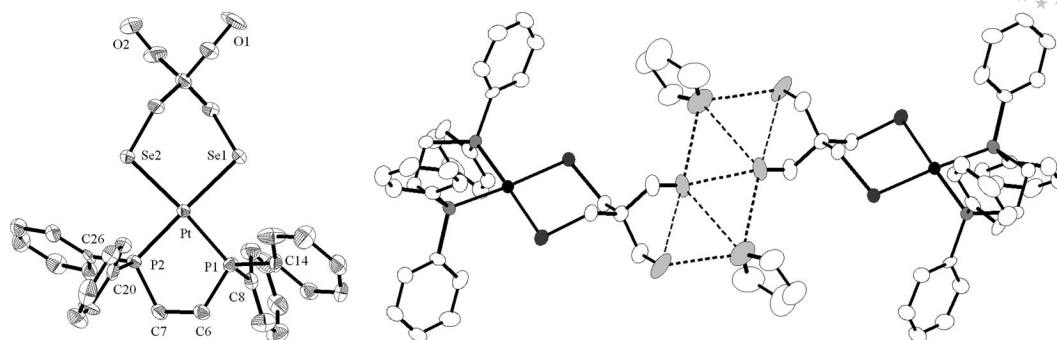


Figure 15. Left: molecular structure of **15** in the crystal. Right: dimeric unit of **15** in the crystal, displaying intra- and intermolecular hydrogen bonding. Ellipsoids are drawn at 50% probability level, hydrogen atoms and non-coordinated solvent molecules have been omitted for clarity. Selected bond lengths [Å] and angles [°]: Pt–P1 2.264(3), Pt–P2 2.248(3), Pt–Se1 2.4520(13), Pt–Se2 2.4621(12), O1...O2 3.27 (intramolecular), O2...O2' 2.79 (intermolecular), O1...OS1 2.94, O2...OS1 3.31, O2'...OS1 3.11 [hydrogen bonds to solvent molecule (thf)]; P1–Pt–P2 85.33(11), Se1–Pt–Se2 92.10(4), P1–Pt–Se1 93.00(7), P2–Pt–Se2 89.57(8); *i*: 2 – *x*, 1 – *y*, 1 – *z*.

Therefore, the platinum atom is coordinated strongly distorted from square planarity. This fact is even more apparent as the P1–Pt–Se1 and P2–Pt–Se2 angles have considerably different values of 93.46(3) and 101.09(5)°, respectively, further reducing the symmetry at the platinum centre. These differences can be explained from the molecular structure, exposing the creation of dimeric units by formation of hydrogen bonds between hydroxy groups [ $d(\text{O1} \cdots \text{O2}) = 3.30 \text{ Å}$ ] of **13**. Furthermore, close contacts between an oxygen atom of one complex and a selenium atom of another molecule were detected. The distance is  $d(\text{O2} \cdots \text{Se2}) = 3.33 \text{ Å}$  and thus clearly shorter than the sum of the van der Waals radii.

The bite angle of the phosphane was further decreased by replacing the methylene bridge in dppe with a methylamine moiety (dppma).<sup>[39]</sup> Both, the  $^{31}\text{P}$  and the  $^{195}\text{Pt}$  resonances of **14** [ $\delta(\text{P}) = 34.5 \text{ ppm}$ ,  $\delta(\text{Pt}) = -4364 \text{ ppm}$ ] are significantly shifted downfield compared to that of **13** [ $\delta(\text{P}) = -49.6 \text{ ppm}$  and  $\delta(\text{Pt}) = -4655 \text{ ppm}$  ( $^1J_{\text{Pt,P}} = 2440 \text{ Hz}$ ), respectively]. The  $^1\text{H}$   $^{77}\text{Se}$  HMBC NMR spectrum showed a multiplet at  $\delta = -47.9 \text{ ppm}$  and that is close to that of the dppm-containing complex **13**. The molecular structure and the supramolecular arrangement of **14** in the crystal are shown in Figure 14. Unexpectedly, the molecules have a twofold axis of rotation along the quaternary carbon atom of the diselenolato ligand, the platinum and nitrogen atom and the carbon atom of the methyl group (space group *Pnma*). Compared to **13** the P1–Pt–P1A angle is expectedly further reduced to 71.71(4)°, distorting the coordination sphere at the platinum atom strongly from square planarity. The intramolecular hydrogen bonds between the hydroxy groups [ $d(\text{O1} \cdots \text{O1A}) = 3.17 \text{ Å}$ ] and the intermolecular contacts between a hydroxy oxygen and a selenium atom of the adjacent molecule [ $d(\text{O1} \cdots \text{Se1}) = 3.36 \text{ Å}$ ] link the complexes into a continuous chain.

In complexes **15** and **16** the spacer between the two phosphorus atoms of the diphosphane is composed by two carbon atoms. The phosphorus atoms in both complexes show an identical resonance at  $\delta = 47.9 \text{ ppm}$ . The respective HMBC NMR spectra yielded signals at  $\delta = -42.6$  and  $-25.2 \text{ ppm}$  for the  $^{77}\text{Se}$  nuclei and at  $\delta = -4787$  and

$-4748 \text{ ppm}$  for the  $^{195}\text{Pt}$  nuclei ( $^1J_{\text{Pt,Pt}}$  is 2721 Hz for **15** and 2736 Hz for **16**). The molecular structures are very similar (see Figures 15 and 16). Both complexes crystallise as solvates. Complex **15** forms dimeric units, linked by two thf molecules through branched hydrogen bonds (see Figure 15). The bite angle of dppe in **15** is 85.33(11)° and the corresponding angle in **16** is 87.81(8)°.

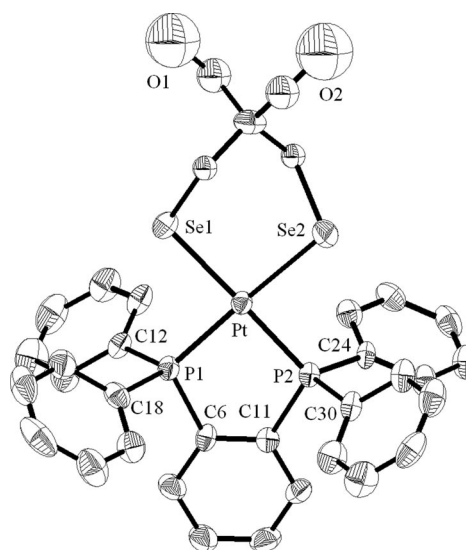


Figure 16. Molecular structure of **16** in the crystal. For the sake of clarity only one conformation is shown, ellipsoids are drawn at 50% probability level, hydrogen atoms and solvent molecules have been omitted for clarity. Selected bond lengths [Å] and angles [°]: Pt–P1 2.248(2), Pt–P2 2.235(2), Pt–Se1 2.4426(9), Pt–Se2 2.4572(10); P1–Pt–P2 87.81(8), Se1–Pt–Se2 92.28(3), P1–Pt–Se1 90.30(6), P2–Pt–Se2 89.60(6).

**[PtL<sub>2</sub>{(SeCH<sub>2</sub>)<sub>2</sub>C(CH<sub>2</sub>OH)<sub>2</sub>}] (L = ½ dppp, ½ dppn) (**17**, **18**)**

The complexes **17** and **18** involve dppp and the naphthyl-bearing dppn, respectively, and contain a spacer of three carbon atoms between the two phosphorus donors. The  $^{31}\text{P}$  resonances are observed at  $\delta = -1.9$  and 8.1 ppm with  $^1J_{\text{Pt,Pt}} = 2652$  and 2573 Hz, for compounds **17** and **18**, respectively. The increased value of  $^1J_{\text{Pt,Pt}}$  in **17** compared to that

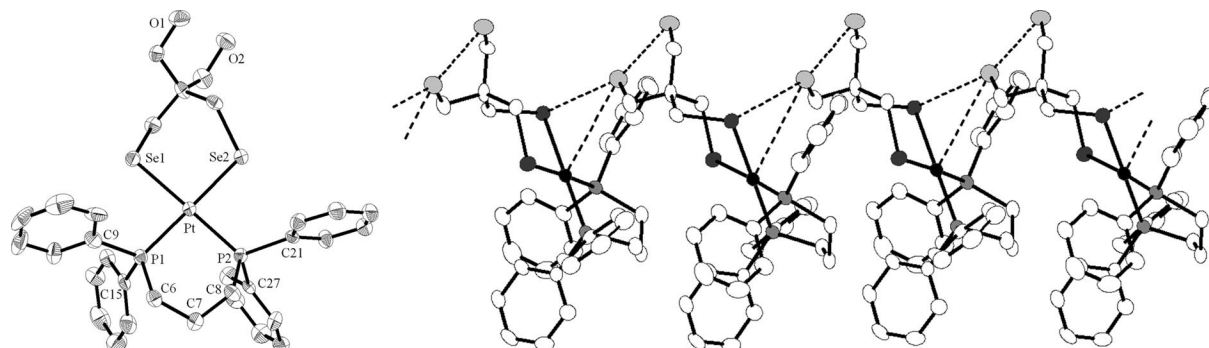


Figure 17. Left: molecular structure of **17** in the crystal. Right: part of the chains of **17** built by intra- and intermolecular hydrogen bonds. Ellipsoids are drawn at 50% probability level, hydrogen atoms and solvent molecules have been omitted for clarity. Selected bond lengths [Å] and angles [°]: Pt–P1 2.268(2), Pt–P2 2.266(2), Pt–Se1 2.4652(9), Pt–Se2 2.4652(8), O1...O2 2.69, O2...Se1<sup>i</sup> 3.46, O2...Pt<sup>i</sup> 3.89; P1–Pt–P2 91.98(8), Se1–Pt–Se2 91.69(3), P1–Pt–Se1 87.39(6), P2–Pt–Se2 88.91(5); *i*: *x*, 0.5 – *y*, –0.5 + *z*.

in **18** indicates a larger bite angle in dppp than in dppn. Both the <sup>77</sup>Se and <sup>195</sup>Pt resonances of **18** are also shifted downfield due to the presence of the naphthalene bridge, appearing at  $\delta = 39.7$  ppm for selenium (**17**:  $\delta = 12.4$  ppm) and at  $\delta = -4686$  ppm for platinum (**17**:  $\delta = -4758$  ppm).

The molecular structures of **17** and **18** show the expected differences in the bite angle (see Figures 17 and 18). The P1–Pt–P2 angle in **17** is 91.98(8)°, while the analogous angle in **18** is only 88.36(10)° due to the rigid backbone in dppn. The coordination sphere of the metal centre in both complexes is close to square planarity. Additionally, the dihedral angle between the phosphorus atoms at the naphthalene moiety is found to be as small as 0.45°, arranging it with the atoms surrounding the platinum centre almost perfectly coplanar. Therefore, the dppn ligand serves well for the formation of complexes close to perfect square-planar coordination.

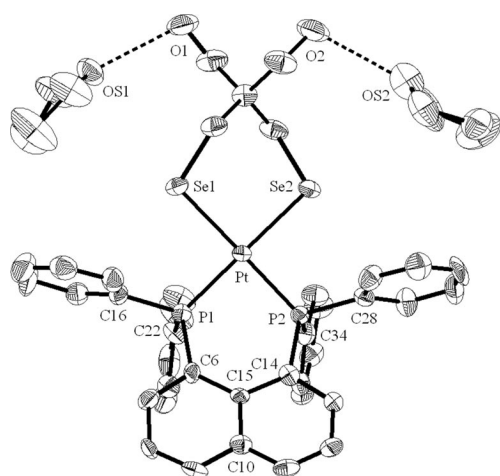


Figure 18. Molecular structure of **18** as thf solvate in the crystal. Ellipsoids are drawn at 50% probability level, hydrogen atoms have been omitted for clarity. Selected bond lengths [Å] and angles [°]: Pt–P1 2.243(3), Pt–P2 2.248(3), Pt–Se1 2.4548(11), Pt–Se2 2.4582(11), O1...OS1 2.85, O2...OS2 2.80 [hydrogen bonds to solvent molecules (thf)]; P1–Pt–P2 88.36(10), Se1–Pt–Se2 91.09(4), P1–Pt–Se1 90.77(8), P2–Pt–Se2 89.55(7), P1–C6...C14–P2 0.45.

As shown in Figure 17, complex **17** forms intramolecular [ $d(\text{O1}\cdots\text{O2}) = 2.69$  Å] hydrogen bonds. In addition, there are intermolecular hydrogen bonds between a hydroxy group and one selenium atom and the platinum centre of an adjacent molecule. The distances  $d(\text{O2}\cdots\text{Se1}) = 3.46$  Å and  $d(\text{O2}\cdots\text{Pt}) = 3.89$  Å are still below the sum of the van der Waals radii and indicate weak interactions. Complex **18** crystallises as a thf solvate, with each hydroxy group forming a hydrogen bond to the oxygen of a thf molecule [ $d(\text{O1}\cdots\text{OS1}) = 2.85$  Å and  $d(\text{O2}\cdots\text{OS2}) = 2.80$  Å].

**[PtL<sub>2</sub>(SeCH<sub>2</sub>)<sub>2</sub>C(CH<sub>2</sub>OH)<sub>2</sub>] (L = ½ dppb, ½ dppo-xyl) (**19**, **20**)**

The complexes **19** and **20**, bearing the bidentate phosphanes dppb and dppo-xyl, both contain a spacer of four atoms. While the dppo-xyl moiety should result in a rather rigid conformation of the metallacycle, the corresponding compound containing the dppb ligand is expected to be more flexible. The NMR spectroscopic data of both compounds are comparable considering the shifts of the resonances, being  $\delta = 13.7$  and 1.2 ppm for the <sup>31</sup>P,  $\delta = 27.9$  and 33.2 ppm for the <sup>77</sup>Se and  $\delta = -4817$  and  $-4834$  ppm for the <sup>195</sup>Pt nuclei, for **19** and **20**, respectively. A first evaluation of the bite angle can be obtained from the phosphorus platinum coupling constants. For **19** and **20** <sup>1</sup>J<sub>Pt</sub> were determined to be 2783 and 2847 Hz, respectively, surpassing all values of the aforementioned complexes bearing bidentate phosphanes. Consequently, the bite angle is expected to be enlarged in **19** and **20**.

As shown in Figure 19 the dppb bridge of **19** seems to be quite flexible, resulting in a bite angle of 95.06(8)° and hence is in agreement with the expectations. In the crystal, **19** arranges in dimeric units built via intra- and intermolecular hydrogen bonds. Both hydroxy groups form triple-branched hydrogen bonds. Two close contacts are observed between oxygen atoms from hydroxy groups [ $d(\text{O1}\cdots\text{O2}) = 3.37$  Å, intramolecular;  $d(\text{O1}\cdots\text{O1}) = 2.78$  Å, intermolecular] and one strong hydrogen bond to chlorine from cocrystallised chloroform, only 2.69 Å [ $d(\text{O2}\cdots\text{Cl})$ ] long. The supramolecular alignment of **20** is comparable to **19**,

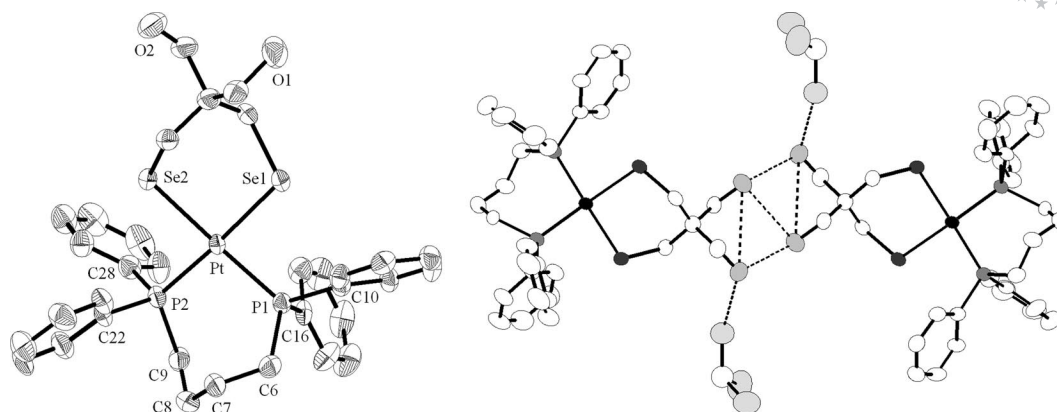


Figure 19. Left: molecular structure of **19** in the crystal. Right: dimeric unit of **19** formed via intra- and intermolecular hydrogen bonds. Ellipsoids are drawn at 50% probability level, hydrogen atoms have been omitted for clarity. Selected bond lengths [Å] and angles [°]: Pt–P1 2.284(2), Pt–P2 2.4430(9), Pt–Se1 2.4737(9), O1...O2 3.37 (intramolecular hydrogen bond), O1...O2<sup>i</sup> 2.78, O1...O1<sup>i</sup> 3.09 (intermolecular hydrogen bonds), O2...C11 2.69 [hydrogen bond to solvent molecule (chloroform)]; P1–Pt–P2 95.06(8), Se1–Pt–Se2 91.25(3), P1–Pt–Se1 87.77(6), P2–Pt–Se2 85.88(6); *i*: –*x*, 4 – *y*, –*z*.

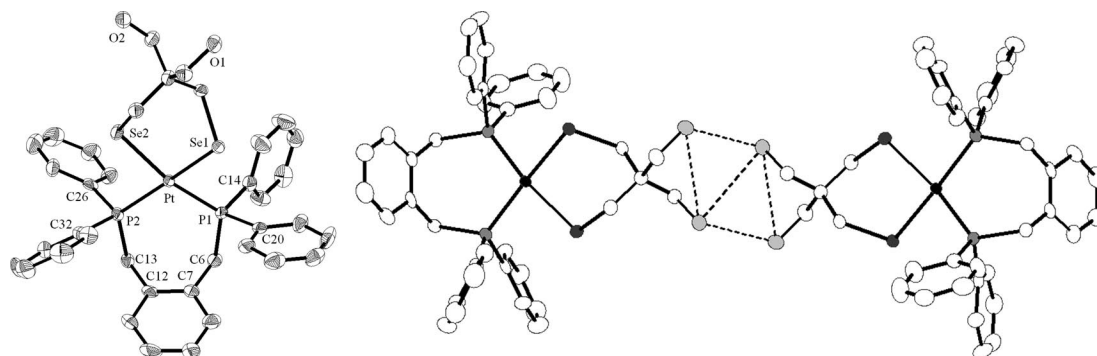


Figure 20. Left: molecular structure of **20** in the crystal. Right: dimeric unit of **20** in the crystal, displaying intra- and intermolecular hydrogen bonding. Ellipsoids are drawn at 50% probability level, hydrogen atoms and solvent molecules have been omitted for clarity. Selected bond lengths [Å] and angles [°]: Pt–P1 2.2564(18), Pt–P2 2.2682(17), Pt–Se1 2.4672(7), Pt–Se2 2.4614(8), O1...O2 3.40 (intramolecular hydrogen bond), O1...O2<sup>i</sup> 2.85, O2...O2<sup>i</sup> 3.34 (intermolecular hydrogen bonds); P1–Pt–P2 101.21(6), Se1–Pt–Se2 90.87(2), P1–Pt–Se1 85.38(5), P2–Pt–Se2 84.55(5); *i*: 1 – *x*, –*y*, 1 – *z*.

just varying in the shape of the branched hydrogen bonds without involvement of solvent molecules (Figure 20). Instead three oxygen...oxygen contacts are monitored, one short intermolecular distance being  $d(\text{O1}\cdots\text{O2}) = 2.85$  Å and one intra- and intermolecular contact each [ $d(\text{O1}\cdots\text{O2}) = 3.40$  Å and  $d(\text{O2}\cdots\text{O2}) = 3.34$  Å, respectively]. Most interesting is the rigidity of the *o*-xylene bridging moiety, expanding the P1–Pt–P2 angle to 101.21(6)° and thus clearly distorting the platinum centre from a square-planar coordination. This enlargement is at the expense of the P–Pt–Se angles, which are reduced to 85.38(5)° and 84.55(5)°, whereas the bite angle of the diselenolato ligand is determined to 90.87(2)°.

#### Attempted Synthesis of $[\text{Pt}\{(\text{SeCH}_2)_2\text{C}(\text{CH}_2\text{OH})_2\}-(\text{xantphos})]$ (**21**)

4,5-Bis(diphenylphosphanyl)-9,9-dimethylxanthene is a diphosphane with a spacer of five atoms. The complex formation, however, led to surprising results. The  $^{31}\text{P}\{^1\text{H}\}$  NMR spectrum showed the expected resonance at

$\delta = 15.1$  ppm ( $^1J_{\text{P,Pt}} = 2886$  Hz) displaying also  $^{77}\text{Se}$  satellites ( $^2J_{\text{P,Se}} = 39.6$  Hz) and the HMBC NMR spectra exhibited resonances at  $\delta = 64.9$  and  $-4892$  ppm for  $^{77}\text{Se}$  and  $^{195}\text{Pt}$ , respectively. However, the elemental analysis and mass spectrum of the solid product were not consistent with the composition of **21** nor did it match with any amount of cocrystallised solvent.

The observed carbon content is 5% smaller than that calculated for **21**. Furthermore, the product contained 9.9% of chlorine that should not be present in **21**. The mass spectrum showed the parent ion at  $m/z = 2298$  with the isotopic pattern consistent with the presence of two platinum and two selenium atoms. The base peak was observed at  $m/z = 1131$  and was inferred to be due to a doubly charged positive ion indicating a mass of 2262 g/mol. Therefore, the difference between the parent ion and the base peak seems to equal HCl or chlorine. Hence, in the solid state some species must have been formed containing at least two platinum centres.

Upon crystallisation, a mixture of two types of crystals was obtained and their investigation exposed two different

molecular structures, neither being the expected complex **21**. One of them showed a doubly charged complex cation bearing two platinum-phosphane moieties and only one diselenolato ligand with chloride counterions (**22**, see Figure 21). Comparable complexes have been prepared by Singhal et al. from the reaction of  $[\text{ML}_2(\text{SeR})_2]$  ( $\text{L} = \frac{1}{2}$  bidentate phosphane) and metal(II) phosphane fragments.<sup>[34c]</sup> Each selenium atom in **22** acts as  $\mu$ -bridging donor between the two platinum centres. Both platinum atoms show a strongly distorted square-planar coordination environment. Xantphos showed two clearly differing bite angles of  $107.65(5)^\circ$  and  $100.61(6)^\circ$  at Pt1A and Pt1B, respectively. The expansion of the P–Pt–P angles is at the expense of a decrease of the Se–Pt–Se angles, which measure  $77.501(19)^\circ$  and  $78.032(19)^\circ$  for Pt1A and Pt1B, respectively. The coordination planes are hinged at the bridging selenium atoms with the angle between the least-squares planes involving the platinum centres (P1A, P2A, Pt1A, Se1, Se2 and P1B, P2B, Pt1B, Se1, Se2) is  $144.09^\circ$ . Another evidence for the asymmetry of **22** in the crystal is seen in the arrangement of the two xanthene moieties indicated by the dihedral angles between the mean planes of the platinum atoms and the planes through the phosphorus and *ipso*-carbon atoms of the according xanthene. While this angle is determined to  $165.0^\circ$  at Pt1A, arranging the xanthene group almost in the platinum plane, the analogous angle at Pt1B measures  $83.5^\circ$ , locating it more perpendicular. One of the chloride counterions is bound by a hydrogen bond to the hydroxy groups with the distances between chlorine and oxygen of  $3.03 \text{ \AA}$  and  $3.10 \text{ \AA}$ . The second chloride ion shows a close contact of  $3.24 \text{ \AA}$  to Pt1B and expanding the coordination sphere of the platinum atom to a pseudo-square pyramid. Consequently, the platinum atom deviates from the least-squares plane by  $0.2 \text{ \AA}$  towards the chloride ion.

The second crop of crystals gave the molecular structure shown in Figure 22 (complex **23**). It shows a doubly positive-charged trinuclear complex cation with two chloride counterions. It can be described as two molecules of **21** linked by a platinum atom. The platinum centres are bridged by selenolato ligands. The cation of **23** is symmetric and the central platinum atom is located at the centre of inversion. The Se1–Pt2–Se2 angle is  $83.91(3)^\circ$ , the Se1–Pt2–Se2A angle is  $96.09(3)^\circ$ .

The bite angle of the xantphos ligand in **23** involving the coordination to Pt1 is  $101.69(8)^\circ$  and the opposite Se1–Pt1–Se2 angle is decreased to  $81.00(3)^\circ$ . The angle between the least-squares planes of the platinum atoms is  $130.14^\circ$  (planes through atoms P1, P2, Pt1, Se1, Se2 and Se1, Se2, Pt2, Se1A, Se2A). The dihedral angle between the platinum coordination plane and the xanthene moiety has a value of  $81.4^\circ$  again arranging it perpendicular. The platinum–selenium bond lengths at the central Pt atom are significantly shorter [ $d(\text{Pt2–Se1}) = 2.4202(8) \text{ \AA}$  and  $d(\text{Pt2–Se2}) = 2.4181(8) \text{ \AA}$ ] than the corresponding bonds involving the phosphane coordinated platinum atom Pt1 [ $d(\text{Pt1–Se1}) = 2.4919(8) \text{ \AA}$  and  $d(\text{Pt1–Se2}) = 2.4890(9) \text{ \AA}$ ]. The two chloride counterions are linked by hydrogen bonds to the hy-

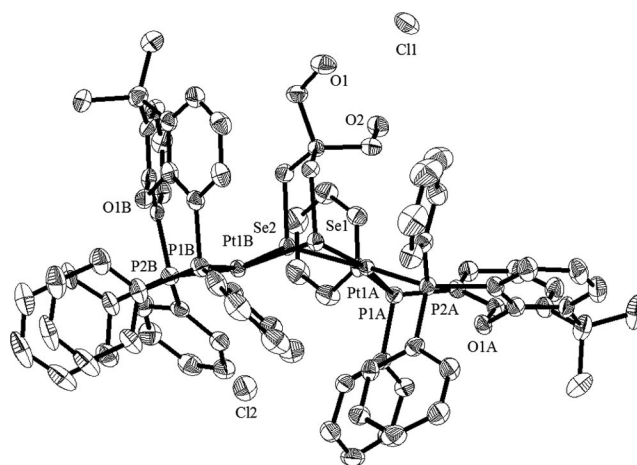


Figure 21. Molecular structure of **22** in the crystal. Ellipsoids are drawn at 50% probability level, hydrogen atoms and solvent molecules have been omitted for clarity. Selected bond lengths [ $\text{\AA}$ ] and angles [ $^\circ$ ]: Pt1A–P1A  $2.3349(14)$ , Pt1A–P2A  $2.3450(16)$ , Pt1A–Se1  $2.4766(6)$ , Pt1A–Se2  $2.4739(6)$ , Pt1B–P1B  $2.3021(15)$ , Pt1B–P2B  $2.3046(16)$ , Pt1B–Se1  $2.4632(6)$ , Pt1B–Se2  $2.4600(6)$ , O1...Cl1  $3.10$ , O2...Cl1  $3.03$ , Pt1B...Cl2  $3.24$ ; P1A–Pt1A–P2A  $107.65(5)$ , Se1–Pt1A–Se2  $77.501(19)$ , P1A–Pt1A–Se2  $88.50(4)$ , P2A–Pt1A–Se1  $85.85(4)$ , P1B–Pt1B–P2B  $100.61(6)$ , Se1–Pt1B–Se2  $78.032(19)$ , P1B–Pt1B–Se1  $90.25(4)$ , P2B–Pt1B–Se2  $88.60(4)$ ; the dihedral angle between the platinum mean planes (P1A, P2A, Pt1A, Se1, Se2) and (P1B, P2B, Pt1B, Se1, Se2) is  $144.09^\circ$ .

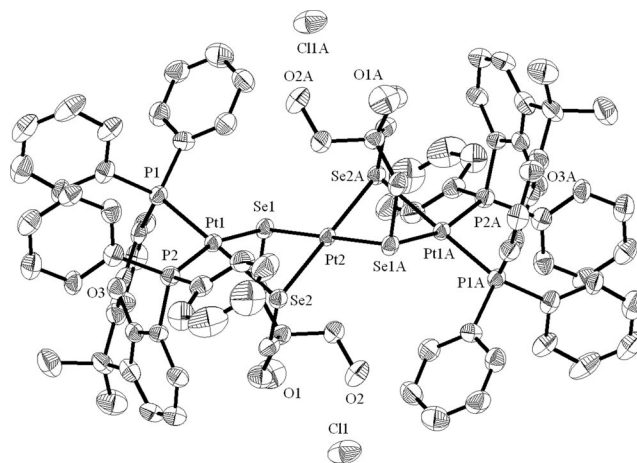


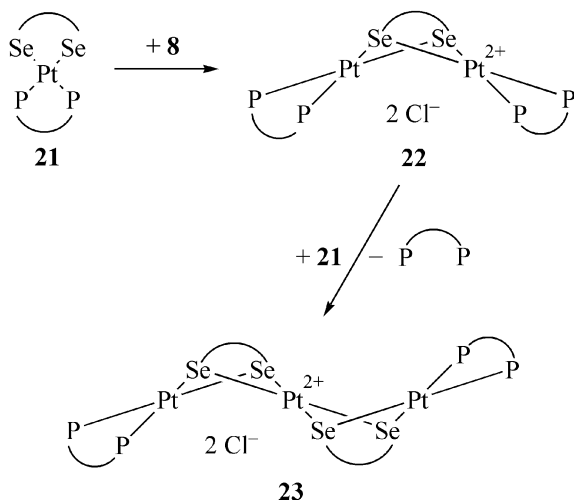
Figure 22. Molecular structure of **23** in the crystal. Ellipsoids are drawn at 50% probability level, hydrogen atoms and solvent molecules have been omitted for clarity. Selected bond lengths [ $\text{\AA}$ ] and angles [ $^\circ$ ]: Pt1–P1  $2.287(2)$ , Pt1–P2  $2.285(2)$ , Pt1–Se1  $2.4919(8)$ , Pt1–Se2  $2.4890(9)$ , Pt2–Se1  $2.4202(8)$ , Pt2–Se2  $2.4181(8)$ , O1...Cl1  $3.05$ , O2...Cl1  $3.28$ ; P1–Pt1–P2  $101.69(8)$ , Se1–Pt1–Se2  $81.00(3)$ , P1–Pt1–Se1  $87.45(5)$ , P2–Pt1–Se2  $88.38(6)$ , Se1–Pt2–Se2  $83.91(3)$ , Se1–Pt2–Se2A  $96.09(3)$ ; the dihedral angle between the least-squares planes (P1, P2, Pt1, Se1, Se2) and (Se1, Se2, Pt2, Se1A, Se2A) is  $130.14^\circ$ .

droxy groups, showing oxygen chlorine contacts of  $3.05 \text{ \AA}$  and  $3.28 \text{ \AA}$ .

The elemental analysis can be explained in terms of a 1:1 mixture of **22** and **23** together with three equivalents of solvent chloroform. The  $m/z = 2298$  in the mass spectrum can be assigned to  $(\mathbf{23})^+$  upon loss of one  $\text{Cl}^-$ , and the base

peak at  $m/z = 1131$  to **(23)**<sup>2+</sup> upon loss of both Cl<sup>−</sup> anions. Still unsettled remains the fact that no evidence for the constitution of **22** and **23** can be obtained from phosphorus, selenium and platinum NMR spectra. As the selenium atoms in **22** and **23** are magnetically equivalent each and their signal appears as multiplet, no hint for the structure can be expected. The <sup>31</sup>P{<sup>1</sup>H} NMR and <sup>1</sup>H <sup>195</sup>Pt HMBC NMR spectra of **21** should differ remarkably from the spectra of **23** as additional coupling to the central platinum atom can be expected. However none of the expected splittings was detected.

A proposed reaction mechanism for the formation of **22** and **23** is shown in Scheme 4. The desired complex **21** might react with one equivalent of **8** giving **22**, which might form **23** on reaction with another molecule of **21** with elimination of xantphos. Repeated experiments gave comparable analytical results, thus it must be concluded that complex **21** is not stable. It is assumed that the instability is due to the large bite angle of xantphos.



Scheme 4. Proposed formation of complexes **22** and **23** from **21** [where the bridged selenium ligand is 2,2-bis(hydroxymethyl)-1,3-diselenolotopropane, the phosphane moiety is xantphos].

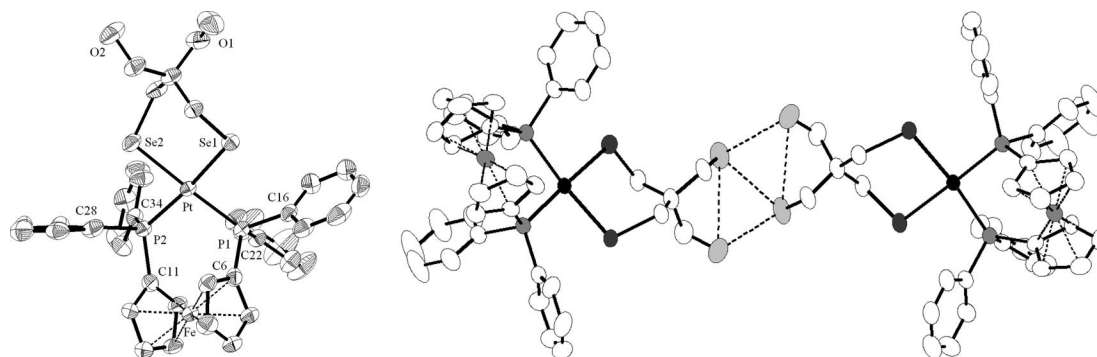


Figure 23. Left: molecular structure of **24** in the crystal. Right: dimeric unit of **24** formed via intra- and intermolecular hydrogen bonds. Ellipsoids are drawn at 50% probability level, hydrogen atoms have been omitted for clarity. Selected bond lengths [Å] and angles [°]: Pt–P1 2.2792(17), Pt–P2 2.2918(18), Pt–Se1 2.4527(7), Pt–Se2 2.4586(7), O1...O2 3.39 (intramolecular hydrogen bond), O1...O2<sup>i</sup> 2.83, O2...O2<sup>i</sup> 2.96 (intermolecular hydrogen bonds); P1–Pt–P2 96.99(6), Se1–Pt–Se2 90.53(3), P1–Pt–Se1 88.12(5), P2–Pt–Se2 84.41(5); *i*: 1 – *x*, *y*, 1.5 – *z*.

### [PtL<sub>2</sub>{(SeCH<sub>2</sub>)<sub>2</sub>C(CH<sub>2</sub>OH)<sub>2</sub>}] (L = ½ dppf) (**24**)

Dppf serves as an example for a diphosphane with a large bite angle, resulting in the stable complex **24**. The <sup>1</sup>J<sub>P,Pt</sub> of the complex **24** obtained from the <sup>31</sup>P{<sup>1</sup>H} NMR spectrum is 2952 Hz and indicates a wide P1–Pt–P2 angle. The HMBC NMR spectra gave the <sup>77</sup>Se and <sup>195</sup>Pt resonances at  $\delta = 61.6$  and  $-4786$  ppm, respectively. Single crystals that were suitable for X-ray structure determination were grown by diffusion of hexane into a concentrated chloroform solution. The molecular structure shows the bite angle of dppe of 96.99(6)° and the Se1–Pt–Se2 angle of 90.53(3)° (see Figure 23). The molecules of **24** are linked into dimeric units by hydrogen bonding. Close inter- and intramolecular oxygen...oxygen contacts are in the range of 2.8 to 3.4 Å. The complex **24** slowly decomposes in chlorinated solvents after several days, as indicated from the colour of the solution and NMR spectra.

### [ML<sub>2</sub>{(SeCH<sub>2</sub>)<sub>2</sub>C(CH<sub>2</sub>OH)<sub>2</sub>}] (M = Pd, Ni; L = ½ dppe, ½ dppn, ½ dppf) (**25–28**)

The effect of the metal centre on the bite angle and stability of the complexes was explored by preparing Pd<sup>II</sup> or Ni<sup>II</sup> complexes that are analogues to the Pt<sup>II</sup> complexes described above. The complex **25** is the palladium analogue of **15** with the bidentate dppe ligand. The <sup>31</sup>P{<sup>1</sup>H} NMR spectrum showed a resonance at  $\delta = 49.2$  ppm with two sets of satellites due to the coupling to two magnetically inequivalent <sup>77</sup>Se nuclei. The two phosphorus atoms exhibit different magnitudes to *cis*- and *trans*-coupling (<sup>2</sup>J<sub>P,Se</sub> = 29.6 and 50.1 Hz). This is in good agreement with reported values, though the assignment to *cis*- and *trans*-coupling cannot be made.<sup>[7b,7d,13,34c,34e,37d,37e]</sup> The <sup>1</sup>H <sup>77</sup>Se HMBC NMR showed a broad resonance at  $\delta = 8.8$  ppm.

Crystals suitable for structure analysis were obtained by slow diffusion of hexane into a concentrated chloroform/methanol solution. There are two symmetry-independent molecules (**A** and **B**) of **25** in the asymmetric unit, as shown in Figure 24. The bond lengths and angles are comparable to the platinum analogue **15**. The bite angle of the dppe ligand is 85.84(7)° and 85.42(7)° for **A** and **B**, respectively.

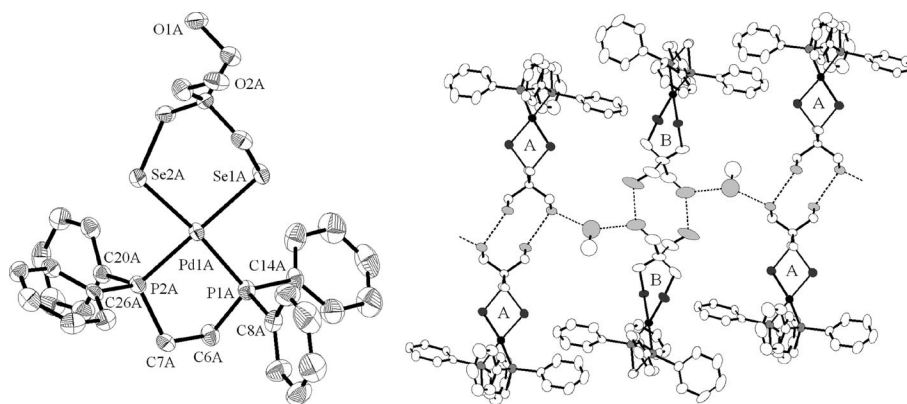


Figure 24. Left: molecular structure of one of the two symmetry-independent molecules of **25** in the crystal. Right: supramolecular arrangement of the independent molecules **A** and **B** in the crystal with intra- and intermolecular hydrogen bonds. Ellipsoids are drawn at 50% probability level, hydrogen atoms and non-coordinated solvent molecules have been omitted for clarity. Selected bond lengths [Å] and angles [°], the first value is assigned to molecule **A**, the second to **B**, respectively: Pd–P1 2.280(2)/2.2640(18), Pd–P2 2.2724(18)/2.2799(19), Pd–Se1 2.4518(8)/2.4437(9), Pd–Se2 2.4573(9)/2.4536(9), O1A...O2A<sup>i</sup> 2.77, O1B<sup>ii</sup>...O2B<sup>iii</sup> 2.68, O2A...OS 2.71, O2B<sup>iii</sup>...OS 2.76 [hydrogen bonds to solvent molecule (methanol)]; P1–Pd–P2 85.84(7)/85.42(7), Se1–Pd–Se2 93.09(3)/92.94(3), P1–Pd–Se1 92.88(5)/85.19(5), P2–Pd–Se2 88.54(5)/96.74(5); *i*:  $-1 - x, -y, 1 - z$ ; *ii*:  $1 + x, 0.5 - y, 0.5 + z$ ; *iii*:  $-1 - x, -0.5 + y, 1.5 - z$ .

The respective Se1–Pd–Se2 angles are widened to 93.09(3)° and 92.94(3)°. The P1–Pd–Se1 and P2–Pd–Se2 angles were significantly different, one being enlarged to 92.88(5)°/96.74(5)° and the other diminished to 88.54(5)°/85.19(5)° for **A/B**, respectively. The independent molecules form dimeric units (each **A/A** and **B/B**) due to hydrogen bonding [ $d(\text{O1A/B} \cdots \text{O2A/B}) = 2.77$  Å and 2.68 Å for **A** and **B**, respectively]. They also align into a double chain-like structure linked by hydrogen bonds to solvent methanol [ $d(\text{O2A/B} \cdots \text{OS}) = 2.71$  Å and 2.76 Å for **A** and **B**, respectively]. The intermolecular hydrogen bonds show oxygen...oxygen distances of 2.77 Å for **A** and 2.68 Å for **B**, respectively, the distances to the oxygen atom of methanol are 2.71 Å and 2.76 Å. We note that **25** decomposes in thf solution within two or three days, as indicated by its NMR spectra.

The  $^{31}\text{P}\{^1\text{H}\}$  resonance of complex **26** ( $\delta = 13.5$  ppm) also shows two sets of  $^{77}\text{Se}$  satellites, giving similar *cis*- and *trans*-coupling constants ( $^2J_{\text{P,Se}} = 33.7$  and 40.8 Hz). The  $^{31}\text{P}\{^1\text{H}\}$  NMR spectrum of **27** revealed a resonance at  $\delta = 20.9$  ppm with only one pair of  $^{77}\text{Se}$  satellites ( $^2J_{\text{P,Se}} = 48.6$  Hz). The  $^{77}\text{Se}$  chemical shifts are found at  $\delta = 93.0$  and 134.7 ppm for **26** and **27**, respectively. Thus, the  $^{77}\text{Se}$  resonance of **26** is shifted downfield more than 50 ppm compared to the platinum analogue **18**, while the downfield shift of **27** compared to the corresponding platinum complex **24** is even larger (>70 ppm). The deshielding of the selenium nuclei might be explained by a better  $\pi$ -acceptor ability of palladium compared with platinum because of a better overlap of the orbitals of selenium and palladium. Unfortunately no crystals suitable for single-crystal X-ray structure determination of **26** could be obtained, as the compound decomposed in thf solutions within two days (the crystals of the platinum analogue **18** could only be grown from thf solutions).

On the other hand, suitable crystals of **27** were grown from concentrated chloroform solution (see Figure 25). The palladium–selenium bonds of 2.4453(8) Å and 2.4287(9) Å

are slightly shorter than the corresponding platinum–selenium bonds of 2.4527(7) Å and 2.4586(7) Å in **24**. The metal–phosphorus bonds of 2.3391(19) Å and 2.3187(17) Å are longer in **27** than in **24** [ $d(\text{Pt–P}) = 2.2792(17)$  Å and 2.2918(18) Å]. The bite angle of dppf in **27** is 99.34(6)° and therefore is enlarged by more than 2° compared to that in **24**. The supramolecular assembly of the dppf-bearing **27** is comparable to that of **13**, containing the dppm moiety (see Figures 25 and 13). Dimeric units are formed through intermolecular hydrogen bonds between a hydroxy group of one molecule and a selenium atom of a neighbouring one. The oxygen...selenium distance is determined to 3.27 Å [cf.  $d(\text{O} \cdots \text{Se}) = 3.33$  Å in **13**]. Like in many of the complexes described in this work, an intramolecular hydrogen bond between the two hydroxy groups of each molecule is detected [ $d(\text{O1} \cdots \text{O2}) = 2.69$  Å].

The palladium complexes **25–27** are less stable than their platinum analogues. This trend continues with the nickel complexes that are quite unstable. The dppe-containing nickel(II) complex **28** readily starts to decompose in chlorinated solvents, the main products being dppe-dioxide and **2**. Apparently, some inorganic nickel species are also developed, as indicated by the green colour of the aqueous solutions. Nonetheless, we were able to obtain **28** in analytical purity. Its  $^{31}\text{P}\{^1\text{H}\}$  NMR spectrum again exhibits a single resonance at  $\delta = 59.9$  ppm with two sets of  $^{77}\text{Se}$  satellites due to the aforementioned inequivalence ( $^2J_{\text{P,Se}} = 48.8$  and 54.2 Hz). The  $^1\text{H}$   $^{77}\text{Se}$  HMBC NMR spectrum showed a multiplet at  $\delta = 24.9$  ppm in which the coupling constants could not be resolved.

Crystals suitable for single-crystal X-ray structure determination were obtained by diffusion of hexane into a concentrated chloroform solution of **28** under non-inert conditions. As shown in Figure 26, the crystals included a half equivalent of dppe dioxide, which was generated by the decomposition of **28**. The bite angle of dppe in the  $\text{Ni}^{\text{II}}$  complex is 87.58(8)° and the opposite Se1–Ni–Se2 angle is wid-

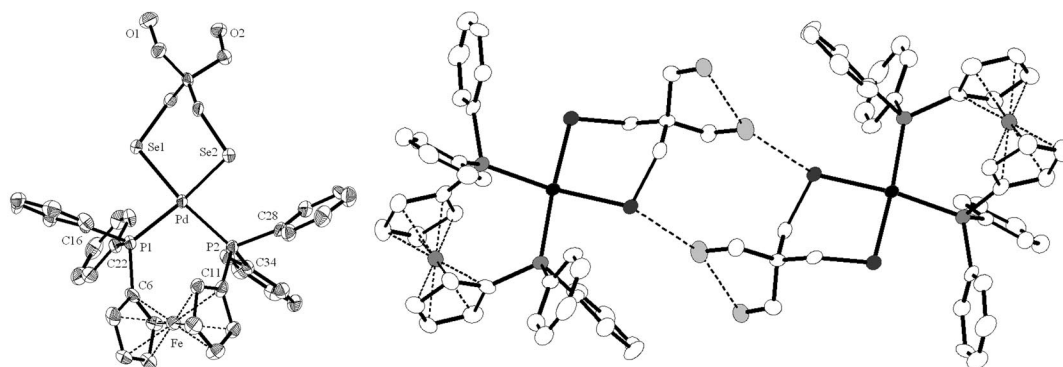


Figure 25. Left: molecular structure of **27** in the crystal. Right: dimeric unit of **27** formed via intermolecular hydrogen bonds. Ellipsoids are drawn at 50% probability level, hydrogen atoms and solvent molecules have been omitted for clarity. Selected bond lengths [Å] and angles [°]: Pd–P1 2.3391(19), Pd–P2 2.3187(17), Pd–Se1 2.4453(8), Pd–Se2 2.4287(9), O1...O2 2.69, O1...Se1<sup>i</sup> 3.27; P1–Pd–P2 99.34(6), Se1–Pd–Se2 90.29(3), P1–Pd–Se1 85.97(5), P2–Pd–Se2 85.85(5); *i*: 1 – *x*, 1 – *y*, 1 – *z*.

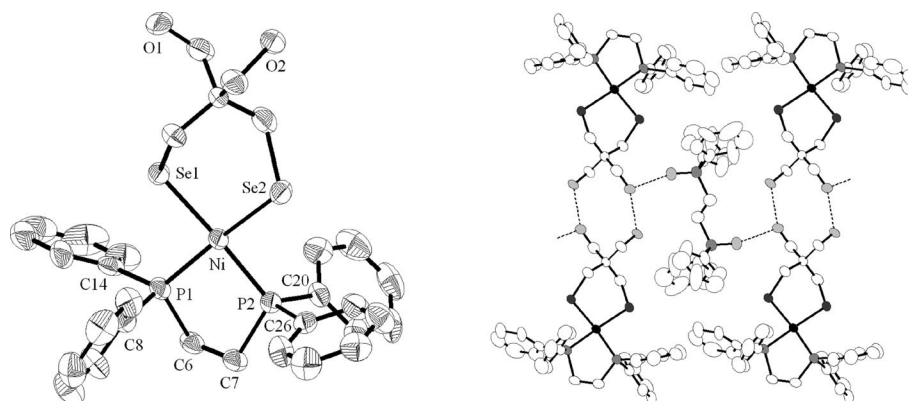


Figure 26. Left: molecular structure of **28** in the crystal. Right: arrangement of the dimeric units of **28** and hydrogen bridging to cocrystallised dppe dioxide. Ellipsoids are drawn at 50% probability level, hydrogen atoms and solvent molecules have been omitted for clarity. Selected bond lengths [Å] and angles [°]: Ni–P1 2.1467(19), Ni–P2 2.152(2), Ni–Se1 2.2977(12), Ni–Se2 2.3081(13), O1...O2<sup>i</sup> 2.66 (intermolecular hydrogen bonds), O1...OP1 2.61 (hydrogen bonds to cocrystallised dppe dioxide); P1–Ni–P2 87.58(8), Se1–Ni–Se2 96.02(5), P1–Ni–Se1 87.43(6), P2–Ni–Se2 89.43(6); *i*: –*x*, 1 – *y*, 1 – *z*.

ened to 96.02(5)° consistent with the distorted square-planar coordination. The intermolecular hydrogen bonds between two molecules of **28** are 2.66 Å and the oxygen...oxygen distance between the hydroxy groups and the dppe dioxide is 2.61 Å. In consequence of the cocrystallisation of dppe dioxide, a chain-like structure is formed, with dimeric units of **28** linked by the phosphane dioxide involving hydrogen bonds.

#### Attempted Synthesis of [Ni(dppn)]{(SeCH<sub>2</sub>)<sub>2</sub>C(CH<sub>2</sub>OH)<sub>2</sub>}

All attempts to synthesise the nickel analogue of **18** and **26** following the established procedure failed due to the fast decomposition of the complex. The desired compound might be rapidly formed, as indicated by the deep red colour of the reaction mixture that fast lightened to orange. After common workup procedures and purification using column chromatography, **2** was obtained in almost a quantitative yield. The second fraction yielded the dppn mono-oxide **29**. As the ethanol might act as an oxygen donor, the

reaction was additionally carried out in dry and degassed diethyl ether using lithium aluminium hydride to reduce **2** to the diselenolato species (see Supporting Information, procedure **B**). Upon addition of **4** dissolved in thf, the colour again changed to deep red and lightened very quickly. The <sup>31</sup>P{<sup>1</sup>H} NMR spectrum only showed resonances due to **29** and a small amount of dppn dioxide. Therefore, no further attempts to purify the crude products were made.

The synthesis of [Ni(dppn)]{(SeCH<sub>2</sub>)<sub>2</sub>C(CH<sub>2</sub>OH)<sub>2</sub>}

 was also attempted by direct oxidative addition of **2** to a freshly prepared zero-valent nickel complex [Ni(cod)(dppn)] (see Supporting Information, procedure **C**) that was prepared from [Ni(cod)<sub>2</sub>] in toluene in order to circumvent the reduction step. Even under an argon atmosphere at –24 °C this unstable dark green, almost black solid decomposed within two weeks. According to the <sup>31</sup>P{<sup>1</sup>H} NMR, [Ni(dppn)<sub>2</sub>] might be formed. It further decomposed to elemental nickel and free dppn. Unfortunately, the decomposition of the Ni<sup>0</sup> complex proceeds faster than the oxidative addition to the diselenide or the formation of **29**.

### Characterisation of dppn Monooxide **29**

Contrary to earlier reports,<sup>[30a]</sup> dppn is not air-stable but is easily oxidised to form the appropriate dioxide, without detectable amounts of the monooxide **29**. On the other hand, we noted that **29** is surprisingly insensitive to further oxidation by oxygen in air. Because only the monosulfide and the related monoselenide have been reported,<sup>[40]</sup> we investigated the spectroscopic properties of **29** and its molecular structure. The  $^1\text{H}$  and  $^{13}\text{C}\{^1\text{H}\}$  NMR spectroscopic data of **29** are in good agreement with those reported for the monosulfide and monoselenide of dppn. The  $^{31}\text{P}$  nuclei showed resonance at  $\delta = -10.3$  and  $39.4$  ppm, assigned to the unoxidised and oxidised phosphorus atom, respectively. Both resonances are split into doublets because of the coupling between the two phosphorus nuclei ( $^4J_{\text{P,P}} = 8.9$  Hz). The molecular structure of **29** (see Figure 27) showed the distance between the unoxidised phosphorus atom and oxygen to be  $2.98$  Å and thus expectedly shorter than the corresponding phosphorus...selenium distance of  $3.41$  Å in dppnSe.<sup>[40a]</sup> The torsion angle  $\text{P1-C1}\cdots\text{C9-P2}$  has a value of  $31.25^\circ$  and is larger than the corresponding angle in the monoselenide that is  $28.87^\circ$ .

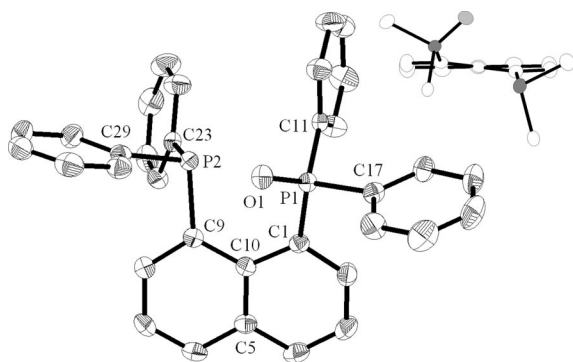


Figure 27. Molecular structure of **29** in the crystal. Upper right corner: view along the plane of the naphthalene ring, displaying the distortion of the two phosphorus atoms. Ellipsoids are drawn at 50% probability level, hydrogen atoms and solvent molecules have been omitted for clarity. Selected bond lengths [Å] and angles [ $^\circ$ ]:  $\text{P1-O1}$   $1.4875(16)$ ,  $\text{P1-C1}$   $1.827(2)$ ,  $\text{P2-C9}$   $1.843(2)$ ,  $\text{P2}\cdots\text{O1}$   $2.98$ ;  $\text{P1-C1}\cdots\text{C9-P2}$   $31.25$ .

We conclude that the oxygen atom of **29** can only come from small traces of air or the hydroxy groups of the selenium ligand itself. Since utmost care was taken to attain inert conditions, the hydroxy group of  $[(\text{SeCH}_2)_2\text{C}(\text{CH}_2\text{OH})_2]^{2-}$  either as a free ligand or coordinated in  $[\text{Ni}(\text{dppn})\{(\text{SeCH}_2)_2\text{C}(\text{CH}_2\text{OH})_2\}]$ , or the solvent in interaction with the nickel centre oxidises one of the phosphorus atoms of the dppn moiety to form **29** and possibly leading to the decomposition of the nickel(0) complex.

### Relationship between Bite Angle and $^1J_{\text{P,Pt}}$ Coupling Constant

The number of complexes reported, allows proving the assumed relationship between the bite angle and the magnitude of  $^1J_{\text{P,Pt}}$ . As shown in Figure 28 a linear correlation is recognisable for diphosphane diselenolato platinum(II)

complexes **13–20** and **24**. Hence, a rough estimation of the bite angle from the  $^1J_{\text{P,Pt}}$  coupling constant is justified. The linear fit possesses a coefficient of correlation of  $0.80$ . It must be noted that the coupling constants are based on solution data, while the bite angles were taken from the solid state arrangement of the respective complexes.

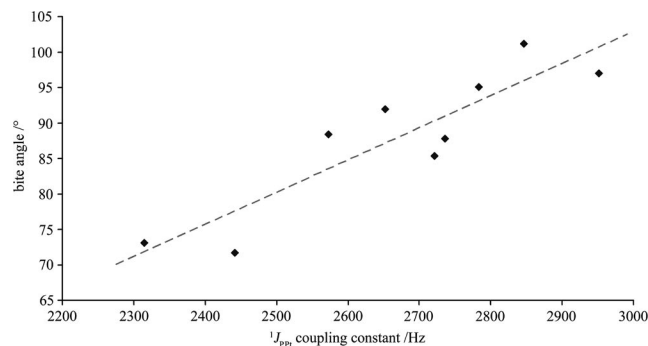


Figure 28. Relationship between the bite angle and the  $^1J_{\text{P,Pt}}$  coupling constant for diphosphane diselenolato platinum(II) complexes **13–20** and **24**. The dashed line represents the linear fit with a coefficient of determination of  $0.80$ .

## Conclusions

During our investigation of the influence of the bite angle of bidentate phosphanes towards their steric demand we determined the molecular structures of some dichlorido-phosphanemetal(II) complexes and prepared the sterically demanding monodentate phosphane 4-dppdbf, which, upon reaction with  $[\text{PtCl}_2(\text{cod})]$ , yielded the appropriate *cis*-complex **3**. Furthermore, we improved the synthesis of 4,4-bis(hydroxymethyl)-1,2-diselenolane **2** using a two-step synthesis starting from 2,2-bis(bromomethyl)propane-1,3-diol. The molecular structure of **2** revealed an interesting supra-molecular assembly caused by the interplay of a hydrogen-bonding network and rather strong chalcogen–chalcogen interactions.

To study the complexation behaviour of the dianion of the air- and moisture-stable 1,2-diselenolane **2** towards group-10 metals, an efficient and straightforward one-pot procedure was established that circumvents the isolation of the malodorous and air-sensitive diselenol. Compound **2** was reduced *in situ* by sodium borohydride in protic media followed by the addition of an appropriate dichloridophosphanemetal(II) yielding complexes of the type  $[\text{ML}_2\{(\text{SeCH}_2)_2\text{C}(\text{CH}_2\text{OH})_2\}]$  ( $\text{M} = \text{Ni}, \text{Pd}, \text{Pt}$ ;  $\text{L} = \text{mono- or } \frac{1}{2} \text{ bidentate phosphane}$ ) (**9–28**) in good yields. The platinum complexes proved to be rather stable, showing slow decomposition only in chlorinated solvents after several weeks. By contrast, the palladium complexes also decomposed in thf, and the nickel complexes proved to be sensitive against oxidation.

All complexes were characterised by multinuclear NMR spectroscopy ( $^1\text{H}$ ,  $^{13}\text{C}\{^1\text{H}\}$ ,  $^{31}\text{P}\{^1\text{H}\}$ ,  $^{77}\text{Se}\{^1\text{H}\}$  and  $^{195}\text{Pt}\{^1\text{H}\}$ , where appropriate), mass spectrometry and elemental analysis. Phosphorus and platinum NMR spec-

troscopy particularly proved to be useful for the prediction of bite angles from  $^1\text{J}_{\text{P-Pt}}$  coupling constants. The  $^{31}\text{P}\{^1\text{H}\}$  NMR spectra of some complexes also showed two sets of  $^{77}\text{Se}$  satellites due to *cis*- and *trans*-coupling to the selenium nuclei. The magnetic non-equivalence of the two phosphorus atoms in the case of one NMR active selenium atom results in further splitting of the selenium resonances in the  $^{77}\text{Se}\{^1\text{H}\}$  NMR spectra resulting in unresolved high-order multiplets.

In order to investigate the dependence of the bite angle on the steric demand of phosphanes, most complexes were investigated by single-crystal X-ray crystallography. As we sought to cover a broad range of P–M–P angles for further investigations, a number of bidentate phosphanes with different bite angles was utilised in the preparation of complexes **9–28**. As revealed by the molecular structures, phosphorus–metal–phosphorus angles range from  $71^\circ$  to  $108^\circ$ . The complexes also show interesting supramolecular arrangements in the solid state due to the presence of hydroxy groups forming a hydrogen-bonding network. A conclusion that is derived from the molecular structures of di- and trinuclear cationic platinum(II) complexes **22** and **23** is the instability of  $[\text{Pt}\{(\text{SeCH}_2)_2\text{C}(\text{CH}_2\text{OH})_2\}(\text{xantphos})]$ . The instability might be due to the large bite angle of the phosphane or its bonding behaviour.

The attempt to synthesise  $[\text{Ni}(\text{dppn})\{(\text{SeCH}_2)_2\text{C}(\text{CH}_2\text{OH})_2\}]$  led to rapid decomposition, affording the so far unknown dppn monooxide **29** that is stable against further oxidation by air. Compound **29** might be an interesting mixed-donor ligand with hemilabile properties.<sup>[40a,41]</sup>

## Experimental Section

**Caution!** All new selenium-containing complexes are potentially highly toxic compounds. The selenium precursors ( $\text{Na}_2\text{Se}_2$ ,  $\text{KSeCN}$ ) are known to be poisonous and must be handled carefully. All operations have to be carried out in a well-ventilated hood. Particular care must be taken in the  $\text{NaBH}_4$  reduction step, as small amounts of hydrogen selenide ( $\text{H}_2\text{Se}$ ), and during the preparation of **2** hydrogen cyanide ( $\text{HCN}$ ) might evolve. Therefore, all gases should be bubbled through concentrated aqueous  $\text{NaOH}$  solution.

**General:** All operations except for the preparation of **1** were carried out under dry argon using standard Schlenk techniques. Solvents were distilled prior to use, other reagents were used without further purification.  $\text{KSeCN}$  and  $\text{NaBH}_4$  were purchased from Acros, 2,2-bis(bromomethyl)propane-1,3-diol, 1,1-bis(diphenylphosphanyl)methane, 1,2-bis(diphenylphosphanyl)ethane, 1,3-bis(diphenylphosphanyl)propane, 1,4-bis(diphenylphosphanyl)butane and 1,1'-bis(diphenylphosphanyl)ferrocene from Aldrich,  $\text{NiCl}_2 \cdot 6\text{H}_2\text{O}$ ,  $\text{K}_2\text{PdCl}_4$ ,  $\text{K}_2\text{PtCl}_4$  and silica gel (silica gel 60, 0.2–0.5 mm) from Merck.  $^1\text{H}$ ,  $^{13}\text{C}\{^1\text{H}\}$  and  $^{31}\text{P}\{^1\text{H}\}$  NMR spectra were recorded with either a Bruker AVANCE 200 or 400, the  $^{77}\text{Se}\{^1\text{H}\}$  and  $^{195}\text{Pt}\{^1\text{H}\}$  NMR spectra were carried out with Bruker AVANCE 400 or Bruker DPX 400.  $^1\text{H}$  NMR spectra were calibrated to the signal of the remaining protons of the solvents ( $\text{CDCl}_3$ :  $\delta = 7.24$  ppm,  $\text{C}_6\text{D}_6$ :  $\delta = 7.15$  ppm,  $\text{CD}_2\text{Cl}_2$ :  $\delta = 5.32$  ppm,  $[\text{D}_6]\text{dmsO}$ :  $\delta = 2.49$  ppm),  $^{13}\text{C}\{^1\text{H}\}$  NMR spectra were determined using the signal of the solvent as internal reference ( $\text{CDCl}_3$ :  $\delta = 77.0$  ppm,  $\text{C}_6\text{D}_6$ :  $\delta = 128.0$  ppm,  $\text{CD}_2\text{Cl}_2$ :  $\delta = 53.8$  ppm,  $[\text{D}_6]\text{dmsO}$ :  $\delta =$

39.5 ppm).  $^{31}\text{P}\{^1\text{H}\}$ ,  $^{77}\text{Se}\{^1\text{H}\}$  and  $^{195}\text{Pt}\{^1\text{H}\}$  NMR spectra were recorded using 85%  $\text{H}_3\text{PO}_4$  ( $\delta = 0.0$  ppm) and concentrated  $\text{SeO}_2$  in  $\text{D}_2\text{O}$  ( $\delta = -1302.6$  ppm) solutions and saturated  $\text{K}_2\text{PtCl}_4$  in 1 M  $\text{NaCl}$  ( $\delta = -1628.0$  ppm)  $\text{D}_2\text{O}$  solution as external references, respectively. The  $^{77}\text{Se}$  chemical shifts are reported relative to neat  $\text{Me}_2\text{Se}$  [ $\delta(\text{Me}_2\text{Se}) = \delta(\text{SeO}_2) + 1302.6$  ppm],<sup>[42]</sup> while the  $^{195}\text{Pt}$  resonances are referenced to  $\text{PtCl}_6^{2-}$  [ $\delta(\text{PtCl}_6^{2-}) = \delta(\text{PtCl}_4^{2-}) + 1628.0$  ppm].<sup>[43]</sup> The  $^{77}\text{Se}\{^1\text{H}\}$  and  $^{195}\text{Pt}\{^1\text{H}\}$  NMR spectra were recorded either directly or indirectly using two dimensional  $^1\text{H}$   $^{77}\text{Se}$  and  $^1\text{H}$   $^{195}\text{Pt}$  HMBNMR experiments. If not mentioned otherwise, couplings to  $^{77}\text{Se}$  were usually not fully resolved in  $^1\text{H}$ ,  $^{13}\text{C}\{^1\text{H}\}$ ,  $^{31}\text{P}\{^1\text{H}\}$  and  $^{195}\text{Pt}\{^1\text{H}\}$  NMR spectra due to the multiplicity of the signals and the low natural abundance of the  $^{77}\text{Se}$  isotope (see results and discussion section for details). Assignments of  $^1\text{H}$  and  $^{13}\text{C}$  signals were confirmed by two-dimensional NMR experiments ( $^1\text{H}$   $^1\text{H}$  COSY,  $^1\text{H}$   $^{13}\text{C}$  HSQC,  $^1\text{H}$   $^{13}\text{C}$  HMBC), in some cases the coupling of protons to other heteroatoms was assigned by special decoupling experiments ( $^1\text{H}\{^{31}\text{P}\}$ ,  $^1\text{H}\{^{77}\text{Se}\}$ ,  $^1\text{H}\{^{195}\text{Pt}\}$  NMR). Mass spectra were performed with either a Finnigan SSQ 710 (DEI, FAB) or a MAT 95 XL (ESI) instrument. All mass spectra showed parent ions with appropriate isotopomer distributions. Elemental analyses have been measured with a Vario EL III CHNS (Elementaranalysensystem GmbH Hanau) as single determinations. Melting points were obtained using an Axiolap microscope (Carl Zeiss Jena GmbH) equipped with heating unit THMS 600 (Linkam) and Linkam LNP and CI 93 control units.

All compounds are stable in the presence of atmospheric oxygen and moisture in the solid state. However, the final complexes show some instability in chlorinated solvents, as indicated by NMR experiments. Especially chloroform solutions show decomposition after several weeks,<sup>[7b]</sup> while the nickel and palladium species showed to be more labile and fast decomposed in thf as well. Additionally the nickel-containing complexes showed to be sensitive against oxidation.

**Preparation of Starting Materials:** For compounds **1**,<sup>[44]</sup> **5**<sup>[30a]</sup> and **6**<sup>[30a]</sup> the literature procedures were modified considerably or were not satisfying, therefore, the synthetic details are given in the Supporting Information. PTA,<sup>[36]</sup> 4-dppdbf,<sup>[45]</sup> dppma,<sup>[39]</sup> dppn,<sup>[30]</sup> dppbe,<sup>[46]</sup> dppo-xy,<sup>[47]</sup> xantphos,<sup>[48]</sup>  $[\text{Ni}(\text{cod})_2]$ ,<sup>[49]</sup>  $[\text{NiCl}_2(\text{dppe})]$ ,<sup>[50]</sup>  $[\text{PdCl}_2(\text{NCPH})_2]$ ,<sup>[51]</sup>  $[\text{PdCl}_2(\text{dppf})]$ ,<sup>[52]</sup>  $[\text{PtCl}_2(\text{PTA})_2]$ <sup>[53]</sup> and  $[\text{PtCl}_2(\text{PPh}_3)_2]$ <sup>[54]</sup> were synthesised following literature procedures.  $[\text{PdCl}_2(\text{dppe})]$  and  $[\text{PtCl}_2(\text{dppe})]$  were prepared in the same manner as reported for the synthesis of  $[\text{PtCl}_2(\text{PPh}_3)_2]$ <sup>[54]</sup> using dppe instead of  $\text{PPh}_3$  and  $\text{K}_2\text{PdCl}_4$  or  $\text{K}_2\text{PtCl}_4$ , respectively.  $[\text{PtCl}_2(\text{PMe}_3)_2]$ ,<sup>[8e]</sup>  $[\text{PtCl}_2(\text{dppm})]$ ,  $[\text{PtCl}_2(\text{dppma})]$ ,  $[\text{PtCl}_2(\text{dppbe})]$ ,  $[\text{PtCl}_2(\text{dppn})]$ ,<sup>[30a]</sup>  $[\text{PtCl}_2(\text{dppb})]$ ,  $[\text{PtCl}_2(\text{dppo-xy})]$  and  $[\text{PtCl}_2(\text{dppf})]$  were synthesised by suspending  $[\text{PtCl}_2(\text{cod})]$ <sup>[55]</sup> in dichloromethane or chloroform and adding an equimolar amount of the phosphane. The reaction mixture was stirred for 2 d at room temp., filtered, washed with a small amount of chloroform and dried in vacuo.

**General Procedure for the Synthesis of Complexes 9–28:** One equivalent of **2** was dissolved in ethanol (6 mL) under argon. Three equivalents of  $\text{NaBH}_4$  were added with stirring, affording the solution to lighten and turning colourless. After 30 min the excess of  $\text{NaBH}_4$  was destroyed by dropwise addition of 4.0 M  $\text{HCl}$  solution. Stirring was continued for 5 min before an excess of  $\text{K}_2\text{CO}_3$  was carefully added. A solution or suspension of the phosphane bearing metal(II) precursor (one equivalent) in acetone, chloroform, dichloromethane or ethanol (6 mL) was added at once and the mixture was stirred at room temp. overnight, resulting in yellow to red solutions. The solvent was removed using a rotary evaporator. Except for compound **10** (see there), the residue was chromatographed on sil-

ica gel, separating some unreacted **2** as less polar fraction and the complexes as second fraction (the eluents are given in the detailed procedures in the Supporting Information). Complexes **9–28** were obtained in 48–86% yield.

**4,4-Bis(hydroxymethyl)-1,2-diselenolane (2):**<sup>[16a]</sup> KSeCN (10.81 g, 75 mmol) was added to a solution of **1** (7.55 g, 25 mmol) in 70 mL of acetone. To maximise the yield, the colourless reaction mixture was heated to reflux for 14 d. During that time a mass of KBr and a small amount of red selenium developed. Due to the precipitated selenium and the formation of some amount of the product the colour changed to deep red. After cooling to room temp., water (70 mL) was added to dissolve the KBr and the solution was filtered to remove the selenium. Ether (150 mL) was added and phases were separated. The organic layer was washed with water (3 × 30 mL), dried with Na<sub>2</sub>SO<sub>4</sub> and the solvents evaporated to dryness, giving a viscous deep red oil. This was dissolved in ethanol/water (90:10, 100 mL) and cooled to 0 °C. NaBH<sub>4</sub> (3.78 g, 100 mmol) was added in small portions during 2 h, while the solution lightened and became colourless. Evolving gases were removed with a slight stream of argon, which was bubbled through a washing bottle with concentrated aqueous NaOH solution. After 1 h water (30 mL) was added and the excess of NaBH<sub>4</sub> was destroyed by drop wise addition of 4.0 M HCl solution until pH 2. The stream of argon was removed and the solution was stirred vigorously under air to aspirate as much oxygen as possible. After 12 h the clear, deep red solution was heated to 75 °C for 4 h before an excess of K<sub>2</sub>CO<sub>3</sub> was added carefully. The solution was slowly cooled to room temp. and extracted with dichloromethane (5 × 30 mL). The combined organic layer was washed with water (10 mL), dried with Na<sub>2</sub>SO<sub>4</sub> and the solvents evaporated in vacuo, giving crude **2** as a brown red solid. Recrystallisation from ethanol yielded deep red crystals. Single crystals were grown from a concentrated ethanol solution at 7 °C; yield 4.72 g (73%); m.p. 134–135 °C (ref.<sup>[16a]</sup> 133–135 °C). <sup>1</sup>H NMR (200.1 MHz, [D<sub>6</sub>]dmsO, 27 °C): δ = 3.17 (s with <sup>77</sup>Se satellites, <sup>2</sup>J<sub>H,Se</sub> = 15.4 Hz, 4 H, SeCH<sub>2</sub>), 3.46 (d, <sup>3</sup>J<sub>H,H</sub> = 5.4 Hz, 4 H, OCH<sub>2</sub>), 4.76 (t, <sup>3</sup>J<sub>H,H</sub> = 5.4 Hz, 2 H, OH) ppm. <sup>13</sup>C{<sup>1</sup>H} NMR (50.3 MHz, [D<sub>6</sub>]dmsO, 27 °C): δ = 35.6 (s with <sup>77</sup>Se satellites, <sup>1</sup>J<sub>C,Se</sub> = 66.2 Hz, SeCH<sub>2</sub>), 59.0 [s, C(CH<sub>2</sub>OH)<sub>2</sub>], 62.6 (s, CH<sub>2</sub>OH) ppm. <sup>77</sup>Se{<sup>1</sup>H} NMR (76.3 MHz, [D<sub>6</sub>]dmsO, 27 °C): δ = 270.0 (s, SeCH<sub>2</sub>) ppm. DEI-MS: m/z = 260 [M<sup>+</sup>].

**Data Collection and Structural Refinement:** The intensity data for the compounds were collected with a Nonius KappaCCD diffractometer using graphite-monochromated Mo-K<sub>α</sub> radiation. Data were corrected for Lorentz and polarisation effects but not for absorption effects.<sup>[56]</sup> Crystallographic data as well as structure solution and refinement details are given in the Supporting Information.

The structures were solved by direct methods (SHELXS<sup>[57]</sup>) and refined by full-matrix least-squares techniques against F<sub>o</sub><sup>2</sup> (SHELXL-97<sup>[58]</sup>). All hydrogen atom positions were included at calculated positions with fixed thermal parameters. All non-hydrogen and non-disordered atoms were refined anisotropically.<sup>[58]</sup>

CCDC-730500 (for **2**), -730501 (for **3**), -730502 (for **4**), -730503 (for **5**), -730504 (for **7**), -730505 (for **6**), -730506 (for **8**), -730507 (for **9**), -730508 (for **10**), -730509 (for **11a**), -730510 (for **11b**), -730511 (for **13**), -730512 (for **14**), -730513 (for **15**), -730514 (for **16**), -730515 (for **17**), -730516 (for **18**), -730517 (for **19**), -730518 (for **20**), -730519 (for **22**), -730520 (for **23**), -730521 (for **24**), -730522 (for **25**), -730523 (for **27**), -730524 (for **28**) and -730525 (for **29**) contain the supplementary crystallographic data for this paper. These data can be obtained free of charge from the Cambridge

Crystallographic Data Centre via [www.ccdc.cam.ac.uk/data\\_request/cif](http://www.ccdc.cam.ac.uk/data_request/cif).

**Supporting Information** (see also the footnote on the first page of this article): Detailed experimental procedures, complete spectroscopic data of all new compounds and full X-ray crystallographic data on all determined molecular structures.

## Acknowledgments

Heraeus GmbH is gratefully acknowledged for a donation of K<sub>2</sub>PtCl<sub>4</sub>. The authors wish to express their gratitude to one of the referees for his helpful remarks. Furthermore we thank Prof. Dr. Fabian Mohr, Bergische Universität Wuppertal, for donating some amount of the PTA ligand. Additionally, we wish to thank Dr. Reinald Fischer for the preparation of xantphos and Thomas Weisheit for the donation of dppbe and dppo-xyI. Financial Support from Academy of Finland is gratefully acknowledged.

- [1] a) E. Fritzmann, *Z. Anorg. Chem.* **1911**, 73, 239–255; b) E. Fritzmann, *Z. Anorg. Allg. Chem.* **1924**, 133, 119–132.
- [2] a) H. Kuniyashi, A. Maruyama, H. Kurosawa, *Organometallics* **1998**, 17, 908–913; b) V. P. Ananikov, I. P. Beletskaya, G. G. Aleksandrov, I. L. Eremenko, *Organometallics* **2003**, 22, 1414–1421.
- [3] a) A. Singhal, V. K. Jain, R. Mishra, B. Varghese, *J. Mater. Chem.* **2000**, 10, 1121–1124; b) S. Dey, V. K. Jain, S. Chaudhury, A. Knoedler, F. Lissner, W. Kaim, *J. Chem. Soc., Dalton Trans.* **2001**, 723–728; c) S. Dey, V. K. Jain, B. Varghese, *J. Organomet. Chem.* **2001**, 623, 48–55.
- [4] a) W. Henderson, B. K. Nicholson, M. B. Dinger, *Inorg. Chim. Acta* **2003**, 355, 428–431; b) J. Ashaks, Y. Bankovsky, D. Zaruma, I. Shestakova, I. Domracheva, A. Nesterova, E. Lukevics, *Chem. Heterocycl. Compd.* **2004**, 40, 776–780.
- [5] for a general survey see: a) S. G. Murray, F. R. Hartley, *Chem. Rev.* **1981**, 81, 365–414; b) E. G. Hope, W. Levason, *Coord. Chem. Rev.* **1993**, 122, 109–170; c) W. Levason, S. D. Orchard, G. Reid, *Coord. Chem. Rev.* **2002**, 225, 159–199.
- [6] for reviews see: a) J. Arnold, *Prog. Inorg. Chem.* **1995**, 43, 353–417; b) V. K. Jain, L. Jain, *Coord. Chem. Rev.* **2005**, 249, 3075–3197.
- [7] a) S. Akabori, T. Kumagai, T. Shirahige, S. Sato, K. Kawazoe, C. Tamura, M. Sato, *Organometallics* **1987**, 6, 526–531; b) S. M. Aucott, H. L. Milton, S. D. Robertson, A. M. Z. Slawin, G. D. Walker, J. D. Woollins, *Chem. Eur. J.* **2004**, 10, 1666–1676; c) M. J. Brown, J. F. Corrigan, *J. Organomet. Chem.* **2004**, 689, 2872–2879; d) S. M. Aucott, P. Kilian, S. D. Robertson, A. M. Z. Slawin, J. D. Woollins, *Chem. Eur. J.* **2006**, 12, 895–902.
- [8] a) N. Sonoda, S. Araki, T. Onishi, T. Tanaka, *J. Inorg. Nucl. Chem.* **1974**, 36, 1985–1989; b) W.-H. Pan, J. P. Fackler Jr., *J. Am. Chem. Soc.* **1978**, 100, 5783–5789; c) W.-H. Pan, J. P. Fackler Jr., H.-W. Chen, *Inorg. Chem.* **1981**, 20, 856–863; d) M. Ebner, H. Werner, *Chem. Ber.* **1986**, 119, 482–487; e) C. J. Burchell, S. M. Aucott, A. M. Z. Slawin, J. D. Woollins, *Dalton Trans.* **2005**, 735–739; f) C. J. Burchell, S. M. Aucott, A. M. Z. Slawin, J. D. Woollins, *Eur. J. Inorg. Chem.* **2005**, 209–213; g) S. M. Aucott, A. M. Z. Slawin, C. J. Burchell, J. D. Woollins, *Phosphorus Sulfur Silicon Relat. Elem.* **2004**, 179, 903–906.
- [9] a) C. M. Bolinger, T. B. Rauchfuss, *Inorg. Chem.* **1982**, 21, 3947–3954; b) P. K. Khanna, C. P. Morley, *J. Chem. Res. Synop.* **1995**, 64–65; c) R. D. McCullough, J. A. Belot, J. Seth, A. L. Rheingold, G. P. A. Yap, D. O. Cowan, *J. Mater. Chem.* **1995**, 5, 1581–1587; d) S. Ford, M. R. Lewtas, C. P. Morley, M. Di Vaira, *Eur. J. Inorg. Chem.* **2000**, 5, 933–938.
- [10] a) H. Werner, M. Ebner, W. Bertleff, *Z. Naturforsch. Teil B: Chem. Sci.* **1985**, 40, 1351–1361; b) H. Otto, M. Ebner, H. Werner, *J. Organomet. Chem.* **1986**, 311, 63–68; c) S. Ford, P. K.

- Khanna, C. P. Morley, M. Di Vaira, *J. Chem. Soc., Dalton Trans.* **1999**, 791–794; d) S. Ford, C. P. Morley, M. Di Vaira, *New J. Chem.* **1999**, 23, 811–813; e) S. Ford, C. P. Morley, M. Di Vaira, *Inorg. Chem.* **2004**, 43, 7101–7110; f) C. Morley, C. Jones, C. Webster, M. Vaira, *Phosphorus Sulfur Silicon Relat. Elem.* **2005**, 180, 801–813; g) K. Rofe, P. Douglas, C. P. Morley, C. A. Webster, J. G. Pichereau, *Inorg. Chem.* **2009**, 48, 4549–4556.
- [11] a) K. A. Jensen, V. Krishnan, *Acta Chem. Scand.* **1970**, 24, 1090–1092; b) K. A. Jensen, V. Krishnan, *Acta Chem. Scand.* **1970**, 24, 1092–1094; c) K. A. Jensen, E. Høge-Jensen, *Acta Chem. Scand.* **1973**, 27, 3605–3606; d) M. S. Thomas, J. Darkwa, E. Y. Osei-Twum, L. A. Litorja Jr., *Polyhedron* **1999**, 18, 2803–2810; e) C. C. McLaughlan, J. A. Ibers, *Inorg. Chem.* **2000**, 39, 1046–1048.
- [12] a) M. Schmidt, G. G. Hoffmann, *Chem. Ber.* **1979**, 112, 2190–2196; b) M. Schmidt, G. G. Hoffmann, *Revue de Chimie Minerale* **1983**, 20, 769–775.
- [13] P. K. Khanna, C. P. Morley, M. B. Hursthouse, K. M. Abdul Malik, O. W. Howarth, *Heteroat. Chem.* **1995**, 6, 519–524.
- [14] J. S. L. Yeo, J. J. Vittal, W. Henderson, T. S. A. Hor, *Organometallics* **2002**, 21, 2944–2949.
- [15] a) G. T. Morgan, F. H. Burstall, *J. Chem. Soc.* **1930**, 1497–1502; b) L. Syper, J. Mlochowski, *Tetrahedron* **1988**, 44, 6119–6130; c) M. K. Harb, T. Niksch, J. Windhager, H. Görls, R. Holze, L. T. Lockett, N. Okumura, D. H. Evans, R. S. Glass, D. L. Lichtenberger, M. El-khateeb, W. Weigand, *Organometallics* **2009**, 28, 1039–1048.
- [16] a) G. Bergson, *Acta Chem. Scand.* **1958**, 12, 582–583; b) G. Bergson, *Arkiv Kemi* **1958**, 13, 11–27.
- [17] W. McFarlane, D. S. Rycroft, *J. Chem. Soc., Chem. Commun.* **1973**, 1, 10–11.
- [18] a) H. J. Reich, C. A. Hoeger, W. W. Willis Jr., *J. Am. Chem. Soc.* **1982**, 104, 2936–2937; b) H. J. Reich, C. A. Hoeger, W. W. Willis Jr., *Tetrahedron* **1985**, 41, 4771–4779.
- [19] W. McFarlane, R. J. Wood, *J. Chem. Soc., Dalton Trans.* **1972**, 13, 1397–1402.
- [20] N. Tonkikh, H. Duddeck, M. Petrova, O. Neilands, A. Strakovs, *Eur. J. Org. Chem.* **1999**, 7, 1585–1588.
- [21] a) M. Mellini, S. Merlino, *Acta Crystallogr., Sect. B: Struct. Sci.* **1976**, 32, 1074–1078; b) K. I. Doudin, R. K. Berge, K. J. Børve, J. Songstad, K. W. Törnroos, *J. Mol. Struct.* **2000**, 554, 149–161; c) K. K. Bhasin, J. Singh, *J. Organomet. Chem.* **2002**, 658, 71–76; d) J.-M. Chen, B. K. Santra, C. W. Liu, *Inorg. Chem. Commun.* **2004**, 7, 1103–1105; e) A. K. Ghosh, D. Ghoshal, M. G. B. Drew, G. Mostafa, N. R. Chaudhuri, *Struct. Chem.* **2006**, 17, 85–90; f) D. B. Werz, T. H. Staeb, C. Benisch, B. J. Rausch, F. Rominger, R. Gleiter, *Org. Lett.* **2002**, 4, 339–342; g) D. B. Werz, R. Gleiter, F. Rominger, *J. Am. Chem. Soc.* **2002**, 124, 10638–10639; h) R. Gleiter, D. B. Werz, B. J. Rausch, *Chem. Eur. J.* **2003**, 9, 2676–2683; i) D. B. Werz, R. Gleiter, F. Rominger, *J. Org. Chem.* **2004**, 69, 2945–2952; j) D. B. Werz, B. J. Rausch, R. Gleiter, *Tetrahedron Lett.* **2002**, 43, 5767–5769; k) C. Bleiholder, D. B. Werz, H. Köppel, R. Gleiter, *J. Am. Chem. Soc.* **2006**, 128, 2666–2674; l) C. Bleiholder, R. Gleiter, D. B. Werz, H. Köppel, *Inorg. Chem.* **2007**, 46, 2249–2260.
- [22] a) L. Pauling, *Die Natur der chemischen Bindung*, 2nd ed., Verlag Chemie, Weinheim, **1964**; b) A. Bondi, *J. Phys. Chem.* **1964**, 68, 441–451.
- [23] a) R. E. Rosenfield Jr., R. Parthasarathy, J. D. Dunitz, *J. Am. Chem. Soc.* **1977**, 99, 4860–4862; b) J. P. Glusker, *Top. Curr. Chem.* **1998**, 198, 1–56.
- [24] Due to the presence of heavy atoms, the hydrogen atoms are fixed at calculated positions in all X-ray structures and were not directly determined from the diffraction. Taking the marginal part of the hydrogen atoms in the electron density into account, their positions are not satisfyingly determinable. Hence, the notation of “hydrogen bond” refers to O···E (E = N, O, Se, Pt) distances throughout this article and short contacts might be explained by the presence of hydrogen bonds. A conclusion about the O–H···E angle cannot be drawn.
- [25] Holleman-Wiberg, *Lehrbuch der Anorganischen Chemie*, 102nd ed., Walter de Gruyter, Berlin, New York, **2007**.
- [26] P. E. Garrou, *Chem. Rev.* **1981**, 81, 229–266.
- [27] J. A. Rahn, L. Baltusis, J. H. Nelson, *Inorg. Chem.* **1990**, 29, 750–755.
- [28] H.-K. Fun, S. Chantrapromma, Y.-C. Liu, Z.-F. Chen, H. Liang, *Acta Crystallogr., Sect. E: Struct. Rep. Online* **2006**, 62, m1252–m1254.
- [29] J. W. Steed, J. L. Atwood, *Supramolecular Chemistry*, John Wiley & Sons, Ltd, Chichester, New York, Weinheim, Brisbane, Singapore, Toronto, **2000**.
- [30] a) R. D. Jackson, S. James, A. G. Orpen, P. G. Pringle, *J. Organomet. Chem.* **1993**, 458, C3–C4; b) A. Karaçar, H. Thönnessen, P. G. Jones, R. Bartsch, R. Schmutzler, *Heteroat. Chem.* **1997**, 8, 539–550.
- [31] a) J.-E. Song, B.-O. Kim, Y. Ha, *Mater. Sci. Eng., Part C* **2004**, C24, 191–194; b) H. Petzold, H. Görls, W. Weigand, *J. Organomet. Chem.* **2007**, 692, 2736–2742.
- [32] M. Gerisch, F. W. Heinemann, U. Markgraf, D. Steinborn, *Z. Anorg. Allg. Chem.* **1997**, 623, 1651–1656.
- [33] R. Oilunkaniemi, R. S. Laitinen, M. Ahlgren, *J. Organomet. Chem.* **1999**, 587, 200–206.
- [34] a) M. Risto, *Titentiate Thesis*, University of Oulu, Finland **2006**; b) M. Risto, E. M. Jahr, M. S. Hannu-Kuure, R. Oilunkaniemi, R. S. Laitinen, *J. Organomet. Chem.* **2007**, 692, 2193–2204; c) A. Singhal, V. K. Jain, B. Varghese, E. R. T. Tiekink, *Inorg. Chim. Acta* **1999**, 285, 190–196; d) M. S. Hannu, R. Oilunkaniemi, R. S. Laitinen, M. Ahlgren, *Inorg. Chem. Commun.* **2000**, 3, 397–399; e) S. Dey, V. K. Jain, A. Knoedler, W. Kaim, *Inorg. Chim. Acta* **2003**, 349, 104–110.
- [35] a) G. G. Messmer, E. L. Amma, J. A. Ibers, *Inorg. Chem.* **1967**, 6, 725–730; b) A. Del Pra, G. Zanotti, *Cryst. Struct. Commun.* **1979**, 8, 737–742.
- [36] a) D. J. Daigle, A. B. Pepperman Jr., S. L. Vail, *J. Heterocycl. Chem.* **1974**, 11, 407–408; b) D. J. Daigle, *Inorg. Synth.* **1998**, 32, 40–45; c) for a review see: A. D. Phillips, L. Gonsalvi, A. Romerosa, F. Vizza, M. Peruzzini, *Coord. Chem. Rev.* **2004**, 248, 955–993.
- [37] a) V. W. Day, D. A. Lesch, T. B. Rauchfuss, *J. Am. Chem. Soc.* **1982**, 104, 1290–1295; b) S. Narayan, V. K. Jain, B. Varghese, *J. Chem. Soc., Dalton Trans.* **1998**, 2359–2366; c) S. Kato, O. Niyomura, Y. Kawahara, T. Kanda, *J. Chem. Soc., Dalton Trans.* **1999**, 1677–1685; d) M. Herberhold, T. Schmalz, W. Milius, B. Wrackmeyer, *Z. Anorg. Allg. Chem.* **2002**, 628, 979–986; e) M. Herberhold, T. Schmalz, W. Milius, B. Wrackmeyer, *Z. Naturforsch., Teil B* **2002**, 57, 53–60.
- [38] N. Bertel, H. W. Roesky, F. T. Edelmann, M. Noltemeyer, H. G. Schmidt, *Z. Anorg. Allg. Chem.* **1990**, 586, 7–18.
- [39] E. J. Sekabunga, M. L. Smith, T. R. Webb, W. E. Hill, *Inorg. Chem.* **2002**, 41, 1205–1214.
- [40] a) A. Karaçar, M. Freytag, H. Thönnessen, J. Omelanczuk, P. G. Jones, R. Bartsch, R. Schmutzler, *Z. Anorg. Allg. Chem.* **2000**, 626, 2361–2372; b) A. Karaçar, V. Klaukien, M. Freytag, H. Thönnessen, J. Omelanczuk, P. G. Jones, R. Bartsch, R. Schmutzler, *Z. Anorg. Allg. Chem.* **2001**, 627, 2589–2603.
- [41] for some examples and reviews on this topic see following and literature cited therein: a) J. C. Jeffrey, T. B. Rauchfuss, *Inorg. Chem.* **1979**, 18, 2858–2866; b) J. A. Davies, F. R. Hartley, *Chem. Rev.* **1981**, 81, 79–90; c) P. Wehman, H. M. A. van Donge, A. Hagos, P. C. J. Kamer, P. W. N. M. van Leeuwen, *J. Organomet. Chem.* **1997**, 535, 183–193; d) M. Hingst, M. Tepper, O. Stelzer, *Eur. J. Inorg. Chem.* **1998**, 1, 73–82.
- [42] R. C. Burns, M. J. Collins, R. J. Gillespie, G. J. Schrobilgen, *Inorg. Chem.* **1986**, 25, 4465–4469.
- [43] N. V. Kaminskaja, N. M. Kostić, *Inorg. Chem.* **2001**, 40, 2368–2377.

- [44] a) N. Nishizono, N. Koike, Y. Yamagata, S. Fujii, A. Matsuda, *Tetrahedron Lett.* **1996**, 37, 7569–7572; b) S. K. Chung, S. H. Ban, S. H. Kim, B. E. Kim, S. H. Woo, *Bioorg. Med. Chem. Lett.* **1995**, 5, 1091–1096; c) P. Bitha, S. G. Carvajal, R. V. Citarella, E. F. Delos Santos, F. E. Durr, J. J. Hlavka, S. A. Lang Jr., J. P. Thomas, R. E. Wallace, Y. Lin, *J. Med. Chem.* **1989**, 32, 2063–2067.
- [45] M. W. Haenel, D. Jakubik, E. Rothenberger, G. Schroth, *Chem. Ber.* **1991**, 124, 1705–1710.
- [46] R.-X. Li, X.-J. Li, N.-B. Wong, K.-C. Tin, Z.-Y. Zhou, T. C. W. Mak, *J. Mol. Catal. A* **2002**, 178, 181–190.
- [47] S. E. Tunney, J. K. Stille, *J. Org. Chem.* **1987**, 52, 748–753.
- [48] M. Kranenburg, Y. E. M. van der Burgt, P. C. J. Kamer, P. W. N. M. van Leeuwen, K. Goubitz, J. Fraanje, *Organometallics* **1995**, 14, 3081–3089.
- [49] B. Heyn, B. Hipler, G. Kreisel, H. Schreer, D. Walther, *Anorganische Synthesechemie – Ein integriertes Praktikum*, 2nd ed., Springer-Verlag, Berlin, **1990**.
- [50] M. J. Hudson, R. S. Nyholm, M. B. H. Stiddard, *J. Chem. Soc. A* **1968**, 40–43.
- [51] J. R. Doyle, P. E. Slade, H. B. Jonassen, *Inorg. Synth.* **1960**, 6, 216–219.
- [52] T. Hayashi, M. Konishi, Y. Kobori, M. Kumada, T. Higuchi, K. Hirotsu, *J. Am. Chem. Soc.* **1984**, 106, 158–163.
- [53] D. A. Krogstad, S. B. Owens, J. A. Halfen, V. G. Young Jr., *Inorg. Chem. Commun.* **2005**, 8, 65–69.
- [54] U. Nagel, *Chem. Ber.* **1982**, 115, 1998–1999.
- [55] J. Chatt, L. M. Vallarino, L. M. Venanzi, *J. Chem. Soc.* **1959**, 2496–2505.
- [56] a) *COLLECT*, Data Collection Software, Nonius B. V., Netherlands, **1998**; b) *Processing of X-ray Diffraction Data Collected in Oscillation Mode*: Z. Otwinowski, W. Minor, in: *Methods in Enzymology* (Eds.: C. W. Carter, R. M. Sweet), vol. 276, *Macromolecular Crystallography*, part A, pp. 307–326, New York, Academic Press, **1997**.
- [57] G. M. Sheldrick, *Acta Crystallogr., Sect. A* **1990**, 46, 467–473.
- [58] G. M. Sheldrick, *SHELXL-97* (rel. 97-2), University of Göttingen, Germany, **1997**.

Received: August 21, 2009

Published Online: November 30, 2009

# The Extension of the Solid-Angle Concept to Bidentate Ligands<sup>[‡]</sup>

Tobias Niksch,<sup>[a]</sup> Helmar Görls,<sup>[a]</sup> and Wolfgang Weigand\*<sup>[a]</sup>

**Keywords:** Phosphane ligands / Selenolato ligands / Steric demand / Solid-angle concept / Steric hindrance / X-ray diffraction

In search of an applicable parameter to express the steric requirement of bidentate ligands, the generalised equivalent cone angle  $\bar{\theta}_b$  is established. It is designed in the style of the solid-angle concept for monodentate ligands, utilising crystal structure data. Its reliability is tested with bidentate phosphanes coordinated to a central platinum atom. Therefore, a detailed evaluation of the Cambridge Database for platinum complexes with bridging phosphanes is performed. Herein, we present the results of the analysis of more than 900 molecular structures and over 280 different bidentate phosphanes. We intend to establish diselenolatoplatinum(II) complexes as

model compounds for the fast prediction of  $\bar{\theta}_b$  instead of calculating a multiplicity of molecular structures that is often not available. The complexes reported in Part 1 of this publication turn out to be rather acceptable for rough estimates of the generalised equivalent cone angle. On the other hand, the compounds are used to demonstrate the practicability of the concept, which is easily extended to other bidentate ligands, as is shown for the 2,2-bis(hydroxymethyl)-1,3-diselenolato moiety. In conclusion, the generalised equivalent cone angle  $\bar{\theta}_b$  proves to be a feasible parameter for the steric demand of bidentate ligands.

## Introduction

The bulkiness of ligands or the steric crowding of the central atom in metal complexes is of utmost interest in catalysis, as this could determine reactions to occur or not. Moreover, the choice of a tailored ligand might provide selectivity in those reactions.<sup>[1]</sup> Furthermore, influences of the ligand steric requirement to coordination modes and supramolecular assembly of molecules might be expected.

Quite a few models for the determination of the steric demand of ligands have been designed during the last decades (for reviews see ref.<sup>[2]</sup>). Best known is the pioneering work of C. A. Tolman, who formulated the cone angle that is also known as the Tolman angle in the 1970s.<sup>[3]</sup> The cone angle  $\theta$  describes the opening angle of the cone that just touches the surface of the outermost atoms of a ligand (phosphane), while flexible parts of the ligand were bent back to yield the smallest cone possible. The apex of the cone is positioned at the central metal atom, with a settled metal–phosphorus bond length of 2.28 Å. Thus,  $\theta$  gives a

value representative for the least required space of a ligand. Nowadays the cone angle still is state of the art and widely used to describe the bulkiness of ligands.<sup>[1]</sup>

As the Tolman model has limitations, as the use of physical molecular models causes, efforts have been done to overcome them. The use of data obtained from single-crystal structure determination was obvious and led to the development of the solid-angle concept by Immirzi and Musco in 1977.<sup>[4]</sup> They used atom coordinates as obtained from diffraction data and calculated the size of the shadow the phosphane causes, when being projected on a unit sphere with the metal atom being its centre and the light source. The value of the solid angle  $\Omega$  thus obtained is not as comprehensible as the calculated angle  $\bar{\theta}$  representing an equivalent circular cone, which is thus comparable with  $\theta$ . Some years later,  $\Omega$  was converted into  $\Omega_s$  (where s stands for shadow) giving the relative value of the unit sphere shaded by the ligand.<sup>[5]</sup>

The increasing interest in the steric demand of ligands and the easy accessibility of a large number of crystallographic data and powerful computers led to numerous publications dealing with the cone and solid-angle concepts<sup>[5a,6]</sup> and their enhancements<sup>[7]</sup> during the last three decades. Although the Tolman model was extended for bidentate phosphanes by approximating their cone via the cones of substituents and the angle between the metal–phosphorus bond and the half angle of P–M–P',<sup>[8]</sup> to the best of our knowledge there is still lack of coverage on this topic.<sup>[9]</sup> Even though the phosphorus–metal–phosphorus angle, also known as the bite angle, may vary widely, it seems to be the

[‡] Determination of the Steric Demand of Bidentate Phosphanes Using X-ray Crystal Structure Data, Part 2. Part 1: T. Niksch, H. Görls, M. Friedrich, R. Oilunkaniemi, R. Laitinen, W. Weigand, *Eur. J. Inorg. Chem.* **2009**, 74–94, preceding paper.

[a] Institut für Anorganische und Analytische Chemie, Friedrich-Schiller-Universität Jena, August-Bebel-Str. 2, 07743 Jena, Germany  
Fax: +49-3641-948102  
E-mail: wolfgang.weigand@uni-jena.de

Supporting information for this article is available on the WWW under <http://dx.doi.org/10.1002/ejic.200900825>.

best steric parameter for bidentate ligands to date as was discussed and reviewed by van Leeuwen and co-workers.<sup>[8,10]</sup>

During our work, the question arose whether the solid-angle concept might be extended to bidentate ligands as well. Therefore, we performed an extensive Cambridge Structural Database (CSD) search at the Cambridge Crystallographic Data Centre (CCDC) for bidentate ligands coordinating via two phosphorus atoms to a platinum centre and calculated their solid angles. Herein, we report the results for calculations of over 900 structures with more than 280 different bidentate phosphorus ligands. We found the solid-angle concept to be transferable to bidentate ligands and established the generalised parameter  $\Omega_b$  (where b means bidentate ligand) taking the phosphorus–metal bond lengths into account. Further conversion into  $\bar{\Theta}_b$  gives an easy manageable tool for the steric demand of these ligands. The reliability of this model and different influences, like bond lengths and angles, on the value of  $\Omega_b$  and  $\bar{\Theta}_b$  were tested and are discussed in this paper. Additionally, bis-(phosphane) 1,3-diselenolotoplatinum(II) complexes (their synthesis and characterisation is described in Part 1 of this publication) are reported as convenient models for the prediction of the steric demand of bidentate ligands.

## Preliminary Considerations

Particularly in regard to the fixed bond lengths and angles as resulting from the use of physical CPK models, the cone-angle approach depicts a good approximation for the steric demand of phosphanes (Figure 1<sup>[11]</sup>). As useful Tolman's concept has proven for monodentate phosphanes, it is scarcely transferable to bidentate ligands. Only approximations via the half-cone angles  $\Theta/2$  of the two substituents at the phosphorus atoms and the half angle of P–M–P' were used and proved quite useful.<sup>[8]</sup> Though more promising for the prediction of the steric demand of bidentate ligands seems the model of Immerzi and Musco.<sup>[4]</sup> For the determination of the solid angle  $\Omega$ , the metal atom is put into the centre of an outer sphere and becomes a light source projecting the shadow of the ligand onto the inner surface of the sphere (Figure 2<sup>[11]</sup>). Nowadays the angle of the equivalent cone  $\bar{\Theta}$  and the relative value of the shaded area of the surface  $\Omega_s$  are used more commonly.

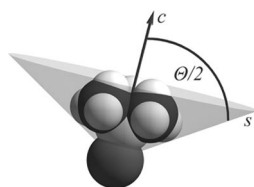


Figure 1. Visualisation of the Tolman cone angle  $\Theta$ , being twice the value of the angle between the cone axis  $c$  and the surface  $s$  of the cone just touching the outer surface of the ligand. For the sake of clarity a trimethylphosphane moiety bonded to a platinum atom is displayed.

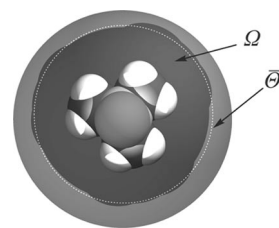


Figure 2. Demonstration of Immerzi's solid-angle concept. The ligand (trimethylphosphane) is projected on an outer sphere with the metal atom (platinum) being the centre and the light source. The shaded area gives the solid angle  $\Omega$  which is easily converted into  $\bar{\Theta}$  giving the angle of a circular equivalent cone.

One problem arising when facing the assignability of the solid-angle concept to bridging ligands is due to the assumption of a fixed metal–phosphorus bond length of 2.28 Å. For monodentate ligands, a dummy atom X at the required distance apart from the phosphorus nucleus is easily introduced along the metal–phosphorus bond and the solid angle is determined using X as the centre of the outer sphere and the light source. Besides the problem where to place the dummy atom, the question is raised whether a bond length of 2.28 Å should be used for bidentate ligands as well.

## Results and Discussion

To respond the question of the assignability of the solid-angle concept to bidentate ligands, we decided to put our focus on bidentate phosphanes, promising a large number of crystallographic data. To exclude effects caused by the central metal atom, we additionally limited our analysis to platinum-containing complexes. Thus a Cambridge Structural Database search was performed<sup>[12]</sup> and the hits were handpicked, with regard to square-planar, *P,P'*-*cis*-coordinated platinum complexes, fulfilling several other criteria as given in detail in the data retrieval part. Thereby, a total of 967 structures, with 282 different chelating phosphanes (in this article the terminus “phosphane” will be used in the broader sense of any moiety bearing two different phosphorus atoms that are coordinating to the same central platinum atom) was yielded and analysed with respect to the solid angle of the bridging phosphanes. Firstly, the platinum–phosphorus bond lengths were investigated, showing an average value of 2.268 Å with a standard deviation of 0.041 Å. The total range of  $d(\text{Pt}–\text{P})$  of all analysed molecular structures varies from 2.149 Å to 2.427 Å (Figure 3). Thus, the bond length of 2.28 Å used in the past, seems to be a good approximation for the investigation of bidentate phosphanes bonded to platinum as well. Therefore a dummy atom for the determination of the solid angle of chelating phosphanes might be placed at the appropriate distance of 2.28 Å. Additionally the plane defined by the metal and the two phosphorus atoms could be made use of to find an adequate position for X. As the solid-angle concept uses data deriving from single-crystal structure determination, mainly packing effects affect the conformation of

a ligand as well as the position of the central metal atom. Hence, it must be noted that for each molecular structure usually only one conformation is frozen in the solid state and was analysed according to the solid angle of the phosphane. Especially the fact that the introduction of a dummy atom influences the value of the bite angle remarkably, led us to the decision to keep the platinum atom as the centre and light source of the sphere for our investigations. The resulting solid angles  $\Omega_b$  thus obtained were converted into  $\bar{\Theta}_b$  following Equation (1).<sup>[4]</sup>

$$\bar{\Theta}_b = 2 \cdot b \cdot \arccos \left( 1 - \frac{\Omega_b}{2\pi} \right) \quad (1)$$

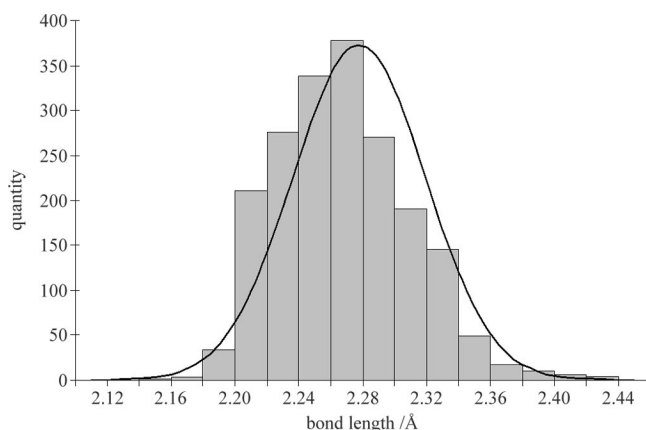


Figure 3. Histogram for the platinum–phosphorus bond lengths of all investigated molecular structures. The Gauss distribution plot has an average value of  $(2.268 \pm 0.041)$  Å for  $d(\text{Pt}–\text{P})$ . Each column has a width of 0.02 Å, i.e. it covers for example all bond lengths between 2.20 Å and 2.219 Å.

The correction factor  $b$  includes the two platinum–phosphorus bond lengths as well as the bite angle  $\beta$  of the appropriate bidentate phosphane [Equation (2), lengths in Å without unit, as indicated by {...}].

$$b = 1 + \frac{1}{2.28 \cdot \cos(\beta/2)} - \frac{\{d(\text{Pt}–\text{P})\} + \{d(\text{Pt}–\text{P}')\}}{2 \cdot \{d(\text{Pt}–\text{P})\} \cdot \{d(\text{Pt}–\text{P}')\} \cdot \cos(\beta/2)} \quad (2)$$

Thereby, the two platinum–phosphorus bond lengths were taken into account and the resulting value might be understood as “generalised equivalent cone angle”  $\bar{\Theta}_b$ , describing the angle of the equivalent cone imbedding the same surface as the shadow of the ligand.

The best phosphane to test the reliability of the aforementioned considerations is 1,2-bis(diphenylphosphanyl)ethane, better known as dppe. We found 175 structures for the analysis fulfilling all criteria and giving more than 200 data points (Figure 4). While the uncorrected relative solid angle  $\Omega_s$  varies from 0.444 to 0.534, the generalised equivalent cone angle  $\bar{\Theta}_b$  varies in the range of  $169.0^\circ$  to  $184.3^\circ$ . As shown in Table 1, the generalised angle  $\bar{\Theta}_b$  obtained following Equation (1) and Equation (2) has a narrow distri-

bution and is more suitable for a conclusion about the steric demand of bidentate phosphanes than the uncorrected  $\bar{\Theta}$  [resulting from Equation (1), with  $b = 1$ ] and the relative solid angle  $\Omega_s$ . Thus, the solid-angle concept seems to be transferable to bidentate phosphanes.

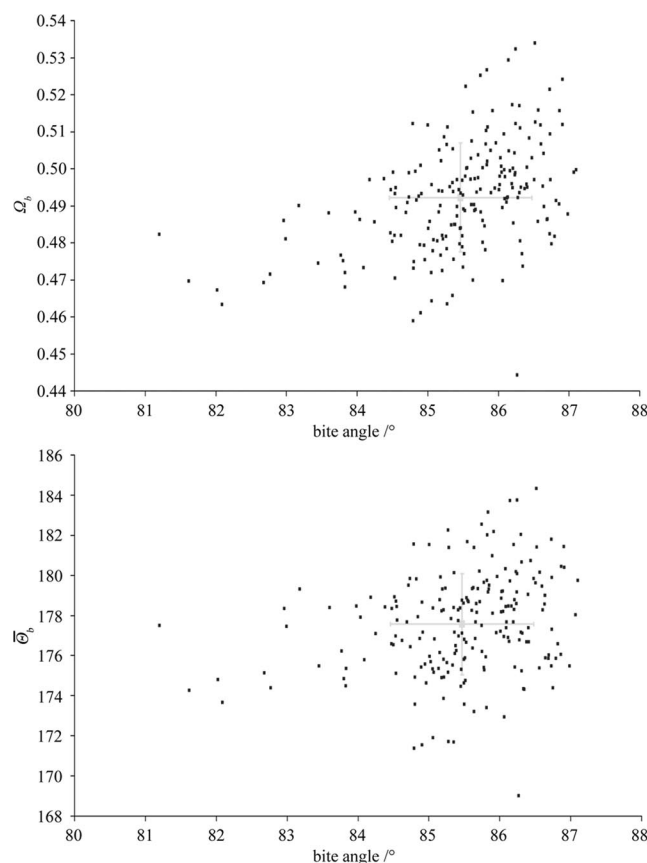


Figure 4. Analysis of dppe containing platinum complexes. Plots against the bite angle of the dppe moiety. Top: relative solid angle  $\Omega_s$  of the phosphane. Bottom: generalised equivalent cone angle  $\bar{\Theta}_b$ . Average values:  $\Omega_s$ :  $0.492 \pm 0.015$ ;  $\bar{\Theta}_b$ :  $177.6 \pm 2.5^\circ$ ; bite angle:  $85.46 \pm 1.01^\circ$ .

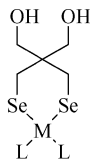
Table 1. Comparison of the different parameters, the relative solid angle  $\Omega_s$ , the equivalent cone angle  $\bar{\Theta}$  and the generalised equivalent cone angle  $\bar{\Theta}_b$  for all investigated dppe containing structures.

|                              | $\Omega_s$  | $\bar{\Theta}$          | $\bar{\Theta}_b$        |
|------------------------------|-------------|-------------------------|-------------------------|
| range                        | 0.444–0.534 | $167.2$ – $187.8^\circ$ | $169.0$ – $184.3^\circ$ |
| average                      | 0.492       | $178.2^\circ$           | $177.6^\circ$           |
| s.d. <sup>[a]</sup>          | 0.015       | $3.4^\circ$             | $2.5^\circ$             |
| relative s.d. <sup>[a]</sup> | 3.0%        | 1.9%                    | 1.4%                    |

[a] s.d. = standard deviation.

These promising results following from the analysis of dppe-containing platinum complexes require a closer look, which parameters influence the generalised equivalent cone angle  $\bar{\Theta}_b$  of bidentate phosphanes. As we intended to use phosphane-bearing diselenolotoplatinum(II) complexes as models for the prediction of the steric demand, a series of 2,2-bis(hydroxymethyl)-1,3-diselenolotoplatinum(II) complexes was prepared and reported in part 1 of this publication (Scheme 1 shows the numbering of the complexes, used

throughout this article). Thus, we took a closer look on the molecular structure of compound **C15** and the resulting steric demand of the dppe moiety. The parameters were determined to  $\Omega_s = 0.496$ ,  $\bar{\theta} = 179.2^\circ$  and  $\bar{\theta}_b = 178.0^\circ$  and all values are within one standard deviation from the average values determined for dppe.



|            | M  | L                |            | M  | L            |            | M  | L          |
|------------|----|------------------|------------|----|--------------|------------|----|------------|
| <b>C9</b>  | Pt | PMe <sub>3</sub> | <b>C15</b> | Pt | ½ dppe       | <b>C21</b> | Pt | ½ xantphos |
| <b>C10</b> | Pt | PTA              | <b>C16</b> | Pt | ½ dppbe      | <b>C24</b> | Pt | ½ dppf     |
| <b>C11</b> | Pt | PPh <sub>3</sub> | <b>C17</b> | Pt | ½ dppp       | <b>C25</b> | Pd | ½ dppe     |
| <b>C12</b> | Pt | 4-dppdbf         | <b>C18</b> | Pt | ½ dppn       | <b>C26</b> | Pd | ½ dppn     |
| <b>C13</b> | Pt | ½ dppm           | <b>C19</b> | Pt | ½ dppb       | <b>C27</b> | Pd | ½ dppf     |
| <b>C14</b> | Pt | ½ dppma          | <b>C20</b> | Pt | ½ dppo-xylyl | <b>C28</b> | Ni | ½ dppe     |

Scheme 1. Numbering of the complexes reported in Part A of this communication [PTA = 1,3,5-triaza-7-phosphaadamantane, 4-dppdbf = 4-(diphenylphosphanyl)dibenzofuran, dppm = 1,1-bis(diphenylphosphanyl)methane, dppma = *N,N*-bis(diphenylphosphanyl)methylamine, dppe = 1,2-bis(diphenylphosphanyl)ethane, dppbe = 1,2-bis(diphenylphosphanyl)benzene, dppp = 1,3-bis(diphenylphosphanyl)propane, dppn = 1,8-bis(diphenylphosphanyl)naphthalene, dppb = 1,4-bis(diphenylphosphanyl)butane, dppo-xylyl =  $\alpha,\alpha'$ -bis(diphenylphosphanyl)-*o*-xylene, xantphos = 4,5-bis(diphenylphosphanyl)-9,9-dimethylxanthene, dppf = 1,1'-bis(diphenylphosphanyl)ferrocene].

Firstly, we investigated the influence of the position of the platinum atom relative to the two phosphorus atoms. Movement of the platinum atom perpendicular to the segment defined by the phosphorus atoms changes the bond length and the resulting equivalent cone angle  $\bar{\theta}$ . As shown in Figure 5 the generalised equivalent cone angle  $\bar{\theta}_b$  is much less affected by changes in the platinum–phosphorus bond length, as requested, and thus proves a sufficient tool for the steric demand. Another factor that influences Tolman's as well as Immirzi's concepts considerably is the hybridisation of the phosphorus atoms. The use of physical CPK models implies perfect  $sp^3$ -hybridised phosphorus atoms, with all angles being  $109.5^\circ$ . Evidently, changes of the Pt–P–X (X = C for dppe) angles affect the steric demand. If the Pt–P–X angles increase, the substituents were folded back into the cone and the cone angle decreases and vice versa. This problem is partially overcome by the solid-angle concept, because only one conformation of each structure is frozen in the solid state. The dimension of the factor becomes explicit in the plot of  $\bar{\theta}_b$  against the average Pt–P–C<sub>Ph</sub> angle (Figure 6).

A quantity that remarkably affects the steric demand of bidentate ligands is the flexibility of substituents, e.g. the phenyl rings in the dppe moiety. This problem is well known for monodentate phosphite ligands.<sup>[6m,6n,13]</sup> The rotation of one of the phenyl rings of **C15** along the phosphorus carbon bond changes  $\bar{\theta}_b$  within a range of  $4\text{--}5^\circ$  (Figure 7). This effect is moderate for rather rigid substituents. All

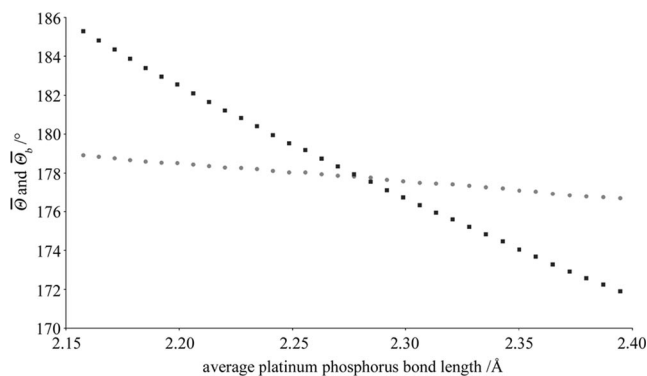


Figure 5. Dependence of the equivalent cone angle  $\bar{\theta}$  (squares) and the generalised equivalent cone angle  $\bar{\theta}_b$  (circles) on the platinum–phosphorus bond length.

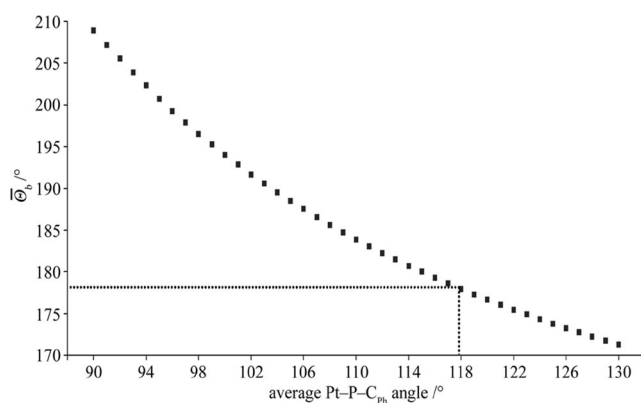


Figure 6. Plot of  $\bar{\theta}_b$  of **C15** against the average Pt–P–C<sub>Ph</sub> angle. Only the angles at one phosphorus atom were changed without considering any meshing in the ligand. The dotted lines represent the value in the original conformation of **C15**.

mentioned considerations led us to the conclusion, that the solid-angle concept might serve useful as steric parameter for bidentate phosphanes as well, whereas the generalised equivalent cone angle  $\bar{\theta}_b$  is best manageable.

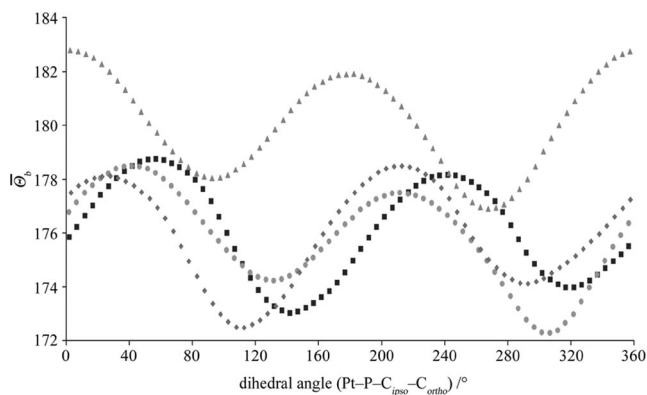


Figure 7. Change of the generalised equivalent cone angle  $\bar{\theta}_b$  on rotation of the phenyl rings along the phosphorus carbon bond (any meshing effects were not considered).

Therefore, the steric demand of all phosphanes meeting the postulated criteria was determined. To give some reliable values, Table 2 contains only bidentate phosphorus li-

Table 2. Summary of the steric parameters of some investigated phosphanes.

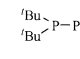
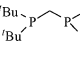
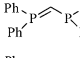
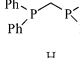
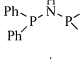
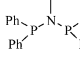
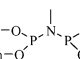
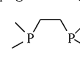
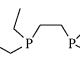
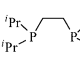
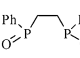
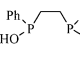
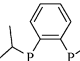
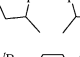
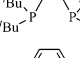
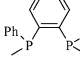
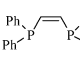
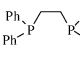
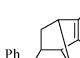
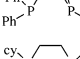
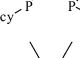
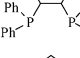
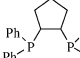
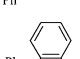
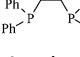
| Entry                      | Ring size <sup>[a]</sup> | Structure of investigated phosphane <sup>[b]</sup>                                  | Molecular formula  | Formula weight /g·mol <sup>-1</sup> | $d(\text{P-Pt})$ <sup>[c,d]</sup> /Å | Bite angle <sup>[d,e]</sup> /°              | Investigated molecular structures <sup>[d,f]</sup> | $\theta$ <sup>[d,g]</sup> /°              | $\theta_b$ <sup>[d,h]</sup> /°            |
|----------------------------|--------------------------|---|--|-------------------------------------|--------------------------------------|---|--|---|---|
| <b>1</b> <sup>[i]</sup>    | 3                        |    | C <sub>8</sub> H <sub>18</sub> P <sub>2</sub>                                | 176.18                              | 2.353                                | 52.16 ± 0.23                                | 3  | 152.3 ± 1.4                               | 154.6 ± 1.2                               |
| <b>14</b>                  | 4                        |    | C <sub>17</sub> H <sub>38</sub> P <sub>2</sub>                               | 304.43                              | 2.301                                | 75.15 ± 0.85                                | 11   | 188.6 ± 4.1                               | 189.5 ± 2.6                               |
| <b>19</b> <sup>[i,j]</sup> | 4                        |    | C <sub>25</sub> H <sub>21</sub> P <sub>2</sub>                               | 383.38                              | 2.262                                | 70.00 ± 0.49                                | 7  | 169.1 ± 2.7                               | 168.3 ± 2.1                               |
| <b>21</b> <sup>[i,j]</sup> | 4                        |    | C <sub>23</sub> H <sub>22</sub> P <sub>2</sub>                               | 384.39                              | 2.283                                | 72.59 ± 1.28                                | 49   | 168.1 ± 4.5                               | 168.1 ± 3.3                               |
| <b>22</b>                  | 4                        |    | C <sub>24</sub> H <sub>21</sub> NP <sub>2</sub>                              | 385.38                              | 2.297                                | 69.52 ± 0.39                                | 7  | 163.4 ± 4.4                               | 164.0 ± 3.9                               |
| <b>24</b> <sup>[j]</sup>   | 4                        |    | C <sub>25</sub> H <sub>23</sub> NP <sub>2</sub>                              | 399.4                               | 2.266                                | 70.76 ± 1.02                                | 9  | 166.6 ± 3.1                               | 166.0 ± 2.6                               |
| <b>33</b> <sup>[j]</sup>   | 4                        |    | C <sub>28</sub> H <sub>33</sub> NO <sub>4</sub> P <sub>2</sub>               | 463.4                               | 2.213                                | 70.59 ± 0.64                                | 5  | (173.8 ± 13.2) <sup>[k]</sup>             | (171.0 ± 13.3) <sup>[k]</sup>             |
| <b>53</b>                  | 5                        |    | C <sub>6</sub> H <sub>16</sub> P <sub>2</sub>                                | 150.14                              | 2.275                                | 85.57 ± 0.76                                | 11   | 155.8 ± 2.9                               | 155.5 ± 1.6                               |
| <b>55</b> <sup>[j]</sup>   | 5                        |    | C <sub>10</sub> H <sub>24</sub> P <sub>2</sub>                               | 206.25                              | 2.271                                | 85.69 ± 0.84                                | 7  | 176.0 ± 5.6                               | 175.5 ± 4.2                               |
| <b>57</b> <sup>[i,j]</sup> | 5                        |    | C <sub>14</sub> H <sub>32</sub> P <sub>2</sub>                               | 262.35                              | 2.287                                | 86.28 ± 0.87                                | 8  | 187.5 ± 2.4                               | 187.6 ± 1.7                               |
| <b>59</b>                  | 5                        |    | C <sub>14</sub> H <sub>15</sub> O <sub>2</sub> P <sub>2</sub>                | 277.22                              | 2.297                                | 85.64 ± 0.46                                | 4  | 165.0 ± 1.5                               | 165.7 ± 1.5                               |
| <b>60</b> <sup>[j]</sup>   | 5                        |   | C <sub>14</sub> H <sub>16</sub> O <sub>2</sub> P <sub>2</sub>                | 278.22                              | 2.274<br>2.302 <sup>[l]</sup>        | 85.23 ± 1.38<br>84.32 ± 0.25 <sup>[l]</sup> | 4<br>3 <sup>[l]</sup>                              | 166.3 ± 3.4<br>158.7 ± 1.9 <sup>[l]</sup> | 165.9 ± 1.5<br>159.6 ± 2.0 <sup>[l]</sup> |
| <b>62</b>                  | 5                        |  | C <sub>18</sub> H <sub>28</sub> P <sub>2</sub>                               | 306.36                              | 2.256                                | 86.67 ± 0.95                                | 23   | 176.9 ± 2.6                               | 175.7 ± 1.4                               |
| <b>64</b> <sup>[j]</sup>   | 5                        |  | C <sub>18</sub> H <sub>40</sub> P <sub>2</sub>                               | 318.46                              | 2.298                                | 88.45 ± 0.57                                | 14   | 201.6 ± 2.0                               | 202.6 ± 1.4                               |
| <b>65</b>                  | 5                        |  | C <sub>20</sub> H <sub>20</sub> P <sub>2</sub>                               | 322.32                              | 2.217                                | 87.17 ± 0.14                                | 4  | 169.4 ± 3.3                               | 166.5 ± 2.4                               |
| <b>78</b> <sup>[i,j]</sup> | 5                        |  | C <sub>26</sub> H <sub>22</sub> P <sub>2</sub>                               | 396.4                               | 2.256                                | 86.01 ± 0.75                                | 17   | 176.6 ± 2.9                               | 175.4 ± 2.3                               |
| <b>79</b> <sup>[i,j]</sup> | 5                        |  | C <sub>26</sub> H <sub>24</sub> P <sub>2</sub>                               | 398.42                              | 2.267                                | 85.46 ± 1.01                                | 203  | 178.2 ± 3.4                               | 177.6 ± 2.5                               |
| <b>80</b>                  | 5                        |  | C <sub>26</sub> H <sub>26</sub> P <sub>2</sub>                               | 400.43                              | 2.326                                | 81.63 ± 0.33                                | 3  | 168.8 ± 1.6                               | 170.8 ± 1.4                               |
| <b>87</b> <sup>[i,j]</sup> | 5                        |  | C <sub>26</sub> H <sub>48</sub> P <sub>2</sub>                               | 422.61                              | 2.273                                | 87.29 ± 1.49                                | 40   | 191.4 ± 2.9                               | 191.0 ± 2.4                               |
| <b>88</b>                  | 5                        |  | C <sub>28</sub> H <sub>28</sub> P <sub>2</sub>                               | 426.47                              | 2.251<br>2.273 <sup>[m]</sup>        | 86.41 ± 0.60<br>84.61 <sup>[m]</sup>        | 13<br>1 <sup>[m]</sup>                             | 180.6 ± 3.2<br>183.2 <sup>[m]</sup>       | 179.1 ± 3.0<br>182.8 <sup>[m]</sup>       |
| <b>89</b>                  | 5                        |  | C <sub>20</sub> H <sub>28</sub> P <sub>2</sub>                               | 438.48                              | 2.265                                | 87.24 ± 0.84                                | 5  | 175.4 ± 2.1                               | 174.6 ± 2.2                               |
| <b>90</b>                  | 5                        |  | C <sub>30</sub> H <sub>24</sub> P <sub>2</sub>                               | 446.46                              | 2.234                                | 86.60 ± 0.23                                | 6  | 179.6 ± 3.8                               | 177.3 ± 2.7                               |
| <b>94</b>                  | 5                        |  | C <sub>25</sub> H <sub>48</sub> N <sub>4</sub> P <sub>2</sub> <sup>[n]</sup> | 466.62                              | 2.256 <sup>[n]</sup>                 | 87.00 ± 0.99 <sup>[n]</sup>                 | 4 <sup>[n]</sup>                                   | 186.8 ± 2.9 <sup>[n]</sup>                | 185.5 ± 2.6 <sup>[n]</sup>                |
| <b>104</b>                 | 5                        |  | C <sub>20</sub> H <sub>28</sub> O <sub>4</sub> P <sub>2</sub> <sup>[o]</sup> | 502.48                              | 2.209 <sup>[o]</sup>                 | 86.07 ± 0.54 <sup>[o]</sup>                 | 4 <sup>[o]</sup>                                   | (202.0 ± 15.7) <sup>[k,o]</sup>           | (198.1 ± 14.8) <sup>[k,o]</sup>           |
| <b>137</b>                 | 6                        |  | C <sub>15</sub> H <sub>34</sub> P <sub>2</sub>                               | 276.38                              | 2.278                                | 97.50 ± 3.47                                | 3  | 192.7 ± 3.7                               | 192.5 ± 1.3                               |

Table 2. (Continued)

| Entry                | Ring size <sup>[a]</sup> | Structure of investigated phosphane <sup>[b]</sup> | Molecular formula  | Formula weight /g·mol <sup>-1</sup> | <i>d</i> (P–Pt) <sup>[c,d]</sup> /Å | Bite angle <sup>[d,e]</sup> /° | Investigated molecular structures <sup>[d,f]</sup> | $\bar{\theta}$ <sup>[d,g]</sup> /° | $\bar{\theta}_b$ <sup>[d,h]</sup> /° |
|----------------------|--------------------------|--|--|-------------------------------------|-------------------------------------|--------------------------------|--|------------------------------------|--------------------------------------|
| 139 <sup>[i]</sup>   | 6                        |  | C <sub>19</sub> H <sub>42</sub> P <sub>2</sub>   | 332.48                              | 2.297                               | 99.03 ± 1.62                   | 4  | 210.1 ± 2.3                        | 211.0 ± 1.3                          |
| 142 <sup>[i,j]</sup> | 6                        |  | C <sub>27</sub> H <sub>26</sub> P <sub>2</sub>   | 412.44                              | 2.266                               | 92.94 ± 1.95                   | 90   | 183.7 ± 3.9                        | 182.9 ± 2.9                          |
| 145                  | 6                        |  | C <sub>29</sub> H <sub>30</sub> P <sub>2</sub> [p]   | 440.5                               | 2.273[p]                            | 94.54 ± 1.79[p]                | 7[p]   | 190.0 ± 2.5[p]                     | 189.6 ± 2.1[p]                       |
| 156                  | 6                        |  | C <sub>30</sub> H <sub>27</sub> NP <sub>2</sub>  | 463.49                              | 2.270                               | 91.77 ± 2.24                   | 3  | 190.5 ± 2.4                        | 189.9 ± 1.3                          |
| 169 <sup>[i,j]</sup> | 6                        |  | C <sub>34</sub> H <sub>28</sub> P <sub>2</sub> Fe  | 554.38                              | 2.286                               | 99.59 ± 1.95                   | 64   | 191.9 ± 2.7                        | 192.2 ± 2.2                          |
| 172                  | 6                        |  | C <sub>38</sub> H <sub>34</sub> BP <sub>2</sub>  | 563.44                              | 2.291                               | 89.58 ± 3.15                   | 3  | 187.3 ± 0.9                        | 187.8 ± 1.3                          |
| 188                  | 6                        |  | C <sub>32</sub> H <sub>38</sub> Cl <sub>2</sub> N <sub>2</sub> P <sub>2</sub> Ti             | 631.38                              | 2.309                               | 103.73 ± 1.35                  | 4  | 209.9 ± 1.3                        | 211.7 ± 0.5                          |
| 204 <sup>[i]</sup>   | 7                        |  | C <sub>28</sub> H <sub>28</sub> P <sub>2</sub>   | 426.47                              | 2.274                               | 96.81 ± 3.17                   | 12   | 188.1 ± 4.2                        | 187.7 ± 2.5                          |
| 216 <sup>[i]</sup>   | 7                        |  | C <sub>31</sub> H <sub>32</sub> O <sub>2</sub> P <sub>2</sub> [q]                            | 498.53                              | 2.275[q]                            | 100.49 ± 4.35[q]               | 11[q]  | 186.0 ± 3.2[q]                     | 185.7 ± 3.1[q]                       |
| 219 <sup>[i]</sup>   | 7                        |  | C <sub>36</sub> H <sub>28</sub> P <sub>2</sub>   | 522.56                              | 2.260                               | 92.40 ± 1.66                   | 5  | 189.3 ± 5.2                        | 188.2 ± 3.2                          |
| 229                  | 7                        |  | C <sub>44</sub> H <sub>32</sub> P <sub>2</sub>   | 622.67                              | 2.287                               | 93.04 ± 1.49                   | 4  | 189.0 ± 2.9                        | 189.4 ± 1.8                          |
| 251                  | 8                        |  | C <sub>44</sub> H <sub>44</sub> N <sub>2</sub> O <sub>6</sub> P <sub>2</sub> Mo <sub>2</sub> | 950.66                              | 2.260                               | 96.70 ± 1.10                   | 3  | 221.6 ± 2.4                        | 220.3 ± 1.6                          |
| 253 <sup>[i]</sup>   | 9                        |  | C <sub>24</sub> H <sub>36</sub> O <sub>2</sub> P <sub>2</sub>                                | 418.49                              | 2.256                               | 109.18 ± 10.28                 | 4  | 205.4 ± 6.1                        | 203.7 ± 6.1                          |

[a] Ring size of the platinacycle upon coordination of the phosphane. [b] The following abbreviations were used in the chemical formulae: Me = methyl, *i*Pr = isopropyl, *t*Bu = *tert*-butyl, Ph = phenyl, cy = cyclohexyl. [c] Average phosphorus–platinum bond length determined from investigated structures with the appropriate phosphane ligand. [d] Discrimination due to stereochemical isomers is only given for phosphanes showing remarkable differences in their steric demand caused by diverse alignment of substituents. [e] Average phosphorus–platinum–phosphorus angle for the investigated phosphane. [f] Quantity of investigated molecular structures bearing the respective phosphane, all values given for only one investigated structure should be used cautiously. [g] Average equivalent cone angle, see text for details. [h] Average generalised equivalent cone angle, taking the phosphorus–platinum bond lengths into account, see text for details. [i] For some structures the positions of hydrogen atoms were calculated with the programs given in ref.<sup>[15]</sup> [j] For some structures the positions of atoms due to symmetry elements within the molecular structure were calculated with the programs given in ref.<sup>[15]</sup> [k] The values for  $\bar{\theta}$  and  $\bar{\theta}_b$  must be taken with great care as the flexibility of substituents at heteroatoms strongly influences them, see text for a detailed discussion. [l] The first value refers to (1*R*,2*R*)- the second to (1*R*,2*S*)-bis(hydroxyphenylphosphanyl)ethane. [m] The first value refers to (2*R*,3*R*)- and (2*S*,3*S*)- the second to (2*R*,3*S*)-bis(diphenylphosphanyl)butane. [n] All investigated molecular structures showed (1*R*,2*R*)- or (1*S*,2*S*)-symmetry of 1,2-bis[bis(piperidin-1-yl)phosphanyl]cyclopentane. [o] All investigated molecular structures showed (1*R*,2*R*)-(+)- or (1*S*,2*S*)-(-)-symmetry of bis[bis(phenoxy)phosphanyl]cyclopentane. [p] All investigated molecular structures showed (2*R*,4*R*)- or (2*S*,4*S*)-symmetry of 2,4-bis(diphenylphosphanyl)pentane. [q] All investigated molecular structures showed (2*R*,3*R*)-(-)- or (2*S*,3*S*)-(+)-symmetry of 2,3-*O*,*O'*-isopropylidene-2,3-dioxy-1,4-bis(diphenylphosphanyl)butane.

gands for which at least three crystallographic data files were accessible (for data on all investigated phosphanes please refer to the Supporting Information). The entries are sorted firstly according to increasing size of the platinacycle built upon coordination and secondly with respect to increasing molecular weight.

As depicted from the standard deviations, the values for the generalised equivalent cone angles  $\bar{\Theta}_b$  show moderate distributions around the related average value and thus further support its suitability as steric parameter for bridging phosphanes. Expectedly, broad distributions are observed for ligands having sterically demanding flexible substituents, namely phosphites (entries **33** and **104**). While the standard deviation varies in the range of 1–2% for most phosphanes, it increases to about 8% for the mentioned phosphites.

The possibility of the phenyl rings to rotate around the oxygen–carbon bond on the one hand and along the P–O bond on the other hand results in tremendous changes of the steric demand. The analysis of one exemplary complex bearing phosphane **104** ([PtCl<sub>2</sub>(**104**)], CCDC code BEQBAA, first published in ref.<sup>[14]</sup>) including both axes of rotation shows the sensitivity of the generalised equivalent cone angle to the torsion angles Pt–P–O–C<sub>ipso</sub> and P–O–C<sub>ipso</sub>–C<sub>ortho</sub>. The three-dimensional plot (Figure 8) clarifies the dimension of the influence of the steric alignment of one phenyl ring. Thus,  $\bar{\Theta}_b$  differs in a range of about 180° to 220° only due to the rotation of one phenyl ring. For this reason, the solid-angle concept yields only rough estimates for the steric demand of ligands with highly flexible groups.

Another conclusion resulting from Table 2 is the increasing steric demand in phosphanes including the same bridging moiety but containing bulkier substituents. This anticipated effect is best seen in the variably substituted 1,2-diphosphanylene ligands. Such,  $\bar{\Theta}_b$  increases in the series methyl (**53**) < ethyl (**55**) ≈ phenyl (**79**) < isopropyl (**57**) <

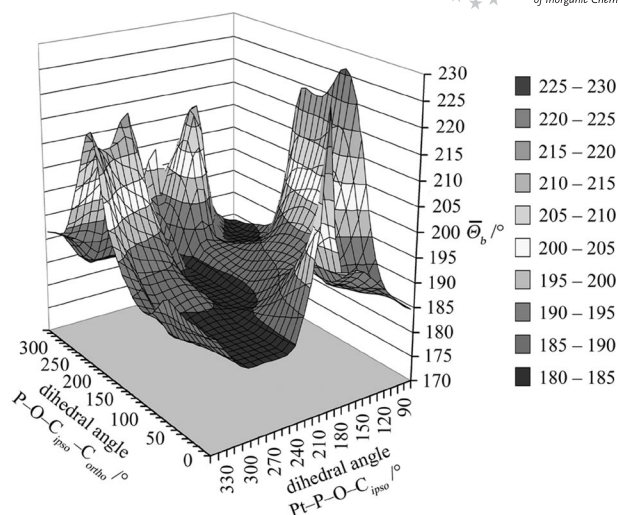


Figure 8. Influence of the rotation of one phenyl ring around the phosphorus–oxygen and the oxygen–carbon bond (data was taken from crystallographic data file BEQBAA<sup>[14]</sup> composited at Cambridge Crystallographic Data Centre; no meshing effects were considered; only the area where the phenyl ring is not overlapping with the platinum atom is displayed).

cyclohexyl (**87**) < *tert*-butyl (**64**) from about 155° for 1,2-bis(dimethylphosphanyl)ethane (Entry **53**) to more than 200° for 1,2-bis(di-*tert*-butylphosphanyl)ethane (Entry **64**). On the other hand, changes within the bridging part of the phosphanes only affect the steric demand remarkably, when bulky substituents show deviations from the central metal mean plane. The steric demand is comparable for identically substituted 1,2-diphosphanylene and 1,2-diphosphanylene derivatives (Table 3, lines 2 to 9). Hence  $\bar{\Theta}_b$  varies only from 174.6° to 179.1° for diphenylphosphanyl-substituted derivatives, including rather big substituents like a phenyl moiety (lines 4 and 8) at the backbone. Unsurpris-

Table 3. Influence of the backbone to the steric demand of bidentate phosphanes (bold numbers follow the entry number of the phosphane used in Table 2 and in the Supporting Information, the values given, refer to  $\bar{\Theta}_b$ ).

| Entry | Backbone   | Methyl                            | Isopropyl                         | Phenyl                            |
|-------|--|-----------------------------------|-----------------------------------|-----------------------------------|
| 1     | 1,1-diphosphanylmethane                                  |                                   | <b>10</b> /177.9° <sup>[a]</sup>  | <b>21</b> /168.1°                 |
| 2     | 1,2-diphosphanylene                                      |                                   |                                   | <b>78</b> /175.4°                 |
| 3     | 1,2-diphosphanyl-1-methylethane                          |                                   |                                   | <b>82</b> /175.7° <sup>[a]</sup>  |
| 4     | 1,2-diphosphanyl-1-phenylethane                          |                                   |                                   | <b>97</b> /178.1° <sup>[a]</sup>  |
| 5     | 1,2-diphosphanylbenzene                                  | <b>54</b> /156.9° <sup>[a]</sup>  | <b>63</b> /192.1°                 | <b>90</b> /177.3°                 |
| 6     | 1,2-diphosphanylene                                      | <b>53</b> /155.5°                 | <b>57</b> /187.6°                 | <b>79</b> /177.6°                 |
| 7     | 2,3-diphosphanylbutane                                   |                                   |                                   | <b>88</b> /179.1° <sup>[b]</sup>  |
| 8     | 1,2-diphosphanyl-1-phenylethane                          |                                   |                                   | <b>99</b> /177.2° <sup>[a]</sup>  |
| 9     | 1,2-diphosphanylcyclopentane                             |                                   |                                   | <b>89</b> /174.6°                 |
| 10    | 1,2-diphosphanyl-1,2-dicarba- <i>closo</i> -dodecaborane |                                   | <b>75</b> /199.5° <sup>[a]</sup>  |                                   |
| 11    | 1,3-diphosphanylpropane                                  | <b>135</b> /158.4° <sup>[a]</sup> | <b>137</b> /192.5°                | <b>142</b> /182.9°                |
| 12    | 1,8-diphosphanylnaphthalene                              |                                   |                                   | <b>163</b> /178.5° <sup>[a]</sup> |
| 13    | 1,4-diphosphanylbutane                                   |                                   | <b>200</b> /199.4° <sup>[a]</sup> | <b>204</b> /187.7°                |
| 14    | $\alpha,\alpha'$ -diphosphanyl- <i>o</i> -xylene         |                                   |                                   | <b>211</b> /189.1° <sup>[a]</sup> |
| 15    | 2,2'-diphosphanyl-1,1'-biphenyl                          |                                   |                                   | <b>219</b> /188.2°                |
| 16    | 2,2'-diphosphanyl-1,1'-binaphthalene                     |                                   |                                   | <b>229</b> /189.4°                |
| 17    | 1,5-diphosphanylpentane                                  |                                   |                                   | <b>241</b> /193.6° <sup>[a]</sup> |
| 18    | 1,8-diphosphanylmethylnaphthalene                        |                                   |                                   | <b>245</b> /196.5° <sup>[a]</sup> |

[a] The values given for  $\bar{\Theta}_b$  refer to less than three structures and thus must be used with caution. [b] Only the value referring to (2*R*,3*R*)- and (2*S*,3*S*)-bis(diphenylphosphanyl)butane is given.

ingly, bulkier substituents at the backbone clearly influence  $\bar{\Theta}_b$ , as shown from the isopropyl derivatives in lines 5, 6 and 10. While the generalised equivalent cone angle increases moderately from 187.6° (**57**) to 192.1° (**63**) by changing the ethane moiety to a benzene ring, it extends to 199.5° in **75**, bearing a bulky borane moiety in the backbone. Additionally, it becomes obvious that the extension of the platina-cyclo formed upon coordination of the phosphanes  $R_2P(CH_2)_n-PR_2$  by one  $CH_2$  group enlarges  $\bar{\Theta}_b$  by about 5° to 7° for  $n = 2-5$  (lines 6, 11, 13 and 17) irrespective of the substituents  $R$ . The difference between  $n = 1$  and 2 (lines 1 and 6) is almost 10° due to the large relative change of the ring size and the average bite angle.

Because the bite angle has been used as steric parameter for bidentate phosphanes during the last years<sup>[10]</sup> a comparison with the generalised equivalent cone angle is mandatory. The bite angles of the phosphanes reported in this paper and that found by Dierkes and van Leeuwen<sup>[10a]</sup> are mostly within one standard deviation.

It must be noted that only platinum complexes have been considered in our studies while all d- and f-block elements were accepted as metal centre in ref.<sup>[10a]</sup> The goodness of the correlation between  $\bar{\Theta}_b$  and the bite angle is shown in Figure 9. On the one hand the recognisable relationship between the two quantities justifies the use of the bite angle as steric parameter, on the other hand it also illustrates the possibility of improvement by the use of  $\bar{\Theta}_b$ .

Because a precise determination of the steric demand of any bidentate phosphane requires crystal structure data and sometimes is quite elaborate, the question for any model compound is raised. In general, most influences due to the alignment of substituents at the phosphane, the conformation at the phosphorus atoms and the platinum–phosphorus bond lengths are averaged in  $\bar{\Theta}_b$ . Despite that, impacts

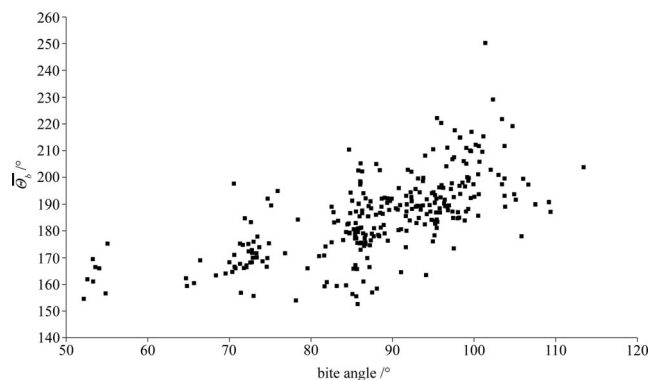


Figure 9. Correlation between the generalised equivalent cone angle  $\bar{\Theta}_b$  and the bite angle of the appropriate phosphane.

resulting from packing effects, the metal–phosphorus bond lengths and the angles at the phosphorus atoms are most influential to the value of the generalised equivalent cone angle. Thus, the substituents opposite to the investigated phosphane play an important role.

We chose diselenolato ligands as opposite substituents for model compounds for several reasons. Firstly, the difference in the electronegativity between selenium and platinum is very small and thus electronic effects should be negligible. Secondly, the resulting diselenolato complexes display platinum–phosphorus bond lengths,  $(2.266 \pm 0.019)$  Å, representative for platinum bisphosphane complexes. Additionally, the use of 4,4-bis(hydroxymethyl)-1,2-diselenolane as ligand proved useful. It is moisture- and air-stable and is easily prepared, as the platinum(II) complexes **C9** to **C24**, too. Most of the prepared complexes were easily crystallised and the single-crystal structure determination gave the desired data for the investigation of the steric demand. Table 4 dis-

Table 4. Comparison of the generalised equivalent cone angles deriving from the database analysis and the appropriate values for complexes **C13** to **C24**, additionally the steric demand of the diselenolato moiety in the compounds **C9** to **C11b** is given.

| Phosphane                       | Entry compd. no. <sup>[a]</sup> | $\bar{\Theta}_b$ <sup>[b]</sup> /° | Complex no. <sup>[c]</sup> | $\bar{\Theta}_b(P \cap P)$ <sup>[d]</sup> /° | $\bar{\Theta}_b(Se \cap Se)$ <sup>[e]</sup> /° |
|---------------------------------|---------------------------------|------------------------------------|----------------------------|--|--|
| PMe <sub>3</sub>                |                                 |                                    | <b>C9</b>                  |  | 139.7  |
| PTA                             |                                 |                                    | <b>C10</b>                 |  | 139.4  |
| PPh <sub>3</sub> <sup>[f]</sup> |                                 |                                    | <b>C11a</b>                |  | 139.5  |
|                                 |                                 |                                    | <b>C11b</b>                |  | 139.3  |
| dppm                            | <b>21</b>                       | 168.1 ± 3.3                        | <b>C13</b>                 | 167.9  | 141.0  |
| dppma                           | <b>24</b>                       | 166.0 ± 2.6                        | <b>C14</b>                 | 166.8  | 140.4  |
| dppe                            | <b>79</b>                       | 177.6 ± 2.5                        | <b>C15</b>                 | 178.0  | 140.4  |
| dppbe                           | <b>90</b>                       | 177.3 ± 2.7                        | <b>C16</b>                 | 174.0  | 140.4  |
| dppp                            | <b>142</b>                      | 182.9 ± 2.9                        | <b>C17</b>                 | 179.3  | 139.9  |
| dppn                            | <b>163</b>                      | 178.5 ± 2.1 <sup>[g]</sup>         | <b>C18</b>                 | 179.8  | 139.6  |
| dppb                            | <b>204</b>                      | 187.7 ± 2.5                        | <b>C19</b>                 | 186.1  | 140.2  |
| dppo-xyI                        | <b>211</b>                      | 189.1 ± 3.6 <sup>[g]</sup>         | <b>C20</b>                 | 186.4  | 139.7  |
| xantphos <sup>[h]</sup>         |                                 |                                    | <b>C22</b> <sup>[i]</sup>  | (191.9/192.8)                                | (153.5/143.1)                                  |
|                                 |                                 |                                    | <b>C23</b> <sup>[j]</sup>  | (196.4)                                      | (142.5)  |
| dppf                            | <b>169</b>                      | 192.2 ± 2.2                        | <b>C24</b>                 | 189.2  | 139.4  |

[a] Numbering according to Table 2 and the Supporting Information part. [b] Average generalised equivalent cone angle for the appropriate phosphane. [c] Numbering of the reported complexes according to Scheme 1. [d] Generalised equivalent cone angle for the bidentate phosphane in the particular complex. [e] Generalised equivalent cone angle for the 2,2-bis(hydroxymethyl)-1,3-diselenolato bridging moiety in the respective complex. [f] Two different samples were investigated, for details see Part 1 of this series (preceding article). [g] The values for less than three structures are implied in these average values. [h] No molecular structure fulfilling the criteria for involvement in our analysis was found, the values in the first line belong to **C22** (with Pt1A/Pt1B being the central atom), that in the second to **C23**, the structure of both complexes disagree distinctly from all other complexes and the values were excluded from all following investigations. [i] Dinuclear complex  $[Pt_2(xantphos)_2\{(SeCH_2)_2C(CH_2OH)_2\}]Cl_2$ . [j] Trinuclear complex  $[Pt_3(xantphos)_2\{(SeCH_2)_2C(CH_2OH)_2\}_2]Cl_2$ .

plays  $\bar{\theta}_b$  of the phosphane moiety in compounds **C13** to **C24** and the average equivalent cone angles as obtained from the database analysis. It becomes obvious that the values from the model compounds are in good agreement with the average values deriving from the database analysis, but the desired intention to establish the diselenolato complexes as standard for the fast and easy prediction of the steric demand of bidentate phosphanes failed. Mainly some apparent deviations from the average values, especially **C16** and **C24**, contradict the use of the reported complexes as standard compounds. Beyond this, we tested whether the solid-angle concept might be further extended to other bidentate ligands. Therefore, we investigated the generalised equivalent cone angle  $\bar{\theta}_b(\text{Se}\cap\text{Se})$  for the diselenolato moiety in complexes **C13–C24** following Equation (1) with the modified factor  $b_{\text{Se}}$  [Equation (3)] implying an average platinum–selenium bond length of 2.458 Å and the bite angle of the diselenolato moiety  $\gamma$ . The average of the platinum–selenium bond length was determined from the crystal-

structure data from complexes **C13–C20** and **C24** to  $(2.458 \pm 0.008)$  Å, the related bite angle is  $(91.75 \pm 1.02)^\circ$ . The results for  $\bar{\theta}_b(\text{Se}\cap\text{Se})$  prove the usefulness of the solid-angle concept for bidentate ligands. For the 2,2-bis-(hydroxymethyl)-1,3-diselenolato ligand,  $\bar{\theta}_b(\text{Se}\cap\text{Se})$  has a value of  $(139.9 \pm 0.5)^\circ$  and so that demonstrates the possibility of expansion of the reported method to other bidentate ligands as well.

$$b_{\text{Se}} = 1 + \frac{1}{2.458 \cdot \cos(\gamma/2)} - \frac{\{d(\text{Pt}-\text{Se})\} + \{d(\text{Pt}-\text{Se}')\}}{2 \cdot \{d(\text{Pt}-\text{Se})\} \cdot \{d(\text{Pt}-\text{Se}')\} \cdot \cos(\gamma/2)} \quad (3)$$

Some results for  $\bar{\theta}_b$  stated in Table 2 can be corrected to the values given in Table 5, including the results for the equivalent cone angle of the phosphanes in **C7**, **C8**, **C13–C20** and **C24**. For xantphos the value must be added to the complete table given in the Supporting Information as no structure matching the criteria was reported so far.

Table 5. Corrections for  $\bar{\theta}_b$  necessary after implementation of **C7**, **C8**, **C13–C20** and **C24**. Entries printed in *italics* are taken from Table 2 and the tables given in the Supporting Information, while the corrected values are printed in **bold**, entry **X283** was added to the table; for footnotes please refer to Table 2.

| Entry                       | Ring size <sup>[a]</sup> | Structure of investigated phosphane <sup>[b]</sup> | Molecular formula                                 | Formula weight /g·mol <sup>−1</sup> | $d(\text{P}-\text{Pt})$ <sup>[c,d]</sup> /Å | Bite angle <sup>[d,e]</sup> /°        | Investigated molecular structures <sup>[d,f]</sup> | $\theta$ <sup>[d,g]</sup> /°      | $\theta_b$ <sup>[d,h]</sup> /°    |
|-----------------------------|--------------------------|--|---|-------------------------------------|---|---------------------------------------|--|-----------------------------------|-----------------------------------|
| <b>21</b> <sup>[i,j]</sup>  | 4                        |  | C <sub>25</sub> H <sub>22</sub> P <sub>2</sub>    | 384.39                              | 2.283<br><b>2.282</b>                       | 72.59 ± 1.28<br><b>72.60 ± 1.27</b>   | 49<br><b>50</b>                                    | 168.1 ± 4.5<br><b>168.1 ± 4.4</b> | 168.1 ± 3.3<br><b>168.1 ± 3.3</b> |
| <b>24</b> <sup>[i]</sup>    | 4                        |  | C <sub>25</sub> H <sub>23</sub> NP <sub>2</sub>   | 399.4                               | 2.266<br><b>2.263</b>                       | 70.76 ± 1.02<br><b>70.86 ± 1.01</b>   | 9<br><b>10</b>                                     | 166.6 ± 3.1<br><b>166.8 ± 3.0</b> | 166.0 ± 2.6<br><b>166.1 ± 2.5</b> |
| <b>79</b> <sup>[i,j]</sup>  | 5                        |  | C <sub>26</sub> H <sub>24</sub> P <sub>2</sub>    | 398.42                              | 2.267<br><b>2.267</b>                       | 85.46 ± 1.01<br><b>85.46 ± 1.01</b>   | 203<br><b>204</b>                                  | 178.2 ± 3.4<br><b>178.2 ± 3.4</b> | 177.6 ± 2.5<br><b>177.6 ± 2.5</b> |
| <b>90</b>                   | 5                        |  | C <sub>30</sub> H <sub>24</sub> P <sub>2</sub>    | 446.46                              | 2.234<br><b>2.235</b>                       | 86.60 ± 0.23<br><b>86.77 ± 0.50</b>   | 6<br><b>7</b>                                      | 179.6 ± 3.8<br><b>179.0 ± 3.7</b> | 177.3 ± 2.7<br><b>176.8 ± 2.7</b> |
| <b>142</b> <sup>[i,j]</sup> | 6                        |  | C <sub>27</sub> H <sub>26</sub> P <sub>2</sub>    | 412.44                              | 2.266<br><b>2.266</b>                       | 92.94 ± 1.95<br><b>92.93 ± 1.94</b>   | 90<br><b>91</b>                                    | 183.7 ± 3.9<br><b>183.6 ± 3.9</b> | 182.9 ± 2.9<br><b>182.9 ± 2.9</b> |
| <b>163</b>                  | 6                        |  | C <sub>34</sub> H <sub>26</sub> P <sub>2</sub>    | 496.52                              | 2.256<br><b>2.244</b>                       | 88.24 ± 0.61<br><b>89.26 ± 2.00</b>   | 2<br><b>4</b>                                      | 179.7 ± 2.4<br><b>182.9 ± 5.5</b> | 178.5 ± 2.1<br><b>181.1 ± 4.5</b> |
| <b>169</b> <sup>[i,j]</sup> | 6                        |  | C <sub>34</sub> H <sub>28</sub> P <sub>2</sub> Fe | 554.38                              | 2.286<br><b>2.286</b>                       | 99.59 ± 1.95<br><b>99.55 ± 1.96</b>   | 64<br><b>65</b>                                    | 191.1 ± 2.7<br><b>191.1 ± 2.7</b> | 192.2 ± 2.2<br><b>192.2 ± 2.2</b> |
| <b>204</b> <sup>[i]</sup>   | 7                        |  | C <sub>28</sub> H <sub>28</sub> P <sub>2</sub>    | 426.47                              | 2.274<br><b>2.274</b>                       | 96.81 ± 3.17<br><b>96.68 ± 3.07</b>   | 12<br><b>13</b>                                    | 188.1 ± 4.2<br><b>188.0 ± 4.0</b> | 187.7 ± 2.5<br><b>187.6 ± 2.5</b> |
| <b>211</b>                  | 7                        |  | C <sub>32</sub> H <sub>28</sub> P <sub>2</sub>    | 474.51                              | 2.263<br><b>2.263</b>                       | 103.82 ± 1.68<br><b>102.95 ± 1.92</b> | 2<br><b>3</b>                                      | 190.2 ± 3.3<br><b>189.3 ± 2.8</b> | 189.1 ± 3.6<br><b>188.2 ± 3.0</b> |
| <b>X283</b>                 | 8                        |  | C <sub>39</sub> H <sub>32</sub> OP <sub>2</sub>   | 578.62                              | —<br><b>2.297</b>                           | —<br><b>102.71 ± 3.33</b>             | —<br><b>4</b>                                      | —<br><b>192.2 ± 3.2</b>           | —<br><b>193.2 ± 2.2</b>           |

Expectedly, the changes are marginal when large numbers of structures were already available at the Cambridge Database, as for instance for **21**, **79**, **142** and **169**, while the result is concretised for **163**, whereof only two structures suitable for analysis were known so far. Evidently, the generalised equivalent cone angle is a useful tool for the steric demand of bidentate phosphanes, but nevertheless its prediction for a specific phosphane deriving from the value of  $\bar{\Theta}_b$  for [2,2-bis(hydroxymethyl)-1,3-diselenolato]platinum(II) complexes can only serve as a first approximation.

## Conclusions

A detailed Cambridge Database search for platinum complexes bearing bidentate phosphanes was conducted in order to find as many bridging phosphane moieties as possible. The findings were handpicked with respect to precise criteria, like square-planar coordination at the central metal atom, a *cis*-coordination of the appropriate phosphane, acceptable accuracy of the crystal-structure determination. In doing so, over 900 molecular structures with 282 different bidentate phosphanes were obtained. To answer the question whether the solid-angle concept is transferable to bidentate ligands, we first investigated 1,2-bis(diphenylphosphanyl)ethane, providing the largest amount of crystal data. Therefore, the solid angles  $\Omega_s$  were calculated and converted into the generalised equivalent cone angles  $\bar{\Theta}_b$ , giving the angle of the cone encircling the same area as the shadow of the ligand and comprising the platinum–phosphorus bond lengths and the bite angle of the phosphane. The influences of changes in the metal–phosphorus distance were minimised, and the resulting value displays a manageable tool for expressing the steric demand. The large quantity of crystal data available – 175 molecular structures containing more than 200 dppe moieties – and the analysis of these data demonstrated the suitability of the solid-angle concept. The generalised equivalent cone angle for dppe was determined to be  $(177.6 \pm 2.5)^\circ$ . As  $\bar{\Theta}_b$  seems to be a practicable parameter for the quantification of the steric demand of bidentate phosphanes, we analysed all suitable molecular structures and present the values of  $\bar{\Theta}_b$  for over 280 different phosphanes. As is known from the literature and is obvious from the results, ligands having bulky flexible parts and hence great latitudes show huge differences in their alignment in the solid state and, consequently, yield scarcely useable values.

During the last decade, the bite angle of bidentate phosphanes was widely used as a parameter for the steric properties of these ligands. Inevitably, we compared the bite angles of the analysed phosphanes and their generalised equivalent cone angles. A correlation between these two quantities was detected, but owing to the possibility of improvement, we conclude that the use of  $\bar{\Theta}_b$  is preferable.

However, the generalised equivalent cone angle cannot be employed without any qualification. The use of crystal structure data implies some restrictions. For example, only one precise conformation of the investigated ligand is fro-

zen in the solid state, packing effects might cause compression or expansion of substituents at the ligand, as intermolecular forces like hydrogen bridges and integration of solvent molecules might as well. The solid-angle concept is not transferable to the behaviour of ligands in solution, as solvent interactions and increasing degrees of freedom come to the fore. Finally, many other factors, especially electronic parameters, influence the steric demand of any ligand.

Since the generalised equivalent cone angle works well for bidentate phosphanes, we hoped to employ diselenolato-platinum(II) complexes as model compounds for the prediction of  $\bar{\Theta}_b$  and therefore to avoid the elaborate analysis of a large number of molecular structures. The values calculated for the diselenato bearing complexes can be used as a first approximation to the average of all available structures. Nevertheless,  $\bar{\Theta}_b$  is not limited to phosphanes, but can easily be extended to other bidentate ligands, as was proven for the 2,2-bis(hydroxymethyl)-1,3-diselenolato ligand in the complexes reported in Part 1 of this publication. We arrive at the conclusion that the generalised equivalent cone angle  $\bar{\Theta}_b$  is an expedient parameter to express the steric demand of bidentate ligands.

## Data Retrieval and Calculations

All data (except for the newly prepared compounds) used for analysis were extracted from the Cambridge Structural Database in January 2009. Searches were performed using the ConQuest software package as updated in November 2008.<sup>[12]</sup> The determination of bond lengths and angles and graphical visualisation was performed with several programs.<sup>[15]</sup> The calculation of the positions of hydrogen atoms in molecular structures and the positions of symmetry-dependent atoms were performed according to ref.<sup>[15a,15c]</sup> while the output of orthonormalised atom positions was done according to ref.<sup>[15a]</sup> Calculations of solid angles and generalised solid angles were performed with a program written in QuickBasic and working under MS-DOS.<sup>[16]</sup> All data obtained from the structure files and solid-angle analysis were collected and processed in Microsoft® Excel.<sup>[17]</sup> The Bondi set of van der Waals radii was used for the calculations as available at the Cambridge Crystallographic Data Centre.<sup>[18]</sup>

The following criteria were used for the selection of appropriate phosphanes from the Cambridge Structural Database: (1) the structure must contain any *cis*- $P,P'$ -coordinated bidentate moiety coordinated to a (distorted) square-planar surrounded platinum atom, not taking its oxidation state into account; (2) information on atomic coordinates must be available in the CSD file and the structure must be adequately precise ( $R$ -factor  $\leq 0.075$ ), structures with  $R$ -factor between 0.075 and 0.100 were examined individually and included into analysis if no gross errors within the molecular structure were identified; (3) in case of multiple available CSD files for the same structure, only that one with the lowest  $R$ -factor fulfilling all other criteria was used; (4) any disordered atoms were fixed in one discrete position; (5) if a molecule contained more than one platinum *cis*- $P,P'$ -moiety, each was included in the analysis separately; (6) in case of two or more symmetry independent molecules in the unit cell of any molecular structure only one molecule was taken into consideration (usually those with the platinum atom identified “Pt” or “Pt1”).

**Supporting Information** (see also the footnote on the first page of this article): Detailed information on the steric demand of more

than 280 phosphanes including average bite angles, equivalent cone angles and generalised equivalent cone angles.

- [1] For some examples on this topic see: a) M. an der Heiden, H. Plenio, *Chem. Commun.* **2007**, 972–974; b) A. Ehrentraut, A. Zapf, M. Beller, *J. Mol. Catal. A* **2002**, 182–183, 515–523; c) V. P. Ananikov, R. Szilagy, K. Morokuma, D. G. Musaev, *Organometallics* **2005**, 24, 1938–1946; d) A. V. Vorogushin, X. Huang, S. L. Buchwald, *J. Am. Chem. Soc.* **2005**, 127, 8146–8149; e) E. Graf, W. Leitner, *Chem. Ber.* **1996**, 129, 91–96.
- [2] a) E. Burello, G. Rothenberg, *Int. J. Mol. Sci.* **2006**, 7, 375–404; b) K. A. Bunten, L. Chen, A. L. Fernandez, A. J. Poë, *Coord. Chem. Rev.* **2002**, 233–234, 41–51; c) T. L. Brown, K. J. Lee, *Coord. Chem. Rev.* **1993**, 128, 89–116.
- [3] a) C. A. Tolman, *J. Am. Chem. Soc.* **1970**, 92, 2953–2956; b) C. A. Tolman, *J. Am. Chem. Soc.* **1970**, 92, 2956–2965; c) C. A. Tolman, W. C. Seidel, L. W. Gosser, *J. Am. Chem. Soc.* **1974**, 96, 53–60; d) C. A. Tolman, *Chem. Rev.* **1977**, 77, 313–348; e) H.-Y. Liu, K. Eriks, A. Prock, W. P. Giering, *Organometallics* **1990**, 9, 1758–1766.
- [4] A. Immirzi, A. Musco, *Inorg. Chim. Acta* **1977**, 25, L41–L42.
- [5] a) T. Komatsuzaki, K. Sakakibara, M. Hirota, *Tetrahedron Lett.* **1989**, 30, 3309–3312; b) M. Hirota, K. Sakakibara, T. Komatsuzaki, I. Akai, *Comput. Chem.* **1991**, 15, 241–248.
- [6] a) T. E. Müller, D. M. P. Mingos, *Transition Met. Chem.* **1995**, 20, 533–539; b) E. C. Alyea, S. A. Dias, G. Ferguson, R. J. Restivo, *Inorg. Chem.* **1977**, 16, 2329–2334; c) K. W. Bagnall, L. Xing-fu, *J. Chem. Soc., Dalton Trans.* **1982**, 1365–1369; d) K. W. Bagnall, *Inorg. Chim. Acta* **1984**, 94, 3–6; e) E. B. Lobkovsky, *J. Organomet. Chem.* **1984**, 277, 53–59; f) J. I. Seeman, J. W. Viers, J. C. Schug, M. D. Stovall, *J. Am. Chem. Soc.* **1984**, 106, 143–151; g) L. Xing-fu, S. Eggers, J. Kopf, W. Jahn, R. D. Fischer, C. Apostolidis, B. Kanellakopulos, F. Benetollo, A. Polo, G. Bombieri, *Inorg. Chim. Acta* **1985**, 100, 183–199; h) L. Xing-fu, G. Ao-Ling, *Inorg. Chim. Acta* **1987**, 131, 129–137; i) L. Xing-fu, G. Ao-Ling, *Inorg. Chim. Acta* **1987**, 134, 143–153; j) R. Chauvin, H. B. Kagan, *Chirality* **1991**, 3, 242–253; k) D. White, B. C. Taverner, P. G. L. Leach, N. J. Coville, *J. Comput. Chem.* **1993**, 14, 1042–1049; l) B. C. Taverner, *J. Comput. Chem.* **1996**, 17, 1612–1623; m) J. M. Smith, N. J. Coville, L. M. Cook, J. C. A. Boeyens, *Organometallics* **2000**, 19, 5273–5280; n) J. M. Smith, N. J. Coville, *Organometallics* **2001**, 20, 1210–1215; o) M. D. Bala, O. G. Adeyemi, D. G. Billing, D. C. Levendis, N. J. Coville, *J. Organomet. Chem.* **2006**, 691, 890–897.
- [7] a) J. T. DeSanto, J. A. Mosbo, B. N. Storhoff, P. L. Bock, R. E. Bloss, *Inorg. Chem.* **1980**, 19, 3086–3092; b) H. C. Clark, M. J. Hampden-Smith, *Coord. Chem. Rev.* **1987**, 79, 229–255; c) J. D. Smith, J. D. Oliver, *Inorg. Chem.* **1978**, 17, 2585–2589; d) D. H. Farrar, N. C. Payne, *Inorg. Chem.* **1981**, 20, 821–828; e) E. C. Alyea, G. Ferguson, A. Somogyvari, *Inorg. Chem.* **1982**, 21, 1369–1371; f) E. Burello, G. Rothenberg, *Adv. Synth. Catal.* **2005**, 347, 1969–1977; g) A. L. Seligson, W. C. Troglor, *J. Am. Chem. Soc.* **1991**, 113, 2520–2527; h) D. Datta, D. Majumdar, *J. Phys. Org. Chem.* **1991**, 4, 611–617; i) B. J. Dunne, R. B. Morris, A. G. Orpen, *J. Chem. Soc., Dalton Trans.* **1991**, 5, 653–661; j) R. P. Hughes, J. M. Smith, L. M. Liable-Sands, T. E. Concolino, K.-C. Lam, C. Incarvito, L. Rheingold, *J. Chem. Soc., Dalton Trans.* **2000**, 24, 873–879; k) J. M. Smith, B. C. Taverner, N. J. Coville, *J. Organomet. Chem.* **1997**, 530, 131–140; l) W. Porzio, A. Musco, A. Immirzi, *Inorg. Chem.* **1980**, 19, 2537–2540; m) H. Schlenkluhn, W. Scheidt, B. Weimann, M. Zähres, *Angew. Chem. Int. Ed. Engl.* **1979**, 18, 401–402; n) A. C. Hillier, W. J. Sommer, B. S. Yong, J. L. Petersen, L. Cavallo, S. P. Nolan, *Organometallics* **2003**, 22, 4322–4326; o) L. Cavallo, A. Correa, C. Costabile, H. Jakobsen, *J. Organomet. Chem.* **2005**, 690, 5407–5413; p) R. Dorta, E. D. Stevens, N. M. Scott, C. Costabile, L. Cavallo, C. D. Hoff, S. P. Nolan, *J. Am. Chem. Soc.* **2005**, 127, 2485–2495; q) N. M. Scott, S. P. Nolan, *Eur. J. Inorg. Chem.* **2005**, 10, 1815–1828; r) R. A. Kelly III, H. Clavier, S. Giudice, N. M. Scott, E. D. Stevens, J. Bordner, I. Samardjiev, C. D. Hoff, L. Cavallo, S. P. Nolan, *Organometallics* **2008**, 27, 202–210; s) H. Clavier, A. Correa, L. Cavallo, E. C. Escudero-Adán, J. Benet-Buchholz, A. M. Z. Slawin, S. P. Nolan, *Eur. J. Inorg. Chem.* **2009**, 1767–1773; t) D. G. Gusev, *Organometallics*, DOI: 10.1021/om900654g.
- [8] P. W. N. M. van Leeuwen, P. C. J. Kamer, J. N. H. Reek, P. Dierkes, *Chem. Rev.* **2000**, 100, 2741–2769.
- [9] E. Holló-Sitkei, G. Tárkányi, L. Párkányi, T. Megyes, G. Besenyei, *Eur. J. Inorg. Chem.* **2008**, 1573–1583.
- [10] a) P. Dierkes, P. W. N. M. van Leeuwen, *J. Chem. Soc., Dalton Trans.* **1999**, 1519–1529; b) P. C. J. Kamer, P. W. N. M. van Leeuwen, J. N. H. Reek, *Acc. Chem. Res.* **2001**, 34, 895–904; c) L. A. van der Veen, P. C. J. Kamer, P. W. N. M. van Leeuwen, *CATTECH* **2002**, 6, 116–120; d) Z. Freixa, P. W. N. M. van Leeuwen, *Dalton Trans.* **2003**, 10, 1890–1901; e) M. Kranenburg, P. C. J. Kamer, P. W. N. M. van Leeuwen, *Eur. J. Inorg. Chem.* **1998**, 1, 25–27; f) K. A. Leñero, M. Kranenburg, Y. Guari, P. C. J. Kamer, P. W. N. M. van Leeuwen, S. Sabo-Etienne, B. Chaudret, *Inorg. Chem.* **2003**, 42, 2859–2866.
- [11] a) Atomic coordinates were taken from the crystal data file of compound **C9**, thus it must be noted, that the bond lengths and angles are not fixed at idealised values as the use of space filling CPK models implies; b) visualisation was performed using *POV-Ray™ for Windows* version 3.6.1.icl8.win32, Persistence of Vision Team, C. Cason, Persistence of Vision Raytracer Pty. Ltd. **2004**.
- [12] *ConQuest* version 1.11, CSD version 5.30, including updates version 5.30 (November **2008**).
- [13] a) L. Stahl, R. D. Ernst, *J. Am. Chem. Soc.* **1987**, 109, 5673–5680; b) L. Stahl, W. Trakarnpruk, J. W. Freeman, A. M. Arif, R. D. Ernst, *Inorg. Chem.* **1995**, 34, 1810–1814; and literature cited therein.
- [14] L. Dahlenburg, C. Becker, J. Höck, S. Mertel, *J. Organomet. Chem.* **1998**, 564, 155–166.
- [15] a) *SHELXL-97* (Release 97-2), G. M. Sheldrick, University of Göttingen, Germany, **1997**; b) *Diamond* version 3.0b, Crystal Impact GbR, Bonn, Germany, **2005**; c) *RESVIEW* Version 2.26, H. Schwenk, **1998**; d) *ORTEP-3* for Windows version 1.08, L. J. Farrugia, *J. Appl. Crystallogr.* **1997**, 30, 565; e) *Mercury*, version 2.2, CCDC, **2008**.
- [16] *QuickBASIC 4.5*, complete German version, Microsoft Corporation **1989**.
- [17] *Microsoft® Excel 2002*, Microsoft Corporation, **2001**.
- [18] a) A. Bondi, *J. Phys. Chem.* **1964**, 68, 441–452; b) available on the WWW under: <http://www.ccdc.cam.ac.uk/products/csd/radii/>.

Received: August 21, 2009

Published Online: November 30, 2009

## C<sub>2</sub>-Symmetric Ferrocene–Bis(ureido)peptides: Synthesis, Conformation and Solid-State Structure

Jasmina Lapić,<sup>[a]</sup> Senka Djaković,<sup>[a]</sup> Mario Cetina,<sup>[b]</sup> Katja Heinze,<sup>\*[c]</sup> and Vladimir Rapić<sup>\*[a]</sup>

**Keywords:** Conformation analysis / Density functional calculations / Hydrogen bonds / Metallocenes / Peptides

The extension of peptide derivatives of ferrocene-1,1'-dicarboxylic acid by formal insertion of NH units between ferrocene and peptide strands results in ferrocene-bis(ureido)peptides. Experimentally, alanine and dialanine methyl esters were attached to the 1- and 1'-position of 1,1'-diisocyanoferrrocene to give the corresponding bis(ureido)peptide derivatives **3** and **4**. The conformation of **3** has been deter-

mined in the solid state by X-ray crystallography. In solution the preferred conformation of **3** and **4** has been elucidated by NMR, IR and CD spectroscopy in concert with DFT calculations. The secondary structure of ferrocene-bis(ureido)peptides **3** and **4** is determined by double bifurcated intramolecular hydrogen bonds (IHBs). The different stability of the secondary structures of **3** and **4** is due to different types of IHBs.

### Introduction

The importance of peptides and proteins in a plethora of immunological, neurological and other bioprocesses is well known. They act as receptors, neurotransmitters, neuromodulators, enzymes, hormones, antigens, antibiotics and much more. In spite of their pronounced bioactivity, the application of peptides as drugs is rather limited by disadvantages affiliated with their use in biological systems: they are easily proteolytically degraded, and they are often too hydrophilic to pass through cell membranes. Therefore, in the last decade the focus of pharmaceutical research has moved away from peptides towards artificial peptidomimetics ("pseudopeptides") out of a desire to remedy the disadvantages mentioned. These compounds are often derived from peptides by side-chain and/or main-chain modifications, as well as by incorporating (non-natural) turn inducers.

An important class of peptidomimetics includes *N*-alkylureas and ureidopeptides, in which some peptide (amide)

groups –NH–CO– are formally replaced by a urea moiety –NH–CO–NH– with elongation of the main strand.<sup>[1,2]</sup> Urea subunits have also been exploited as pharmacophores in peptide-based inhibitors. Recent investigations have shown that urea-derived small molecules can act as molecular scaffolds for studies of protein folding. The formation of a bioactive folded protein conformation depends upon secondary-structure elements such as  $\alpha$  helices,  $\beta$  sheets and turns.<sup>[3]</sup> Stable turn mimics were achieved by introduction of appropriately designed urea subunits. North et al. prepared conformationally defined peptide analogues on the basis of constrained  $\beta$ -amino acids in synergism with ureylene groups.<sup>[4–6]</sup> Nowick constructed "pure" urea-containing scaffolds, that is, diurea derivatives of oligomethylene diamines. In such a way frameworks for peptide attachment or peptidomimetic chains were obtained. The resulting type **I** conjugates form an intramolecularly hydrogen-bonded (IHB) U-turn, which induces an artificial parallel  $\beta$  sheet (Scheme 1).<sup>[7–10]</sup>

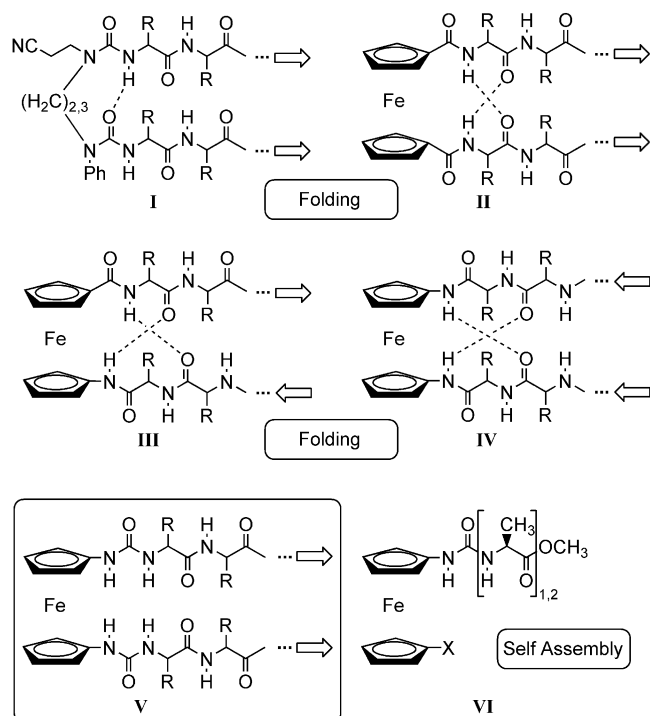
A large number of ferrocene-peptide bioconjugates have been prepared to induce ordered conformations of peptides and to develop new biomaterials. A lot of work has been devoted to ferrocene-peptide conjugates and the results have been summarised in recent reviews and monographs.<sup>[11–17]</sup> Due to the suitable distance between its cyclopentadienyl (Cp) rings (ca. 3.3 Å) and its rotational flexibility, ferrocene is perfectly suited for peptidomimetic purposes. IHBs between attached peptide chains at the 1- and 1'-position principally allow for ordered structures, and thus the ferrocene unit can act as a reliable turn inducer in peptidomimetics. Furthermore, the ferrocene moiety in these bioconjugates imparts reversible redox chemistry to such artificial biomaterials.

[a] Department of Chemistry and Biochemistry, Faculty of Food Technology and Biotechnology, Pierottijeva 6, 10000 Zagreb, Croatia  
Fax: +385-4836-082  
E-mail: vrapic@pbf.hr

[b] Department of Applied Chemistry, Faculty of Textile Technology, University of Zagreb, Prilaz Baruna Filipovića 30, 10000 Zagreb, Croatia

[c] Institute of Inorganic Chemistry and Analytical Chemistry, Johannes Gutenberg University of Mainz, Duesbergweg 10–14, 55128 Mainz, Germany  
Fax: +49-6131-3927277  
E-mail: katja.heinze@uni-mainz.de

Supporting information for this article is available on the WWW under <http://dx.doi.org/10.1002/ejic.200900679>.



Scheme 1. Conjugates of *N,N*-linked diureas with peptides (type **I** forming 9- and 10-membered rings); Fcd- (type **II**), Fca- (type **III**) and Fcda- (type **IV**) linked peptides (forming 9-, 10- and 11-membered rings); symmetric ureidopeptides (type **V**); and simplified “desymmetrised” single-strand Fc-ureidopeptides (type **VI**; X = H, COOCH<sub>3</sub>). Arrows point from *N* to *C* termini of peptide chains.

The coupling of ferrocene-1,1'-dicarboxylic acid (Fcd) to amino acids and peptides is probably the most extensively studied bioorganometallic conjugation reaction<sup>[16–24]</sup> giving preponderantly symmetrically substituted bioconjugates of type **II** (Scheme 1), which is characterised by two 10-membered IHBs that form a so-called “Herrick conformation”, that is, a  $\beta$  turn.<sup>[16–18]</sup> In previous investigations bioconjugates of 1'-aminoferrocene-1-carboxylic acid (Fca, type **III**) were studied in some detail and antiparallel peptide chains were observed.<sup>[25–35]</sup> Symmetrical and unsymmetrical bioconjugates of ferrocene-1,1'-diamine (Fcda, type **IV**) have been recently reported by Kraatz and by our groups.<sup>[36,37]</sup> Ferrocene bioconjugates of types **II–IV** show a specific secondary structure through involvement of IHBs between the peptide chains both in the solid state and in solution. These ferrocene bioconjugates are quite reliable mimetics of  $\beta$ -sheet conformations in natural peptides.

Owing to *two* amino groups as hydrogen-bond-donating sites and one carbonyl group as a hydrogen-bond-accepting site, ureylene groups have a great potential for the robust formation of hydrogen bonds. Fc-containing ureidopeptides of type **V** are formally derived from type **II** conjugates by insertion of NH groups between ferrocene and adjacent carbonyl groups (Scheme 1). First explorations revealed that in simplified models (type **VI**) without hydrogen acceptors at the 1'-substituent (X = H) or a single H acceptor (X = COOCH<sub>3</sub>) intramolecular hydrogen bonding is absent or negligible and intermolecular hydrogen bonds prevail,

which results in self-assembly of the ferrocene derivatives in the solid state.<sup>[38]</sup> Anion binding and anion sensing with ferrocene urea receptors<sup>[39,40]</sup> – usually ferrocenyl ureas or symmetrically disubstituted ferrocene bis(ureas) – have been investigated by the groups of Tucker,<sup>[41]</sup> Beer,<sup>[42,43]</sup> Kaifer<sup>[44]</sup> and Molina<sup>[45–48]</sup> with ferrocene as an electrochemical detection unit.

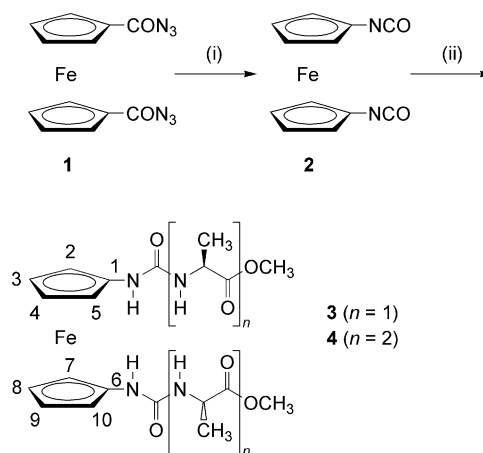
In this study we address the question of folding versus self-assembly of C<sub>2</sub>-symmetrical ferrocene-containing ureido-peptides of type **V** (Scheme 1).

## Results and Discussion

### Synthesis and Characterisation of Ferrocene-Ureidopeptides **3** and **4**

The general methods for the preparation of ureidopeptides involve treating either an N<sup>α</sup>-unprotected peptide with an isocyanate R–NCO or a peptide isocyanate OCN–CHR'CO–(NHCHR''CO)<sub>n</sub> with an amine R–NH<sub>2</sub>. As 1,1'-Fn(NH<sub>2</sub>)<sub>2</sub> is rather sensitive and peptide isocyanates are commercially unavailable, the first option was applied, namely, conjugation of 1,1'-Fn(NCO)<sub>2</sub> with Ala–OCH<sub>3</sub> and with Ala–Ala–OCH<sub>3</sub> (Fn = ferrocene-1,1'-diyl).

The synthesis of ferrocene-ureidopeptides **3** and **4** is depicted in Scheme 2. The starting ferrocene-1,1'-dicarboxazide **1** was prepared in 75% yield from ferrocene-1,1'-dicarboxylic acid Fc(COOH)<sub>2</sub> by the successive action of ClCOOEt/NEt<sub>3</sub> in acetone and an aqueous solution of NaN<sub>3</sub> via the intermediate mixed anhydride.<sup>[49]</sup> Curtius rearrangement of **1** in benzene gave the corresponding diisocyanate **2**.<sup>[49]</sup> Crude **2** was coupled with L-Ala–OCH<sub>3</sub> (obtained from L-Ala–OCH<sub>3</sub>·HCl by treatment with NEt<sub>3</sub>) to give ureidopeptide **3** in 36% isolated yield after thin-layer chromatography (TLC). Deprotection of Boc-L-Ala-L-Ala–OCH<sub>3</sub> was performed by the action of gaseous hydrochloric acid in ethyl acetate; the resulting hydrochloride was treated with an excess amount of NEt<sub>3</sub> and coupled with crude **2** to give ureidopeptide **4** in 42% isolated yield after TLC.



Scheme 2. Synthesis of **3** and **4**. Reagents and conditions: (i) Benzene, 80 °C; (ii) Ala–OCH<sub>3</sub>·HCl (*n* = 1)/Ala–Ala–OCH<sub>3</sub>·HCl (*n* = 2), NEt<sub>3</sub>, CH<sub>2</sub>Cl<sub>2</sub>.

The new complexes **3** and **4** were fully characterised by IR and NMR spectroscopy, as well as by low- and high-resolution mass spectrometry and elemental analysis (see the Experimental Section and Tables 1–4). Mass spectrometry and elemental analysis were used to prove the composition and the purity of **3** and **4**.

In the IR spectra, characteristic group frequencies are observed for NH and CO groups (Table 1). In the solid state all NH groups of **3** and **4** are involved in NH bonds as seen from the low-energy NH stretching vibrations below  $\tilde{\nu} = 3400\text{ cm}^{-1}$ . In a solution of the complexes in  $\text{CH}_2\text{Cl}_2$ , free NH groups are also present ( $\tilde{\nu} = 3441/3414\text{ cm}^{-1}$ ). In conjugate **3** the ester carbonyl is hydrogen bonded both in solution and in the solid state ( $\tilde{\nu} = 1728/1729\text{ cm}^{-1}$ ), whereas in bis(alanine) derivative **4** the ester group ( $\tilde{\nu} = 1740/1744\text{ cm}^{-1}$ ) is free and the amide carbonyl group ( $\tilde{\nu} = 1661/1648\text{ cm}^{-1}$ ) is hydrogen bonded.

Table 1. IR spectroscopic data ( $c = 10^{-2}\text{ M}$  in  $\text{CH}_2\text{Cl}_2$ /in KBr) of **3** and **4**.

| $\tilde{\nu} [\text{cm}^{-1}]$    | <b>3</b> ( $\text{CH}_2\text{Cl}_2$ ) | <b>3</b> (KBr) | <b>4</b> ( $\text{CH}_2\text{Cl}_2$ ) | <b>4</b> (KBr) |
|-----------------------------------|---------------------------------------|----------------|---------------------------------------|----------------|
| $\tilde{\nu}_{\text{NH,free}}$    | 3441                                  | —              | 3414                                  | —              |
| $\tilde{\nu}_{\text{NH,bound}}$   | 3398, 3355                            | 3366, 3308     | 3363, 3314                            | 3354, 3302     |
| $\tilde{\nu}_{\text{CO,ester}}$   | 1728                                  | 1729           | 1740                                  | 1744           |
| $\tilde{\nu}_{\text{CO,amide I}}$ | 1686                                  | 1671           | 1661                                  | 1648           |

The  $^1\text{H}$  and  $^{13}\text{C}\{^1\text{H}\}$  NMR spectroscopic data fully confirm the proposed structures of **3** and **4** (Tables 2, 3 and 4). All of the resonances of the protons and carbon atoms were observed in typical spectral regions.<sup>[38]</sup>

Table 2.  $^1\text{H}$  NMR spectroscopic data ( $c = 10^{-2}\text{ M}$  in  $\text{CDCl}_3$ ) of **3** and **4** (for atom numbering see Scheme 2).<sup>[a]</sup>

|  | <b>3</b>                                    | <b>4</b>                                    |
|--|---|---|
| 1-NH                                   | 6.10 (s, 2 H)                               | 6.42 (s, 2 H)                               |
| NH <sub>Ala1</sub>                     | 6.36 (d, $J = 7.08\text{ Hz}$ , 2 H)        | 6.80 (d, $J = 7.14\text{ Hz}$ , 2 H)        |
| NH <sub>Ala2</sub>                     | —   | 7.05 (d, $J = 5.67\text{ Hz}$ , 2 H)        |
| CH <sub><math>\alpha</math>,Ala1</sub> | 4.44 (dq, $J = 7.38, 7.35\text{ Hz}$ , 2 H) | 4.23 (dq, $J = 7.02, 7.11\text{ Hz}$ , 2 H) |
| CH <sub><math>\alpha</math>,Ala2</sub> | —   | 4.59 (dq, $J = 7.23, 7.23\text{ Hz}$ , 2 H) |
| H2, H5 H7, H10                         | 4.93 (br. s, 2 H), 4.15 (br. s, 2 H)        | 4.81 (br. s, 2 H), 4.07 (br. s, 2 H)        |
| H3, H4, H8, H9                         | 3.92 (br. s, 2 H), 3.84 (br. s, 2 H)        | 3.89 (br. s, 2 H), 3.80 (br. s, 2 H)        |
| OCH <sub>3</sub>                       | 3.85 (s, 6 H)                               | 3.77 (s, 6 H)                               |
| CH <sub>3,Ala1</sub>                   | 1.40 (d, $J = 7.38\text{ Hz}$ , 6 H)        | 1.53 (d, $J = 7.17\text{ Hz}$ , 6 H)        |
| CH <sub>3,Ala2</sub>                   | —   | 1.40 (d, $J = 7.17\text{ Hz}$ , 6 H)        |

[a] Chemical shift ( $\delta$ ) values are given in ppm.

Table 3.  $^1\text{H}$  NMR spectroscopic data ( $c = 10^{-2}\text{ M}$  in  $[\text{D}_6]\text{DMSO}$ ) of **3** and **4** (for atom numbering see Scheme 2).<sup>[a]</sup>

|  | <b>3</b>                              | <b>4</b>   |
|--|---------------------------------------|--|
| 1-NH                                   | 7.52 (s, 2 H)                         | 7.47 (s, 2 H)  |
| NH <sub>Ala1</sub>                     | 6.32 (d, $J = 5.94\text{ Hz}$ , 2 H)  | 6.31 (d, $J = 7.59\text{ Hz}$ , 2 H)                 |
| NH <sub>Ala2</sub>                     | —                                     | 8.52 (d, $J = 7.02\text{ Hz}$ , 2 H)                 |
| CH <sub><math>\alpha</math>,Ala1</sub> | 4.20 (dq, $J = 5.82\text{ Hz}$ , 2 H) | 4.22–4.30 (m, 4 H)                                   |
| CH <sub><math>\alpha</math>,Ala2</sub> | —                                     | —  |
| H2, H5, H7, H10                        | 4.32 (br. s, 2 H), 4.25 (br. s, 2 H)  | 4.43 (pt, 2 H), 4.36 (br. s, 1 H), 4.32 (br. s, 1 H) |
| H3, H4, H8, H9                         | 3.81 (br. s, 4 H)                     | 4.20 (pt, 2 H), 4.19 (pt, 2 H)                       |
| OCH <sub>3</sub>                       | 3.62 (s, 6 H)                         | 3.80 (s, 6 H)  |
| CH <sub>3,Ala1</sub>                   | 1.27 (d, $J = 5.88\text{ Hz}$ , 6 H)  | 1.30 (d, $J = 7.29\text{ Hz}$ , 6 H)                 |
| CH <sub>3,Ala2</sub>                   | —                                     | 1.23 (d, $J = 6.93\text{ Hz}$ , 6 H)                 |

[a] Chemical shift ( $\delta$ ) values are given in ppm.

Table 4.  $^{13}\text{C}$  NMR spectroscopic data ( $c = 10^{-2}\text{ M}$  in  $\text{CDCl}_3$ ) of **3** and **4** (for atom numbering see Scheme 2).<sup>[a]</sup>

|                                       | <b>3</b>   | <b>4</b>   |
|---------------------------------------|------------|------------|
| CO <sub>ester</sub>                   | 177.84 (s) | 176.26 (s) |
| CO <sub>urea</sub>                    | 154.82 (s) | 155.67 (s) |
| CO <sub>amide</sub>                   | —          | 172.41 (s) |
| C <sub><math>\alpha</math>,Ala1</sub> | 48.49 (s)  | 49.91 (s)  |
| C <sub><math>\alpha</math>,Ala2</sub> | —          | 48.11 (s)  |
| C1, C6                                | 97.093 (s) | 97.07 (s)  |
| C2, C5                                | 59.54 (s)  | 59.26 (s)  |
| C3, C4                                | 60.73 (s)  | 60.92 (s)  |
| C7, C10                               | 62.10 (s)  | 61.66 (s)  |
| C8, C9                                | 64.59 (s)  | 64.47 (s)  |
| OCH <sub>3</sub>                      | 52.40 (s)  | 51.98 (s)  |
| CH <sub>3,Ala1</sub>                  | 18.59 (s)  | 17.58 (s)  |
| CH <sub>3,Ala2</sub>                  | —          | 17.30 (s)  |

[a] Chemical shift ( $\delta$ ) values are given in ppm.

### X-ray Crystal Structure Analysis of Ferrocene Derivative **3**

An orange crystal of the alanyl-substituted ferrocene derivative **3** was grown from a solution of **3** in  $\text{CH}_2\text{Cl}_2$  at room temperature. Complex **3** crystallises in the chiral orthorhombic space group  $P2_12_12_1$ . The absolute configuration of the stereogenic carbon atoms C12 and C17 of the L-Ala substituents is *S* as expected (Figure 1).

The torsion angle of the ferrocene defined as C1–C<sub>g1</sub>–C<sub>g2</sub>–C6 is  $+16^\circ$ , that is, a positive helical chirality (*P*) is observed (C<sub>g1</sub> = centroid of Cp ring C1–C5 and C<sub>g2</sub> = centroid of Cp ring C6–C10). The Cp rings are thus oriented approximately halfway between a staggered ( $36^\circ$ ) and an eclipsed ( $0^\circ$ ) conformation. The Cp rings are almost parallel to each other, with a tilt angle of  $2.81(13)^\circ$ .

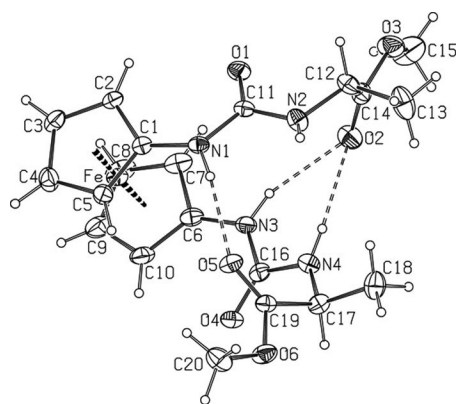


Figure 1. Molecular structure of **3** in the crystal. Displacement ellipsoids for non-hydrogen atoms are drawn at the 20% probability level. NH $\cdots$ O intramolecular hydrogen bonds are shown by dashed lines.

The bond lengths in the two peptide strands attached to the cyclopentadienyl rings as well as within the ferrocene core present no unexpected features and agree very well with equivalent ones in *N*-(1'-methoxycarbonylferrocene-1-carbamoyl)alanylalanine methyl ester.<sup>[38]</sup>

The direction of the 1- and 1'-substituents of **3** is a consequence of intramolecular NH $\cdots$ O hydrogen bonds that link the juxtaposed strands. These IHBs are formed between amide NH groups and ester carbonyl oxygen atoms (Figure 1, Table 5). The N1 $\cdots$ O5 and N3 $\cdots$ O2 hydrogen bonds form two 10-membered rings of the *R*<sub>1</sub><sup>1</sup>(10) type,<sup>[50]</sup> thus inducing a  $\beta$  turn. In addition, the N4 $\cdots$ O2 hydrogen bond generates a 12-membered ring of the *R*<sub>1</sub><sup>1</sup>(12) type (Figure 1). The combinations of these three IHBs form three new rings of the *R*<sub>2</sub><sup>2</sup>(14) (N1 $\cdots$ O5 and N3 $\cdots$ O2), *R*<sub>2</sub><sup>2</sup>(12) (N1 $\cdots$ O5 and N4 $\cdots$ O2) and *R*<sub>2</sub><sup>2</sup>(6) (N3 $\cdots$ O2 and N4 $\cdots$ O2) type in which the O2 atom acts as a double hydrogen acceptor (bifurcated hydrogen bond). In **3**, three intramolecular CH $\cdots$ O hydrogen contacts are also observed (C2 $\cdots$ O1, C10 $\cdots$ O4 and C20 $\cdots$ O5; Table 5).

Table 5. Selected bond lengths [Å] and angles [°] of **3**.

| D–H $\cdots$ A       | H $\cdots$ A | D $\cdots$ A | D–H $\cdots$ A        |
|----------------------|--------------|--------------|-----------------------|
| N1–H1N $\cdots$ O5   | 2.14(2)      | 2.993(2)     | 168(2)                |
| N3–H3N $\cdots$ O2   | 2.22(2)      | 3.060(3)     | 160(2)                |
| N4–H4N $\cdots$ O2   | 2.52(2)      | 3.232(3)     | 144(2)                |
| C2–H2 $\cdots$ O1    | 2.50         | 2.907(3)     | 107                   |
| C10–H10 $\cdots$ O4  | 2.46         | 2.920(3)     | 111                   |
| C20–H20C $\cdots$ O5 | 2.30         | 2.676(3)     | 102                   |
| N2–H2N $\cdots$ O4   | 2.22(2)      | 2.998(2)     | 164(2) <sup>[a]</sup> |
| C20–H20B $\cdots$ O1 | 2.48         | 3.334(3)     | 149 <sup>[b]</sup>    |

[a] Symmetry code 1 – *x*, 0.5 + *y*, 1.5 – *z*. [b] Symmetry code 1 + *x*, *y*, *z*.

In the crystal, the molecules of **3** are self-assembled by N2 $\cdots$ O4 hydrogen bonds into infinite C<sub>9</sub> chains parallel to the *b* axis (Figure 2). This hydrogen bond is accompanied by a CH $\cdots$ O hydrogen contact, C20 $\cdots$ O1, which produces a C<sub>13</sub> chain parallel to the *a* axis. The combination of these two orthogonal chains generates (001) sheets and leads to a (4,4) net.<sup>[51]</sup>

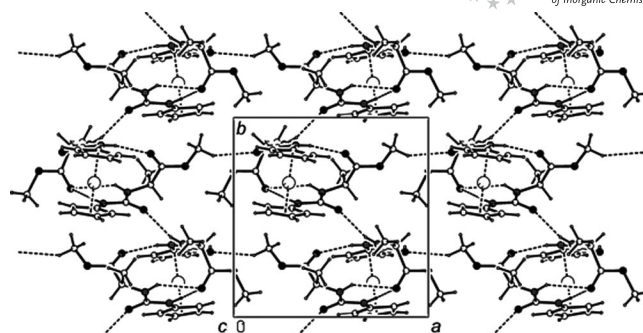


Figure 2. A crystal packing diagram of **3**, viewed along the *c* axis, showing intramolecular and intermolecular NH $\cdots$ O and CH $\cdots$ O hydrogen contacts. Hydrogen bonds are indicated by dashed lines.

### Conformational Analysis of **3** and **4**

To elucidate the preferred conformation of **3** and **4** in solution, IR, NMR and CD spectroscopy together with DFT calculations were employed. This combination of methods has been previously successfully applied for analysing bioconjugates of ferrocene derivatives.<sup>[19,23,25–27,31,33,36,38]</sup>

The hydrogen-acceptor site of hydrogen bonds is easily seen by IR spectroscopy. The IR data of **3** indicate hydrogen bonds to the ester carbonyl CO<sub>ester</sub>, whereas in **4** hydrogen bonds to the amide carbonyl CO<sub>amide</sub> are observed (Table 1). The NH donor site cannot be extracted straightforwardly from IR data alone but some hints can be gained from <sup>1</sup>H NMR spectroscopy in CDCl<sub>3</sub> (noncoordinating solvent) and in DMSO (hydrogen-bond-disrupting solvent). <sup>1</sup>H NMR chemical shifts relevant to the hydrogen bonding of **3** and **4** as well as of reference complexes Fc-NHCO-NH-Ala-OCH<sub>3</sub> (**5**) and Fc-NHCO-NH-Ala-Ala-OCH<sub>3</sub> (**6**)<sup>[38]</sup> (which are expected to be unable to form IHBs) are compiled in Table 6.

Table 6. <sup>1</sup>H NMR spectroscopic data of **3** and **4** and of reference compounds **5** and **6**.<sup>[a]</sup>

| Complex  | $\delta_{\text{NH}}(1)$ [ppm]<br>(CDCl <sub>3</sub> ) | $\delta_{\text{NH}}(2)$ [ppm]<br>([D <sub>6</sub> ]DMSO) | $\Delta\delta_{\text{NH}}$ [ppm]<br>[ $\delta_{\text{NH}}(2) - \delta_{\text{NH}}(1)$ ] |
|----------|---|--|---|
| <b>3</b> | 6.10/6.36   | 7.52/6.32  | 1.42/–0.04  |
| <b>5</b> | 5.63/5.70   | 7.68/6.31  | 2.05/0.61   |
| <b>4</b> | 6.42/6.80/7.05  | 7.47/6.31/8.15   | 1.05/–0.49/1.10   |
| <b>6</b> | 6.48/6.09/7.07  | 7.73/6.17/8.44   | 1.25/0.08/1.37  |

[a] The resonances are given in the sequence 1-NH, NH<sub>Ala1</sub>, NH<sub>Ala2</sub>.

The NH resonances of **3** in CDCl<sub>3</sub> are shifted to lower field relative to those of **5**, which suggests IHBs in **3** that involve both 1-NH and NH<sub>Ala1</sub>. The NH shifts of **3** and **5** in DMSO (100%) are very similar, which suggests full solvation of **3** and **5** in this solvent with disruption of IHBs. A similar situation is found for the pair **4** and **6** in CDCl<sub>3</sub> – except for 1-NH, which also appears hydrogen bonded in **6**. The NH<sub>Ala2</sub> group does not engage in hydrogen bonds in CDCl<sub>3</sub>. In pure DMSO all NH groups participate in hydrogen bonds to DMSO as expected. These data led us to conclude that 1-NH and NH<sub>Ala1</sub> are the hydrogen-donor

groups in IHBs of **3** and **4** in  $\text{CDCl}_3$ .  $\text{NH}_{\text{Ala}2}$  of **4** remains noncoordinating, although this proton experiences the largest low-field shift of the NH resonances of **4**. This cautions against interpretation of absolute NH chemical shifts without consideration of the environment (e.g., amide, urea, aliphatic/aromatic substituents, concentration, see below), that is, it is always advisable to refer to reference compounds under similar conditions.<sup>[28]</sup>

A further result should be noted: the resonances of  $\text{NH}_{\text{Ala}1}$  are shifted to lower field in the IHB structures of **3** and **4** as compared with the DMSO-solvated structure. Slightly negative  $\Delta\delta = -0.04$  ppm values in **3** and significantly negative  $\Delta\delta = -0.49$  ppm values of **4** are measured (Table 6). The IHB involving  $\text{NH}_{\text{Ala}1}$  appears slightly (**3**) or significantly (**4**) stronger than the respective intermolecular  $\text{NH}_{\text{Ala}1} \cdots \text{OSMe}_2$  hydrogen bond to DMSO. Thus a further result of the NMR spectroscopic analysis is the conclusion that the IHB  $\text{NH}_{\text{Ala}1} \cdots \text{OC}_{\text{amide}}$  of **4** is stronger than the IHB  $\text{NH}_{\text{Ala}1} \cdots \text{OC}_{\text{ester}}$  of **3** (with reference to the intermolecular hydrogen bond to DMSO).

Dilution experiments conducted using solutions of **3** and **4** in  $\text{CDCl}_3$  revealed that resonances of 1-NH and  $\text{NH}_{\text{Ala}1}$  are independent of the concentration in the regime 1.5–100 mM, whereas the signal of  $\text{NH}_{\text{Ala}2}$  of **4** dramatically shifts to lower field at higher concentration (Figures 3 and 4). Thus amide proton  $\text{NH}_{\text{Ala}2}$  is mainly involved in intermolecular hydrogen bonds at higher concentration and the other amide protons are mainly involved in IHBs. Association phenomena to give dimers and oligomers by means of hydrogen bonding have been previously observed in ferrocenyl ureas (see ref.<sup>[38]</sup> and cited literature).

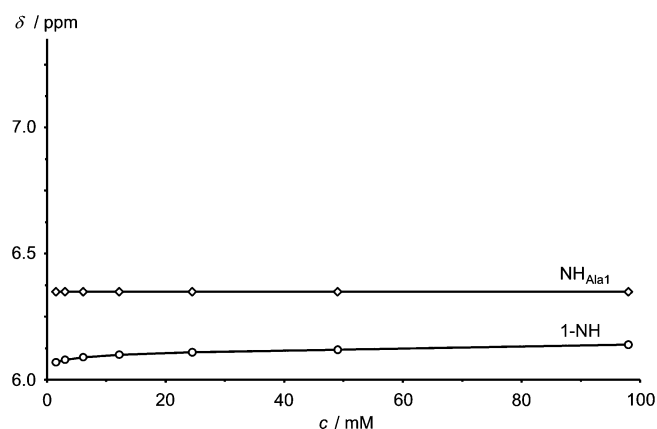


Figure 3.  $\delta$  versus  $c$  plot of NH resonances of **3**.

Information on the ferrocene helical chirality can be gained from circular dichroism spectroscopy. UV/Vis and CD spectroscopic data of **3** and **4** are collected in Table 7. The characteristic ferrocene absorption is found at  $\lambda_{\text{max}} = 447$  nm in  $\text{CH}_2\text{Cl}_2$  (noncoordinating solvent) as well as in  $\text{CH}_2\text{Cl}_2/\text{DMSO}$  mixtures (20% v/v DMSO as hydrogen-bond-disrupting solvent). Positive Cotton effects were observed at the ferrocene absorption, which is usually associated with a (*P*)-helical chirality of the metallocene (Figures 5 and 6). The positive Cotton effect is also observed in

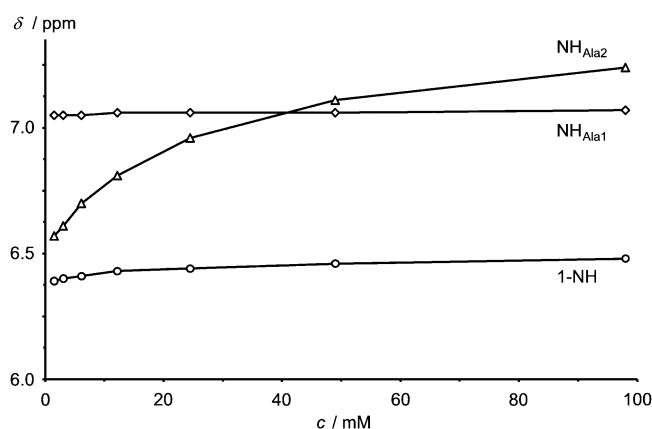


Figure 4.  $\delta$  versus  $c$  plot of NH resonances of **4**.

the solid state (KBr disks of **3** and **4**; bottom of Figures 5 and 6) and is in accordance with the X-ray crystal structure analysis results for **3** (vide supra). With DMSO present in solution, the strength of the Cotton effect is reduced by factors of 4.5 (**3**) and 1.3 (**4**), which suggests some disruption of the IHBs that determine the conformation. The observed decrease is stronger for **3** with an ester carbonyl as hydrogen-acceptor group than for **4** with an amide carbonyl hydrogen acceptor, which suggests stronger IHBs in **4** and supports the NMR spectroscopic results (vide supra).

Table 7. UV/Vis and CD spectroscopic data of **3** and **4** ( $c = 10^{-3}$  M).<sup>[a]</sup>

|                                       | Solvent  | <b>3</b>    | <b>4</b>    |
|---------------------------------------|--|-------------|-------------|
| $\lambda_{\text{max}}$ (ε)            | $\text{CH}_2\text{Cl}_2$                       | 447 (920)   | 447 (900)   |
| $\lambda_{\text{max}}$ (ε)            | $\text{CH}_2\text{Cl}_2/\text{DMSO}$ (20% v/v) | 447 (950)   | 447 (930)   |
| $\lambda_{\text{max}}$ ( $M_\theta$ ) | $\text{CH}_2\text{Cl}_2$                       | 460 (15100) | 460 (12000) |
| $\lambda_{\text{max}}$ ( $M_\theta$ ) | $\text{CH}_2\text{Cl}_2/\text{DMSO}$ (20% v/v) | 463 (3300)  | 463 (9200)  |
| $\lambda_{\text{max}}$ (CD)           | KBr  | 475         | 470         |

[a] The units are as follows:  $\lambda_{\text{max}}$  [nm] (ε [ $\text{M}^{-1} \text{cm}^{-1}$ ];  $M_\theta$  [ $^\circ \text{M}^{-1} \text{cm}^{-1}$ ]).

DFT calculations have been quite successful in describing the energetics of IHBs in 1,1'-disubstituted ferrocenes.<sup>[19,23,25–27,31,33,36,38]</sup> To gain some further insight, DFT calculations (B3LYP/LanL2DZ<sup>[52]</sup>) and optimisations were performed on full complexes **3** and **4** without any symmetry constraints (Figures 7 and 8). In fact, highly unsymmetrical starting geometries converged to almost  $C_2$ -symmetric optimised conformations in both cases (bottom of Figures 7 and 8). Two bifurcated IHBs were observed between 1-NH/ $\text{NH}_{\text{Ala}1}$  and  $\text{CO}_{\text{ester}}$  of different chains for **3** and between 1-NH/ $\text{NH}_{\text{Ala}1}$  and  $\text{CO}_{\text{amide}}$  for **4** (Figures 7 and 8, Table 8).

The DFT-calculated conformation of **3** with IHBs is very similar to the X-ray structure of **3** but more symmetric (almost perfect  $C_2$  symmetry) with two essentially identical bifurcated IHBs (Table 8, Figure 7). Clearly, in the solid state the  $C_2$  symmetry of **3** is broken due to the intermolecular hydrogen bond  $\text{N2-H2N} \cdots \text{O4}$  (which is naturally absent in the gas-phase DFT calculation). The DFT-calculated conformation of **4** is basically similar to that of **3** (Figures 7 and 8). However, the hydrogen acceptor in **4** is now an amide carbonyl group instead of an ester carbonyl

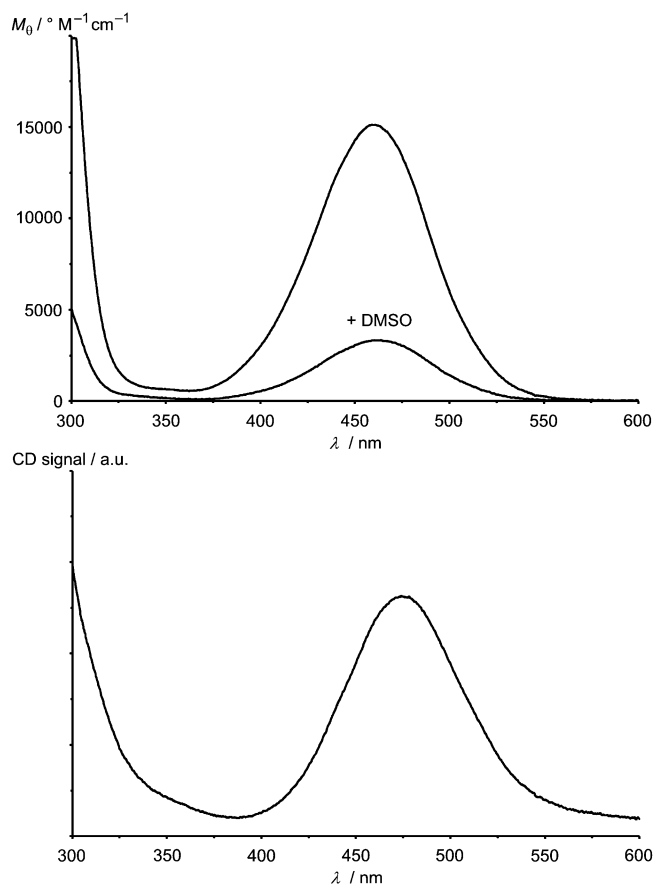


Figure 5. CD spectra of **3** in solution (top; in CH<sub>2</sub>Cl<sub>2</sub> and in CH<sub>2</sub>Cl<sub>2</sub>/DMSO) and as KBr disk (bottom) at room temperature.

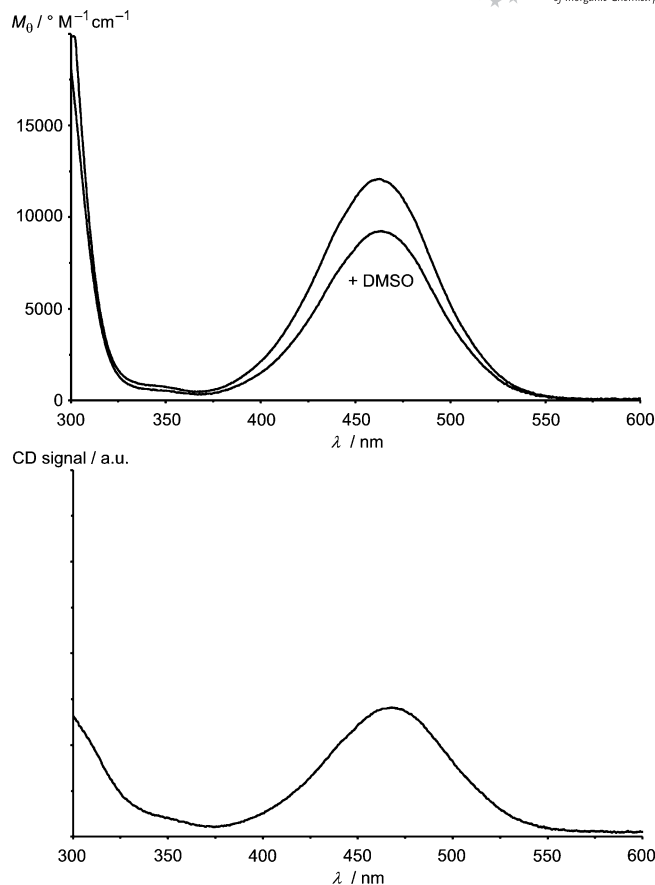


Figure 6. CD spectra of **4** in solution (top; in CH<sub>2</sub>Cl<sub>2</sub> and in CH<sub>2</sub>Cl<sub>2</sub>/DMSO) and as KBr disk (bottom) at room temperature.

group. This is fully in accord with the experimental IR analysis, which suggests a free ester carbonyl (1740 cm<sup>-1</sup>) and a hydrogen-bonded amide carbonyl (1661 cm<sup>-1</sup>) in CH<sub>2</sub>Cl<sub>2</sub> (Table 1). Similar to the solid-state structure of **3**, the ferrocene helicity is calculated as positive for **3** (torsion C1–C<sub>g1</sub>–C<sub>g2</sub>–C6 = +9°) and also for **4** (torsion C1–C<sub>g1</sub>–C<sub>g2</sub>–C6 = +12°). These torsion angles are in agreement with the experimentally observed positive Cotton effects at around λ<sub>max</sub> = 460 nm (Table 7).

The <sup>3</sup>J<sub>H,H</sub> coupling constants between NH<sub>Ala1</sub> and CH<sub>α,Ala1</sub> of around 7 Hz in CDCl<sub>3</sub> (Table 2) fit to a torsion angle C(O)–N<sub>Ala1</sub>–C<sub>α,Ala1</sub>–C(O) in the range –70 to –85° [calculated –70° (**3**) and –66° (**4**)], which supports the DFT-optimised structures. Unfortunately, NOE spectra did not reveal any unambiguous contacts *between* the strands in **3** or **4**, which could have helped to substantiate the assumptions.

If H···O distances are taken as a criterion for hydrogen-bond strengths, then the IHBs in **4** should be somewhat stronger than those in **3**, which would be in accord with the NMR spectroscopic and chiroptical measurements with added DMSO. Furthermore, the stronger NH···OC<sub>amide</sub> bonds in **4** relative to the NH···OC<sub>ester</sub> IHBs are also documented by the lower experimental NH stretching vibration energies of **4** (3314/3363 cm<sup>-1</sup>) relative to those of **3** (3355/3398 cm<sup>-1</sup>). This trend is also reproduced by the DFT cal-

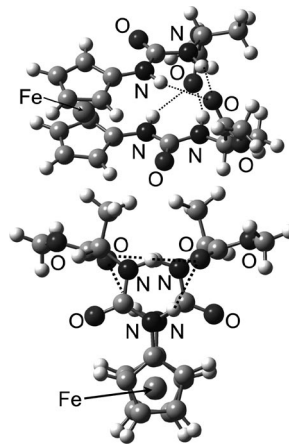


Figure 7. DFT-calculated conformation of **3** (top: side view; bottom: top view illustrating the approximate C<sub>2</sub> symmetry).

culations (Table 8). For **3**, the scaled (by 0.9614<sup>[53]</sup>) average NH stretching vibrations are found at 3383/3451 cm<sup>-1</sup> (NH<sub>Ala1</sub>/1-NH) and the corresponding values for **4** amount to 3323/3425 cm<sup>-1</sup> (NH<sub>Ala1</sub>/1-NH). Thus the difference in stability of the secondary structure of **3** and **4** as experimentally observed by CD spectroscopy is ascribed to the different stability of the NH···OC hydrogen bond rather than to a different hydrogen-bonding motif, that is, an amide

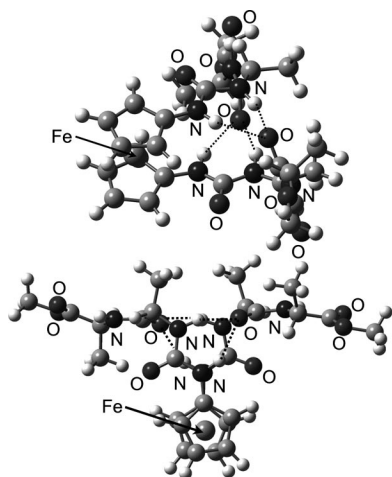


Figure 8. DFT-calculated conformation of **4** (top: side view; bottom: top view illustrating the approximate  $C_2$  symmetry).

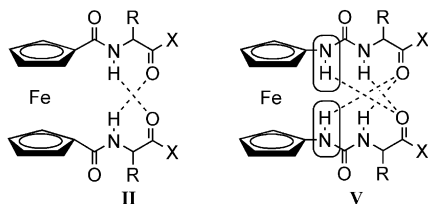
Table 8. DFT-calculated selected bond lengths [Å], angles [°] and relevant scaled<sup>[a]</sup> NH vibrational wavenumbers [cm<sup>-1</sup>] of **3** and **4**.

| D–H...A                                  | H...A     | D...A     | D–H...A | $\tilde{\nu}_{\text{NH}}$ |
|--|-----------|-----------|---------|---------------------------|
| <b>3</b>                                 |           |           |         |                           |
| 1-NH...O <sub>ester</sub>                | 2.35/2.35 | 3.23/3.23 | 145/145 | 3450/3451                 |
| NH <sub>Ala1</sub> ...O <sub>ester</sub> | 1.96/1.96 | 2.94/2.94 | 160/160 | 3379/3386                 |
| <b>4</b>                                 |           |           |         |                           |
| 1-NH...O <sub>amide</sub>                | 2.24/2.17 | 3.14/3.08 | 146/148 | 3421/3429                 |
| NH <sub>Ala1</sub> ...O <sub>amide</sub> | 1.91/1.94 | 2.89/3.08 | 159/156 | 3313/3332                 |

[a] Scaled by 0.9614.<sup>[53]</sup>

carbonyl is a better hydrogen acceptor than an ester carbonyl.

Thus, the observed conformation of type **V** conjugates represented by **3** and **4** resembles very much the robust “Herrick conformation” of type **II** conjugates with two 10-membered IHBs (Scheme 3). The  $C_2$ -symmetric urea derivatives of type **V** feature four IHBs (two 10-membered and two 12-membered rings). This motif can be termed an “expanded Herrick conformation” (Scheme 3).



Scheme 3. “Herrick conformation” of type **II** conjugates (left) and “expanded Herrick conformation” of type **V** conjugates (right).

## Conclusion

$C_2$ -Symmetric ferrocene-bis(ureido)peptides with alanyl and bis(alanyl) substituents (**3**, **4**) were successfully prepared from 1,1'-diisocyanoferrocene. In the crystal structure of the alanyl derivative **3** an asymmetric double IHB

motif  $\text{NH}\cdots\text{OC}_{\text{ester}}$  spanning the two substituents was found along with an intermolecular  $\text{NH}\cdots\text{OC}$  hydrogen bond. In solutions of noncoordinating solvents a more symmetric double IHB pattern was observed for **3**, which results in a quite stable secondary structure with positive helical ferrocene units. For the bis(alanyl)-substituted derivative **4**, a fully analogous (but slightly more stable) motif is suggested, with two  $\text{NH}\cdots\text{OC}_{\text{amide}}$  IHBs determined on the basis of NMR, IR and CD spectroscopic results and DFT calculations.

The double IHB motif – also observed in  $C_2$ -symmetric amino acid derivatives of Fcd and Fcda as well as in bis(amino acid) derivatives of Fca or covalent organic backbones such as 1,4-diamino-2-butyne<sup>[54]</sup> – appears to be quite robust. A single amino acid substituent in the 1-position at the urea unit and a weak acceptor in the 1'-position (e.g., an ester group) in ferrocene mono(ureido)peptides allows only for a single  $\text{NH}\cdots\text{OC}$  bond spanning the two substituents and thus an ensemble of several conformers is observed in solution.<sup>[38]</sup> The ferrocene-1,1'-bis(urea) motif explored in this study is thus a further member of stable turn elements with parallel  $\beta$  strands based on a ferrocene scaffold.

## Experimental Section

**General:** The syntheses were carried out under argon.  $\text{CH}_2\text{Cl}_2$  used for synthesis and FTIR spectroscopy was dried ( $\text{P}_2\text{O}_5$ ), distilled from  $\text{CaH}_2$  and stored over molecular sieves (4 Å).  $\text{C}_6\text{H}_6$  used for synthesis was dried and distilled from  $\text{CaH}_2$  and  $\text{LiAlH}_4$ . Products were purified by preparative thin-layer chromatography on silica gel (Merck, Kieselgel 60 HF254) using  $\text{CH}_2\text{Cl}_2$ /ethyl acetate. Melting points were determined with a Buechi apparatus. IR spectra were recorded for samples as solutions in  $\text{CH}_2\text{Cl}_2$  or as KBr disks with a Bomem MB 100 mid FTIR spectrometer.  $^1\text{H}$  and  $^{13}\text{C}\{^1\text{H}\}$  NMR spectra were recorded with a Varian Gemini 300 spectrometer for solutions of the samples in  $\text{CDCl}_3$  and  $[\text{D}_6]\text{DMSO}$  with  $\text{Me}_4\text{Si}$  as the internal standard. ESI and HR-ESI mass spectra were recorded with a Micromass Q-TOF-Ultima-API spectrometer. UV/Vis and CD spectra were recorded for solutions of the samples in  $\text{CH}_2\text{Cl}_2$  or DMSO with a JASCO-810 CD spectrometer.

**Computational Methods:** Density functional calculations were carried out with the Gaussian 03/DFT<sup>[52]</sup> series of programs. The B3LYP formulation of density functional theory was used by employing the LanL2DZ basis set.<sup>[52]</sup> All points were characterised as minima ( $N_{\text{imag}} = 0$ ) by frequency analysis.

**Crystal Structure Determination:** An orange irregular crystal of **3** with dimensions  $0.54 \times 0.62 \times 0.69 \text{ mm}^3$  was obtained from a solution of **3** in dichloromethane by partial evaporation at room temperature. Intensities were collected at 295 K with an Oxford Diffraction Xcalibur2 diffractometer using graphite-monochromated  $\text{Mo-K}_\alpha$  radiation ( $\lambda = 0.71073 \text{ Å}$ ). CrysAlis<sup>[55]</sup> programs were used for data collection and reduction. Intensities were corrected for Lorentz and polarisation effects, and for absorption using the multiscan absorption correction method (CrysAlis RED).<sup>[55]</sup>

Formula:  $\text{C}_{20}\text{H}_{26}\text{FeN}_4\text{O}_6$  ( $M_r = 474.30$ ); orthorhombic;  $P2_12_12_1$ ;  $a = 10.8909(2) \text{ Å}$ ,  $b = 11.1217(3) \text{ Å}$ ,  $c = 17.9019(5) \text{ Å}$ ;  $V = 2168.37(9) \text{ Å}^3$ ;  $Z = 4$ ;  $\rho_{\text{calcd.}} = 1.453 \text{ g cm}^{-3}$ ;  $\mu = 0.740 \text{ mm}^{-1}$ ;  $F(000) = 992$ ;  $\theta = 3.91\text{--}30.00^\circ$ ;  $h\ k\ l = -15 \text{ to } 15; -15 \text{ to } 15; -25 \text{ to } 24$ ;

reflections collected/independent/observed [ $I \geq 2\sigma(I)$ ] = 17476/6294/3096; 296 refined parameters; transmission factors,  $T_{\min}/T_{\max}$  = 0.82454/1.00000; Flack parameter,  $x = -0.038(11)$ ; goodness-of-fit on  $F^2$ ,  $S = 0.998$ ;  $R$  [ $I \geq 2\sigma(I)$ ]/ $R$  (all data) = 0.0333/0.0758;  $wR$  [ $I \geq 2\sigma(I)$ ]/ $wR$  (all data) = 0.0624/0.0674; max./min. electron density = 0.304/−0.368 e Å<sup>−3</sup>. The crystal structure was solved by direct methods.<sup>[56]</sup> All non-hydrogen atoms were refined anisotropically by full-matrix least-squares calculations based on  $F^2$ .<sup>[56]</sup> The hydrogen atoms of N1, N2, N3 and N4 have been found in a difference Fourier map and refined freely. All other hydrogen atoms were included in calculated positions as riding atoms, with SHELXL97<sup>[56]</sup> defaults. The PLATON<sup>[57]</sup> program was used for structure analysis and drawings preparation. CCDC-740342 contains the supplementary crystallographic data for this paper. These data can be obtained free of charge from The Cambridge Crystallographic Data Centre via [www.ccdc.cam.ac.uk/data\\_request/cif](http://www.ccdc.cam.ac.uk/data_request/cif).

**Ferrocene-1,1'-dicarboxazide (1):** Ferrocene-1,1'-dicarboxylic acid (500 mg, 1.80 mmol) was suspended in water (0.3 mL), and acetone (6.3 mL) was added to dissolve it. After cooling to 0 °C, triethylamine (404 mg, 4.0 mmol) in acetone (5 mL) was added. While maintaining the temperature at 0 °C, a solution of ethyl chloroformate (500 mg, 4.61 mmol) in acetone (2 mL) was added. After stirring for 30 min at 0 °C, a solution of sodium azide (360 mg, 5.44 mmol) in water (1.3 mL) was added. After stirring for 1 h at 0 °C, the mixture was poured into ice water and extracted with dichloromethane. The extracts were washed with a 5% aqueous solution of NaHCO<sub>3</sub> and a saturated aqueous solution of NaCl and then dried with Na<sub>2</sub>SO<sub>4</sub>. Evaporation under reduced pressure at room temperature to dryness gave red crystals (332 mg, 75%). M.p. 112–115 °C. IR (CH<sub>2</sub>Cl<sub>2</sub>):  $\tilde{\nu}$  = 2138 cm<sup>−1</sup> (s, N<sub>3</sub>), 1687 (s, CO) cm<sup>−1</sup>. <sup>1</sup>H NMR (300 MHz, CDCl<sub>3</sub>):  $\delta$  = 4.91 (s, 4 H, Cp-H), 4.56 (s, 4 H, Cp-H) ppm. <sup>13</sup>C NMR (75 MHz, CDCl<sub>3</sub>):  $\delta$  = 175.68 (s, CO), 74.36 (s, C1), 74.14 (s, Cp-C), 72.11 (s, Cp-C) ppm.

**1,1'-Diisocyanoferrocene (2):** A solution of **1** (400 mg, 1.56 mmol) in dry benzene (20 mL) was heated at 85 °C for 4 h. The course of the reaction was monitored by IR spectroscopy as characteristic absorption bands of **1** decreased while the band for the NCO substituent of **2** increased. As prolonged heating results in the formation of *N,N'*-diferrocenyl ureas, the reaction could not be driven to completion.<sup>[38]</sup> After cooling to room temperature, the reaction mixture was evaporated to dryness under reduced pressure at room temperature to give a brown resin. IR (CH<sub>2</sub>Cl<sub>2</sub>):  $\tilde{\nu}$  = 2173 [s, NCO (2)], 1687 [s, CO (residual 1)] cm<sup>−1</sup>.

**Fn(NH-CO-Ala-OCH<sub>3</sub>)<sub>2</sub> (3):** Ala-OCH<sub>3</sub> [obtained from Ala-OCH<sub>3</sub>·HCl (540 mg, 4 mmol) by treatment with Et<sub>3</sub>N in CH<sub>2</sub>Cl<sub>2</sub>] was added to a suspension of crude **2** (500 mg) in dry dichloromethane. The mixture was stirred for 1 h at room temperature. The reaction mixture was washed with saturated aqueous NaHCO<sub>3</sub> and water. The organic layer was dried with Na<sub>2</sub>SO<sub>4</sub> and the solvents evaporated in vacuo. TLC purification with CH<sub>2</sub>Cl<sub>2</sub>/ethyl acetate (10:1) gave compound **3** as orange crystals (230 mg, 36%) and compound **1** (50 mg). M.p. 137–139 °C. MS (ES<sup>+</sup>):  $m/z$  (%) = 474.09 (100) [M]<sup>+</sup>, 497.09 (80) [M + Na]<sup>+</sup>, 513.09 (5) [M + K]<sup>+</sup>, 971.21 (59) [2M + Na]<sup>+</sup>. HRMS (ESI<sup>+</sup>): calcd. for C<sub>20</sub>H<sub>26</sub>N<sub>4</sub>O<sub>6</sub>FeNa 497.1100; found 497.1100. C<sub>20</sub>H<sub>26</sub>N<sub>4</sub>O<sub>6</sub>Fe (474.30): calcd. C 50.65, H 5.53, N 11.81; found C 50.59, H 5.77, N 11.91. For NMR spectroscopic data see Tables 2–4.

**Fn(NH-CO-Ala-Ala-OCH<sub>3</sub>)<sub>2</sub> (4):** A solution of Boc-Ala-Ala-OCH<sub>3</sub> (986 mg, 4 mmol) in ethyl acetate was deprotected by treatment with gaseous HCl. The hydrochloride Ala-Ala-CH<sub>3</sub>·HCl that resulted after evaporation of the solvent was treated with Et<sub>3</sub>N in CH<sub>2</sub>Cl<sub>2</sub> and coupled with crude **2** (500 mg). The mixture was

stirred for 1 h at room temperature, washed with saturated aqueous NaHCO<sub>3</sub> and water. The organic layer was dried with Na<sub>2</sub>SO<sub>4</sub> and the solvents evaporated in vacuo. TLC purification with CH<sub>2</sub>Cl<sub>2</sub>/ethyl acetate (10:1) gave compound **4** as yellow crystals (280 mg, 42%) and **1** (100 mg). M.p. 142–145 °C. MS (ES<sup>+</sup>):  $m/z$  (%) = 616.14 (100) [M]<sup>+</sup>, 639.18 (16) [M + Na]<sup>+</sup>, 655.17 (2) [M + K]<sup>+</sup>, 1255.39 (3) [2M + Na]<sup>+</sup>. HRMS (ESI<sup>+</sup>): calcd. for C<sub>26</sub>H<sub>37</sub>N<sub>6</sub>O<sub>8</sub>Fe 617.2022; found 617.1995. C<sub>26</sub>H<sub>37</sub>N<sub>6</sub>O<sub>8</sub>Fe (616.45): calcd. C 50.66, H 5.89, N 13.63; found C 50.58, H 5.93, N 13.41. For NMR spectroscopic data see Tables 2–4.

**Supporting Information** (see footnote on the first page of this article): DFT-calculated Cartesian coordinates of conformers of **3** and **4**.

## Acknowledgments

We thank the Ministry for Science, Education and Sport of Croatia for support through grant numbers 058-1191344-3122 and 119-1193079-3069. We are indebted to PhD Leo Frkanec (Rudjer Bošković Institute) for measuring UV/Vis and CD spectra.

- [1] R. M. J. Liskamp, *Angew. Chem.* **1994**, *106*, 313–315; *Angew. Chem. Int. Ed. Engl.* **1994**, *33*, 305–307.
- [2] A. Boeijen, R. M. J. Liskamp, *Eur. J. Org. Chem.* **1999**, 2127–2135.
- [3] N. Sewald, H.-D. Jakubke, *Peptides: Chemistry and Biology*, Wiley-VCH, Weinheim, **2002**.
- [4] M. North, *J. Pept. Sci.* **2000**, *6*, 301–313.
- [5] I. G. Jones, W. Jones, M. North, *J. Org. Chem.* **1998**, *63*, 1505–1513.
- [6] D. E. Hibbs, M. B. Hursthouse, I. G. Jones, W. Jones, K. M. A. Malik, M. North, *J. Org. Chem.* **1998**, *63*, 1496–1504.
- [7] J. S. Nowick, E. M. Smith, G. Noronha, *J. Org. Chem.* **1995**, *60*, 7386–7387.
- [8] K. D. Stigers, M. J. Soth, J. S. Nowick, *Curr. Opin. Chem. Biol.* **1999**, *3*, 714–723.
- [9] J. S. Nowick, M. Abdi, K. A. Bellamo, J. A. Love, E. J. Martinez, G. Noronha, E. M. Smith, J. W. Ziller, *J. Am. Chem. Soc.* **1995**, *117*, 89–99.
- [10] O. Khakshoor, J. S. Nowick, *Curr. Opin. Chem. Biol.* **2008**, *12*, 1–8.
- [11] *Bioorganometallics: Biomolecules, Labeling, Medicine* (Ed.: G. Jaouen), Wiley-VCH, Weinheim, **2006**.
- [12] A. Lataifeh, S. Beheshti, H.-B. Kraatz, *Eur. J. Inorg. Chem.*, DOI: 10.1002/ejic.200900268.
- [13] N. Metzler-Nolte, M. Salmain, “The Bioorganometallic Chemistry of Ferrocene” in *Ferrocenes: Ligands, Materials and Biomolecules* (Ed.: P. Štěpnička), Wiley, New York, **2008**, pp. 499–639.
- [14] D. N. Van Staveren, N. Metzler-Nolte, *Chem. Rev.* **2004**, *104*, 5931–5985.
- [15] S. I. Kirin, H.-B. Kraatz, N. Metzler-Nolte, *Chem. Soc. Rev.* **2006**, *35*, 348–354.
- [16] T. Moriuchi, T. Hirao, *Chem. Soc. Rev.* **2004**, *33*, 294–301.
- [17] T. Hirao, *J. Organomet. Chem.* **2009**, *694*, 806–811.
- [18] R. S. Herrick, R. M. Jarret, T. P. Curran, D. R. Dragoli, M. B. Flaherty, S. E. Lindyberg, R. A. Slate, L. C. Thornton, *Tetrahedron Lett.* **1996**, *37*, 5289–5292.
- [19] V. Kovač, K. Radolović, I. Habuš, D. Siebler, K. Heinze, V. Rapić, *Eur. J. Inorg. Chem.* **2009**, 389–399.
- [20] S. I. Kirin, U. Schatzschneider, S. D. Köster, D. Siebler, N. Metzler-Nolte, *Inorg. Chim. Acta* **2009**, *362*, 894–906.
- [21] S. Chowdhury, G. Schatte, H.-B. Kraatz, *Angew. Chem.* **2008**, *120*, 7164–7167; *Angew. Chem. Int. Ed.* **2008**, *47*, 7056–7059.
- [22] S. Chowdhury, D. A. R. Sanders, G. Schatte, H.-B. Kraatz, *Angew. Chem.* **2006**, *118*, 765–768; *Angew. Chem. Int. Ed.* **2006**, *45*, 751–754.

- [23] G. Lapić, D. Siebler, K. Heinze, V. Rapić, *Eur. J. Inorg. Chem.* **2007**, 2014–2024.
- [24] T. Moriuchi, T. Nagai, T. Hirao, *Org. Lett.* **2005**, 7, 5265–5268.
- [25] M. Čakić-Semenčić, D. Siebler, K. Heinze, V. Rapić, *Organometallics* **2009**, 28, 2028–2037.
- [26] K. Heinze, D. Siebler, *Z. Anorg. Allg. Chem.* **2007**, 633, 2223–2233.
- [27] K. Heinze, U. Wild, M. Beckmann, *Eur. J. Inorg. Chem.* **2007**, 617–623.
- [28] L. Barišić, M. Čakić, K. A. Mahmoud, Y. Liu, H.-B. Kraatz, H. Pritzkow, S. I. Kirin, N. Metzler-Nolte, V. Rapić, *Chem. Eur. J.* **2006**, 12, 4965–4980.
- [29] L. Barišić, V. Rapić, N. Metzler-Nolte, *Eur. J. Inorg. Chem.* **2006**, 4019–4021.
- [30] S. Chowdhury, G. Schatte, H.-B. Kraatz, *Angew. Chem.* **2006**, 118, 7036–7038; *Angew. Chem. Int. Ed.* **2006**, 45, 6882–6884.
- [31] K. Heinze, M. Schlenker, *Eur. J. Inorg. Chem.* **2005**, 66–71.
- [32] L. Barišić, M. Dropučić, V. Rapić, H. Pritzkow, S. I. Kirin, N. Metzler-Nolte, *Chem. Commun.* **2004**, 2004–2005.
- [33] K. Heinze, M. Schlenker, *Eur. J. Inorg. Chem.* **2004**, 2974–2988.
- [34] L. Barišić, V. Rapić, V. Kovač, *Croat. Chem. Acta* **2002**, 75, 199–210.
- [35] T. Okamura, K. Sakauye, N. Ueyama, A. Nakamura, *Inorg. Chem.* **1998**, 37, 6731–6736.
- [36] S. Djaković, D. Siebler, M. Čakić-Semenčić, K. Heinze, V. Rapić, *Organometallics* **2008**, 27, 1447–1453.
- [37] S. Chowdhury, K. A. Mahmoud, G. Schatte, H.-B. Kraatz, *Org. Biomol. Chem.* **2005**, 3, 3018–3023.
- [38] J. Lapić, G. Pavlović, D. Siebler, K. Heinze, V. Rapić, *Organometallics* **2008**, 27, 726–735.
- [39] S. R. Bayly, P. D. Beer, G. Z. Chen, “Ferrocene Sensors” in *Ferrocenes: Ligands, Materials and Biomolecules* (Ed.: P. Štěpnička), Wiley, New York, **2008**, pp. 281–318.
- [40] P. Molina, A. Tárraga, A. Caballero, *Eur. J. Inorg. Chem.* **2008**, 3401–3417.
- [41] H. Miyaji, S. R. Collonson, I. Prokeš, J. H. R. Tucker, *Chem. Commun.* **2003**, 64–65.
- [42] A. J. Evans, S. E. Matthews, A. R. Cowley, P. D. Beer, *Dalton Trans.* **2003**, 4644–4650.
- [43] M. D. Pratt, P. D. Beer, *Polyhedron* **2003**, 22, 649–653.
- [44] K. Moon, A. E. Kaifer, *J. Am. Chem. Soc.* **2004**, 126, 15016–15017.
- [45] F. Otón, A. Tárraga, A. Espinosa, M. D. Velasco, P. Molina, *Dalton Trans.* **2006**, 3685–3692.
- [46] F. Otón, A. Tárraga, A. Espinosa, M. D. Velasco, P. Molina, *J. Org. Chem.* **2006**, 71, 4590–4598.
- [47] F. Otón, A. Tárraga, M. D. Velasco, P. Molina, *Dalton Trans.* **2005**, 1159–1161.
- [48] F. Otón, A. Tárraga, A. Espinosa, M. D. Velasco, D. Bautista, P. Molina, *J. Org. Chem.* **2005**, 70, 6603–6608.
- [49] K. Schlögl, H. Seiler, *Naturwissenschaften* **1958**, 45, 337.
- [50] J. Bernstein, R. E. Davis, L. Shimoni, N.-L. Chang, *Angew. Chem.* **1995**, 107, 1689–1708; *Angew. Chem. Int. Ed. Engl.* **1995**, 34, 1555–1573.
- [51] S. R. Batten, R. Robson, *Angew. Chem.* **1998**, 110, 1558–1595; *Angew. Chem. Int. Ed.* **1998**, 37, 1460–1494.
- [52] M. J. Frisch, G. W. Trucks, H. B. Schlegel, G. E. Scuseria, M. A. Robb, J. R. Cheeseman, J. A. Montgomery Jr, T. Vreven, K. N. Kudin, J. C. Burant, J. M. Millam, S. S. Iyengar, J. Tomasi, V. Barone, B. Mennucci, M. Cossi, G. Scalmani, N. Rega, G. A. Petersson, H. Nakatsuji, M. Hada, M. Ehara, K. Toyota, R. Fukuda, J. Hasegawa, M. Ishida, T. Nakajima, Y. Honda, O. Kitao, H. Nakai, M. Klene, X. Li, J. E. Knox, H. P. Hratchian, J. B. Cross, C. Adamo, J. Jaramillo, R. Gomperts, R. E. Stratmann, O. Yazyev, A. J. Austin, R. Cammi, C. Pomelli, J. W. Ochterski, P. Y. Ayala, K. Morokuma, G. A. Voth, P. Salvador, J. J. Dannenberg, V. G. Zakrzewski, S. Dapprich, A. D. Daniels, M. C. Strain, O. Farkas, D. K. Malick, A. D. Rabuck, K. Raghavachari, J. B. Foresman, J. V. Ortiz, Q. Cui, A. G. Baboul, S. Clifford, J. Cioslowski, B. B. Stefanov, G. Liu, A. Liashenko, P. Piskorz, I. Komaromi, R. L. Martin, D. J. Fox, T. Keith, M. A. Al-Laham, C. Y. Peng, A. Nanayakkara, M. Challacombe, P. M. W. Gill, B. Johnson, W. Chen, M. W. Wong, C. Gonzalez, J. A. Pople, *Gaussian 03*, Revision B.03, Gaussian, Inc., Pittsburgh, PA, **2003**.
- [53] W. Koch, M. C. Holthausen, *A Chemist's Guide to Density Functional Theory*, Wiley-VCH, Weinheim, **2001**, p. 134.
- [54] T. P. Curran, K. A. Marques, M. V. Silva, *Org. Biomol. Chem.* **2005**, 3, 4134–4138.
- [55] Xcalibur CCD System, *CrysAlis CCD and CrysAlis RED*, Version 1.171.32.4, Oxford Diffraction, Oxford, United Kingdom, **2007**.
- [56] G. M. Sheldrick, *Acta Crystallogr., Sect. A* **2008**, 64, 112–122.
- [57] A. L. Spek, *J. Appl. Crystallogr.* **2003**, 36, 7–13.

Received: July 20, 2009

Published Online: November 20, 2009

# Syntheses of the First Coordination Compounds of the New Strong Molecular Electron Donor and Double Proton Sponge 1,4,5,8-Tetrakis(tetramethylguanidino)naphthalene

Viktoriia Vitske,<sup>[a]</sup> Carolin König,<sup>[a]</sup> Olaf Hübner,<sup>[a]</sup> Elisabeth Kaifer,<sup>[a]</sup> and  
Hans-Jörg Himmel<sup>\*[a]</sup>

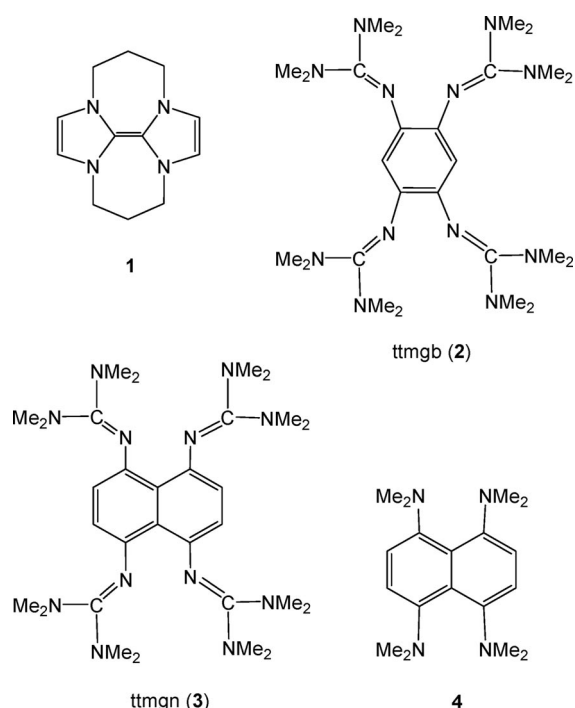
**Keywords:** Electron donor ligands / Cobalt / Aluminum / N ligands

Herein we report on the synthesis and properties of a new electron donor featuring an aromatic system to which four guanidino groups are attached, namely, 1,4,5,8-tetrakis(tetramethylguanidino)naphthalene (ttmgn). The molecule is a double proton sponge with an asymmetric N–H···N bridge being formed in the protonated form. Oxidation is followed electrochemically, and two oxidation waves at  $E_{1/2}(\text{CH}_3\text{CN}) = -0.25$  and  $+0.50$  V vs. SCE are observed. Chemical oxidation with  $\text{I}_2$  yields ttmgn( $\text{I}_3$ )<sub>2</sub>, in which the  $\text{I}_3^-$  units interact with the ttmgn<sup>2+</sup> cations through I···C contacts. Reaction with an excess amount of  $\text{Br}_2$  leads to removal of four electrons from the aromatic system and formation of the salt (ttmgn)- $\text{Br}_4$  with a chair-type conformation of the  $\text{C}_{10}$  core. The binuclear Al alkyl complex [(ttmgn)(AlMe<sub>2</sub>)<sub>2</sub>][BPh<sub>4</sub>]<sub>2</sub> can be pre-

pared by reaction between the diprotonated ttmgn molecule and AlMe<sub>3</sub> and serves as a benchmark system for the understanding of dynamic effects. Magnetic superexchange through the ligand unit is studied for the binuclear Co<sup>II</sup> complex [(ttmgn)(CoCl<sub>2</sub>)<sub>2</sub>]. SQUID measurements show an extremely weak antiferromagnetic coupling. The coupling might be affected by the unusual geometry of the coordination compounds of ttmgn, in which the metal ions are significantly displaced from the plane defined by the aromatic ring of the ttmgn ligand. We also report the analogous Co complex of ttmb [ttmb = 1,2,4,5-tetrakis(tetramethylguanidino)-benzene], namely, [(ttmb)(CoCl<sub>2</sub>)<sub>2</sub>], in which the bonding situation is quite different.

## Introduction

There is a still increasing interest in new strong molecular organic electron donors, which can be combined with electron acceptors to give electrical conducting materials. The first compounds have been already known for more than three decades.<sup>[1]</sup> In the past, some effort was devoted to the synthesis of new representatives of imidazole-derived donors. Bisimidazolyliene (tetraazafulvalene) (**1**; Scheme 1)<sup>[2]</sup> was denoted “organic sodium” due to its facile oxidation<sup>[3]</sup> and was applied as a mild and selective reducing agent in a number of reactions; for example, reductive cleavage of sulfones and sulfonamides<sup>[4]</sup> and reduction of aryl iodides.<sup>[5–7]</sup> In contrast, donor **1** is, in difference to conventional strong reducing agents such as Mg or sodium naphthalene, not capable of reducing ketones. Recently, we reported the synthesis and properties of a first molecular electron donor consisting of an aromatic system to which four strongly basic guanidino ligands were attached, namely,

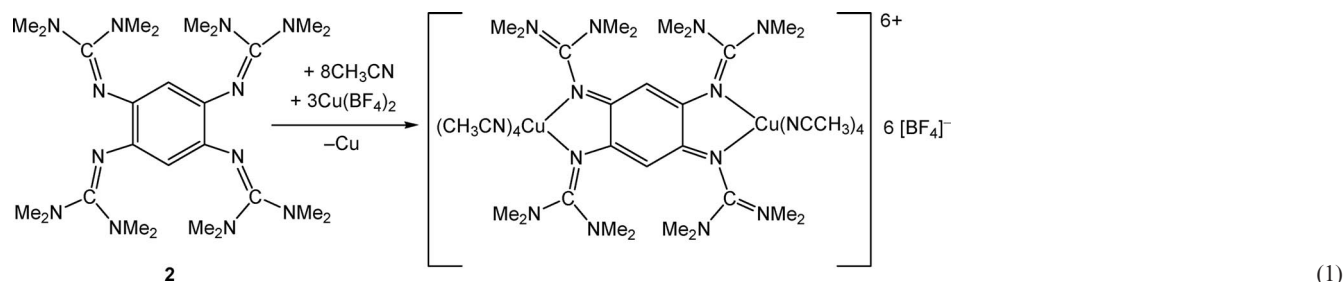


Scheme 1.

[a] Anorganisch-Chemisches Institut, Ruprecht-Karls-Universität Heidelberg, Im Neuenheimer Feld 270, 69120 Heidelberg, Germany  
Fax: +49-6221-545707

E-mail: hans-jorg.himmel@aci.uni-heidelberg.de

Supporting information for this article is available on the WWW under <http://dx.doi.org/10.1002/ejic.200900724>.



1,2,4,5-tetrakis(tetramethylguanidino)benzene (**2**; Scheme 1).<sup>[8]</sup> Quantum chemical calculations suggest this molecule to be an even better electron donor than **1** in the gas phase. Here, we now report on the synthesis of a second representative of aromatic compounds with four guanidino groups, namely, 1,4,5,8-tetrakis(tetramethylguanidino)naphthalene (**3**). The properties of the new compound will be compared with those of **2** and also related compounds like the double proton sponge 1,4,5,8-tetrakis(dimethylamino)naphthalene (**4**; Scheme 1).<sup>[9]</sup> In contrast to **4**, new guanidine electron donors **2**<sup>[10]</sup> and **3** are capable of acting as redox-active complex ligands in the same way as shown recently by us for the related 1,8-bis(tetramethylguanidino)naphthalene (btmgn).<sup>[11]</sup>

Because of their high basicity,<sup>[12]</sup> guanidines are interesting complex ligands. Herres-Pawlis, Henkel et al. published a valuable work on the synthetic routes to such ligands.<sup>[13]</sup> A number of chelating bisguanidine complexes have already been prepared and characterised.<sup>[14,15]</sup> Just to name a few examples, Fe and Cu complexes of chelating guanidines were synthesised by Henkel, Tamm et al.<sup>[16,17]</sup> Recently, the first 1:1 Cu/O<sub>2</sub> complex featuring end-on coordinated O<sub>2</sub> and its interesting chemistry were reported.<sup>[18,19]</sup> In this complex, the Cu is coordinated by the tripodal, superbasic and sterically encumbered tris(tetramethylguanidino)trien (TMG3tren) ligand. Furthermore, guanidine-stabilised zinc complexes were shown to be promising catalysts for the synthesis of polylactide.<sup>[20]</sup> Previous studies by our group focussed on the preparation of a variety of binuclear metal complexes of **2**.<sup>[10]</sup> Magnetic superexchange was studied for the complex [Cu<sub>2</sub>(MeCN)<sub>4</sub>(ttmgb)][BF<sub>4</sub>]<sub>6</sub>, in which the ligand is oxidised [Equation (1)]. Herein we now analyse magnetic coupling in binuclear Co<sup>II</sup> complexes of **3**.

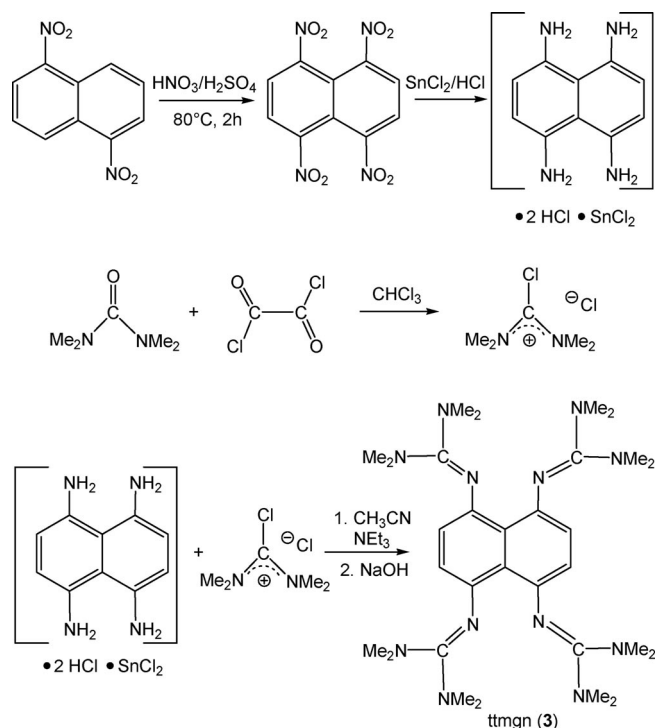
## Results and Discussion

In the following, we report on the synthesis and characterisation of **3** and its protonation and oxidation. Subsequently, the binuclear metal complexes [3(AlMe<sub>2</sub>)<sub>2</sub>]<sup>2+</sup> and 3(CoCl<sub>2</sub>)<sub>2</sub> as well as the analogue 2(CoCl<sub>2</sub>)<sub>2</sub> will be discussed.

### Synthesis and Characterisation

The synthesis of **3** turned out to be much more difficult than that of **2**. Nevertheless, its preparation was achieved

in acceptable yield (Scheme 2) starting with 1,5-dinitronaphthalene. Nitration led to 1,4,5,8-tetranitronaphthalene,<sup>[21]</sup> which had to be separated from its isomer 1,3,5,8-tetranitronaphthalene. Reduction with SnCl<sub>2</sub>/HCl then gave the corresponding protonated tetraamine (as SnCl<sub>2</sub> adduct).<sup>[22]</sup> The neutral tetraamine is a highly unstable, intensively blue-coloured compound.<sup>[23]</sup> Therefore, we directly reacted the protonated 1,4,5,8-tetrakis(tetraamino)naphthalene with 2-chloro-1,1',3,3'-tetramethylformamidinium chloride (freshly prepared from tetramethylurea and oxalyl chloride) to give protonated **3**. Treatment with NaOH then finally yielded neutral **3**.



Scheme 2.

The compound turned out to be a yellow-coloured solid, which is soluble in H<sub>2</sub>O, CH<sub>3</sub>CN and CH<sub>2</sub>Cl<sub>2</sub>. The solutions have to be stored under an inert gas atmosphere, as O<sub>2</sub> causes rapid oxidation. At room temperature, compound **3** exhibits only two signals in the <sup>1</sup>H NMR spectrum. In CD<sub>3</sub>CN solutions, the methyl groups show at δ = 2.65 ppm, and the four aromatic protons give rise to a singlet at δ = 6.01 ppm. The <sup>13</sup>C NMR spectrum contains a signal at δ =

154.26 ppm due to the central C atoms (bonded to three N atoms) of the four guanidino groups. This chemical shift compares with  $\delta = 158.4$  and  $155.0$  ppm as measured for **2** and 1,8-bis(tetramethylguanidino)naphthalene (btmgn),<sup>[24]</sup> respectively. The variable-temperature  $^1\text{H}$  NMR spectra of a  $\text{CH}_2\text{Cl}_2$  solution of **3** showed the splitting of the methyl signals at lower temperatures into two signals (see Supporting Information). No changes were observed in the aromatic region. Thus, the situation is comparable to that found in 1,8-bis(tetramethylguanidino)naphthalene (btmgn),<sup>[24]</sup> and the splitting arises from the freezing of the rotations around the four C=N bonds.

The UV/Vis spectrum of **3** (0.1 mM in  $\text{H}_2\text{O}$ ) is shown in Figure 1. The spectra of the two guanidino compounds 1,2-bis(tetramethylguanidino)benzene (btmgb) and **2**, which were both studied previously in our group,<sup>[25]</sup> are also included for comparison. All three compounds exhibit, in addition to the typical features of the aromatic system, an extra absorption at lower energy. The absorption maximum of this extra band shifts in the order btmgb (292 nm) > **2** (329 nm) > **3** (404 nm) towards lower energy, in line with the increasing extent of the  $\pi$  system. In the case of btmgn, a corresponding absorption was observed at 349 nm.<sup>[24]</sup> The IR spectrum (see Supporting Information) is dominated by a large group of bands in the region  $1650\text{--}1550\text{ cm}^{-1}$ , which is characteristic of guanidino compounds and arises from vibrational modes with significant character from the  $\nu(\text{C}=\text{N})$  stretches. However, heavy mode coupling prohibits any straightforward mode description. In addition, a sharp band occurs at  $1140\text{ cm}^{-1}$ , signalling the presence of  $\text{CH}_2$  groups. Furthermore, relatively strong bands (with maxima of absorption at  $2926$  and  $2884\text{ cm}^{-1}$ ) and weaker ones ( $2999$  and  $2803\text{ cm}^{-1}$ ) appear in the region characteristic for the  $\nu(\text{C}\text{--}\text{H})$  stretching modes.

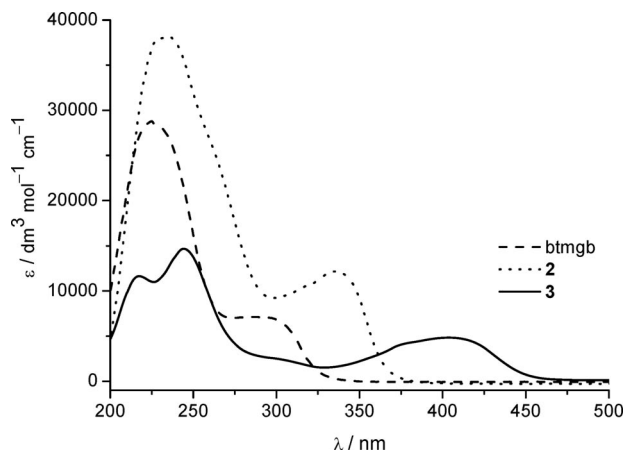


Figure 1. UV/Vis spectra as recorded for bis(tetramethylguanidino)-benzene, **2** and **3**.

Crystals of compound **3** were obtained from  $\text{CH}_3\text{CN}$  solutions. Figure 2 displays the molecular structure of the new electron donor in the crystalline state as derived from X-ray diffraction measurements. Whereas in Figure 2a all atoms are drawn, the view along the naphthalene plane in Figure 2b intends to highlight the propeller-like conforma-

tion of the four C–N bonds, C1–N1, C4–N10, C6–N7 and C9–N4, and all methyl and hydrogen atoms were omitted for the sake of clarity. The angles between the pairs of bonds C1–N1/C9–N4 and C4–N10/C6–N7 measure  $27.6$  and  $30.9^\circ$ , respectively. Interestingly, with  $271.7(2)$  and  $268.8(3)$  pm the N1...N4 and N7...N10 separations are shorter than the two shortest N...N separations in 1,4,5,8-tetrakis(dimethylamino)naphthalene [**4**;  $274.5(1)$  pm]<sup>[26]</sup> and compare with a value of  $271.7$  pm in btmgn.<sup>[24]</sup> The reason for the larger N...N separation in **4** can be found in the steric encumbrance at the N atoms. In difference to the situation in **4**, the aromatic unit is only very slightly twisted, showing again that the steric encumbrance of the guanidino groups is much smaller. Informative indicators of the bonding properties also are the relatively small angles C4–C5–C6 and C9–C10–C1 of  $120.92(15)$  and  $121.59(15)^\circ$ , respectively, which compare with  $122.6^\circ$  as measured in btmgn,<sup>[24]</sup> and are slightly but significantly smaller than the  $123.6^\circ$  adopted in **4**.<sup>[26]</sup>

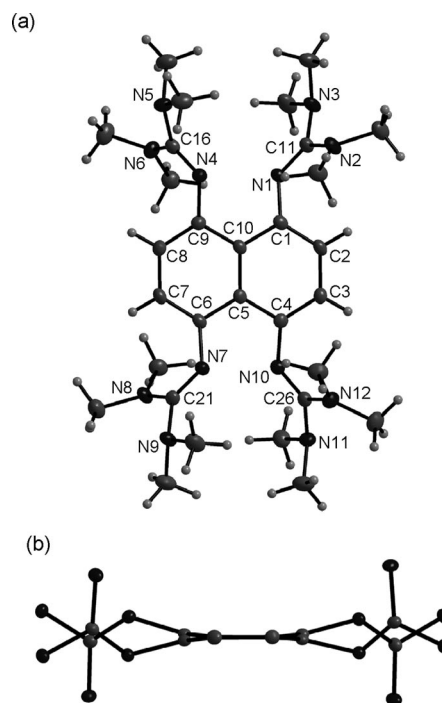
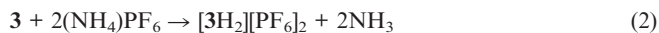


Figure 2. (a) Molecular structure of **3**; thermal ellipsoids are drawn at the 50% probability level. (b) View along the naphthalene plane showing the twisting of the four guanidino groups (hydrogen and methyl groups were omitted for the sake of better clarity).

### Protonation and Oxidation

An aqueous solution of **3** (5.0 mM) was titrated with a 0.1 M HCl solution (see the titration curve in the Supporting Information). Addition of two equivalents of HCl to an  $\text{H}_2\text{O}$  solution of **3** brings about a decrease in the pH value from 11.6 at the start to ca. 7. A pH value of ca. 2 is reached after addition of four equivalents of HCl. The  $\text{p}K(\text{BH}^+)$  value of **3** should be in the same region as that of 1,8-bis(tetramethylguanidino)naphthalene [btmgn;  $\text{p}K$ -

(BH<sup>+</sup>) = 25.1 in MeCN].<sup>[24]</sup> Due to the high reactivity and air sensitivity of **3** (oxidation, see below) we have, however, set aside an exact determination for **3**. Reaction of **3** with (NH<sub>4</sub>)PF<sub>6</sub> proceeded smoothly to give the salt of the diprotonated guanidino compound, [3H<sub>2</sub>][PF<sub>6</sub>]<sub>2</sub> [see Equation (2)].



The <sup>1</sup>H NMR spectrum of [3H<sub>2</sub>][PF<sub>6</sub>]<sub>2</sub> in CH<sub>3</sub>CN solution displays signals at  $\delta$  = 2.83, 6.45 and 14.45 ppm, which can be assigned to the methyl groups, the aromatic protons and the N–H protons, respectively. The  $\delta$  value of 14.45 compares with  $\delta$  = 14.28 for btmg<sup>[24]</sup> and shows that a nonsymmetrical N–H⋯N bridge is adopted. A symmetric N–H–N bridge was previously shown to give rise to a signal at even lower field (e.g.,  $\delta$  = 18.80 in [4H<sub>2</sub>][BF<sub>4</sub>]<sub>2</sub>).<sup>[27]</sup> Orange-coloured crystals were grown from CH<sub>3</sub>CN solutions. The molecular structure from X-ray diffraction is visualised in Figure 3. Protonation leads to further reduction of the N⋯N separations between the imino N atoms of two adjacent guanidino groups (N1⋯N4 and N7⋯N10) to 252.3(3)/252.5(3) pm. In agreement with the results of the NMR spectroscopic data, X-ray diffraction analysis points to the presence of a nonsymmetrical N–H⋯N bridge. Of course we are, in the absence of neutron diffraction data, not in the position to determine the exact position of the H atoms. However, quantum chemical calculations (B3LYP/6-311++G\*\*) also predict a nonsymmetrical N–H⋯N bridge (e.g., with bond lengths of 104.9 pm for N1–H and 166.9 pm for H⋯N4, see also the Supporting Information). Furthermore, the N=C bond lengths increase significantly. Hence, whereas the N1–C11, N4–C16, N7–C21 and N10–C26 distances in **3** cover the range 127.7–128.6 pm before protonation, the range is 131.9–134.3 pm after protonation. At the same time, the average C–N bond lengths from the central C atom to the NMe<sub>2</sub> groups in the

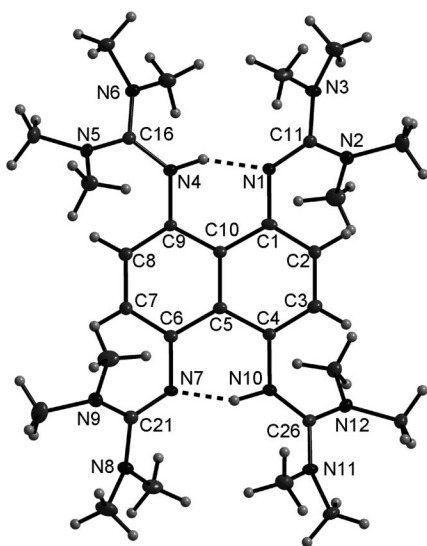


Figure 3. Molecular structure of [3H<sub>2</sub>][PF<sub>6</sub>]<sub>2</sub> (only the cationic part is shown). Thermal ellipsoids are drawn at the 50% probability level.

guanidino units decrease upon protonation. These changes indicate delocalisation of the positive charge. Selected structural parameters for [3H<sub>2</sub>][PF<sub>6</sub>]<sub>2</sub> are given in the Supporting Information (Table S2).

In further experiments, we treated [3H<sub>2</sub>](PF<sub>6</sub>)<sub>2</sub> with three equivalents of HCl to obtain the tetraprotonated guanidine [3H<sub>4</sub>]Cl<sub>4</sub>. The <sup>1</sup>H NMR spectrum recorded after the reaction indeed contained a singlet at  $\delta$  = 10.84 ppm, which can be assigned to the four N–H protons. Crystals were grown at –18 °C. Figure 4 illustrates the molecular structure as obtained from XRD analysis. The crystalline phase contains 8 equivalents of crystal water, and a fraction of the extended hydrogen-bonded network established in the crystal is also shown in Figure 4. The N1⋯N4 separation in the tetraprotonated ttmg molecule increases to 277.1 pm. As a result of tetraprotonation, all N–C bond lengths within the guanidino groups (involving atoms C6 or C11) become almost equal, indicating stabilisation of the positive charge by delocalisation over all non-hydrogen atoms. The C–C bond lengths within the naphthalene group indicate that the aromatic system remains intact.

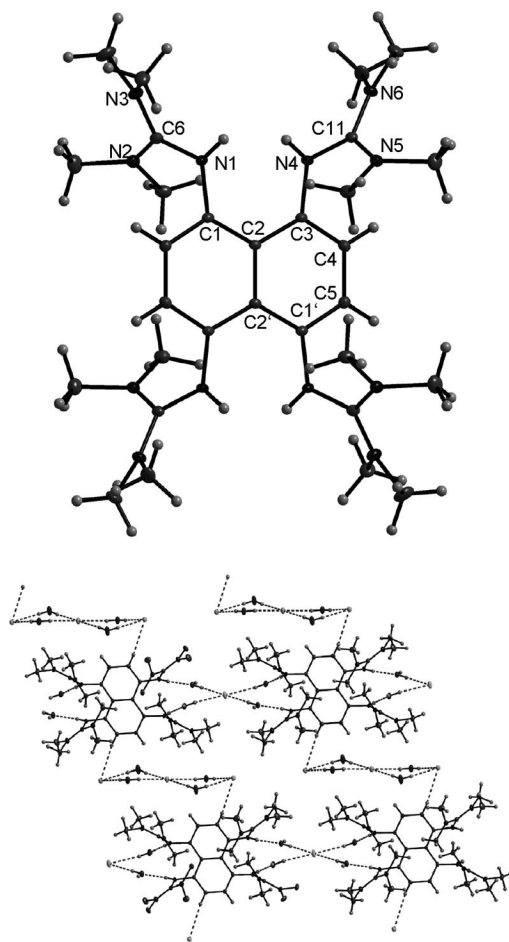


Figure 4. Molecular structure of [3H<sub>4</sub>]Cl<sub>4</sub>·8H<sub>2</sub>O. The cationic part and a fraction of the network connecting the cations through hydrogen bonding are shown. Thermal ellipsoids are drawn at the 50% probability level.

CV measurements show the existence of two relatively sharp and well-separated oxidation waves at  $E_{1/2}(\text{CH}_3\text{CN}) = -0.25$  (presumably oxidation to  $3^{2+}$ ) and  $+0.50$  V (presumably oxidation to  $3^{4+}$ ) vs. SCE (at a scan rate of  $25 \text{ mV s}^{-1}$ , see Figure 5).<sup>[28]</sup> Variation of the scan rate (see Supporting Information) had little effect on the half-width of the oxidation peaks, arguing for relatively fast processes. Like **2** and **4**, new electron donor **3** can easily be oxidised chemically. Reaction with  $\text{I}_2$  was followed by UV/Vis, IR and NMR spectroscopy [Equation (3)].

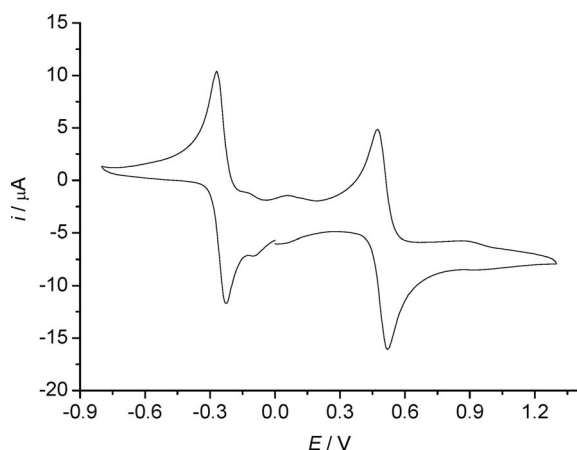
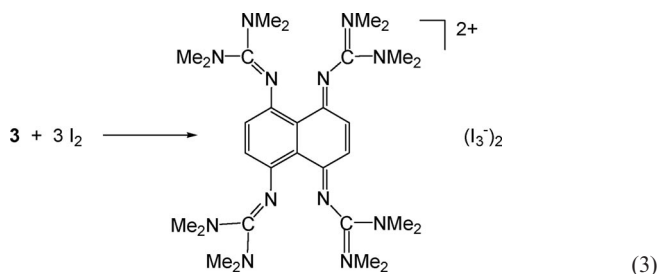


Figure 5. CV curve for **3** in  $\text{CH}_3\text{CN}$  (measured vs. SCE at a scan rate of  $25 \text{ mV s}^{-1}$ ).



in  $3(\text{I}_3)_2$  [293.05(9) pm in one and 294.07(7) pm in the other  $\text{I}_3^-$  unit]. This interaction has also consequences for the structural parameters within the  $3^{2+}$  dication. Hence, the shortest C–N bond lengths connecting the guanidino groups with the central C10 unit (C1–N1 and C3–N4) are not equal. However, both are significantly shorter than the corresponding distances in neutral **3**, indicating extended delocalisation of the positive charges. The presence of cation–anion interactions should lead to large differences in the electrical conductivity between **2** and **3**. Such measurements are currently in progress.<sup>[30]</sup>

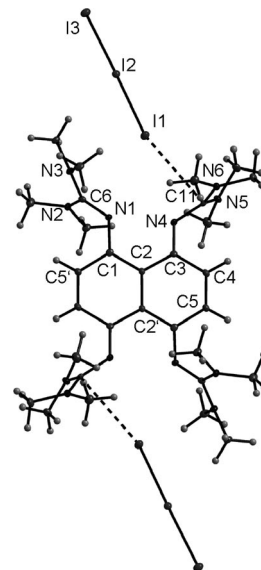


Figure 6. Molecular structure of  $[3(\text{I}_3)_2]$  as derived from X-ray diffraction. Thermal ellipsoids are drawn at the 50% probability level.

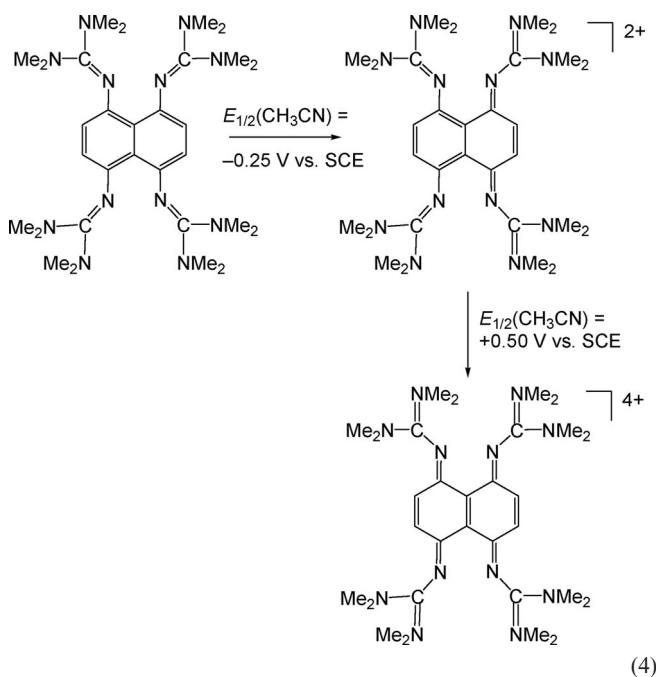
The structures of neutral **3** and dication  $3^{2+}$  were calculated by using the B3LYP functional in combination with a SV(P) basis set. According to these calculations, **3** and its dication adopt  $\text{C}_{2h}$  symmetric structures. A comparison between experimental and calculated bond parameters is given in Table 1. It can be seen that the general level of agreement between calculated and experimentally observed bond parameters for **3** is very pleasing. Hence, for all bond lengths the deviations between calculated and observed value is smaller than 2 pm. The calculated bond angles differ by less than  $2^\circ$  from the experimental ones. In the case of the torsional angles the deviations are slightly larger ( $<5^\circ$ ). Due to the absence of  $\text{I}_3^-$  units, the calculated structure of an isolated  $3^{2+}$  dication deviates slightly from that derived from X-ray diffraction. This shows the modulations in the structural details resulting from  $\text{I}_3^-$  coordination. The variations of the C–C bond lengths within the naphthalene ring in oxidised molecule  $3^{2+}$  indicate loss of aromaticity. Hence, the largest calculated C–C distance in the dication is 145.2 pm and the smallest one is 135.7 pm. The C–N bond lengths between C naphthyl atoms and the N atoms of the guanidino groups shrink considerably upon oxidation (from calculated 140.0 pm in **3** to 133.3 pm in  $3^{2+}$ ). All these variations are in line with the expectations from the Lewis formula [see Equation (4)].

The UV/Vis spectrum shows two strong absorptions at 294 and 367 nm, which can be assigned to the  $\text{I}_3^-$  anion.<sup>[29]</sup> Unfortunately, the large intensity of these bands mask any possible band of oxidised **3**. Nevertheless, the UV/Vis spectra indicate that a redox reaction occurred in the course of which the iodine gets reduced, however, without providing direct proof for the oxidation of **3**. Further analysis showed that a reaction occurs according to Equation (3). Crystals of  $3(\text{I}_3)_2$  were grown from  $\text{CH}_3\text{CN}$ . Figure 6 sketches the molecular structure (see Table S4 in the Supporting Information for a list of structural parameters). Interestingly, each of the two  $\text{I}_3^-$  units interacts with one guanidino unit through  $\text{I}\cdots\text{C}$  contacts [of 351.9(1) pm (I1 $\cdots$ C11)]. This leads to a stabilisation of the positive charge at the C11 atom (carbocation character) by the donation of electron density from  $\text{I}_3^-$ . This donation causes the two I–I bond lengths within the  $\text{I}_3^-$  unit to be significantly different [284.39(6) and 300.51(7) pm]. For comparison, in  $2(\text{I}_3)_2$  both I–I bond lengths are equal and in between the values

Table 1. Comparison between some observed and calculated [B3LYP/SV(P)] bond lengths (in pm) for **3** before and after oxidation.

|          | <b>3</b><br>exp. <sup>[a]</sup> | <b>3</b><br>calcd. <sup>[a]</sup> |           | <b>3(I<sub>3</sub>)<sub>2</sub></b><br>exp. <sup>[b]</sup> | <b>3<sup>2+</sup></b><br>calcd. <sup>[b]</sup> |
|----------|---------------------------------|-----------------------------------|-----------|--|--|
| C1–N1    | 141.5(2)                        | 140.0                             | C1–N1     | 135.3(4)   | 133.3  |
| C9–N4    | 140.9(2)                        | 140.0                             | C3–N4     | 132.5(4)   | 133.3  |
| C6–N7    | 141.4(2)                        | 140.0                             | C1'–N1'   | 135.3(4)   | 133.3  |
| C4–N10   | 140.5(2)                        | 140.0                             | C3'–N4'   | 132.5(4)   | 133.3  |
| N1–C11   | 127.7(2)                        | 128.7                             | N1–C6     | 131.3(5)   | 133.0  |
| N4–C16   | 127.9(2)                        | 128.7                             | N4–C11    | 135.3(5)   | 133.0  |
| N7–C21   | 128.6(2)                        | 128.7                             | N1'–C6'   | 131.3(5)   | 133.0  |
| N10–C26  | 128.0(2)                        | 128.7                             | N4'–C11'  | 135.3(5)   | 133.0  |
| N2–C11   | 138.19(19)                      | 139.8                             | N2–C6     | 137.1(5)   | 136.9  |
| N3–C11   | 140.7(2)                        | 139.8                             | N3–C6     | 134.5(4)   | 135.8  |
| N5–C16   | 140.2(2)                        | 139.8                             | N5–C11    | 133.9(5)   | 135.8  |
| N6–C16   | 138.62(19)                      | 139.8                             | N6–C11    | 134.1(5)   | 136.9  |
| N8–C21   | 138.13(19)                      | 139.8                             | N5'–C11'  | 133.9(5)   | 136.9  |
| N9–C21   | 139.7(2)                        | 139.8                             | N6'–C11'  | 134.1(5)   | 135.8  |
| N11–C26  | 140.5(2)                        | 139.8                             | N3'–C6'   | 134.5(4)   | 135.8  |
| N12–C26  | 138.35(19)                      | 139.8                             | N2'–C6'   | 137.1(5)   | 136.9  |
| C1–C2    | 137.5(2)                        | 139.2                             | C1–C5'    | 143.5(5)   | 145.2  |
| C2–C3    | 140.1(2)                        | 140.4                             | C4–C5     | 135.6(5)   | 135.7  |
| C3–C4    | 137.9(2)                        | 139.2                             | C5–C1'    | 143.5(5)   | 145.2  |
| C4–C5    | 144.0(2)                        | 144.3                             | C1'–C2'   | 142.6(5)   | 144.1  |
| C5–C6    | 143.4(2)                        | 144.3                             | C2'–C3'   | 143.4(5)   | 144.1  |
| C6–C7    | 137.7(2)                        | 139.2                             | C3'–C4'   | 144.7(5)   | 145.2  |
| C7–C8    | 139.8(2)                        | 140.4                             | C4'–C5'   | 135.6(5)   | 135.7  |
| C8–C9    | 137.7(2)                        | 139.2                             | C5'–C1    | 143.5(5)   | 145.2  |
| C9–C10   | 143.5(2)                        | 144.3                             | C1–C2     | 142.6(5)   | 144.1  |
| C10–C1   | 144.8(4)                        | 144.3                             | C2–C3     | 143.4(5)   | 144.1  |
| C5–C10   | 143.8(2)                        | 145.1                             | C2–C2'    | 144.6(7)   | 145.3  |
| N1...N4  | 271.7(2)                        | 271.3                             | N1...N4   | 266.3(7)   | 267.0  |
| N7...N10 | 268.8(3)                        | 271.3                             | N1'...N4' | 266.3(7)   | 267.0  |

[a] Atom numbering given in Figure 2. [b] Atom numbering given in Figure 6.



Reaction of **3** with an excess amount of Br<sub>2</sub> yielded **3Br<sub>4</sub>** [see Equation (5)]. The salt was crystallised together with

four equivalents of H<sub>2</sub>O. Figure 7 shows the molecular structure, and Table S5 (Supporting Information) contains some structural parameters. As anticipated, the bond lengths N1–C1 and N4–C3' of 129.1(3) and 128.5(3) pm, respectively, signal double-bond character, whereas the N1–C6 and N4–C11 bonds changed from double bonds in neutral **3** [127.7(2) and 127.9(2) pm] to single bonds [138.5(3) and 140.3(3) pm]. A consequence of the removal of four electrons from the naphthalene unit is the loss of planarity. Figure 7b,c illustrate the chair-type conformation of the C<sub>10</sub> ring in **3Br<sub>4</sub>**. The possibility to form a **3<sup>4+</sup>** cation by oxidation with Br<sub>2</sub> is in sharp contrast to the reactivity of **2**, for which only dication **2<sup>2+</sup>** was obtained.

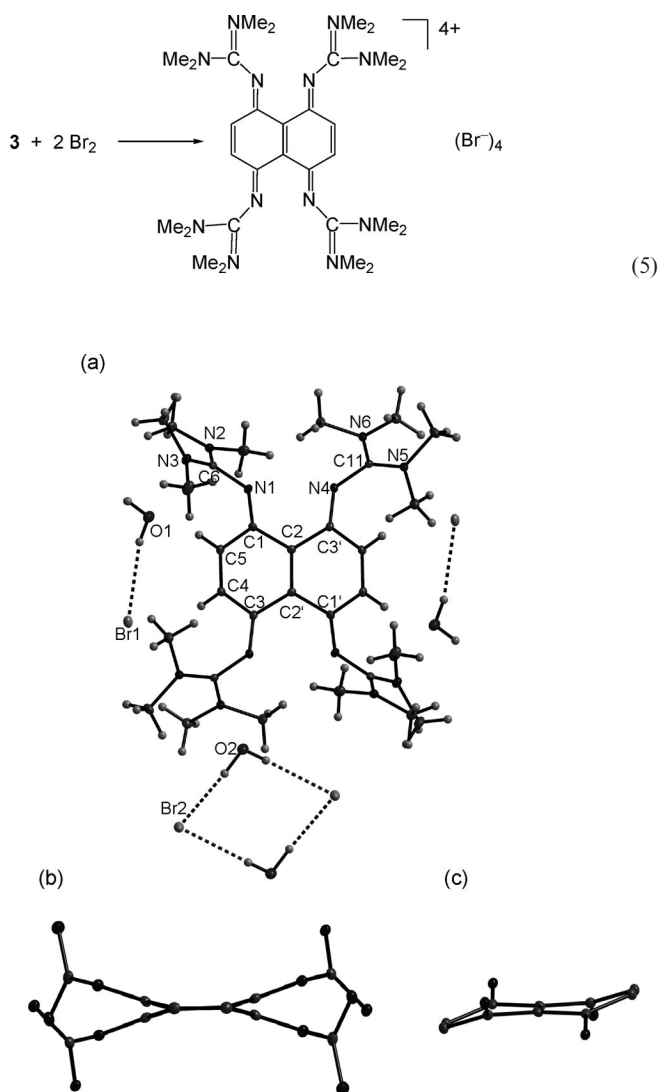
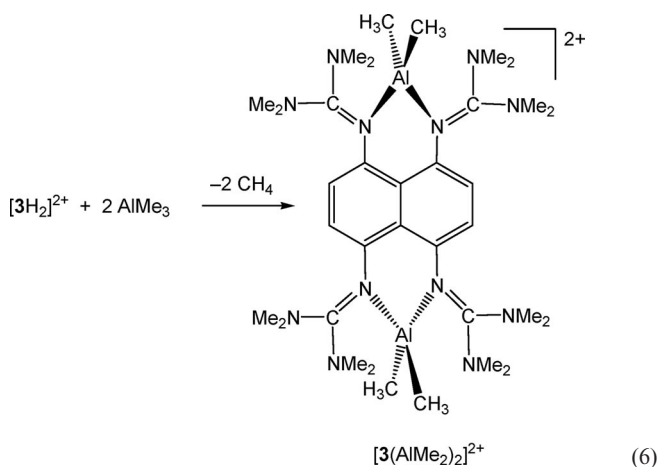


Figure 7. (a) Molecular structure of **[3]Br<sub>4</sub>·4H<sub>2</sub>O** as derived from X-ray diffraction; thermal ellipsoids are drawn at the 50% probability level. (b and c) Illustration of the nonplanarity of the central C<sub>10</sub>H<sub>4</sub> unit; all hydrogen atoms were omitted for sake of clarity. In (b) the guanidine CH<sub>3</sub> groups and in (c) the C(NMe<sub>2</sub>)<sub>2</sub> units were also omitted to better see the chair-type conformation of the C<sub>10</sub> scaffold.

### Binuclear Metal Complexes with **3** as Ligand

Having analysed the response of the new tetraguanidine to protonation and oxidation, we next tested the possibility to use **3** as a ligand in binuclear metal complexes. We first decided to prepare a dicationic Al alkyl complex, because these complexes are useful benchmark systems to study dynamic behaviour.<sup>[31]</sup> We will see that the knowledge about the conformation adopted at low temperatures is important to appreciate the superexchange in paramagnetic complexes of **3**. Reaction between  $[3H_2]^{2+}[BPh_4]_2$  and an excess amount of  $AlMe_3$  at 60 °C yielded, with elimination of two equivalents of methane, the dicationic complex  $[3(AlMe_2)_2]^{2+}$  [see Equation (6)]. The mass spectra (FAB) confirmed that Al has coordinated to both sides of **3**.



Crystals of  $[3(AlMe_2)_2][BPh_4]_2$  suitable for XRD analysis were obtained by layering of a  $CH_3CN$  solution with toluene. The unit cell of the crystal contained two slightly different  $[3(AlMe_2)_2]^{2+}$  complex dicationic units. Figure 8 illustrates the structure of the binuclear Al complex from two perspectives (see Table S6 in the Supporting Information for a list of structural parameters). The Al–C and Al–N distances are 195.9(3)/196.3(3) and 190.8(2)/191.6(2) pm, respectively, for the unit depicted in Figure 8. For comparison, the recently synthesised mononuclear salt  $[5(BPh_4)]$  (see Scheme 3) features Al–C and Al–N bond lengths of 197.0(4)/196.4(3) and 190.7(2)/192.0(2) pm, respectively.<sup>[32]</sup> With 90.74(9)°, the angle N1–Al1–N4 is significantly smaller than the angle C16–Al1–C17 [122.04(14)°]. The Al atoms are located at opposite sides of the plane defined by the naphthalene group [*trans*-type conformation, with the Al atoms being 96.2 or 84.4 pm (for the two slightly different molecules in the unit cell) below and above this plane, respectively]. The  $^1H$  NMR spectrum showed only one signal due to the methyl groups attached to the Al atoms at  $\delta = -0.89$  ppm. At low temperatures this signal splits into two (see Supporting Information). The presence of only one signal due to the methyl group in the  $^1H$  NMR spectra indicates that the metal moves fast relative to the NMR time

scale from one side to the other at room temperature. At very low temperatures, this movement is frozen and consequently two signals appear.

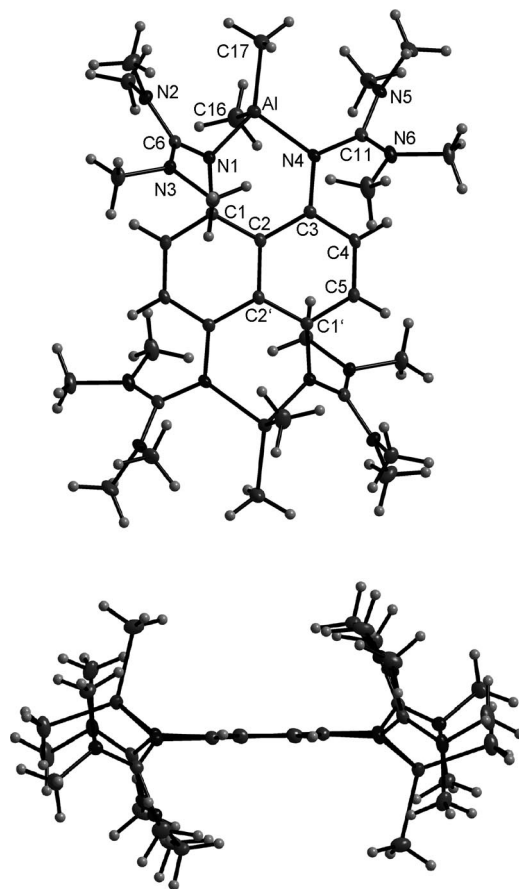
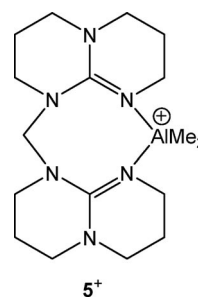


Figure 8. Molecular structure of  $[3(AlMe_2)_2](BPh_4)_2$  (only the cationic part is shown). Thermal ellipsoids are drawn at the 50% probability level.



Scheme 3.

To further evaluate the properties of the new ligand, we prepared the first paramagnetic transition metal complex of **3**, namely,  $3(CoCl_2)_2$  [see Equation (7)]. For comparison, we also prepared the corresponding complex **2**( $CoCl_2$ )<sub>2</sub>. The structures of both complexes as derived from X-ray diffraction experiments are visualised in Figures 9 and 10. Like in the previously discussed dicationic Al dimethyl complex, the Co atoms in  $3(CoCl_2)_2$  are not in the same plane as the aromatic core, but adopt a *trans*-type conformation in which the Co atoms are 103.4 pm above and below this

plane. The Co atoms are separated by 805.7 pm. In contrast to the situation in  $3(\text{CoCl}_2)_2$ , the Co atoms in  $2(\text{CoCl}_2)_2$  are located in the plane of the  $\text{C}_6$  ring. With 795.2 pm, the Co...Co separation is smaller than in  $3(\text{CoCl}_2)_2$ . The Co–N distances in both complexes are similar [199.6(2) pm in  $3(\text{CoCl}_2)_2$  and 201.7(1) pm in  $2(\text{CoCl}_2)_2$ ]. The angle N–Co–N is slightly smaller in  $2(\text{CoCl}_2)_2$  (83.5 vs. 87.8°).

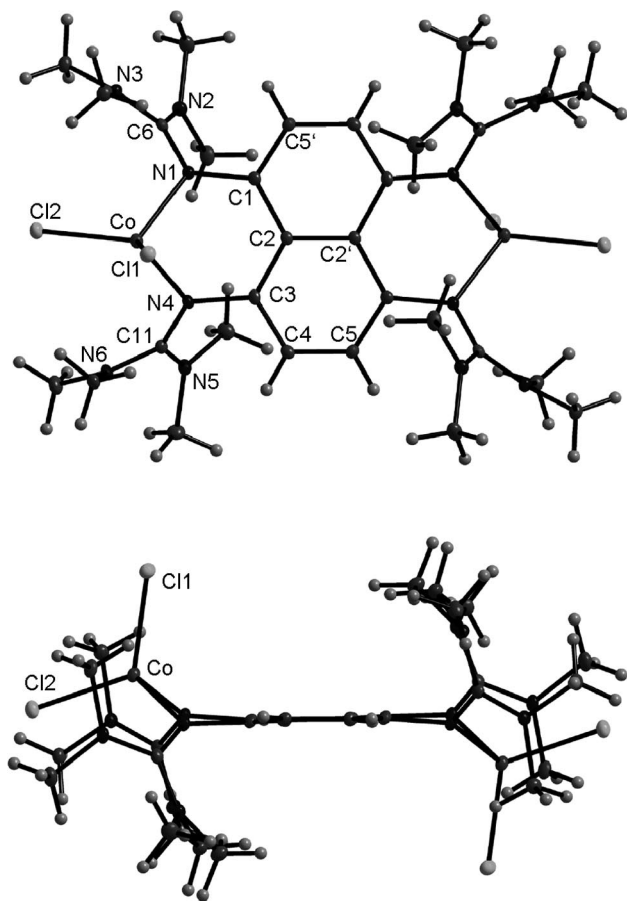
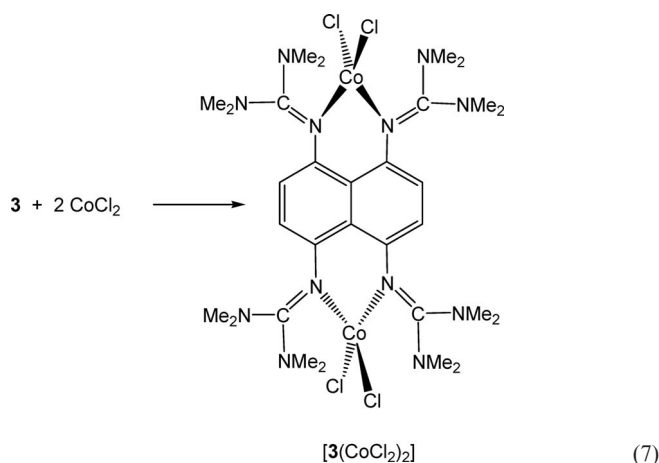


Figure 9. Molecular structure of  $3(\text{CoCl}_2)_2$  as derived from X-ray diffraction. Thermal ellipsoids are drawn at the 50% probability level.

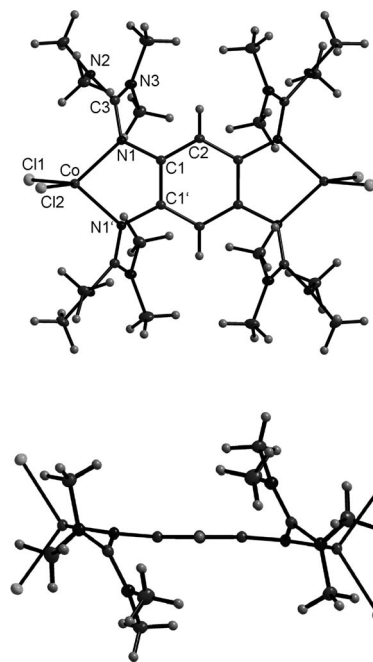


Figure 10. Molecular structure of  $2(\text{CoCl}_2)_2$  as derived from X-ray diffraction. Thermal ellipsoids are drawn at the 50% probability level.

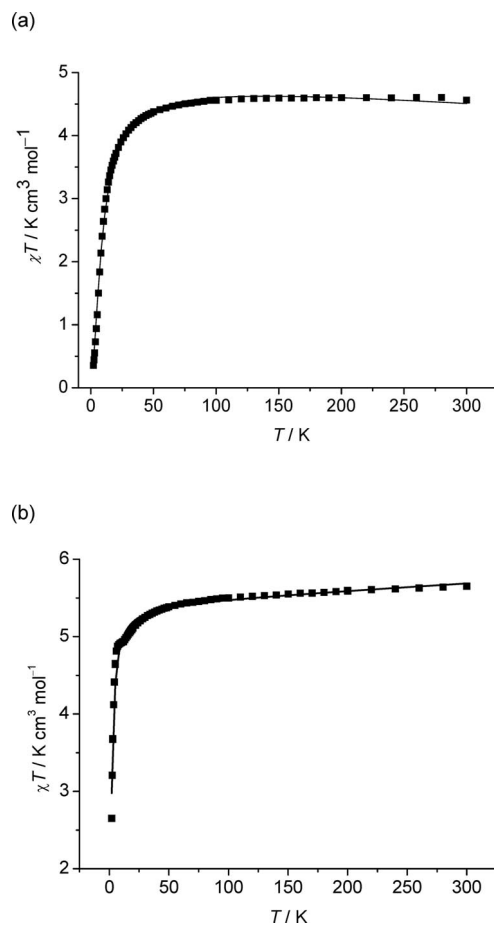


Figure 11. Plot of  $\chi T$  vs.  $T$  (at 500 Oe) for a polycrystalline powder sample of (a)  $3(\text{CoCl}_2)_2$  and (b)  $2(\text{CoCl}_2)_2$ .

Figure 11 shows the dependence of  $\chi T$  on the temperature  $T$  as derived from SQUID magnetic data for polycrystalline powder samples of **3**(CoCl<sub>2</sub>)<sub>2</sub> and also **2**(CoCl<sub>2</sub>)<sub>2</sub>. The curves can be fitted with the standard analytical expression for a coupled  $S = 3/2$  dimer [Equation (8),  $H = -2JS_1S_2$ ], providing values for  $g$ ,  $J$  and  $TIP$  (the temperature-independent paramagnetism). However, it has to be stressed that this equation neglects zero-field splitting, which certainly is important in this case. We obtained  $g = 2.3$ ,  $J = -1.5 \text{ cm}^{-1}$  and  $TIP = 136 \times 10^{-5} \text{ emu mol}^{-1}$  for complex **3**(CoCl<sub>2</sub>)<sub>2</sub> ( $\Theta = 0 \text{ K}$ ). The negative sign of  $J$  indicates antiferromagnetic coupling. However, the absolute value of  $J$  is very small, indicating that the superexchange through **3** is extremely weak. In the case of **2**(CoCl<sub>2</sub>)<sub>2</sub>, a fit was achieved with  $g = 2.4$ ,  $J = -0.3 \text{ cm}^{-1}$  and  $TIP = 92 \times 10^{-5} \text{ emu mol}^{-1}$ . For comparison, in [(TPyA)Co<sup>II</sup>(DBQ<sup>2-</sup>)Co<sup>II</sup>(TPyA)](BF<sub>4</sub>)<sub>2</sub> [TPyA = tris(2-pyridylmethyl)amine, DBQ<sup>2-</sup> = 2,5-di-*tert*-butyl-3,6-dihydroxy-1,4-benzoquinonate] a value of  $J = -2.2 \text{ cm}^{-1}$  was obtained by using the same fit formula.<sup>[33]</sup>

$$\chi = \left[ \frac{Ng^2\mu^2}{k_B(T-\Theta)} \right] \cdot \left[ \frac{2\exp\left(\frac{2J}{k_BT}\right) + 10\exp\left(\frac{6J}{k_BT}\right) + 28\exp\left(\frac{12J}{k_BT}\right)}{1 + 3\exp\left(\frac{2J}{k_BT}\right) + 5\exp\left(\frac{6J}{k_BT}\right) + 7\exp\left(\frac{12J}{k_BT}\right)} \right] + TIP \quad (8)$$

## Conclusions

Herein we reported on the protonation, oxidation and coordination chemistry of new aromatic tetraguanidine **3**. There are important differences between the chemistry of **3** and **2**, which can be summarised as follows: In difference to **2**, **3** represents a proton sponge. However, in difference to **4**, a nonsymmetric N–H···N bridge is adopted. Whereas **2** can only be oxidised with I<sub>2</sub> or Br<sub>2</sub> to dication, **3**<sup>2+</sup> as well as **3**<sup>4+</sup> can be obtained by reaction of **3** with I<sub>2</sub> or Br<sub>2</sub>, respectively. Both **2** and **3** can be used as ligands in dinuclear metal complexes. However, the geometry differs. Hence, in complexes of **2** the metal ions are generally located in the plane defined by the C<sub>6</sub> ring. In contrast, the metal ions in complexes of **3** are largely displaced from the plane of the C<sub>10</sub> rings (by 103.4 pm). A plot of the magnetic susceptibility  $\chi$  in dependence of the temperature (see Supporting Information) shows a maximum at  $T = 9.5 \text{ K}$  in the case of **3**(CoCl<sub>2</sub>)<sub>2</sub>. For **2**(CoCl<sub>2</sub>)<sub>2</sub> this maximum is absent. Magnetic exchange in both complexes seems to be very weak.

Future work will focus on (1) the evaluation of the influence of the coordination mode and symmetry of the magnetic orbitals on the magnetic properties in paramagnetic complexes; (2) changes in the magnetic coupling caused by oxidation of the tetraguanidine electron donor ligands; (3) magnetic coupling in binuclear complexes of other paramagnetic metals and (4) synthesis of coordination polymers of different dimensionalities by introduction of a second bridging ligand.

## Experimental Section

**General:** All experiments were carried out by using standard Schlenk techniques. The starting compounds 1,5-dinitronaphthalene and SnCl<sub>2</sub> were purchased from Aldrich and Strem, respectively. In addition, the following chemicals were used as delivered: tetramethyl urea (Aldrich, 99%), oxalyl chloride (Aldrich, 98%), AlMe<sub>3</sub> (Aldrich, 2 M in toluene, 97%), CoCl<sub>2</sub> (Acros Organics, anhydrous, 97%), NH<sub>4</sub>PF<sub>6</sub> (Fluka, 98%). NMR spectra were recorded with a Bruker DBX 200 and an AVII 400 spectrometer at a temperature of 23 °C and referenced to known standards; IR spectra were recorded with a Bruker Vertex 80v spectrometer. A Perkin–Elmer Lambda 19 spectrometer was used for UV/Vis, and an EG&G Princeton 273 apparatus for the CV measurements. Magnetic measurements were made with a Quantum Design MPMS-XL-5 apparatus.

**Tetrakis(tetramethylguanidino)naphthalene (3):** 1,5-Dinitronaphthalene (4.90 g, 22.5 mmol) was added to a solution of fuming nitric acid (14 mL) and concentrated sulfuric acid (12.5 mL). The reaction mixture was kept at 20 °C during the addition. Subsequently, the reaction mixture was slowly heated to 80 °C and kept there for 2 h. After cooling the reaction mixture to 5 °C, it was filtered to give a mixture of the two isomers 1,4,5,8- and 1,3,5,8-tetranitronaphthalene. 1,4,5,8-Tetranitronaphthalene was separated from its isomer by filtration from hot ethanol and then recrystallised from acetone. Yield of 1,4,5,8-tetranitronaphthalene: 1.814 g (52.4%). <sup>1</sup>H NMR (199.92 MHz, DMSO):  $\delta = 8.83$  (s) ppm. Then a suspension of 1,4,5,8-tetranitronaphthalene (1.814 g, 5.90 mmol) in ethanol (60 mL) was added to a solution of SnCl<sub>2</sub> (22.4 g, 118 mmol, 20 equiv.) dissolved in concentrated HCl (90 mL). The mixture was stirred for 2.5 h at 40 °C. After cooling, the volume of the mixture was condensed to 100 mL. The product precipitated from this solution. The solution was filtered off and the product dried under vacuum. Yield of 1,4,5,8-tetraaminonaphthalene complexed with SnCl<sub>2</sub>: 2.27 g (86.2%). <sup>1</sup>H NMR (199.92 MHz, DMSO):  $\delta = 4.422$  (s), 6.847–7.357 (m) ppm.

**Tetramethylchloroformamidinium Chloride:** Prepared as outlined above. Oxalyl chloride (11 mL, 127.9 mmol) was added dropwise to a solution of *N,N,N',N'*-tetramethyl urea (3 mL, 25.4 mmol) in dry CHCl<sub>3</sub> (15 mL). The reaction mixture was stirred for 16 h under reflux under an inert atmosphere. After removal of the solvent under vacuum, 2-chloro-1,1,3,3-tetramethylformamidinium chloride was washed with Et<sub>2</sub>O (15 mL), then dissolved in CH<sub>3</sub>CN (50 mL) and added slowly and dropwise to a CH<sub>3</sub>CN solution (30 mL) containing the tetraamino salt (2.27 g, 5.08 mmol) and triethylamine (9.3 mL, 67.3 mmol) at 0 °C. After stirring the mixture for 2 h at the same temperature, the solvent was removed under vacuum. The precipitate was redissolved in 10% HCl (15 mL) and an excess amount of 25% NaOH (40 mL) was added whilst stirring to deprotonate the product. Subsequently, the solution was extracted three times with diethyl ether. The combined phases were dried with K<sub>2</sub>CO<sub>3</sub> and diethyl ether was removed under vacuum. The precipitate was washed with cooled acetonitrile to give **3** as a yellow powder. Needle-shaped crystals of **3** were grown from acetonitrile. Yield: 0.627 g (1.08 mmol, 21.3%). C<sub>32</sub>H<sub>55</sub>N<sub>13</sub> (621.890): calcd. C 61.81, H 8.92, N 29.29; found C 61.83, H 8.96, N 28.60. <sup>1</sup>H NMR (199.92 MHz, C<sub>6</sub>D<sub>6</sub>):  $\delta = 2.70$  (s, 48 H, CH<sub>3</sub>), 6.50 (s, 4 H) ppm. <sup>1</sup>H NMR (399.89 MHz, CD<sub>3</sub>CN):  $\delta = 2.66$  (s, 48 H, CH<sub>3</sub>), 6.02 (s, 4 H) ppm. <sup>1</sup>H NMR (199.92 MHz, CD<sub>2</sub>Cl<sub>2</sub>):  $\delta = 2.711$  (s, 48 H, CH<sub>3</sub>), 6.140 (s, 4 H) ppm. <sup>13</sup>C NMR (100.56 MHz, CD<sub>2</sub>Cl<sub>2</sub>):  $\delta = 154.26$ , 143.06, 125.15, 116.33 (CH), 39.76 (CH<sub>3</sub>) ppm. IR (CsI):  $\tilde{\nu} = 2999$  (w), 2930 (w), 2879 (w), 2802 (w), 1612 (vs), 1560 (vs), 1491 (s), 1460 (s), 1427 (s 1367vs), 1314 (w), 1236 (s), 1134

(vs), 1070 (w), 1024 (s), 945 (w), 886 (w), 835 (w), 821 (w), 705 (w), 657 (w)  $\text{cm}^{-1}$ . UV/Vis ( $\text{CH}_3\text{CN}$ ,  $c = 7.34 \times 10^{-5} \text{ mol L}^{-1}$ ):  $\lambda_{\text{max}}$  ( $\epsilon$ ) = 394 ( $2.47 \times 10^4$ ) nm. UV/Vis ( $\text{CH}_2\text{Cl}_2$ ,  $c = 8.65 \times 10^{-5} \text{ mol L}^{-1}$ ):  $\lambda_{\text{max}}$  ( $\epsilon$ ) = 393 ( $2.28 \times 10^4$ ) nm. UV/Vis ( $\text{H}_2\text{O}$ ,  $c = 10^{-4} \text{ mol L}^{-1}$ ):  $\lambda_{\text{max}}$  ( $\epsilon$ ) = 404 ( $0.95 \times 10^4$ ), 245 ( $2.95 \times 10^4$ ) nm. MS (FAB):  $m/z$  (%) = 581.6 (100)  $[\text{3H}]^+$ , 567.4 (9)  $[\text{3} - \text{CH}]^+$ , 536.5 (2)  $[\text{3} - \text{NMe}_2]^+$ , 468.4 (5)  $[\text{3} - \text{NC}(\text{NMe}_2)_2\text{H}_2]^+$ , 436.4 (18)  $[\text{3} - \text{NC}(\text{NMe}_2)_2 - 2\text{CH}_3]^+$ . MS (ESI):  $m/z$  (%) = 581.5 (20)  $[\text{3H}]^+$ , 468.3 (3)  $[\text{3} - \text{NC}(\text{NMe}_2)_2\text{H}_2]^+$ , 291.3 (100)  $[\text{3H}_2]^{2+}$ , 268.7 (18)  $[\text{3} - \text{NMe}_2\text{H}]^{2+}$ , 246.2 (7)  $[\text{3} - 2\text{NMe}_2]^{2+}$ , 234.6 (3)  $[\text{3} - \text{NC}(\text{NMe}_2)_2\text{H}_3]^{2+}$ . Crystal data for **3**:  $\text{C}_{30}\text{H}_{52}\text{N}_{12} \cdot \text{MeCN}$ ,  $M_r = 621.89$ ,  $0.30 \times 0.20 \times 0.15 \text{ mm}^3$ , monoclinic, space group  $P2_1/c$ ,  $a = 16.328(3) \text{ \AA}$ ,  $b = 16.441(3) \text{ \AA}$ ,  $c = 13.217(3) \text{ \AA}$ ,  $\beta = 100.95(3)^\circ$ ,  $V = 1789.9(6) \text{ \AA}^3$ ,  $Z = 4$ ,  $d_{\text{calcd.}} = 1.186 \text{ Mg m}^{-3}$ , Mo- $K_\alpha$  radiation (graphite monochromated,  $\lambda = 0.71073 \text{ \AA}$ ),  $T = 100 \text{ K}$ ,  $\theta_{\text{range}} 1.77$  to  $27.47^\circ$ . Reflections measured 15838, indep. 7970,  $R_{\text{int}} = 0.0423$ . Final  $R$  indices [ $I > 2\sigma(I)$ ]:  $R_1 = 0.0536$ ,  $wR_2 = 0.1605$ .

**[3H<sub>2</sub>][PF<sub>6</sub>]<sub>2</sub>**: A solution of  $\text{NH}_4\text{PF}_6$  (0.0163 g, 0.1 mmol) in  $\text{CH}_3\text{CN}$  (10 mL) was added to a solution of **3** (0.0290 g, 0.05 mmol) in  $\text{CH}_3\text{CN}$  (10 mL). The mixture was stirred for 1 h at room temperature. After 3 d orange crystals of  $[\text{3H}_2][\text{PF}_6]_2$  were obtained from this solution. They were washed with diethyl ether and dried in vacuo. Yield: 0.0356 g (0.04 mmol, 81.7%).  $\text{C}_{30}\text{H}_{54}\text{F}_{12}\text{N}_{12}\text{P}_2$  (872.306): calcd. C 41.30, H 6.20, N 19.26; found C 41.36, H 6.40, N 18.96.  $^1\text{H}$  NMR (399.89 MHz,  $\text{CD}_3\text{CN}$ ):  $\delta = 2.83$  (s, 48 H,  $\text{CH}_3$ ), 6.45 (s, 4 H), 14.45 (s, 2 H) ppm.  $^{13}\text{C}$  NMR (100.56 MHz,  $\text{CD}_3\text{CN}$ ):  $\delta = 159.09$ , 136.79, 120.04, 115.19 (CH), 39.44 ( $\text{CH}_3$ ) ppm.  $^{19}\text{F}$  NMR (376.27 MHz):  $\delta = -72.85$  [d,  $^2J(\text{F,P}) = 706.51 \text{ Hz}$ ,  $\text{PF}_6$ ] ppm.  $^{31}\text{P}$  NMR (161.88 MHz,  $\text{CD}_3\text{CN}$ ):  $\delta = -144.61$  [sept,  $J(\text{P,F}) = 706.52 \text{ Hz}$ ,  $\text{PF}_6$ ] ppm. UV/Vis ( $\text{CH}_3\text{CN}$ ,  $c = 5.34 \times 10^{-5} \text{ mol L}^{-1}$ ):  $\lambda_{\text{max}}$  ( $\epsilon$ ) = 414 ( $1.84 \times 10^4$ ), 248 ( $4.83 \times 10^4$ ) nm. UV/Vis ( $\text{H}_2\text{O}$ ,  $c = 4.58 \times 10^{-5} \text{ mol L}^{-1}$ ):  $\lambda_{\text{max}}$  ( $\epsilon$ ) = 380 ( $0.79 \times 10^4$ ), 239 ( $2.12 \times 10^4$ ) nm. MS (ESI):  $m/z$  (%) = 873.4 (7)  $[(\text{3} + 2\text{PF}_6^-)\text{H}_3]^+$ , 727.4 (100)  $[(\text{3} + \text{PF}_6^-)\text{H}_2]^+$ , 291.2 (57)  $[\text{3H}_2]^{2+}$  nm. IR (CsI):  $\tilde{\nu} = 3005$  (w), 2935 (w), 2896 (w), 2809 (w), 1602 (s), 1561 (s), 1476 (s), 1429 (s), 1410 (s 1363s), 1319 (w), 1233 (w), 1171 (s), 1070 (w), 1042 (w), 949 (w), 840 (vs), 705 (w), 657 (w), 556 (vs)  $\text{cm}^{-1}$ . Crystal data for  $[\text{3H}_2][\text{PF}_6]_2$ :  $\text{C}_{30}\text{H}_{54}\text{F}_{12}\text{N}_{12}\text{P}_2$ ,  $M_r = 872.79$ ,  $0.30 \times 0.20 \times 0.20 \text{ mm}^3$ , triclinic, space group  $P\bar{1}$ ,  $a = 14.226(3) \text{ \AA}$ ,  $b = 14.679(3) \text{ \AA}$ ,  $c = 21.284(4) \text{ \AA}$ ,  $\alpha = 88.98(3)^\circ$ ,  $\beta = 81.35(3)^\circ$ ,  $\gamma = 70.27(3)^\circ$ ,  $V = 4133.6(14) \text{ \AA}^3$ ,  $Z = 4$ ,  $d_{\text{calcd.}} = 1.402 \text{ Mg m}^{-3}$ , Mo- $K_\alpha$  radiation (graphite monochromated,  $\lambda = 0.71073 \text{ \AA}$ ),  $T = 100 \text{ K}$ ,  $\theta_{\text{range}} 1.47$  to  $27.46^\circ$ . Reflections measured 18743, indep. 18743,  $R_{\text{int}} = 0.1023$ . Final  $R$  indices [ $I > 2\sigma(I)$ ]:  $R_1 = 0.0705$ ,  $wR_2 = 0.1659$ .

**[3H<sub>4</sub>]Cl<sub>4</sub>**: A solution of HCl (1.25 M in ethanol, 0.12 mL, 0.15 mmol, 3 equiv.) was added slowly and dropwise to a solution of  $[\text{3H}_2](\text{PF}_6)_2$  (43.6 mg, 0.05 mmol) in  $\text{CH}_3\text{CN}$  (10 mL). During the addition of HCl the yellow colour of the solution disappeared. In one week colourless crystals of  $[\text{3H}_4]\text{Cl}_4$  were obtained from this solution at  $-18^\circ\text{C}$ . Yield: 0.0207 g (0.029 mmol, 57.2%).  $^1\text{H}$  NMR (399.89 MHz,  $\text{CD}_3\text{CN}$ ):  $\delta = 2.937$  (s, 48 H,  $\text{CH}_3$ ), 7.049 (s, 4 H), 10.837 (s, 4 H) ppm.  $^{13}\text{C}$  NMR (100.56 MHz,  $\text{CD}_3\text{CN}$ ):  $\delta = 160.19$ , 132.81, 125.84, 124.05, 40.64 ( $\text{CH}_3$ ) ppm. IR (CsI):  $\tilde{\nu} = 3025$  (w), 2939 (w), 2933 (w), 2790 (w), 1638 (s), 1547 (s), 1468 (s), 1412 (s), 1363 (s 1297s), 1228 (w), 1171 (w), 1068 (s), 957 (w), 767 (w), 677 (w)  $\text{cm}^{-1}$ . Crystal data for  $[\text{3H}_4]\text{Cl}_4 \cdot 8\text{H}_2\text{O}$ :  $\text{C}_{30}\text{H}_{72}\text{Cl}_4\text{N}_{12}\text{O}_8$ ,  $M_r = 870.80$ ,  $0.40 \times 0.30 \times 0.25 \text{ mm}^3$ , monoclinic, space group  $P2_1/n$ ,  $a = 12.960(3) \text{ \AA}$ ,  $b = 12.961(3) \text{ \AA}$ ,  $c = 14.864(3) \text{ \AA}$ ,  $\beta = 114.10(3)^\circ$ ,  $V = 2279.1(10) \text{ \AA}^3$ ,  $Z = 2$ ,  $d_{\text{calcd.}} = 1.269 \text{ Mg m}^{-3}$ , Mo- $K_\alpha$  radiation (graphite-monochromated,  $\lambda = 0.71073 \text{ \AA}$ ),  $T = 100 \text{ K}$ ,  $\theta_{\text{range}} 1.76$  to  $30.05^\circ$ . Reflections measured 12930, indep. 6669,  $R_{\text{int}} = 0.0538$ . Final  $R$  indices [ $I > 2\sigma(I)$ ]:  $R_1 = 0.0504$ ,  $wR_2 = 0.1416$ .

**3(I<sub>3</sub>)<sub>2</sub>**: A solution of  $\text{I}_2$  (0.016 g, 0.063 mmol) in  $\text{CH}_3\text{CN}$  (5 mL) was added to a solution of **3** (0.0174 g, 0.03 mmol) in  $\text{CH}_3\text{CN}$  (5 mL). The solution turned to a deep-green colour. In one week black crystals of **3(I<sub>3</sub>)<sub>2</sub>** were obtained from this solution at  $-18^\circ\text{C}$ . Yield: 0.021 g (0.016 mmol, 52.2%).  $^1\text{H}$  NMR (199.92 MHz,  $\text{CD}_3\text{CN}$ ):  $\delta = 2.89$  (s, 48 H,  $\text{CH}_3$ ), 6.62 (s, 4 H) ppm.  $^{13}\text{C}$  NMR (100.56 MHz,  $\text{CD}_3\text{CN}$ ):  $\delta = 163.32$ , 156.14, 131.68, 116.14 (CH), 39.85 ( $\text{CH}_3$ ) ppm. IR (CsI):  $\tilde{\nu} = 3019$  (w), 2968 (w), 2932 (w), 2858 (w), 1632 (vs), 1592 (m), 1556 (w), 1529 (s), 1467 (m), 1407 (s), 1363 (w), 1270 (s), 1166 (s), 1070 (w), 1040 (w), 886 (w), 836 (w), 783 (w), 657 (w), 690 (w)  $\text{cm}^{-1}$ . Crystal data for **3(I<sub>3</sub>)<sub>2</sub>**:  $\text{C}_{30}\text{H}_{52}\text{I}_6\text{N}_{12}$ ,  $M_r = 1342.24$ ,  $0.25 \times 0.10 \times 0.05 \text{ mm}^3$ , monoclinic, space group  $C2/c$ ,  $a = 25.760(5) \text{ \AA}$ ,  $b = 7.7160(15) \text{ \AA}$ ,  $c = 22.991(5) \text{ \AA}$ ,  $\beta = 106.31(3)^\circ$ ,  $V = 4385.9(15) \text{ \AA}^3$ ,  $Z = 4$ ,  $d_{\text{calcd.}} = 2.033 \text{ Mg m}^{-3}$ , Mo- $K_\alpha$  radiation (graphite-monochromated,  $\lambda = 0.71073 \text{ \AA}$ ),  $T = 100 \text{ K}$ ,  $\theta_{\text{range}} 1.65$  to  $27.54^\circ$ . Reflections measured 36714, indep. 5031,  $R_{\text{int}} = 0.0630$ . Final  $R$  indices [ $I > 2\sigma(I)$ ]:  $R_1 = 0.0317$ ,  $wR_2 = 0.0663$ .

**3(Br<sub>4</sub>)**:  $\text{Br}_2$  (0.003 mL, 0.06 mmol) was added to a solution of **3** (0.0174 g, 0.03 mmol) in  $\text{CH}_3\text{CN}$  (5 mL). The solution turned to a deep-brown colour. In 1 d plate-like crystals of  $\text{LBr}_4$  were obtained from this solution at  $-18^\circ\text{C}$ . Yield: 0.019 g (0.021 mmol, 70.4%).  $^1\text{H}$  NMR (199.92 MHz,  $\text{CD}_3\text{CN}$ ):  $\delta = 3.282$  (s, 48 H,  $\text{CH}_3$ ), 7.100 (s, 4 H) ppm.  $^1\text{H}$  NMR (399.89 MHz,  $\text{CD}_3\text{CN}$ ):  $\delta = 3.170$  (s, 48 H,  $\text{CH}_3$ ), 7.072 (s, 4 H);  $^{13}\text{C}$  (100.56 MHz,  $\text{CD}_3\text{CN}$ ):  $\delta = 162.91$ , 159.09, 130.51, 116.47 (CH), 42.05 ( $\text{CH}_3$ ) ppm. IR (CsI):  $\tilde{\nu} = 3028$  (w), 2967 (w), 2930 (w), 1632 (vs), 1594 (m), 1524 (w), 1455 (m), 1401 (s), 1357 (w), 1275 (s), 1188 (w), 1164 (s), 1052 (w), 1035 (w), 883 (w), 827 (w), 790 (w), 688 (w)  $\text{cm}^{-1}$ . MS (FAB):  $m/z$  (%) = 580.8 (22)  $[\text{3}]^+$ , 462.9 (95)  $[\text{3} - \text{NC}(\text{NMe}_2)_2 - 4\text{H}]^+$ , 432.7 (100)  $[\text{3} - \text{NC}(\text{NMe}_2)_2 - 2\text{CH}_3 - 4\text{H}]^+$ . Crystal data for **3(Br<sub>4</sub>)**:  $\text{C}_{30}\text{H}_{52}\text{Br}_4\text{N}_{12} \cdot 4\text{H}_2\text{O}$ ,  $M_r = 972.54$ ,  $0.30 \times 0.30 \times 0.20 \text{ mm}^3$ , monoclinic, space group  $P2_1/c$ ,  $a = 13.420(3) \text{ \AA}$ ,  $b = 14.285(3) \text{ \AA}$ ,  $c = 11.025(2) \text{ \AA}$ ,  $\beta = 101.94(3)^\circ$ ,  $V = 2067.8(7) \text{ \AA}^3$ ,  $Z = 2$ ,  $d_{\text{calcd.}} = 1.562 \text{ Mg m}^{-3}$ , Mo- $K_\alpha$  radiation (graphite monochromated,  $\lambda = 0.71073 \text{ \AA}$ ),  $T = 100 \text{ K}$ ,  $\theta_{\text{range}} 2.11$  to  $30.12^\circ$ . Reflections measured 34736, indep. 6079,  $R_{\text{int}} = 0.0565$ . Final  $R$  indices [ $I > 2\sigma(I)$ ]:  $R_1 = 0.0373$ ,  $wR_2 = 0.0904$ .

**[3(AlMe<sub>2</sub>)<sub>2</sub>][BPh<sub>4</sub>]<sub>2</sub>**: To a suspension of  $[\text{3H}_2][\text{PF}_6]_2$  (0.150 g, 17 mmol) in THF (50 mL) was added  $\text{NaBPh}_4$  (0.236 g, 0.68 mmol, 4 equiv.). The mixture was stirred under reflux for 2 h. Subsequently, the solution was filtered off and the product of the reaction was dissolved in  $\text{CH}_3\text{CN}$  (20 mL). Then, a solution of  $\text{Al}(\text{CH}_3)_3$  (2 M in toluene, 0.68 mL, 1.36 mmol, 8 equiv.) was added dropwise to this solution. The mixture was stirred for 12 h at  $60^\circ\text{C}$ . After removing the solvent under vacuum the precipitate was washed three times with THF. A yellow powder of  $[\text{3(AlMe}_2)_2][\text{BPh}_4]_2$  was obtained. Yield: 0.186 g (0.14 mmol, 82%). Needle-shaped crystals of this compound were grown by layering  $\text{CH}_3\text{CN}$  solution with toluene at room temperature.  $^1\text{H}$  NMR (199.92 MHz,  $\text{CD}_3\text{CN}$ ):  $\delta = -0.89$  (s, 12 H,  $\text{Al-CH}_3$ ), 2.73 (s, 24 H,  $\text{CH}_3$ ), 2.95 (s, 24 H,  $\text{CH}_3$ ), 6.52 (s, 4 H), 6.842 (t,  $J = 6.53 \text{ Hz}$ , 8 H), 7.00 (t,  $J = 6.57 \text{ Hz}$ , 16 H), 7.28 (s, 16 H) ppm.  $^{13}\text{C}$  NMR (100.56 MHz,  $\text{CD}_3\text{CN}$ ):  $\delta = 165.39$  (CN), 164.06, 163.57, 137.87, 135.76, 125.60, 122.92, 121.79, 119.81 ( $\text{C}_{\text{arom}}$ ), 40.76, 39.74 ( $\text{CH}_3$ ), 25.28 ppm.  $^{11}\text{B}$  NMR (128.30 MHz,  $\text{CD}_3\text{CN}$ ):  $\delta = -18.60$  (s) ppm.  $^{27}\text{Al}$  NMR (104.20 MHz,  $\text{CD}_3\text{CN}$ ):  $\delta = 156.0$  (s) ppm. IR (CsI):  $\tilde{\nu} = 3051$  (w), 3005 (w), 2940 (w), 2896 (w), 2800 (w), 1577 (vs), 1527 (vs), 1466 (s), 1406 (s), 1380 (s 1312s), 1288 (s), 1232 (w), 1193 (w), 1163 (s), 1058 (w), 965 (w), 891 (ms), 846 (s), 812 (w), 736 (s), 706 (vs), 677 (vs), 612 (ms), 576 (w), 480 (w), 428 (w)  $\text{cm}^{-1}$ . UV/Vis ( $\text{CH}_3\text{CN}$ ,  $c = 6.42 \times 10^{-5} \text{ mol L}^{-1}$ ):  $\lambda_{\text{max}}$  ( $\epsilon$ ) = 396 ( $0.67 \times 10^4$ ), 244 ( $2.76 \times 10^4$ ) nm. MS (FAB):  $m/z$  (%) = 679.3 (10)  $[\text{3Al}_2\text{Me}_3]^+$ , 637.4 (55)

$[3\text{AlMe}_2]^+$ , 581.3 (48)  $[3\text{H}]^+$ , 436.4 (10)  $[3 - \text{NC}(\text{NMe}_2)_2 - 2\text{CH}_3]^+$ , 355.2 (100)  $\{[3 - 2\text{NC}(\text{NMe}_2)_2]\text{H}_3\}^+$ . Crystal data for  $[3(\text{AlMe}_2)_2][\text{BPh}_4] \cdot 0.4\text{CH}_3\text{CN}$ :  $\text{C}_{82.80}\text{H}_{105.20}\text{Al}_2\text{B}_2\text{N}_{12.40}$ ,  $M_r = 1349.78$ ,  $0.40 \times 0.20 \times 0.20 \text{ mm}^3$ , triclinic, space group  $P\bar{1}$ ,  $a = 15.726(3) \text{ \AA}$ ,  $b = 16.187(3) \text{ \AA}$ ,  $c = 19.191(4) \text{ \AA}$ ,  $\alpha = 96.70(3)^\circ$ ,  $\beta = 99.56(3)^\circ$ ,  $\gamma = 118.22(3)^\circ$ ,  $V = 4136.0(2) \text{ \AA}^3$ ,  $Z = 2$ ,  $d_{\text{calcd.}} = 1.084 \text{ Mg m}^{-3}$ , Mo- $K_\alpha$  radiation (graphite-monochromated,  $\lambda = 0.71073 \text{ \AA}$ ),  $T = 100 \text{ K}$ ,  $\theta_{\text{range}} 1.47$  to  $28.00^\circ$ . Reflections measured 43866, indep. 19975,  $R_{\text{int}} = 0.0388$ . Final  $R$  indices  $[I > 2\sigma(I)]$ :  $R_1 = 0.0737$ ,  $wR_2 = 0.2212$ .

**3(CoCl<sub>2</sub>)<sub>2</sub>**: Compound **3** (0.070 g, 0.12 mmol) was added to a solution of  $\text{CoCl}_2$  (0.0268 g, 0.21 mmol) in  $\text{CH}_3\text{CN}$  (20 mL). The mixture was stirred under reflux for 4 h. After cooling the solution, the green precipitate of  $3\text{Co}_2\text{Cl}_4$  was filtered off and washed three times with  $\text{CH}_2\text{Cl}_2$ . Yield: 0.0659 g (0.078 mmol, 74.7%). The dark-green crystals of the compound were obtained by layering  $\text{CH}_3\text{CN}$  solution with toluene at room temperature.  $\text{C}_{30}\text{H}_{52}\text{Cl}_4\text{Co}_2\text{N}_{12}$  (840.80): calcd. C 42.85, H 6.25, N 19.99; found C 42.60, H 6.26, N 19.71. IR (CsI):  $\tilde{\nu} = 3015$  (w), 2928 (w), 2882 (w), 2790 (w), 1555 (vs), 1529 (vs), 1458 (s), 1401 (vs), 1371 (vs), 1318 (s), 1283 (vs), 1238 (w), 1190 (w), 1155 (vs), 1109 (w), 1049 (m), 894 (s), 860 (m), 820 (m), 772 (w), 712 (m), 635 (w)  $\text{cm}^{-1}$ . UV/Vis ( $\text{CH}_3\text{CN}$ ,  $c = 5.73 \times 10^{-5} \text{ mol L}^{-1}$ ):  $\lambda_{\text{max}}$  ( $\epsilon$ ) = 451 ( $1.88 \times 10^4$ ), 376 ( $1.50 \times 10^4$ ) nm. MS (ESI):  $m/z$  (%) = 803.2 (14)  $[3\text{Co}_2\text{Cl}_3]^+$ , 710.3 (100)  $[3\text{CoCl}_2]^+$ . Crystal data for  $[3(\text{CoCl}_2)_2] \cdot 2\text{CH}_3\text{CN}$ :  $\text{C}_{34}\text{H}_{58}\text{Cl}_4\text{Co}_2\text{N}_{14}$ ,  $M_r = 922.60$ ,  $0.20 \times 0.20 \times 0.12 \text{ mm}^3$ , triclinic, space group  $P\bar{1}$ ,  $a = 9.4950(19) \text{ \AA}$ ,  $b = 11.382(2) \text{ \AA}$ ,  $c = 11.438(2) \text{ \AA}$ ,  $\alpha = 63.81(3)^\circ$ ,  $\beta = 74.29(3)^\circ$ ,  $\gamma = 78.11(3)^\circ$ ,  $V = 1062.4(5) \text{ \AA}^3$ ,  $Z = 1$ ,  $d_{\text{calcd.}} = 1.442 \text{ Mg m}^{-3}$ , Mo- $K_\alpha$  radiation (graphite-monochromated,  $\lambda = 0.71073 \text{ \AA}$ ),  $T = 100 \text{ K}$ ,  $\theta_{\text{range}} 2.00$  to  $30.00^\circ$ . Reflections measured 16691, indep. 6172,  $R_{\text{int}} = 0.0555$ . Final  $R$  indices  $[I > 2\sigma(I)]$ :  $R_1 = 0.0465$ ,  $wR_2 = 0.1110$ .

**2(CoCl<sub>2</sub>)<sub>2</sub>**: Compound **2** (0.111 g, 0.2 mmol) was dissolved in  $\text{CH}_3\text{CN}$  (8 mL) at  $60^\circ\text{C}$ . The obtained solution was added to a solution of  $\text{CoCl}_2$  (65.6 mg, 0.5 mmol) in  $\text{CH}_3\text{CN}$  (6 mL). The dark-green reaction mixture was stirred for 30 min at  $70^\circ\text{C}$ . After the solvent was removed in vacuo, the solid was redissolved in  $\text{CH}_2\text{Cl}_2$  (16 mL). Then, *n*-hexane (8 mL) was added. At  $-20^\circ\text{C}$ , the product precipitates in the form of a dark green solid. One obtains 80.4 mg (0.1 mmol, yield 46%) of  $[2(\text{CoCl}_2)_2 \cdot \text{CH}_2\text{Cl}_2]$ , which can be recrystallised from  $\text{CH}_3\text{CN}$ .  $\text{C}_{27}\text{H}_{50}\text{Cl}_6\text{Co}_2\text{N}_{12}$  (875.37): calcd. C 37.05, H 5.99, N 19.20; found C 36.99, H 6.17, N 19.70. IR (CsI):  $\tilde{\nu} = 3009$  (w), 2943 (m), 2878 (w), 2797 (w), 1555 (vs), 1520 (vs), 1485 (s), 1481 (vs), 1331 (m), 1180 (m), 1157 (m), 1030 (m), 891 (m) 814 (m) 718 (m)  $\text{cm}^{-1}$ . MS (FAB):  $m/z$  (%) = 659 (8)  $[2\text{CoCl}_2]$ , 531 (52)  $[2(\text{H})]^+$ , 486 (27)  $[2 - \text{N}(\text{CH}_3)_2]$ . Crystal data for  $[2(\text{CoCl}_2)_2] \cdot \text{CH}_3\text{CN}$ :  $\text{C}_{30}\text{H}_{56}\text{Cl}_4\text{Co}_2\text{N}_{14}$ ,  $M_r = 872.55$ ,  $0.40 \times 0.40 \times 0.40 \text{ mm}^3$ , monoclinic, space group  $C2/m$ ,  $a = 16.794(3) \text{ \AA}$ ,  $b = 12.988(3) \text{ \AA}$ ,  $c = 9.6140(19) \text{ \AA}$ ,  $\beta = 99.82(3)^\circ$ ,  $V = 2066.3(7) \text{ \AA}^3$ ,  $Z = 2$ ,  $d_{\text{calcd.}} = 1.402 \text{ Mg m}^{-3}$ , Mo- $K_\alpha$  radiation (graphite-monochromated,  $\lambda = 0.71073 \text{ \AA}$ ),  $T = 100 \text{ K}$ ,  $\theta_{\text{range}} 1.99$  to  $32.09^\circ$ . Reflections measured 6924, indep. 3718,  $R_{\text{int}} = 0.0349$ . Final  $R$  indices  $[I > 2\sigma(I)]$ :  $R_1 = 0.0370$ ,  $wR_2 = 0.0973$ .

**X-ray Crystallographic Study:** Suitable crystals were taken directly out of the mother liquor, immersed in perfluorinated polyether oil, and fixed on top of a glass capillary. Measurements were made with a Nonius-Kappa CCD diffractometer with a low-temperature unit with the use of graphite-monochromated Mo- $K_\alpha$  radiation. The temperature was set to 100 K. The data collected were processed using the standard Nonius software.<sup>[34]</sup> All calculations were performed using the SHELXT-PLUS software package. Structures were solved by direct methods with the SHELXS-97 program and

refined with the SHELXL-97 program.<sup>[35,36]</sup> Graphical handling of the structural data during solution and refinement was performed with XPLA.<sup>[37]</sup> Atomic coordinates and anisotropic thermal parameters of non-hydrogen atoms were refined by full-matrix least-squares calculations. CCDC-729982 (for  $[3\text{H}_2][\text{PF}_6]_2$ ), -729983 (for **3**), -729984 [for  $3(\text{I}_3)_2$ ], -729985 (for  $[3\text{H}_4]\text{Cl}_4 \cdot 8\text{H}_2\text{O}$ ), -729986 [for  $[3(\text{AlMe}_2)_2][\text{BPh}_4]_2$ ], -740703 (for  $3\text{Br}_4 \cdot 4\text{H}_2\text{O}$ ), -740704 [for  $2(\text{CoCl}_2)_2$ ] and -740705 [for  $3(\text{CoCl}_2)_2$ ] contain the supplementary crystallographic data for this paper. These data can be obtained free of charge from The Cambridge Crystallographic Data Centre via [www.ccdc.cam.ac.uk/data\\_request/cif](http://www.ccdc.cam.ac.uk/data_request/cif).

**Supporting Information** (see also the footnote on the first page of this article): Selected structural parameters of **3**,  $[3\text{H}_2][\text{PF}_6]_2$ ,  $[3\text{H}_4]\text{Cl}_4 \cdot 8\text{H}_2\text{O}$ ,  $3(\text{I}_3)_2$ ,  $3\text{Br}_4 \cdot 4\text{H}_2\text{O}$ ,  $[3(\text{AlMe}_2)_2][\text{BPh}_4]_2$ ,  $3(\text{CoCl}_2)_2$  and  $2(\text{CoCl}_2)_2$  as derived from X-ray diffraction measurements; comparison of structural experimental and calculated parameters for  $[3\text{H}_2]^{2+}$  and  $[3\text{H}_4]^{4+}$ ; CV curves for **3**; VT  $^1\text{H}$  NMR of **3**; titration curve for **3** (5.0 mM) with 0.1 M HCl; UV/Vis spectra and IR spectra of **3**,  $[3\text{H}_2][\text{PF}_6]_2$  and  $3(\text{I}_3)_2$ ; plot of  $\chi$  vs.  $T$  for  $2(\text{CoCl}_2)_2$  and  $3(\text{CoCl}_2)_2$ .

## Acknowledgments

The authors thank the Deutsche Forschungsgemeinschaft (DFG) for continuous financial support.

- [1] J. Ferraris, D. O. Cowan, V. Walatka, J. H. Perlstein, *J. Am. Chem. Soc.* **1973**, *95*, 948–949.
- [2] T. A. Taton, P. Chen, *Angew. Chem.* **1996**, *108*, 1098–1100; *Angew. Chem. Int. Ed. Engl.* **1996**, *35*, 1011–1013.
- [3] R. D. Richardson, T. Wirth, *Chem. Unserer Zeit* **2008**, *42*, 190–191.
- [4] F. Schoenebeck, J. A. Murphy, S.-ze Zhou, Y. Uenoyama, Y. Miclo, T. Tuttle, *J. Am. Chem. Soc.* **2007**, *129*, 13368–13369.
- [5] J. A. Murphy, S.-ze Zhou, D. W. Thomson, F. Schoenebeck, M. Mahesh, S. R. Park, T. Tuttle, L. E. A. Berlouis, *Angew. Chem.* **2007**, *119*, 5270–5275; *Angew. Chem. Int. Ed. Engl.* **2007**, *46*, 5178–5183.
- [6] R. D. Richardson, T. Wirth, *Chem. Unserer Zeit* **2008**, *42*, 186–191.
- [7] G. P. McGlacken, T. A. Khan, *Angew. Chem.* **2008**, *120*, 1843–1847; *Angew. Chem. Int. Ed.* **2008**, *47*, 1819–1823.
- [8] A. Peters, E. Kaifer, H.-J. Himmel, *Eur. J. Org. Chem.* **2008**, 5907–5914.
- [9] T. Barth, C. Krieger, F. A. Neugebauer, H. A. Staab, *Angew. Chem.* **1991**, *103*, 1006–1008; *Angew. Chem. Int. Ed. Engl.* **1991**, *30*, 1028–1030.
- [10] A. Peters, C. Trumm, M. Reinmuth, D. Emeljanenko, E. Kaifer, H.-J. Himmel, *Eur. J. Inorg. Chem.* **2009**, 3791–3800.
- [11] a) U. Wild, O. Hübner, A. Maronna, M. Enders, E. Kaifer, H. Wadepohl, H.-J. Himmel, *Eur. J. Inorg. Chem.* **2008**, 4440–4447; b) D. Domide, C. Neuhäuser, E. Kaifer, H. Wadepohl, H.-J. Himmel, *Eur. J. Inorg. Chem.* **2009**, 2170–2178.
- [12] R. Schwesinger, *Nachr. Chem. Tech. Lab.* **1990**, *38*, 1214–1226; and references given therein.
- [13] S. Herres-Pawlis, A. Neuba, O. Seewald, T. Seshadri, H. Egold, U. Flörke, G. Henkel, *Eur. J. Org. Chem.* **2005**, 4879–4890.
- [14] F. T. Edelmann, *Adv. Organomet. Chem.* **2008**, *57*, 183–352.
- [15] S. Herres-Pawlis, *Nachr. Chem.* **2009**, *57*, 20–23.
- [16] S. Pohl, M. Harmjan, J. Schneider, W. Saak, G. Henkel, *J. Chem. Soc., Dalton Trans.* **2000**, 3473–3479.
- [17] D. Petrovic, L. M. R. Hill, P. G. Jones, W. B. Tolman, M. Tamm, *Dalton Trans.* **2008**, 887–894.
- [18] C. Würtele, E. Gaoutchenova, K. Harms, M. C. Holthausen, J. Sundermeyer, S. Schindler, *Angew. Chem.* **2006**, *118*, 3951–3954; *Angew. Chem. Int. Ed.* **2006**, *45*, 3867–3869.

- [19] a) D. Maiti, D.-H. Lee, K. Gaoutchenova, C. Würtele, M. C. Hothausen, A. A. N. Sarjeant, J. Sundermeyer, S. Schindler, K. D. Karlin, *Angew. Chem.* **2007**, *120*, 88–91; *Angew. Chem. Int. Ed.* **2007**, *47*, 82–85; b) M. P. Lanci, V. V. Smirnov, C. J. Cramer, E. V. Gauchenova, J. Sundermeyer, J. P. Roth, *J. Am. Chem. Soc.* **2007**, *129*, 14697–14709; c) D. Maiti, D.-H. Lee, K. Gaoutchenova, C. Würtele, M. C. Holthausen, A. A. N. Sarjeant, J. Sundermeyer, S. Schindler, K. D. Karlin, *Angew. Chem.* **2008**, *120*, 88–91; *Angew. Chem. Int. Ed.* **2008**, *47*, 82–85.
- [20] a) J. Börner, S. Herres-Pawlis, U. Flörke, K. Huber, *Eur. J. Inorg. Chem.* **2007**, 5645–5651; b) J. Börner, U. Flörke, K. Huber, A. Döring, D. Kuckling, S. Herres-Pawlis, *Chem. Eur. J.* **2009**, *15*, 2362–2376.
- [21] W. L. Hinze, L.-J. Liu, J. H. Fendler, *J. Chem. Soc. Perkin Trans. 2* **1975**, 1751–1767.
- [22] O. Dimroth, H. Roos, *Justus Liebigs Ann. Chem.* **1927**, 456, 177–192.
- [23] V. I. Sorokin, V. A. Ozeryanskii, A. F. Pozharskii, *Russ. J. Org. Chem. C S.* **2002**, *38*, 699–708.
- [24] V. Raab, J. Kipke, R. M. Gschwind, J. Sundermeyer, *Chem. Eur. J.* **2002**, *8*, 1682–1693.
- [25] A. Peters, U. Wild, O. Hübner, E. Kaifer, H.-J. Himmel, *Chem. Eur. J.* **2008**, *14*, 7813–7821.
- [26] a) T. Barth, C. Krieger, F. A. Neugebauer, H. A. Staab, *Angew. Chem.* **1991**, *103*, 1006–10088; *Angew. Chem. Int. Ed. Engl.* **1991**, *30*, 1028–1030; b) H. A. Staab, A. Kirsch, T. Barth, C. Krieger, F. A. Neugebauer, *Eur. J. Org. Chem.* **2000**, 1617–1622.
- [27] G. Miehe, P. Süsse, V. Kupcik, E. Egert, M. Nieger, G. Kunz, R. Gerke, B. Knieriem, M. Niemeyer, W. Lüttke, *Angew. Chem.* **1991**, *103*, 1006–1008; *Angew. Chem. Int. Ed. Engl.* **1991**, *30*, 964–967.
- [28] In addition, the CV curves show weak features that we were not in the position to assign.
- [29] H. Isci, W. R. Mason, *Inorg. Chem.* **1985**, *24*, 271–274.
- [30] J. Beck, V. Vitske, H.-J. Himmel, unpublished results.
- [31] See also: M. Reinmuth, U. Wild, D. Rudolph, E. Kaifer, M. Enders, H. Wadepohl, H.-J. Himmel, *Eur. J. Inorg. Chem.* **2009**, 4795–4808.
- [32] P. J. A. Sáez, S. H. Oakley, M. P. Coles, P. B. Hitchcock, *Chem. Commun.* **2007**, 816–818.
- [33] See, for example: K. S. Min, A. G. DiPasquale, A. L. Rheingold, H. S. White, J. S. Miller, *J. Am. Chem. Soc.* **2009**, *131*, 6229–6236.
- [34] DENZO-SMN, Data processing software, Nonius **1998**; <http://www.noniuss.com>.
- [35] a) G. M. Sheldrick, *SHELXS-97, Program for Crystal Structure Solution*, University of Göttingen, **1997**; <http://shelx.uni-ac.gwdg.de/SHELX/index.html>; b) G. M. Sheldrick, *SHELXL-97, Program for Crystal Structure Refinement*, University of Göttingen, **1997**; <http://shelx.uni-ac.gwdg.de/SHELX/index.html>.
- [36] *International Tables for X-ray Crystallography*, Vol. 4, Kynoch Press, Birmingham, UK, **1974**.
- [37] L. Zsolnai, G. Huttner, *XPMA*, University of Heidelberg, **1994**; <http://www.uni-eidelberg.de/institute/fak12/AC/huttner/software/software.html>.

Received: July 27, 2009

Published Online: November 20, 2009

# Formation of Metastable $\text{Na}_2\text{CrO}_4$ -Type $\text{LiNiPO}_4$ from a Phosphate–Formate Precursor

Violeta Koleva,<sup>\*,[a]</sup> Radostina Stoyanova,<sup>[a]</sup> and Ekaterina Zhecheva<sup>[a]</sup>

**Keywords:** Lithium / Nickel / Organic–inorganic hybrid composites / Metastable compounds / X-ray diffraction

High-pressure modification of  $\text{LiNiPO}_4$  with a  $\text{Na}_2\text{CrO}_4$ -type structure was obtained at ambient pressure and low temperature from a mixed LiNi–phosphate–formate precursor,  $\text{LiNiPO}_4\text{H}_x(\text{HCOO})_y\cdot y\text{H}_2\text{O}$  (where  $x \approx 1.2$  and  $y \approx 2.5$ ). The structural and thermal characterization of the precursor and the  $\text{LiNiPO}_4$  compositions were carried out by powder XRD analysis, IR spectroscopy, and DSC analysis. Thermal treatment of  $\text{LiNiPO}_4\text{H}_x(\text{HCOO})_y\cdot y\text{H}_2\text{O}$  precursors between 450

and 650 °C yields a mixture of the two structural modifications of  $\text{LiNiPO}_4$ : the  $\text{Na}_2\text{CrO}_4$  type and the olivine type. It was established that the obtained  $\text{Na}_2\text{CrO}_4$ -type  $\text{LiNiPO}_4$  is a metastable phase, which completely transforms at 700 °C into the olivine-type phase. The enthalpy of the phase transition is  $\Delta H = -43.40 \text{ kJ mol}^{-1}$ . The mechanism of formation of the two forms of  $\text{LiNiPO}_4$  from the LiNi–phosphate–formate precursor is discussed.

## Introduction

Lithium transition-metal orthophosphates with the general formula  $\text{LiMPO}_4$  ( $M = \text{Fe, Ni, and Co}$ ) exhibit three structural modifications. The stable modification at ambient pressure adopts the olivine-type structure. This structure can be described as hexagonal oxygen close packing, where lithium and transition-metal ions occupy half of the available octahedral sites with  $C_i$  and  $C_s$  symmetry, respectively. The  $\text{MO}_6$  octahedra are ordered in a way to form zigzag chains in the  $bc$  plane, which are cross-linked by  $\text{PO}_4^{3-}$  groups. Lithium ions fall in the rows (running along the  $a$  direction) between the transition metal chains. The lithium arrangement in the olivine structure favors the 1D mobility of the  $\text{Li}^+$  ions along the  $a$  direction.<sup>[1]</sup> The ability of the olivine structure to intercalate and deintercalate lithium reversibly determines phosphoolivines as potential cathode materials for lithium-ion batteries.<sup>[2,3]</sup> The best electrochemical performance is achieved with the iron analogues,  $\text{LiFePO}_4$ . The reversible electrochemical intercalation of  $\text{Li}^+$  from the olivine structure takes place concomitantly with the oxidation/reduction of  $\text{M}^{2+}/\text{M}^{3+}$  ions. This allows manipulating the potential, where Li intercalation takes place, replacing iron by manganese, cobalt, and nickel.<sup>[4–6]</sup>

The second structural modification of  $\text{LiMPO}_4$  possesses a spinel-type structure.<sup>[7]</sup> While the olivine modification is stable at ambient pressure, the spinel modification is formed under high pressures (above 20 GPa) only.

At an intermediate pressure (between 4 and 20 GPa), a new structural modification of  $\text{LiMPO}_4$  with a  $\text{Na}_2\text{CrO}_4$ -like structure (denoted also as  $\beta'$ -phase in <sup>[8]</sup>) has been obtained by Amador et al.<sup>[7,8]</sup> The  $\text{Na}_2\text{CrO}_4$ -like structure consists of layers with the composition  $[(\text{MO}_6)(\text{LiO}_4)(\text{PO}_4)]_\infty$  in the  $ac$  plane, where every  $\text{MO}_6$  octahedron shares two opposite edges with neighboring  $\text{MO}_6$  and two apical oxygen atoms with two  $\text{LiO}_4$  and two  $\text{PO}_4$  tetrahedra. Contrary to the olivine-type structure,  $\text{Li}^+$  ions occupy isolated tetrahedral positions, as a result of which the lithium mobility is hindered. This determines the lack of electrochemical activity of the  $\text{Na}_2\text{CrO}_4$ -type structure. On the basis of first-principle calculations at the DFT level, it is calculated that, for the Co analogue, both structural modifications possess close to total energies, with an enthalpy difference of 0.05 eV/f.u.<sup>[7]</sup> However, to the best of our knowledge, there is no data on the preparation of a  $\text{Na}_2\text{CrO}_4$ -type modification at ambient pressure of Fe, Ni, or Co analogues.

In this paper, the preparation of  $\text{Na}_2\text{CrO}_4$ -type modification of the Ni analogue from the  $\text{LiMPO}_4$  family at ambient pressure is reported. The method of synthesis is based on the formation of metal–organic precursors, where  $\text{Li}^+$  and  $\text{Ni}^{2+}$  ions are bonded by  $\text{PO}_4^{3-}$  and  $\text{HCOO}^-$  anions. Metal–organic precursors are isolated by freeze drying aqueous solutions of  $\text{Li}^+$ ,  $\text{M}^{2+}$ ,  $\text{PO}_4^{3-}$ , and  $\text{HCOO}^-$  ions. At ambient pressure the thermal decomposition of metal–organic precursors yields a  $\text{Na}_2\text{CrO}_4$ -type modification of  $\text{LiNiPO}_4$ . This method was recently applied to the preparation of  $\text{LiFePO}_4$  compositions. A pure olivine modification of  $\text{LiFePO}_4$  is only obtained at ambient pressure.<sup>[9]</sup> The structural characterization of the  $\text{LiNiPO}_4$  samples was carried out by powder X-ray diffraction (XRD) analysis and

[a] Institute of General and Inorganic Chemistry, Bulgarian Academy of Sciences, Acad. G. Bonchev St, bl. 11, 1113 Sofia, Bulgaria  
Fax: +359-2-8705024  
E-mail: vkoleva@svr.igic.bas.bg

IR spectroscopy. The thermal stability of the  $\text{Na}_2\text{CrO}_4$ -type modification of  $\text{LiNiPO}_4$  was determined by differential scanning calorimetry (DSC) analysis.

## Results and Discussion

Freeze drying solutions containing  $\text{Ni}(\text{HCOO})_2 \cdot 2\text{H}_2\text{O}$  and  $\text{LiH}_2\text{PO}_4$  yields amorphous, pale-green powders with a  $\text{LiNiPO}_4\text{H}_x(\text{HCOO})_x \cdot y\text{H}_2\text{O}$  composition ( $x \approx 1.2$  and  $y \approx 2.5$ ), where the Ni(Li) to HCOO ratio decreases from 1:2 to 1:1. This indicates that about 0.8 mol of formic acid is sublimated during the freeze-drying process. The same process of sublimation of formic acid was observed when iron and manganese phosphate-formate precursors are obtained.<sup>[9,10]</sup>

To rationalize the coordination of formate and phosphate groups, IR spectroscopy was undertaken (Figure 1). For the sake of comparison, the same figure shows the IR spectra of  $\text{Ni}(\text{HCOO})_2 \cdot 2\text{H}_2\text{O}$  and  $\text{Ni}(\text{H}_2\text{PO}_4)_2 \cdot 2\text{H}_2\text{O}$ .

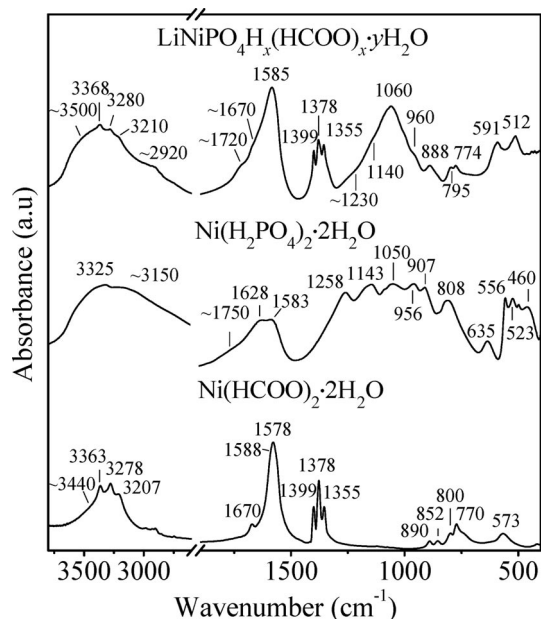


Figure 1. IR spectra of LiNi-phosphate-formate precursor,  $\text{Ni}(\text{HCOO})_2 \cdot 2\text{H}_2\text{O}$ , and  $\text{Ni}(\text{H}_2\text{PO}_4)_2 \cdot 2\text{H}_2\text{O}$ .

In the IR spectra of LiNi-phosphate-formate precursors, the IR modes due to the formate, phosphate, and OH groups are clearly resolved. The characteristic IR bands for the formate ion vibrations are assigned on the basis of IR studies of formate salts.<sup>[11–13]</sup> These vibrations are:  $\nu_{\text{as}}(\text{COO})$  at  $1585 \text{ cm}^{-1}$ ;  $\delta(\text{CH})$  at  $1399 \text{ cm}^{-1}$ ;  $\nu_{\text{s}}(\text{COO})$  at  $1378/1355 \text{ cm}^{-1}$ , and  $\delta_{\text{s}}(\text{OCO})$  at  $795/774 \text{ cm}^{-1}$ . Further on, the  $\delta(\text{CH})$  and  $\nu_{\text{s}}(\text{COO})$  vibrations in the Ni precursor are the same as those detected for pure  $\text{Ni}(\text{HCOO})_2 \cdot 2\text{H}_2\text{O}$ . Therefore, one can suppose that the formate ions are preferentially coordinated around the  $\text{Ni}^{2+}$  ions in LiNi precursors.

In addition, the low intensity of the IR bands at 960, 1230, and  $1720 \text{ cm}^{-1}$  cannot be unambiguously attributed. In this region, the characteristic bands for protonated

$\text{HCOOH}$  groups appear:  $\nu(\text{C}=\text{O})$  at about  $1700 \text{ cm}^{-1}$ ,  $\nu(\text{C}-\text{O})$  at  $1260 \text{ cm}^{-1}$ , and  $\gamma(\text{OH})$  at  $975 \text{ cm}^{-1}$ .<sup>[15]</sup> The protonated phosphate ions such as  $\text{H}_2\text{PO}_4^-$  or  $\text{HPO}_4^{2-}$  also display bands at  $1230\text{--}1260$  and  $800\text{--}900 \text{ cm}^{-1}$  due to out-of-plane  $\delta(\text{OH})$  and in-plane  $\gamma(\text{OH})$  bending POH vibrations, respectively.<sup>[16,17]</sup> Close inspection of the IR spectra of LiNi precursors,  $\text{Ni}(\text{HCOO})_2 \cdot 2\text{H}_2\text{O}$ , and  $\text{Ni}(\text{H}_2\text{PO}_4)_2 \cdot 2\text{H}_2\text{O}$  shows that the additional three bands at 1720, 1230, and  $960 \text{ cm}^{-1}$  are due more to  $\text{HCOOH}$  than to the protonated phosphate ions.

In the region of stretching OH vibrations, the IR spectrum of the LiNi precursor consists of four bands with positions close to those of  $\text{Ni}(\text{HCOO})_2 \cdot 2\text{H}_2\text{O}$ . For the sake of comparison, we shall mention that the stretching OH vibrations for  $\text{LiHCOO} \cdot \text{H}_2\text{O}$  appear at 3398 and  $3109 \text{ cm}^{-1}$ .<sup>[13]</sup> It seems that water molecules are predominantly coordinated to the nickel ions.

In summary, two features concerning the manner of coordination of the phosphate and formate groups and water molecules in  $\text{LiNiPO}_4\text{H}_x(\text{HCOO})_x \cdot y\text{H}_2\text{O}$  precursors can be outlined. It appears that the formate and phosphate groups are mainly deprotonated. The formate groups and water molecules prefer to coordinate around the  $\text{Ni}^{2+}$  ions, whereas the phosphate groups prefer to coordinate around the  $\text{Li}^+$  ions. This is a specific feature of LiNi precursors obtained by freeze drying of mixed formate-phosphate solutions. When the same freeze drying method is used for the preparation of LiM-phosphate-formate ( $\text{M} = \text{Fe}, \text{Mn}, \text{Co}$ ) compositions, both formate and phosphate groups are protonated, and they are coordinated to the  $\text{Fe}^{2+}$  and  $\text{Li}^+$  ions in a nonpreferential way.<sup>[9,10,18]</sup> The different types of coordinations of  $\text{PO}_4^{3-}$  and  $\text{HCOO}^-$  to  $\text{M}^{2+}$  and  $\text{Li}^+$  in the phosphate-formate precursors determines their different thermal behavior.

Thermal decomposition of LiNi-phosphate-formate precursors leads to the formation of a target  $\text{LiNiPO}_4$  composition at temperature higher than  $450^\circ\text{C}$ . To elucidate the mechanism of  $\text{LiNiPO}_4$  formation, Figure 2 shows the XRD patterns of the lithium-nickel-phosphate-formate precursor heated at selected temperatures in the range of 350 to  $750^\circ\text{C}$ . At  $350^\circ\text{C}$ , the sample is still amorphous. However, XRD peaks due to  $\text{Li}_3\text{PO}_4$  (JCPDS 25–1030) and hexagonal Ni metal (JCPDS 45–1027) become visible. Going from 350 to  $400^\circ\text{C}$ , new phases such as NiO (JCPDS 4–835) and  $\text{Li}_4\text{P}_2\text{O}_7$  (JCPDS 87–409) also crystallize. This means that at  $350\text{--}400^\circ\text{C}$  the thermal decomposition of freeze-dried LiNi-formate-phosphate precursors yields a mixture between Ni/NiO and lithium phosphate phases. For comparison, in this temperature range, pure  $\text{LiFePO}_4$  with an olivine-type structure is obtained. This results from the different structures of the precursors. When  $\text{PO}_4^{3-}$  and  $\text{HCOO}^-$  ions are preferentially coordinated around the  $\text{Li}^+$  and  $\text{Ni}^{2+}$  ions, respectively, then mixtures of lithium phosphates and metal phases are obtained during thermal decomposition.

Structural parameters of both modifications were determined by Rietveld analysis of the XRD pattern of lithium nickel phosphate obtained at  $500^\circ\text{C}$  (Figure 3).

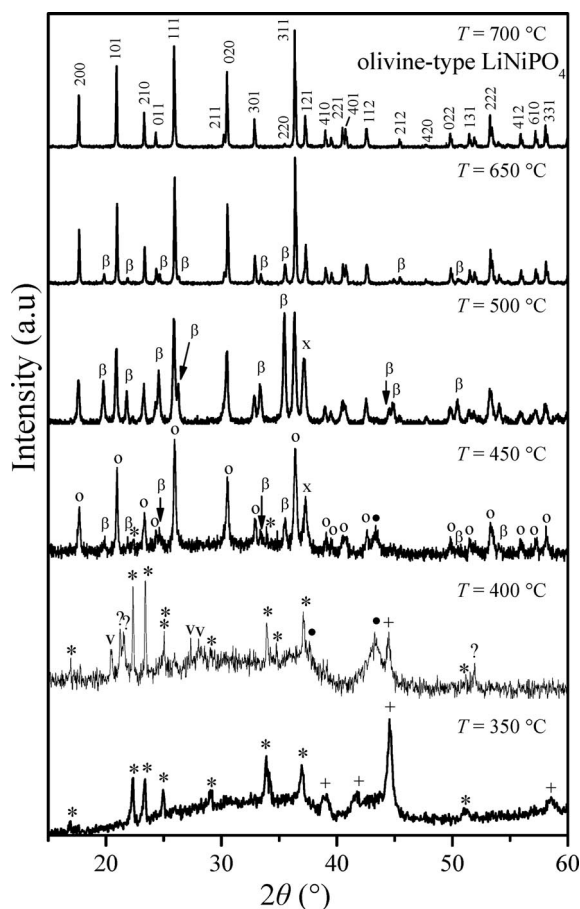


Figure 2. XRD patterns of LiNi-phosphate-formate precursor annealed at different temperatures. Symbols: Li<sub>3</sub>PO<sub>4</sub> (\*), metal Ni (+), NiO (●), Li<sub>4</sub>P<sub>2</sub>O<sub>7</sub> (v), unknown phase (?), Na<sub>2</sub>CrO<sub>4</sub>-type LiNiPO<sub>4</sub> (β), olivine-type LiNiPO<sub>4</sub> (o), common peak (x).

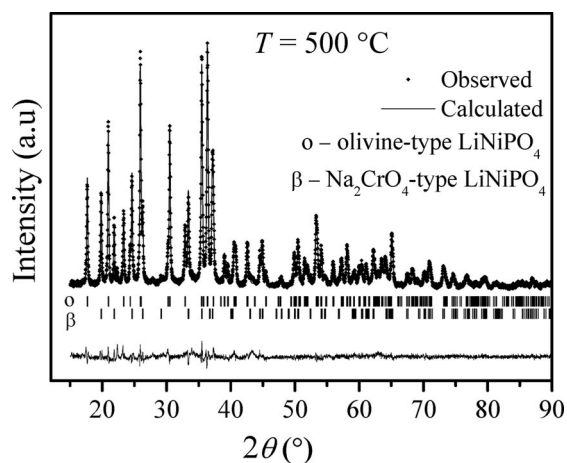


Figure 3. Rietveld refinement of the XRD pattern of lithium nickel phosphate obtained at 500 °C. Bragg reflections for olivine-type LiNiPO<sub>4</sub> (o) and Na<sub>2</sub>CrO<sub>4</sub>-type LiNiPO<sub>4</sub> (β) are shown. The difference between the observed and calculated profiles is plotted.

The atomic coordinates of olivine-type LiNiPO<sub>4</sub> and the high-pressure form of Na<sub>2</sub>CrO<sub>4</sub>-type LiNiPO<sub>4</sub> determined in ref.<sup>[8]</sup> were used as a starting model for Rietveld refinement. The structural parameters are listed in Table 1. It is

worth mentioning that the lattice parameters of the Na<sub>2</sub>CrO<sub>4</sub> form obtained by us at ambient pressure are close to those for the phase obtained under high pressure (6.5 GPa).<sup>[8]</sup> In addition, the lattice volume is expanded by 2.9% during the transformation from the Na<sub>2</sub>CrO<sub>4</sub> form to the olivine form at ambient pressure. Under high pressure the change in the lattice volumes is 2.8%.<sup>[8]</sup>

Table 1. Structural parameters of olivine-type and Na<sub>2</sub>CrO<sub>4</sub>-type LiNiPO<sub>4</sub> determined from Rietveld analysis of the XRD pattern of a sample annealed at 500 °C.

|                            | Olivine-type<br>LiNiPO <sub>4</sub><br>(this work) | Na <sub>2</sub> CrO <sub>4</sub> -type<br>LiNiPO <sub>4</sub> ,<br>ambient pressure<br>(this work) | Na <sub>2</sub> CrO <sub>4</sub> -type<br>LiNiPO <sub>4</sub> ,<br>high pressure<br>(6.5 GPa) <sup>[8]</sup> |
|----------------------------|--|--|--|
| <i>a</i> [Å]               | 10.0426(3)   | 5.3628(3)  | 5.3580(2)  |
| <i>b</i> [Å]               | 5.8582(2)  | 8.1344(3)  | 8.1272(3)  |
| <i>c</i> [Å]               | 4.6804(2)  | 6.1279(2)  | 6.1241(3)  |
| <i>V</i> [Å <sup>3</sup> ] | 275.364(17)  | 267.325(17)  | 266.7(1)   |
| <i>SG</i>                  | <i>Pnma</i>  | <i>Cmcm</i>  | <i>Cmcm</i>  |
| <i>Z</i>                   | 4  | 4  | 4  |
| <i>R<sub>B</sub></i>       | 0.043  | 0.041  | 0.033  |
| <i>R<sub>F</sub></i>       | 0.033  | 0.031  |  |
| <i>R<sub>exp</sub></i>     | 0.024  | 0.024  | 0.028  |
| <i>R<sub>wp</sub></i>      | 0.10   | 0.10   | 0.09   |
| χ <sup>2</sup>             | 2.49   | 2.49   | 5.7  |

Two structural modifications are, further on, characterized by IR spectroscopy (Figure 4). The sample annealed at 700 °C exhibits a typical IR spectrum for well-crystallized olivine-type LiNiPO<sub>4</sub>.<sup>[14,19]</sup> The band at 943 cm<sup>−1</sup> is due to ν<sub>1</sub>(PO<sub>4</sub>), the bands in the region of 1147–980 correspond to ν<sub>3</sub>(PO<sub>4</sub>), and those in the region of 662–550 cm<sup>−1</sup> correspond to ν<sub>4</sub>(PO<sub>4</sub>) vibrations. The bands at 525 and 476 cm<sup>−1</sup> are suggested to originate mainly from Li<sup>+</sup> translations.<sup>[19]</sup> In the IR spectra of the samples annealed at 500 °C three additional bands are observed at 934, 609, and 501 cm<sup>−1</sup>, which are attributed to the Na<sub>2</sub>CrO<sub>4</sub>-type form. According to factor group analysis, these bands are assigned as follows: the band at 934 cm<sup>−1</sup> to the ν<sub>1</sub> mode, that at 609 cm<sup>−1</sup> as a component from ν<sub>4</sub>(PO<sub>4</sub>) vibrations, and that at 501 cm<sup>−1</sup> as originating from ν<sub>2</sub>(PO<sub>4</sub>) and/or Li<sup>+</sup> and Ni<sup>2+</sup> translations.

The formation of the Na<sub>2</sub>CrO<sub>4</sub>-like modification at ambient pressure was unexpected if we take into account the previously reported data on high-pressure synthesis of the LiNiPO<sub>4</sub> modification.<sup>[8]</sup> Evidently, under the conditions of our experiments the Na<sub>2</sub>CrO<sub>4</sub>-type modification obtained is a metastable phase, which transforms upon heating at *T* > 650 °C into thermodynamically stable olivine modification. To prove the phase transformation, a DSC experiment was performed on a sample annealed at 500 °C (Figure 5). A broad exothermic peak between 580 and 650 °C was clearly resolved due to the Na<sub>2</sub>CrO<sub>4</sub>-type→olivine-type transformation. The experimentally measured enthalpy of this process was −19.1 kJ mol<sup>−1</sup> for the mixture containing Na<sub>2</sub>CrO<sub>4</sub>-type and olivine-type LiNiPO<sub>4</sub> in a ratio of 0.44:0.56 (determined by Rietveld analysis). The recalculated enthalpy for the phase transformation of pure Na<sub>2</sub>CrO<sub>4</sub>-type to olivine-type LiNiPO<sub>4</sub> was Δ*H* = −43.40 kJ mol<sup>−1</sup>.

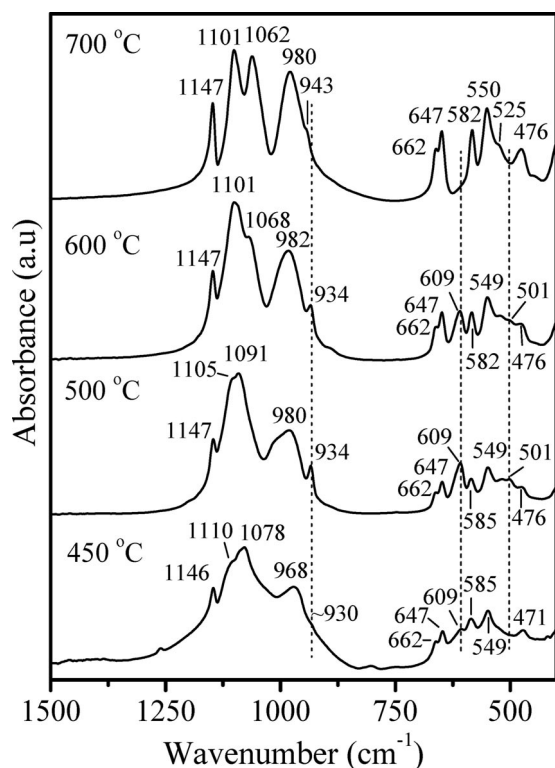


Figure 4. IR spectra of LiNi-phosphate-formate precursor annealed at different temperatures.

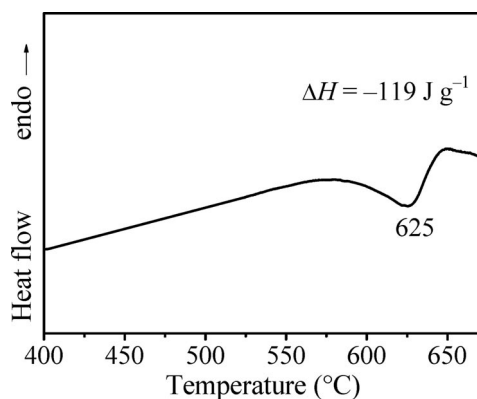


Figure 5. DSC curve of lithium nickel phosphate obtained at 500 °C (mixture of olivine-type  $\text{LiNiPO}_4$  and  $\text{Na}_2\text{CrO}_4$ -type  $\text{LiNiPO}_4$  in a ratio of 0.56:0.44).

For the iron, cobalt, and nickel members of the  $\text{LiMPO}_4$  family, it is worth mentioning that both  $\text{Na}_2\text{CrO}_4$ -type and olivine-type forms exhibit common structural features with respect to the “metallic” framework arrangement (Li, M, and P).<sup>[8]</sup> In Figure 6 the arrangement of the cations in the two types of structures is depicted for  $\text{LiNiPO}_4$ . In both structures, hexagonal sheets composed of P atoms and Li/Ni atoms are ordered in an ABAB sequence. In the olivine phase, the hexagonal sheets consist of P and Ni atoms, whereas in the  $\text{Na}_2\text{CrO}_4$  phase these sheets are formed by P and Li atoms (Figure 6). In both cases, the P atoms from two neighboring sheets build distorted octahedra, which are

occupied either by Ni ( $\text{Na}_2\text{CrO}_4$  phase, Figure 6a) or by Li (olivine phase, Figure 6b). Irrespective of this structural similarity, the formation of the  $\text{Na}_2\text{CrO}_4$ -type phase is observed for the Ni analogues only.

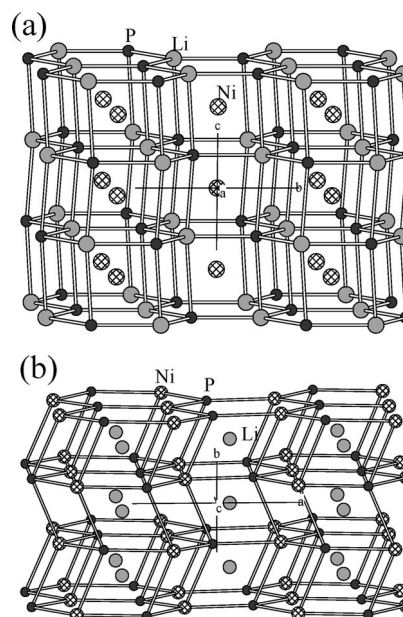


Figure 6. Structure of the metal sheets in  $\text{Na}_2\text{CrO}_4$ -type  $\text{LiNiPO}_4$  (a) and olivine-type  $\text{LiNiPO}_4$  (b).

The simultaneous appearance of the two structural modifications of  $\text{LiNiPO}_4$  after the solid-state reaction between lithium phosphates and Ni/NiO at 450 °C allows the mechanism of their formation to be explained. On the basis of the available reports in the literature,<sup>[6,8,20,21]</sup> the preparation of the thermodynamically stable olivine-type  $\text{LiNiPO}_4$  is realized at temperatures higher than 750 °C, even in the case when solution-based methods are used. This temperature is significantly higher than that of the Fe- (350 °C<sup>[9]</sup>), Mn- (450 °C<sup>[10]</sup>), and Co- (450 °C<sup>[18]</sup>) analogues. The formation of the olivine-type  $\text{LiNiPO}_4$  at higher temperature implies some kinetics limitations. It appears that these kinetic difficulties give rise to the formation of the  $\text{Na}_2\text{CrO}_4$ -type metastable  $\text{LiNiPO}_4$  at low temperature and ambient pressure.

## Conclusions

Freeze drying solutions containing  $\text{Ni}(\text{HCOO})_2$  and  $\text{LiH}_2\text{PO}_4$  yields precursors with compositions  $\text{LiNiPO}_4 \cdot x\text{H}_x(\text{HCOO})_x \cdot y\text{H}_2\text{O}$  ( $x \approx 1.2$  and  $y \approx 2.5$ ). In the precursor, the formate and phosphate ions are mainly deprotonated and exhibit preferential coordination:  $\text{Li}^+$  prefers phosphate ions, whereas  $\text{Ni}^{2+}$  prefers formate ions. Below 400 °C the thermal decomposition of the precursors results in the formation of a mixture of lithium phosphates and Ni/NiO. After further annealing, two structural modifications of  $\text{LiNiPO}_4$  are simultaneously formed. A  $\text{Na}_2\text{CrO}_4$ -type  $\text{LiNiPO}_4$  is stabilized as a metastable phase at 450 °C,

whereas pure olivine-type LiNiPO<sub>4</sub> is obtained at 700 °C. The lattice parameters of Na<sub>2</sub>CrO<sub>4</sub>-type LiNiPO<sub>4</sub> obtained at ambient pressure are close to that of Na<sub>2</sub>CrO<sub>4</sub>-type LiNiPO<sub>4</sub> obtained at high pressure (6.5 GPa). The enthalpy of the phase transition Na<sub>2</sub>CrO<sub>4</sub>-type → olivine-type LiNiPO<sub>4</sub> is  $\Delta H = -43.40 \text{ kJ mol}^{-1}$ . Within the LiMPO<sub>4</sub> family (M = Fe, Co, Mn, Ni), the appearance of the metastable Na<sub>2</sub>CrO<sub>4</sub>-type modification at ambient pressure is a specific feature of the Ni analogue. The much higher temperature of formation of the olivine-type LiNiPO<sub>4</sub> (700 °C) as compared to the Co and Fe olivines (350–450 °C) is most probably a consequence of kinetic limitations.

## Experimental Section

The homogeneous lithium–nickel–phosphate–formate precursors were prepared following the procedure developed earlier for the iron and manganese compounds, respectively.<sup>[9,10]</sup>

Transparent phosphate–formate solutions of lithium and nickel were obtained by mixing solutions of Ni(HCOO)<sub>2</sub>·2H<sub>2</sub>O and LiH<sub>2</sub>PO<sub>4</sub>, keeping a stoichiometric 1:1:1 = Ni/Li/P ratio. The pH value of both solutions before mixing was adjusted to pH ≈ 3 with addition of a small quantity of HCOOH (1:1). Solutions with concentrations of 0.05 and 0.1 M with respect to the metal ions were prepared. As-prepared solutions were frozen instantly with liquid nitrogen and dried in vacuo (20–30 mbar) at –20 °C with an Alpha-Christ Freeze Dryer. After drying, the solid precursors were predecomposed at 350 °C for 3 h and then further annealed at temperatures from 350 to 750 °C for 10 h under a static air atmosphere.

The starting Ni(HCOO)<sub>2</sub>·2H<sub>2</sub>O was prepared by dissolving nickel carbonate with dilute formic acid at 60–70 °C. The solution was then filtered and concentrated. Crystals were obtained by cooling to room temperature. Ni(HCOO)<sub>2</sub>·2H<sub>2</sub>O is very stable during storage, which ensures an exact stoichiometry in the final product.

The chemical composition of the precursors and of the LiNiPO<sub>4</sub> samples was determined by using data from the chemical analyses of Ni (complexometrically), Li (atomic absorption analysis), C and H (Elementar Analysensysteme GmbH), and thermal analysis (“Stanton Redcroft” apparatus). X-ray structural analysis was made with a Bruker Advance 8 diffractometer (Cu-K<sub>α</sub> radiation). Step-scan recordings for structure refinement by the Rietveld method were carried out using by 0.02° 2θ steps of 10 s duration. The computer program FULLPROF was used in the calculations. The DSC curve was recorded using DSC 20 of Mettler TA 3000 system at a heating rate of 10 °C min<sup>–1</sup>.

## Acknowledgments

Authors are grateful for the financial support of the National Science Fund of Bulgaria (Ch 1701/2007) and to the National Centre for New Materials (DO-02-82/2008). Thanks to Prof. T. Spassov (Sofia University, Bulgaria) for the DSC measurement.

- [1] A. S. Anderson, J. O. Thomas, *J. Power Sources* **2001**, 97–98, 498–502.
- [2] A. K. Padhi, K. S. Nanjundaswamy, J. B. Goodenough, *J. Electrochem. Soc.* **1997**, 144, 1188–1194.
- [3] M. S. Whittingham, Y. Song, S. Lutta, P. Y. Zavalij, N. Chernova, *J. Mater. Chem.* **2005**, 15, 3362–3379.
- [4] G. Li, H. Azuma, M. Tohda, *Electrochem. Solid-State Lett.* **2002**, 5, A135–137.
- [5] K. Amine, H. Yasuda, M. Yamachi, *Electrochem. Solid-State Lett.* **2000**, 3, 178–179.
- [6] J. Wolfenstine, J. Allen, *J. Power Sources* **2005**, 14, 389–390.
- [7] U. Amador, J. M. Gallardo-Amores, G. Neymann, H. Hupertz, E. Morán, M. E. Arroyo y de Dompablo, *Solid State Sci.* **2009**, 1, 343–348.
- [8] O. García-Moreno, M. Álvarez-Vega, F. García-Alvarado, J. García-Jaca, J. M. Gallardo-Amores, M. L. Sanjuán, U. Amador, *Chem. Mater.* **2001**, 13, 1570–1576.
- [9] V. Koleva, E. Zhecheva, R. Stoyanova, *J. Alloys Compd.* **2009**, 476, 950–957.
- [10] V. Koleva, R. Stoyanova, E. Zhecheva, *Mater. Chem. Phys.*, submitted.
- [11] K. G. Kidd, H. H. Mantsch, *J. Mol. Spectrosc.* **1981**, 85, 375–389.
- [12] A. Heyns, *J. Mol. Struct.* **1985**, 127, 9–20.
- [13] K. Mouaïne, P. Becker, C. Carabatos-Nédelec, *Phys. Status Solidi B* **1997**, 200, 273–287.
- [14] A. Ait Salah, P. Jozwiak, K. Zaghib, J. Garbarczyk, F. Gendron, A. Manger, C. M. Julien, *Spectrochim. Acta* **2006**, 65A, 1007–1113.
- [15] A. Novak, *Struct. Bonding (Berlin)* **1974**, 18, 177–216.
- [16] J. Baran, T. Lis, M. Drozd, H. Ratajczak, *J. Mol. Struct.* **2000**, 516, 185–202.
- [17] J. Xu, D. F. R. Gilson, I. S. Butler, *Spectrochim. Acta Part A* **1998**, 54, 1869–1878.
- [18] V. Koleva, E. Zhecheva, R. Stoyanova, *unpublished data*.
- [19] M. Th. Paques-Ledent, P. Tarte, *Spectrochim. Acta Part A* **1974**, 30, 673–689.
- [20] K. Rissouli, K. Benkhoulja, J. R. Ramos-Barrado, C. Julien, *Mater. Sci. Eng.* **2003**, B98, 185–189.
- [21] Gangulibabu, D. Bhuvaneswari, N. Kalaiselvi, N. Jayaprakash, P. Periasamy, *J. Sol-Gel Sci. Technol.* **2009**, 49, 137–144.

Received: July 28, 2009

Published Online: December 1, 2009

# Solvent Effects on Coordination Chemistry – Stepwise Synthesis and Structural Properties of Monometallic Palladium(II) Complexes and Bimetallic Palladium(II)/Platinum(II) Complexes

Tae Hwan Noh,<sup>[a]</sup> Young-A Lee,<sup>[b]</sup> and Ok-Sang Jung\*<sup>[a]</sup>

**Keywords:** Bimetallic complexes / Coordination modes / Crystal engineering / NMR spectroscopy / Palladium

Stepwise syntheses of monometallic palladium(II) and bimetallic palladium(II)/platinum(II) complexes were carried out in order to measure the metallophilicity of potential tetradentate bis(alkylthio)ylidenemalonato ligands. The reaction of [Pd](SO<sub>4</sub>) ([Pd] = (Me<sub>4</sub>en)Pd; Me<sub>4</sub>en = *N,N,N',N'*-tetramethylethylenediamine) with Ba[L] {L: bis(methylthio)methylenepropanedioato (**1**); bis(ethylthio)methylenepropanedioato (**2**); 1,3-dithiapan-2-ylidene-malonato (**3**)} produced [[Pd]-O,O'-L]. Successive reactions of [[Pd]-O,O'-L] with {M}(NO<sub>3</sub>)<sub>2</sub> ({M} = (en)M; en = ethylenediamine; M = Pd<sup>II</sup>, Pt<sup>II</sup>), followed by anion exchange with PF<sub>6</sub><sup>-</sup>, yielded banana-shaped bimetallic complexes [[Pd]-O,O'-L-S,S'-{M}](PF<sub>6</sub>)<sub>2</sub>. In case of [[Pd]-O,O'-**1**], the bis(alkylthio)methylene group of **1** was bent strikingly from the palladium square plane (dihedral angle = 78.26°), in contrast to the cases of [[Pd]-O,O'-**3**] (120.84°) and [[Pd]-O,O'-L-S,S'-{M}](PF<sub>6</sub>)<sub>2</sub> (101.75–103.54°).

[[Pd]-O,O'-L] (L = **1**, **2**) in Me<sub>2</sub>SO existed as a mixture of [[Pd]-O,O'-L] and [(Me<sub>4</sub>en-*N*)(Me<sub>2</sub>SO-S)-Pd-O,O'-L] in a mol ratio of 1:1. For the labile species, a linkage isomeric equilibrium between [[Pd]-O,O'-L] and [[Pd]-O,S-L] in D<sub>2</sub>O was observed. [[Pd]-O,O'-**3**] and [[Pd]-O,O'-L-S,S'-{M}](PF<sub>6</sub>)<sub>2</sub>, however, were found to be inert in Me<sub>2</sub>SO or D<sub>2</sub>O. Such notably different solution behavior possibly can be explained by the steric hindrance occurring via the dihedral angles between the palladium square plane and the ylidene moiety. Variable-temperature <sup>1</sup>H NMR spectra of the banana-shaped bimetallic complexes [[Pd]-O,O'-L-S,S'-{M}](PF<sub>6</sub>)<sub>2</sub> in CD<sub>3</sub>CN solution revealed that the amine proton resonances are sensitive to the fluxional motion of the remote bis(alkylthio)ylidene groups, suggesting the occurrence of interconversion between the two “bent-up” and “bent-down” forms.

## Introduction

The synthesis of designed polymetallic complexes promising specific catalysts, enzyme-mimics, molecular materials, and pharmaceutical applications is a pressing issue in inorganic and organometallic chemistry.<sup>[1]</sup> Short-bridged polymetallic complexes are of particular interest owing to their “communicating” properties suitable for photoelectrochemical applications, magnetic properties, self-assembling nanocages, efficient catalysts, nanowire precursors, chemical sensors, and superconducting materials.<sup>[2]</sup> A general synthetic strategy for achieving (hetero)polymetallic topology and conformation turns on the use of “metalloligands”.<sup>[3]</sup> This procedure exploits heterotopic ligands already bound to one metal by means of free donors that can bind them to a second metal, via stepwise synthesis utilizing the different reactivities of the various donor sites. Many discrete mono-

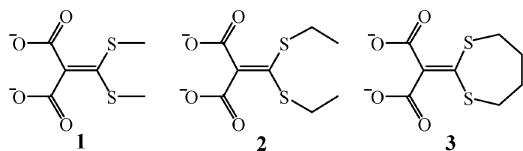
metallic Pd<sup>II</sup> or Pt<sup>II</sup> complexes with bidentate donors have been investigated with an eye to achieving more effective anticancer drugs, catalysts,<sup>[4,5]</sup> and morphology control.<sup>[6]</sup> The structure, conformation, and topology of those monometallic complexes are functions of the nature of the organic backbone as well as the nature of the metal–ligand interaction. In particular, palladium(II) complexes of N-donor ligands have significantly contributed to the synthesis of coordination materials such as catalysts, rectangle building blocks, submicrospheres, task-specific morphology, and the “magic ring” with associative/dissociative dual character Pd–N bonds.<sup>[7]</sup>

Platinum(II) complexes of a series of potential tetradentate bis(alkylthio)ylidenemalonato ligands<sup>[8]</sup> were prepared and investigated in our group;<sup>[9]</sup> however, monometallic palladium(II) complexes as well as Pd<sup>II</sup>/Pt<sup>II</sup> or Pd<sup>II</sup>/Pd<sup>II</sup> bimetallic complexes of the bis(alkylthio)ylidenemalonato ligands remain unexplored. In this context, we report the stepwise syntheses along with the crystal structures and solution-dynamic properties of monometallic palladium(II) and bimetallic Pd<sup>II</sup>/Pt<sup>II</sup> or Pd<sup>II</sup>/Pd<sup>II</sup> complexes containing ligands **1–3**. The coordination-behavior of the monometallic or bimetallic complexes will be a useful information in the design and synthesis of anticancer agents, luminescent materials, catalysts, and photophysical materials.<sup>[5c]</sup>

[a] Department of Chemistry, Pusan National University, Pusan 609-735, Republic of South Korea  
Fax: +82-51-510-3522  
E-mail: oksjung@pusan.ac.kr

[b] Department of Chemistry, Chonbuk National University, Jeonju 561-756, Republic of South Korea

Supporting information for this article is available on the WWW under <http://dx.doi.org/10.1002/ejic.200900804>.

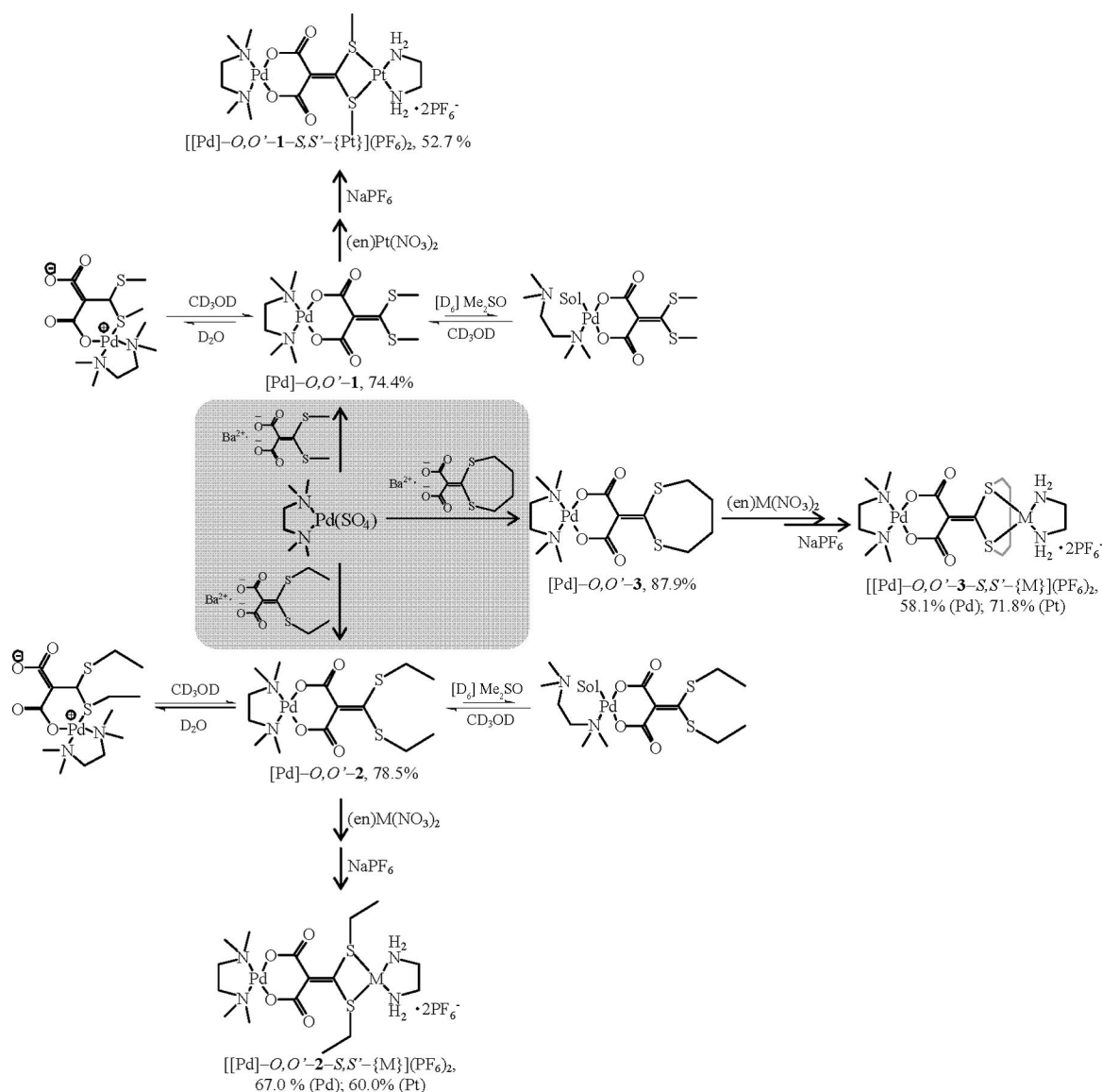


## Results and Discussion

### Synthesis

The monometallic palladium(II) complexes were synthesized by the reaction of *cis*-protected palladium(II) sulfate with barium salts of appropriate ligands (Scheme 1) in water, and then were recrystallized from a mixture of water and acetone to obtain thin yellow crystalline products. The products are soluble in water, dimethyl sulfoxide (Me<sub>2</sub>SO), and *N,N*-dimethylformamide, and are slightly soluble in

methanol, ethanol, and acetonitrile, but are insoluble in chloroform, *n*-hexane, tetrahydrofuran, and diethyl ether. For [[Pd]-*O*,*O'*-1], the asymmetric and symmetric stretching frequencies of the carboxylate moiety of the product appeared at 1612 and 1335 cm<sup>-1</sup>, respectively, unlike those (1585 and 1348 cm<sup>-1</sup>) of **1** itself, indicating that the complexation had been accomplished. The successive reaction of [{M}(NO<sub>3</sub>)<sub>2</sub>] ({M} = (en)M<sup>II</sup>; en = ethylenediamine; M<sup>II</sup> = Pd<sup>II</sup>, Pt<sup>II</sup>) with the above monometallic palladium(II) complexes as a metalloligand, followed by an anion exchange with sodium hexafluorophosphate, yielded new bimetallic complexes. The bimetallic complexes were recrystallized to obtain single crystals suitable for analysis by single-crystal X-ray diffraction. The crystals proved to be soluble in water, acetone, and nitromethane, and slightly soluble in methanol and ethanol. The elemental analyses, IR, and NMR spectra of the products were consistent with the proposed structures.



Scheme 1. [Pd] = (Me<sub>4</sub>en)Pd; {M} = (en)M; M = Pd<sup>II</sup> and Pt<sup>II</sup>; Sol = [D<sub>6</sub>]Me<sub>2</sub>SO.

Crystal Structures of Monometallic Pd<sup>II</sup> Complexes

The molecular structures of monometallic palladium(II) complexes  $[[\text{Pd}]\text{-O},\text{O}'\text{-1}]$  and  $[[\text{Pd}]\text{-O},\text{O}'\text{-3}]$  are depicted in Figures 1 and 2, respectively, and the relevant bond lengths and angles are listed in Table 1. For  $[[\text{Pd}]\text{-O},\text{O}'\text{-1}]$ , the local geometry around the palladium(II) approximates a square planar arrangement [Pd–O1 2.037(2) Å; Pd–O3 2.032(2) Å; Pd–N1 2.035(3) Å; Pd–N2 2.037(2) Å] with two carboxylates in the *cis*-position [O1–Pd–O3 89.81(1)°]. Concomitantly, the neutral Me<sub>4</sub>en ligand is bonded to the palladium(II) in a *cis* bidentate fashion [N1–Pd–N2 86.71(1)°]. Ligand **1** is coordinated with Pd<sup>II</sup> in *O,O'*-fashion in contrast to the *S,S'*-mode of  $[(\text{DACH})\text{Pt}(\text{I})]$  (DACH = 1,2-diaminocyclohexane).<sup>[9d]</sup> The most interesting feature is that the bis(methylthio)methylene group of ligand **1** is strikingly bent from the palladium square plane (the dihedral angle between the two planes is 78.24(6)°). Even though ligand **1** is an  $\alpha,\beta$ -unsaturated carboxylic acid, the bending prevents delocalization of its  $\pi$  electrons. As a proof of the localization, the bond length [1.340(4) Å] of the double bond C2–C4 corresponds to that (1.34 Å) of a normal ethylene group.<sup>[10]</sup> No other exceptional features, including those of either bond lengths or angles, were observed. For  $[[\text{Pd}]\text{-O},\text{O}'\text{-3}]$ ,

the structure including the local geometry around the palladium(II) atom [Pd1–O3 2.009(2) Å; Pd1–O1 2.011(2) Å; Pd1–N2 2.039(2) Å; Pd1–N1 2.045(2) Å; O3–Pd1–O1 91.59(7)°; O3–Pd1–N2 174.99(8)°; O1–Pd1–N2 90.93(7)°; O3–Pd1–N1 91.21(7)°; O1–Pd1–N1 176.92(7)°; N2–Pd1–N1 86.18(8)°] is very similar to the structure of  $[[\text{Pd}]\text{-O},\text{O}'\text{-1}]$  except for the dihedral angles between the 1,3-dithiapan-2-ylidenemalonate group and the palladium square plane. The dihedral angle between the two planes of Pd1, N1, N2, O1, and O3, and C1, C2, C3, C4, S1, and S2 is 121.52(6)°.

Table 1. Selected bond lengths [Å] and angles [°] of  $[[\text{Pd}]\text{-O},\text{O}'\text{-1}]$  and  $[[\text{Pd}]\text{-O},\text{O}'\text{-3}]$ .

| $[[\text{Pd}]\text{-O},\text{O}'\text{-1}]$ |           | $[[\text{Pd}]\text{-O},\text{O}'\text{-3}]$ |           |
|---|-----------|---|-----------|
| Pd1–N1                                      | 2.035(3)  | Pd1–N1                                      | 2.045(2)  |
| Pd1–N2                                      | 2.037(2)  | Pd1–N2                                      | 2.039(2)  |
| Pd1–O1                                      | 2.037(2)  | Pd1–O1                                      | 2.011(2)  |
| Pd1–O3                                      | 2.032(2)  | Pd1–O3                                      | 2.009(2)  |
| N1–Pd1–N2                                   | 86.71(1)  | N1–Pd1–N2                                   | 86.18(8)  |
| O1–Pd1–O3                                   | 89.81(8)  | O1–Pd1–O3                                   | 91.59(7)  |
| N1–Pd1–O3                                   | 177.24(9) | N1–Pd1–O1                                   | 176.92(7) |
| N2–Pd1–O1                                   | 178.47(9) | N2–Pd1–O3                                   | 174.99(8) |

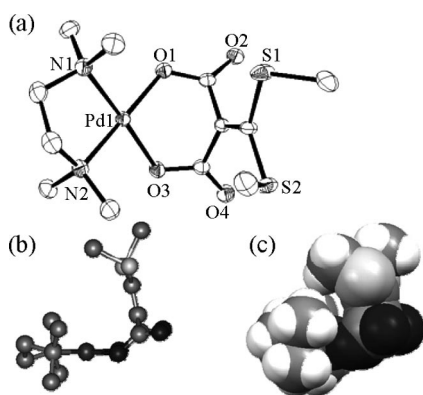


Figure 1. ORTEP (a), ball-and-stick drawing (b), and space-filling diagram (c) of  $[[\text{Pd}]\text{-O},\text{O}'\text{-1}]$ . The space-filling diagram shows the steric hindrance. Solvated water molecules are omitted for clarity.

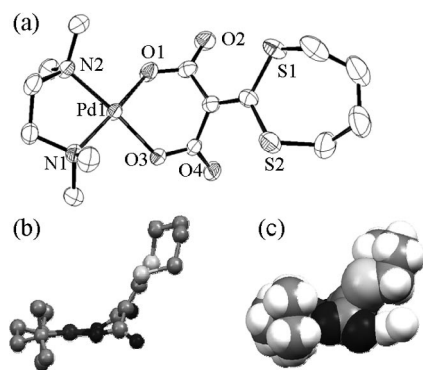


Figure 2. ORTEP (a), ball-and-stick drawing (b), and space-filling diagram (c) of  $[[\text{Pd}]\text{-O},\text{O}'\text{-3}]$ . Solvated water molecule is omitted for clarity.

Crystal Structures of Bimetallic Pd<sup>II</sup>/Pt<sup>II</sup> Complexes

The crystal structures of  $[[\text{Pd}]\text{-O},\text{O}'\text{-2-}S,S'\text{-}\{\text{Pd}\}](\text{PF}_6)_2$ ,  $[[\text{Pd}]\text{-O},\text{O}'\text{-2-}S,S'\text{-}\{\text{Pt}\}](\text{PF}_6)_2$ , and  $[[\text{Pd}]\text{-O},\text{O}'\text{-3-}S,S'\text{-}\{\text{Pt}\}](\text{PF}_6)_2$  are depicted in Figures 3, 4, and 5, respectively, and the relevant bond lengths and angles are listed in Table 2. For these complexes, the second metal ions were coordinated with each L in an essential *cis-S,S'*-fashion in the solid state [Pd1–S1 2.282(2) Å, Pd1–S2 2.295(2) Å for  $[[\text{Pd}]\text{-O},\text{O}'\text{-2-}S,S'\text{-}\{\text{Pd}\}](\text{PF}_6)_2$ ; Pt1–S1 2.272(9) Å, Pt1–S2 2.273(1) Å for  $[[\text{Pd}]\text{-O},\text{O}'\text{-2-}S,S'\text{-}\{\text{Pt}\}](\text{PF}_6)_2$ ; Pt1–S1 2.274(1) Å, Pt1–S2 2.259(1) Å for  $[[\text{Pd}]\text{-O},\text{O}'\text{-3-}S,S'\text{-}\{\text{Pt}\}](\text{PF}_6)_2$ ], resulting in the formation of bimetallic complexes. The dihedral angles [101.75(7)° for  $[[\text{Pd}]\text{-O},\text{O}'\text{-2-}S,S'\text{-}\{\text{Pd}\}](\text{PF}_6)_2$ ; 103.25(7)° for  $[[\text{Pd}]\text{-O},\text{O}'\text{-2-}S,S'\text{-}\{\text{Pt}\}](\text{PF}_6)_2$ ; 103.53(9)° for  $[[\text{Pd}]\text{-O},\text{O}'\text{-3-}S,S'\text{-}\{\text{Pt}\}](\text{PF}_6)_2$ ]

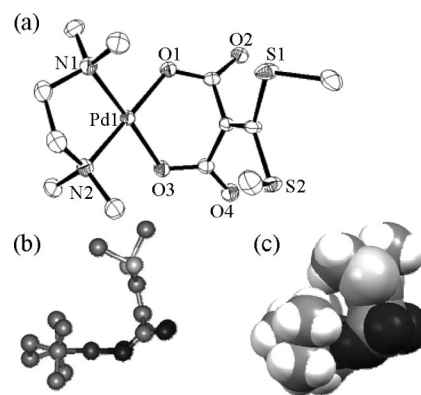


Figure 3. ORTEP (a) and ball-and-stick drawing (b) of  $[[\text{Pd}]\text{-O},\text{O}'\text{-2-}S,S'\text{-}\{\text{Pd}\}](\text{PF}_6)_2$ . Hydrogen atoms and counteranions are omitted for clarity.

between the (Me<sub>4</sub>en)Pd square plane and the (en)M<sup>II</sup> (M = Pd, Pt) square plane yield a banana-shaped conformation in the solid state.

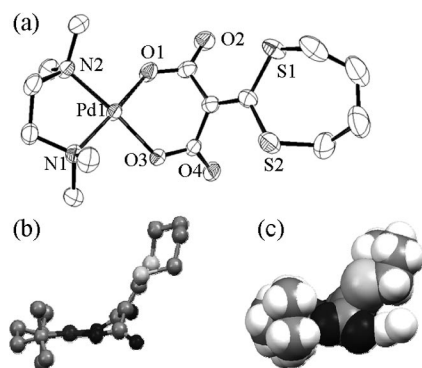


Figure 4. ORTEP (a) and ball-and-stick drawing (b) of [[Pd]-O,O'-2-S,S'-{Pt}](PF<sub>6</sub>)<sub>2</sub>. Hydrogen atoms, counteranions, and solvated solvent molecules are omitted for clarity.

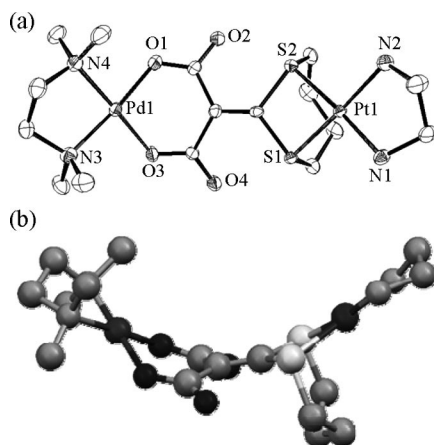


Figure 5. ORTEP (a) and ball-and-stick drawing (b) of [[Pd]-O,O'-3-S,S'-{Pt}](PF<sub>6</sub>)<sub>2</sub>. Hydrogen atoms, counteranions, and solvated solvent molecules are omitted for clarity.

## Solution Behavior of Monometallic Complexes

The solvent-dependent <sup>1</sup>H NMR spectra (D<sub>2</sub>O, [D<sub>6</sub>]-Me<sub>2</sub>SO, [D<sub>7</sub>]-DMF, CD<sub>3</sub>OD, and CD<sub>3</sub>CN) of [[Pd]-O,O'-1] were measured (Figure 6). The NMR spectra in CD<sub>3</sub>OD or CD<sub>3</sub>CN were consistent with the X-ray structure, whereas the NMR spectra in D<sub>2</sub>O, [D<sub>6</sub>]-Me<sub>2</sub>SO, or [D<sub>7</sub>]-DMF confirm the coexistence of two species, including the original product, in the solutions. The spectrum in D<sub>2</sub>O shows that the new species is an asymmetric **1** product (chemical shift: 2.92, 2.73, 2.72, 2.52 ppm; see Figure 7). Another interesting feature is that the new peaks gradually disappear upon the addition of CD<sub>3</sub>OD into the D<sub>2</sub>O solution, indicating that the new species returns to its original structure (Figure 7). The addition of [D<sub>6</sub>]-Me<sub>2</sub>CO into the D<sub>2</sub>O solution caused the same phenomena. These evidences indicate that the reversible linkage isomerism process can be explained by the equilibrium between [[Pd]-O,O'-1] and [[Pd]-O,S-1], as shown in Scheme 1 and Figure 7. Such a facile structural restoration suggests that the stability between the original and the new species is only slightly different. The <sup>13</sup>C NMR spectrum in D<sub>2</sub>O also supports such phenomena (Supporting Information). Three <sup>13</sup>C NMR resonances at 172.93 (O,O'-), 170.83 (O,S-), and 167.23 (O,S-) ppm for the carboxylate group indicated the presence of the two species in D<sub>2</sub>O. The <sup>13</sup>C NMR resonances of the two ethylene moiety pairs at 146.62, 145.41 and 136.83, 132.62 ppm along with those of the methyl moiety at δ = 16.94 (O,O'-) and 24.32 ppm; 16.55 ppm (O,S-) indicate the coexistence of the two species in a mol ratio of 1:1. That is, a zwitterionic O,S-chelate species forms in D<sub>2</sub>O in addition to the O,O'-chelate. That is, a solvent with a high dielectric constant (the dielectric constant of water is 78.54 at 20 °C; that of methanol is 32.63 at 20 °C)<sup>[11]</sup> favors the zwitterionic species. Thus, the nature of solvents is an important factor in the shift of the equilibrium.<sup>[4d]</sup>

The NMR spectrum of [[Pd]-O,O'-1] in [D<sub>6</sub>]-Me<sub>2</sub>SO showed different patterns as illustrated in Figure 8. The main peaks of the original structure at 2.78 (N-CH<sub>2</sub>), 2.54

Table 2. Selected bond lengths (Å) and angles [°] of [[Pd]-O,O'-2-S,S'-{Pd}](PF<sub>6</sub>)<sub>2</sub>, [[Pd]-O,O'-2-S,S'-{Pt}](PF<sub>6</sub>)<sub>2</sub>, and [[Pd]-O,O'-3-S,S'-{Pt}](PF<sub>6</sub>)<sub>2</sub>.

| [[Pd]-O,O'-2-S,S'-{Pd}](PF <sub>6</sub> ) <sub>2</sub> |          | [[Pd]-O,O'-2-S,S'-{Pt}](PF <sub>6</sub> ) <sub>2</sub> |           | [[Pd]-O,O'-3-S,S'-{Pt}](PF <sub>6</sub> ) <sub>2</sub> |           |
|--|----------|--|-----------|--|-----------|
| Pd1–N1   | 2.074(8) | Pt1–N1   | 2.056(3)  | Pt1–N1   | 2.066(5)  |
| Pd1–N2   | 2.053(8) | Pt1–N2   | 2.067(3)  | Pt1–N2   | 2.073(5)  |
| Pd1–S1   | 2.282(2) | Pt1–S1   | 2.272(9)  | Pt1–S1   | 2.274(1)  |
| Pd1–S2   | 2.295(2) | Pt1–S2   | 2.273(1)  | Pt1–S2   | 2.259(1)  |
| Pd2–O1   | 2.023(9) | Pd1–O1   | 2.031(3)  | Pd1–O1   | 2.004(4)  |
| Pd2–O2   | 2.011(8) | Pd1–O3   | 2.019(3)  | Pd1–O3   | 2.016(4)  |
| Pd2–N5   | 2.04(1)  | Pd1–N3   | 2.035(3)  | Pd1–N3   | 2.034(5)  |
| Pd2–N6   | 2.04(1)  | Pd1–N4   | 2.033(4)  | Pd1–N4   | 2.047(5)  |
| N1–Pd1–N2  | 82.6(3)  | N1–Pt1–N2  | 82.42(1)  | N1–Pt1–N2  | 82.6(2)   |
| S1–Pd1–S2  | 76.67(7) | S1–Pt1–S2  | 76.66(3)  | S1–Pt1–S2  | 76.83(5)  |
| N1–Pd1–S1  | 177.5(3) | N1–Pt1–S2  | 171.56(1) | N1–Pt1–S2  | 173.76(2) |
| N2–Pd1–S2  | 171.3(4) | N2–Pt1–S1  | 177.56(1) | N2–Pt1–S1  | 176.30(1) |
| O1–Pd2–O2  | 90.4(4)  | O1–Pd1–O3  | 90.72(1)  | O1–Pd1–O3  | 91.20(2)  |
| N5–Pd2–N6  | 85.9(4)  | N3–Pd1–N4  | 85.87(2)  | N3–Pd1–N4  | 86.0(2)   |
| O1–Pd2–N5  | 178.2(4) | O1–Pd1–N4  | 176.91(1) | O1–Pd1–N3  | 174.42(2) |
| O2–Pd2–N6  | 174.7(3) | O3–Pd1–N3  | 174.24(1) | O3–Pd1–N4  | 178.2(2)  |

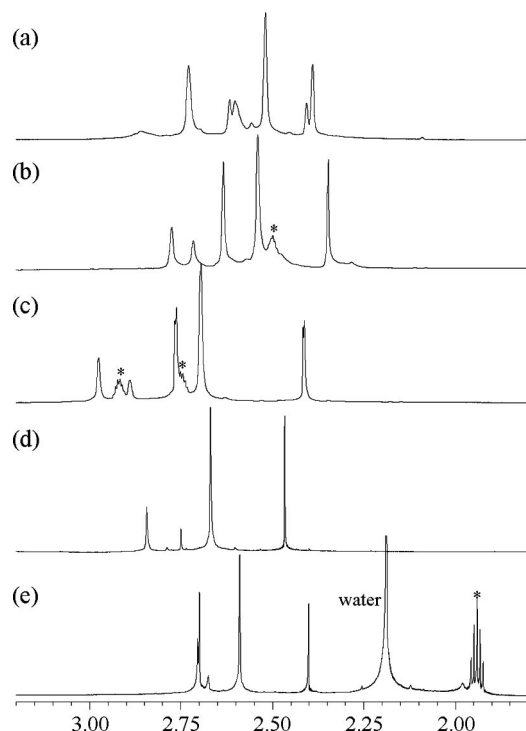


Figure 6.  $^1\text{H}$  NMR spectra of  $[\text{Pd}]\text{-O,O'-1}$  in  $\text{D}_2\text{O}$  (a),  $[\text{D}_6]\text{Me}_2\text{SO}$  (b),  $[\text{D}_7]\text{DMF}$  (c),  $\text{CD}_3\text{OD}$  (d), and  $\text{CD}_3\text{CN}$  (e). The asterisks indicate the respective solvent peaks.

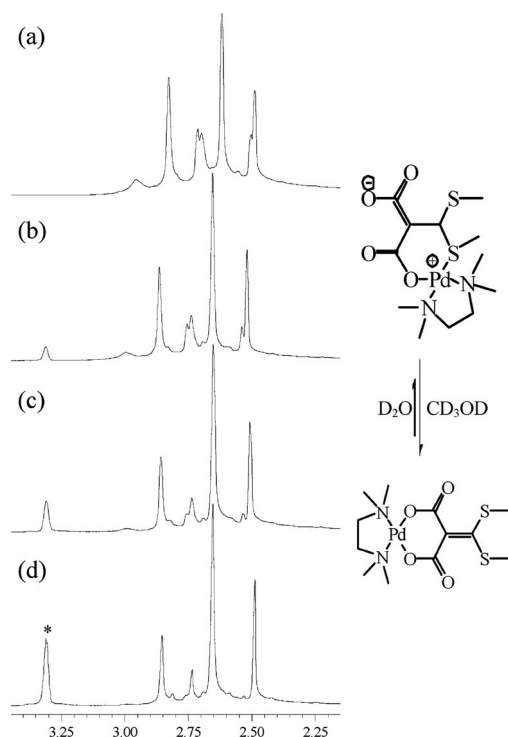


Figure 7.  $^1\text{H}$  NMR spectra of  $[\text{Pd}]\text{-O,O'-1}$  for gradual addition of  $\text{CD}_3\text{OD}$  into  $\text{D}_2\text{O}$  solution.  $[\text{D}_2\text{O}]/[\text{CD}_3\text{OD}] = 10:0$  (a);  $10:2$  (b);  $10:5$  (c);  $10:12$  (d) and corresponding equilibrium with assignments. The asterisk indicates the resonances of  $\text{CD}_3\text{OD}$ .

( $\text{N-CH}_3$ ), and 2.35 ( $\text{S-CH}_3$ ) ppm along with those of the new species at 2.72 (ethylene) and 2.64 (methyl) ppm from  $\text{Me}_4\text{en}$  in a mol ratio of 1:1 appeared. The addition of  $\text{CD}_3\text{OD}$  into the  $[\text{D}_6]\text{Me}_2\text{SO}$  solution restored the original  $[\text{Pd}]\text{-O,O'-1}$  complex (Figure 8). In contrast to the NMR spectrum in  $\text{D}_2\text{O}$ , the addition of acetone did not allow restoration to the original complex. According to the  $^{13}\text{C}$  NMR spectrum (Figure 9, Supporting Information), the  $^{13}\text{C}$  NMR resonances of **1** at 168.77, 144.54, 131.73, and 16.65 ppm appeared, but the resonances of  $\text{Me}_4\text{en}$  appeared as two pairs at  $\delta = 61.78$  and 61.07 ppm ( $\text{N-CH}_2$ ); 50.49 and 49.09 ppm ( $\text{N-CH}_3$ ), indicating an equilibrium between the original structure,  $[\text{Pd}]\text{-O,O'-1}$ , and the “ring-opened  $\text{Me}_2\text{SO}$  adduct”  $[(\text{Me}_4\text{en-N})(\text{Me}_2\text{SO-S})\text{Pd}]\text{-O,O'-1}$  species shown in Scheme 1 and Figure 8. The NMR spectrum of  $[\text{Pd}]\text{-O,O'-1}$  in  $[\text{D}_7]\text{DMF}$  showed a similar pattern as that in  $[\text{D}_6]\text{Me}_2\text{SO}$  (Figure 6). As mentioned earlier, the structure of  $[\text{Pd}]\text{-O,O'-1}$  is retained in  $\text{CD}_3\text{OD}$  or  $\text{CD}_3\text{CN}$ .

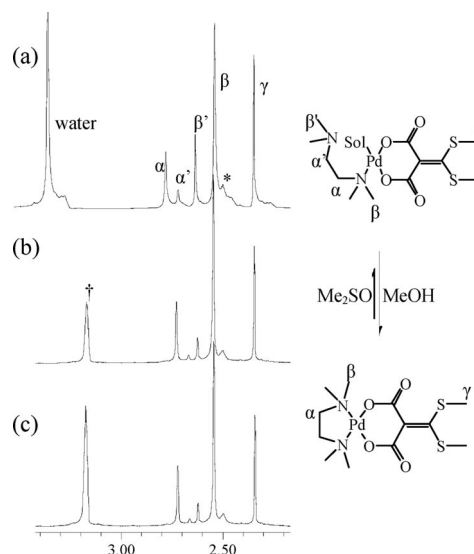


Figure 8.  $^1\text{H}$  NMR spectra of  $[\text{Pd}]\text{-O,O'-1}$  for gradual addition of  $\text{CD}_3\text{OD}$  into  $[\text{D}_6]\text{Me}_2\text{SO}$  solution  $\{[\text{D}_6]\text{Me}_2\text{SO}/[\text{CD}_3\text{OD}] = 1:0$  (a);  $1:4$  (b);  $1:8$  (c)\} and corresponding equilibrium with assignments. The asterisk and dagger indicate the resonances of  $[\text{D}_6]\text{Me}_2\text{SO}$  and  $\text{CD}_3\text{OD}$ , respectively.

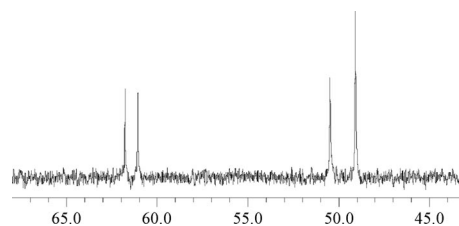


Figure 9. Partial  $^{13}\text{C}$  NMR spectrum of  $[\text{Pd}]\text{-O,O'-1}$  in  $[\text{D}_6]\text{-Me}_2\text{SO}$ .

$[\text{Pd}]\text{-O,O'-2}$  in  $\text{D}_2\text{O}$  exists as a mixture of  $\text{O,O'}$ - vs.  $\text{O,S}$ -chelate in a mol ratio of 2:5 (Supporting Information) in contrast to the 1:1 mol ratio of  $[\text{Pd}]\text{-O,O'-1}$ . Such a different mol ratio can be explained in that  $\text{S-Et}$  is more fluxional than  $\text{S-Me}$ , and thus the coplanar character of the sulfur-containing ethylene plane might be broken, resulting

in the enhancement of the donor strength of sulfur.<sup>[9c]</sup> The gradual addition of CD<sub>3</sub>OD into the D<sub>2</sub>O solution resulted in interconversion between *O,S*- and *O,O'*-chelate (Supporting Information). Of course, [[Pd]-*O,O'*-**2**] in [D<sub>6</sub>]-Me<sub>2</sub>SO coexists as a mixture of the species [[Pd]-*O,O'*-**2**] and [(Me<sub>4</sub>en-*N*)(Me<sub>2</sub>SO-*S*)Pd-*O,O'*-**2**] (Supporting Information).

By contrast, the structure of [[Pd]-*O,O'*-**3**], which contains the seven-membered ring, is preserved even in D<sub>2</sub>O or [D<sub>6</sub>]-Me<sub>2</sub>SO (Supporting Information).

### Solution Behavior of Bimetallic Complexes

The <sup>1</sup>H NMR spectra of [[Pd]-*O,O'*-**2**-*S,S'*-{M}](PF<sub>6</sub>)<sub>2</sub> in [D<sub>6</sub>]-Me<sub>2</sub>CO are depicted in Figure 10 (see Supporting Information for the solvent-dependent NMR spectra). The <sup>1</sup>H resonances of N-CH<sub>3</sub> (Me<sub>4</sub>en), S-CH<sub>2</sub>-, and NH<sub>2</sub> (en) in [D<sub>6</sub>]-Me<sub>2</sub>CO, [D<sub>6</sub>]-Me<sub>2</sub>SO, or CD<sub>3</sub>CN show two pairs of signals of 1:1 integral ratio. The two pairs of signals can be explained by the conformational fluxionality in the solution. Of course, NH<sub>2</sub> peaks disappear in protic solvents such as D<sub>2</sub>O and CD<sub>3</sub>OD. For [[Pd]-*O,O'*-**2**-*S,S'*-{Pd}](PF<sub>6</sub>)<sub>2</sub> in [D<sub>6</sub>]-Me<sub>2</sub>CO, NH<sub>2</sub> (en), S-CH<sub>2</sub>-, and N-CH<sub>3</sub> (Me<sub>4</sub>en) appeared at δ = 5.45 and 5.27 ppm as a singlet, 3.51 and 3.41 ppm as a multiplet, and 2.75 and 2.73 ppm as a singlet, respectively. For [[Pd]-*O,O'*-**2**-*S,S'*-{Pt}](PF<sub>6</sub>)<sub>2</sub> in the same solvent, NH<sub>2</sub> (en), S-CH<sub>2</sub>-, and N-CH<sub>3</sub> (Me<sub>4</sub>en) appeared at δ = 6.07 and 5.87 ppm as a singlet, and 3.67 and 3.51 ppm as a multiplet, and 2.75 and 2.73 ppm as a singlet, respectively. The amine protons of [[Pd]-*O,O'*-**2**-*S,S'*-{Pt}](PF<sub>6</sub>)<sub>2</sub> in CD<sub>3</sub>CN consisted of three singlets of ratio 2:1:1 at δ = 5.08, 4.85, and 4.65 ppm at 5 °C. The amine region of the proton spectra exhibited a marked temperature dependence in the range 5–60 °C, as shown in Figure 11. The banana-shaped conformational structure was fluxional in solution at high temperatures. The low-temperature spectrum showed three resonances (the resonance

at δ = 5.05 ppm came from the two N-H protons). Warming the sample resulted in a broadening of the resonance peaks at δ = 4.70 and 4.82 ppm, each pair coalescing at 60 °C. The process of exchange of the amine protons can be interpreted as reflecting an interconversion of the equilibration between the banana-type bent structures shown in Figure 11. Similarly, for [[Pd]-*O,O'*-**3**-*S,S'*-{Pt}](PF<sub>6</sub>)<sub>2</sub> in [D<sub>6</sub>]-Me<sub>2</sub>CO, NH<sub>2</sub> (en), S-CH<sub>2</sub>-, and N-CH<sub>3</sub> (Me<sub>4</sub>en) appeared at δ = 5.77 and 5.71 ppm as a singlet, 3.72 and 3.63 ppm as a multiplet, and 2.76 and 2.69 ppm as a singlet, respectively.

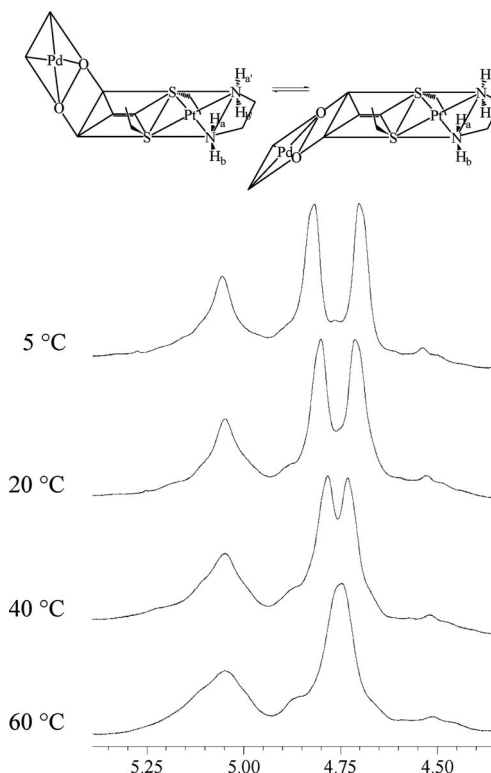


Figure 11. Variable-temperature amine <sup>1</sup>H NMR spectra of [[Pd]-*O,O'*-**2**-*S,S'*-{Pt}](PF<sub>6</sub>)<sub>2</sub> in CD<sub>3</sub>CN (600 MHz).

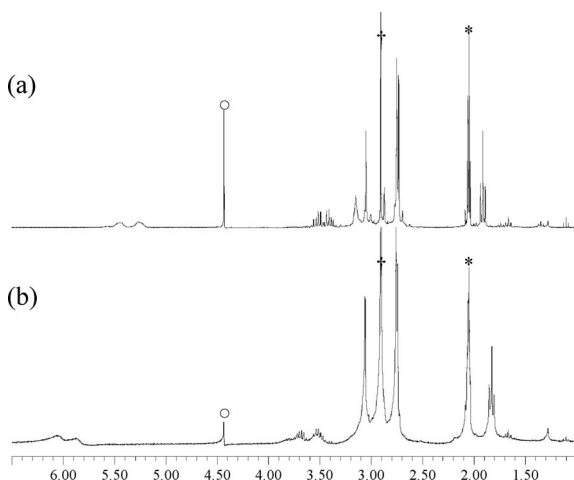


Figure 10. <sup>1</sup>H NMR spectra of [[Pd]-*O,O'*-**2**-*S,S'*-{Pd}](PF<sub>6</sub>)<sub>2</sub> (a) and [[Pd]-*O,O'*-**2**-*S,S'*-{Pt}](PF<sub>6</sub>)<sub>2</sub> (b) in [D<sub>6</sub>]-Me<sub>2</sub>CO. The asterisk, dagger, and circle indicate the resonances of [D<sub>6</sub>]-Me<sub>2</sub>CO, water, and solvated nitromethane, respectively.

### Effect of Coordination Chemistry on Solution Behavior

The present single-crystal X-ray structures show that Pd<sup>II</sup> favors the *O,O'*-chelate, whereas Pt<sup>II</sup> favors the *S,S'*-chelate in the solid state, indicating that Pt<sup>II</sup> is softer than Pd<sup>II</sup> in acidity. Actually, Pd<sup>II</sup> is very similar to Pt<sup>II</sup> chemically, but the present results discriminate the delicate difference between the Pd<sup>II</sup> and Pt<sup>II</sup> ions. Even though the reaction was conducted in water, in which [[Pd]-*O,O'*-L] exists as a mixture of the *O,S*- and *O,O'*-chelates, the reaction of [[Pd]-*O,O'*-L] with [(en)M<sup>II</sup>]<sup>2+</sup> yielded a product of [[Pd]-*O,O'*-L-*S,S'*-{M}]<sup>2+</sup>. Furthermore, the monometallic Pd<sup>II</sup> complexes of the ring-free ligands, **1** and **2**, in Me<sub>2</sub>SO, DMF, and H<sub>2</sub>O are labile on both sides of the neutral amine and anionic L ligands, but the monometallic compound of the ring containing ligand **3** is relatively resistant to solvent. Such a notably different behavior in solution might be explained by the steric constraints via the bent dihedral angles

(78.26° for  $[[\text{Pd}]\text{-O},\text{O}'\text{-1}]$ , 120.84° for  $[[\text{Pd}]\text{-O},\text{O}'\text{-3}]$ ). Furthermore, the dihedral angles of the bimetallic complexes corroborate that the complexes are inert in  $\text{Me}_2\text{SO}$  and  $\text{D}_2\text{O}$ . These results indicate that the labile properties result from a delicate combination of the steric strain via the dihedral angles and the nature of the solvents. Thus, a suitable combination of ring constraint, media, and dihedral angles can be considered to be the driving force behind the unusual isomerization and solvation.

The present banana-shaped bimetallic complexes are inert to linkage isomerism in solution, but variable temperature  $^1\text{H}$  NMR spectra in  $\text{CD}_3\text{CN}$  revealed that the amine proton resonances are sensitive to the fluxional motion of the remote ylidene moiety, suggesting that interconversion occurs between two “bent-up” and “bent-down” forms. Its amine proton resonance is clearly observable at  $\delta = 4.70$  and 4.82 ppm at room temperature, but as the sample temperature is increased, the resonance peaks become broadened, coalescing at 60 °C. In particular, the fact that there are two coalescing temperatures ( $T_c = 5^\circ\text{C}$ ,  $\Delta G^\ddagger = 13.8$  kcal/mol;  $T_c = 60^\circ\text{C}$ ,  $\Delta G^\ddagger = 16.6$  kcal/mol)<sup>[12]</sup> implies that interconversion occurs through an asymmetric fluxional process.<sup>[4c]</sup> Further studies on analogues will provide more detailed information on the pervasive influences and applications of task-specific bimetallic molecular materials. Such striking solution behavior including linkage isomerism, solvation, and interconversion seems to be attributed to the conformational properties of the present monometallic and bimetallic complexes.

## Conclusions

Procedures for efficient stepwise syntheses of monometallic palladium(II) and cognate bimetallic  $\text{Pd}^{\text{II}}/\text{Pt}^{\text{II}}$  complexes containing potential tetradentate bis(alkylthio)ylidenemalonate ligands were established. Notably, the crystalline structures indicate that palladium(II) favors the oxygen carboxylate donor and platinum(II) favors the S donor, which will be very useful information for the discrimination of metal properties. In contrast, the configuration of the big-size banana-shaped bimetallic complexes did not change, though conformational dynamics occurred in solution. The dihedral angles significantly affected the solution behavior. Studies on the structural nonrigidity of the present monometallic and bimetallic complexes will certainly contribute to the design and synthesis of molecular materials.

## Experimental Section

**Materials and Measurements:** All chemicals, including potassium tetrachloropalladate(II), potassium tetrachloroplatinate(II), diethylmalonate, ethylenediamine (en), *N,N,N',N'*-tetramethylethylenediamine ( $\text{Me}_4\text{en}$ ), and silver sulfate, were purchased from Aldrich and used without further purification. ( $\text{Me}_4\text{en}$ ) $\text{PdCl}_2$ <sup>[5c]</sup> and  $\text{Ba}[\text{L}]$ <sup>[13]</sup> were prepared according to the procedures outlined in the literature. Infrared spectra were obtained with a Nicolet 380 FTIR spectrophotometer, and samples were prepared as KBr pellets.  $^1\text{H}$

(300 MHz) and  $^{13}\text{C}$  NMR (75 MHz) spectra were recorded with a Varian Mercury Plus 300 instrument, and  $^{13}\text{C}$  NMR (125 MHz) spectra were recorded with an Inova 500 spectrometer. Temperature-dependent  $^1\text{H}$  NMR (600 MHz) spectra were recorded with a Varian Unity Plus 600 instrument. Elemental analyses were performed on crystalline samples by using a Vario-EL III analyzer at Pusan center, KBSI. The melting points were determined with a Thomas-Hoover capillary melting point apparatus and are uncorrected. Mass spectrometric analysis by a fast atom bombardment technique was performed in chloroform by using a KMS-700 Mstation Mass Spectrometer (Jeol, Japan) and an MS-MP9020D data system.

**$[[\text{Pd}]\text{-O},\text{O}'\text{-1}]$ :** Silver sulfate (2 mmol, 0.624 g) in water (10 mL) was added to a suspension of ( $\text{Me}_4\text{en}$ ) $\text{PdCl}_2$  (2 mmol, 0.587 g) in water (10 mL). The reaction mixture was stirred for 6 h, after which the silver chloride precipitate was filtered off. To this filtrate was added an aqueous solution of  $\text{Ba}[\text{I}]$  (2 mmol, 0.687 g), and the reaction solution was stirred for 8 h at room temperature in darkness. After the barium sulfate was filtered off, the filtrate was condensed to 3 mL at 40 °C, to which an excess amount of acetone was added. The resulting yellow crystalline product was filtered and washed with acetone. Single crystals suitable for single-crystal X-ray diffraction analysis were formed in a 74.4% yield (0.636 g) in a mixture of water and acetone. Mp: 169 °C (dec). IR (KBr pellet):  $\tilde{\nu} = 3406$  (br), 3282 (br), 1612 (s), 1466 (w), 1387 (w), 1335 (w) and 1117 (s)  $\text{cm}^{-1}$ .  $^1\text{H}$  NMR (300 MHz,  $\text{CD}_3\text{OD}$ , 25 °C):  $\delta = 2.84$  (s, 4 H, N- $\text{CH}_2$ ), 2.67 (s, 12 H, N- $\text{CH}_3$ ), 2.47 (s, 6 H, S- $\text{CH}_3$ ) ppm.  $^{13}\text{C}$  NMR (125 MHz,  $\text{D}_2\text{O}$ , 25 °C):  $\delta = 172.93$ , 170.83, 167.23, 146.62, 145.41, 136.83, 132.62, 64.24, 63.04, 62.32, 62.26, 61.59, 60.89, 51.81, 51.36, 51.22, 49.84, 49.72, 48.65, 24.32, 16.94, 16.55 ppm. MS (FAB):  $m/z = 426.1$  [ $\text{M} + \text{H}^+$ ]<sup>+</sup>, 385.2 [ $\text{M} + \text{H}^+ - \text{CO}_2$ ]<sup>+</sup>.  $\text{C}_{12}\text{H}_{30}\text{N}_2\text{O}_3\text{PdS}_2$  ( $[[\text{Pd}]\text{-O},\text{O}'\text{-1}]\cdot 4\text{H}_2\text{O}$ , 500.05): calcd. C 28.77, H 6.04, N 5.59; found C 28.50, H 6.01, N 5.62.

**$[[\text{Pd}]\text{-O},\text{O}'\text{-2}]$ :**  $[[\text{Pd}]\text{-O},\text{O}'\text{-2}]$  was obtained in the same manner as  $[[\text{Pd}]\text{-O},\text{O}'\text{-1}]$  in a 78.5% (0.715 g) yield. Mp: 157 °C (dec). IR (KBr pellet):  $\tilde{\nu} = 3417$  (br), 2922 (w), 1645 (s), 1624 (s), 1460 (w), 1321 (w), 1122 (w), 808 (w)  $\text{cm}^{-1}$ .  $^1\text{H}$  NMR (300 MHz,  $\text{CD}_3\text{NO}_2$ , 25 °C):  $\delta = 2.90$  (q,  $J = 7.5$  Hz, 4 H, S- $\text{CH}_2$ ), 2.86 (s, 4 H, N- $\text{CH}_2$ ), 2.68 (s, 12 H, N- $\text{CH}_3$ ), 1.35 (t,  $J = 7.5$  Hz, 6 H,  $\text{CH}_3$ ) ppm.  $\text{C}_{14}\text{H}_{26}\text{N}_2\text{O}_4\text{PdS}_2$  (456.92): calcd. C 36.80, H 5.74, N 6.13; found C 36.20, H 5.60, N 6.18.

**$[[\text{Pd}]\text{-O},\text{O}'\text{-3}]$ :**  $[[\text{Pd}]\text{-O},\text{O}'\text{-3}]$  was obtained in the same manner as  $[[\text{Pd}]\text{-O},\text{O}'\text{-1}]$  in an 87.9% (0.799 g) yield. Mp: 155 °C (dec). IR (KBr pellet):  $\tilde{\nu} = 3400$  (br), 2902 (w), 1639 (br), 1578 (w), 1342 (w), 1122 (w), 808 (w)  $\text{cm}^{-1}$ .  $^1\text{H}$  NMR (300 MHz,  $\text{D}_2\text{O}$ , 25 °C):  $\delta = 3.16$  (br., 4 H, S- $\text{CH}_2$ ), 2.85 (s, 4 H, N- $\text{CH}_2$ ), 2.64 (s, 12 H, N- $\text{CH}_3$ ), 2.06 (br., 4 H,  $\text{CH}_2$ ) ppm.  $^{13}\text{C}$  NMR (75 MHz,  $\text{D}_2\text{O}$ , 25 °C):  $\delta = 173.35$ , 148.76, 131.26, 62.31, 49.83, 33.14, 30.30 ppm.  $\text{C}_{14}\text{H}_{26}\text{N}_2\text{O}_3\text{PdS}_2$  ( $[[\text{Pd}]\text{-O},\text{O}'\text{-3}]\cdot \text{H}_2\text{O}$ , 472.03): calcd. C 35.56, H 5.54, N 5.92; found C 35.30, H 5.41, N 5.88.

**$[[\text{Pd}]\text{-O},\text{O}'\text{-1-S,S'}\text{-}\{\text{Pt}\}](\text{PF}_6)_2$ :** To a suspension of ( $\text{en}$ ) $\text{PtI}_2$  (0.5 mmol, 0.254 g) in  $\text{H}_2\text{O}$  (10 mL) was added  $\text{AgNO}_3$  (1 mmol, 0.170 g) in  $\text{H}_2\text{O}$  (10 mL), after which the mixture was stirred at 50 °C for 6 h. The silver iodide precipitate was removed, an aqueous solution (30 mL) of  $[[\text{Pd}]\text{-O},\text{O}'\text{-1}]$  (0.5 mmol, 0.227 g) was added dropwise to the filtrate, and the mixture was stirred at room temperature for 12 h in darkness. The solution was condensed to 2 mL, and an aqueous solution (0.5 mL) of  $\text{NaPF}_6$  (2 mmol, 0.222 g) was added, after which the solution was stirred for a further 1 h to obtain a pale yellow precipitate in a 52.7% (0.257 g) yield. Mp: 126 °C (dec). IR (KBr pellet):  $\tilde{\nu} = 3437$  (br), 1614 (br), 1464 (w), 1381 (w), 1338 (w), 843 (s,  $\text{PF}_6$ ), 561 (w,  $\text{PF}_6$ )  $\text{cm}^{-1}$ .  $^1\text{H}$

NMR (300 MHz,  $[D_6]Me_2CO$ , 25 °C):  $\delta$  = 5.95 (br., 2 H,  $NH_2$ ), 5.73 (br., 2 H,  $NH_2$ ), 3.39 (s, 4 H, N- $CH_2$ ), 3.21 (s, 4 H, N- $CH_2$ ), 3.01 (s, 6 H, S- $CH_3$ ), 2.73 (m, 12 H, N- $CH_3$ ) ppm.  $C_{14}H_{30}F_{12}N_4O_4P_2PdPtS_2$  (972.97): calcd. C 17.26, H 3.10, N 5.75; found C 17.40, H 3.18, N 5.60.

**[[Pd]-O,O'-2-S,S'-{Pd}](PF<sub>6</sub>)<sub>2</sub>:** [[Pd]-O,O'-2-S,S'-{Pd}](PF<sub>6</sub>)<sub>2</sub> was obtained in the same manner as [[Pd]-O,O'-1-S,S'-{Pt}](PF<sub>6</sub>)<sub>2</sub> and recrystallized from a mixture of  $CH_3NO_2$  and  $Et_2O$  to obtain single crystals in a 67.0% (0.306 g) yield. Mp: 168 °C (dec). IR (KBr pellet):  $\tilde{\nu}$  = 3437 (br), 3282 (w), 2928 (w), 1624 (s), 1464 (w), 1348 (s), 1057 (w), 1009 (w), 957 (w), 843 (s, PF<sub>6</sub>), 559 (w, PF<sub>6</sub>)  $cm^{-1}$ .  $^1H$  NMR (300 MHz,  $[D_6]Me_2CO$ , 25 °C):  $\delta$  = 5.45 (br., 2 H,  $NH_2$ ), 5.27 (br., 2 H,  $NH_2$ ), 3.51 (m, 2 H, S- $CH_2$ ), 3.41 (m, 2 H, S- $CH_2$ ), 3.14 (s, 4 H, N- $CH_2$ ), 3.04 (s, 4 H, N- $CH_2$ ), 2.75 (s, 6 H, N- $CH_3$ ), 2.73 (s, 6 H, N- $CH_3$ ), 1.91 (t,  $J$  = 7.5 Hz, 6 H,  $CH_3$ ) ppm.  $C_{16}H_{34}F_{12}N_4O_4P_2PdS_2$  (913.32): calcd. C 21.04, H 3.75, N 6.13; found C 20.90, H 3.66, N 6.30.

**[[Pd]-O,O'-2-S,S'-{Pt}](PF<sub>6</sub>)<sub>2</sub>:** [[Pd]-O,O'-2-S,S'-{Pt}](PF<sub>6</sub>)<sub>2</sub> was obtained in the same manner as [[Pd]-O,O'-1-S,S'-{Pt}](PF<sub>6</sub>)<sub>2</sub> and recrystallized from a mixture of  $CH_3NO_2$  and  $Et_2O$  to obtain crystals in a 60.0% (0.301 g) yield. Mp: 173 °C (dec). IR (KBr pellet):  $\tilde{\nu}$  = 3444  $cm^{-1}$  (br), 1618 (s), 1458 (w), 1354 (w), 845 (s, PF<sub>6</sub>), 559 (w)  $cm^{-1}$ .  $^1H$  NMR (300 MHz,  $[D_6]Me_2CO$ , 25 °C):  $\delta$  = 6.07 (br., 2 H,  $NH_2$ ), 5.87 (br., 2 H,  $NH_2$ ), 3.67 (m, 2 H, S- $CH_2$ ), 3.51 (m, 2 H, S- $CH_2$ ), 3.05 (s, 4 H, N- $CH_2$ ), 2.75 (s, 6 H, N- $CH_3$ ), 2.73 (s, 6 H, N- $CH_3$ ), 1.82 (t,  $J$  = 7.2 Hz, 6 H,  $CH_3$ ) ppm.

$C_{17}H_{37}F_{12}N_5O_6P_2PdPtS_2$  ([[Pd]-O,O'-2-S,S'-{Pd}](PF<sub>6</sub>)<sub>2</sub>· $CH_3NO_2$ , 1062.02): calcd. C 19.21, H 3.51, N 6.59; found C 19.10, H 3.55, N 6.60.

**[[Pd]-O,O'-3-S,S'-{Pd}](PF<sub>6</sub>)<sub>2</sub>:** [[Pd]-O,O'-3-S,S'-{Pd}](PF<sub>6</sub>)<sub>2</sub> was obtained in the same manner as [[Pd]-O,O'-1-S,S'-{Pt}](PF<sub>6</sub>)<sub>2</sub> in a 58.1% (0.264 g) yield. Mp: 165 °C (dec). IR (KBr pellet):  $\tilde{\nu}$  = 2922 (w), 1649 (s), 1579 (w), 1354 (w), 843 (s, PF<sub>6</sub>), 559 (w)  $cm^{-1}$ .  $^1H$  NMR (300 MHz,  $[D_6]Me_2CO$ , 25 °C):  $\delta$  = 5.23 (s, 2 H,  $NH_2$ ), 4.95 (s, 2 H,  $NH_2$ ), 3.43 (t,  $J$  = 5.7 Hz, 4 H, S- $CH_2$ ), 3.12 (s, 4 H, N- $CH_2$ ), 2.99 (s, 4 H, N- $CH_2$ ), 2.75 (s, 6 H, N- $CH_3$ ), 2.67 (s, 6 H, N- $CH_3$ ), 2.41 (m, 4 H,  $CH_2$ ) ppm.  $C_{16}H_{32}F_{12}N_4O_4P_2PdS_2$  (909.92): calcd. C 21.09, H 3.54, N 6.15; found C 21.50, H 3.52, N 6.30.

**[[Pd]-O,O'-3-S,S'-{Pt}](PF<sub>6</sub>)<sub>2</sub>:** [[Pd]-O,O'-3-S,S'-{Pt}](PF<sub>6</sub>)<sub>2</sub> was obtained in the same manner as [[Pd]-O,O'-1-S,S'-{Pt}](PF<sub>6</sub>)<sub>2</sub> and recrystallized via slow evaporation in acetone solution to obtain single crystals in a 71.8% (0.359 g) yield. Mp: 194 °C (dec). IR (KBr pellet):  $\tilde{\nu}$  = 1643 (br), 1626 (br), 1365 (w), 845 (s, PF<sub>6</sub>), 559 (w)  $cm^{-1}$ .  $^1H$  NMR (300 MHz,  $[D_6]Me_2CO$ , 25 °C):  $\delta$  = 5.9–5.6 (br., 4 H,  $NH_2$ ), 3.72 (m, 2 H, S- $CH_2$ ), 3.63 (m, 2 H, S- $CH_2$ ), 3.05–3.01 (m, 4 H, N- $CH_2$ ), 2.76 (s, 6 H, N- $CH_3$ ), 2.69 (s, 6 H, N- $CH_3$ ), 2.27 (m, 4 H,  $CH_2$ ) ppm.  $^{13}C$  NMR (75 MHz,  $[D_6]Me_2CO$ , 25 °C):  $\delta$  = 165.56, 155.74, 139.05, 62.75, 50.17, 49.87, 48.36, 41.34, 20.38 ppm.  $C_{19}H_{38}F_{12}N_4O_5P_2PdPtS_2$  ([[Pd]-O,O'-3-S,S'-{Pt}](PF<sub>6</sub>)<sub>2</sub>· $Me_2CO$ , 1057.03): calcd. C 21.57, H 3.62, N 5.30; found C 21.40, H 3.66, N 5.50.

Table 3. Crystallographic data for [[Pd]-O,O'-1]·4H<sub>2</sub>O, [[Pd]-O,O'-3]·H<sub>2</sub>O, [[Pd]-O,O'-2-S,S'-{Pd}](PF<sub>6</sub>)<sub>2</sub>, [[Pd]-O,O'-2-S,S'-{Pt}](PF<sub>6</sub>)<sub>2</sub>· $CH_3NO_2$ , and [[Pd]-O,O'-3-S,S'-{Pt}](PF<sub>6</sub>)<sub>2</sub>· $Me_2CO$ .

|   | [[Pd]-O,O'-1]·4H <sub>2</sub> O                                     | [[Pd]-O,O'-3]·H <sub>2</sub> O                                    | [[Pd]-O,O'-2-S,S'-{Pd}](PF <sub>6</sub> ) <sub>2</sub> |
|---|---|---|--|
| Formula                                   | $C_{12}H_{30}N_2O_8PdS_2$   | $C_{14}H_{26}N_2O_5PdS_2$   | $C_{16}H_{34}F_{12}N_4O_4P_2PdS_2$                     |
| $M_w$ [g mol <sup>-1</sup> ]              | 500.90  | 472.89  | 913.32   |
| Crystal system                            | monoclinic  | monoclinic  | triclinic  |
| Space group                               | $P2_1/c$  | $P2_1/c$  | $P\bar{1}$   |
| $a$ [Å]                                   | 8.699(9)  | 14.105(7)   | 11.981(1)  |
| $b$ [Å]                                   | 27.240(3)   | 8.712(4)  | 12.988(1)  |
| $c$ [Å]                                   | 11.532(1)   | 15.807(8)   | 14.389(1)  |
| $\alpha$ [°]                              | 90  | 90  | 65.780(2)  |
| $\beta$ [°]                               | 131.26(2)   | 94.397(1)   | 66.462(2)  |
| $\gamma$ [°]                              | 90  | 90  | 60.525(2)  |
| $V$ [Å <sup>3</sup> ]                     | 2054.3(4)   | 1936.8(2)   | 1721.8(3)  |
| $Z$                                       | 4   | 4   | 2  |
| $\mu$ [mm <sup>-1</sup> ]                 | 1.145   | 1.198   | 1.352  |
| GOF on $F^2$                              | 1.075   | 1.239   | 1.050  |
| $R_1$ [ $I > 2\sigma(I)$ ] <sup>[a]</sup> | 0.0361  | 0.0231  | 0.0920   |
| $wR_2$ (all data) <sup>[b]</sup>          | 0.0952  | 0.0748  | 0.2830   |
|   | [[Pd]-O,O'-2-S,S'-{Pt}](PF <sub>6</sub> ) <sub>2</sub> · $CH_3NO_2$ | [[Pd]-O,O'-3-S,S'-{Pt}](PF <sub>6</sub> ) <sub>2</sub> · $Me_2CO$ |  |
| Formula                                   | $C_{17}H_{37}F_{12}N_5O_6P_2PdPtS_2$                                | $C_{19}H_{38}F_{12}N_4O_5P_2PdPtS_2$                              |  |
| $M_w$ [g mol <sup>-1</sup> ]              | 1063.07   | 1058.08   |  |
| Crystal system                            | triclinic   | monoclinic  |  |
| Space group                               | $P\bar{1}$  | $P2_1/n$  |  |
| $a$ [Å]                                   | 11.632(8)   | 12.769(7)   |  |
| $b$ [Å]                                   | 12.452(9)   | 12.545(7)   |  |
| $c$ [Å]                                   | 14.429(1)   | 21.203(1)   |  |
| $\alpha$ [°]                              | 92.595(1)   | 90  |  |
| $\beta$ [°]                               | 113.360(1)  | 100.50(1)   |  |
| $\gamma$ [°]                              | 115.615(1)  | 90  |  |
| $V$ [Å <sup>3</sup> ]                     | 1667.7(2)   | 3339.6(3)   |  |
| $Z$                                       | 2   | 4   |  |
| $\mu$ [mm <sup>-1</sup> ]                 | 5.052   | 5.048   |  |
| GOF on $F^2$                              | 1.187   | 1.376   |  |
| $R_1$ [ $I > 2\sigma(I)$ ] <sup>[a]</sup> | 0.0294  | 0.0411  |  |
| $wR_2$ (all data) <sup>[b]</sup>          | 0.0615  | 0.0994  |  |

[a]  $R_1 = \Sigma ||F_o| - |F_c|| / \Sigma |F_o|$ . [b]  $wR_2 = \{ \Sigma [w(F_o^2 - F_c^2)^2] / \Sigma [w(F_o^2)^2] \}^{1/2}$ .

**Crystal Structure Determination:** X-ray data were collected with a Bruker SMART automatic diffractometer with graphite-monochromated Mo- $K_{\alpha}$  radiation ( $\lambda = 0.71073 \text{ \AA}$ ) and a CCD detector at ambient temperature. Forty five frames of two-dimensional diffraction images were collected and processed to obtain the cell parameters and orientation matrix. The data were corrected for the Lorentz and polarization effects. The absorption effects were corrected by using the empirical  $\psi$ -scan method. The structures were solved by using the direct method (SHELXS 97) and refined by using the full-matrix least-squares techniques (SHELXL 97).<sup>[14]</sup> The non-hydrogen atoms were refined anisotropically, and the hydrogen atoms were placed in calculated positions and refined only for the isotropic thermal factors. The crystal parameters and procedural information corresponding to the data collection and structure refinement are listed in Table 3. CCDC-739529 (for [[Pd]-O, O'-1]·4H<sub>2</sub>O), -739530 (for [[Pd]-O, O'-3]·H<sub>2</sub>O), -739531 (for [[Pd]-O, O'-2-S, S'-{Pd}](PF<sub>6</sub>)<sub>2</sub>), -739532 (for [[Pd]-O, O'-2-S, S'-{Pt}](PF<sub>6</sub>)<sub>2</sub>·CH<sub>3</sub>NO<sub>2</sub>), and -739533 (for [[Pd]-O, O'-3-S, S'-{Pt}](PF<sub>6</sub>)<sub>2</sub>·Me<sub>2</sub>CO) contain the supplementary crystallographic data for this paper. These data can be obtained free of charge from The Cambridge Crystallographic Data Centre via [http://www.ccdc.cam.ac.uk/data\\_request/cif](http://www.ccdc.cam.ac.uk/data_request/cif).

**Supporting Information** (see footnote on the first page of this article): NMR spectra of [[Pd]-O, O'-1] in D<sub>2</sub>O (<sup>1</sup>H, <sup>13</sup>C) and [D<sub>6</sub>]-Me<sub>2</sub>SO (<sup>13</sup>C). Solvent-dependent <sup>1</sup>H NMR spectra of [[Pd]-O, O'-2]. <sup>1</sup>H NMR spectra of [[Pd]-O, O'-2] during gradual addition of CD<sub>3</sub>OD into the D<sub>2</sub>O solution. <sup>1</sup>H NMR spectra of [[Pd]-O, O'-2] during gradual addition of D<sub>2</sub>O into the CD<sub>3</sub>OD solution of [[Pd]-O, O'-2]. <sup>1</sup>H NMR spectra of [[Pd]-O, O'-2] during gradual addition of CD<sub>3</sub>OD into the [D<sub>6</sub>]-Me<sub>2</sub>SO solution of [[Pd]-O, O'-2]. Solvent-dependent <sup>1</sup>H NMR spectra of [[Pd]-O, O'-3]. <sup>1</sup>H NMR spectra of [[Pd]-O, O'-1-S, S'-{Pt}](PF<sub>6</sub>)<sub>2</sub>, [[Pd]-O, O'-3-S, S'-{Pd}](PF<sub>6</sub>)<sub>2</sub>, and [[Pd]-O, O'-3-S, S'-{Pt}](PF<sub>6</sub>)<sub>2</sub> in [D<sub>6</sub>]-Me<sub>2</sub>CO. Solvent-dependent <sup>1</sup>H NMR spectra of [[Pd]-O, O'-2-S, S'-{Pd}](PF<sub>6</sub>)<sub>2</sub>, and [[Pd]-O, O'-2-S, S'-{Pt}](PF<sub>6</sub>)<sub>2</sub>.

## Acknowledgments

This research was supported by the Korea Science and Engineering Foundation (KOSEF) R01-2007-000-20245-0.

- [1] a) C. Azerraf, S. Cohen, D. Gelman, *Inorg. Chem.* **2006**, *45*, 7010–7017; b) A. K. Justice, R. C. Linck, T. B. Rauchfuss, *Inorg. Chem.* **2006**, *45*, 2406–2412; c) E. Bukhaltsev, L. Frish, Y. Cohen, A. Vigalok, *Org. Lett.* **2005**, *7*, 5123–5126; d) C. Metcalfe, M. Webb, J. A. Thomas, *Chem. Commun.* **2002**, 2026–2027; e) S. Tabassum, I. H. Bhat, *Transition Met. Chem.* **2005**, *30*, 998–1007.
- [2] a) T. E. Bitterwolf, *Coord. Chem. Rev.* **2000**, 206–207, 419–450; b) K. T. Szacilowski, P. Xie, A. Y. S. Malkhasian, M. J. Heeg, M. Y. Udugala-Ganeheneg, L. E. Wenger, J. F. Endicott, *Inorg. Chem.* **2005**, *44*, 6019–6033; c) V. Balzani, A. Credi, M. Venturi, *Molecular Devices and Machines: A Journey into the Nano World*, Wiley-VCH, Weinheim, Germany, **2003**; d) K. Kubo, A. Nakao, H. M. Yamamoto, R. Kato, *J. Am. Chem. Soc.* **2006**, *128*, 12358–12359.
- [3] a) G. R. Newkome, E. He, C. N. Moorefield, *Chem. Rev.* **1999**, *99*, 1689–1746; b) S. Lanza, G. Callipari, F. Loiseau, S. Serroni, G. Tresoldi, *Inorg. Chem.* **2005**, *44*, 6717–6724.
- [4] a) I. S. Chun, S. J. Moon, Y. M. Na, Y.-A. Lee, K. H. Yoo, O.-S. Jung, *Inorg. Chem. Commun.* **2007**, *10*, 967–970; b) Y.-A. Lee, O.-S. Jung, *Angew. Chem. Int. Ed.* **2001**, *40*, 3868–3870; c) Y.-A. Lee, O.-S. Jung, S. J. Kang, K. B. Lee, Y. S. Sohn, *Inorg. Chem.* **1996**, *35*, 1641–1646; d) T. H. Noh, S. J. Moon, Y. M. Na, B. J. Ha, O.-S. Jung, *Inorg. Chem. Commun.* **2008**, *11*, 1334–1336.
- [5] a) S. S. Kwon, M. S. Cha, J. E. Lee, S. S. Lee, O.-S. Jung, *Cryst. Growth Des.* **2008**, *8*, 2073–2075; b) Y. M. Na, T. H. Noh, I. S. Chun, Y.-A. Lee, J. Hong, O.-S. Jung, *Inorg. Chem.* **2008**, *47*, 1391–1396; c) V. K. Jain, L. Jain, *Coord. Chem. Rev.* **2005**, *249*, 3075–3197.
- [6] a) T. H. Noh, I. S. Chun, Y.-A. Lee, S. Ahn, J. Hong, O.-S. Jung, *Bull. Chem. Soc. Jpn.* **2008**, *81*, 1461–1464; b) H. J. Kang, T. H. Noh, J. S. Jin, O.-S. Jung, *Inorg. Chem.* **2008**, *47*, 5528–5530; c) I. S. Chun, J. A. Kwon, H. J. Yoon, M. N. Bae, J. Hong, O.-S. Jung, *Angew. Chem. Int. Ed.* **2007**, *46*, 4960–4963; d) H. J. Yoon, I. S. Chun, Y. M. Na, Y.-A. Lee, O.-S. Jung, *Chem. Commun.* **2007**, 492–494.
- [7] a) Q. Yao, E. P. Kinney, C. Zheng, *Org. Lett.* **2004**, *6*, 2997–2999; b) M. Fujita, F. Ibukuro, H. Hagihara, K. Ogura, *Nature* **1994**, *367*, 720–723; c) I. S. Chun, K. S. Lee, J. Hong, Y. Do, O.-S. Jung, *Chem. Lett.* **2007**, 548–549; d) S. R. Seidel, P. J. Stang, *Acc. Chem. Res.* **2002**, *35*, 972–983.
- [8] K. M. Kim, S. S. Lee, O.-S. Jung, Y. S. Sohn, *Inorg. Chem.* **1996**, *35*, 3077–3078.
- [9] a) K. M. Kim, J. S. Park, Y.-S. Kim, Y. J. Jun, T. Y. Kang, Y. S. Sohn, M. J. Jun, *Angew. Chem. Int. Ed.* **2001**, *40*, 2458–2460; b) K. H. Kim, R. Song, K. M. Kim, *J. Am. Chem. Soc.* **2003**, *125*, 7170–7171; c) R. Song, K. M. Kim, Y. S. Sohn, *Inorg. Chem.* **2003**, *42*, 821–826; d) Y. S. Sohn, K. M. Kim, S. J. Kang, O.-S. Jung, *Inorg. Chem.* **1996**, *35*, 4274–4276; e) K. M. Kim, S. S. Lee, O.-S. Jung, M. J. Jun, Y. S. Sohn, *Inorg. Chim. Acta* **1997**, *256*, 217–222.
- [10] F. H. Allen, O. Kennard, D. G. Watson, L. Brammer, A. G. Orpen, R. Taylor, *J. Chem. Soc., Perkin Trans. 2* **1987**, S1–S19.
- [11] D. R. Lide, *CRC Handbook of Chemistry and Physics*, 71st ed., CRC Press, Boston, **1990–1991**, pp. 8–44.
- [12]  $\Delta G^\ddagger$  values were calculated from  $k_c = \pi \Delta v / 2^{1/2}$ ;  $\Delta G^\ddagger = 2.3RT_c(10.32 + \log T_c/k_c)$ . The value of  $\Delta v$  at 5 °C was supposed to be the same as that at 60 °C.
- [13] a) N. Katagiri, S. Ise, N. Watanabe, C. Kaneko, *Chem. Pharm. Bull.* **1990**, *38*, 3242–3248; b) T. Kosakada, K. Taninaka, H. Kurono, *Jpn. Patent*, 78 03519, **1978**.
- [14] G. M. Sheldrick, *SHELXS-97: A Program for Structure Determination*; University of Göttingen, Germany, **1997**; G. M. Sheldrick, *SHELXL-97: A Program for Structure Refinement*, University of Göttingen, Germany, **1997**.

Received: August 18, 2009

Published Online: November 11, 2009

# Fréchet-Type Pallado-Dendrimers Containing Bis(pyrazolyl)methane Ligands

Alberto Sánchez-Méndez,<sup>[a]</sup> Ernesto de Jesús,<sup>\*[a]</sup> Juan C. Flores,<sup>\*[a]</sup> and Pilar Gómez-Sal<sup>[a]</sup>

**Keywords:** Dendrimers / N ligands / Palladium / Heck reaction / Pyrazolyl ligands

Neutral and cationic {bis(3,5-dimethylpyrazol-1-yl)methane}-palladium(II) complexes of general formula  $[\text{PdClX}\{\text{RCH}(3,5\text{-Me}_2\text{pz})_2\}]$  ( $\text{X} = \text{Cl}$  or  $\text{Me}$ ) or  $[\text{PdMe}(\text{MeCN})\{\text{RCH}(3,5\text{-Me}_2\text{pz})_2\}][\text{BAr}^f_4]$ , where R is a benzyl or benzyloxycarbonyl group or a poly(aryl ether) Fréchet-type dendron, have been synthesized and fully characterized, including by X-ray diffraction

methods in some cases. These palladium complexes have been evaluated as catalyst precursors in the Heck reaction between *para*-iodotoluene and methyl acrylate. The active catalytic species formed from these precursors are apparently not coordinated to the bis(pyrazolyl)methane ligands.

## Introduction

The incorporation of transition metal atoms into dendrimers has attracted much attention in the light of possible applications in advanced materials, biomedicine, and catalysis.<sup>[1–4]</sup> Metal binding is achieved by means of a large variety of anchoring ligands, which themselves modulate the steric and electronic properties of the first coordination sphere of the metal centers. Our recent work in this field has focused on metal–dendrimer linkages based on N-donor ligands, such as diketiminato,<sup>[5]</sup> imido,<sup>[6]</sup> or (pyridin-2-yl)methanimine.<sup>[7]</sup>

Poly(pyrazol-1-yl)borates and related compounds constitute an important and versatile class of N-donor ligands with an extensively developed coordination chemistry.<sup>[8]</sup> Their neutral and isoelectronic counterparts, poly(pyrazol-1-yl)alkanes, have also received significant attention during the last few years<sup>[9]</sup> encouraged by synthetic advances<sup>[10]</sup> and a wide range of attractive applications.<sup>[11,12]</sup> Despite their availability, however, poly(pyrazolyl) ligands have rarely been used in the chemistry of dendrimers or related compounds. We have combined scorpionato ligands with dendrimers according to the strategy used by Reger and co-workers to prepare multitopic ligands and polynuclear compounds by taking advantage of the facile functionalization of the methine bridging carbon atom in tris(pyrazol-1-yl)methanes.<sup>[13,14]</sup> According to a similar strategy, we functionalized the bridging methylene carbon atom of bis(pyrazol-1-yl)methanes with poly(aryl ether) dendrons (Fréchet dendrons) and used these ligands to form monometallic nickel(II)<sup>[15]</sup> or molybdenum complexes.<sup>[16]</sup> Ciriano and Ca-

sado used a different approach to synthesize carbosilane dendrimers with bis- or tris(pyrazolyl)borate rhodium complexes.<sup>[17]</sup>

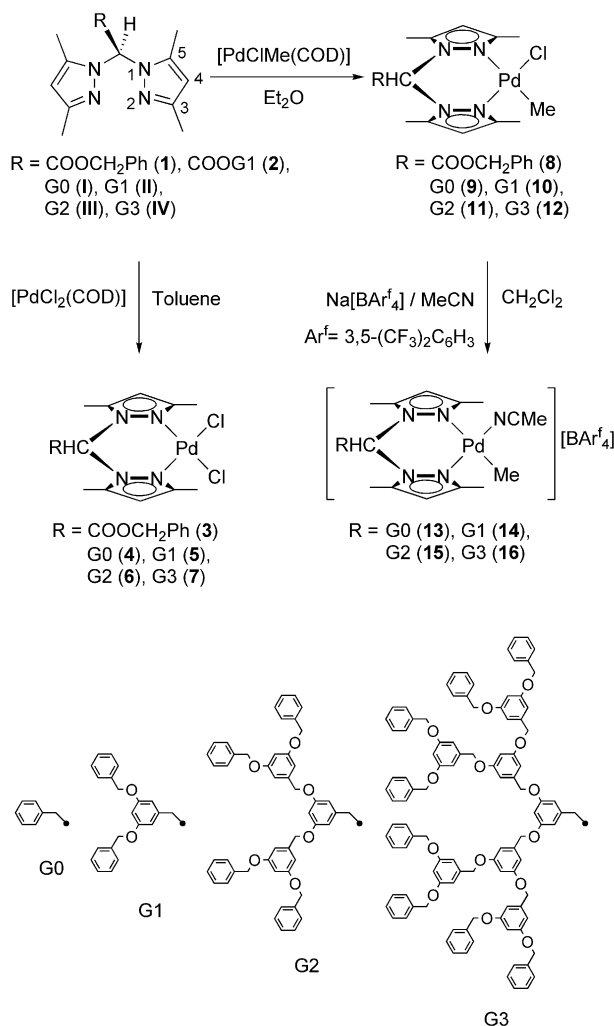
The application of dendrimers containing transition metal atoms in catalysis has been stimulated by the possibility of catalyst recovery, especially by using nanofiltration techniques,<sup>[18,19]</sup> and the likelihood of obtaining specific dendrimer effects.<sup>[3,20]</sup> A stable dendritic ligand–metal coordination is usually a prerequisite for most of these applications. We recently reported the X-ray structures of the {bis(pyrazol-1-yl)methane}palladium complexes **4–6** (Scheme 1), which differ in the size of the poly(aryl ether) substituents (zeroth, first, and second generation, respectively).<sup>[21]</sup> As the accessibility of metal centers varies with the size of the dendritic ligand coordinated to them, we reasoned that these complexes might be useful for examining the stability of bis(pyrazol-1-yl)methane coordination to palladium under the reductive conditions of a Heck reaction. The results of this study are reported herein together with full details of the synthesis and characterization of **4–6** and other related neutral and cationic palladium(II) complexes.

## Results and Discussion

### Synthesis of Ligands and Palladium Compounds

The (benzyl)bis(3,5-dimethylpyrazol-1-yl)methane ligand **I** and the related first- to third-generation Fréchet dendrons **II–IV** used in this work were obtained by alkylation of the bromobenzyl derivatives  $G_n\text{-Br}$ <sup>[22]</sup> with  $\text{LiCH}(3,5\text{-Me}_2\text{pz})_2$ , as reported elsewhere (Scheme 1).<sup>[15]</sup> Ester **1** was synthesized from benzyl bromide and the carboxylate  $\text{Na}[\text{CH}(3,5\text{-Me}_2\text{pz})_2(\text{COO})]$  in a reaction which took 2 d to complete in refluxing thf. In contrast, formation of the G1 analogue **2** was not possible under the same conditions, and the maxi-

[a] Departamento de Química Inorgánica, Universidad de Alcalá, Campus Universitario, 28871 Alcalá de Henares (Madrid), Spain  
Fax: +34-91-885-4683  
E-mail: ernesto.dejesus@uah.es  
juanc.flores@uah.es



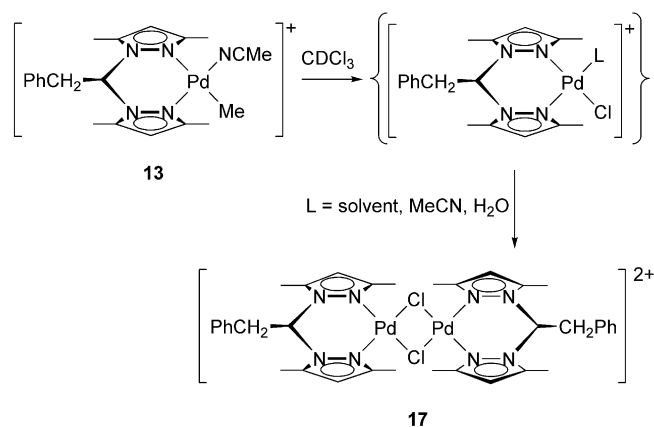
Scheme 1. Synthesis of the palladium complexes.

mum yield of this ligand (21%) was achieved after 4 d in refluxing acetone. Moreover, compound **2** was always isolated contaminated with small amounts of the carboxylic acid CH(3,5-Me<sub>2</sub>pz)<sub>2</sub>(COOH). In view of these results, the preparation of higher-generation analogues of ligands **1** and **2** was not attempted.

The palladium(II) dichlorido complexes **3–7** were synthesized by treating the corresponding bis(pyrazolyl)methanes with 1 equiv. of [PdCl<sub>2</sub>(COD)] in warm toluene, whereas the chlorido(methyl)palladium(II) complexes **8–12** were obtained from [PdClMe(cod)] at room temperature in diethyl ether (cod = η<sup>4</sup>-1,5-cyclooctadiene; Scheme 1). The addition of Na[Barf<sub>4</sub>] [Ar<sup>f</sup> = 3,5-(CF<sub>3</sub>)<sub>2</sub>C<sub>6</sub>H<sub>3</sub>] to dichloromethane solutions of **9–12** in the presence of acetonitrile afforded the cationic methyl(acetonitrile) complexes **13–16** by chloride abstraction. All these complexes were obtained in good to excellent yields as air-stable, hygroscopic, yellow-orange (**3–7** and **13–16**) or white solids (**8–12**). They are insoluble in alkanes, scarcely soluble in diethyl ether, soluble in aromatics, and very soluble in chlorinated solvents.

The solubility of these compounds in the above solvents increases with the molecular size of the dendritic substituent.

The neutral methyl complexes **8–12** are fairly stable in chlorinated solvents despite the tendency of methylpalladium complexes to decompose in such solvents by Pd–Me/Pd–Cl exchange, with concomitant precipitation of black Pd<sup>0</sup>.<sup>[7c,23]</sup> Cationic methyl complexes **13–16** are somewhat less stable under such conditions and, for instance, complex **13** partially decomposes after several weeks in CDCl<sub>3</sub> to give a complex mixture of products from which single crystals of the dimer **17** were obtained. The molecular structure of **17** was obtained by X-ray diffraction methods and is discussed below. The formation of this dimer probably occurs via an intermediate similar to that proposed in Scheme 2. Indeed, a new group of two resonances, as would be expected for the two nonequivalent CH<sub>2</sub> protons of the proposed intermediate, were found to appear at δ = 4.80 [dd, <sup>2</sup>J<sub>H,H</sub> = 13.5, <sup>3</sup>J<sub>H,H</sub> = 7.2 Hz] and 5.08 (dd, <sup>2</sup>J<sub>H,H</sub> = 13.5, <sup>3</sup>J<sub>H,H</sub> = 7.5 Hz) ppm in the <sup>1</sup>H NMR spectrum of samples of **13** in CDCl<sub>3</sub> after 2–3 weeks.

Scheme 2. Proposed pathway for the formation of the dimetallic complex **17** by decomposition of **13** in [D<sub>1</sub>]chloroform (counteranion = [Barf<sub>4</sub>]<sup>−</sup>).

Both pyrazolyl rings are equivalent in the <sup>1</sup>H and <sup>13</sup>C{<sup>1</sup>H} NMR spectra of the dichlorido complexes **3–7** but give rise to two sets of resonances in monomethyl derivatives **8–16** due to the absence of a mirror plane in the latter complexes. Thus, the resonance for the Me<sup>3</sup> protons at δ ≈ 2.5 ppm in **3–7** is split into two singlets in **8–16**, with that at higher field corresponding to the Me<sup>3</sup> group adjacent to the Pd–Me (δ ≈ 2.3 ppm) or Pd–NCMe groups (δ ≈ 2.1 ppm). For the same reason, the methylene protons of the benzyl group or their analogues in the G<sub>n</sub> dendrons are diastereotopic in the asymmetrically substituted complexes **8–16**. The chemical shifts corresponding to the dendron nuclei remain basically unmodified upon coordination of the free ligands to the metal center, with the exception of those belonging to the most internal moieties [–ArCH<sub>2</sub>CH(3,5-Me<sub>2</sub>pz)<sub>2</sub> or >–CH<sub>2</sub>OC(O)CH(3,5-Me<sub>2</sub>pz)<sub>2</sub>]. The most significant changes involve the 3-Me (Δδ ≈ +0.5 ppm), methylene (Δδ ≈ +1.7 ppm), and *ortho*-protons of the inner benzyl group (Δδ ≈ +0.5 ppm), and the methylene (Δδ ≈ +3 ppm),

methine ( $\Delta\delta \approx -3$  ppm), pz-C<sup>5</sup> ( $\Delta\delta \approx +2$  ppm), pz-C<sup>3</sup> ( $\Delta\delta \approx +5$  ppm), and *ipso*-carbon atoms of the same benzyl group ( $\Delta\delta \approx -3$  ppm) for **4–7** and **9–16**, respectively. These changes are more pronounced for the dichlorido complexes and are attributed to a combination of deshielding and anisotropic effects caused by the chlorido ligand and the positioning upon coordination of the pyrazolyl rings, respectively.

The anisotropy resulting from the increasing number of aryl groups surrounding the metal center in a G0–G3 series of complexes also has a small effect on the chemical shifts of nuclei situated at the focal point of the molecules. The general trend is a small, but steady and consistent, shift of the proton and carbon resonances to higher field, as can be seen, for instance, for the Me<sup>3</sup> group of the G0–G3 series **4–7**:  $\delta_{\text{average}} = 2.59, 2.57, 2.52$ , and  $2.51$  ppm for <sup>1</sup>H and  $\delta_{\text{average}} = 15.4, 15.3, 15.3$ , and  $15.2$  ppm for <sup>13</sup>C.

Compounds **1–16** were also characterized by IR spectroscopy, where an intense  $\nu_{\text{as}}(\text{C}=\text{N})$  absorption at around  $1560\text{ cm}^{-1}$  was observed, and mass spectrometry (APCI<sup>+</sup>/MS for **1–6** and **8–11**, ESI<sup>+</sup>/MS for **7**, and ESI<sup>+</sup>-TOF/MS for **12–16**). However, whereas the molecular cation  $[\text{M} - \text{BAR}^f_4]^+$  was detected in the case of the ionic compounds **12–16**, only typical fragmentation patterns of  $[\text{L}_2\text{PdXY}]$  complexes were observed for the neutral complexes **3–11**. For instance, dichlorido complexes **3–7** fragmented by loss of one or two chloro atoms, followed in some cases by coordination of methanol or by recombination to give dimetallic halide-bridged structures such as  $[\text{M}_2 - \text{Cl}]^+$  or  $[\{\text{M} - \text{Cl}\}_2 - \text{Cl}]^{2+}$ . Chlorido(methyl) derivatives **8–12** produced comparable fragments by loss of methyl groups or chloro atoms. In addition, peaks corresponding to the bis(pyrazolyl) ligands and their fragmentation by loss of a pyrazolyl ring were generally observed for all palladium complexes.

### Crystal Structures of **3–6** and **17**

The molecular structures of the G0–G2 series of  $\text{PdCl}_2$  complexes **4–6** have been reported previously<sup>[21]</sup> and data are given here for comparative purposes only. The molecular structure of **3** consists of discrete monometallic molecules (Figure 1), whereas that of **17** contains a cationic dimer (Figure 2). The structural parameters defining the  $[\text{CH}(3,5\text{-Me}_2\text{pz})_2]\text{PdCl}_2$  moieties are fairly similar for the five complexes compared in Table 1 (**3–6** and **17**), with the palladium atoms exhibiting rather square-planar geometries. The  $\text{Pd}[(\text{NN})_2\text{C}]$  palladacycles adopt pronounced boat

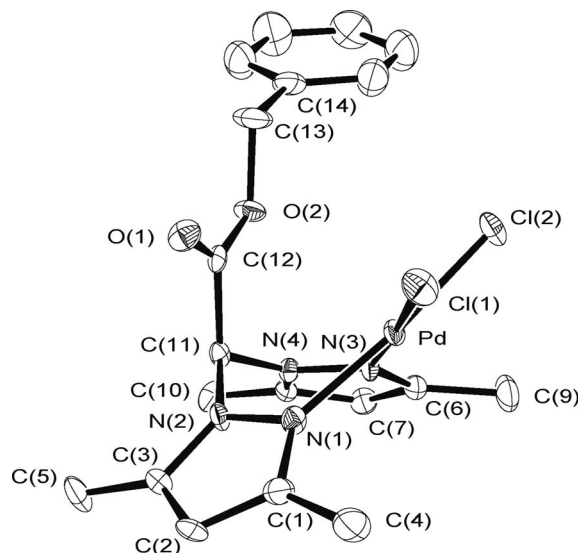


Figure 1. Molecular structure of  $[\text{PdCl}_2\{\text{PhCH}_2\text{OC}(\text{O})\text{CH}(3,5\text{-Me}_2\text{pz})_2\}]$  (**3**).

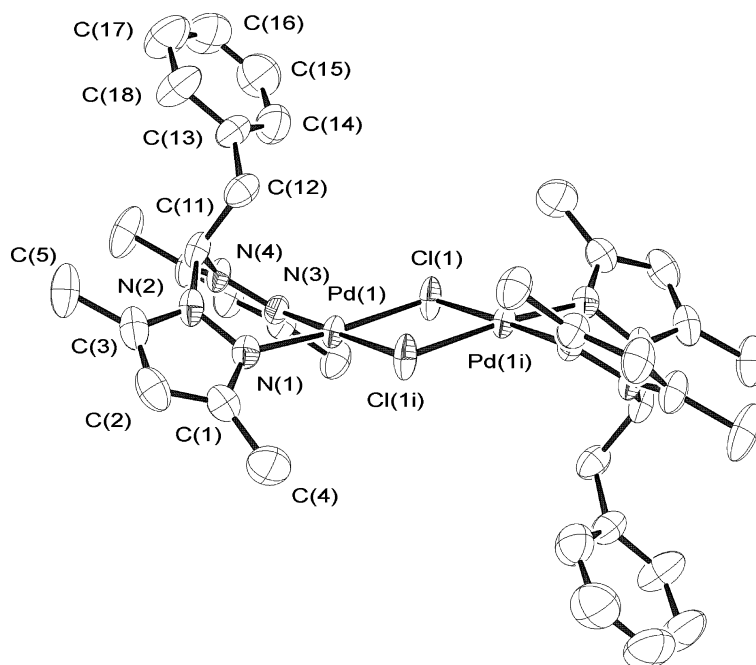


Figure 2. Molecular structure of  $[(\text{Pd}(\mu\text{-Cl})\{\text{PhCH}_2\text{CH}(3,5\text{-Me}_2\text{pz})_2\})_2][\text{BAR}^f_4]_2$  (**17**). The  $\text{BAR}^f_4^-$  ions have been omitted for clarity.

Table 1. Selected bond lengths [Å] and angles [°] for compounds **3–6** and **17**.

|                            | <b>3</b>  | <b>4</b>   | <b>5</b>  | <b>6</b>   | <b>17</b> <sup>[a]</sup> |
|----------------------------|-----------|------------|-----------|------------|--------------------------|
| Pd–Cl(1)                   | 2.2734(9) | 2.2883(16) | 2.281(2)  | 2.2826(12) | 2.3419(12)               |
| Pd–Cl(2)                   | 2.2894(9) | 2.2797(16) | 2.292(2)  | 2.2852(15) |                          |
| Pd–Cl(1i)                  |           |            |           |            | 2.3365(12)               |
| Pd(1)···Pd(1i)             |           |            |           |            | 3.42                     |
| Pd–N(1)                    | 2.032(3)  | 2.031(5)   | 2.046(7)  | 2.038(3)   | 2.017(4)                 |
| Pd–N(3)                    | 2.021(3)  | 2.027(5)   | 2.012(6)  | 2.018(3)   | 2.015(4)                 |
| C(11)–N(2)                 | 1.441(4)  | 1.458(7)   | 1.451(9)  | 1.451(5)   | 1.466(7)                 |
| C(11)–N(4)                 | 1.443(5)  | 1.457(7)   | 1.463(10) | 1.454(5)   | 1.465(6)                 |
| Cl(1)–Pd–Cl(2)             | 90.00(3)  | 89.10(6)   | 90.29(8)  | 89.43(5)   |                          |
| Cl(1)–Pd–Cl(1i)            |           |            |           |            | 86.16(5)                 |
| N(1)–Pd–N(3)               | 86.13(11) | 85.69(19)  | 86.3(3)   | 85.92(14)  | 87.43(16)                |
| Cl(2)–Pd–N(3)              | 91.16(8)  | 91.87(15)  | 91.05(19) | 92.34(10)  |                          |
| Cl(1)–Pd–N(1)              | 92.56(8)  | 93.16(14)  | 92.2(2)   | 92.10(10)  |                          |
| Cl(1)–Pd–N(3)              |           |            |           |            | 92.95(12)                |
| Cl(1i)–Pd–N(1)             |           |            |           |            | 93.36(12)                |
| N(2)–C(11)–N(4)            | 110.6(3)  | 109.6(4)   | 110.3(6)  | 108.9(3)   | 109.2(4)                 |
| Pd···C(11)···C(12)···C(13) | 91.9      | 112.0      | 115.6     | 114.5      | 127.7                    |
| Pd(1)–Cl(1)–Pd(1i)         |           |            |           |            | 93.84(5)                 |

[a] Symmetry i is  $-x + 1, -y + 2, -z + 1$ .

conformations in which the ester or benzyl group attached to the methine carbon atom C(11) occupies an axial position, thereby avoiding the steric hindrance that would arise in the equatorial positions with the adjacent methyl groups at the 5-position of the pyrazolyl rings. This steric repulsion confers rigidity on the metallacycle as no boat-to-boat conformational exchange is observed in solution. The substituents on C(11) are oriented asymmetrically in relation to the palladacycle, with the dihedral angle defined by the Pd···C(11) molecular axes and the C(12)–C(13) bonds (or axis for **3**) being in the range of 112.0–115.6° for **4–6**, somewhat wider (127.6°) for **17**, and narrower (91.9°) for ester **3**. The same asymmetrical arrangement of the benzyl group observed for **4** is found in structures of tetrahedral nickel(II)<sup>[15]</sup> and octahedral molybdenum(0)<sup>[16]</sup> complexes containing ligand **I**, although their different coordination environment yields broader or narrower N–M–N angles (approx. 94 and 79°, respectively) than those found in the structures of the square-planar Pd complexes listed in Table 1 (approx. 86°).

The structure of **17** is centrosymmetric, consisting of a dimetallic central cation, formed by two chlorido-bridged subunits, and two [BAr<sup>f</sup><sub>4</sub>]<sup>−</sup> counterions (see Figure 2). The most remarkable differences between this structure and those of the neutral compounds **3–6** are the longer Pd–Cl bonds (approx. 2.34 vs. 2.28 Å), the narrower Cl–Pd–Cl angle (approx. 86° vs. 90°), and the above-mentioned dihedral angle due to the asymmetric positioning of the benzyl group.

### Evaluation of Dendronized Ligands in the Pd-Catalyzed Heck Reaction

The Heck–Mizoroki reaction<sup>[24]</sup> is a fundamental palladium-catalyzed reaction for the olefination of aryl halides that has found widespread use in organic synthesis.<sup>[25]</sup> The pioneering work by Reetz and co-workers<sup>[26]</sup> using Pd den-

drimers<sup>[4]</sup> in this process has been followed by several studies on peripheral<sup>[27–30]</sup> or core-metalated<sup>[31]</sup> dendrimers, as well as on composite materials obtained by anchoring the latter to inorganic or organic supports<sup>[32,33]</sup> or encapsulating Pd nanoparticles inside dendrimers.<sup>[34]</sup>

Complexes **3–16** were tested as catalysts in the Heck reaction between *para*-iodotoluene and methyl acrylate in the presence of NEt<sub>3</sub> as base under the conditions summarized in Table 2. Methyl (*E*)-3-(4-methylphenyl)-2-propenoate (methyl 4-methylcinnamate) was the unique reaction product, with neither the  $\beta$ -disubstituted nor the (*Z*) isomer being detected by GC or <sup>1</sup>H NMR analysis. It is important to note that the precipitation of varying amounts of Pd black was observed in all cases. The conversions observed after 23 h are summarized in Table 2 except for those for the ester compounds **3** and **8**, which showed the lowest conversions (62 and 83 %, respectively). The conversions after 2 h are also given for the **G1** complexes. The performance of the remaining catalysts after 23 h is similar and independent of the size or nature of the precursor.

Table 2. Heck coupling of methyl acrylate and 4-iodotoluene.<sup>[a]</sup>

| Catalyst                                  | Conversions (%) after 23 h <sup>[b]</sup> |                       |           |           |           |
|---|---|-----------------------|-----------|-----------|-----------|
|   | <b>G0</b>                                 | <b>G1</b> (after 2 h) | <b>G1</b> | <b>G2</b> | <b>G3</b> |
| <b>4–7</b> ([PdCl <sub>2</sub> ])         | 90  | 57                    | 90        | 90        | 94        |
| <b>9–12</b> ([PdMeCl])                    | 93  | 80                    | 94        | 86        | 94        |
| <b>13–16</b> ([PdMe(NCMe)] <sup>+</sup> ) | 90  | 81                    | 95        | 93        | 95        |

[a] Conditions: 5 mL MeCN; *n*(Pd) = 5  $\mu$ mol (1 mol-% based on Pd); [4-iodotoluene] = [methyl acrylate] = [NEt<sub>3</sub>] = 0.1 M; *t*<sub>r</sub> = 23 h; *T*<sub>r</sub> = 80 °C. [b] % Determined by GC.

The reaction profiles were determined by periodic GC monitoring, and some of them are shown in Figure 3. The dashed line in Figure 3a represents the profile of a control reaction obtained under the same conditions by using

$\text{PdCl}_2$  in the absence of ligand as catalyst. The profiles differ appreciably with the nature of the palladium precursor, as illustrated by the G1 complexes **5**, **10**, and **14** in Figure 3a. Thus,  $\text{PdCl}_2$  complexes **4–7** (and also **3** and  $\text{PdCl}_2$ ) afforded slower rates at early reaction stages than the neutral or cationic  $\text{PdMeX}$  complexes **9–16**. For instance, the conversions reached after 2 h with the G1 complexes **10** and **14** were around 80% compared with 57% for **5** or 40% for  $\text{PdCl}_2$ . In contrast, the generation of the dendron was essentially irrelevant, as exemplified by the G0–G3 series **9–12** in Figure 3b.

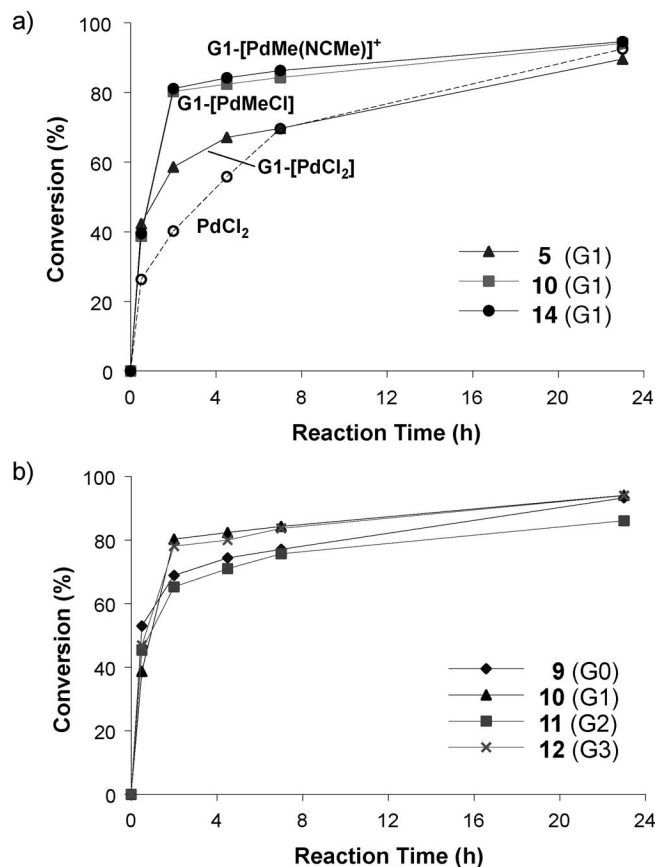


Figure 3. Effect of the nature of the palladium precursor and the dendron generation on the conversion profiles exemplified by (a) the G1 complexes **5**, **10**, and **14**, and (b) the G0–G3 series **9–12**, respectively. The dashed line represents the profile obtained under the same conditions for  $\text{PdCl}_2$ .

The slower initial rates observed for the  $\text{PdCl}_2$  complexes might be explained by their higher resistance to undergo reduction to form the  $\text{Pd}^0$  active species involved in the  $\text{Pd}^0/\text{Pd}^{\text{II}}$  catalytic cycle.<sup>[35]</sup> The almost invariant reaction profile with dendritic generation is, however, more intriguing. The reactivity of core-substituted dendrimers should be affected, at least after a critical size,<sup>[4]</sup> by the restricted accessibility to the metal center imposed by the dendritic substituents. Indeed, we have shown in previous studies how [bis(pyrazol-1-yl)methane] $\text{Ni}^{\text{II}}$  or  $-\text{Pd}^{\text{II}}$  complexes are partially enclosed in  $\text{CDCl}_3$  solution or the solid state by the dendritic arms of the poly(aryl ether) dendrons to which they are linked.<sup>[15,21]</sup> Moreover, the Heck reactions were performed in acetonitrile,

which is a poor solvent for poly(aryl ether) dendrons and promotes the collapse of their structures, as has been shown by PGSE diffusion NMR experiments (PGSE = pulse-gradient spin-echo) and fluorescence techniques.<sup>[36,37]</sup> Thus, studies carried out with pyrene-cored poly(aryl ether) monodendrons have revealed that G3 and G4 poly(aryl ether)s dissolved in acetonitrile are only partially permeable to the passage of small oxygen molecules. We therefore propose that the initial reduction of  $\text{Pd}^{\text{II}}$  to  $\text{Pd}^0$  is accompanied by decoordination of the bis(pyrazolyl)methane ligand from the palladium center to explain the similar behavior of all the catalytic precursors. In the absence of good stabilizing ligands, the observed formation of  $\text{Pd}^0$  aggregates and metallic Pd precipitates is easily explainable.

The mechanistic considerations made by Reetz and de Vries for the Heck reaction under ligand-free conditions are therefore applicable here.<sup>[38]</sup> A key point of their argument is the existence of equilibria between higher-order palladium species (i.e., palladium nanoparticles) of low reactivity and lower-order species (such as monomeric or dimeric species) of high reactivity.<sup>[39]</sup> The effect of these equilibria is that high concentrations of Pd are counterproductive and result in decreased turnover frequencies because of a shift of these equilibria towards the formation of aggregates and Pd black.<sup>[40]</sup> The behavior of the above complexes at Pd concentrations ranging from 1 to 0.01 mol-% is illustrated with complex **14** in Figure 4. A reduction in metal loading from 1 to 0.1 mol-% barely alters the reaction profile, and the catalytic system is fairly active even at 0.01 mol-%. Of more interest, however, is that the turnover frequencies increase notably upon lowering the Pd concentrations. Thus, for metal concentrations of 1, 0.5, 0.1, and 0.01 mol-%, the respective TOF values are 80, 133, 667, and 1050  $\text{h}^{-1}$ , respectively, at a fixed conversion of 20%, and 4.1, 8.3, 39.5, and 244.8  $\text{h}^{-1}$ , respectively, after 23 h.

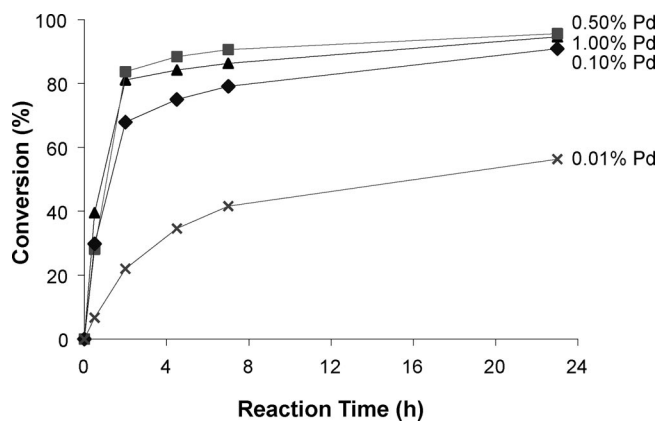


Figure 4. Effect of the Pd concentration on the conversion by using the cationic precursor **14**.

We noted above the existence of slight differences in the reaction profiles in Figure 3 at early reaction stages depending on the nature of the Pd precursor. For that reason, we performed a final experiment involving the repeated addition of fresh substrate to the reaction medium once the previous catalytic cycle was complete (48–72 h). These re-

loading cycles were repeated up to six times, and the conversions were measured by GC after 2 and 24 h after re-addition of substrates in each cycle. The results obtained with the G0–G3 series of cationic complexes **9–12** (Figure 5a) and plain  $\text{PdCl}_2$  (Figure 5b) are quite similar. Thus, the conversions reached after 2 h tend to decrease from one to the next cycle (for instance, average TOFs are 295, 175, 95, 61, 75, and  $33 \text{ h}^{-1}$  for **12**) but remain fairly constant after 24 h, with somewhat higher values for the odd-generation dendrons G1 (**10**) and G3 (**12**). It is worth mentioning that, after storing the reaction vials for 1.5 months, the last run yielded comparable conversions for each generation of catalytic system derived from **9–12**. These results show that the influence of the precursor nature on the reaction kinetics is essentially limited to the first cycle, probably because decomposition of the precursors after this initial cycle leads to catalytic systems with a similar composition. The ligands might nevertheless play some minor role in the equilibria between Pd species by interacting, to different degrees, with, for instance, the Pd nanoparticles, thus explaining the small differences observed between dendron generations.

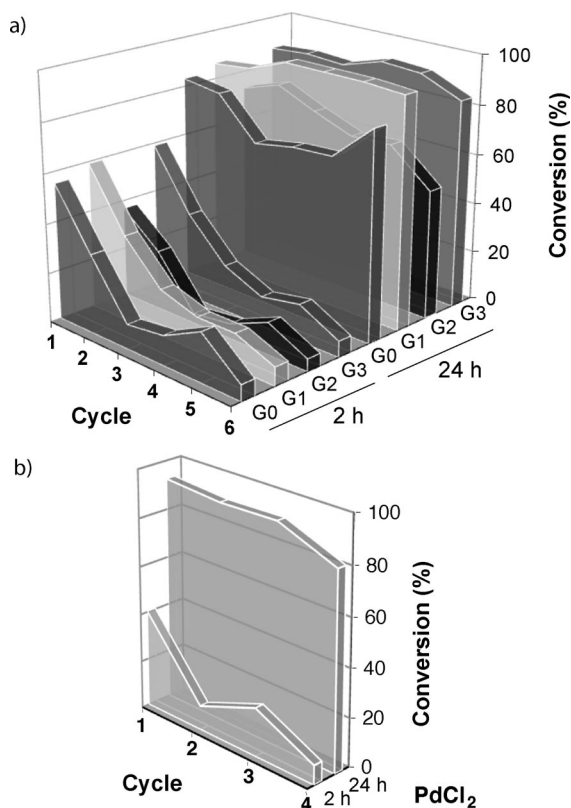


Figure 5. Catalytic conversions (%) after 2 and 24 h in successive cycles after reloading the reaction media with fresh substrate. Catalysts: (a) G0–G3 series of complexes **9–12** at 0.1 mol-% Pd and (b)  $\text{PdCl}_2$  at 1 mol-% Pd.

## Conclusions

We have reported the synthesis of a series of neutral and cationic palladium coordination compounds with bis(pyrazol-1-yl)methane ligands embedded in poly(benzyl ether)

dendrons of up to the third generation. These complexes have been studied as catalysts in the Heck reaction of *para*-iodotoluene and methyl acrylate in acetonitrile. Several observations point to decoordination of the dendronized bis(pyrazolyl) ligands at earlier stages of the catalytic reaction and to a “ligand-free” Heck mechanism involving the formation of Pd aggregates: (a) the reaction profiles are essentially independent of the dendron size, (b) the precipitation of Pd black is observed in all cases, (c) the turnover frequencies increase at lower catalyst concentrations, and (d) the conversions attained with these complexes and palladium dichloride are quite similar, except in the initial stages of the reaction, as shown in the consecutive cycles involving the addition of fresh substrate.

There is considerable evidence that phosphanes, N-heterocyclic carbenes, and other ligands used in the Heck and other Pd-catalyzed C–C coupling reactions form part of the truly active catalytic species under certain conditions, especially at low temperatures. Nevertheless, many metal–ligand complexes decompose to form  $\text{Pd}^0$  aggregates that are precursors of the true molecular catalysts. This fact complicates the design of, for instance, dendritic catalysts that are recoverable by nanofiltration as these techniques rely on stable ligand coordination.

## Experimental Section

**Reagents and General Techniques:** All operations were performed under argon by using Schlenk or dry-box techniques. Unless otherwise stated, reagents were obtained from commercial sources and used as received. Compounds  $\text{Na}[\text{BAR}^f_4]$  [ $\text{Ar}^f = 3,5\text{-(CF}_3)_2\text{C}_6\text{H}_3$ ],<sup>[41]</sup>  $\text{CH}_2(3,5\text{-Me}_2\text{pz})_2$ ,<sup>[10]</sup> and  $\text{CH}(3,5\text{-Me}_2\text{pz})_2\text{COOH}$ ,<sup>[42]</sup> dendrons *Gn*-Br<sup>[22]</sup> and *Gn*-CH(3,5-Me<sub>2</sub>pz)<sub>2</sub> (**I–IV**, *n* = 0–3),<sup>[15]</sup> and complexes  $[\text{PdCl}_2(\text{cod})]$  (cod =  $\eta^4$ -1,5-cyclooctadiene),<sup>[43]</sup>  $[\text{PdClMe}(\text{cod})]$ ,<sup>[44]</sup> and  $[\text{PdCl}_2(\text{Gn-CH}(3,5\text{-Me}_2\text{pz})_2)]$  (**4–7**)<sup>[21]</sup> were prepared according to literature procedures. Solvents were dried prior to use and distilled under argon as described elsewhere.<sup>[45]</sup> NMR spectra were recorded with Varian Unity 500+, Varian Unity VR-300, or Varian Unity 200 NMR spectrometers. Chemical shifts ( $\delta$ ) are reported in ppm relative to  $\text{SiMe}_4$  and were measured relative to the  $^{13}\text{C}$  and residual  $^1\text{H}$  resonances of the deuterated solvents. The following abbreviations/notations are used: Ph refers to the aromatic ring of terminal benzyl groups, Ar to internal rings of benzyl ethers, and *ipso* refers to the first ring position on going from the didentate pyrazolyl ligand. IR spectra were recorded with a Perkin–Elmer FT-IR Spectrum-2000 spectrophotometer. Elemental analyses and mass spectra were performed by the Microanalytical Laboratories of the University of Alcalá (MLUAH) with a Heraeus CHN-O-Rapid microanalyzer and a Thermoquest–Finnigan Automass Multi (APCI) or Agilent G3250AA LC/MSD TOF Multi (ESI) mass spectrometer. The progress of the Heck reactions was determined with a Chrompack CP 9001 gas chromatograph by using a CP-WAX 52 CB FS-capillary column (15 m, 0.25 mm i.d., 0.25  $\mu\text{m}$  film thickness) under the following conditions: injector and detector temperatures: 250 and 260 °C, respectively; oven temperature program: 100 °C/1 min, 10 °C/min ramp, 240 °C/10 min.

**Preparation of Benzyl Bis(3,5-dimethylpyrazol-2-yl)acetate [G0-OC(O)CH(3,5-Me<sub>2</sub>pz)<sub>2</sub>] (**1**):** A solution of  $\text{CH}(3,5\text{-Me}_2\text{pz})_2\text{COOH}$  (735 mg, 2.96 mmol) in thf (20 mL) was added to a suspension of NaH (71 mg, 2.96 mmol) in the same solvent (15 mL) at 0 °C. After stirring for 2 h, an excess of benzyl bromide was added from a

syringe (0.42 mL, 3.5 mmol) and the mixture maintained at reflux for 2 d. The resulting solution was then cooled, the solvent removed in vacuo, and the crude solid extracted with pentane ( $2 \times 25$  mL). Compound **1** precipitated as a white solid after concentration and cooling of the solution, and was recrystallized from pentane to eliminate the excess of BzBr. Compound **1** is soluble in alkanes, ethers, and aromatic and chlorinated organic solvents. Yield: 502 mg (50%).  $\text{C}_{19}\text{H}_{22}\text{N}_4\text{O}_2$  (338.41): calcd. C 67.44, H 6.55, N 16.56; found C 67.43, H 6.61, N 16.35.  $^1\text{H}$  NMR ( $\text{CDCl}_3$ ):  $\delta$  = 2.07 (s, 6 H, pz-Me<sup>3</sup>), 2.18 (s, 6 H, pz-Me<sup>5</sup>), 5.31 (s, 2 H, CH<sub>2</sub>), 5.82 (s, 2 H, pz-H<sup>4</sup>), 6.94 (s, 1 H, CH), 7.25–7.40 (m, 5 H, Ph) ppm.  $^{13}\text{C}\{^1\text{H}\}$  NMR ( $\text{CDCl}_3$ ):  $\delta$  = 11.0 (pz-Me<sup>5</sup>), 13.6 (pz-Me<sup>3</sup>), 68.1 (CH), 73.3 (CH<sub>2</sub>), 107.5 (pz-C<sup>4</sup>), 128.3 and 128.4 (*o*-, *m*- and *p*-Ph), 134.8 (*ipso*-Ph), 141.1 (pz-C<sup>5</sup>), 148.3 (pz-C<sup>3</sup>), 164.7 (C=O) ppm. IR (KBr):  $\tilde{\nu}$  = 1761 (vs, C=O), 1563 (s, C=N), 1456 (m, C=C)  $\text{cm}^{-1}$ . MS (APCI in  $\text{CH}_2\text{Cl}_2$  + MeOH/ $\text{H}_2\text{O}$ , 3:1):  $m/z$  = 339 [ $\text{M} + \text{H}$ ]<sup>+</sup>, 243 [ $\text{M} - \text{Me}_2\text{pz}$ ]<sup>+</sup>.

**Preparation of G1-OC(O)CH(3,5-Me<sub>2</sub>pz)<sub>2</sub> (2):** Na[CH(3,5-Me<sub>2</sub>pz)<sub>2</sub>-COO] (353 mg, 1.31 mmol), prepared as described above and isolated as a white solid, and dendritic wedge G1-Br (500 mg, 1.30 mmol) were refluxed in acetone (30 mL) for 4 d. A white solid precipitated during the course of the reaction. The solvent was then removed in vacuo and the crude solid extracted with dichloromethane ( $2 \times 15$  mL) to give an oily residue after removal of the solvent, which was treated and washed with cold pentane ( $2 \times 15$  mL) to give compound **2** as a white solid. Compound **2** is partially soluble in alkanes, and soluble in ether, acetone, and chlorinated organic solvents. Persistent small amounts of CH(3,5-Me<sub>2</sub>pz)<sub>2</sub>COOH remained after purification of **2**. Yield: 151 mg (21%).  $^1\text{H}$  NMR ( $\text{CDCl}_3$ ):  $\delta$  = 2.08 (s, 6 H, pz-Me<sup>3</sup>), 2.16 (s, 6 H, pz-Me<sup>5</sup>), 4.97 (s, 4 H, PhCH<sub>2</sub>O), 5.26 (s, 2 H, ArCH<sub>2</sub>), 5.82 (s, 2 H, pz-H<sup>4</sup>), 6.53 (t,  $^4J_{\text{H,H}} = 2.0$  Hz, 1 H, *p*-Ar), 6.57 (d,  $^4J_{\text{H,H}} = 2.0$  Hz, 2 H, *o*-Ar), 6.96 (s, 1 H, CH), 7.25–7.40 (m, 10 H, Ph) ppm.  $^{13}\text{C}\{^1\text{H}\}$  NMR ( $\text{CDCl}_3$ ):  $\delta$  = 11.0 (pz-Me<sup>5</sup>), 13.5 (pz-Me<sup>3</sup>), 67.9 (CH), 70.1 (PhCH<sub>2</sub>O), 73.3 (CH<sub>2</sub>), 101.9 (*p*-Ar), 106.9 (*o*-Ar), 107.6 (pz-C<sup>4</sup>), 127.6, 128.0, 128.6 (*o*-, *m*-, *p*-Ph), 136.6 (*ipso*-Ph), 137.1 (*ipso*-Ar), 141.2 (pz-C<sup>5</sup>), 148.5 (pz-C<sup>3</sup>), 160.0 (*m*-Ar), 164.7 (C=O) ppm. IR (KBr):  $\tilde{\nu}$  = 1767 (vs, C=O), 1563 (s, C=N), 1597, 1453 (vs, C=C), 1164, 1060 (vs, C–O–C)  $\text{cm}^{-1}$ . MS (ESI<sup>+</sup>-TOF in  $\text{CH}_2\text{Cl}_2/\text{MeOH}/\text{NH}_4\text{HCOO}$  5 mm):  $m/z$  = 573.25 [ $\text{M} + \text{Na}$ ]<sup>+</sup>, 551.26 [ $\text{M} + \text{H}$ ]<sup>+</sup>.

**Preparation of [PdCl<sub>2</sub>{G0-OC(O)CH(3,5-Me<sub>2</sub>pz)<sub>2</sub>}] (3):** Ester **1** (68 mg, 0.2 mmol) and [PdCl<sub>2</sub>(cod)] (50 mg, 0.175 mmol) were mixed in toluene (40 mL) and the mixture refluxed for 2 h. After cooling the resulting orange solution to room temp., the solvent was removed in vacuo and the residue washed with pentane ( $2 \times 10$  mL) to eliminate the cod by-product and the unreacted ligand. Compound **3** was isolated as a yellow-orange solid, which is insoluble in alkanes and slightly and readily soluble in aromatic and chlorinated solvents, respectively. Orange monocrystals were obtained after recrystallization from  $\text{CH}_2\text{Cl}_2$ /pentane by the two-layer diffusion technique. Yield: 82 mg (91%).  $\text{C}_{19}\text{H}_{22}\text{Cl}_2\text{N}_4\text{O}_2\text{Pd}$  (515.73): calcd. C 44.25, H 4.30, N 10.86; found C 44.02, H 4.30, N 10.74.  $^1\text{H}$  NMR ( $\text{CDCl}_3$ ):  $\delta$  = 2.37 (s, 6 H, pz-Me<sup>5</sup>), 2.59 (s, 6 H, pz-Me<sup>3</sup>), 5.70 (s, 2 H, CH<sub>2</sub>), 5.96 (s, 2 H, pz-H<sup>4</sup>), 6.43 (s, 1 H, CH), 7.3 (m, 3 H, Ph), 7.4 (m, 2 H, Ph) ppm.  $^{13}\text{C}\{^1\text{H}\}$  NMR ( $\text{CDCl}_3$ ):  $\delta$  = 11.6 (pz-Me<sup>5</sup>), 15.2 (pz-Me<sup>3</sup>), 66.6 (CH), 71.3 (CH<sub>2</sub>), 108.6 (pz-C<sup>4</sup>), 128.3, 128.6, 129.4 (*o*-, *m*-, *p*-Ph), 133.9 (*ipso*-Ph), 141.7 (pz-C<sup>5</sup>), 155.0 (pz-C<sup>3</sup>), 162.9 (C=O) ppm. IR (KBr):  $\tilde{\nu}$  = 1755 (vs, C=O), 1617 (m, C=C), 1567 (s, C=N), 1470 (m, C=C), 1315, 1234 (s, C–O)  $\text{cm}^{-1}$ . MS (APCI in  $\text{CH}_2\text{Cl}_2$  + MeOH/ $\text{H}_2\text{O}$ , 3:1):  $m/z$  = 995 [ $\text{M}_2 - \text{Cl}$ ]<sup>+</sup>, 512 [ $\text{M} - \text{Cl} + \text{MeOH}$ ]<sup>+</sup>, 477 [ $\text{M} - \text{Cl}_2 + \text{MeOH}$ ]<sup>+</sup>, 339 [ $\text{M} - \text{PdCl}_2 + \text{H}$ ]<sup>+</sup>, 243 [ $\text{M} - \text{PdCl}_2 - \text{Me}_2\text{pz}$ ]<sup>+</sup>.

**Preparation of [PdClMe{G0-OC(O)CH(3,5-Me<sub>2</sub>pz)<sub>2</sub>}] (8):** Diethyl ether (30 mL) was added to [PdClMe(cod)] (50 mg, 0.19 mmol) and ligand **1** (68 mg, 0.20 mmol) in a Schlenk tube at room temp. After a few minutes, a solid started to precipitate from the solution. The mixture was stirred overnight, then the solvent was removed under vacuum, and the unreacted ligand and free cod were removed by washing the residue with pentane ( $2 \times 15$  mL). Compound **8** was isolated as a white solid, which is insoluble in alkanes and slightly and very soluble in diethyl ether and chlorinated solvents, respectively. Yield: 86 mg (91%).  $\text{C}_{20}\text{H}_{25}\text{ClN}_4\text{O}_2\text{Pd}$  (495.32): calcd. C 48.50, H 5.09, N 11.31; found C 48.22, H 4.95, N 11.21.  $^1\text{H}$  NMR ( $\text{CDCl}_3$ ):  $\delta$  = 0.88 (s, 3 H, PdMe), 2.28 (s, 3 H, pz-Me<sup>3</sup> adjacent to PdMe), 2.36 (s, 3 H, pz-Me<sup>5</sup>), 2.37 (s, 3 H, pz-Me<sup>5</sup>), 2.45 (s, 3 H, pz-Me<sup>3</sup> adjacent to PdCl), 5.50 (s, 2 H, CH<sub>2</sub>), 5.84 (s, 2 H, pz-H<sup>4</sup>), 6.00 (s, 2 H, pz-H<sup>4</sup>), 6.35 (s, 1 H, CH), 7.3 (m, 3 H, Ph), 7.4 (m, 2 H, Ph) ppm.  $^{13}\text{C}\{^1\text{H}\}$  NMR ( $\text{CDCl}_3$ ):  $\delta$  = –6.0 (PdMe), 11.0, 11.5 (pz-Me<sup>5</sup>), 13.9, 14.8 (pz-Me<sup>3</sup>), 66.3 (CH), 70.2 (CH<sub>2</sub>), 107.5, 108.0 (pz-C<sup>4</sup>), 128.5, 128.6, 129.1 (*o*-, *m*-, *p*-Ph), 134.5 (*ipso*-Ph), 139.8, 141.2 (pz-C<sup>5</sup>), 152.7, 152.8 (pz-C<sup>3</sup>), 163.9 (C=O) ppm. IR (KBr):  $\tilde{\nu}$  = 1749 (vs, C=O), 1620 (w, C=C), 1564 (s, C=N), 1465 (m, C=C), 1311, 1228 (s, C–O)  $\text{cm}^{-1}$ . MS (APCI in  $\text{CH}_2\text{Cl}_2$  + MeOH/ $\text{H}_2\text{O}$ , 3:1):  $m/z$  = 512 [ $\text{M} - \text{Me} + \text{MeOH}$ ]<sup>+</sup>, 477 [ $\text{M} - \text{Me} - \text{Cl} + \text{MeOH}$ ]<sup>+</sup>, 339 [ $\text{M} - \text{PdClMe} + \text{H}$ ]<sup>+</sup>, 243 [ $\text{M} - \text{PdClMe} - \text{Me}_2\text{pz}$ ]<sup>+</sup>.

**Preparation of [PdClMe{Gn-CH(3,5-Me<sub>2</sub>pz)<sub>2</sub>}] (9–12):** These compounds were synthesized as described above for **8**, starting from the amount of the corresponding chelating ligand Gn-CH(3,5-Me<sub>2</sub>pz)<sub>2</sub> [*n* = 0 (**I**), 1 (**II**), 2 (**III**), 3 (**IV**)] indicated below and [PdClMe(cod)]. The reaction was very slow with ligand **III**, due to its limited solubility, and the preparation of compound **12** was carried out similarly but in warm (80 °C) toluene and in the dark. Purification of **11** and **12** also included washing with cold diethyl ether. Compounds **9–12** were isolated as white solids, which are insoluble in alkanes, methanol, and diethyl ether and soluble in toluene and chlorinated solvents.

**[PdClMe{G0-CH(3,5-Me<sub>2</sub>pz)<sub>2</sub>}] (9):** G0-CH(3,5-Me<sub>2</sub>pz)<sub>2</sub> (**I**; 70 mg, 0.24 mmol) and [PdClMe(cod)] (54 mg, 0.20 mmol). Yield: 85 mg (94%).  $\text{C}_{19}\text{H}_{25}\text{ClN}_4\text{Pd}$  (451.31): calcd. C 50.57, H 5.58, N 12.41; found C 50.52, H 5.59, N 11.92.  $^1\text{H}$  NMR ( $\text{CDCl}_3$ ):  $\delta$  = 1.03 (s, 3 H, PdMe), 1.95 (s, 3 H, pz-Me<sup>5</sup>), 2.03 (s, 3 H, pz-Me<sup>5</sup>), 2.38 (s, 3 H, pz-Me<sup>3</sup> adjacent to PdMe), 2.50 (s, 3 H, pz-Me<sup>3</sup> adjacent to PdCl), 4.98 (dd,  $^2J_{\text{H,H}} = 13.6$ ,  $^3J_{\text{H,H}} = 6.9$  Hz, 1 H, CH<sub>2</sub>), 5.66 (dd,  $^2J_{\text{H,H}} = 13.6$ ,  $^3J_{\text{H,H}} = 8.6$  Hz, 1 H, CH<sub>2</sub>), 5.74 (s, 1 H, pz-H<sup>4</sup>), 5.83 (s, 1 H, pz-H<sup>4</sup>), 6.04 (dd,  $^3J_{\text{H,H}} = 6.9$ ,  $^3J_{\text{H,H}} = 8.6$  Hz, 1 H, CH), 7.1 (m, 2 H, Ph), 7.2 (m, 3 H, Ph) ppm.  $^{13}\text{C}\{^1\text{H}\}$  NMR ( $\text{CDCl}_3$ ):  $\delta$  = –6.7 (PdMe), 10.9, 11.2 (pz-Me<sup>5</sup>), 14.3, 15.3 (pz-Me<sup>3</sup>), 42.8 (CH<sub>2</sub>), 69.0 (CH), 106.9, 107.4 (pz-C<sup>4</sup>), 127.6, 128.8, 129.2 (*o*-, *m*-, *p*-Ph), 134.6 (*ipso*-Ph), 138.7, 140.6 (pz-C<sup>5</sup>), 152.8 (pz-C<sup>3</sup>) ppm. IR (KBr):  $\tilde{\nu}$  = 1618 (m, C=C), 1561 (s, C=N), 1460 (s, C=C)  $\text{cm}^{-1}$ . MS (APCI in  $\text{CH}_2\text{Cl}_2$  + MeOH/ $\text{H}_2\text{O}$ , 3:1):  $m/z$  = 468 [ $\text{M} - \text{Me} + \text{MeOH}$ ]<sup>+</sup>, 447 [ $\text{M} - \text{Cl} + \text{MeOH}$ ]<sup>+</sup>, 433 [ $\text{M} - \text{Cl} - \text{Me} + \text{MeOH}$ ]<sup>+</sup>, 199 [ $\text{M} - \text{PdClMe} - \text{Me}_2\text{pz}$ ]<sup>+</sup>.

**[PdClMe{G1-CH(3,5-Me<sub>2</sub>pz)<sub>2</sub>}] (10):** G1-CH(3,5-Me<sub>2</sub>pz)<sub>2</sub> (**II**; 229 mg, 0.45 mmol), [PdClMe(cod)] (120 mg, 0.45 mmol). Yield: 270 mg (90%).  $\text{C}_{33}\text{H}_{37}\text{ClN}_4\text{O}_2\text{Pd}$  (663.56): calcd. C 59.73, H 5.62, N 8.44; found C 59.43, H 5.77, N 8.21.  $^1\text{H}$  NMR ( $\text{CDCl}_3$ ):  $\delta$  = 1.00 (s, 3 H, PdMe), 1.94 (s, 3 H, pz-Me<sup>5</sup>), 2.00 (s, 3 H, pz-Me<sup>5</sup>), 2.35 (s, 3 H, pz-Me<sup>3</sup> adjacent to PdMe), 2.46 (s, 3 H, pz-Me<sup>3</sup> adjacent to PdCl), 4.88 (A part of an AB system,  $^2J_{\text{H,H}} = 11.8$  Hz, 2 H, PhCH<sub>2</sub>O), 4.95 (B part of an AB system,  $^2J_{\text{H,H}} = 11.8$  Hz, 2 H, PhCH<sub>2</sub>O), 5.06 (dd,  $^2J_{\text{H,H}} = 13.6$ ,  $^3J_{\text{H,H}} = 7.3$  Hz, 1 H, CH<sub>2</sub>), 5.38 (dd,  $^2J_{\text{H,H}} = 13.6$ ,  $^3J_{\text{H,H}} = 8.6$  Hz, 1 H, CH<sub>2</sub>), 5.68 (s, 1 H, pz-H<sup>4</sup>), 5.81 (s, 1 H, pz-H<sup>4</sup>), 6.00 (dd,  $^3J_{\text{H,H}} = 7.3$ ,  $^3J_{\text{H,H}} = 8.6$  Hz, 1 H,

CH), 6.42 (d,  $^4J_{\text{H,H}} = 2.0$  Hz, 2 H, *o*-Ar), 6.48 (t,  $^4J_{\text{H,H}} = 2.0$  Hz, 1 H, *p*-Ar), 7.25–7.45 (m, 10 H, Ph) ppm.  $^{13}\text{C}\{^1\text{H}\}$  NMR ( $\text{CDCl}_3$ ):  $\delta = -7.0$  (PdMe), 10.8, 11.2 (pz-Me<sup>5</sup>), 14.1, 15.2 (pz-Me<sup>3</sup>), 42.7 (CH<sub>2</sub>), 68.6 (CH), 70.0 (PhCH<sub>2</sub>O), 102.0 (*p*-Ar), 106.9, 107.5 (pz-C<sup>4</sup>), 108.1 (*o*-Ar), 127.4, 128.0, 128.6 (*o*-, *m*-, *p*-Ph), 136.8 (*ipso*-Ar, *ipso*-Ph), 139.0, 140.8 (pz-C<sup>5</sup>), 152.1, 152.2 (pz-C<sup>3</sup>), 160.0 (*m*-Ar) ppm. IR (KBr):  $\tilde{\nu} = 1561$  (s, C=N), 1595, 1450 (vs, C=C), 1154, 1047 (vs, C–O–C)  $\text{cm}^{-1}$ . MS (APCI in  $\text{CH}_2\text{Cl}_2$  + MeOH/ $\text{H}_2\text{O}$ , 3:1):  $m/z = 680$  [ $\text{M} - \text{Me} + \text{MeOH}$ ]<sup>+</sup>, 507 [ $\text{M} - \text{PdClMe} + \text{H}$ ]<sup>+</sup>, 411 [ $\text{M} - \text{PdClMe} - \text{Me}_2\text{pz}$ ]<sup>+</sup>.

**[PdClMe{G2-CH(3,5-Me<sub>2</sub>pz)<sub>2</sub>}] (11):** G2-CH(3,5-Me<sub>2</sub>pz)<sub>2</sub> (III; 171 mg, 0.18 mmol), [PdClMe(cod)] (49 mg, 0.18 mmol). Yield: 270 mg (90%). C<sub>61</sub>H<sub>61</sub>ClN<sub>4</sub>O<sub>6</sub>Pd (1088.05): calcd. C 67.34, H 5.65, N 5.15; found C 66.84, H 5.50, N 5.17.  $^1\text{H}$  NMR ( $\text{CDCl}_3$ ):  $\delta = 1.00$  (s, 3 H, PdMe), 1.93 (s, 3 H, pz-Me<sup>5</sup>), 1.97 (s, 3 H, pz-Me<sup>5</sup>), 2.33 (s, 3 H, pz-Me<sup>3</sup> adjacent to PdMe), 2.45 (s, 3 H, pz-Me<sup>3</sup> adjacent to PdCl), 4.82 (A part of an AB system,  $^2J_{\text{H,H}} = 12.3$  Hz, 2 H, ArCH<sub>2</sub>O), 4.90 (B part of an AB system,  $^2J_{\text{H,H}} = 12.3$  Hz, 2 H, ArCH<sub>2</sub>O), 5.01 (s, 8 H, PhCH<sub>2</sub>O), 5.08 (dd,  $^2J_{\text{H,H}} = 13.4$ ,  $^3J_{\text{H,H}} = 7.3$  Hz, 1 H, CH<sub>2</sub>), 5.38 (dd,  $^2J_{\text{H,H}} = 13.4$ ,  $^3J_{\text{H,H}} = 8.3$  Hz, 1 H, CH<sub>2</sub>), 5.67 (s, 1 H, pz-H<sup>4</sup>), 5.78 (s, 1 H, pz-H<sup>4</sup>), 5.99 (dd,  $^2J_{\text{H,H}} = 7.3$ ,  $^3J_{\text{H,H}} = 8.3$  Hz, 1 H, CH), 6.40 (d,  $^4J_{\text{H,H}} = 1.8$  Hz, 2 H, G0-*o*-Ar), 6.45 (t,  $^4J_{\text{H,H}} = 1.8$  Hz, 1 H, G0-*p*-Ar), 6.55 (t,  $^4J_{\text{H,H}} = 2.2$  Hz, 2 H, G1-*p*-Ar), 6.62 (d,  $^4J_{\text{H,H}} = 2.2$  Hz, 4 H, G1-*o*-Ar), 7.25–7.45 (m, 20 H, Ph) ppm.  $^{13}\text{C}\{^1\text{H}\}$  NMR ( $\text{CDCl}_3$ ):  $\delta = -7.0$  (PdMe), 10.7, 11.1 (pz-Me<sup>5</sup>), 14.1, 15.1 (pz-Me<sup>3</sup>), 42.7 (CH<sub>2</sub>), 68.6 (CH), 69.8 (ArCH<sub>2</sub>O), 70.0 (PhCH<sub>2</sub>O), 101.4 (G1-*p*-Ar), 101.9 (G0-*p*-Ar), 106.3 (G1-*o*-Ar), 106.9 (pz-C<sup>4</sup>), 107.4 (pz-C<sup>4</sup>), 108.1 (G0-*o*-Ar), 127.6, 128.0, 128.6 (*o*-, *m*-, *p*-Ph), 134.8 (G0-*ipso*-Ar), 136.7 (*ipso*-Ph), 139.3 (G1-*ipso*-Ar), 139.0, 140.8 (pz-C<sup>5</sup>), 152.1, 152.2 (pz-C<sup>3</sup>), 159.9 (G0-*m*-Ar), 160.2 (G1-*m*-Ar) ppm. IR (KBr):  $\tilde{\nu} = 1560$  (s, C=N), 1596, 1451 (vs, C=C), 1154, 1046 (vs, C–O–C)  $\text{cm}^{-1}$ . MS (APCI in  $\text{CH}_2\text{Cl}_2$  + MeOH/ $\text{H}_2\text{O}$ , 3:1):  $m/z = 1104$  [ $\text{M} - \text{Me} + \text{MeOH}$ ]<sup>+</sup>, 931 [ $\text{M} - \text{PdClMe} + \text{H}$ ]<sup>+</sup>, 835 [ $\text{M} - \text{PdClMe} - \text{Me}_2\text{pz}$ ]<sup>+</sup>.

**[PdClMe{G3-CH(3,5-Me<sub>2</sub>pz)<sub>2</sub>}] (12):** G3-CH(3,5-Me<sub>2</sub>pz)<sub>2</sub> (IV; 276 mg, 0.15 mmol) and [PdClMe(cod)] (41 mg, 0.15 mmol). Yield: 255 mg (88%). C<sub>117</sub>H<sub>109</sub>ClN<sub>4</sub>O<sub>14</sub>Pd (1937.04): calcd. C 72.55, H 5.67, N 2.89; found C 72.14, H 5.42, N 2.46.  $^1\text{H}$  NMR ( $\text{CDCl}_3$ ):  $\delta = 1.00$  (s, 3 H, PdMe), 1.93 (s, 3 H, pz-Me<sup>5</sup>), 1.94 (s, 3 H, pz-Me<sup>5</sup>), 2.32 (s, 3 H, pz-Me<sup>3</sup> adjacent to PdMe), 2.45 (s, 3 H, pz-Me<sup>3</sup> adjacent to PdCl), 4.81 (A part of an AB system,  $^2J_{\text{H,H}} = 12.2$  Hz, 2 H, G1-ArCH<sub>2</sub>O), 4.88 (B part of an AB system,  $^2J_{\text{H,H}} = 12.3$  Hz, 2 H, G1-ArCH<sub>2</sub>O), 4.94 (s, 8 H, G2-ArCH<sub>2</sub>O), 5.00 (s, 16 H, PhCH<sub>2</sub>O), 5.22 (br. m, 1 H, CH<sub>2</sub>), 5.65 (s, 1 H, pz-H<sup>4</sup>), 5.77 (s, 1 H, pz-H<sup>4</sup>), 5.98 (br. t,  $^3J_{\text{H,H}} \approx 8.0$  Hz, 1 H, CH), 6.41 (d,  $^4J_{\text{H,H}} = 2.0$  Hz, 2 H, G0-*o*-Ar), 6.47 (t,  $^4J_{\text{H,H}} = 2.0$  Hz, 1 H, G0-*p*-Ar), 6.50 (t,  $^4J_{\text{H,H}} = 2.0$  Hz, 2 H, G1-*p*-Ar), 6.55 (t,  $^4J_{\text{H,H}} = 2.2$  Hz, 4 H, G2-*p*-Ar), 6.60 (d,  $^4J_{\text{H,H}} = 2.0$  Hz, 4 H, G1-*o*-Ar), 6.65 (d,  $^4J_{\text{H,H}} = 2.2$  Hz, 8 H, G2-*o*-Ar), 7.25–7.40 (m, 40 H, Ph) ppm.  $^{13}\text{C}\{^1\text{H}\}$  NMR ( $\text{CDCl}_3$ ):  $\delta = -7.0$  (PdMe), 10.7, 11.1 (pz-Me<sup>5</sup>), 14.1, 15.1 (pz-Me<sup>3</sup>), 42.6 (CH<sub>2</sub>), 68.5 (CH), 69.8 (G1-ArCH<sub>2</sub>O), 70.0 (G2-ArCH<sub>2</sub>O), 70.1 (PhCH<sub>2</sub>O), 101.3 (G1-*p*-Ar), 101.5, (G2-*p*-Ar), 101.8 (G0-*p*-Ar), 106.3 (G1-*o*-Ar), 106.4 (G2-*o*-Ar), 106.8, 107.4 (pz-C<sup>4</sup>), 108.0 (G0-*o*-Ar), 127.5, 128.0, 128.6 (*o*-, *m*-, *p*-Ph), 136.7 (G0-*ipso*-Ar, *ipso*-Ph), 139.1 (G2-*ipso*-Ar), 139.2 (G1-*ipso*-Ar), 139.0, 140.8 (pz-C<sup>5</sup>), 152.0, 152.1 (pz-C<sup>3</sup>), 159.9 (G0-*m*-Ar), 160.0 (G1-*m*-Ar), 160.1 (G2-*m*-Ar) ppm. IR (KBr):  $\tilde{\nu} = 1560$  (m, C=N), 1596, 1451 (vs, C=C), 1154, 1048 (vs, C–O–C)  $\text{cm}^{-1}$ . MS (ESI<sup>+</sup>-TOF in  $\text{CH}_2\text{Cl}_2/\text{MeOH}$ ):  $m/z = 1939.66$  [ $\text{M} - \text{Cl} + \text{K}$ ]<sup>+</sup>, 1917.70 [ $\text{M} - \text{Me} - \text{Cl} + \text{MeOH}$ ]<sup>+</sup>, 1900.70 [ $\text{M} - \text{Cl}$ ]<sup>+</sup>, 1884.67 [ $\text{M} - \text{Cl} - \text{CH}_4$ ]<sup>+</sup>, 1802.77 [ $\text{M} - \text{PdClMe} + \text{Na} + \text{H}$ ]<sup>+</sup>, 1762.74 [ $\text{M} - \text{PdClMe} - \text{CH}_4$ ]<sup>+</sup>.

**Preparation of [PdMe(MeCN){Gn-CH(3,5-Me<sub>2</sub>pz)<sub>2</sub>}][BAR<sup>f</sup><sub>4</sub>] (13–16):** The cationic compounds 13–16 were synthesized by using the following general procedure starting from the amounts indicated below: 1 equiv. of Na[BAR<sup>f</sup><sub>4</sub>] was added to a solution of the corresponding precursor [PdClMe{Gn-CH(3,5-Me<sub>2</sub>pz)<sub>2</sub>}] (9–12) in  $\text{CH}_2\text{Cl}_2$  (25 mL) in the presence of an excess of  $\text{CH}_3\text{CN}$ . The solution was stirred at room temp. for 1 h and the NaCl precipitate removed by filtration. The solvent was evaporated under reduced pressure and the crude solid washed with pentane (2 × 15 mL). Compounds 13–16 were isolated as orange solids, which are insoluble in alkanes and diethyl ether, although the third-generation compound is slightly soluble, and soluble in toluene and chlorinated solvents. As corresponds to a noncoordinating anion, identical spectroscopic data were obtained for the [BAR<sup>f</sup><sub>4</sub>]<sup>−</sup> ion for all four compounds. These data are as follows and will not be reproduced later.  $^1\text{H}$  NMR ( $\text{CDCl}_3$ ):  $\delta = 7.49$  (br. s, 4 H, Ar<sup>f</sup>-H<sub>p</sub>), 7.68 (br. s, Ar<sup>f</sup>-H<sub>o</sub>) ppm.  $^{13}\text{C}\{^1\text{H}\}$  NMR ( $\text{CDCl}_3$ ):  $\delta = 117.4$  (Ar<sup>f</sup>-C<sub>p</sub>), 124.4 (q,  $J_{\text{C,F}} = 272.1$  Hz, CF<sub>3</sub>), 129.0 (q,  $^2J_{\text{C,F}} = 29.0$  Hz, Ar<sup>f</sup>-C<sub>m</sub>), 134.7 (Ar<sup>f</sup>-C<sub>o</sub>), 161.6 (q,  $J_{\text{C,B}} = 50.7$  Hz, Ar<sup>f</sup>-C<sub>ipso</sub>) ppm. IR (KBr):  $\tilde{\nu} = 1357$  (s), 1279 (vs), 1128 (vs, B–C, C–F)  $\text{cm}^{-1}$ .

**[PdMe(MeCN){G0-CH(3,5-Me<sub>2</sub>pz)<sub>2</sub>}][BAR<sup>f</sup><sub>4</sub>] (13):** Compound 9 (51 mg, 0.11 mmol), Na[BAR<sup>f</sup><sub>4</sub>] (101 mg, 0.11 mmol), and  $\text{CH}_3\text{CN}$  (2 mL). Yield: 136 mg (94%). C<sub>53</sub>H<sub>40</sub>BF<sub>24</sub>N<sub>5</sub>Pd (1320.1): calcd. C 48.22, H 3.05, N 5.30; found C 47.84, H 2.97, N 5.12.  $^1\text{H}$  NMR ( $\text{CDCl}_3$ ):  $\delta = 1.08$  (s, 3 H, PdMe), 1.89 (s, 3 H, pz-Me<sup>5</sup>), 1.98 (s, 3 H, pz-Me<sup>5</sup>), 2.18 (s, 3 H, pz-Me<sup>3</sup> adjacent to Pd-NCMe), 2.28 (s, 3 H, MeCN), 2.30 (s, 3 H, pz-Me<sup>3</sup> adjacent to PdMe), 4.50 (dd,  $^2J_{\text{H,H}} = 14.0$ ,  $^3J_{\text{H,H}} = 6.5$  Hz, 1 H, CH<sub>2</sub>), 5.16 (dd,  $^2J_{\text{H,H}} = 14.0$ ,  $^3J_{\text{H,H}} = 8.8$  Hz, 1 H, CH<sub>2</sub>), 5.76 (s, 1 H, pz-H<sup>4</sup>), 5.86 (s, 1 H, pz-H<sup>4</sup>), 6.04 (dd,  $^3J_{\text{H,H}} = 6.5$ ,  $^3J_{\text{H,H}} = 8.8$  Hz, 1 H, CH), 6.9 (m, 2 H, Ph), 7.2 (m, 3 H, Ph) ppm.  $^{13}\text{C}\{^1\text{H}\}$  NMR ( $\text{CDCl}_3$ ):  $\delta = -3.6$  (PdMe), 3.0 (CH<sub>3</sub>CN), 10.5, 10.9 (pz-Me<sup>5</sup>), 13.5, 15.1 (pz-Me<sup>3</sup>), 42.9 (CH<sub>2</sub>), 68.9 (CH), 107.3, 108.3 (pz-C<sup>4</sup>), 121.3 (MeCN), 128.5, 128.7, 129.3 (*o*-, *m*-, *p*-Ph), 133.3 (*ipso*-Ph), 140.9, 142.6 (pz-C<sup>5</sup>), 151.1, 153.3 (pz-C<sup>3</sup>) ppm. IR (KBr):  $\tilde{\nu} = 1611$  (m, C=C), 1568 (m, C=N), 1465 (m, C=C)  $\text{cm}^{-1}$ . MS (ESI<sup>+</sup>-TOF in  $\text{CH}_2\text{Cl}_2/\text{MeOH}/\text{NH}_4\text{HCOO}$  5 mM):  $m/z = 457.12$  [ $\text{M} - \text{BAR}^f_4$ ]<sup>+</sup>, 446.09 [ $\text{M} - \text{CH}_4 - \text{MeCN} - \text{BAR}^f_4 + \text{HCOO}$ ]<sup>+</sup>, 416.11 [ $\text{M} - \text{MeCN} - \text{BAR}^f_4$ ]<sup>+</sup>, 400.08 [ $\text{M} - \text{CH}_4 - \text{MeCN} - \text{BAR}^f_4$ ]<sup>+</sup>, 294.39 [ $\text{M} - \text{PdMe}(\text{MeCN}) - \text{BAR}^f_4$ ]<sup>+</sup>, 199.28 [ $\text{M} - \text{PdMe}(\text{MeCN}) - \text{BAR}^f_4 - \text{Me}_2\text{pz}$ ]<sup>+</sup>.

**[PdMe(MeCN){G1-CH(3,5-Me<sub>2</sub>pz)<sub>2</sub>}][BAR<sup>f</sup><sub>4</sub>] (14):** Compound 10 (91 mg, 0.14 mmol), Na[BAR<sup>f</sup><sub>4</sub>] (121 mg, 0.14 mmol), and  $\text{CH}_3\text{CN}$  (2 mL). Yield: 163 mg (76%). C<sub>67</sub>H<sub>52</sub>BF<sub>24</sub>N<sub>5</sub>O<sub>2</sub>Pd (1532.4): calcd. C 52.52, H 3.42, N 4.57; found C 52.35, H 3.45, N 4.62.  $^1\text{H}$  NMR ( $\text{CDCl}_3$ ):  $\delta = 1.03$  (s, 3 H, PdMe), 1.83 (s, 3 H, pz-Me<sup>5</sup>), 1.98 (s, 3 H, pz-Me<sup>5</sup>), 2.14 (s, 3 H, pz-Me<sup>3</sup> adjacent to Pd-NCMe), 2.23 (s, 3 H, MeCN), 2.27 (s, 3 H, pz-Me<sup>3</sup> adjacent to PdMe), 4.26 (dd,  $^2J_{\text{H,H}} = 13.5$ ,  $^3J_{\text{H,H}} = 6.2$  Hz, 1 H, CH<sub>2</sub>), 4.95 (s, 4 H, PhCH<sub>2</sub>O), 5.16 (dd,  $^2J_{\text{H,H}} = 13.5$ ,  $^3J_{\text{H,H}} = 9.1$  Hz, 1 H, CH<sub>2</sub>), 5.75 (s, 1 H, pz-H<sup>4</sup>), 5.83 (s, 1 H, pz-H<sup>4</sup>), 5.96 (dd,  $^3J_{\text{H,H}} = 9.1$  Hz, 1 H, CH), 6.17 (d,  $^4J_{\text{H,H}} = 2.1$  Hz, 2 H, *o*-Ar), 6.56 (t,  $^4J_{\text{H,H}} = 2.1$  Hz, 1 H, *p*-Ar), 7.25–7.40 (m, 10 H, Ph) ppm.  $^{13}\text{C}\{^1\text{H}\}$  NMR ( $\text{CDCl}_3$ ):  $\delta = -3.6$  (PdMe), 2.9 (CH<sub>3</sub>CN), 10.6, 11.0 (pz-Me<sup>5</sup>), 13.5, 15.1 (pz-Me<sup>3</sup>), 43.1 (CH<sub>2</sub>), 68.6 (CH), 70.0 (PhCH<sub>2</sub>O), 101.6 (*p*-Ar), 107.3, 108.2 (pz-C<sup>4</sup>), 108.1 (*o*-Ar), 121.3 (MeCN), 127.3, 128.2, 128.7 (*o*-, *m*-, *p*-Ph), 135.5 (*ipso*-Ar), 136.3 (*ipso*-Ph), 140.7, 142.7 (pz-C<sup>5</sup>), 151.1, 153.2 (pz-C<sup>3</sup>), 160.4 (*m*-Ar) ppm. IR (KBr):  $\tilde{\nu} = 1609$  (m, C=C), 1564 (m, C=N), 1466 (m, C=C), 1154, 1048 (s, C–O–C)  $\text{cm}^{-1}$ . MS (ESI<sup>+</sup>-TOF in  $\text{CH}_2\text{Cl}_2/\text{MeOH}/\text{NH}_4\text{HCOO}$  5 mM):  $m/z = 669.22$  [ $\text{M} - \text{BAR}^f_4$ ]<sup>+</sup>, 627.28 [ $\text{M} - \text{MeCN} - \text{BAR}^f_4$ ]<sup>+</sup>, 612.17 [ $\text{M} - \text{CH}_4 - \text{MeCN} - \text{BAR}^f_4$ ]<sup>+</sup>, 411.21 [ $\text{M} - \text{PdMe}(\text{MeCN}) - \text{BAR}^f_4 - \text{Me}_2\text{pz}$ ]<sup>+</sup>.

**[PdMe(MeCN){G2-CH(3,5-Me<sub>2</sub>pz)<sub>2</sub>}[BARf<sub>4</sub>] (15):** Compound **11** (91 mg, 0.08 mmol), Na[BARf<sub>4</sub>] (72 mg, 0.08 mmol), and CH<sub>3</sub>CN (2 mL). Yield: 130 mg (83%). C<sub>95</sub>H<sub>76</sub>BF<sub>24</sub>N<sub>5</sub>O<sub>6</sub>Pd (1956.9): calcd. C 58.31, H 3.91, N 3.58; found C 57.99, H 3.53, N 3.47. <sup>1</sup>H NMR (CDCl<sub>3</sub>): δ = 1.01 (s, 3 H, PdMe), 1.81 (s, 3 H, pz-Me<sup>5</sup>) 1.95 (s, 3 H, pz-Me<sup>5</sup>), 2.10 (s, 3 H, pz-Me<sup>3</sup> adjacent to Pd-NCMe), 2.18 (s, 3 H, MeCN), 2.24 (s, 3 H, pz-Me<sup>3</sup> adjacent to PdMe), 4.26 (dd, <sup>2</sup>J<sub>H,H</sub> = 13.3, <sup>3</sup>J<sub>H,H</sub> = 6.5 Hz, 1 H, CH<sub>2</sub>), 4.88 (s, 4 H, ArCH<sub>2</sub>O), 4.99 (s, 8 H, PhCH<sub>2</sub>O), 5.10 (dd, <sup>2</sup>J<sub>H,H</sub> = 13.3, <sup>3</sup>J<sub>H,H</sub> = 8.8 Hz, 1 H, CH<sub>2</sub>), 5.70 (s, 1 H, pz-H<sup>4</sup>), 5.79 (s, 1 H, pz-H<sup>4</sup>), 5.95 (dd, <sup>3</sup>J<sub>H,H</sub> = 6.5, <sup>3</sup>J<sub>H,H</sub> = 8.8 Hz, 1 H, CH), 6.14 (d, <sup>4</sup>J<sub>H,H</sub> = 2.2 Hz, 2 H, G0-*o*-Ar), 6.49 (t, <sup>4</sup>J<sub>H,H</sub> = 2.2 Hz, 1 H, G0-*p*-Ar), 6.56 (br. s, 6 H, G1-*p*-Ar, G1-*o*-Ar), 7.25–7.40 (m, 20 H, Ph) ppm. <sup>13</sup>C{<sup>1</sup>H} NMR (CDCl<sub>3</sub>): δ = –3.6 (PdMe), 2.9 (CH<sub>3</sub>CN), 10.5, 10.9 (pz-Me<sup>5</sup>), 13.5, 15.1 (pz-Me<sup>3</sup>), 43.1 (CH<sub>2</sub>), 68.6 (CH), 69.9 (ArCH<sub>2</sub>O), 70.2 (PhCH<sub>2</sub>O), 101.0 (G1-*p*-Ar), 101.6 (G0-*p*-Ar), 106.2 (G1-*o*-Ar), 107.3, 108.3 (pz-C<sup>4</sup>), 108.0 (G0-*o*-Ar), 121.4 (MeCN), 127.5, 128.2, 128.7 (*o*-, *m*-, *p*-Ph), 135.5 (G0-*ipso*-Ar), 136.4 (*ipso*-Ph), 138.9 (G1-*ipso*-Ar), 140.8, 142.7 (pz-C<sup>5</sup>), 152.1, 153.2 (pz-C<sup>3</sup>), 160.2 (G0-*m*-Ar), 160.3 (G1-*m*-Ar) ppm. IR (KBr): ν̄ = 1596 (m, C=C), 1560 (w, C=N), 1454 (m, C=C), 1160, 1051 (s, C–O–C) cm<sup>–1</sup>. MS (ESI<sup>+</sup>-TOF in CH<sub>2</sub>Cl<sub>2</sub>/MeOH/NH<sub>4</sub>HCOO 5 mM): *m/z* = 1093.39 [M – BARf<sub>4</sub>]<sup>+</sup>, 1052.36 [M – MeCN – BARf<sub>4</sub>]<sup>+</sup>, 1036.33 [M – CH<sub>4</sub> – MeCN – BARf<sub>4</sub>]<sup>+</sup>, 931.44 [M – PdMe(MeCN) – BARf<sub>4</sub> + H]<sup>+</sup>.

**[PdMe(MeCN){G3-CH(3,5-Me<sub>2</sub>pz)<sub>2</sub>}[BARf<sub>4</sub>] (16):** Compound **12** (86 mg, 0.04 mmol), Na[BARf<sub>4</sub>] (39 mg, 0.04 mmol), and CH<sub>3</sub>CN (2 mL). Yield: 109 mg (97%). C<sub>151</sub>H<sub>124</sub>BF<sub>24</sub>N<sub>5</sub>O<sub>14</sub>Pd (2805.9): calcd. C 64.64, H 4.45, N 2.50; found C 64.19, H 4.26, N 2.31. <sup>1</sup>H NMR (CDCl<sub>3</sub>): δ = 1.00 (s, 3 H, PdMe), 1.81 (s, 3 H, pz-Me<sup>5</sup>) 1.96 (s, 3 H, pz-Me<sup>5</sup>), 2.09 (s, 3 H, pz-Me<sup>3</sup> adjacent to Pd-NCMe), 2.12 (s, 3 H, MeCN), 2.22 (s, 3 H, pz-Me<sup>3</sup> adjacent to PdMe), 4.22 (br. dd, <sup>2</sup>J<sub>H,H</sub> ≈ 14, <sup>3</sup>J<sub>H,H</sub> ≈ 6 Hz, 1 H, CH<sub>2</sub>), 4.86 (s, 4 H, G1-ArCH<sub>2</sub>O),

4.91 (s, 8 H, G2-ArCH<sub>2</sub>O), 4.98 (s, 16 H, PhCH<sub>2</sub>O), 5.08 (overlapped m, CH<sub>2</sub>), 5.70 (s, 1 H, pz-H<sup>4</sup>), 5.78 (s, 1 H, pz-H<sup>4</sup>), 5.95 (br. dd, <sup>3</sup>J<sub>H,H</sub> ≈ 9, 7 Hz, 1 H, CH), 6.14 (br. d, <sup>4</sup>J<sub>H,H</sub> ≈ 2 Hz, 2 H, G0-*o*-Ar), 6.51 (br. t, <sup>4</sup>J<sub>H,H</sub> ≈ 2 Hz, 1 H, G0-*p*-Ar), 6.55 (m, 6 H, G1-*p*-Ar, G2-*p*-Ar), 6.62 (br. resonance, 12 H, G1-*o*-Ar, G2-*o*-Ar), 7.25–7.40 (m, 40 H, Ph) ppm. <sup>13</sup>C{<sup>1</sup>H} NMR (CDCl<sub>3</sub>): δ = –3.6 (PdMe), 2.7 (CH<sub>3</sub>CN), 10.6, 10.9 (pz-Me<sup>5</sup>), 13.5, 15.0 (pz-Me<sup>3</sup>), 43.0 (CH<sub>2</sub>), 68.6 (CH), 69.7 (G1-ArCH<sub>2</sub>O), 70.0 (G2-ArCH<sub>2</sub>O), 70.1 (PhCH<sub>2</sub>O), 101.0 (G1-*p*-Ar), 101.3, (G2-*p*-Ar), 101.5 (G0-*p*-Ar), 106.2 (G1-*o*-Ar), 106.4 (G2-*o*-Ar), 107.3, 108.2 (pz-C<sup>4</sup>), 108.1 (G0-*o*-Ar), 121.4 (MeCN), 127.5, 128.1, 128.6 (*o*-, *m*-, *p*-Ph), 135.6 (G0-*ipso*-Ar), 136.6 (*ipso*-Ph), 138.8 (G1-*ipso*-Ar), 138.9 (G2-*ipso*-Ar), 140.7, 142.7 (pz-C<sup>5</sup>), 151.1, 153.2 (pz-C<sup>3</sup>), 160.1 (G0-*m*-Ar, G1-*m*-Ar overlapping), 160.2 (G2-*m*-Ar) ppm. IR (KBr): ν̄ = 1595 (m, C=C), 1561 (w, C=N), 1452 (m, C=C), 1159, 1050 (s, C–O–C) cm<sup>–1</sup>. MS (ESI<sup>+</sup>-TOF in CH<sub>2</sub>Cl<sub>2</sub>/MeOH/NH<sub>4</sub>HCOO 5 mM): *m/z* = 1941.72 [M – BARf<sub>4</sub>]<sup>+</sup>, 1900.70 [M – MeCN – BARf<sub>4</sub>]<sup>+</sup>, 1884.67 [M – CH<sub>4</sub> – MeCN – BARf<sub>4</sub>]<sup>+</sup>.

**X-ray Crystallographic Studies:** Single crystals of **3–6** suitable for X-ray diffraction studies were obtained by slow diffusion of pentane or hexane into a dichloromethane solution of the palladium complex at room temperature, whereas crystals of **17** incidentally formed from a sample of **13** in CDCl<sub>3</sub> upon standing in an NMR tube for several weeks. A summary of crystal data, data collection, and refinement parameters for the structural analysis of **3** and **17** is given in Table 3, whereas those corresponding to **4**, **5**, and **6** have been reported previously.<sup>[21]</sup> Suitable crystals were covered with mineral oil and mounted in the N<sub>2</sub> stream of a Bruker-Nonius Kappa-CCD diffractometer with area detector, and equipped with an Oxford Cryostream 700 unit; data were collected by using graphite-monochromated Mo-K<sub>α</sub> radiation (λ = 0.71073 Å), at 200 K, with an exposure time of 20 s per frame (nine sets); 467

Table 3. Crystal data and structure refinement for compounds **3** and **17**.

|  | <b>3</b>  | <b>17</b>   |
|--|---|---|
| Empirical formula  | C <sub>19</sub> H <sub>22</sub> Cl <sub>2</sub> N <sub>4</sub> O <sub>2</sub> Pd                      | C <sub>50</sub> H <sub>34</sub> BClF <sub>24</sub> N <sub>4</sub> Pd  |
| Formula mass   | 515.71  | 1299.47   |
| Color  | orange  | orange  |
| Temperature  | 200(2) K  | 150(2) K  |
| Wavelength   | 0.71073 Å   | 0.71073 Å   |
| Crystal system, space group  | monoclinic, P2 <sub>1</sub> /n  | triclinic, P $\bar{1}$  |
| Unit cell dimensions   | <i>a</i> = 8.5493(8) Å<br><i>b</i> = 15.0228(14) Å<br><i>c</i> = 16.9694(7) Å<br>$\beta$ = 90.608(7)° | <i>a</i> = 12.4379(12) Å<br><i>b</i> = 13.0254(11) Å<br><i>c</i> = 17.5787(12) Å<br><i>a</i> = 82.859(7)<br>$\beta$ = 88.324(7)<br>$\gamma$ = 88.559(7) |
| Volume   | 2179.3(3) Å <sup>3</sup>  | 2823.9(4) Å <sup>3</sup>  |
| Z, calculated density  | 4, 1.572 g cm <sup>–3</sup>   | 2, 1.528 g cm <sup>–3</sup>   |
| Absorption coefficient   | 11.18 cm <sup>–1</sup>  | 4.93 cm <sup>–1</sup>   |
| <i>F</i> (000)   | 1040  | 1292  |
| Crystal size   | 0.8 × 0.30 × 0.2 mm   | 0.35 × 0.35 × 0.25 mm   |
| $\theta$ range   | 5.09–27.50°   | 2.04–27.50°   |
| Limiting indices   | –11 ≤ <i>h</i> ≤ 10, –19 ≤ <i>k</i> ≤ 19, –22 ≤ <i>l</i> ≤ 21   | –16 ≤ <i>h</i> ≤ 16, –16 ≤ <i>k</i> ≤ 16, –22 ≤ <i>l</i> ≤ 22   |
| Reflections collected/unique                                       | 17234/4955 [ <i>R</i> (int) = 0.0886]   | 96548/12938 [ <i>R</i> (int) = 0.1534]  |
| Reflections observed   | 3562  | 8918 [ <i>I</i> > 2s( <i>I</i> )]   |
| Absorption correction  | semiempirical   | none  |
| Max. and min. transmission   | 1.566 and 0.739   | –   |
| Refinement method  | Full-matrix least squares on <i>F</i> <sup>2</sup>  | Full-matrix least squares on <i>F</i> <sup>2</sup>  |
| Data/restraints/parameters   | 4955/0/341  | 12938/0/730   |
| Goodness of fit on <i>F</i> <sup>2</sup>                           | 0.951   | 1.024   |
| Final <i>R</i> <sup>[a]</sup> indices [ <i>I</i> > 2s( <i>I</i> )] | <i>R</i> 1 = 0.0401, <i>wR</i> 2 = 0.0816   | <i>R</i> 1 = 0.0694, <i>wR</i> 2 = 0.1775   |
| <i>R</i> indices (all data)  | <i>R</i> 1 = 0.0711, <i>wR</i> 2 = 0.0904   | <i>R</i> 1 = 0.1087, <i>wR</i> 2 = 0.2080   |
| Largest diff. peak and hole  | 0.930 and –1.092 e Å <sup>–3</sup>  | 1.673 and –1.058 e Å <sup>–3</sup>  |

[a] *R*1 = Σ||*F*<sub>o</sub>| – |*F*<sub>c</sub>||/Σ|*F*<sub>o</sub>|; *wR*2 = {Σω(*F*<sub>o</sub><sup>2</sup> – *F*<sub>c</sub><sup>2</sup>)/[Σω(*F*<sub>o</sub><sup>2</sup>)]<sup>1/2</sup>.

frames; phi and omega scan 2.0° scan-width) for compound **3**, and at 150 K, with an exposure time of 10 s per frame (three sets; 186 frames; phi and omega scans 2° scan-width) for compound **17**. Raw data were corrected for Lorenz and polarization effects. Structures were solved by direct methods, completed by subsequent difference Fourier techniques, and refined by full-matrix least squares on  $F^2$  (SHELXL-97).<sup>[46]</sup> Anisotropic thermal parameters were used in the last cycles of refinement for the non-hydrogen atoms in both structures. In the case of compound **3**, the hydrogen atoms were found in the difference Fourier map and refined with isotropic thermal parameters, whereas the hydrogen atoms for **17** were introduced in the last cycle of refinement from geometrical calculations and refined by using a riding model. All the calculations were made by using the WINGX program.<sup>[47]</sup> CCDC-738727 (**3**) and -738728 (**17**) contain the supplementary crystallographic data for this paper. These data can be obtained free of charge from The Cambridge Crystallographic Data Centre via [www.ccdc.cam.ac.uk/data\\_request/cif](http://www.ccdc.cam.ac.uk/data_request/cif).

**General Procedure for Heck Reactions:** The corresponding catalyst precursor was weighed (2.0–20.0 mg, adjusted for catalytic [Pd] = 1.0–0.1 mM) into 10 mL screw-capped glass vials equipped with a magnetic stirrer. Alternatively, acetonitrile-diluted solutions were used in order to achieve a lower catalytic [Pd] ( $10^{-2}$  mM). The vial was capped and sealed with a septum, purged by repeated argon/vacuum operations, and an acetonitrile solution (5 mL) of methyl acrylate (0.1 M), 4-iodotoluene (0.1 M), and triethylamine (0.1 M) added from a syringe. The vial was immediately placed in a sand bath thermostatted at 80 °C, with vigorous stirring, taking that instant as the starting time of the reaction. Stirring of the mixture was maintained and 1 µL samples were withdrawn periodically and analyzed by GC using mesitylene as internal standard. Once the reaction was complete, the vial was reloaded with methyl acrylate, 4-iodotoluene, and triethylamine in amounts identical to those initially added (specified above). The vial was then again placed in the sand bath at 80 °C taking that instant as the new starting time. Samples (1 µL) were withdrawn after 2 and 24 h and analyzed by GC. These reloading operations were repeated up to six consecutive times.

## Acknowledgments

We gratefully acknowledge financial support from the DGI – Ministerio de Educación y Ciencia of Spain (project CTQ2008-02918/BQU) and the Comunidad de Madrid (project S-0505/PPQ/0328-03). A. S.-M. and P. G.-S. are also indebted to the Universidad de Alcalá for financial support (FPI grant) and to the “Factoría de Cristalización” (Consolider-Ingenio 2010), respectively.

- [1] a) G. R. Newkome, C. N. Moorefield, F. Vögtle, *Dendrimers and Dendrons: Concepts, Syntheses, Applications*, Wiley-VCH, Weinheim, 1996; b) J. M. J. Fréchet, D. A. Tomalia, *Dendrimers and Other Dendritic Polymers*, John Wiley & Sons, Chichester, 2002.
- [2] Some reviews on the chemistry and applications of metallodendrimers: a) C. Gorman, *Adv. Mater.* **1998**, *10*, 295; b) M. Venturi, S. Serroni, A. Juris, S. Campagna, V. Balzani, *Top. Curr. Chem.* **1998**, *197*, 193; c) G. R. Newkome, E. He, C. N. Moorefield, *Chem. Rev.* **1999**, *99*, 1689; d) F. J. Stoddart, T. Welton, *Polyhedron* **1999**, *18*, 3575; e) M. A. Hearshaw, J. R. Moss, *Chem. Commun.* **1999**, *1*; f) I. Cuadrado, M. Morán, C. M. Casado, B. Alonso, J. Losada, *Coord. Chem. Rev.* **1999**, *193–195*, 395; g) D. Astruc, J.-C. Blais, E. Cloutet, L. Djakovitch, S. Rigaut, J. Ruiz, V. Sartor, C. Valério, *Top. Curr. Chem.* **2000**, *210*, 229; h) H.-J. van Manen, F. C. J. M. van Vergel, D. N. Reinhoudt, *Top. Curr. Chem.* **2001**, *217*, 121; i) K. Onitsuka, S. Takahashi, *Top. Curr. Chem.* **2003**, *228*, 39; j) O. Rossell, M. Seco, I. Angurell, *C. R. Chim.* **2003**, *6*, 803; k) P. A. Chase, R. J. M. K. Gebbink, G. van Koten, *J. Organomet. Chem.* **2004**, *689*, 4016; l) S.-H. Hwang, C. D. Shreiner, C. N. Moorefield, G. R. Newkome, *New J. Chem.* **2007**, *31*, 1192.
- [3] Selected reviews on catalysis with dendrimers: a) G. E. Oosterom, J. N. H. Reek, P. C. J. Kamer, P. W. N. M. van Leeuwen, *Angew. Chem. Int. Ed.* **2001**, *40*, 1828; b) D. Astruc, F. Char-dac, *Chem. Rev.* **2001**, *101*, 2991; c) R. Kreiter, A. W. Kleij, R. J. M. K. Gebbink, G. van Koten, *Top. Curr. Chem.* **2001**, *217*, 163; d) A. M. Caminade, V. Maraval, R. Laurent, J. P. Majoral, *Curr. Org. Chem.* **2002**, *6*, 739; e) A. Dahan, M. Portnoy, *J. Polym. Sci., Part A: Polym. Chem.* **2005**, *43*, 235; f) R. van de Coevering, R. J. M. Klein Gebbink, G. van Koten, *Prog. Polym. Sci.* **2005**, *30*, 474; g) D. Méry, D. Astruc, *Coord. Chem. Rev.* **2006**, *250*, 1965; h) J. N. H. Reek, S. Arévalo, R. van Heerbeek, P. C. J. Kamer, P. W. N. M. van Leeuwen, *Adv. Catal.* **2006**, *49*, 71; i) L. H. Gade (Ed.), *Dendrimer Catalysis*, Springer, Berlin, 2006.
- [4] For a recent review of palladium dendrimers in catalysis, see: R. Andrés, E. de Jesús, J. C. Flores, *New J. Chem.* **2007**, *31*, 1161.
- [5] R. Andrés, E. de Jesús, F. J. de la Mata, J. C. Flores, R. Gómez, *J. Organomet. Chem.* **2005**, *690*, 939.
- [6] a) J. M. Benito, S. Arévalo, E. de Jesús, F. J. de la Mata, J. C. Flores, R. Gómez, *J. Organomet. Chem.* **2000**, *610*, 42; b) J. M. Benito, E. de Jesús, F. J. de la Mata, J. C. Flores, R. Gómez, P. Gómez-Sal, *J. Organomet. Chem.* **2002**, *664*, 258; c) J. M. Benito, E. de Jesús, F. J. de la Mata, J. C. Flores, R. Gómez, P. Gómez-Sal, *J. Organomet. Chem.* **2006**, *691*, 3602.
- [7] a) J. M. Benito, E. de Jesús, F. J. de la Mata, J. C. Flores, R. Gómez, *Chem. Commun.* **2005**, 5217; b) J. M. Benito, E. de Jesús, F. J. de la Mata, J. C. Flores, R. Gómez, P. Gómez-Sal, *Organometallics* **2006**, *25*, 3876; c) J. M. Benito, E. de Jesús, F. J. de la Mata, J. C. Flores, R. Gómez, *Organometallics* **2006**, *25*, 3045; d) J. M. Benito, E. de Jesús, F. J. de la Mata, J. C. Flores, R. Gómez, *J. Organomet. Chem.* **2008**, *693*, 278.
- [8] S. Trofimenko, *Scorpionates – The Coordination Chemistry of Polypyrazolylborate Ligands*, Imperial College Press, London, 1999.
- [9] a) A. Otero, J. Fernández-Baeza, A. Antiñolo, J. Tejada, A. Lara-Sánchez, *Dalton Trans.* **2004**, 1499; b) C. Pettinari, R. Pettinari, *Coord. Chem. Rev.* **2005**, *249*, 663; c) C. Pettinari, R. Pettinari, *Coord. Chem. Rev.* **2005**, *249*, 525; d) H. R. Bigmore, S. C. Lawrence, P. Mountford, C. S. Tredget, *Dalton Trans.* **2005**, 635.
- [10] a) D. L. Reger, T. C. Grattan, K. J. Brown, C. A. Little, J. J. S. Lamba, A. L. Rheingold, R. D. Sommer, *J. Organomet. Chem.* **2000**, *607*, 120; b) S. Juliá, P. Sala, J. del Mazo, M. Sancho, C. Ochoa, J. Elguero, J.-P. Fayet, M.-C. Vertut, *J. Heterocycl. Chem.* **1982**, *19*, 1141; c) S. Juliá, J. M. del Mazo, L. Avila, J. Elguero, *Org. Prep. Proced. Int.* **1984**, *16*, 299.
- [11] a) H. R. Bigmore, S. R. Dubberley, M. Kranenburg, S. C. Lawrence, A. J. Sealey, J. D. Selby, M. A. Zuideveld, A. R. Cowley, P. Mountford, *Chem. Commun.* **2006**, 436; b) S. C. Lawrence, B. D. Ward, S. R. Dubberley, C. M. Kozak, P. Mountford, *Chem. Commun.* **2003**, 2880; c) S. Milione, C. Montefusco, T. Cuenca, A. Grassi, *Chem. Commun.* **2003**, 1176.
- [12] For leading references, see the following and references cited therein: a) S. C. Lawrence, M. E. G. Skinner, J. C. Green, P. Mountford, *Chem. Commun.* **2001**, 705; b) A. Otero, J. Fernández-Baeza, A. Antiñolo, J. Tejada, A. Lara-Sánchez, L. Sánchez-Barba, A. M. Rodríguez, M. A. Maestro, *J. Am. Chem. Soc.* **2004**, *126*, 1330; c) D. L. Reger, R. F. Semeniuc, V. Rassolov, M. D. Smith, *Inorg. Chem.* **2004**, *43*, 537; d) D. L. Reger, J. R. Gardinier, M. D. Smith, *Inorg. Chem.* **2004**, *43*, 3825; e) A. Otero, J. Fernández-Baeza, A. Antiñolo, J. Tejada, A. Lara-Sánchez, L. Sánchez-Barba, E. Martínez-Caballero, A. M. Rodríguez, I. López-Solera, *Inorg. Chem.* **2005**, *44*, 5336;

- f) R. G. Howe, C. S. Tredget, S. C. Lawrence, S. Subongkoj, A. R. Cowley, P. Mountford, *Chem. Commun.* **2006**, 223; g) A. Otero, J. Fernández-Baeza, A. Antiñolo, J. Tejada, A. Lara-Sánchez, L. Sánchez-Barba, M. Sánchez-Molina, S. Franco, I. López-Solera, A. M. Rodríguez, *Eur. J. Inorg. Chem.* **2006**, 707; h) D. Adhikari, G. Zhao, F. Basuli, J. Tomaszewski, J. C. Huffman, D. J. Mindiola, *Inorg. Chem.* **2006**, 45, 1604; i) D. L. Reger, R. F. Semeniuc, J. R. Gardinier, J. O'Neal, B. Reinecke, M. D. Smith, *Inorg. Chem.* **2006**, 45, 4337; j) D. L. Reger, J. R. Gardinier, J. D. Elgin, M. D. Smith, *Inorg. Chem.* **2006**, 45, 8862; k) E. Caverio, S. Uriel, P. Romero, J. L. Serrano, R. Giménez, *J. Am. Chem. Soc.* **2007**, 129, 11608; l) M. P. Conley, C. T. Bruns, R. F. Jordan, *Organometallics* **2007**, 26, 6750; m) H.-J. Xu, Y. Cheng, J.-F. Sun, B. A. Dougan, Y.-Z. Li, X.-T. Chen, Z.-L. Xue, *J. Organomet. Chem.* **2008**, 693, 3851; n) A. D. Schofield, M. L. Barros, M. G. Cushion, A. D. Schwarz, P. Mountford, *Dalton Trans.* **2009**, 85; o) D. L. Reger, E. A. Foley, M. D. Smith, *Inorg. Chem.* **2009**, 48, 936; p) T. Godau, F. Platzmann, F. W. Heinemann, N. Burzlaff, *Dalton Trans.* **2009**, 254; q) L. Maria, C. Fernandes, R. García, L. Gano, A. Paulo, I. C. Santos, I. Santos, *Dalton Trans.* **2009**, 603.
- [13] A. Sánchez-Méndez, G. F. Silvestri, E. de Jesús, F. J. de la Mata, J. C. Flores, R. Gómez, P. Gómez-Sal, *Eur. J. Inorg. Chem.* **2004**, 3287.
- [14] a) D. L. Reger, R. F. Semeniuc, M. D. Smith, *J. Organomet. Chem.* **2003**, 666, 87; b) D. L. Reger, R. F. Semeniuc, M. D. Smith, *J. Chem. Soc., Dalton Trans.* **2002**, 476.
- [15] A. Sánchez-Méndez, J. M. Benito, E. de Jesús, F. J. de la Mata, J. C. Flores, R. Gómez, P. Gómez-Sal, *Dalton Trans.* **2006**, 5379.
- [16] A. Sánchez-Méndez, A. M. Ortiz, E. de Jesús, J. C. Flores, P. Gómez-Sal, *Dalton Trans.* **2007**, 5658.
- [17] a) M. A. Casado, V. Hack, J. A. Camerano, M. A. Ciriano, C. Tejel, L. A. Oro, *Inorg. Chem.* **2005**, 44, 9122; b) J. A. Camerano, M. A. Casado, M. A. Ciriano, L. A. Oro, *Dalton Trans.* **2006**, 5287.
- [18] J. W. J. Knapen, A. W. van der Made, J. C. de Wilde, P. W. N. M. van Leeuwen, P. Wijkens, D. M. Grove, G. van Koten, *Nature* **1994**, 372, 659.
- [19] a) H. P. Dijkstra, G. P. M. van Klink, G. van Koten, *Acc. Chem. Res.* **2002**, 35, 798; b) R. van Heerbeek, P. C. J. Kamer, P. W. N. M. van Leeuwen, J. N. H. Reek, *Chem. Rev.* **2002**, 102, 3717; c) G. P. M. van Klink, H. P. Dijkstra, G. van Koten, *C. R. Chim.* **2003**, 6, 1079; d) C. Müller, M. G. Nijkamp, D. Vogt, *Eur. J. Inorg. Chem.* **2005**, 4011; e) A. Berger, R. J. M. Klein Gebbink, G. van Koten, *Top. Organomet. Chem.* **2006**, 20, 1; f) E. de Jesús, J. C. Flores, *Ind. Eng. Chem. Res.* **2008**, 47, 7968.
- [20] B. Helms, J. M. J. Fréchet, *Adv. Synth. Catal.* **2006**, 348, 1125.
- [21] A. Sánchez-Méndez, E. de Jesús, J. C. Flores, P. Gómez-Sal, *Inorg. Chem.* **2007**, 46, 4793.
- [22] a) C. Hawker, J. M. J. Fréchet, *J. Chem. Soc., Chem. Commun.* **1990**, 1010; b) C. J. Hawker, J. M. J. Fréchet, *J. Am. Chem. Soc.* **1990**, 112, 7638.
- [23] a) S. Tsuji, D. C. Swenson, R. F. Jordan, *Organometallics* **1999**, 18, 4758; b) W. de Graaf, J. Boersma, W. J. J. Smeets, A. L. Spek, G. van Koten, *Organometallics* **1989**, 8, 2907.
- [24] a) T. Mizoroki, K. Mori, A. Ozaki, *Bull. Chem. Soc. Jpn.* **1971**, 44, 581; b) R. F. Heck, J. P. Nolley Jr., *J. Org. Chem.* **1972**, 37, 2330.
- [25] a) W. A. Herrmann in *Applied Homogeneous Catalysis with Organometallic Compounds* (Eds.: B. Cornils, W. A. Herrmann), 2nd ed., Wiley-VCH, Weinheim, **2002**, vol. 2, pp. 775–793; b) S. Bräse, A. de Meijere in *Metal-Catalyzed Cross-Coupling Reactions* (Eds.: A. de Meijere, F. Diederich), 2nd ed., Wiley-VCH, Weinheim, **2004**, vol. 1, pp. 217–315; c) A. M. Trzeciak, J. J. Ziolkowski, *Coord. Chem. Rev.* **2005**, 249, 2308.
- [26] M. T. Reetz, G. Lohmer, R. Schwickardi, *Angew. Chem. Int. Ed. Engl.* **1997**, 36, 1526.
- [27] M. Ooe, M. Murata, T. Mizugaki, K. Ebitani, K. Kaneda, *J. Am. Chem. Soc.* **2004**, 126, 1604.
- [28] a) D. P. Catsoulacos, B. R. Steele, G. A. Heropoulos, M. Micha-Screttas, C. G. Screttas, *Tetrahedron Lett.* **2003**, 44, 4575; b) T. R. Krishna, N. Jayaraman, *Tetrahedron* **2004**, 60, 10325; c) J. Kuehnert, M. Lamac, J. Demel, A. Nicolai, H. Lang, P. Stepnicka, *J. Mol. Catal. A* **2008**, 285, 41; d) P. Servin, R. Laurent, A. Romerosa, M. Peruzzini, J. P. Majoral, A. M. Caminade, *Organometallics* **2008**, 27, 2066.
- [29] G. S. Smith, S. F. Mapolie, *J. Mol. Catal. A* **2004**, 213, 187.
- [30] F. Martínez-Olíd, J. M. Benito, J. C. Flores, E. de Jesús, *Isr. J. Chem.* **2009**, 49, 99.
- [31] F. Montilla, A. Galindo, R. Andrés, M. Córdoba, E. de Jesús, C. Bo, *Organometallics* **2006**, 25, 4138.
- [32] a) H. Alper, P. Arya, S. C. Bourque, G. R. Jefferson, L. E. Manzer, *Can. J. Chem.* **2000**, 78, 920; b) R. Chanthateyanonth, H. Alper, *J. Mol. Catal. A* **2003**, 201, 23.
- [33] a) A. Dahan, M. Portnoy, *Org. Lett.* **2003**, 5, 1197; b) A. Dahan, M. Portnoy, *J. Am. Chem. Soc.* **2007**, 129, 5860.
- [34] a) L. K. Yeung, R. M. Crooks, *Nano Lett.* **2001**, 1, 14; b) L. K. Yeung, C. T. Lee, K. P. Johnston, R. M. Crooks, *Chem. Commun.* **2001**, 2290; c) E. H. Rahim, F. S. Kamounah, J. Frederiksen, J. B. Christensen, *Nano Lett.* **2001**, 1, 499; d) K. R. Gopidas, J. K. Whitesell, M. A. Fox, *Nano Lett.* **2003**, 3, 1757.
- [35] C. Amatore, A. Jutand, *Acc. Chem. Res.* **2000**, 33, 314.
- [36] J. M. Riley, S. Alkan, A. Chen, M. Shapiro, W. A. Khan, W. R. Murphy Jr., J. E. Hanson, *Macromolecules* **2001**, 34, 1797.
- [37] S. De Backer, Y. Prinzie, W. Verheijen, M. Smet, K. Desmedt, W. Dehaen, F. C. De Schryver, *J. Phys. Chem. A* **1998**, 102, 5451.
- [38] M. T. Reetz, J. G. de Vries, *Chem. Commun.* **2004**, 1559.
- [39] See also: a) C. S. Consorti, F. R. Flores, J. Dupont, *J. Am. Chem. Soc.* **2005**, 127, 12054; b) J. G. de Vries, *Dalton Trans.* **2006**, 421; c) N. T. S. Phan, M. Van der Sluys, C. W. Jones, *Adv. Synth. Catal.* **2006**, 348, 609; d) D. Astruc, *Inorg. Chem.* **2007**, 46, 1884; e) K. Köhler, W. Kleist, S. S. Pröckl, *Inorg. Chem.* **2007**, 46, 1876; f) M. Weck, C. W. Jones, *Inorg. Chem.* **2007**, 46, 1865; g) A. V. Gaikwad, A. Holuigue, M. B. Thathagar, J. E. ten Elshof, G. Rothenberg, *Chem. Eur. J.* **2007**, 13, 6908; h) L. Durán Pachón, G. Rothenberg, *Appl. Organomet. Chem.* **2008**, 22, 288; i) J. Durand, E. Teuma, M. Gómez, *Eur. J. Inorg. Chem.* **2008**, 3577; j) M. Diéguez, O. Pàmies, Y. Mata, E. Teuma, M. Gómez, F. Ribaudo, P. W. N. M. van Leeuwen, *Adv. Synth. Catal.* **2008**, 350, 2583; k) L. Wu, Z.-W. Li, F. Zhang, Y.-M. He, Q.-H. Fan, *Adv. Synth. Catal.* **2008**, 350, 846.
- [40] A. H. M. de Vries, J. M. C. A. Mulders, H. H. M. Mommers, H. J. W. Hendricks, J. G. de Vries, *Org. Lett.* **2003**, 5, 3285.
- [41] M. Brookhart, B. Grant, A. F. Volpe Jr., *Organometallics* **1992**, 11, 3920.
- [42] a) A. Otero, J. Fernández-Baeza, J. Tejada, A. Antiñolo, F. Carrillo-Hermosilla, E. Díez-Barra, A. Lara-Sánchez, M. Fernández-López, *J. Chem. Soc., Dalton Trans.* **2000**, 2367; b) B. S. Hammes, M. T. Kieber-Emmons, J. A. Letizia, Z. Shirin, C. J. Carrano, L. N. Zakharov, A. L. Rheingold, *Inorg. Chim. Acta* **2003**, 346, 227.
- [43] D. Drew, J. R. Doyle in *Inorganic Syntheses* (Ed.: F. A. Cotton), McGraw-Hill, New York, **1972**, vol. 13, p. 47.
- [44] R. E. Rülke, J. M. Ernsting, A. L. Spek, C. J. Elsevier, P. W. N. M. van Leeuwen, K. Vrieze, *Inorg. Chem.* **1993**, 32, 5769.
- [45] D. P. Perrin, W. L. F. Armarego, *Purification of Laboratory Chemicals*, 3rd ed., Pergamon Press, Oxford, **1988**.
- [46] G. M. Sheldrick, *SHELXL-97, Program for Crystal Structure Refinement*, University of Göttingen, Germany, **1997**.
- [47] WinGX system: L. J. Farrugia, *J. Appl. Crystallogr.* **1999**, 32, 837.

Received: September 2, 2009

Published Online: November 25, 2009

# Synthesis, Characterization and Hydrolysis of Osmium Tetrphosphorus Complexes

Maria Caporali,<sup>[a]</sup> Massimo Di Vaira,<sup>[b]</sup> Maurizio Peruzzini,<sup>\*[a]</sup> Stefano Seniori Costantini,<sup>[b]</sup> Piero Stoppioni,<sup>\*[b]</sup> and Fabrizio Zanolini<sup>[a]</sup>

**Keywords:** Phosphorus / Coordination / Hydrolysis / Cyclopentadienyl ligands / Osmium

The reaction of  $[\text{CpOs}(\text{PPh}_3)_2\text{Cl}]$  (**1**) with one equivalent of white phosphorus in the presence of  $\text{AgOTf}$  ( $\text{OTf} = \text{triflate}$ ,  $\text{OSO}_2\text{CF}_3$ ) as chloride scavenger affords the stable metal complex  $[\text{CpOs}(\text{PPh}_3)_2(\eta^1\text{-P}_4)]\text{OTf}$  (**2**), which contains the tetrahedral  $\text{P}_4$   $\eta^1$ -bound to the  $\text{CpOs}(\text{PPh}_3)_2$  metal fragment. Addition of  $[\text{CpRu}(\text{PPh}_3)_2(\text{OTf})]$  to **2** yields the heterobimetallic species  $[\{\text{CpRu}(\text{PPh}_3)_2\}\{\text{CpOs}(\text{PPh}_3)_2(\mu, \eta^{1:1}\text{-P}_4)\}](\text{OTf})_2$  (**3**), in which the tetrahedral  $\text{P}_4$  is bound to two different metal

fragments through two phosphorus atoms. The compounds have been characterized by elemental analysis, IR and NMR spectroscopy, and their crystal structures have been determined by X-ray diffraction. The coordinated  $\text{P}_4$ , at variance with the free ligand, reacts with an excess amount of water in *thf* under mild conditions to yield several products, most of which have been characterized.

## Introduction

In recent years, the reactivity of white phosphorus,  $\text{P}_4$ , towards different transition metal fragments has been widely investigated.<sup>[1–5]</sup> The efforts of several research groups in this field have led to the synthesis of an amazing variety of transition metal complexes containing  $\text{P}_n$  units originating from either the degradation of white phosphorus or from the recombination of smaller fragments into polyatomic aggregates.<sup>[6,7]</sup> Indeed, while the range of  $\text{P}_x$  topologies which may be generated from  $\text{P}_4$  is enormous, the number of coordination complexes featuring the intact cage molecule as a ligand was, until a few years ago, limited to very few examples of species thermally unstable and/or difficult to handle.<sup>[8–11]</sup> Accordingly, the reactivity of the coordinated molecule has been scarcely investigated. In contrast to this general belief, we have found recently that 16-electron  $d^7$ -metal complexes of rhenium,<sup>[12]</sup> iron<sup>[13]</sup> and ruthenium<sup>[13–15]</sup> may coordinate the intact  $\text{P}_4$  molecule to readily form mono- and bimetallic compounds in good yield. The high stability and relatively good availability of these complexes have allowed to investigate the reactivity of the coordinated molecule towards a variety of different organic and inorganic reagents. Such a topic deserves particular interest in view of the attractive possibility of ob-

taining organophosphorus derivatives from white phosphorus through the mild and controllable activation of the coordinated intact molecule. The results we have obtained in this field are particularly intriguing, as we found that the  $\text{P}_4$  molecule in the monometallic  $[\text{CpRu}(\text{PPh}_3)_2(\eta^1\text{-P}_4)]\text{Y}$  ( $\text{Y} = \text{PF}_6$ ,  $\text{OTf}$ )<sup>[14]</sup> (**4**) and bimetallic  $[\{\text{CpRu}(\text{PPh}_3)_2\}_2(\mu, \eta^{1:1}\text{-P}_4)](\text{OTf})_2$ <sup>[15]</sup> (**5**) complexes readily undergoes disproportionation with water under mild conditions. Detailed investigations of the hydrolysis have outlined some points of great interest. Monometallic compound **4** yields phosphane and oxygenated phosphorus compounds;<sup>[14]</sup> fine tuning the properties of the metal fragment plays an important role in determining the reactivity of the coordinated  $\text{P}_4$  tetrahedron. For example, the structurally related  $[\text{Cp}^*\text{Ru}(\text{PPh}_3)_2(\eta^1\text{-P}_4)]^+$  ( $\text{Cp}^* = \text{pentamethylcyclopentadienyl}$ ) does not undergo hydrolysis under the same conditions.<sup>[13]</sup> The hydrolysis of the doubly metallated  $\text{P}_4$  in **5** is even more intriguing, as the products are strongly affected by the ratio of complex and water. Thus, diphosphane  $\text{P}_2\text{H}_4$ ,<sup>[15]</sup> 1-hydroxytriphosphane  $\text{PH}(\text{OH})\text{P}(\text{H})\text{P}(\text{H})_2$ <sup>[16]</sup> and 1,1,4-tris(hydroxy)tetrphosphane  $\text{P}(\text{OH})_2\text{P}(\text{H})\text{P}(\text{H})\text{P}(\text{H})_2$ <sup>[17]</sup> form by the reaction of **5** with different amounts of water. Such molecules, which are either quite unstable ( $\text{P}_2\text{H}_4$ )<sup>[18]</sup> or unknown as free molecules,<sup>[19]</sup> are highly stabilized through coordination to two ruthenium fragments.

The above results have clearly highlighted that the coordination of the intact  $\text{P}_4$  molecule may be accomplished in the presence of metal fragments with proper coordinating properties. However, these have been, up to now, exploited only for a limited number of 16-electron fragments, while the activation of the coordinated molecule has been obtained for an even more restricted number of complexes. To

[a] ICCOM CNR,  
Via Madonna del Piano 10, 50019, Sesto Fiorentino, Firenze,  
Italy

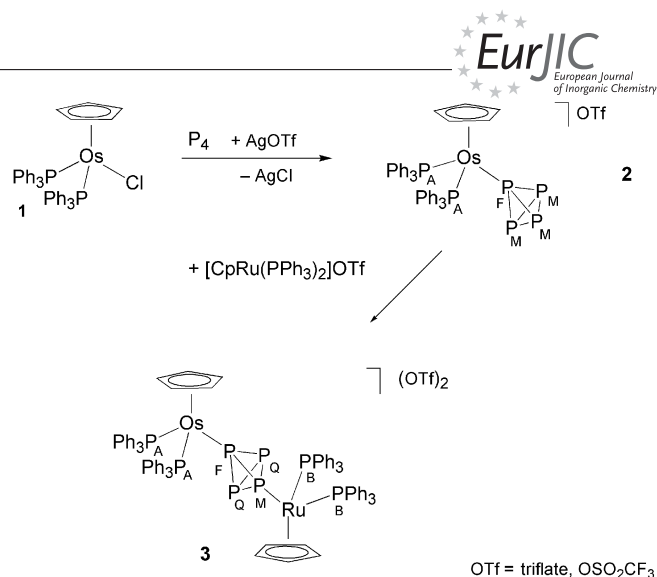
[b] Dipartimento di Chimica, Università di Firenze,  
Via della Lastruccia 3, 50019 Sesto Fiorentino, Firenze, Italy  
Fax: +39-0554573385  
E-mail: mperuzzini@iccom.cnr.it  
piero.stoppioni@unifi.it

investigate further this field and, particularly, to address the possible role played by the transition metal in driving the hydrolysis of coordinated  $P_4$ , we have now considered the chemistry of  $P_4$  in the presence of the related  $CpOs(PPh_3)_2$  fragment. Here we report on the synthesis of the highly stable monometallic  $[CpOs(PPh_3)_2(\eta^1-P_4)]OTf$  (**2**) and heterobimetallic  $[\{CpRu(PPh_3)_2\}\{CpOs(PPh_3)_2\}(\mu, \eta^{1:1}-P_4)](OTf)_2$  (**3**). In *thf* at room temperature, these complexes readily react with an excess amount of water to yield several products, most of which have been isolated and characterized. The crystal structures of **2** and **3**, which are the first examples of osmium complexes coordinating white phosphorus, have been determined by X-ray diffraction.

## Results and Discussion

The reaction of  $[CpOs(PPh_3)_2Cl]$  (**1**) in a 1:1 *thf*/ $CH_2Cl_2$  mixture with one equivalent of  $P_4$  in the presence of silver triflate as chloride scavenger leads to the precipitation of  $AgCl$  and affords complex  $[CpOs(PPh_3)_2(\eta^1-P_4)]OTf$  (**2**), which can be isolated as orange microcrystals after workup. The addition of one equivalent of  $[CpRu(PPh_3)_2(OTf)]$  in  $CH_2Cl_2$  to a solution of **2** in *thf*/ $CH_2Cl_2$  mixture yields the heterobimetallic compound  $[\{CpRu(PPh_3)_2\}\{CpOs(PPh_3)_2\}(\mu, \eta^{1:1}-P_4)](OTf)_2$  (**3**) as red microcrystals. Both compounds, which are obtained in good yield, are stable under an inert atmosphere and soluble in common organic solvents (Scheme 1). The  $^31P\{^1H\}$  NMR spectra of both **2** and **3** ( $CDCl_3$ , r.t.) clearly show that the  $P_4$  molecule is firmly coordinated to the metal(s) also in solution. No high-field resonance attributable to  $P_4$  dissociation is observed in solution at room temperature. Compound **2** exhibits an  $A_2FM_3$  spin system in which A denotes the two equivalent triphenylphosphane phosphorus atoms, F is the atom bound to the metal and M stands for the three atoms of the tetraphosphorus tetrahedron not involved in coordination (see Scheme 1 for labels). The phosphane ligands yield resonances in the range expected for cationic osmium half-sandwich compounds.<sup>[20]</sup> The four phosphorus atoms of the coordinated tetraphosphorus ligand form the  $FM_3$  part of the spectrum. These resonances are shifted downfield with respect to the free  $P_4$  molecule ( $\Delta\delta P_F = 149.57$ ,  $\Delta\delta P_M = 48.37$  ppm), and this shift, as found for the analogous ruthenium  $[CpRu(PPh_3)_2(\eta^1-P_4)]Y$  derivative **4**,<sup>[14]</sup> is particularly enhanced for the atom bound to the metal centre.

Complex **3** yields a first-order  $A_2B_2FMQ_2$ , where A and B are the triphenylphosphane phosphorus atoms of the  $CpOs(PPh_3)_2$  and  $CpRu(PPh_3)_2$  fragments, respectively, F and M are the  $P_4$  atoms bound to osmium and ruthenium, respectively, and Q denotes the two atoms of the tetraphosphorus tetrahedron not involved in the coordination (see Scheme 1 for labels). Both the chemical shifts and the coupling constants of the phosphane ligands show values in the range expected for cationic osmium<sup>[20]</sup> and ruthenium<sup>[14,15]</sup> half-sandwich compounds. The signals of the coordinated  $P_4$  are shifted downfield with respect to the free molecule. The resonance ascribable to the two phosphorus atoms of



Scheme 1.

the cage not involved in the coordination occurs at higher field ( $-462.76$  ppm) with a coordination chemical shift ( $\Delta\delta P_F = 63.22$  ppm) comparable to that observed for diruthenium compound **5**.<sup>[15]</sup> The two phosphorus atoms bound to the metal fragments undergo higher downfield shifts with that of  $P_M$  being more enhanced ( $\Delta\delta P_M = 247.81$  ppm) than that of  $P_F$  ( $\Delta\delta P_F = 211.06$  ppm).

The structure of **2** consists of  $[CpOs(PPh_3)_2(\eta^1-P_4)]^+$  complex cations and triflate anions. The compound is isomorphous with the  $[CpRu(PPh_3)_2(P_4)](PF_6)$  ruthenium analogue **4**,<sup>[14]</sup> irrespective of the different nature of the anions in the two compounds. The geometry of the osmium cation in **2** (Figure 1) is closely similar to that of the ruthenium complex, which may be mostly attributed to the similarity in the atomic radii of the two metals. The  $Os-P(PPh_3)$  distances (Table 1) are slightly shorter, by  $0.024$  Å on average, than the corresponding distances in the ruthenium cation, and the  $Os-P(P_4)$  distance,  $2.263(1)$  Å, almost matches the  $Ru-P(P_4)$  one [ $2.269(2)$  Å]. The values of the  $P-P$  distances in the  $P_4$  cage of **2** are, overall, slightly larger than those found for the ruthenium complex **4**: in particular, the mean value of the three  $P-P$  distances formed by the coordinating phosphorus atom and that of the three  $P-P$  distances between the distal P atoms of the cage in **2** are larger than the corresponding mean values for the ruthenium complex by  $0.008$  Å and  $0.025$  Å, respectively. Such differences may be considered to result from effects of apparent bond shortening because of thermal motion, significantly affecting the  $P_4$  dangling group in the room-temperature structure of the ruthenium derivative. Indeed, in the structure of **2** refined from room temperature data,<sup>[21]</sup> the mean values of the same groups of  $P-P$  distances are found to be in line, within  $0.001$  Å, with those of the ruthenium compound. The structure of compound **3** comprises bimetallic cations, triflate anions and solvate chloroform molecules, some of which are in highly disordered arrangement. Also the cation (Figure 2), which possesses apparent twofold rotational symmetry, the twofold axis passing through the  $P-P$  bond of the bridging phosphorus atoms and through the opposite

bond in the cage, is affected by orientational disorder, each metal site (M) having 50% Ru and 50% Os character. However, this type of disorder is expected to have minor consequences on the values of derived structural parameters, because of the similarity in the values of the atomic radii of Ru and Os, which is consistent with the above results of the comparison between the monometallic  $P_4$  derivatives. The (metal-mediated) geometry of the cation in **3** (Table 2) closely corresponds to that of the diruthenium cation in the structure of the previously reported  $[\{CpRu(PPh_3)_2\}_2(\mu, \eta^{1:1}-P_4)](OTf)_2$  (**5**).<sup>[15]</sup> The M–P( $PPh_3$ ) distances in **3** are shorter, by 0.018 Å on average, than those of the diruthenium complex, and the M–P( $P_4$ ) bond length in **3** is only 0.004 Å smaller than the mean of the two values in the other compound. There is also close agreement, within 0.002 Å, between the mean values of the six P–P distances in the  $P_4$  cages of the two compounds (effects of thermal motion should be smaller for the cage in bridging position than for the monodentate one; moreover, the data sets of both bimetallic compounds were collected at low temperature). In detail, a feature already noticed for the structure of the diruthenium complex is found also for **3**: the P–P bond formed by the bridging phosphorus atoms is the shortest among all bonds in the cage, whereas the opposite bond is the longest one. Remarkably, the  $-26.9(6)^\circ$  M–P3–P3'–M' torsion angle in **3** is quite close to the  $-27.4(6)^\circ$  value found for the diruthenium cation, in spite of the different packing and local symmetries of the cations in the two structures. This suggests that the overall conformation of the bimetallic cation is primarily dictated by the steric requirements of the bulky triphenylphosphane ligands.

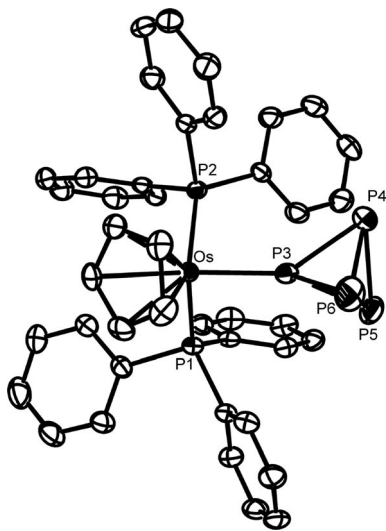


Figure 1. A view of the cation in the structure of **2** with 50% probability ellipsoids. Hydrogen atoms are omitted for clarity.

When a solution of **2** or **3** in thf was treated with an excess amount of water, hydrolysis of the  $P_4$  ligand occurred at room temperature. Reactions carried out on different batches are reproducible, both with respect to the amount and nature of the products obtained. The  $^{31}P\{^1H\}$  NMR spectra of the solids obtained from the hydrolysis of **2** and

Table 1. Selected bond lengths [Å] and angles [ $^\circ$ ] for **2**.<sup>[a]</sup>

|          |           |          |             |
|----------|-----------|----------|-------------|
| Os–P1    | 2.345(1)  | P3–P6    | 2.151(1)    |
| Os–P2    | 2.327(1)  | P4–P5    | 2.198(2)    |
| Os–P3    | 2.263(1)  | P4–P6    | 2.214(2)    |
| P3–P4    | 2.146(1)  | P5–P6    | 2.231(2)    |
| P3–P5    | 2.167(1)  | Os–C(Cp) | 2.215–2.263 |
| P1–Os–P2 | 103.56(3) | P2–Os–P3 | 91.31(3)    |
| P1–Os–P3 | 93.73(3)  |          |             |

[a] 150 K data.

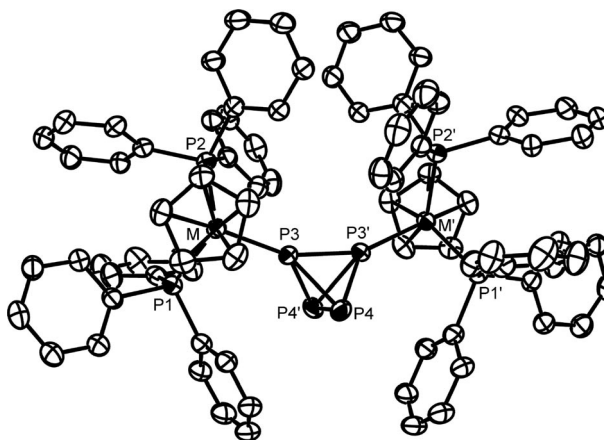


Figure 2. A view of the cation in the structure of **3** with 30% probability ellipsoids. The metal sites M have 50% Ru and 50% Os occupancies. Primed atoms are related to the corresponding unprimed ones by a twofold axis bisecting the P3–P3' and P4–P4' bonds. Hydrogen atoms are omitted for clarity.

Table 2. Selected bond lengths [Å] and angles [ $^\circ$ ] for **3**.<sup>[a]</sup>

|                      |          |                        |             |
|----------------------|----------|------------------------|-------------|
| M–P1                 | 2.353(1) | P3–P4                  | 2.197(2)    |
| M–P2                 | 2.346(1) | P3–P4 <sup>‡</sup>     | 2.189(2)    |
| M–P3                 | 2.285(1) | P4–P4 <sup>‡</sup>     | 2.224(4)    |
| P3–P3 <sup>[b]</sup> | 2.168(3) | M–C(Cp)                | 2.226–2.249 |
| P1–M–P2              | 99.49(5) | P2–M–P3                | 98.76(5)    |
| P1–M–P3              | 92.51(5) | M–P3–P3 <sup>[b]</sup> | 158.41(4)   |

[a] The metal site has 50% Ru and 50% Os occupancy. [b] Symmetry operation:  $1 - x, y, 1/2 - z$ .

**3** after workup show the presence of a mixture of several compounds, most of which have been identified and whose percentages were estimated with respect to the four phosphorus atoms in **2** and **3** by careful integration of the corresponding resonances.

Compound **2** is completely hydrolyzed within one day in the presence of 100 equiv. of water. The hydrolysis of **2** is significantly slowed down with respect to that of the ruthenium derivative **4**, which is completely transformed within a few hours. The products include free hypophosphorous (20%) and phosphorous (55%) acids, and the cationic species of compounds **6** and **8**,  $[CpOs(PPh_3)_2(PH_3)]^+$  (55%) and  $[CpOs(PPh_3)_2\{P(OH)_3\}]^+$  (22%), respectively. Further products, for which no structure can be assigned by NMR spectroscopic analysis, are also formed. The oxyacids were identified by comparison of the  $^{31}P$  NMR spectra of the hydrolyzed mixture with those of the pure specimen in the same solvent. Cations **6** and **8** were identified by compari-

son of the NMR ( $^1\text{H}$  and  $^{31}\text{P}$ ) spectroscopic data of the mixture with those of the pure compounds, which have been synthesized and characterized by elemental analysis and NMR spectroscopy separately (see below). Thus, the hydrolysis of **2** yields substantially the same products that have been observed from the reaction of the analogous ruthenium derivative **4**;<sup>[14]</sup> the main difference consists in the formation of a small amount of complex **8**, containing the phosphorous acid, which was not observed in the hydrolysis of **4**.

Compounds  $[\text{CpOs}(\text{PPh}_3)_2(\text{PH}_3)]\text{CF}_3\text{SO}_3$  (**6**) and  $[\text{CpOs}(\text{PPh}_3)_2\{\text{PR}(\text{OH})_2\}]\text{CF}_3\text{SO}_3$  [**R** = H, (**7**), OH (**8**)] are obtained in high yield by adding either the stoichiometric amount of the acid ( $\text{H}_3\text{PO}_2$  or  $\text{H}_3\text{PO}_3$ ) or by bubbling gaseous  $\text{PH}_3$  through a solution of  $[\text{CpOs}(\text{PPh}_3)_2\text{Cl}]$  in a  $\text{CH}_2\text{Cl}_2/\text{thf}$  mixture in the presence of the stoichiometric amount of thallium triflate to scavenge the chloride ligand. The white complexes are stable under an inert atmosphere and are soluble in common organic solvents.

The  $^{31}\text{P}\{^1\text{H}\}$  NMR spectrum of **6** exhibits an  $\text{A}_2\text{F}$  pattern in which the lower field doublet is assigned to the phosphorus atoms of triphenylphosphane ligands ( $\text{P}_\text{A}$ ) and the higher field triplet ( $\delta = -152.22$ ) to the phosphorus atom of the coordinated phosphane ( $\text{P}_\text{F}$ ). The triplet of the phosphane is resolved in a quartet of triplets in the  $^{31}\text{P}-^1\text{H}$  coupled spectrum, as expected for a P-coordinated  $\text{PH}_3$ . The observed value of  $^1J(\text{P}_\text{F}, \text{H}) = 368.5$  Hz is in the range of those found for coordinated  $\text{PH}_3$ .<sup>[14]</sup> The hydrogen atoms directly bound to phosphorus show in the  $^1\text{H}$  NMR spectrum a doublet of triplets ( $\delta = 4.38$  ppm), characterized by the above strong  $^1J(\text{H}, \text{P}_\text{F})$  coupling and a weak  $^3J(\text{H}, \text{P}_\text{A})$  one (4.0 Hz). The elemental analysis and the NMR spectroscopic data allow to conclude unambiguously that  $\text{PH}_3$  is bound to the  $\text{CpOs}(\text{PPh}_3)_2$  fragment.

The  $^{31}\text{P}\{^1\text{H}\}$  NMR spectra of **7** and **8** consist of  $\text{A}_2\text{F}$  spin systems in which the lower field triplet is assigned to the phosphorus atom ( $\text{P}_\text{F}$ ) of the hypophosphorous or phosphorous acid and the higher field doublet to the triphenylphosphane atoms ( $\text{P}_\text{A}$ ). The  $^{31}\text{P}$  resonance of the coordinated hypophosphorous acid occurs at a lower field than that of the phosphorous acid. The triplet of hypophosphorous derivative **7** is doubled in the  $^{31}\text{P}-^1\text{H}$  coupled spectrum, showing that only one hydrogen is bound to the P atom; the observed value of  $^1J(\text{P}, \text{H}) = 425.5$  Hz is similar to that found for tetracoordinate P–H systems.<sup>[22]</sup> The hydrogen atom directly bound to phosphorus yields in the  $^1\text{H}$  NMR spectrum a doublet of triplets ( $\delta = 8.84$  ppm), characterized by the above strong  $^1J(\text{H}, \text{P}_\text{F})$  coupling and a weak  $^3J(\text{H}, \text{P}_\text{A})$  one (3 Hz). On the other hand, no P–H coupling is observed for the coordinated  $\text{H}_3\text{PO}_3$ , clearly showing that no hydrogen atom is bound to the  $\text{P}_\text{F}$  phosphorus in that case. The NMR spectroscopic data for complexes **7** and **8** parallel those of the ruthenium analogues  $[\text{CpRu}(\text{PPh}_3)_2\{\text{PR}(\text{OH})_2\}]\text{OTf}$  (**R** = H, OH), which have been found, by X ray analysis, to contain the unstable hydroxyphosphane tautomers of the hypophosphorous  $[\text{HP}(\text{OH})_2]$  and phosphorous  $[\text{P}(\text{OH})_3]$  acids stabilized by coordination through their P atom to the metal.<sup>[22]</sup> Accordingly, the same coordi-

nation geometry is assigned to the present osmium derivatives. Compounds **6**, **7** and **8**, in addition to their essential value in assessing the nature of the products from the hydrolysis of **2** and **3**, have an intrinsic interest. Indeed, compound **6** adds to the rare examples of metal– $\text{PH}_3$  derivatives,<sup>[23]</sup> and the formation of compounds **7** and **8** provides true examples of hypo- and phosphorous acid isomerization, which has been observed only for the analogous ruthenium derivatives.<sup>[22]</sup>

The hydrolysis of  $[\{\text{CpRu}(\text{PPh}_3)_2\}_2(\mu, \eta^{1:1}\text{-P}_4)](\text{OTf})_2$  (**5**), in which two phosphorus atoms of the cage bridge two  $\text{CpRu}(\text{PPh}_3)_2$  moieties, had been studied in detail.<sup>[15–17]</sup> The reaction follows several routes depending on the reaction conditions, particularly on the amount of added water, and a mixture of products is usually obtained. By adding 500 equiv. of water to **5**, only two compounds were obtained: phosphorous acid and 1-hydroxytriphosphane. The latter molecule is stabilized through coordination to two equivalent ruthenium fragments.<sup>[16]</sup> Therefore, the selectivity of this reaction suggested that the hydrolysis of **3** should be repeated under the same conditions. In keeping with our expectation, addition of 500 equiv. of water to a solution of **3** completely hydrolyzes the dimer within 1 h. The  $^{31}\text{P}\{^1\text{H}\}$  NMR spectrum of the solid obtained from the hydrolysis shows the presence of several compounds, including free phosphorous acid and the cations  $[\text{CpM}(\text{PPh}_3)_2(\text{PH}_3)]^+$  and  $[\text{CpM}(\text{PPh}_3)_2\{\text{PR}(\text{OH})_2\}]^+$  (**M** = Ru, Os; **R** = H, OH), which were identified by comparison of their NMR ( $^1\text{H}$  and  $^{31}\text{P}$ ) spectroscopic data with those of the pure compounds previously described. Remarkably, and at variance with the homo bimetallic ruthenium derivative, no polyphosphorus compound is formed, and only those mononuclear species that are considered as the thermodynamic sinks along the degradation pathway of the heterobimetallic complex are obtained. The hydrolysis performed with a smaller amount (100 equiv.) of water reaches completion much more slowly (one day) still substantially yielding single phosphorus species.

## Conclusions

$[\text{CpOs}(\text{PPh}_3)_2]^+$ , generated in situ by chloride removal from  $[\text{CpOs}(\text{PPh}_3)_2\text{Cl}]$ , is a suitable synthon for the preparation of osmium complexes containing tetrakisphosphorus as a ligand. The monometallic  $[\text{CpOs}(\text{PPh}_3)_2(\eta^1\text{-P}_4)]\text{OTf}$  and the heterobimetallic  $[\{\text{CpRu}(\text{PPh}_3)_2\}\{\text{CpOs}(\text{PPh}_3)_2\}(\mu, \eta^{1:1}\text{-P}_4)](\text{OTf})_2$  were prepared and characterized by elemental analysis, IR, NMR spectroscopy and X-ray crystallography. The latter technique allowed to collect important metrical parameters for this class of compounds. Remarkably, double metallation of the  $\text{P}_4$  with different metal fragments does not result in any significant deformation with respect to the geometry of either the free ligand or the homobimetallic diruthenium compound.

Both compounds react with an excess amount of water to undergo complete hydrolysis of the  $\text{P}_4$  cage. The hydrolysis products of the monometallic compound substantially

parallel those obtained from the ruthenium analogue, while the products obtained from the hydrolysis of the heterobimetallic OsRu complex encompass only single phosphorus species, in this case diverging from the behaviour of the RuRu analogue. In fact, at variance with the ruthenium homobimetallic derivative, the hydrolysis of the OsRu dimer is driven to single P compounds that are at the end of the P<sub>4</sub> hydrolytic degradation.

Studies are in progress to further expand the reactivity of coordinated P<sub>4</sub> and to better understand the mechanism of its hydrolytic cleavage.

## Experimental Section

All reactions and manipulations were performed under an atmosphere of dry, oxygen-free argon. The solvents were purified according to standard procedures.<sup>[24]</sup> <sup>1</sup>H, <sup>19</sup>F and <sup>31</sup>P NMR spectra were obtained with a Bruker Avance 400 plus spectrometer. <sup>19</sup>F and <sup>31</sup>P chemical shifts are relative to external CFCl<sub>3</sub> and to 85% H<sub>3</sub>PO<sub>4</sub>, respectively. <sup>1</sup>H chemical shifts are relative to tetramethylsilane as external reference and were calibrated against the residual solvent resonance. Downfield values are reported as positive, coupling constants are in Hertz. <sup>19</sup>F NMR spectra of all compounds yielded a singlet at −75.5 ppm for the triflate anion. Nujol mull infrared spectra were obtained with a Perkin–Elmer Spectrum BX FTIR spectrometer with samples between NaCl discs. Microanalyses were carried out at the Microanalytical Laboratory of the Department of Chemistry of the University of Florence. [CpRu(PPh<sub>3</sub>)<sub>2</sub>-(OTf)] was prepared according to the literature.<sup>[25]</sup> Aqueous solutions of H<sub>3</sub>PO<sub>2</sub>, H<sub>3</sub>PO<sub>3</sub> (Aldrich), TlOTf and AgOTf (Strem Chemicals) were used as received.

**[CpOs(PPh<sub>3</sub>)<sub>2</sub>Cl] (1):** The compound has been synthesized through an improved procedure with respect to that previously described.<sup>[26]</sup> Freshly cracked and distilled cyclopentadiene (2.7 cm<sup>3</sup>) was added to [Os(PPh<sub>3</sub>)<sub>3</sub>Cl]<sub>2</sub><sup>[27]</sup> (0.530 mg, 0.50 mmol) in thf (25 cm<sup>3</sup>), and the solution was refluxed for 2 h; in the meantime the green solution became yellow. Half of the solvent was removed under reduced pressure, and yellow microcrystals of **1** were obtained by adding ethanol. The solid was recrystallized from a mixture of CH<sub>2</sub>Cl<sub>2</sub>/ethanol (2:1). Yield 830 mg (80%). Both elemental analysis and NMR spectroscopic data agree with those given in the literature.<sup>[26]</sup>

**[CpOs(PPh<sub>3</sub>)<sub>2</sub>(η<sup>1</sup>-P<sub>4</sub>)](CF<sub>3</sub>SO<sub>3</sub>) (2):** AgOTf (128 mg, 0.50 mmol) was added to a solution of [CpOs(PPh<sub>3</sub>)<sub>2</sub>Cl] (**1**) (407 mg, 0.50 mmol) dissolved in a mixture of CH<sub>2</sub>Cl<sub>2</sub> (30 cm<sup>3</sup>) and thf (30 cm<sup>3</sup>); the resulting slurry was stirred for 2 h at room temperature and filtered. The filtrate was added to P<sub>4</sub> (80 mg, 0.70 mmol) dissolved in thf (20 cm<sup>3</sup>); the resulting solution was stirred 1 h at room temperature, and then the solvent was removed under vacuum. The orange solid was washed with toluene (2 × 10 cm<sup>3</sup>), pentane (2 × 10 cm<sup>3</sup>) and dried. Yield 420 mg (85%). The complex may be recrystallized from CHCl<sub>3</sub>/*n*-hexane. C<sub>42</sub>H<sub>35</sub>F<sub>3</sub>O<sub>3</sub>OsP<sub>6</sub>S (1052.8): calcd. C 47.91, H 3.35, P 17.65; found C 47.80, H 3.50, P 17.50. <sup>1</sup>H NMR (400.13 MHz, CDCl<sub>3</sub>, 21 °C): δ = 7.60–6.90 (m, 30 H, C<sub>6</sub>H<sub>5</sub>), 4.83 (s, 5 H, C<sub>5</sub>H<sub>5</sub>) ppm. <sup>31</sup>P{<sup>1</sup>H} NMR (161.89, CDCl<sub>3</sub>, 21 °C): A<sub>2</sub>FM<sub>3</sub> spin system, δ = −5.94 (d, <sup>2</sup>J(P<sub>A</sub>,P<sub>F</sub>) = 38.4 Hz, 2 P, P<sub>A</sub>), −376.43 (tq, <sup>1</sup>J(P<sub>F</sub>,P<sub>M</sub>) = 238.0 Hz, 1 P, P<sub>F</sub>), −477.63 (d, 3 P, P<sub>M</sub>) ppm.

**[{CpRu(PPh<sub>3</sub>)<sub>2</sub>}{CpOs(PPh<sub>3</sub>)<sub>2</sub>}(μ,η<sup>1:1</sup>-P<sub>4</sub>)](CF<sub>3</sub>SO<sub>3</sub>)<sub>2</sub> (3):** A solution of [CpRu(PPh<sub>3</sub>)<sub>2</sub>OTf] (252 mg, 0.3 mmol) in CH<sub>2</sub>Cl<sub>2</sub> (8 cm<sup>3</sup>) was added to [CpOs(PPh<sub>3</sub>)<sub>2</sub>(η<sup>1</sup>-P<sub>4</sub>)]OTf (**2**) (316 mg, 0.3 mmol) dissolved in a mixture of CH<sub>2</sub>Cl<sub>2</sub> (25 cm<sup>3</sup>) and thf (25 cm<sup>3</sup>). The re-

sulting brick-red solution was stirred for 30 min at room temperature, and then the solvent was removed under vacuum. The solid was recrystallized from CHCl<sub>3</sub>/*n*-hexane. Yield 450 mg (80%). C<sub>84</sub>H<sub>70</sub>F<sub>6</sub>O<sub>6</sub>OsP<sub>8</sub>RuS<sub>2</sub> (1892.5): calcd. C 53.30, H 3.73, P 13.09; found C 53.20, H 3.80, P 12.90. <sup>1</sup>H NMR (400.13 MHz; (CD<sub>3</sub>)<sub>2</sub>CO, 21 °C): δ = 7.60–6.90 (m, 60 H, C<sub>6</sub>H<sub>5</sub>), 5.11 (s, 5 H, C<sub>5</sub>H<sub>5</sub>), 4.97 (s, 5 H, C<sub>5</sub>H<sub>5</sub>) ppm. <sup>31</sup>P{<sup>1</sup>H} NMR [161.89 MHz, (CD<sub>3</sub>)<sub>2</sub>CO, 21 °C]: A<sub>2</sub>B<sub>2</sub>FMQ<sub>2</sub> spin system, δ = 38.24 [d, <sup>2</sup>J(P<sub>B</sub>,P<sub>M</sub>) = 51.3 Hz, 2 P, P<sub>B</sub>], −5.23 [d, <sup>2</sup>J(P<sub>A</sub>,P<sub>F</sub>) = 31.3 Hz, 2 P, P<sub>A</sub>], −278.19 [dtt, <sup>1</sup>J(P<sub>M</sub>,P<sub>Q</sub>) = 145.8, <sup>1</sup>J(P<sub>M</sub>,P<sub>F</sub>) = 229.0 Hz, 1 P, P<sub>M</sub>], −314.94 [dtt, <sup>1</sup>J(P<sub>F</sub>,P<sub>Q</sub>) = 163.0 Hz, 1 P, P<sub>F</sub>], −462.78 (dd, P<sub>Q</sub>)ppm.

**Hydrolysis of 2:** Water (40 mmol) was added to compound **2** (420 mg, 0.40 mmol) in thf (60 cm<sup>3</sup>), and the system was stirred at room temperature for 1 d; the orange colour of the solution changed to yellow. Mass spectra of the gas phase did not show any volatile hydrolysis products. The solvent was then removed under reduced pressure to yield a yellow solid whose spectrum in (CD<sub>3</sub>)<sub>2</sub>-CO exhibited resonances assigned to H<sub>3</sub>PO<sub>2</sub>, H<sub>3</sub>PO<sub>3</sub>, [CpRu(PPh<sub>3</sub>)<sub>2</sub>-(PH<sub>3</sub>)]OTf and [CpRu(PPh<sub>3</sub>)<sub>2</sub>{P(OH)<sub>3</sub>}]OTf.

**Hydrolysis of 3:** The reaction was carried out as for **2** by adding to **3** (570 mg, 0.30 mmol) in thf (60 cm<sup>3</sup>) either 500 or 100 equiv. of water.

**[CpOs(PPh<sub>3</sub>)<sub>2</sub>(PH<sub>3</sub>)]CF<sub>3</sub>SO<sub>3</sub> (6):** Gaseous PH<sub>3</sub> was gently bubbled for 5 min through a solution of [CpOs(PPh<sub>3</sub>)<sub>2</sub>Cl] (122 mg, 0.15 mmol) and AgOTf (38 mg, 0.15 mmol) in a mixture of thf (15 cm<sup>3</sup>) and CH<sub>2</sub>Cl<sub>2</sub> (15 cm<sup>3</sup>). The resulting slurry was stirred at room temperature for 1 h; the solid was filtered off, and pale yellow microcrystals were obtained by evaporating the solvent under reduced pressure. The solid was recrystallized from CH<sub>2</sub>Cl<sub>2</sub>/*n*-hexane. Yield 120 mg (85%). C<sub>42</sub>H<sub>38</sub>F<sub>3</sub>O<sub>3</sub>OsP<sub>3</sub>S (962.9): calcd. C 52.38, H 3.98, P 9.65; found C 52.28, H 4.10, P 9.40. <sup>1</sup>H NMR [400.13 MHz; (CD<sub>3</sub>)<sub>2</sub>CO, 21 °C]: δ = 7.4–7.10 (m, 30 H, C<sub>6</sub>H<sub>5</sub>), 4.89 (s, 5 H, C<sub>5</sub>H<sub>5</sub>), 4.38 [dt, <sup>1</sup>J(H,P<sub>F</sub>) = 368.5, <sup>3</sup>J(H,P<sub>A</sub>) = 4.0 Hz, 3 H, PH<sub>3</sub>] ppm. <sup>31</sup>P{<sup>1</sup>H} NMR [161.89 MHz, (CD<sub>3</sub>)<sub>2</sub>CO, 21 °C]: A<sub>2</sub>F spin system, δ = −1.69 [d, <sup>2</sup>J(P<sub>A</sub>,P<sub>F</sub>) = 30.8 Hz, 2 P, P<sub>F</sub>], −152.22 (t, 1 P, P<sub>F</sub>) ppm.

**[CpOs(PPh<sub>3</sub>)<sub>2</sub>(PR(OH)<sub>2</sub>)]CF<sub>3</sub>SO<sub>3</sub> [R = H (**7**); R = OH (**8**):** The two compounds were obtained by the same procedure. To a suspension of [CpOs(PPh<sub>3</sub>)<sub>2</sub>Cl] (**1**) (122 mg, 0.15 mmol) and AgOTf (38 mg, 0.15 mmol) in a mixture of thf (15 cm<sup>3</sup>) and CH<sub>2</sub>Cl<sub>2</sub> (15 cm<sup>3</sup>) was added at room temperature whilst stirring one equivalent of either H<sub>3</sub>PO<sub>2</sub> or H<sub>3</sub>PO<sub>3</sub>. The resulting slurry was stirred for 2 h at room temperature, and in the meantime the yellow colour faded. The solid was filtered off, and light yellow microcrystals of [CpOs(PPh<sub>3</sub>)<sub>2</sub>{PR(OH)<sub>2</sub>}]OTf (R = H, OH) were obtained by solvent evaporation under reduced pressure. The solid was recrystallized from (CH<sub>3</sub>)<sub>2</sub>CO/*n*-hexane. Yield 80%. **7:** C<sub>42</sub>H<sub>38</sub>F<sub>3</sub>O<sub>5</sub>OsP<sub>3</sub>S (994.9): calcd. C 50.70, H 3.85, P 9.34; found C 50.54, H 3.89, P 9.10. FTIR: ν<sub>max</sub> = (PH) 2302 (s) cm<sup>−1</sup>. <sup>1</sup>H NMR [400.13 MHz; (CD<sub>3</sub>)<sub>2</sub>CO, 21 °C]: δ = 8.84 [dt, <sup>1</sup>J(H,P<sub>F</sub>) = 425.0, <sup>3</sup>J(H,P<sub>A</sub>) = 3.0 Hz, 1 H, HP(OH)<sub>2</sub>], 7.50–7.10 (m, 30 H, C<sub>6</sub>H<sub>5</sub>), 4.89 (s, 5 H, C<sub>5</sub>H<sub>5</sub>) ppm. <sup>31</sup>P{<sup>1</sup>H} NMR [161.89 MHz, (CD<sub>3</sub>)<sub>2</sub>CO, 21 °C]: A<sub>2</sub>F spin system, δ = −0.25 [d, <sup>2</sup>J(P<sub>A</sub>,P<sub>F</sub>) = 32.1 Hz, 2 P, P<sub>A</sub>], 87.37 (t, 1 P, P<sub>F</sub>) ppm. **8:** C<sub>42</sub>H<sub>38</sub>F<sub>3</sub>O<sub>6</sub>OsP<sub>3</sub>S (1010.9): calcd. C 49.90, H 3.79, P 9.19; found C 49.54, H 3.89, P 9.05. <sup>1</sup>H NMR [400.13 MHz; (CD<sub>3</sub>)<sub>2</sub>CO, 21 °C]: δ = 7.50–7.00 (m, 30 H, C<sub>6</sub>H<sub>5</sub>), 4.92 (s, 5 H, C<sub>5</sub>H<sub>5</sub>) ppm. <sup>31</sup>P{<sup>1</sup>H} NMR [161.89, (CD<sub>3</sub>)<sub>2</sub>CO, 21 °C]: A<sub>2</sub>F spin system, δ = 84.28 [t, <sup>2</sup>J(P<sub>F</sub>,P<sub>A</sub>) = 37.5 Hz, 1 P, P<sub>F</sub>], −2.05 (d, 2 P, P<sub>A</sub>) ppm.

**Crystallographic Data Collection and Refinement Procedures:** Data collections were performed with an Oxford Diffraction Xcalibur 3 CCD diffractometer, with graphite-monochromated Mo-K<sub>α</sub> radi-

tion for **2**, and with an Oxford Diffraction Xcalibur PX Ultra CCD diffractometer equipped with Enhance Ultra optics, by using Cu- $K_{\alpha}$  radiation for **3**. For **2**, data collections were performed both at 150 K and, for comparison, at room temperature; results for the latter are summarized in a CIF file.<sup>[21]</sup> Absorption corrections were performed by the ABSPACK multiscan procedure of the *CrysAlis* data reduction package.<sup>[28]</sup> The structures were solved by direct methods with SIR2004,<sup>[29]</sup> and the structural models were completed and refined with SHELXL97.<sup>[30]</sup> Since the bimetallic cation in **3** possesses twofold rotational symmetry, the metal site was assigned 50% Ru and 50% Os populations. In the final refinement cycles on both structural models, all non-hydrogen atoms (including those of the disordered solvent molecule in the structure of **3**; see below) were refined anisotropically, and the hydrogen atoms were in calculated positions, riding, with  $U_{\text{H}} = 1.2U_{\text{C}}^{\text{eq}}$ . One of the chloroform solvate molecules in the structure of **3** was highly affected by disorder and was modelled as being distributed among three distinct orientations within a confined volume, whose fractional occupancy factors were refined with the restraint of overall unit value. Geometrical restraints were applied in the course of the refinement on both solvate molecules and the anion in the structure of **3** (Table 3). The highest peaks of residual density in the final difference Fourier analysis of both structures were in the proximity of the heavy atom positions or of the parts affected by disorder and could not be assigned any chemical meaning. Programs used in the crystallographic calculations included WinGX<sup>[31]</sup> and ORTEP for graphics.<sup>[32]</sup>

Table 3. Crystal and structure refinement parameters for compounds **2** and **3**.

|  | <b>2</b>   | <b>3</b>   |
|--|--|--|
| Empirical formula  | $\text{C}_{42}\text{H}_{35}\text{F}_3\text{O}_3\text{OsP}_6\text{S}$ | $\text{C}_{88}\text{H}_{74}\text{Cl}_{12}\text{F}_6\text{O}_6\text{OsP}_8\text{RuS}_2$ |
| $M_r$  | 1052.78  | 2370.02  |
| Crystal system   | monoclinic   | monoclinic   |
| Space group  | $P2_1/c$   | $C2/c$   |
| $T$ [K]  | 150(2)   | 173(2)   |
| $a$ [Å]  | 11.3805(2)   | 22.3510(3)   |
| $b$ [Å]  | 14.8883(2)   | 18.3381(2)   |
| $c$ [Å]  | 24.0308(3)   | 24.4186(3)   |
| $\beta$ [°]  | 94.423(1)  | 108.186(2)   |
| $V$ [Å <sup>3</sup> ]  | 4059.6(1)  | 9508.6(2)  |
| $Z$  | 4  | 4  |
| $d_{\text{calcd.}}$ [g cm <sup>-3</sup> ]                                  | 1.723  | 1.656  |
| Absorption coefficient [mm <sup>-1</sup> ]                                 | 3.483  | 9.092  |
| $F(000)$   | 2080   | 4720   |
| $\theta$ range [°]   | 3.75–26.37   | 3.81–72.64   |
| Reflections measured   | 39587  | 60084  |
| Independent reflections  | 8275   | 9382   |
| Observed reflections   |  |  |
| $[I > 2\sigma(I)]$ , $R_{\text{int}}$                                      | 6810, 0.0323   | 7945, 0.0500   |
| No. of parameters/restraints   | 505/0  | 635/79   |
| Final $R$ indices $[I > 2\sigma(I)]$ $R_1$ , $wR_2$                        | 0.0248, 0.0656   | 0.0589, 0.1618   |
| Final $R$ indices (all data) $R_1$ , $wR_2$                                | 0.0339, 0.0675   | 0.0679, 0.1715   |
| Goodness on $F^2$  | 1.077  | 1.025  |
| $\Delta\rho_{\text{max}}$ , $\Delta\rho_{\text{min}}$ [e Å <sup>-3</sup> ] | 2.507, -0.558  | 2.051, -0.962  |

CCDC-746584 (for **2** at 150 K), -746585 (for **2** at 293 K) and -746586 (for **3**) contain the supplementary crystallographic data for this paper. These data can be obtained free of charge from the Cambridge Crystallographic Data Centre via [www.ccdc.cam.ac.uk/data\\_request/cif](http://www.ccdc.cam.ac.uk/data_request/cif).

## Acknowledgments

Financial support by the Italian Ministero dell'Istruzione, dell'Università e della Ricerca is gratefully acknowledged (PRIN2007). This work has been carried out within the frame of COST ACTION CM0802 "PHOSCINET" of the European Community.

- [1] K. H. Whitmire, *Adv. Organomet. Chem.* **1998**, *42*, 1–145.
- [2] O. J. Scherer, *Acc. Chem. Res.* **1999**, *32*, 751–762.
- [3] M. Peruzzini, I. de los Rios, A. Romerosa, F. Vizza, *Eur. J. Inorg. Chem.* **2001**, 593–608.
- [4] M. P. Ehses, A. Romerosa, M. Peruzzini, *Top. Curr. Chem.* **2002**, *220*, 107–140.
- [5] M. Peruzzini, L. Gonsalvi, A. Romerosa, *Chem. Soc. Rev.* **2005**, *34*, 1038–1047.
- [6] E. Urnėžius, W. W. Brennessel, C. J. Cramer, J. E. Ellis, P. von Schleyer, *Science* **2002**, *295*, 832–834.
- [7] J. Bai, A. V. Virovets, M. Scheer, *Science* **2003**, *300*, 781–783.
- [8] P. Dapporto, S. Midollini, L. Sacconi, *Angew. Chem. Int. Ed. Engl.* **1979**, *18*, 469–470.
- [9] P. Dapporto, L. Sacconi, P. Stoppioni, F. Zanobini, *Inorg. Chem.* **1981**, *20*, 3834–3839.
- [10] M. Di Vaira, M. P. Ehses, M. Peruzzini, P. Stoppioni, *Eur. J. Inorg. Chem.* **2000**, 2193–2198.
- [11] T. Gröer, G. Baum, M. Scheer, *Organometallics* **1998**, *17*, 5916–5919.
- [12] M. Peruzzini, M. Marvelli, A. Romerosa, R. Rossi, F. Vizza, F. Zanobini, *Eur. J. Inorg. Chem.* **1999**, 931–933.
- [13] I. de los Rios, J.-R. Hamon, P. Hamon, C. Lapinte, L. Toupet, A. Romerosa, M. Peruzzini, *Angew. Chem. Int. Ed.* **2001**, *40*, 3910–3912.
- [14] M. Di Vaira, P. Frediani, S. Seniori Costantini, M. Peruzzini, P. Stoppioni, *Dalton Trans.* **2005**, 2234–2236.
- [15] P. Barbaro, M. Di Vaira, M. Peruzzini, S. Seniori Costantini, P. Stoppioni, *Chem. Eur. J.* **2007**, *13*, 6682–6690.
- [16] P. Barbaro, M. Di Vaira, M. Peruzzini, S. Seniori Costantini, P. Stoppioni, *Angew. Chem. Int. Ed.* **2008**, *47*, 4425–4427.
- [17] P. Barbaro, M. Di Vaira, M. Peruzzini, S. Seniori Costantini, P. Stoppioni, *Inorg. Chem.* **2009**, *48*, 1091–1096.
- [18] M. Baudler, L. Schmidt, *Z. Anorg. Allg. Chem.* **1957**, *289*, 219.
- [19] M. Baudler, K. Glinka, *Chem. Rev.* **1994**, *94*, 1273–1297.
- [20] P. W. Wanandi, T. Don Tilley, *Organometallics* **1997**, *16*, 4299–4313; M. I. Bruce, P. J. Low, B. W. Skelton, E. R. T. Tiekink, A. Werth, A. H. White, *Aust. J. Chem.* **1995**, *48*, 1887–1892.
- [21] Results of the refinement of the structure of **2** by using room temperature data have been deposited as a CIF file: see the Experimental Section.
- [22] D. N. Akbaieva, M. Di Vaira, S. Seniori Costantini, M. Peruzzini, P. Stoppioni, *Dalton Trans.* **2006**, 389–395.
- [23] N. I. Kirillova, A. I. Gusev, A. A. Pasynskii, Yu. T. Struchkov, *J. Organomet. Chem.* **1973**, *63*, 311; G. Huttner, S. Schelle, *J. Organomet. Chem.* **1973**, *47*, 383–390; J. Bould, P. Brint, X. L. R. Fontaine, J. D. Kennedy, M. Thornton-Pett, *J. Chem. Soc., Chem. Commun.* **1989**, 1763–1765; W. A. Herrmann, B. Koumbouris, E. Herdtweck, M. L. Ziegler, P. Weber, *Chem. Ber.* **1987**, *120*, 931; J. Deeming, S. Doherty, J. E. Marshall, J. L. Powell, A. M. Senior, *J. Chem. Soc., Dalton Trans.* **1993**, 1093–1100; E. J. Ditzel, G. B. Robertson, *Aust. J. Chem.* **1995**, *48*, 1277; H.-J. Haupt, O. Krampe, U. Florke, *Z. Anorg. Allg. Chem.* **1996**, *622*, 807.
- [24] D. D. Perrin, W. L. F. Armarego, *Purification of Laboratory Chemicals*, 3rd ed., Pergamon, New York, **1988**.
- [25] J. Amarasekera, T. B. Rauchfuss, S. R. Wilson, *J. Am. Chem. Soc.* **1988**, *110*, 2332–2334.
- [26] G. J. Perkins, M. I. Bruce, B. W. Skelton, A. H. White, *Inorg. Chim. Acta* **2006**, *359*, 2644–2649.
- [27] P. R. Hoffman, K. G. Caulton, *J. Am. Chem. Soc.* **1975**, *97*, 4221–4228.

- [28] Oxford Diffraction, *CrysAlis RED* (version 171.32.29), **2006**, Oxford Diffraction Ltd., Abingdon, Oxfordshire, England.
- [29] M. C. Burla, R. Caliendo, M. Camalli, B. Carrozzini, G. L. Casciarano, L. De Caro, C. Giacovazzo, G. Polidori, R. Spagna, *J. Appl. Crystallogr.* **2005**, 38, 381–388.
- [30] G. M. Sheldrick, *Acta Crystallogr., Sect. A* **2008**, 64, 112–122.
- [31] L. J. Farrugia, *J. Appl. Crystallogr.* **1999**, 32, 837–838.
- [32] L. J. Farrugia, *J. Appl. Crystallogr.* **1997**, 30, 565.

Received: October 19, 2009

Published Online: November 25, 2009

# Exfoliated Titanosilicate Material UZAR-S1 Obtained from JDF-L1

César Rubio,<sup>[a]</sup> Clara Casado,<sup>[a]</sup> Patricia Gorgojo,<sup>[a]</sup> Fernando Etayo,<sup>[a]</sup> Santiago Uriel,<sup>[b]</sup> Carlos Téllez,<sup>[a]</sup> and Joaquín Coronas<sup>\*[a]</sup>

**Keywords:** Intercalations / Layered compounds / Membranes / Organic–inorganic hybrid composites / Zeolite analogues

A new material, UZAR-S1, has been obtained by exfoliation of the layered precursor microporous titanosilicate JDF-L1. The exfoliation consists of a first stage of proton exchange with histidine followed by intercalation with nonylamine and final extraction in HCl/water/ethanol solution. UZAR-S1 is an exfoliated material composed of sheets of a few nanome-

ters of thickness with a high aspect ratio, a BET specific surface area of 160 m<sup>2</sup>/g (JDF-L1 scarcely adsorbs N<sub>2</sub>), and a Si/Ti atomic ratio below 6. The dispersion of this material in commercial polysulfone results in an improved H<sub>2</sub>-selective mixed matrix membrane.

## Introduction

Exfoliated materials obtained from layered silicates and zeolites, due to the fine particles produced (with high aspect ratios and with a theoretical thickness as low as that of a single layer), are useful for catalysis,<sup>[1,2]</sup> enhancing the permselectivity of polymer–zeolite nanocomposite membranes,<sup>[3]</sup> the immobilization of enzymes,<sup>[4]</sup> and producing polymer-layered silicate nanocomposites with improved tensile properties.<sup>[5]</sup>

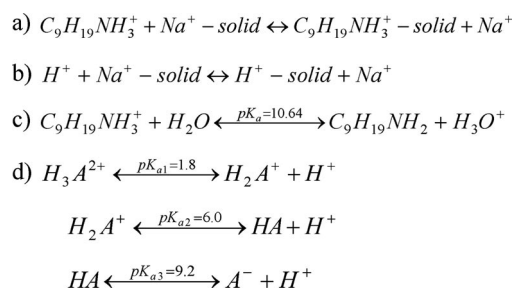
JDF-L1 refers to a microporous titanosilicate with the empirical formula Na<sub>4</sub>Ti<sub>2</sub>Si<sub>8</sub>O<sub>22</sub>·4H<sub>2</sub>O. JDF-L1 contains TiO<sub>5</sub> square pyramids in which each oxygen atom at the base is linked to SiO<sub>4</sub> tetrahedra to form continuous sheets.<sup>[6]</sup> The layers (see Figure S1 in the Supporting Information) have five-membered rings running parallel to them ([100] or [010] equivalent directions) consisting of four SiO<sub>4</sub> tetrahedra and one TiO<sub>5</sub> pyramid. The layers also contain, running along the [001] direction, six-membered rings composed of two square pyramids and two pairs of tetrahedra. One Na atom coordinated with two water molecules is placed inside such a ring. JDF-L1 possesses the same structure as the AM-1<sup>[7]</sup> and NTS<sup>[8]</sup> materials (in fact, all of them were prepared on the same Na<sub>2</sub>O–TiO<sub>2</sub>–SiO<sub>2</sub> basis) and can be considered to be a member of the microporous OPT (octahedral–pentahedral–tetrahedral) family of framework silicates.<sup>[9]</sup>

The exfoliation of this material has not been reported to date; therefore, we present in this paper the synthesis,

characterization, and mixed-matrix membrane application of a new exfoliated titanosilicate obtained from the exfoliation of JDF-L1.

## Results and Discussion

The lamellar precursor JDF-L1 was synthesized by a seeded secondary growth procedure previously established.<sup>[10]</sup> Reaction (a) in Scheme 1 represents the expected exchange reaction between Na<sup>+</sup> cations in JDF-L1 and protonated nonylamine molecules. To favor the intercalation of nonylamine molecules, a proton exchange procedure was initiated at pH = 6.0 by using histidine amino acid.



Scheme 1. (a) Ion exchange reaction between the solid JDF-L1 and nonylamine, (b) ion exchange reaction between the solid and histidine (i.e. protonation), (c) acid–base equilibrium for nonylamine, and (d) dissociation equilibria for histidine (HA being the zwitterion).

After 10 min of reaction with histidine, the pH, initially at 6.0, slightly increased to about 6.1, as some protons from the solution were exchanged by Na<sup>+</sup> cations (reaction b in

[a] Chemical and Environmental Engineering Department and Nanoscience Institute of Aragon, Universidad de Zaragoza, María de Luna 3, 50018 Zaragoza, Spain  
Fax: +34-976-76-1871  
E-mail: coronas@unizar.es

[b] Organic Chemistry Department, Universidad de Zaragoza, María de Luna 3, 50018 Zaragoza, Spain

Supporting information for this article is available on the WWW under <http://dx.doi.org/10.1002/ejic.200900915>.

Scheme 1). The necessary amount of nonylamine was then added to the solution. When the reaction with histidine continued for about 30 min, steady state was quickly reached for the proton exchange reaction in terms of pH (6.15–6.20). This situation led to proton-exchanged JDF-L1 (H-JDF-L1). The H-JDF-L1 whose XRD pattern is shown in Figure 1 was obtained after 120 min of protonation with histidine. All the XRD reflections in the starting material are present in H-JDF-L1 even though small changes in the baseline are evident. This is the reason why surfactant molecules for swelling were added at a pH relatively far from the final value. In agreement with the idea that the proton exchange process itself may produce structural changes, it has been reported that layered silicate AMH-3 became XRD-amorphous upon proton exchange with histidine,<sup>[11]</sup> whereas the crystallinity of JDF-L1 was seriously affected in 0.1 M HCl.<sup>[12]</sup> The layered characteristics of swollen JDF-L1 are revealed in Figure 1 by a series of new peaks at  $2\theta = 2.94^\circ$ ,  $5.91^\circ$ , and  $8.89^\circ$  with indexations of (001), (002), and (003), respectively. Figure S2 also shows the first two reflections as revealed by low-angle XRD analysis. The separation between the layers of swollen JDF-L1 was estimated for 6 samples in  $29.6 \pm 1.4$  Å.

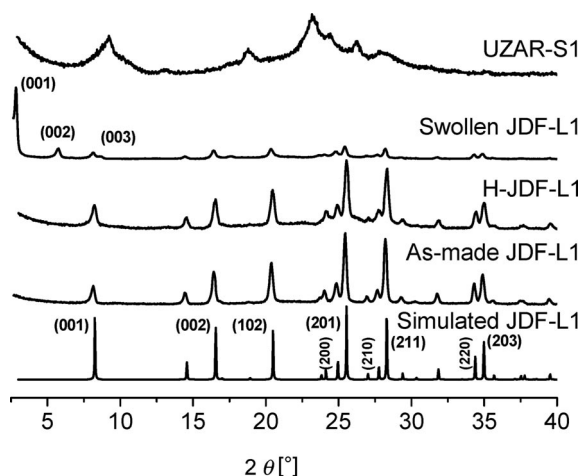


Figure 1. XRD patterns of JDF-L1 and its derivatives. The simulated pattern was obtained by using data from Roberts et al.<sup>[6]</sup>

After adding the amine to the solution with the amino acid and the JDF-L1, the pH suddenly increased to 8.9 and then to only 9.0 after 12 h of swelling reaction. At pH = 9.0,  $[BH^+]/[B]$  equals 44 (equation c in Scheme 1), and nonylamine is present in the swelling solution basically in its protonated form, favoring the exchange process. In any event, the intercalation of neutral nonylamine molecules should not be disregarded. The working pH is close to the  $pK_{a3}$  of the amino acid (9.2), which might be attributed to its buffering action (see reactions d in Scheme 1). It is worth mentioning that, by keeping the same amine concentration, swelling was produced without protonation to a lesser extent in terms of decreasing intensities coming from JDF-L1 (see Figure S3). In addition, the amino acid was not adsorbed on the layered material. The XRD pattern, in which no peaks could be found at low angles, and the TGA analy-

sis, from which only dehydration effects could be inferred (9.2 wt.-% of weight loss at  $900^\circ\text{C}$ ) are in agreement with this conclusion.

The amount of amine can be calculated by TGA (Figure 2) as approximately 28 wt.-%. This is comparable to the amount of dodecylamine intercalated in layered silicate AMH-3 with higher basal spacing (41 Å), consistent with a bilayer surfactant configuration.<sup>[11]</sup> This total amount of amine can be divided into two parts: that coming from protonated amine (removed at about  $150$ – $275^\circ\text{C}$ ) and that from nonprotonated amine (removed at temperatures higher than approximately  $275^\circ\text{C}$ ), similar to the distinction made in lamellar zeolite MCM-22P.<sup>[13]</sup> UZAR-S1 was obtained by extracting the amine with an HCl/H<sub>2</sub>O/ethanol (5:17:870, molar ratio) solution (Figure 2). Protonated amine molecules were only removed from the interlayer space by ion exchange, whereas the repeated washing (10 washings and ultrasound curve in Figure 2) would only be effective for part of the nonprotonated amine. UZAR-S1, similar to other delaminated porous materials,<sup>[2,14,15]</sup> is essentially XRD-amorphous or exhibits broad reflections (Figure 1).

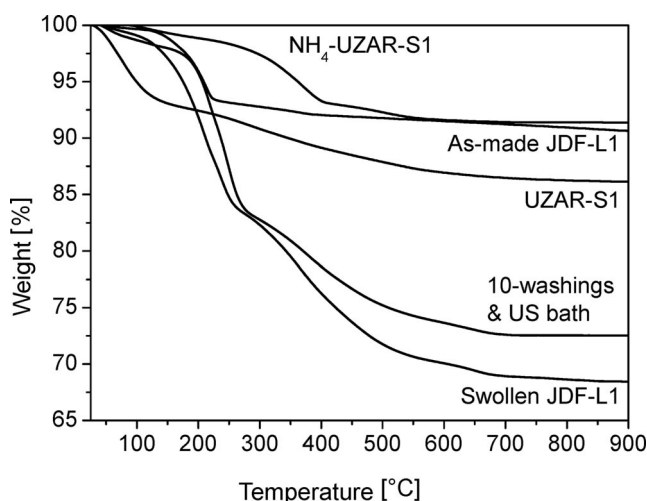


Figure 2. Weight losses as obtained by TGA of (from bottom to top): swollen JDF-L1, ultrasound-treated swollen JDF-L1, UZAR-S1 obtained from swollen JDF-L1 upon HCl treatment, as-made JDF-L1, NH<sub>4</sub>-UZAR-S1 obtained from swollen JDF-L1 upon NH<sub>4</sub>Cl treatment.

The amount of ammonium in NH<sub>4</sub>-UZAR-S1, upon treatment with NH<sub>4</sub>Cl/H<sub>2</sub>O/ethanol (5:17:870, molar ratio) solution, calculated as approximately 8.8 wt.-% (Figure 2), gave rise to an ammonium/nonylamine molar ratio of 2.7, indicating that the swelling of the material was produced without exhausting its ion exchange capacity. This is in agreement with the Na values in the EDX analyses in Table 1, which show important remains of Na after swelling and low Na contents after HCl extraction. UZAR-S1 maintains a high Si/Ti ratio lower than 6, while delaminated titanosilicate Del-Ti-MWW had a Si/Ti atomic ratio in the range 35–46,<sup>[2]</sup> and TiTQ-6 a Ti content of 1.0 wt.-%.<sup>[14]</sup>

Table 1. Atomic coefficients as obtained by EDX analysis in more than 20 different particles for each sample.<sup>[a]</sup>

| Sample   | Na                | Ti | Si                 |
|--|-------------------|----|--------------------|
| Theoretical ( $\text{Na}_4\text{Ti}_2\text{Si}_8\text{O}_{22}$ ) | 4                 | 2  | 8                  |
| As-made  | 2.0 ( $\pm 1.0$ ) | 2  | 5.6 ( $\pm 1.8$ )  |
| Swollen JDF-L1   | 1.3 ( $\pm 0.3$ ) | 2  | 6.4 ( $\pm 1.8$ )  |
| UZAR-S1 (II) <sup>[b]</sup>                                      | 0.2 ( $\pm 0.0$ ) | 2  | 11.3 ( $\pm 3.4$ ) |

[a] The ICP analysis carried out for swollen JDF-L1 gave Na and Ti atomic coefficients of 1.8 and 2. [b] Obtained after two stages of swelling/extraction with HCl.

The as-made JDF-L1 sample shows micrometric crystals with a sheet growth habit (Figure 3a). The TEM image in Figure 3b corresponds to swollen JDF-L1, where an approximate atomic spacing of 3 nm is observed. Similar to other exfoliated porous materials, UZAR-S1 consists of sheets of JDF-L1 only a few nanometers thick (images 3c,d). In the higher magnification Figure 3d, each approximately 5 nm thick sheet of UZAR-S1 is composed of only three to five layers. As in the situation described for MCM22-P,<sup>[16]</sup> each layer appears as two dark bands separated by a bright band that corresponds to the gallery space. The two orthogonal five-membered channels of JDF-L1 may constitute the dark bands. Note that after the HCl extraction treatment (Figure 3d) the fine particles tend to be more aggregated and their edges are less sharp than before.

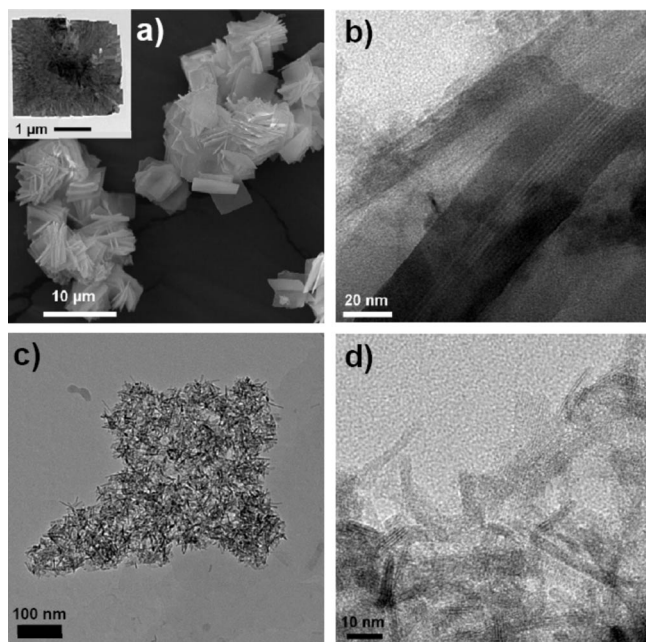


Figure 3. SEM or TEM images of: as-made JDF-L1, the inset corresponding to a single particle (a), swollen JDF-L1 (b), exfoliated JDF-L1 before acid extraction (c), exfoliated and extracted JDF-L1 (UZAR-S1) (d).

JDF-L1 scarcely adsorbs  $\text{N}_2$ , and this is reflected by a BET specific surface area of  $29.6 \text{ m}^2/\text{g}$  ( $29.8 \text{ m}^2/\text{g}$  for the protonated sample). The protonated form of JDF-L1 produced in the presence of HCl has a BET specific surface area of only  $5.0 \text{ m}^2/\text{g}$ .<sup>[12]</sup> Activation of UZAR-S1 was car-

ried out either by calcination at  $200\text{--}650^\circ\text{C}$  or by HCl extraction. With calcination, an optimum BET specific surface area of  $59.1 \text{ m}^2/\text{g}$  was found at  $400^\circ\text{C}$ , whereas the chemical extraction of UZAR-S1 produced a surface area of  $116 \text{ m}^2/\text{g}$ . This means a BET specific surface area four times higher for UZAR-S1 than for JDF-L1. Furthermore, two and three sequential cycles of swelling and extraction gave rise to a BET specific surface area of 160 and  $204 \text{ m}^2/\text{g}$ , respectively. However, there are structural differences between these samples, as will be discussed next. In any event, this was mainly external surface area, as the *t*-plot analysis demonstrated. This suggests that the five- and six-membered rings of JDF-L1 and UZAR-S1, supposing that the layer porosity is preserved upon delamination, are not accessible to  $\text{N}_2$ . On the other hand, even though the level of delamination in terms of surface area is not as high as in other exfoliation examples,<sup>[1]</sup> the avoidance of agglomeration by calcination can be important when the homogeneous dispersion of the exfoliated material in the polymer matrix is pursued, as will be shown later.

From the point of view of solid-state  $^{29}\text{Si}$  NMR spectroscopic analysis, unlike titanosilicate ETS-10, which displays four lines associated with three different Si(3Si, 1Ti) sites and one Si(4Si, 0Ti) site,<sup>[17]</sup> JDF-L1 displays a single peak at  $-109.1 \text{ ppm}$  related to a single Si(3Si, 1Ti) site,<sup>[7,8]</sup> as shown in Figure 4. The swollen JDF-L1 also has a single resonance at the same chemical shift, which indicates that the layered Si and Ti coordination was maintained. After delamination two new lines appeared for sample UZAR-S1 at about  $-102.9$  and  $-111.9 \text{ ppm}$ , the first attributed to Si(3Si, 0Ti) and Si(2Si, 1Ti) sites and the second to Si(4Si, 0Ti) sites. The Si(2Si, 1Ti) sites would have been generated from the breaking of Si–O–Si bonds, consistent with the fine, high length/width ratio particles observed by TEM. The Si(3Si, 0Ti) and Si(4Si, 0Ti) sites would be the result of the leaching of Ti (see Table 1) during the amine extraction in HCl/ $\text{H}_2\text{O}$ /ethanol. A second swelling and subsequent acid extraction treatment [UZAR-S1(II)] led to a high Si(4Si, 0Ti) contribution, associated to the condensation of silica tetrahedra.<sup>[11]</sup> Note the resonances at  $-108.3$  and  $-106.7 \text{ ppm}$  for samples UZAR-S1(I) and UZAR-S1(II) related to unconverted JDF-L1.

The performance of UZAR-S1 was tested as a mixed-matrix membrane filler. The same nanometer-like particles produced upon the exfoliation of JDF-L1 observed before are shown in Figure 5a,b. The aggregate in Figure 5a indicates that, even though the swelling and exfoliation affect most of the precursor material (as inferred from XRD and NMR), some particles with relatively large sizes would be retained. A sheet surrounded by nanometer-like particles was characterized by tilting to confirm their high aspect ratio nature (Figure 5c). The dark-contrast areas changed as the tilting angle evolved from  $0^\circ$  to  $20^\circ$ , thus indicating the presence of sheet-like particles.

Since kinetic diameters of  $\text{H}_2$  and  $\text{CH}_4$  are 0.289 and 0.38 nm, respectively, the bare polysulfone and the UZAR-S1–polysulfone composite membranes were tested for the  $\text{H}_2/\text{CH}_4$  separation (Table 2). While the  $\text{H}_2$  permeability

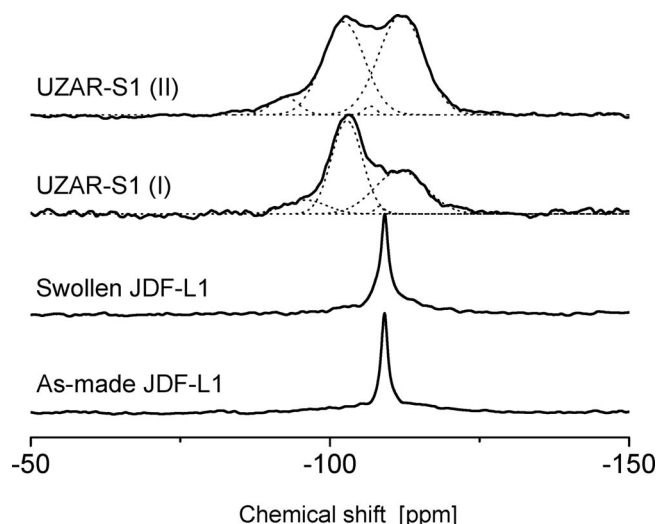


Figure 4.  $^{29}\text{Si}$  MAS NMR spectra of JDF-L1 and derived materials.

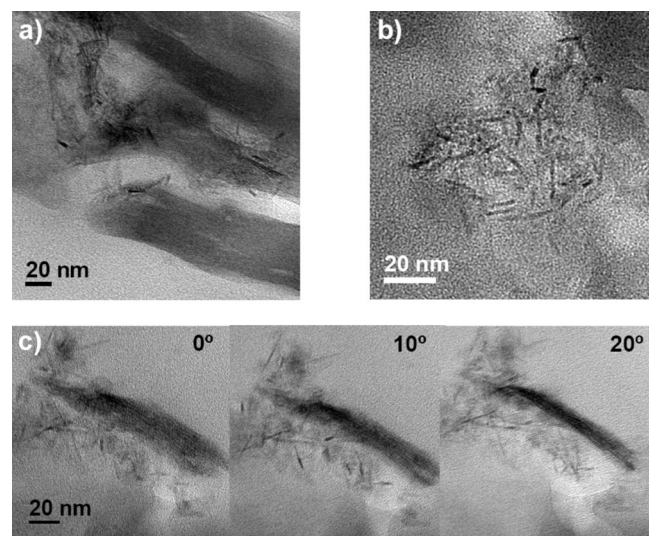


Figure 5. TEM images of a 4 wt.-% UZAR-S1-polysulfone nano-composite membrane: large aggregate (a), nanometer-like particles (b), and observations with tilting (from  $0^\circ$  to  $20^\circ$ ) (c).

showed a small decrease from 11.8 to 11.5 Barrer, the  $\text{H}_2/\text{CH}_4$  selectivity increased from 58.9 for pure polysulfone to 69.2 for 4 wt.-% UZAR-S1-polysulfone membrane. The improvement in the membrane separation ability resides in the six-membered rings that UZAR-S1 has along the [001] direction, supposing that this new material keeps the layer porosity of JDF-L1. In consequence, the molecular sieving ability of the sheets of UZAR-S1 is transferred to the composite membrane, favoring the transport of the smallest molecule ( $\text{H}_2$ ). Other polymers to fabricate the mixed matrix membranes and other gas mixtures to be separated are under investigation using UZAR-S1. Finally, the fact that JDF-L1, after treatment with a mixture of dilute acid and hydrogen peroxide, could selectively oxidize phenol to quinone<sup>[6]</sup> suggests that delaminated titanosilicate UZAR-1 with a larger specific surface area than JDF-L1 may be use-

ful in analogous situations. Besides, the material could be tested in the acylation processes where ETS-10-based catalysts similar in chemical composition have successfully been applied.<sup>[19]</sup> In this case, a good performance of UZAR-S1 may be expected due to an easier access to the protons than in other catalysts with larger particle size or smaller aspect ratio than UZAR-S1.

Table 2.  $\text{H}_2/\text{CH}_4$  separation performance at  $35^\circ\text{C}$  for pure polysulfone Udel® and 4 wt.-% UZAR-S1-Udel® membranes. Average values correspond to 3 (pure Udel®<sup>[18]</sup>) and 4 (mixed matrix) different membranes.

| Sample                | Permeability [Barrer] |                     | $\text{H}_2/\text{CH}_4$ |
|-----------------------|-----------------------|---------------------|--------------------------|
|                       | $\text{H}_2$          | $\text{CH}_4$       | Selectivity              |
| Pure Udel®            | 11.8 ( $\pm 0.2$ )    | 0.2 ( $\pm 0.01$ )  | 58.9 ( $\pm 0.1$ )       |
| 4 wt.-% UZAR-S1-Udel® | 11.5 ( $\pm 0.5$ )    | 0.17 ( $\pm 0.01$ ) | 69.2 ( $\pm 3.7$ )       |

## Conclusions

UZAR-S1, a new delaminated material, has been produced by the exfoliation of layered microporous titanosilicate JDF-L1. The delamination process used here comprises four stages: protonation with amino acid histidine, swelling with nonylamine, the delamination itself, and activation. UZAR-S1, after being activated by chemical extraction with an ethanol solution of HCl, which minimizes the loss of texture as compared with calcination, has an external specific surface area of  $160\text{ m}^2/\text{g}$ , more than five times greater than that of the JDF-L1 precursor. The extraction with an ethanol solution of  $\text{NH}_4\text{Cl}$  indicates that the swelling of JDF-L1 was achieved without exhausting the ion exchange capacity of the latter. In agreement with this, the EDX analysis shows a significant amount of sodium after swelling. One important feature of UZAR-S1, also revealed by EDX, is that the extracted material, in spite of undergoing some Ti leaching, maintained a Si/Ti atomic ratio lower than 6. This reinforces the titanosilicate nature of UZAR-S1.

$^{29}\text{Si}$  NMR spectroscopy and especially TEM analysis, which provides evidence for the existence of nanometer-like, high aspect ratio particles, confirm that UZAR-S1 is a delaminated material. As a first attempt to exploit UZAR-S1, 4 wt.-% UZAR-S1-polysulfone mixed matrix membranes have been shown to achieve a better performance in the separation of a  $\text{H}_2/\text{CH}_4$  mixture than the pure polymer.

## Experimental Section

The lamellar precursor JDF-L1 was synthesized at  $230^\circ\text{C}$  for 24 h by a seeded secondary growth procedure using the following molar composition:  $\text{SiO}_2/\text{TiO}_2/\text{Na}_2\text{O}/\text{H}_2\text{O}$  4.2:1:2.9:101.<sup>[10]</sup> The swollen JDF-L1 was prepared by intercalation of nonylamine (97 wt.-%, Fluka) molecules after proton exchange in the presence of an amino acid. In a typical procedure, L-histidine (0.2 M, 99% min., Sigma-Aldrich) was prepared by dissolving the amino acid (2.561 g) in deionized water (82.5 g) at  $60^\circ\text{C}$  whilst stirring until a transparent solution was achieved and a pH of 7.5 was measured.

Then, once at room temperature, HCl (6 M, Scharlau) was added dropwise to adjust the pH to 6. Proton exchange occurred upon addition of JDF-L1 (660 mg) over 10 min before adding an aqueous nonylamine solution (0.23 M, 5.419 g of the amine in 165 g of deionized water). The pH then increased abruptly to a value of about 9, maintained during the reaction, which was carried out with stirring at 60 °C for 12 h. Once the reaction was completed, the white, viscous and homogeneous dispersion was destabilized in an ultrasound bath for 15 min with the same amount in volume of acetone. The resulting product was centrifuged at 10000 rpm for 15 min, the solid (about 500 mg) being recovered in acetone and dried at 70 °C for 3 h. To remove the amine and then produce what is referred to as UZAR-S1 in this paper, the latter solid (200 mg) was mixed with a solution (50 mL) with molar composition HCl/H<sub>2</sub>O/ethanol 5:17:870. This solution was prepared by using HCl (37%, Scharlau) and ethanol (min. 99.8%, Scharlau), and the reaction proceeded under reflux at 55 °C for 8 h. The dispersion obtained was washed five times with deionized water and centrifuged. The solid recovered was dried at 100 °C for 20 h.

The materials were characterized by X-ray diffraction using a D-Max Rigaku X-ray diffractometer (Cu-K<sub>α</sub> radiation,  $\lambda = 1.5418 \text{ \AA}$ ). Certain samples were calcined under vacuum at 200–650 °C for 10 h. After degassing at 200 °C for 10 h, a Micromeritics Tristar 3000 instrument was used to analyze the BET specific surface area. SEM (JEOL 6400) images were obtained on Au-coated specimens operating at 20 kV. This equipment allowed EDX analysis of C-coated samples. TEM (JEOL-2000 FXII) observations at 200 kV were carried out on samples (powders and sliced sections of composite membranes) prepared by repeated dispersion in deionized water before being poured onto the carbon grid. Solid-state MAS <sup>29</sup>Si NMR spectra were recorded with a Bruker AV400 WB spectrometer operating at a resonance frequency of 79.49 MHz and with a 4 mm probe. The measurements were carried out with a contact time of 3.5 ms, a pulse width of 4  $\mu$ s, a recycle delay of 5 s, and a spinning rate of 10 kHz. Chemical shifts referred to 3-(trimethylsilyl)-1-propanesulfonic acid. For the membrane preparation, polysulfone Udel® P-3500 (kindly supplied by Solvay Advanced Polymers) was degassed at 120 °C for 4 h under vacuum to remove adsorbed water.

For the pure membrane, polysulfone (0.4 g) was dissolved in dichloromethane (3.6 mL) and stirred for 1 d, leading to a viscous solution. The fabrication procedure for the mixed matrix membrane with UZAR-S1 (obtained after one stage of swelling/extraction) involved a previous dispersion stage of the filler in the solvent (in a proportion of 90/10 wt.-% solvent/UZAR-S1-polymer mixture) for 15 min in an ultrasound bath. Polysulfone was then added, and the whole mixture was magnetically stirred for 1 d. Subsequently, the membranes were cast on flat glass plates and then left overnight partially closed to slow down the natural evaporation of solvent under ambient conditions. The solutions were dried for 1 d at room temperature. Once dried, the films were placed for the same period under 10 mbar pressure at 120 °C to remove the remaining solvent. Membranes around 100  $\mu$ m in thickness with 4 wt.-% of inorganic charge were prepared. The permeation characterization of the membranes at 35 °C was performed in a previously described setup.<sup>[18]</sup>

**Supporting Information** (see footnote on the first page of this article): Views of the JDF-L1 structure (Figure S1); low-angle X-ray

diffraction pattern of swollen JDF-L1 (Figure S2); X-ray diffraction pattern of swollen JDF-L1 without previous protonation (Figure S3); SEM images of swollen JDF-L1 and UZAR-S1 (Figure S4).

## Acknowledgments

Financial support from the Spanish Science and Innovation Ministry (MAT2007-61028) and the Aragon Government (PI035/09) is gratefully acknowledged. C. C. and P. G. also acknowledge their respective grants from the Spanish Juan de la Cierva and FPU programs.

- [1] a) A. Corma, V. Fornes, J. Martinez-Triguero, S. B. Pergher, *J. Catal.* **1999**, *186*, 57–63; b) G. Centi, S. Perathoner, *Microporous Mesoporous Mater.* **2008**, *107*, 3–15.
- [2] P. Wu, D. Nuntasri, J. F. Ruan, Y. M. Liu, M. Y. He, W. B. Fan, O. Terasaki, T. Tatsumi, *J. Phys. Chem. B* **2004**, *108*, 19126–19131.
- [3] a) H. K. Jeong, W. Krych, H. Ramanan, S. Nair, E. Marand, M. Tsapatsis, *Chem. Mater.* **2004**, *16*, 3838–3845; b) S. Choi, J. Coronas, E. Jordan, W. Oh, S. Nair, F. Onorato, D. F. Shantz, M. Tsapatsis, *Angew. Chem. Int. Ed.* **2008**, *47*, 552–555.
- [4] A. Corma, V. Fornes, J. L. Jorda, F. Rey, R. Fernandez-Lafuente, J. M. Guisan, B. Mateo, *Chem. Commun.* **2001**, 419–420.
- [5] Z. Wang, T. J. Pinnavaia, *Chem. Mater.* **1998**, *10*, 1820–1826.
- [6] M. A. Roberts, G. Sankar, J. M. Thomas, R. H. Jones, H. Du, J. Chen, W. Pang, R. Xu, *Nature* **1996**, *381*, 401–404.
- [7] Z. Lin, J. Rocha, P. Brandao, A. Ferreira, A. P. Esculcas, J. D. P. deJesus, A. Philippou, M. W. Anderson, *J. Phys. Chem. B* **1997**, *101*, 7114–7120.
- [8] M. Veltri, D. Vuono, P. De Luca, J. B. Nagy, A. Nastro, *J. Therm. Anal.* **2006**, *84*, 247–252.
- [9] J. Rocha, Z. Lin, *Rev. Mineral. Geochem.* **2005**, *57*, 173–201.
- [10] C. Rubio, C. Casado, S. Uriel, C. Téllez, J. Coronas, *Mater. Lett.* **2009**, *63*, 113–115.
- [11] S. Choi, J. Coronas, J. A. Sheffel, E. Jordan, W. Oh, S. Nair, D. F. Shantz, M. Tsapatsis, *Microporous Mesoporous Mater.* **2008**, *115*, 75–84.
- [12] K.-W. Park, J. H. Jung, J. D. Kim, S.-K. Kim, O.-Y. Kwon, *Microporous Mesoporous Mater.* **2009**, *118*, 100–105.
- [13] S. B. C. Pergher, A. Corma, V. Fornes, *Quim. Nova* **2003**, *26*, 795–802.
- [14] A. Corma, U. Diaz, M. E. Domine, V. Fornes, *J. Am. Chem. Soc.* **2000**, *122*, 2804–2809.
- [15] a) A. Corma, V. Fornes, U. Diaz, *Chem. Commun.* **2001**, 2642–2643; b) A. Corma, V. Fornes, J. M. Guil, S. Pergher, T. L. M. Maesen, J. G. Buglass, *Microporous Mesoporous Mater.* **2000**, *38*, 301–309.
- [16] S. Maheshwari, E. Jordan, S. Kumar, F. S. Bates, R. L. Penn, D. F. Shantz, M. Tsapatsis, *J. Am. Chem. Soc.* **2008**, *130*, 1507–1516.
- [17] M. W. Anderson, O. Terasaki, T. Ohsuna, A. Philippou, S. P. Mackay, A. Ferreira, J. Rocha, S. Lidin, *Nature* **1994**, *367*, 347–351.
- [18] B. Zornoza, S. Irusta, C. Tellez, J. Coronas, *Langmuir* **2009**, *25*, 5903–5909.
- [19] S. B. Waghmode, V. V. Thakur, A. Sudalai, S. Sivasanker, *Tetrahedron Lett.* **2001**, *42*, 3145.

Received: September 15, 2009

Published Online: November 20, 2009

# Synthesis and Photophysical Properties of Copper(I) Complexes Obtained from 1,10-Phenanthroline Ligands with Increasingly Bulky 2,9-Substituents

Gianluca Accorsi,<sup>[a]</sup> Nicola Armaroli,<sup>\*[a]</sup> Carine Duhayon,<sup>[b]</sup> Alix Saquet,<sup>[b]</sup> Béatrice Delavaux-Nicot,<sup>\*[b]</sup> Richard Welter,<sup>[c]</sup> Omar Moudam,<sup>[b,d]</sup> Michel Holler,<sup>[d]</sup> and Jean-François Nierengarten<sup>\*[d]</sup>

**Keywords:** Luminescence / Copper / Electrochemistry / Electronic structure / Phenanthroline

In this paper, we describe the synthesis and the electronic properties of a series of  $[\text{Cu}(\text{NN})_2]^+$  systems. The NN ligands investigated are 2,9-bis[(*tert*-butyldimethylsilyloxy)methyl]-1,10-phenanthroline (**1**), 2,9-bis[(triisopropylsilyloxy)methyl]-1,10-phenanthroline (**2**), 2,9-bis[(*tert*-butyldiphenylsilyloxy)ethyl]-1,10-phenanthroline (**3**), 2,9-bis[2,6-bis(benzyl-oxy)phenethyl]-1,10-phenanthroline (**4**) and 2-(1,3-diphenylpropan-2-yl)-9-phenethyl-1,10-phenanthroline (**5**). The electrochemical properties and the ground state electronic

absorption spectra of  $\text{Cu}(\mathbf{1})_2\text{--Cu}(\mathbf{5})_2$  are in line with the classical behaviour of such  $[\text{Cu}(\text{NN})_2]^+$  derivatives. Whereas all the compounds exhibit MLCT luminescence centered around 630–650 nm, the emission quantum yields and the lifetimes are dramatically different as a function of stereo-electronic effects and/or the possibility of internal exciplex quenching when oxygen-containing functional groups are attached to the phenanthroline ligands.

## Introduction

1,10-Phenanthroline and its derivatives have been studied for decades as versatile chelating agents,<sup>[1,2]</sup> analytical probes,<sup>[3]</sup> DNA intercalators,<sup>[4]</sup> building blocks for multi-component architectures<sup>[5–10]</sup> and molecular machines.<sup>[11]</sup> One of the most successful fields of exploitation of these ligands in coordination chemistry is concerned with the preparation of  $\text{Cu}^{\text{I}}$  complexes.  $\text{Cu}^{\text{I}}$ -bisphenanthroline complexes,  $[\text{Cu}(\text{NN})_2]^+$ , display distorted tetrahedral geometries due to intra- and intermolecular (in solid state crystals)  $\pi$ -stacking interactions which are dictated by the size, chemical nature, and position of the phenanthroline substituents.<sup>[12–16]</sup>

$\text{Cu}^{\text{I}}$  is characterized by a  $d^{10}$  electronic configuration<sup>[17]</sup> and exhibits a low oxidation potential, whereas phen-

anthroline is a good  $\pi^*$  electron accepting molecule. Accordingly,  $[\text{Cu}(\text{NN})_2]^+$  may exhibit metal-to-ligand-charge-transfer (MLCT) absorption bands at relatively low energy, typically in the range 380–700 nm.<sup>[15–16]</sup> These features impart a marked color to these complexes which range from orange, to deep red to magenta, depending on the relative intensity of the various MLCT transitions, in turn related to the specific symmetry of the complex.  $[\text{Cu}(\text{NN})_2]^+$  with properly substituted phenanthroline ligands are also characterized by a relatively long-lived MLCT emission in the visible (Vis) spectral region. Over the years, substantial elongation of the excited state lifetime has been pursued by rational ligand design that has made  $[\text{Cu}(\text{NN})_2]^+$  potential alternatives to popular  $\text{Ru}^{\text{II}}$ -polypyridine complexes,<sup>[14,16,18]</sup> because of the larger abundance and smaller environmental impact of Cu compared to Ru. Thus Cu complexes are by far more attractive for potential applications such as dye-sensitized solar cell complex,  $[\text{Cu}(\text{dtbp})_2]^+$  (dtbp = 2,9-di-*tert*-butyl-1,10-phenanthroline), which exhibits the longest MLCT emission lifetime ( $\tau = 3260$  ns) and largest emission quantum yield ( $\Phi = 5.6\%$ ) ever reported for  $[\text{Cu}(\text{NN})_2]^+$  derivatives.<sup>[21,22]</sup> However, despite its outstanding photophysical properties,  $[\text{Cu}(\text{dtbp})_2]^+$  undergoes facile ligand replacement reactions, where one dtbp ligand is lost. Thus, this compound is not very stable in the presence of nucleophiles and coordinating solvents. Indeed, even weakly coordinating solvents such as acetone are capable of displacing one dtbp ligand.<sup>[22]</sup> Therefore, substantial research efforts are still needed to develop stable luminescent  $[\text{Cu}(\text{NN})_2]^+$  derivatives.

[a] Molecular Photoscience Group, Istituto per la Sintesi Organica e la Fotoreattività, Consiglio Nazionale delle Ricerche, Via Gobetti 101, 40129 Bologna, Italy  
E-mail: nicola.armaroli@isof.cnr.it

[b] Laboratoire de Chimie de Coordination du CNRS, 205 route de Narbonne, 31077 Toulouse Cedex 4, France  
E-mail: beatrice.delavaux-nicot@lcc-toulouse.fr

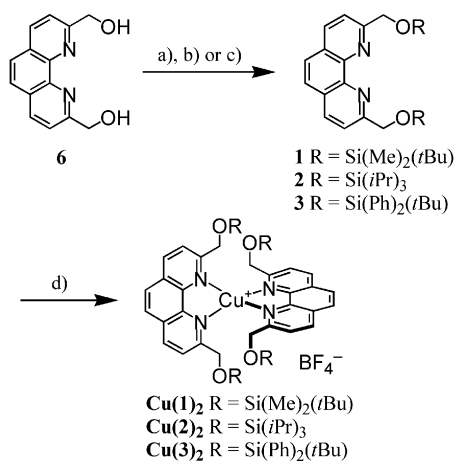
[c] Laboratoire DECOMET, Université de Strasbourg, 4 rue Blaise Pascal, 67000 Strasbourg, France  
E-mail: welter@chimie.u-strasbg.fr

[d] Laboratoire de Chimie des Matériaux Moléculaires, Université de Strasbourg et CNRS (UMR 7509), Ecole Européenne de Chimie, Polymères et Matériaux (ECPM), 25 rue Becquerel, 67087 Strasbourg Cedex 2, France  
E-mail: nierengarten@chimie.u-strasbg.fr

Supporting information for this article is available on the WWW under <http://dx.doi.org/10.1002/ejic.200900954>.

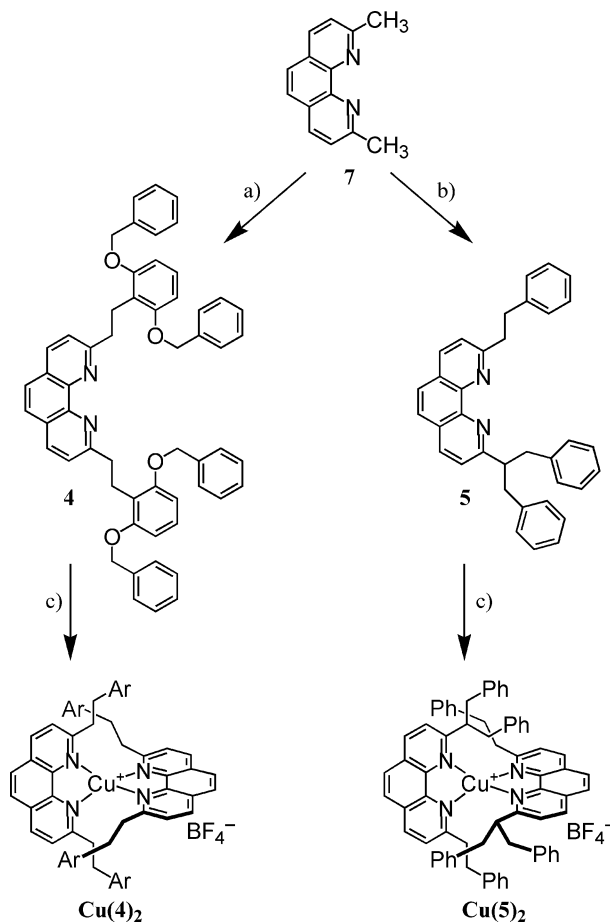
The effects on the intensity and color of the MLCT luminescence band and on its related lifetime is attributed to geometric distortions that occur upon light excitation, when the metal center changes its formal oxidation state from  $\text{Cu}^{\text{I}}$  to  $\text{Cu}^{\text{II}}$  and tend to assume a more flattened geometry.<sup>[15–16]</sup> The flattening process was proposed by McMillin and co-workers 20 years ago on the basis of classical photochemical experiments on series of  $[\text{Cu}(\text{NN})_2]^+$  complexes with increasingly nucleophilic counteranions.<sup>[23]</sup> In recent years it has been confirmed by means of ultrafast transient absorption and light-initiated time-resolved X-ray absorption spectroscopy (LITR-XAS).<sup>[24]</sup> The latter pump-and-probe technique allows one to catch the transient oxidation state of a metal atom as well as its surrounding structures following photoexcitation via an ultrafast laser source. Practically, the information obtained via LITR-XAS is a sort of snapshot of electronic excited states in disordered media (e.g. solution), which are generated via a UV/Vis femtosecond pump laser and subsequently probed with a 30–100 ps intense X-ray pulse produced by 3rd generation large synchrotron facilities.<sup>[25]</sup> Analogous investigations can be carried out also on  $\text{Cu}^{\text{I}}$  complexes as solid crystals (“photo-crystallography”).<sup>[26]</sup>

Recent fluorescence upconversion studies conclude that flattening distortions in  $[\text{Cu}(\text{NN})_2]^+$  occur on a timescale below 100 fs,<sup>[27]</sup> i.e. shorter than proposed before.<sup>[28–29]</sup> Importantly, the distortion tends to reduce the excited state lifetime of the luminescent level, due to parasite non radiative quenching processes that involve binding of solvent molecules and counterions to form pentacoordinate species. To limit these undesired effects two strategies are typically followed, i.e. choosing bulky substituents at the phenanthroline ligands that shield the metal site from intermolecular attack and selecting poor electron donor solvents such as toluene or  $\text{CH}_2\text{Cl}_2$  instead of  $\text{CH}_3\text{CN}$  or  $\text{CH}_3\text{OH}$ .<sup>[14]</sup>



Scheme 1. *Reagents and conditions:* (a) TBDMSCl, DMF, imidazole (80%); (b) TIPSCl, DMF, imidazole (73%); (c) TBDPSCl, DMF, imidazole (84%); (d)  $\text{Cu}(\text{CH}_3\text{CN})_4\text{BF}_4$ ,  $\text{CH}_2\text{Cl}_2$ ,  $\text{CH}_3\text{CN}$  [ $\text{Cu(1)}_2$ : 73%;  $\text{Cu(2)}_2$ : 76%;  $\text{Cu(3)}_2$ : 73%].

A completely different approach to improve substantially the luminescence performance of  $\text{Cu}^{\text{I}}$  complexes is that of using heteroleptic coordination with imine- and phosphane-type ligands,  $[\text{Cu}(\text{NN})(\text{PP})]^+$ .<sup>[30,17]</sup> Unfortunately,  $[\text{Cu}(\text{NN})(\text{PP})]^+$  complexes often exhibit poor stability in solution and are more difficult to handle, making  $[\text{Cu}(\text{NN})_2]^+$  still preferable in this regard. Here we present the synthesis, X-ray crystal structures, electrochemistry, and photophysical properties of five novel  $[\text{Cu}(\text{NN})_2]^+$  complexes, exhibiting rather different luminescence performance (see Schemes 1 and 2). To the best of our knowledge and by excluding the unique and outstanding  $[\text{Cu}(\text{dtbp})_2]$ ,<sup>[22]</sup>  $\text{Cu(5)}_2$  is one of the longest-lived  $[\text{Cu}(\text{NN})_2]^+$  emitters reported so far, with  $\tau = 420$  ns in oxygen-free  $\text{CH}_2\text{Cl}_2$  solution.



Scheme 2. *Reagents and conditions:* (a) KDA, THF,  $-78^\circ\text{C}$  then 2,6-dibenzyloxybenzyl bromide (49%); (b) KDA (3 equiv.), THF,  $-78^\circ\text{C}$  then benzyl bromide (4 equiv.) (44%); (c)  $\text{Cu}(\text{CH}_3\text{CN})_4\text{BF}_4$ ,  $\text{CH}_2\text{Cl}_2$ ,  $\text{CH}_3\text{CN}$  [ $\text{Cu(4)}_2$ : 60%;  $\text{Cu(5)}_2$ : 50%].

## Results and Discussion

### Synthesis

The preparation of complexes  $\text{Cu(1)}_2$ – $\text{Cu(3)}_2$  is depicted in Scheme 1. Compound **6** was prepared according to a previously published procedure.<sup>[31]</sup> Protection of the two alcohol groups of **6** with silylated protecting groups appear

indeed as an easy way to increase the size of the 2,9-substituents of the 1,10-phenanthroline ligand. Reaction of **6** with *tert*-butyldimethylchlorosilane (TBDMSCl) in the presence of imidazole gave the TBDMS-protected ligand **1** in 80% yield. Ligands **2** and **3** were prepared under similar conditions from the reaction of **6** with tri-isopropylchlorosilane (TIPSCl) and *tert*-butyldiphenylchlorosilane (TBDPSCl), respectively. The corresponding Cu<sup>I</sup> complexes **Cu(1)<sub>2</sub>**–**Cu(3)<sub>2</sub>** were obtained in 73 to 76% by treatment of ligands **1–3** with Cu(CH<sub>3</sub>CN)<sub>4</sub>BF<sub>4</sub> in CH<sub>2</sub>Cl<sub>2</sub>/CH<sub>3</sub>CN at room temperature. The coordination of the phenanthroline ligand to the Cu<sup>I</sup> cation was easily observed by an instantaneous color change of the solution upon addition of the Cu<sup>I</sup> salt. Actually, the colorless ligand solution became orange-red due to the apparition of the MLCT band characteristic of bis(2,9-disubstituted-1,10-phenanthroline)Cu<sup>I</sup> derivatives (vide infra). Compounds **Cu(1)<sub>2</sub>**–**Cu(3)<sub>2</sub>** were characterized by <sup>1</sup>H- and <sup>13</sup>C-NMR spectroscopy and elemental analysis.

Crystals suitable for X-ray crystal-structure analysis were obtained by slow diffusion of Et<sub>2</sub>O into a CH<sub>2</sub>Cl<sub>2</sub> solution of **Cu(1)<sub>2</sub>**. The ORTEP drawing of the cationic moiety of **Cu(1)<sub>2</sub>** is depicted in part A of Figure 1. As typically seen for copper phenanthroline complexes,<sup>[32]</sup> packing induced distortions from an idealized pseudotetrahedral geometry are observed. However, unlike what is typically seen in the solid-state structures of related copper(I) complexes,<sup>[32]</sup> there is no flattening of the two ligands relative to one another (towards a square-planar geometry) as a consequence of the packing. Indeed, close inspection of the crystal packing reveals columnar arrays in which intermolecular  $\pi$ - $\pi$  stacking interactions between the phenanthroline rings of neighboring **Cu<sup>+</sup>(1)<sub>2</sub>** cations take place (Figure 1, B). The

resulting packing forces induce a significant rocking (ca. 16.6°) of both phenanthroline ligands as schematically shown in Figure 1 (C–D). This rocking distortion facilitates the intermolecular phenanthroline-phenanthroline interactions in the crystal lattice and produce an exceptionally large N(1)–Cu(1)–N(4) bond angle (139.40°) as well as a lengthening of the Cu(1)–N(2) and Cu(1)–N(3) bonds when compared to the Cu(1)–N(1) and Cu(1)–N(4) bonds (Table 1).

Table 1. Bond lengths [Å] and angles [°] within the coordination spheres for **Cu(1)<sub>2</sub>** and **Cu(5)<sub>2</sub>** (see Figures 1 and 2 for the numbering).

|                 | <b>Cu(1)<sub>2</sub></b> | <b>Cu(5)<sub>2</sub></b> |
|-----------------|--------------------------|--------------------------|
| Cu(1)–N(1)      | 2.007(3)                 | 2.031(7)                 |
| Cu(1)–N(2)      | 2.064(3)                 | 2.032(6)                 |
| Cu(1)–N(3)      | 2.053(3)                 | 2.026(7)                 |
| Cu(1)–N(4)      | 2.010(3)                 | 2.040(6)                 |
| N(1)–Cu(1)–N(2) | 82.5(1)                  | 82.6(3)                  |
| N(1)–Cu(1)–N(3) | 121.4(1)                 | 126.9(3)                 |
| N(1)–Cu(1)–N(4) | 139.4(1)                 | 120.3(3)                 |
| N(2)–Cu(1)–N(3) | 126.3(3)                 | 126.3(3)                 |
| N(2)–Cu(1)–N(4) | 120.4(1)                 | 123.9(3)                 |
| N(3)–Cu(1)–N(4) | 82.6(1)                  | 82.5(3)                  |

The synthesis of compounds **Cu(4)<sub>2</sub>** and **Cu(5)<sub>2</sub>** is depicted in Scheme 2. Ligand **4** was obtained from the reaction of the dicarbanion derived from neocuproine (**7**)<sup>[33]</sup> with 2,6-dibenzoyloxybenzyl bromide. When the dicarbanion was prepared from treatment of **7** with lithium diisopropyl amide (LDA) in THF, the desired dialkylated product was obtained in low yields (<20%). In an attempt to optimize the preparation of ligand **4**, the reaction was performed un-

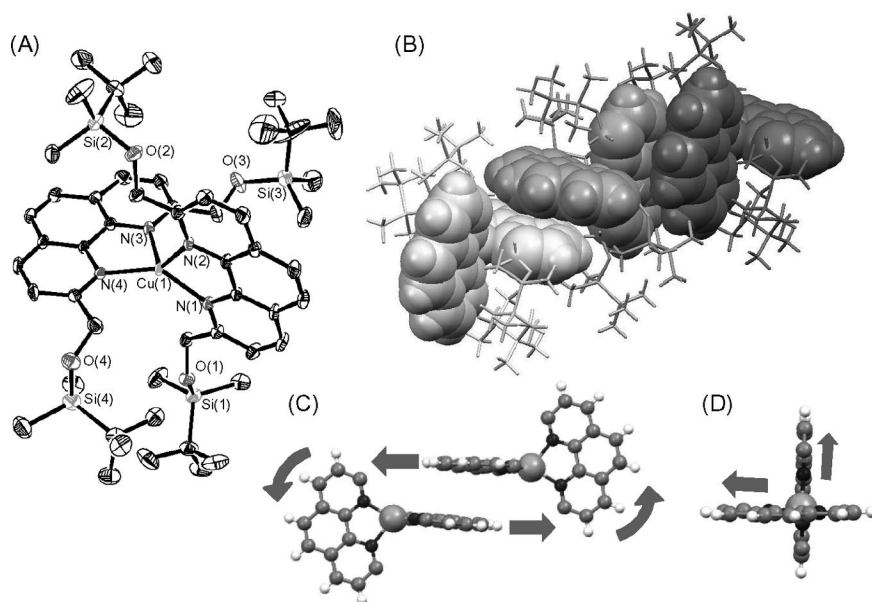


Figure 1. (A) ORTEP view with partial numbering of the cationic part of complex **Cu(1)<sub>2</sub>**. The hydrogen atoms have been omitted for clarity. Thermal ellipsoids include 30% of the electron density. (B) Stacking within the **Cu(1)<sub>2</sub>** lattice highlighting the intramolecular  $\pi$ - $\pi$  stacking interactions between neighboring cations. (C) Schematic view showing how the packing forces induce the rocking distortion. (D) Detailed view of the coordination sphere around the Cu<sup>I</sup> cation highlighting the rocking of both phenanthroline ligands.

der the conditions developed in the group of Gorman for the synthesis of dialkylated bipyridines.<sup>[34]</sup> Indeed, the use of potassium diisopropyl amide (KDA) as base to deprotonate **7** followed by reaction with 2,6-dibenzoyloxybenzyl bromide led to an acceptable yield (49%) of the desired product **4**. By applying the same reaction conditions with benzyl bromide (2.5 equiv.) as electrophile, 2,9-diphenethyl-1,10-phenanthroline<sup>[33]</sup> was isolated as the main product in 40% yield. Under these conditions, mono- and tri-alkylated derivatives were also produced. When an excess of KDA (3 equiv.) and benzyl bromide (4 equiv.) was used, the desired trialkylated product **5** was isolated in 44% yield. It can be noted that with larger excesses of KDA (4 equiv.) and benzyl bromide (6 to 8 equiv.), the trialkylated derivative **5** was always the major product (40 to 45%) and no traces of tetraalkylated products were detected. Finally, treatment of ligands **4** and **5** with  $\text{Cu}(\text{CH}_3\text{CN})_4\text{BF}_4$  in  $\text{CH}_2\text{Cl}_2/\text{CH}_3\text{CN}$  at room temperature gave the  $\text{Cu}^{\text{I}}$  complexes **Cu(4)<sub>2</sub>** and **Cu(5)<sub>2</sub>**, respectively.

The air stable complexes **Cu(4)<sub>2</sub>** and **Cu(5)<sub>2</sub>** were characterized by  $^1\text{H}$ - and  $^{13}\text{C}$ -NMR spectroscopy and their purity confirmed by elemental analysis. Complex **Cu(5)<sub>2</sub>** was further characterized by X-ray crystallography. The ORTEP drawing of the cationic moiety of **Cu(5)<sub>2</sub>** is shown in Figure 2 (A). The dihedral angle between the ligands plane is almost  $90^\circ$ . As a consequence, the four  $\text{Cu}-\text{N}$  distances are similar and the geometry of the copper/nitrogen framework quite regular (Table 1) by comparison with other  $\text{Cu}^{\text{I}}$  bis-(phenanthroline) complexes.<sup>[32]</sup> Close inspection of the crystal packing reveals a network of intermolecular  $\pi$ -stacking interactions between the different phenyl rings of neigh-

boring **Cu<sup>+</sup>(5)<sub>2</sub>** cations. Importantly, the six peripheral phenyl groups prevent intermolecular  $\pi$ -interactions involving the phenanthroline subunits and thus the distortion of the coordination sphere around the  $\text{Cu}^{\text{I}}$  cation. Further stabilization is also provided by several intramolecular face-to-edge  $\pi$ -stacking interactions involving the phenanthroline moiety of one ligand and two phenyl subunits of the other one (Figure 2, B–C).

### Electrochemistry

The electrochemical properties of **Cu(1)<sub>2</sub>–Cu(5)<sub>2</sub>** were determined by cyclic voltammetry (CV) and Osteryoung Square Wave Voltammetry (OSWV). All the experiments were performed at room temperature in  $\text{CH}_2\text{Cl}_2$  solutions containing tetra-*n*-butylammonium tetrafluoroborate (0.1 M) as supporting electrolyte and ferrocene (Fc) as internal reference, with a Pt disk as the working electrode and a saturated calomel electrode (SCE) as a reference. Potential data for all of the complexes are collected in Table 2. In the anodic region, all the copper(I) complexes **Cu(1)<sub>2</sub>–Cu(5)<sub>2</sub>** show a reversible one-electron process assigned to the oxidation of the metal center.<sup>[35]</sup> As far as the cathodic region is concerned, the typical reduction centered on the phenanthroline ligand<sup>[35]</sup> could not be observed in the available potential window.

The oxidation of  $\text{Cu}^{\text{I}}$  to  $\text{Cu}^{\text{II}}$  is accompanied by the rearrangement from a pseudotetrahedral coordination geometry to a distorted square planar one.<sup>[35]</sup> This process is strongly affected by the size of the substituent attached to

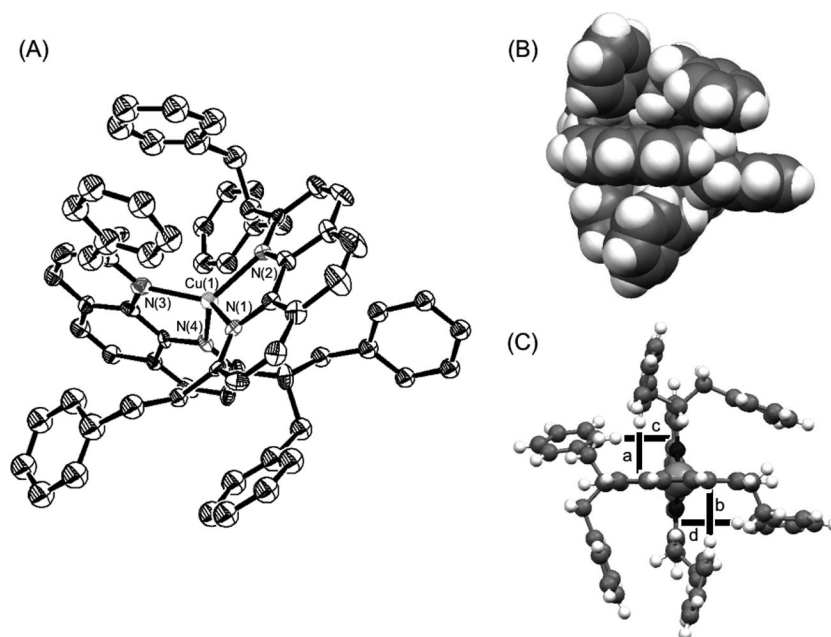


Figure 2. (A) ORTEP view with partial numbering of the cationic part of complex **Cu(5)<sub>2</sub>**. The hydrogen atoms have been omitted for clarity. Thermal ellipsoids include 30% of the electron density. Space filling (B), and ball and stick (C) representations of the cationic part of **Cu(5)<sub>2</sub>** highlighting the intramolecular face-to-edge  $\pi$ -stacking interactions; a: 2.75 Å [distance from C(31)–H to the plane of the phenanthroline]; b: 2.86 Å [distance from C(1)–H to the plane of the phenanthroline]; c: 2.83 Å [distance from C(70)–H to the plane of the phenanthroline]; d: 2.86 Å [distance from C(40)–H to the plane of the phenanthroline].

Table 2. Electrochemical data on the oxidation of the copper(I) complexes determined by CV and OSWV on a Pt working electrode in  $\text{CH}_2\text{Cl}_2 + 0.1 \text{ M } n\text{Bu}_4\text{NBF}_4$  at room temperature.

|                          | CV <sup>[a]</sup> | OSWV <sup>[b]</sup> |
|--------------------------|-------------------|---------------------|
| <b>Cu(1)<sub>2</sub></b> | +0.99 (110)       | +0.99               |
| <b>Cu(2)<sub>2</sub></b> | +1.15 (100)       | +1.16               |
| <b>Cu(3)<sub>2</sub></b> | +1.19 (110)       | +1.20               |
| <b>Cu(4)<sub>2</sub></b> | +0.98 (100)       | +0.98               |
| <b>Cu(5)<sub>2</sub></b> | +1.28 (90)        | +1.28               |

[a] Values for  $(E_{\text{pa}} + E_{\text{pc}})/2$  given in Volt vs. SCE and  $\Delta E_{\text{p}}$  in mV (in parenthesis) at a scan rate of  $100 \text{ mVs}^{-1}$ . [b] OSWV values were obtained using a sweep width of 20 mV, a frequency of 10 Hz, and a step potential of 5 mV; values are given in Volt vs. SCE.

the phenanthroline ligand. Indeed, bulkier substituents on the phenanthroline ligand hinder the formation of a more flattened structure appropriate for the  $\text{Cu}^{\text{II}}$  oxidation state. This rationale perfectly explains the positive shift when going from **Cu(1)<sub>2</sub>** to **Cu(3)<sub>2</sub>** as a result of the increasing size of the silyl protecting groups. This effect is even stronger in the case of **Cu(5)<sub>2</sub>** for which the oxidation is the most difficult. Indeed, this is in good agreement with the X-ray crystal structure analysis of **Cu(5)<sub>2</sub>** which revealed how the six peripheral phenyl subunits prevent significant distortion of the coordination geometry of the copper center. In contrast, the oxidation process is almost not affected by substituents that are attached too far from the phenanthroline ligand. Effectively, the benzyloxy subunits of **Cu(4)<sub>2</sub>** have no significant effect on the redox potential of the  $\text{Cu}^{\text{II}}/\text{Cu}^{\text{I}}$  couple. Indeed, the potential value observed for **Cu(4)<sub>2</sub>** is similar to the one observed for the corresponding unsubstituted copper(I) complex prepared from the 2,9-diphenethyl-1,10-phenanthroline.<sup>[36]</sup> It appears that the benzyloxy groups of **Cu(4)<sub>2</sub>** are not capable of significantly preventing the distortion of the coordination sphere around the copper center.

### Photophysical Properties

In Figure 3 are depicted the absorption spectra of **Cu(1)<sub>2</sub>–Cu(5)<sub>2</sub>** in toluene or dichloromethane solutions. The UV spectral window is characterized by intense ligand-centered (LC) bands typical of the  $\pi\pi^*$  transitions of the phenanthroline ligands, with molar absorption coefficients ( $\epsilon$ ) of the order of  $50,000\text{--}60,000 \text{ M}^{-1} \text{ cm}^{-1}$ .<sup>[2]</sup> The bands lying in the VIS spectral region ( $\approx 380\text{--}600 \text{ nm}$ ) are much weaker than those in the UV and are assigned to MLCT electronic transitions.<sup>[15,16]</sup> Their shape and relatively high intensity are typical of phenanthrolines with alkyl-type substituents at the 2 and 9 position,<sup>[37]</sup> which are substantially different from those with phenyl residues.<sup>[38]</sup> The substantial similarity between the MLCT absorption features [**Cu(1)<sub>2</sub>–Cu(3)<sub>2</sub>** and **Cu(4)<sub>2</sub>–Cu(5)<sub>2</sub>**, in particular, are virtually identical] suggests that the ground state symmetry and electronic configuration of the complexes is pretty much the same along the series. By contrast (vide infra) luminescence properties suggest marked differences in the excited state behaviour.

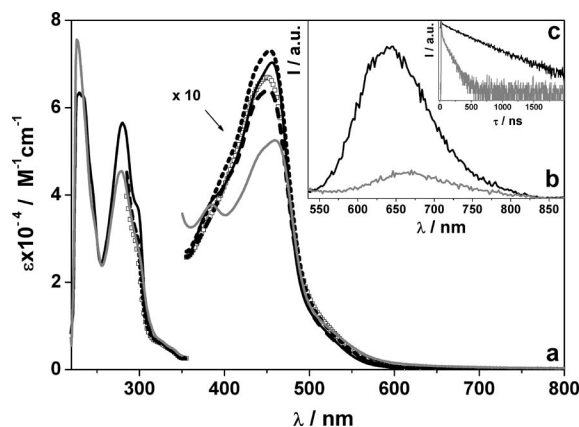


Figure 3. (a) Absorption spectra of **Cu(1)<sub>2</sub>** (empty square), **Cu(2)<sub>2</sub>** (dotted line), **Cu(3)<sub>2</sub>** (dashed line) in toluene and **Cu(4)<sub>2</sub>** (grey line) and **Cu(5)<sub>2</sub>** (black line) in  $\text{CH}_2\text{Cl}_2$ . For the sake of clarity the visible spectral region is multiplied by a factor of ten. The spectra of **Cu(1)<sub>2</sub>** and **Cu(2)<sub>2</sub>** are truncated at 290 nm, limit of the optical window of toluene. (b) Emission spectra of **Cu(4)<sub>2</sub>** and **Cu(5)<sub>2</sub>** in  $\text{CH}_2\text{Cl}_2$  (298 K,  $\lambda_{\text{exc}} = 450 \text{ nm}$ ); relative intensities reflect the magnitude of the corresponding quantum yields. The emission spectra of **Cu(1)<sub>2</sub>–Cu(3)<sub>2</sub>** are extremely weak and have been omitted. (c) Luminescence decays of **Cu(4)<sub>2</sub>** and **Cu(5)<sub>2</sub>**,  $\lambda_{\text{exc}} = 407 \text{ nm}$ , oxygen-free solutions.

As detailed above, the MLCT emissive excited state of  $[\text{Cu}(\text{NN})_2]^+$  complexes is populated after extensive molecular rearrangements, in particular flattening distortion of the initial pseudo-tetrahedral Franck-Condon geometry and expansion of the coordination number.<sup>[29,15]</sup> When the ligand skeleton provides stronger rigidity to the complex, i.e. limited chance of rearrangement, the emission performance and excited state lifetime tend to increase.

In the present case the emission bands of **Cu(1)<sub>2</sub>–Cu(3)<sub>2</sub>** are barely detectable in  $\text{CH}_2\text{Cl}_2$ , which is the classical solvent for  $[\text{Cu}(\text{NN})_2]^+$ , because it offers the best compromise between solubility power and little emission quenching by nucleophilic attack.<sup>[14]</sup> Less nucleophilic solvents such as toluene can hardly solubilize ionic species like  $[\text{Cu}(\text{NN})_2]^+$ , which could thus be studied in this solvent only very rarely.<sup>[29]</sup> Quite unexpectedly, **Cu(1)<sub>2</sub>–Cu(3)<sub>2</sub>** turned out to be reasonably soluble in toluene, so as to enable the determination of molar absorption coefficient values (Figure 3). However, also in this solvent, very weak emission bands were detected with quantum yields lower than  $1 \times 10^{-5}$  (Figure S1) and lifetimes of just a few nanoseconds (Table 3). These values are even much smaller than those of  $[\text{Cu}(\text{dmp})_2]^+$  ( $\text{dmp} = 2,9\text{-dimethyl-1,10-phenanthroline}$ , 72 ns)<sup>[37]</sup> that, in principle, is expected to offer a more limited steric protection to the excited molecule, compared to **Cu(1)<sub>2</sub>–Cu(3)<sub>2</sub>**, with its tiny methyl residue. This suggests an active role of the silyloxy groups in depressing the emission performance, most likely via internal nucleophilic quenching by the oxygen atom. This effect has been already observed earlier, both at room temperature<sup>[37]</sup> and at 77 K,<sup>[39]</sup> in  $[\text{Cu}(\text{NN})_2]^+$  with appended fragments bearing N or O atoms.

Table 3. Photophysical data in solution, low-temperature rigid matrix and solid state as powder.

|                          | Solution (298 K)                  |  |  | Rigid matrix (77 K)               |                         | Solid state (298 K)               |                         |
|--------------------------|-----------------------------------|--|--|-----------------------------------|-------------------------|-----------------------------------|-------------------------|
|                          | $\lambda_{\text{max}}^{[a]}$ [nm] | $\Phi_{\text{em}}^{[b]}$   | $\tau^{[c]}$ [ns]  | $\lambda_{\text{max}}^{[a]}$ [nm] | $\tau^{[c]}$ [ $\mu$ s] | $\lambda_{\text{max}}^{[a]}$ [nm] | $\tau^{[c]}$ [ $\mu$ s] |
| <b>Cu(1)<sub>2</sub></b> | 652 <sup>[d]</sup>                | $< 1 \times 10^{-5}$ <sup>[d]</sup><br>( $< 1 \times 10^{-5}$ ) <sup>[d]</sup> | 2.8 <sup>[d]</sup>   | 650 <sup>[d]</sup>                | 3.4 <sup>[d]</sup>      | 652                               | 0.024                   |
| <b>Cu(2)<sub>2</sub></b> | 644 <sup>[d]</sup>                | $< 1 \times 10^{-5}$ <sup>[d]</sup><br>( $< 1 \times 10^{-5}$ ) <sup>[d]</sup> | 2.4 <sup>[d]</sup>   | 632 <sup>[d]</sup>                | 5.2 <sup>[d]</sup>      | 648                               | 0.030                   |
| <b>Cu(3)<sub>2</sub></b> | 650 <sup>[d]</sup>                | $< 1 \times 10^{-5}$ <sup>[d]</sup><br>( $< 1 \times 10^{-5}$ ) <sup>[d]</sup> | 6.0 <sup>[d]</sup>   | 640 <sup>[d]</sup>                | 4.9 <sup>[d]</sup>      | 622                               | 0.87                    |
| <b>Cu(4)<sub>2</sub></b> | 668 <sup>[e]</sup>                | $2.2 \times 10^{-4}$ <sup>[e]</sup><br>( $2.5 \times 10^{-4}$ ) <sup>[e]</sup> | 6.1, 15% <sup>[e,f]</sup><br>85.9, 85% <sup>[e,f]</sup><br>(6.1, 19%) <sup>[e,f]</sup><br>(95.3, 81%) <sup>[e,f]</sup> | 642 <sup>[e]</sup>                | 5.4 <sup>[e]</sup>      | 645                               | 0.49                    |
| <b>Cu(5)<sub>2</sub></b> | 638 <sup>[e]</sup>                | $1.9 \times 10^{-3}$ <sup>[e]</sup><br>( $2.6 \times 10^{-3}$ ) <sup>[e]</sup> | 9.3, 2% <sup>[e,f]</sup><br>309, 98% <sup>[e,f]</sup><br>(420)   | 638 <sup>[e]</sup>                | 6.3 <sup>[e]</sup>      | 626                               | 1.3                     |

[a] Emission maxima from spectra uncorrected for the detector response. [b] Emission quantum yields in air-equilibrated and, in brackets, in oxygen-free solution. [c] Excited state lifetimes in air-equilibrated and, in brackets, in oxygen-free solution. [d] Toluene. [e] CH<sub>2</sub>Cl<sub>2</sub>. [f] The percentage value is the relative amplitude of the decay components.

The emission spectra of **Cu(4)<sub>2</sub>–Cu(5)<sub>2</sub>** in CH<sub>2</sub>Cl<sub>2</sub> solution at room temperature are reported in Figure 3. The related quantum yields and excited state lifetimes are gathered in Table 3 and are at least one order of magnitude larger than those of **Cu(1)<sub>2</sub>–Cu(3)<sub>2</sub>**. This substantially different performance can be explained with the better protection offered by the bulkier phenanthroline substituents in **4** and **5** relative to **1–3**. It has to be emphasized that **Cu(5)<sub>2</sub>** exhibits a particularly good MLCT luminescence quantum yield for a conventional bisphenanthroline copper(I) complex<sup>[15]</sup> ( $\Phi = 2.6 \times 10^{-3}$  in oxygen free solution), whereas the value of **Cu(4)<sub>2</sub>** is 10 times lower (Figure 3). This remarkably different emission behavior could be related again to the presence of oxygen atoms in the phenanthroline substituents of **4**, which may prompt internal exciplex quenching, as discussed above for **Cu(1)<sub>2</sub>–Cu(3)<sub>2</sub>**. Electrochemical data are in line with the good performance of **Cu(5)<sub>2</sub>**, which exhibits the highest oxidation potential, i.e. it is the least prone to undergo molecular rearrangements upon oxidation.<sup>[40]</sup> The remarkable differences in the emission quantum yields between **Cu(1)<sub>2</sub>–Cu(3)<sub>2</sub>** and **Cu(4)<sub>2</sub>–Cu(5)<sub>2</sub>** are in line with the trend of MLCT excited state lifetimes. **Cu(1)<sub>2</sub>–Cu(3)<sub>2</sub>** exhibit a lifetime of a few ns in toluene solution, unaffected by the removal of oxygen. In the case of **Cu(4)<sub>2</sub>–Cu(5)<sub>2</sub>** double exponential luminescence decays are found, with minor (relative amplitude  $\leq 15\%$ ) shorter components of a few ns (Table 3). Bicomponent emission decays were already found earlier for [Cu(NN)<sub>2</sub>]<sup>+</sup> but, in these cases, the shorter lifetimes were much smaller than found here ( $\ll 1$  ns) and associated with emission from the singlet level (<sup>1</sup>MLCT)<sup>[41]</sup> or to excited states that have not yet undergone structural rearrangements.<sup>[42]</sup> The longer values in the present complexes (ca. 6 ns) can be hardly related to dynamic structural phenomena also because, recently, it has been suggested that they occur in the sub picosecond timescale.<sup>[27]</sup> The multiexponential luminescence decays observed for **Cu(4)<sub>2</sub>** [the effect in **Cu(5)<sub>2</sub>** is much less pronounced, see Table 3] seem to be related to the cumbersome phenanthroline residues

which might foster peculiar intramolecular (see above) and perhaps even intermolecular quenching effect for this complex, yielding complex decay kinetics.

Notably, for **Cu(5)<sub>2</sub>**, the emission decay detected in oxygen free CH<sub>2</sub>Cl<sub>2</sub> solution exhibits a negligibly weak short component and can be well fitted monoexponentially (Figure 3). A lifetime of 420 ns is thus calculated, i.e. one of the longest detected to date for conventional [Cu(NN)<sub>2</sub>]<sup>+</sup> homoleptic complexes.<sup>[14,15]</sup> The longer lifetime component of the less sterically protected **Cu(4)<sub>2</sub>** is substantially shorter, i.e. 95.3 ns.

**Cu(1)<sub>2</sub>–Cu(5)<sub>2</sub>** were also investigated in solid state as powder (room temperature) and in rigid matrix at 77 K (Figure 4, Table 3). The most notable result is the substantial increase of the excited state lifetime of **Cu(1)<sub>2</sub>–Cu(3)<sub>2</sub>** at 77 K, compared to solutions. Hence, for the whole series, lifetime values of a few  $\mu$ s are measured, in line with MLCT lifetimes of [Cu(NN)<sub>2</sub>]<sup>+</sup> in low temperature matrices.<sup>[37]</sup> The emission intensity, albeit non obtainable quantitatively un-

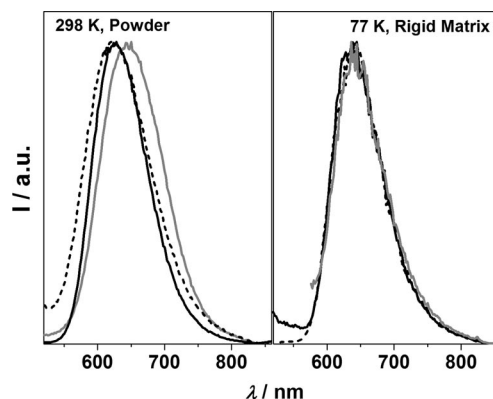


Figure 4. Emission spectra of **Cu(3)<sub>2</sub>** (dashed line), **Cu(4)<sub>2</sub>** (grey line) and **Cu(5)<sub>2</sub>** (black line) in the solid state as powder (left; 298 K,  $\lambda_{\text{exc}} = 450$  nm) and at 77 K rigid matrix (right;  $\lambda_{\text{exc}} = 450$  nm). The emission spectra of **Cu(1)<sub>2</sub>** and **Cu(2)<sub>2</sub>** have been omitted for the sake of clarity (see Supporting Information).

der these conditions, is quite comparable for the whole series. This strengthens the hypothesis that internal exciplex quenching by oxygen is relevant for **Cu(1)<sub>2</sub>–Cu(4)<sub>2</sub>** and particularly abates the luminescence performance in fluid solution at room temperature. Notably, lifetimes in solid state as powder are very short for **Cu(1)<sub>2</sub>** and **Cu(2)<sub>2</sub>** in line with the behaviour in fluid solution at room temperature. Hence, taken together, photophysical data in the solid state indicate that low temperature is essential to limit parasite luminescence quenching processes.

## Conclusions

The ground state electronic absorption spectra of **Cu(1)<sub>2</sub>–Cu(5)<sub>2</sub>** show the typical MLCT pattern in the Vis spectra region. Their shape and intensity is in line with the behaviour of  $[\text{Cu}(\text{NN})_2]^+$  with 2,9-dialkylphenanthroline ligands. All the compounds exhibit MLCT luminescence centered around 630–650 nm, but emission quantum yields and lifetimes are dramatically different along the series. **Cu(1)<sub>2</sub>–Cu(3)<sub>2</sub>** exhibit vanishingly weak emission features even in a solvent of low nucleophilicity such as toluene ( $\Phi < 1 \times 10^{-5}$ ,  $\tau$  in the range 2.4–6.0 ns). **Cu(4)<sub>2</sub>** is a substantially better luminophore ( $\Phi = 2.5 \times 10^{-4}$ ,  $\tau = 95.3$  ns in oxygen-free solution), but the best performer is **Cu(5)<sub>2</sub>** which exhibits one of the longest MLCT lifetimes detected so far for conventional Cu<sup>I</sup>-bisphenanthroline complexes (420 ns). The poor luminescence behaviour of **Cu(1)<sub>2</sub>–Cu(4)<sub>2</sub>** compared to **Cu(5)<sub>2</sub>** in solution is attributed to a combination of factors, i.e. internal exciplex quenching by oxygen atoms on the phenanthroline residues and a more pronounced tendency to undergo flattening distortion upon light excitation, thanks to smaller steric hindrance.

## Experimental Section

**General:** Reagents and solvents were purchased as reagent grade and used without further purification. Compound **6**,<sup>[31]</sup> and 2,6-dibenzoyloxybenzyl bromide<sup>[43]</sup> were prepared according to the literature. THF was distilled from sodium benzophenone ketyl. All reactions were performed in standard glassware under an inert Ar atmosphere. Evaporation and concentration were done at water aspirator pressure and drying in vacuo at  $10^{-2}$  Torr. Column chromatography: silica gel 60 (230–400 mesh, 0.040–0.063 mm) was purchased from E. Merck. Thin Layer Chromatography (TLC) was performed on glass sheets coated with silica gel 60 F<sub>254</sub> purchased from E. Merck, visualization by UV light. NMR spectra were recorded on a Bruker AC 300 with solvent peaks as reference. Elemental analyses were performed by the analytical service at the Institut Charles Sadron, Strasbourg.

**2,9-Bis[(*tert*-butyldimethylsilyloxy)methyl]-1,10-phenanthroline (1):** A mixture of TBDMSCl (660 mg, 4.38 mmol), imidazole (380 mg, 5.56 mmol) and **6** (500 mg, 2.08 mmol) in DMF (20 mL) was stirred at 0 °C for 4 h and the solvents evaporated. The residue was taken up with CH<sub>2</sub>Cl<sub>2</sub>, washed with brine, dried (MgSO<sub>4</sub>), filtered and the solvents evaporated. Column chromatography (SiO<sub>2</sub>, CH<sub>2</sub>Cl<sub>2</sub>/1% MeOH) yielded **1** (780 mg, 80%). Colourless glassy product. <sup>1</sup>H NMR (CDCl<sub>3</sub>, 300 MHz):  $\delta$  = 8.16 (d,  $J$  = 7 Hz, 2 H, H<sup>4–7</sup>), 7.85 (d,  $J$  = 7 Hz, 2 H, H<sup>3–8</sup>), 7.64 (s, 2 H, H<sup>5–6</sup>), 5.19 (s, 4 H,

CH<sub>2</sub>O), 0.91 (s, 18 H, *t*Bu), 0.10 (s, 12 H, Me) ppm. C<sub>26</sub>H<sub>40</sub>N<sub>2</sub>O<sub>2</sub>Si<sub>2</sub> (468.79): calcd. C 66.62, H 8.60, N 5.98; found C 66.66, H 8.79, N 5.69.

**2,9-Bis[(*triisopropylsilyloxy*)methyl]-1,10-phenanthroline (2):** A mixture of TIPSCl (1.1 mL, 5.19 mmol), imidazole (380 mg, 5.56 mmol) and **6** (500 mg, 2.08 mmol) in DMF (20 mL) was stirred at 0 °C for 24 h and the solvents evaporated. The residue was taken up with CH<sub>2</sub>Cl<sub>2</sub>, washed with brine, dried (MgSO<sub>4</sub>), filtered and the solvents evaporated. Column chromatography (SiO<sub>2</sub>, CH<sub>2</sub>Cl<sub>2</sub>/0.5% MeOH) yielded **2** (836 mg, 73%). Colourless glassy product. <sup>1</sup>H NMR (CDCl<sub>3</sub>, 300 MHz):  $\delta$  = 8.28 (d,  $J$  = 8 Hz, 2 H, H<sup>4–7</sup>), 8.02 (d,  $J$  = 8 Hz, 2 H, H<sup>3–8</sup>), 7.75 (s, 2 H, H<sup>5–6</sup>), 5.36 (s, 4 H, CH<sub>2</sub>O), 1.14 (s, 42 H, *i*Pr) ppm. C<sub>32</sub>H<sub>52</sub>N<sub>2</sub>O<sub>2</sub>Si<sub>2</sub> (552.95): calcd. C 69.51, H 9.48, N 5.07; found C 69.19, H 9.71, N 4.88.

**2,9-Bis[(*tert*-butyldiphenylsilyloxy)methyl]-1,10-phenanthroline (3):** A mixture of TBDPSCl (1.1 mL, 4.22 mmol), imidazole (290 mg, 4.22 mmol) and **6** (406 mg, 1.69 mmol) in DMF (20 mL) was stirred at 0 °C for 48 h and the solvents evaporated. The residue was taken up with CH<sub>2</sub>Cl<sub>2</sub>, washed with brine, dried (MgSO<sub>4</sub>), filtered and the solvents evaporated. Column chromatography (SiO<sub>2</sub>, CH<sub>2</sub>Cl<sub>2</sub>/0.5% MeOH) yielded **3** (1.02 g, 84%). Colourless glassy product. <sup>1</sup>H NMR (CDCl<sub>3</sub>, 300 MHz):  $\delta$  = 8.24 (d,  $J$  = 8 Hz, 2 H, H<sup>4–7</sup>), 8.05 (d,  $J$  = 8 Hz, 2 H, H<sup>3–8</sup>), 7.70 (s, 2 H, H<sup>5–6</sup>), 7.58 (m, 8 H, Ph), 7.35 (m, 12 H, Ph), 5.28 (s, 4 H, CH<sub>2</sub>O), 1.02 (s, 18 H, *t*Bu) ppm. C<sub>46</sub>H<sub>48</sub>N<sub>2</sub>O<sub>2</sub>Si<sub>2</sub> (717.07): calcd. C 77.05, H 6.75, N 3.91; found C 77.00, H 6.86, N 3.82.

**2,9-Bis[2,6-bis(benzoyloxy)phenethyl]-1,10-phenanthroline (4):** A 1.6 M *n*BuLi solution (8.8 mL, 14.1 mmol) was added by syringe at room temperature to an argon-flushed, stirred solution of diisopropylamine (2.2 mL, 16.0 mmol) and *t*BuOK (1.68 g, 15.0 mmol) in dry THF (60 mL) at –78 °C under Ar. After 1 h, the resulting solution was added slowly by means of a double-ended needle to a solution of **7** (1.04 g, 5.0 mmol) in dry THF (80 mL) at –78 °C. After 1 h, a solution of 2,6-dibenzoyloxybenzyl bromide (1.98 g, 14.0 mmol) in THF (25 mL) was added dropwise. The resulting mixture was stirred 2 h at –78 °C, then 12 h at room temperature. The solution was then poured into ice water (150 mL). The mixture was extracted with CH<sub>2</sub>Cl<sub>2</sub> (3 × 100 mL) and the combined organic layers dried (MgSO<sub>4</sub>), filtered and the solvents evaporated. Column chromatography (SiO<sub>2</sub>, CH<sub>2</sub>Cl<sub>2</sub>) yielded **4** (1.98 g, 49%). Colourless glassy product. <sup>1</sup>H NMR (CDCl<sub>3</sub>, 300 MHz):  $\delta$  = 7.86 (d,  $J$  = 8 Hz, 2 H, H<sup>4–7</sup>), 7.54 (s, 2 H, H<sup>5–6</sup>), 7.12–7.02 (m, 24 H, H<sup>3–8</sup> and Ph), 7.00 (t,  $J$  = 7 Hz, 2 H, Ar-H<sub>4</sub>), 6.51 (d,  $J$  = 7 Hz, 4 H, Ar-H<sup>3–5</sup>), 4.97 (s, 8 H, OCH<sub>2</sub>), 3.40 (m, 4 H, CH<sub>2</sub>), 3.29 (m, 4 H, CH<sub>2</sub>) ppm. C<sub>56</sub>H<sub>48</sub>N<sub>2</sub>O<sub>4</sub> (813.01): calcd. C 82.73, H 5.95, N 3.45; found C 82.44, H 6.13, N 3.12.

**2-(1,3-Diphenylpropan-2-yl)-9-phenethyl-1,10-phenanthroline (5):** A 1.6 M *n*BuLi solution (8.8 mL, 14.1 mmol) was added by syringe at room temperature to an argon-flushed, stirred solution of diisopropylamine (2.2 mL, 16.0 mmol) and *t*BuOK (1.68 g, 15.0 mmol) in dry THF (60 mL) at –78 °C under Ar. After 1 h, the resulting solution was added slowly by means of a double-ended needle to a solution of **7** (1.04 g, 5.0 mmol) in dry THF (80 mL) at –78 °C. After 1 h, a solution of benzyl bromide (2.40 mL, 20.0 mmol) in THF (25 mL) was added dropwise. The resulting mixture was stirred 2 h at –78 °C, then 12 h at room temperature. The solution was then poured into ice water (150 mL). The mixture was extracted with CH<sub>2</sub>Cl<sub>2</sub> (3 × 100 mL) and the combined organic layers dried (MgSO<sub>4</sub>), filtered and the solvents evaporated. Column chromatography (SiO<sub>2</sub>, CH<sub>2</sub>Cl<sub>2</sub>) yielded **5** (1.06 g, 44%). Colourless glassy product. <sup>1</sup>H NMR (CD<sub>2</sub>Cl<sub>2</sub>, 300 MHz):  $\delta$  = 8.12 (d,  $J$  = 8 Hz, 1 H, H<sub>4</sub>), 7.97 (d,  $J$  = 8 Hz, 1 H, H<sup>7</sup>), 7.68 (AB,  $J$  = 8 Hz, 2

H,  $H^{5-6}$ ), 7.47 (d,  $J = 8$  Hz, 1 H,  $H^3$ ), 7.44 (d,  $J = 8$  Hz, 1 H,  $H^8$ ), 7.20 (m, 15 H, Ph), 3.88 (m, 1 H, phen-CH), 3.50 (m, 6 H,  $3 \times CH_2$ ), 3.25 (m, 2 H,  $CH_2$ ) ppm.  $C_{35}H_{30}N_2$  (478.64): calcd. C 87.83, H 6.32, N 5.85; found C 87.60, H 6.60, N 5.80.

**General Procedure for the Preparation of the  $Cu^I$  Complexes:** A solution of  $Cu(CH_3CN)_4 \cdot BF_4$  (1 equiv.) in  $CH_3CN$  was added under an argon atmosphere at room temperature to a stirred, degassed solution of the appropriate ligand (2 equiv.) in  $CH_2Cl_2$ . The solution turned orange-red instantaneously, indicating the formation of the complex. After 1 h, the solvents were evaporated. The resulting complexes were purified by recrystallization from  $CH_2Cl_2/Et_2O$ . The  $Cu^I$  complexes were thus obtained as their  $BF_4$  salts in 50–76% yields.

**$Cu(1)_2$ :**  $^1H$  NMR ( $CDCl_3$ , 300 MHz):  $\delta = 8.73$  (d,  $J = 8$  Hz, 4 H,  $H^{4-7}$ ), 8.20 (s, 4 H,  $H^{5-6}$ ), 8.11 (d,  $J = 8$  Hz, 4 H,  $H^{3-8}$ ), 4.47 (s, 8 H,  $CH_2O$ ), 0.59 (s, 36 H,  $tBu$ ),  $-0.37$  (s, 24 H, Me) ppm.  $^{13}C$  NMR ( $CDCl_3$ , 75 MHz):  $\delta = 160.1$ , 142.4, 138.5, 128.9, 127.0, 122.6, 66.2, 25.4, 18.5,  $-6.0$  ppm.  $C_{52}H_{80}BCuF_4N_4O_4Si_4$  (1087.92): calcd. C 57.41, H 7.41, N 5.15; found C 57.55, H 7.44, N 5.34.

**$Cu(2)_2$ :**  $^1H$  NMR ( $CDCl_3$ , 300 MHz):  $\delta = 8.71$  (d,  $J = 8$  Hz, 4 H,  $H^{4-7}$ ), 8.22 (s, 4 H,  $H^{5-6}$ ), 8.12 (d,  $J = 8$  Hz, 4 H,  $H^{3-8}$ ), 4.51 (s, 8 H,  $CH_2O$ ), 0.60 (s, 84 H,  $iPr$ ) ppm.  $^{13}C$  NMR ( $CDCl_3$ , 75 MHz):  $\delta = 160.2$ , 142.3, 138.4, 128.9, 126.9, 122.3, 66.7, 17.4, 11.6 ppm.  $C_{64}H_{104}BCuF_4N_4O_4Si_4$  (1256.25): calcd. C 61.19, H 8.34, N 4.46; found C 61.43, H 8.51, N 4.32.

**$Cu(3)_2$ :**  $^1H$  NMR ( $CDCl_3$ , 300 MHz):  $\delta = 8.55$  (d,  $J = 8$  Hz, 4 H,  $H^{4-7}$ ), 8.01 (s, 4 H,  $H^{5-6}$ ), 7.96 (d,  $J = 8$  Hz, 4 H,  $H^{3-8}$ ), 7.19 (t,  $J = 7$  Hz, 8 H, Ph), 7.02 (m, 16 H, Ph), 6.94 (m, 16 H, Ph), 4.01 (s, 8 H,  $CH_2O$ ), 0.82 (s, 36 H,  $tBu$ ) ppm.  $^{13}C$  NMR ( $CDCl_3$ , 75 MHz):  $\delta = 158.9$ , 141.7, 137.9, 134.7, 131.6, 131.1, 129.9, 128.3, 127.5, 127.1, 126.7, 121.9, 66.3, 26.5, 18.9 ppm.  $C_{92}H_{96}BCuF_4N_4O_4Si_4$  (1584.49): calcd. C 69.74, H 6.11, N 3.54; found C 69.69, H 6.25, N 3.33.

**$Cu(4)_2$ :**  $^1H$  NMR ( $CDCl_3$ , 300 MHz):  $\delta = 7.84$  (d,  $J = 8$  Hz, 4 H,  $H^{4-7}$ ), 7.68 (s, 4 H,  $H^{5-6}$ ), 7.10 (m, 28 H,  $H^{3-8}$  and Ph), 6.80 (m, 20 H, Ph and Ar- $H_4$ ), 6.15 (d,  $J = 7$  Hz, 8 H), 2.84 (m, 8 H,  $CH_2$ ), 2.71 (m, 8 H,  $CH_2$ ) ppm.  $^{13}C$  NMR ( $CDCl_3$ , 75 MHz):  $\delta = 161.6$ , 156.8, 142.8, 136.9, 136.2, 128.3, 127.4, 126.4, 125.8, 116.9, 104.9, 69.5, 39.2, 22.6 ppm.  $C_{112}H_{96}BCuF_4N_4O_8 \cdot H_2O$  (1794.38): calcd. C 74.97, H 5.50, N 3.12; found C 74.76, H 5.47, N 3.12.

**$Cu(5)_2$ :**  $^1H$  NMR ( $CDCl_3$ , 300 MHz):  $\delta = 8.68$  (d,  $J = 8$  Hz, 2 H,  $H_4$ ), 8.63 (d,  $J = 8$  Hz, 2 H,  $H_7$ ), 8.02 (s, 4 H,  $H^{5-6}$ ), 7.80 (d,  $J = 8$  Hz, 2 H,  $H^3$ ), 7.70 (d,  $J = 8$  Hz, 2 H,  $H^8$ ), 6.80 (m, 14 H, Ph), 6.68 (m, 4 H, Ph), 6.22 (m, 4 H, Ph), 6.13 (m, 4 H, Ph), 6.04 (m, 4 H, Ph), 3.50 (m, 2 H, phen-CH), 2.71 (m, 4 H,  $2 \times CH_2$ ), 2.50 (m, 8 H,  $4 \times CH_2$ ) ppm.  $^{13}C$  NMR ( $CDCl_3$ , 75 MHz):  $\delta = 163.5$ , 160.6, 143.4, 143.1, 139.2, 137.9, 137.8, 137.75, 128.7, 128.5, 128.3, 128.1, 127.9, 127.1, 126.9, 126.7, 126.3, 125.0, 123.9, 52.3, 41.1, 39.9, 38.5, 34.5 ppm.  $C_{70}H_{60}BCuF_4N_4$  (1107.62): calcd. C 75.91, H 5.46, N 5.06; found C 75.81, H 5.51, N 5.02.

**Electrochemistry:** The cyclic voltammetric measurements were carried out with a potentiostat Autolab PGSTAT100. Experiments were performed at room temperature in a homemade airtight three-electrode cell connected to a vacuum/argon line. The reference electrode consisted of a saturated calomel electrode (SCE) separated from the solution by a bridge compartment. The counter electrode was a platinum wire of ca 1 cm<sup>2</sup> apparent surface. The working electrode was a Pt microdisk (0.5 mm diameter). The supporting electrolyte [ $nBu_4N$ ][ $BF_4$ ] (Fluka, 99% electrochemical grade) was used as received and simply degassed under argon. Dichloromethane was freshly distilled from  $CaH_2$  prior to use. The

solutions used during the electrochemical studies were typically  $10^{-3}$  M in compound and 0.1 M in supporting electrolyte. Before each measurement, the solutions were degassed by bubbling Ar and the working electrode was polished with a polishing machine (Presi P230). Under these experimental conditions,  $Fe^+/Fe$  is observed at  $+0.54 \pm 0.01$  V vs. SCE.

**Spectroscopic Measurements:** Absorption spectra were recorded with a Perkin–Elmer  $\lambda 9$  spectrophotometer. For luminescence experiments, the samples were placed in fluorimetric 1-cm path cuvettes and, when necessary, purged from oxygen by bubbling with argon. Uncorrected emission spectra were obtained with an Edinburgh FLS920 spectrometer equipped with a peltier-cooled Hamamatsu R928 photomultiplier tube (185–850 nm). An Edinburgh Xe900 450 W Xenon arc lamp was used as exciting light source. Corrected spectra were obtained via a calibration curve supplied with the instrument. Luminescence quantum yields ( $\Phi_{em}$ ) in solution obtained from spectra on a wavelength scale [nm] were measured according to the approach described by Demas and Crosby<sup>[44]</sup> using air-equilibrated  $[Ru(bpy)_3]Cl_2$  in water solution,  $\Phi_{em} = 0.028$ <sup>[45]</sup> as standard. Emission lifetimes were determined with the single photon counting technique by means of the same Edinburgh FLS920 spectrometer using a laser diode as excitation source (1 MHz,  $\lambda_{exc} = 407$  nm, 200 ps time resolution after deconvolution) and the above-mentioned PMTs as detectors. Or, with an IBH single-photon counting spectrometer equipped with a thyatron-gated nitrogen lamp working in the range 2–40 kHz (0.5 ns time resolution); the detector was a red-sensitive (185–850 nm) Hamamatsu R-3237–01 photomultiplier tube. To record the 77 K luminescence spectra, the samples were put in glass tubes (2 mm diameter) and inserted in a special quartz dewar, filled up with liquid nitrogen. Experimental uncertainties are estimated to be  $\pm 8\%$  for lifetime determinations,  $\pm 20\%$  for emission quantum yields,  $\pm 2$  nm and  $\pm 5$  nm for absorption and emission peaks respectively.

**X-ray Crystal Structure of  $Cu(1)_2$ :** The orange crystal used for the diffraction study ( $0.15 \times 0.10 \times 0.05$  mm) was produced by slow diffusion of  $Et_2O$  into a  $CH_2Cl_2$  solution of  $Cu(5)_2$ . Single crystals of complex  $Cu(1)_2$  was mounted on a Nonius Kappa-CCD area detector diffractometer ( $\lambda_{Mo-K\alpha} = 0.71073$  Å). The structure was solved by direct methods (SHELXS97)<sup>[46]</sup> and refined against  $F^2$  using the SHELXL97 software (Table 4).<sup>[47]</sup> The absorption was non-corrected. Excepted for the F atoms of the  $BF_4$  counter anion, all non-hydrogen atoms were refined anisotropically. Hydrogen atoms were generated according to stereo-chemistry and refined using a riding model in SHELXL97.

**X-ray Crystal Structure of  $Cu(5)_2$ :** The red crystal used for the diffraction study ( $0.20 \times 0.25 \times 0.35$  mm) was produced by slow diffusion of  $Et_2O$  into a  $CH_2Cl_2$  solution of  $Cu(5)_2$ . Data were collected at low temperature on an Oxford-Diffraction XCALIBUR CCD diffractometer using a graphite-monochromated Mo- $K\alpha$  radiation ( $\lambda = 0.71073$  Å) and equipped with an Oxford Cryosystems Cryostream Cooler Device. The structure was solved by direct methods using SIR92,<sup>[48]</sup> and refined by means of least-squares procedures on  $F$  using the programs of the PC version of CRYSTALS (Table 4).<sup>[49]</sup> Atomic scattering factors were taken from the International tables for X-ray Crystallography.<sup>[50]</sup> All non-hydrogen atoms were refined anisotropically. Hydrogen atoms were refined using a riding model.

CCDC-739310 [for  $Cu(1)_2$ ] and -737783 [for  $Cu(5)_2$ ] contain the supplementary crystallographic data for this paper. These data can be obtained free of charge from The Cambridge Crystallographic Data Centre via [www.ccdc.cam.ac.uk/data\\_request/cif](http://www.ccdc.cam.ac.uk/data_request/cif).

Table 4. Crystallographic and structure refinement data for compounds **Cu(1)<sub>2</sub>** and **Cu(5)<sub>2</sub>**.

|  | <b>Cu(1)<sub>2</sub></b>  | <b>Cu(5)<sub>2</sub></b>  |
|--|---|---------------------------|
| Chemical formula   | C <sub>52</sub> H <sub>80</sub> BCuF <sub>4</sub> N <sub>4</sub> O <sub>4</sub> Si <sub>4</sub> ·Et <sub>2</sub> O·C <sub>70</sub> H <sub>60</sub> BCuF <sub>4</sub> N <sub>4</sub> |                           |
| Formula weight   | 1162.03   | 1107.62                   |
| Crystal system   | monoclinic  | orthorhombic              |
| Space group  | <i>P</i> 2 <sub>1</sub> / <i>n</i>  | <i>Pna</i> 2 <sub>1</sub> |
| <i>a</i> [Å]   | 11.6980(10)   | 23.1526(6)                |
| <i>b</i> [Å]   | 32.578(5)   | 11.7421(3)                |
| <i>c</i> [Å]   | 17.806(2)   | 20.9595(5)                |
| <i>α</i> [°]   | 90  | 90                        |
| <i>β</i> [°]   | 107.86(5)   | 90                        |
| <i>γ</i> [°]   | 90  | 90                        |
| <i>V</i> [Å <sup>3</sup> ]                               | 6458.8(13)  | 5698.1(2)                 |
| <i>Z</i>   | 4   | 4                         |
| Density  | 1.195   | 1.291                     |
| <i>μ</i> (Mo- <i>K<sub>α</sub></i> ) [mm <sup>-1</sup> ] | 0.469   | 0.443                     |
| <i>F</i> (000)   | 2480  | 2312                      |
| <i>T</i> [K]   | 173   | 160                       |
| Reflections collected                                    | 18686   | 52557                     |
| Independent reflections                                  | 18686   | 14050                     |
| Reflections used in the calculation                      | 8645 [ <i>I</i> > 2σ]   | 4878 [ <i>I</i> > 3σ]     |
| Parameters   | 673   | 466                       |
| Goodness-of-fit on <i>F</i>                              | 1.154   | 1.0773                    |
| <i>R</i>   | 0.0920  | 0.0733                    |
| <i>wR</i>  | 0.2403  | 0.0857                    |

**Supporting Information** (see also the footnote on the first page of this article): Emission spectra of **Cu(1)<sub>2</sub>**, **Cu(2)<sub>2</sub>** and **Cu(3)<sub>2</sub>** in toluene.

## Acknowledgments

This work was supported by the Italian National Research Council (PM.P04.010, MACOL), the Centre National de la Recherche Scientifique (CNRS) (UMR 7509, UPR 8241) and the European Commission (OLLA IST-2002-004607, ITN FINELUMEN, PITN-GA-2008-215399). We thank Mr. Roberto Cortesi for technical assistance.

- [1] P. G. Sammes, G. Yahiolglu, *Chem. Soc. Rev.* **1994**, 23, 327–334.
- [2] G. Accorsi, A. Listorti, K. Yoosaf, N. Armaroli, *Chem. Soc. Rev.* **2009**, 38, 1690–1700.
- [3] A. Bencini, M. A. Bernardo, A. Bianchi, V. Fusi, C. Giorgi, F. Pina, B. Valtancoli, *Eur. J. Inorg. Chem.* **1999**, 1911–1918.
- [4] K. Hayashi, H. Akutsu, H. Ozaki, H. Sawai, *Chem. Commun.* **2004**, 1386–1387.
- [5] F. Vögtle, I. Lüer, V. Balzani, N. Armaroli, *Angew. Chem. Int. Ed. Engl.* **1991**, 30, 1333–1336.
- [6] D. J. Cardenas, J. P. Collin, P. Gaviña, J. P. Sauvage, A. De Cian, J. Fischer, N. Armaroli, L. Flamigni, V. Vicinelli, V. Balzani, *J. Am. Chem. Soc.* **1999**, 121, 5481–5488.
- [7] N. Armaroli, G. Accorsi, J. P. Gisselbrecht, M. Gross, J. F. Eckert, J. F. Nierengarten, *New J. Chem.* **2003**, 27, 1470–1478.
- [8] Y. Leydet, D. M. Bassani, G. Jonusauskas, N. D. McClenaghan, *J. Am. Chem. Soc.* **2007**, 129, 8688–8689.
- [9] M. Schmittel, B. He, *Chem. Commun.* **2008**, 4723–4725.
- [10] M. Schmittel, P. Mal, *Chem. Commun.* **2008**, 960–962.
- [11] S. Bonnet, J. P. Collin, M. Koizumi, P. Mobian, J. P. Sauvage, *Adv. Mater.* **2006**, 18, 1239–1250.
- [12] D. R. McMillin, K. M. McNett, *Chem. Rev.* **1998**, 98, 1201–1219.
- [13] D. V. Scaltrito, D. W. Thompson, J. A. O'Callaghan, G. J. Meyer, *Coord. Chem. Rev.* **2000**, 208, 243–266.
- [14] N. Armaroli, *Chem. Soc. Rev.* **2001**, 30, 113–124.
- [15] N. Armaroli, G. Accorsi, F. Cardinali, A. Listorti, *Top. Curr. Chem.* **2007**, 280, 69–115.
- [16] A. Lavie-Cambot, M. Cantuel, Y. Leydet, G. Jonusauskas, D. M. Bassani, N. D. McClenaghan, *Coord. Chem. Rev.* **2008**, 252, 2572–2584.
- [17] A. Barbieri, G. Accorsi, N. Armaroli, *Chem. Commun.* **2008**, 2185–2193.
- [18] N. Robertson, *ChemSusChem* **2008**, 1, 977–979.
- [19] N. Alonso-Vante, J.-F. Nierengarten, J.-P. Sauvage, *J. Chem. Soc., Dalton Trans.* **1994**, 1649–1654; T. Bessho, E. C. Constable, M. Graetzel, A. H. Redondo, C. E. Housecroft, W. Klyberg, M. K. Nazeeruddin, M. Neuburger, S. Schaffner, *Chem. Commun.* **2008**, 3717–3719.
- [20] M. T. Miller, P. K. Gantzel, T. B. Karpishin, *J. Am. Chem. Soc.* **1999**, 121, 4292–4293.
- [21] B. A. Gandhi, O. Green, J. N. Burstyn, *Inorg. Chem.* **2007**, 46, 3816–3825.
- [22] O. Green, B. A. Gandhi, J. N. Burstyn, *Inorg. Chem.* **2009**, 48, 5704–5714.
- [23] R. M. Everly, D. R. McMillin, *Photochem. Photobiol.* **1989**, 50, 711–716.
- [24] L. X. Chen, *Annu. Rev. Phys. Chem.* **2005**, 56, 221–254.
- [25] L. X. Chen, *Angew. Chem. Int. Ed.* **2004**, 43, 2886–2905.
- [26] P. Coppens, I. I. Vorontsov, T. Graber, A. Y. Kovalevsky, Y. S. Chen, G. Wu, M. Gembicky, I. V. Novozhilova, *J. Am. Chem. Soc.* **2004**, 126, 5980–5981.
- [27] G. B. Shaw, C. D. Grant, H. Shirota, E. W. Castner, G. J. Meyer, L. X. Chen, *J. Am. Chem. Soc.* **2007**, 129, 2147–2160.
- [28] T. Gunaratne, M. A. J. Rodgers, D. Felder, J. F. Nierengarten, G. Accorsi, N. Armaroli, *Chem. Commun.* **2003**, 3010–3011.
- [29] L. X. Chen, G. B. Shaw, I. Novozhilova, T. Liu, G. Jennings, K. Attenkofer, G. J. Meyer, P. Coppens, *J. Am. Chem. Soc.* **2003**, 125, 7022–7034.
- [30] D. G. Cuttall, S. M. Kuang, P. E. Fanwick, D. R. McMillin, R. A. Walton, *J. Am. Chem. Soc.* **2002**, 124, 6–7; L. Yang, J. K. Feng, A. M. Ren, M. Zhang, Y. G. Ma, X. D. Liu, *Eur. J. Inorg. Chem.* **2005**, 1867–1879; N. Armaroli, G. Accorsi, M. Holler, O. Moudam, J.-F. Nierengarten, Z. Zhou, R. T. Wegh, R. Welter, *Adv. Mater.* **2006**, 18, 1313–1316; A. J. M. Miller, J. L. Dempsey, J. C. Peters, *Inorg. Chem.* **2007**, 46, 7244–7246.
- [31] C. J. Chandler, L. W. Deady, J. A. Reiss, *J. Heterocycl. Chem.* **1981**, 18, 599–601.
- [32] C. T. Cunningham, J. J. Moore, K. L. H. Cunningham, P. E. Fanwick, D. R. McMillin, *Inorg. Chem.* **2000**, 39, 3638–3644, and references cited therein.
- [33] E. Gumienna-Kontecka, Y. Rio, C. Bourgogne, M. Elhabiri, R. Louis, A.-M. Albrecht-Gary, J.-F. Nierengarten, *Inorg. Chem.* **2004**, 43, 3200–3209.
- [34] Y.-R. Hong, C. B. Gorman, *J. Org. Chem.* **2003**, 68, 9019–9025.
- [35] P. Federlin, J.-M. Kern, A. Rastegar, C. O. Dietrich-Buchecker, P. A. Marnot, J.-P. Sauvage, *New J. Chem.* **1990**, 14, 9–12.
- [36] Y. Rio, G. Accorsi, N. Armaroli, D. Felder, E. Levillain, J.-F. Nierengarten, *Chem. Commun.* **2002**, 2830–2831.
- [37] D. Felder, J. F. Nierengarten, F. Barigelletti, B. Ventura, N. Armaroli, *J. Am. Chem. Soc.* **2001**, 123, 6291–6299.
- [38] V. Kalsani, M. Schmittel, A. Listorti, G. Accorsi, N. Armaroli, *Inorg. Chem.* **2006**, 45, 2061–2067.
- [39] R. M. Everly, R. Ziessel, J. Suffert, D. R. McMillin, *Inorg. Chem.* **1991**, 30, 559–561.
- [40] M. T. Miller, P. K. Gantzel, T. B. Karpishin, *Angew. Chem. Int. Ed.* **1998**, 37, 1556–1558.
- [41] Z. A. Siddique, Y. Yamamoto, T. Ohno, K. Nozaki, *Inorg. Chem.* **2003**, 42, 6366–6378.
- [42] M. Holler, F. Cardinali, H. Mamlouk, J. F. Nierengarten, J. P. Gisselbrecht, M. Gross, Y. Rio, F. Barigelletti, N. Armaroli, *Tetrahedron* **2006**, 62, 2060–2073.
- [43] C. Rosini, S. Superchi, H. W. I. Peerlings, E. W. Meijer, *Eur. J. Org. Chem.* **2000**, 61–71.
- [44] J. N. Demas, G. A. Crosby, *J. Phys. Chem.* **1971**, 75, 991–1024.
- [45] K. Nakamaru, *Bull. Chem. Soc. Jpn.* **1982**, 55, 2697–2705.

- [46] *Kappa CCD Operation Manual*, B. V. Nonius, Delft, The Netherlands, **1997**.
- [47] G. M. Sheldrick, *SHELXL97*, Program for the refinement of crystal structures; University of Göttingen, Germany, **1997**.
- [48] A. Altomare, G. Cascarano, C. Giacovazzo, A. Guagliardi, *J. Appl. Crystallogr.* **1993**, 26, 343–350.
- [49] P. W. Betteridge, J. R. Carruthers, R. I. Cooper, K. Prout, D. J. Watkin, *J. Appl. Crystallogr.* **2003**, 36, 1487.
- [50] *International Tables for X-ray Crystallography*, Kynoch Press, Birmingham, England, **1974**, vol. IV.

Received: September 23, 2009  
Published Online: December 2, 2009

# Neutral Trinuclear Palladium(II) Metalloclusters with Mixed Phosphane/Pyridine-4-thiolato Ligands and Their Catalytic Tests in Suzuki–Miyaura Coupling Reactions

Hui Wang,<sup>[a]</sup> Rui Zhong,<sup>[a]</sup> Xu-Qing Guo,<sup>[a]</sup> Xiao-Yan Feng,<sup>[a]</sup> and Xiu-Feng Hou\*<sup>[a]</sup>

**Keywords:** Palladium / Metalloclusters / Pyridinethiolate / Phosphanes / Catalytic tests / Suzuki–Miyaura cross-coupling reactions

Three neutral trinuclear palladium(II) complexes  $[\text{Ph}_3\text{PPdCl}(\mu\text{-4-PyS})]_3$  (**1**),  $[\text{Cy}_3\text{PPdCl}(\mu\text{-4-PyS})]_3$  (**2**) and  $[(\text{PhO})_3\text{PPdCl}(\mu\text{-4-PyS})]_3$  (**3**) (4-PyS = pyridine-4-thiolate) were self-assembled from corresponding metal fragments  $[\text{R}_3\text{PPdCl}_2]_2$  with lithium pyridine-4-thiolate (PySLi). The crystal structure reveals that complex **1** possesses a triangular macrocyclic structure in which the distances of Pd(1)⋯Pd(2), Pd(2)⋯Pd(3) and Pd(3)⋯Pd(1) are 7.764, 7.684 and

7.944 Å, respectively. An equilibrium between trinuclear complex **1** and mononuclear complex  $(\text{Ph}_3\text{P})_2\text{PdCl}(4\text{-PyS})$  (**4**) in solution through coordination and de-coordination of the  $\text{PPh}_3$  ligand is confirmed by  $^{31}\text{P}$  NMR spectroscopy. A comparative study on the Suzuki–Miyaura coupling reaction showed that complexes **1** and **2** are more active precatalysts than  $[\text{R}_3\text{PPdCl}_2]_2$  complexes without a PyS group.

## Introduction

In the past few years, there has been great interest in supramolecular chemistry, since self-assembly of discrete molecular architectures by using polytopic organic ligands and transition metal complexes has proven a powerful tool for constructing rings, polymers and networks. Some of these compounds have potential applications in molecular recognition, catalysis, optical materials, molecular magnetism, semiconductors, etc.<sup>[1]</sup> In particular, square-planar palladium(II) complexes have been widely used to construct numerous polygons, cages and catenanes with suitable linear, angular or flexible bridging ligands.<sup>[2]</sup> Within the wide range of supramolecular architectures reported, the number of molecular triangles is relatively small due to the lack of suitable building blocks with proper turning angles.<sup>[3]</sup>

To the best of our knowledge, pyridinethiolato ligands display a great versatility of coordination chemistry with metal centers through their tautomeric and mesomeric forms,<sup>[4]</sup> in which pyridine-4-thiolato is a potential bridge ligand, since the sulfur atom and nitrogen atom can act as terminal coordination donors. The less rigid structure and proper turning angle both mean that the pyridine-4-thiolato ligand is a suitable building block for the self-assembly of triangular supramolecules.<sup>[5]</sup> In this paper, we report our successful preparation of three neutral triangular macro-

cycles with  $(\text{R}_3\text{P})\text{PdCl}$  at the corner and pyridine-4-thiolato as the bridging ligand. We also find that these triangular palladium complexes exhibit catalytic activity in the Suzuki–Miyaura cross-coupling reactions.

## Results and Discussion

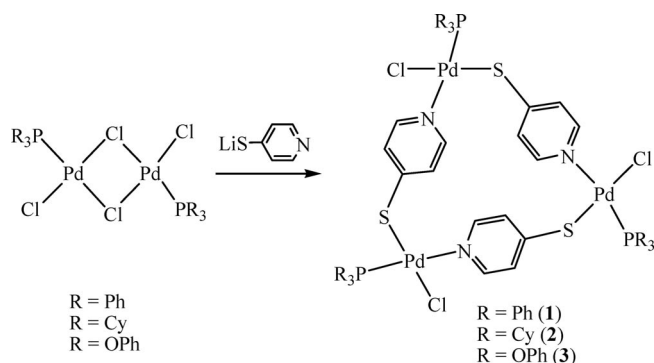
### Self-Assembly Reactions of **1**, **2** and **3** with 4-Pyridinethiolate

The treatment of  $[\text{Ph}_3\text{PPdCl}_2]_2$  with 2 equiv. of lithium pyridine-4-thiolate in thf resulted in the formation of  $[\text{Ph}_3\text{PPdCl}(\mu\text{-4-PyS})]_3$  (**1**) as orange crystals in good yield (Scheme 1). The  $^{31}\text{P}$  NMR spectrum shows a unique signal at  $\delta = 32.35$  ppm. Two doublet peaks ( $\delta = 8.18, 6.95$  ppm) for the pyridine-4-thiolato ligand and three peaks ( $\delta = 7.68, 7.44, 7.38$  ppm) for  $\text{PPh}_3$  are displayed in the aromatic hydrogen region of the  $^1\text{H}$  NMR spectrum.

Single crystals of complex **1** suitable for X-ray diffraction analysis were obtained by slow diffusion of hexane into a concentrated solution of the complex in dichloromethane at low temperature. As shown in Figure 1, the crystal structure reveals that complex **1** possesses a triangular macrocyclic structure in which the  $(\text{PPh}_3)\text{PdCl}$  moiety holds the vertices, and as a nonlinear bridging motif, the 4-PyS ligand is the edge of the triangle through the coordination of the sulfur atom and the nitrogen atom to two palladium atoms. The distances of Pd(1)⋯Pd(2), Pd(2)⋯Pd(3) and Pd(3)⋯Pd(1) are 7.764, 7.684 and 7.944 Å, respectively. The slightly distorted square-planar geometry around each palladium center comprises the Cl atom, the P atom of  $\text{PPh}_3$ , and the S

[a] Department of Chemistry, Fudan University, Han Dan Road 220, Shanghai 200433, P. R. China  
Fax: +86-21-65641740  
E-mail: xfhou@fudan.edu.cn

Supporting information for this article is available on the WWW under <http://dx.doi.org/10.1002/ejic.200900895>.

Scheme 1. Synthesis of complexes **1**, **2** and **3**.

and N atoms from different 4-PyS bridges, in which the two coordinating bonds, Pd–P and Pd–N, are opposite. Three Pd–S–C angles within the macrocycle (105.2, 106.8 and 111.7°, respectively) are smaller than the M–S–C angles in similar Rh and Ir complexes,<sup>[5e,5f]</sup> which means a bigger strain. In some cases, there exists an equilibrium between trinuclear and tetranuclear cycles in solution because of such a strain,<sup>[3g,3h,6]</sup> but the unique signal in the <sup>31</sup>P NMR spectrum proves that only the triangular structure exists in this system. As shown in Figure 2, the molecular rectangles stack along the *a* axis to form triangle channels due to the  $\pi$ – $\pi$  interactions between the independent molecules.

When [Cy<sub>3</sub>PPdCl<sub>2</sub>]<sub>2</sub> was used in place of [Ph<sub>3</sub>PPdCl<sub>2</sub>]<sub>2</sub>, the reaction solution changed from a brown mixture to a clear yellow solution after about 3 h, and yellow acicular crystals of [Cy<sub>3</sub>PdCl(μ-4-PyS)]<sub>3</sub> (**2**) formed by slow diffusion of hexane into a concentrated dichloromethane solution at low temperature. There is only one peak at  $\delta = 45.52$  ppm in the <sup>31</sup>P NMR spectrum of complex **2**. Two doublet peaks ( $\delta = 8.23, 7.12$  ppm) for the pyridine-4-thiolato ligand at low field and multiple peaks ( $\delta = 2.57, 1.96$ – $1.64$  ppm) for PCy<sub>3</sub> at high field are appear in the <sup>1</sup>H NMR spectrum.

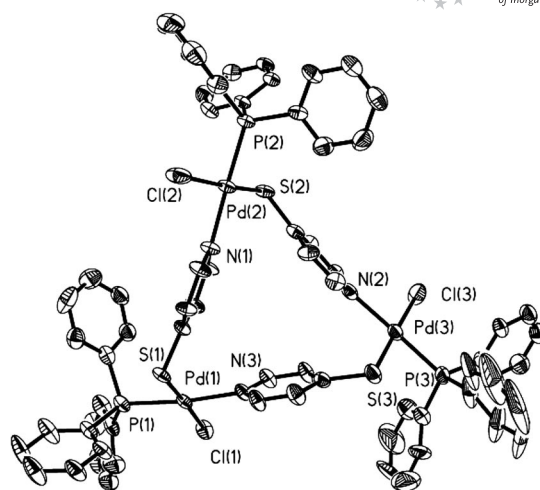


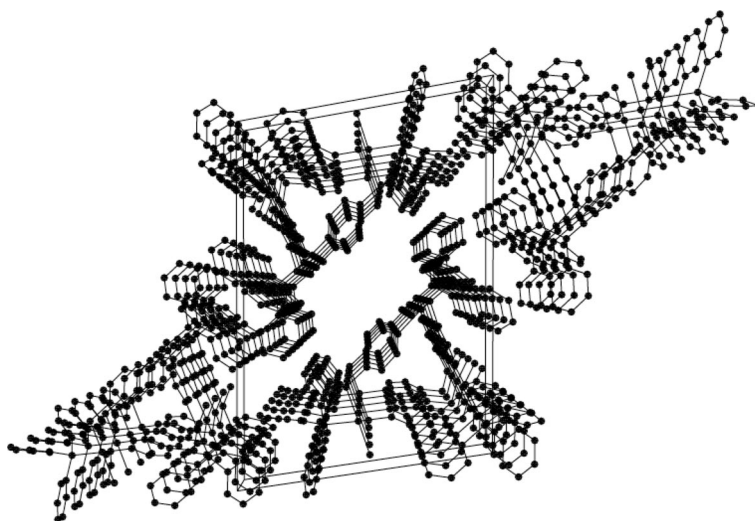
Figure 1. Molecular structure of **1**, ellipsoids at the 30% probability level. H atoms are omitted for clarity. Selected bond lengths [Å] and angles [°]: Pd(1)–Cl(1) 2.311(3), Pd(1)–N(3) 2.118(8), Pd(1)–S(1) 2.293(3), Pd(1)–P(1) 2.241(3), S(1)–C(1) 1.722(10); N(3)–Pd(1)–S(1) 90.6(2), N(3)–Pd(1)–Cl(1) 90.1(3), Cl(1)–Pd(1)–S(1) 176.48(11), N(3)–Pd(1)–P(1) 173.5(3), Pd(1)–S(1)–C(1) 106.8(4).

A similar reaction of [(PhO)<sub>3</sub>PPdCl<sub>2</sub>]<sub>2</sub> with lithium pyridine-4-thiolate gave [(PhO)<sub>3</sub>PPdCl(μ-4-PyS)]<sub>3</sub> (**3**) as an orange solid. Although complexes **1** and **2** have a high solubility in common organic solvents, complex **3** is insoluble in common solvents.

### Equilibrium between Trinuclear and Mononuclear Complexes

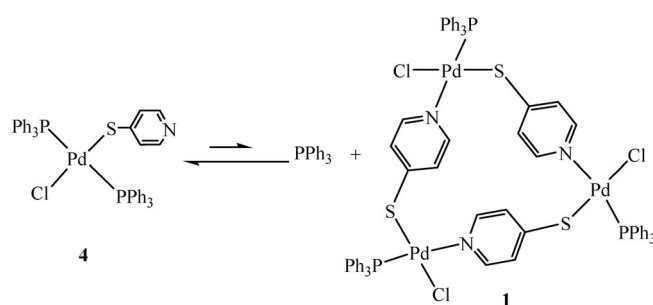
When excess PPh<sub>3</sub> was added to a solution of [Ph<sub>3</sub>PPdCl(μ-4-PyS)]<sub>3</sub> (**1**) in CDCl<sub>3</sub>, the color of the mixture turned from orange to red immediately.

In the <sup>31</sup>P NMR spectrum, the signal at  $\delta = 32.35$  ppm for complex **1** disappeared, and two new peaks appeared. One is for PPh<sub>3</sub> at  $\delta = -4.42$  ppm, and the other ( $\delta =$

Figure 2. Crystal packing diagram of **1** viewed along the *a* axis.

25.39 ppm) is assigned the mononuclear palladium complex ( $\text{Ph}_3\text{P}$ )<sub>2</sub>PdCl(4-PyS) (**4**). However, all efforts to obtain pure samples of **4** failed.

In order to clarify our results, we tried to synthesize the mononuclear complex **4** by direct reaction of ( $\text{Ph}_3\text{P}$ )<sub>2</sub>PdCl<sub>2</sub> with 1 equiv. of lithium pyridine-4-thiolate. However, although the product was isolated and recrystallized repeatedly, it still was a mixture of **4**, **1** and  $\text{PPh}_3$  as confirmed by <sup>31</sup>P NMR spectroscopy ( $\delta$  = 25.39 ppm for **4**,  $\delta$  = 32.31 ppm for **1**,  $\delta$  = -4.42 ppm for  $\text{PPh}_3$ ). It is likely that the complex **4** produced decomposed partially in solution to give  $\text{PPh}_3$ , and the residual  $\text{Ph}_3\text{PPdCl}(4\text{-PyS})$  moiety reassembled through coordination of the nitrogen atom of the pyridine ring with the palladium center to give trinuclear complex **1** (Scheme 2). The conversion of complex **4** to **1** can be observed in their <sup>31</sup>P NMR spectra by washing the solid mix-



Scheme 2. Equilibrium between complexes **4** and **1**.

ture repeatedly with  $\text{Et}_2\text{O}$  (see Supporting Information). Reasonably pure **4** may be isolated in the presence of excess  $\text{PPh}_3$ , but analytically pure samples could not be obtained. A similar equilibrium was also found in  $\text{Pt}^{\text{II}}$  compounds by Krinsky.<sup>[7]</sup>

### Suzuki–Miyaura Cross-Coupling Reactions by Using Palladium Complexes

It is now well established that palladium complexes containing bulky phosphanes, which combine both a good  $\sigma$ -donor strength and a  $\pi$ -accepting capacity, always have a high catalytic activity in Suzuki–Miyaura cross-coupling reactions;<sup>[8]</sup> therefore we attempted to use our palladium(II) metallocycles **1** or **2** in this well-known process.

The palladium complexes catalyze the cross-coupling reactions of aryl bromide and aryl boronic acid to afford the desired biaryls in good yields at 100 °C by using toluene as solvent (Table 1).

Complexes **1** and **2** bearing the PyS ligand are quite effective precatalysts in these reactions to give the corresponding coupled products in better yields than [ $\text{R}_3\text{PPdCl}_2$ ], which indicates that no metal-poisoning occurs in the presence of a sulfide group in the catalyst. Side products derived from the reduction or homocoupling of the aryl halides were not detected at all or were observed only in trace amounts. The higher activities of the  $\text{PCy}_3$  complexes (Entries 3 and 4) relative to the  $\text{PPh}_3$  complexes (Entries 1

Table 1. Suzuki–Miyaura cross-coupling of aryl bromide with aryl boronic acid.<sup>[a]</sup>

| Entry | Precatalysts                  | Halide + boronic acid |                     | Products | Yield <sup>[b]</sup> (%) |
|-------|-------------------------------|-----------------------|---------------------|----------|--------------------------|
| 1     | $[\text{Ph}_3\text{PPdCl}_2]$ | Br-                   | -B(OH) <sub>2</sub> |          | 46                       |
| 2     | $[\text{Ph}_3\text{PPdCl}_2]$ | Br-                   | -B(OH) <sub>2</sub> |          | 32                       |
| 3     | $[\text{Cy}_3\text{PPdCl}_2]$ | Br-                   | -B(OH) <sub>2</sub> |          | 62                       |
| 4     | $[\text{Cy}_3\text{PPdCl}_2]$ | Br-                   | -B(OH) <sub>2</sub> |          | 50                       |
| 5     | <b>1</b>                      | Br-                   | -B(OH) <sub>2</sub> |          | 69                       |
| 6     | <b>1</b>                      | Br-                   | -B(OH) <sub>2</sub> |          | 58                       |
| 7     | <b>1</b>                      | Br-                   | -B(OH) <sub>2</sub> |          | 92                       |
| 8     | <b>1</b>                      | Br-                   | -B(OH) <sub>2</sub> |          | 76                       |
| 9     | <b>1</b>                      | Br-                   | -B(OH) <sub>2</sub> |          | 97                       |
| 10    | <b>1</b>                      | Br-                   | -B(OH) <sub>2</sub> |          | 96                       |
| 11    | <b>1</b>                      | Br-                   | -B(OH) <sub>2</sub> |          | 77                       |
| 12    | <b>1</b>                      | Br-                   | -B(OH) <sub>2</sub> |          | 98                       |
| 13    | <b>2</b>                      | Br-                   | -B(OH) <sub>2</sub> |          | 70                       |
| 14    | <b>2</b>                      | Br-                   | -B(OH) <sub>2</sub> |          | 59                       |

[a] Reaction conditions: Aryl bromide (1 mmol), aryl boronic acid (1.5 mmol),  $\text{K}_2\text{CO}_3$  as base (2 mmol), catalyst (0.1% Pd), toluene (5 mL), 100 °C, 10 h. [b] Yields were determined by <sup>1</sup>H NMR spectroscopy.

and 2) can be attributed to the faster de-coordination of the labile  $\text{PCy}_3$  ligand and facile formation of the  $\text{Pd}^0$  species.<sup>[9]</sup> However, the close activities of complex **1** and **2** should result from the presence of the PyS group. Without any attempt to optimize the reaction conditions, these experiments have demonstrated that the trinuclear palladium(II) complexes **1** and **2** with mixed phosphane and pyridine-4-thiolato ligands are effective precatalysts for the cross-coupling of aryl bromides containing both electron-donating and electron-withdrawing substituents.

## Conclusions

Three neutral trinuclear palladium(II) complexes with mixed phosphane and pyridine-4-thiolato ligands are synthesized. Single-crystal X-ray diffraction shows a triangular structure in which the 4-PyS ligand plays a role as a nonlinear bridging motif, and a unique signal in the  $^{31}\text{P}$  NMR spectrum proves that only the triangle exists in this system. With the help of  $^{31}\text{P}$  NMR spectroscopy, we found an equilibrium between the trinuclear complex **1** and the mononuclear complex **4** in solution through coordination and de-coordination of the  $\text{PPh}_3$  ligand. A preliminary study on Suzuki–Miyaura couplings shows that the novel trinuclear  $\text{Pd}^{\text{II}}$  complexes with a PyS bridge are more active precatalysts than  $[\text{R}_3\text{PPdCl}_2]_2$  complexes. Research in our laboratory is underway to extend the synthetic methodology to other transition metals as well as to widen the scope of these palladium complexes in catalysis.

## Experimental Section

**General:** All reactions and manipulations were carried out under nitrogen by using standard Schlenk techniques. Solvents were dried and deoxygenated by an M. Braun Solvent Purification System (4464) and collected just before use.  $[\text{Ph}_3\text{PPdCl}_2]_2$ ,  $[\text{Cy}_3\text{PPdCl}_2]_2$ ,  $[(\text{PhO})_3\text{PPdCl}_2]_2$  and  $(\text{Ph}_3\text{P})_2\text{PdCl}_2$  were prepared according the literature methods.<sup>[10]</sup> 4-Mercaptopyridine, phenylboronic acid, *p*-tolylboronic acid and 4-bromoanisole were used as purchased without further purification. Elemental analyses were performed with an Elementar III Vario EI Analyzer. Infrared spectra were recorded with a Nicolet AVATAR-360IR spectrometer.  $^1\text{H}$  (500 MHz,  $\text{CDCl}_3$ , TMS),  $^{13}\text{C}$  (125 MHz,  $\text{CDCl}_3$ , TMS) and  $^{31}\text{P}$  NMR spectra (202 MHz,  $\text{CDCl}_3$ ,  $\text{H}_3\text{PO}_4$ ) were obtained with a Bruker DMX-500 spectrophotometer.

**Synthesis of  $[\text{Ph}_3\text{PPdCl}(\mu\text{-4-PyS})]_3$  (**1**):** A solution of *n*BuLi (1.6 M, 0.14 mL, 0.22 mmol) in hexane was added dropwise to a solution of 4-mercaptopyridine (22 mg, 0.2 mmol) in thf (5 mL) at 0 °C. The suspension was stirred at room temperature for another 1 h. Then the solution was slowly added to a solution of  $[\text{Ph}_3\text{PPdCl}_2]_2$  (88 mg, 0.1 mmol) in thf (20 mL) at –78 °C. After it had been stirred for 1 d, the solvent was removed under reduced pressure, and the residue was extracted with  $\text{CH}_2\text{Cl}_2$ . The filtrate was concentrated to about 5 mL, and hexane was added to give **1** as orange solid. Yield: 84 mg, 82%.  $\text{C}_{69}\text{H}_{57}\text{Cl}_3\text{N}_3\text{P}_3\text{Pd}_3\text{S}_3$  (1542.95): calcd. C 53.71, H 3.72, N 2.72; found C 53.66, H 3.75, N 2.70.  $^1\text{H}$  NMR (500 MHz,  $\text{CDCl}_3$ ):  $\delta$  = 8.18 (d,  $J_{\text{H,H}} = 6.5$  Hz, 6 H,  $\mu\text{-4-PyS}$ ), 6.95 (d,  $J_{\text{H,H}} = 5.7$  Hz, 6 H,  $\mu\text{-4-PyS}$ ), 7.70–7.66 (m, 18 H, Ph), 7.45–7.44 (m, 9 H, Ph), 7.43–7.36 (m, 18 H, Ph) ppm.  $^{13}\text{C}$  NMR (125 MHz,  $\text{CDCl}_3$ ):

$\delta$  = 162.19, 147.86, 125.35 ( $\mu\text{-4-PyS}$ ), 134.23, 130.97, 129.73, 128.31 (Ph) ppm.  $^{31}\text{P}$  NMR (202 MHz,  $\text{CDCl}_3$ ):  $\delta$  = 32.35 (s) ppm. IR (KBr disk):  $\tilde{\nu}$  = 3056, 1591, 1480, 1435, 1110, 1060, 1024, 810, 730, 692, 532, 511  $\text{cm}^{-1}$ .

**Synthesis of  $[\text{Cy}_3\text{PPdCl}(\mu\text{-4-PyS})]_3$  (**2**):** A solution of *n*BuLi (1.6 M, 0.14 mL, 0.22 mmol) in hexane was added dropwise to a solution of 4-mercaptopyridine (22 mg, 0.2 mmol) in thf (8 mL) at 0 °C. The suspension was stirred at room temperature for another 1 h. Then the solution was slowly added to a solution of  $[\text{Cy}_3\text{PPdCl}_2]_2$  (91 mg, 0.1 mmol) in thf (20 mL) at –78 °C. After it had been stirred for 1 d, the solvent was removed under reduced pressure, and the residue was extracted with  $\text{CH}_2\text{Cl}_2$ . The filtrate was concentrated to about 5 mL, and hexane was added to give **2** as yellow solid. Yield: 81 mg, 76%.  $\text{C}_{69}\text{H}_{111}\text{Cl}_3\text{N}_3\text{P}_3\text{Pd}_3\text{S}_3$  (1597.38): calcd. C 51.88, H 7.00, N 2.63; found C 51.90, H 7.06, N 2.61.  $^1\text{H}$  NMR (500 MHz,  $\text{CDCl}_3$ ):  $\delta$  = 8.23 (d,  $J_{\text{H,H}} = 6.8$  Hz, 6 H,  $\mu\text{-4-PyS}$ ), 7.12 (d,  $J_{\text{H,H}} = 5.6$  Hz, 6 H,  $\mu\text{-4-PyS}$ ), 2.57 (m, 9 H, Cy), 1.96–1.64 (m, 90 H, Cy) ppm.  $^{13}\text{C}$  NMR (125 MHz,  $\text{CDCl}_3$ ):  $\delta$  = 162.29, 147.68, 125.55 ( $\mu\text{-4-PyS}$ ), 34.33, 29.98, 27.51, 26.37 (Cy) ppm.  $^{31}\text{P}$  NMR (202 MHz,  $\text{CDCl}_3$ ):  $\delta$  = 45.52 (s) ppm. IR (KBr disk):  $\tilde{\nu}$  = 2932, 2847, 1594, 1472, 1445, 1424, 1110, 1058, 1026, 809, 730, 516  $\text{cm}^{-1}$ .

**Synthesis of  $[(\text{PhO})_3\text{PPdCl}(\mu\text{-4-PyS})]_3$  (**3**):** A solution of *n*BuLi (1.6 M, 0.14 mL, 0.22 mmol) in hexane was added dropwise to a solution of 4-mercaptopyridine (22 mg, 0.2 mmol) in thf (8 mL) at 0 °C. The suspension was stirred at room temperature for another 1 h. Then the solution was slowly added to a solution of  $[(\text{PhO})_3\text{PPdCl}_2]_2$  (97 mg, 0.1 mmol) in thf (20 mL) at –78 °C. After it had been stirred for 1 d, the solvent was removed under reduced pressure, and the residue was extracted with  $\text{CH}_2\text{Cl}_2$ . The filtrate was concentrated to about 5 mL, and hexane was added to give **3** as orange solid. Yield: 64 mg, 56%.  $\text{C}_{69}\text{H}_{57}\text{Cl}_3\text{N}_3\text{O}_9\text{P}_3\text{Pd}_3\text{S}_3$  (1686.95): calcd. C 49.13, H 3.41, N 2.49; found C 49.15, H 3.45, N 2.50.  $^{31}\text{P}$  NMR (202 MHz,  $\text{CDCl}_3$ ):  $\delta$  = 51.96 (s) ppm. IR (KBr disk):  $\tilde{\nu}$  = 3060, 1618, 1589, 1487, 1466, 1261, 1185, 1159, 1109, 1024, 927, 807, 763, 729, 698, 457  $\text{cm}^{-1}$ .

**Reaction of  $(\text{Ph}_3\text{P})_2\text{PdCl}_2$  with 4-LiSPy:** A solution of *n*BuLi (1.6 M, 0.14 mL, 0.22 mmol) in hexane was added dropwise to a solution of 4-mercaptopyridine (22 mg, 0.2 mmol) in thf (8 mL) at 0 °C. The suspension was stirred at room temperature for another 1 h. Then the solution was slowly added to a solution of  $(\text{Ph}_3\text{P})_2\text{PdCl}_2$  (140 mg, 0.2 mmol) in thf (20 mL) at –78 °C. After it had been stirred for 1 d, the solvent was removed under reduced pressure, and the residue was extracted with  $\text{CH}_2\text{Cl}_2$ . The filtrate was concentrated to about 5 mL, and hexane was added to give red solid.

**Crystal Structure Determination:** Diffraction data of complex **1**·3 $\text{CH}_2\text{Cl}_2$  were measured at room temperature with a Bruker SMART APEX CCD diffractometer with graphite-monochromated Mo- $K_\alpha$  radiation ( $\lambda = 0.71073$  Å). The structure was solved by direct methods, and refined on  $F^2$  by full-matrix least-squares methods (SHELXL).<sup>[11]</sup> The non-hydrogen atoms were refined anisotropically, and the hydrogen atoms were included but not refined. Compound **1**·3 $\text{CH}_2\text{Cl}_2$  crystallized with highly disordered interstitial solvent molecules. The diffuse electron density created by the interstitial molecules in **1**·3 $\text{CH}_2\text{Cl}_2$  was analyzed by using the program SQUEEZE in the PLATON software package.<sup>[12]</sup> CCDC-746894 (for **1**·3 $\text{CH}_2\text{Cl}_2$ ) contains the supplementary crystallographic data for this paper. These data can be obtained free of charge from The Cambridge Crystallographic Data Centre via [www.ccdc.cam.ac.uk/data\\_request/cif](http://www.ccdc.cam.ac.uk/data_request/cif).

**Suzuki–Miyaura Cross-Coupling Reactions:** In a typical run, a mixture of 4-bromoanisole (1 mmol), arylboronic acid (1.5 mmol),

K<sub>2</sub>CO<sub>3</sub> (2 mmol) and palladium(II) precatalyst (0.1% Pd) in toluene (5 mL) was stirred at 100 °C for 10 h. The solvent was removed under reduced pressure, and the residue was extracted with hexane (2 × 5 mL). The solvent of the organic fractions was removed under vacuum to give a crude product, which was analyzed by <sup>1</sup>H NMR spectroscopy.

**Supporting Information** (see also the footnote on the first page of this article): Crystal data of complex **1**·3CH<sub>2</sub>Cl<sub>2</sub>, NMR spectra (<sup>1</sup>H, <sup>13</sup>C, and <sup>31</sup>P) of all new complexes, and <sup>1</sup>H NMR spectra of Suzuki–Miyaura cross-coupling reactions.

## Acknowledgments

Financial support by the National Science Foundation of China (Grant No. 20871032, 20971026) and the Shanghai Leading Academic Discipline Project (Project Number B108) is gratefully acknowledged. We thank Professor Jie Wu for helpful discussions.

- [1] a) S. R. Seidel, P. J. Stang, *Acc. Chem. Res.* **2002**, *35*, 972; b) F. A. Cotton, C. Lin, C. A. Murillo, *Acc. Chem. Res.* **2001**, *34*, 759; c) S. Leininger, B. Olenyuk, P. J. Stang, *Chem. Rev.* **2000**, *100*, 853; d) D. L. Caulder, K. N. Raymond, *Acc. Chem. Res.* **1999**, *32*, 975; G. F. Swiegers, T. J. Malefetse, *Chem. Rev.* **2000**, *100*, 3483; M. Fujita, M. Tominaga, A. Hori, B. Therrien, *Acc. Chem. Res.* **2005**, *38*, 369; F. Würthner, C. C. You, C. R. Saha-Möller, *Chem. Soc. Rev.* **2004**, *33*, 133–146.
- [2] a) M. Fujita, K. Umemoto, M. Yoshizawa, N. Fujita, T. Kusakawa, K. Biradha, *Chem. Commun.* **2001**, 509; b) B. J. Holliday, C. A. Mirkin, *Angew. Chem. Int. Ed.* **2001**, *40*, 2022; c) J. Hall, S. J. Loeb, G. K. H. Shimizu, G. P. A. Yap, *Angew. Chem. Int. Ed.* **1998**, *37*, 121; d) A. Thompson, S. J. Rettig, D. Dolphin, *Chem. Commun.* **1999**, 631; e) S.-W. Lai, M. C.-W. Chan, S.-M. Peng, C.-M. Che, *Angew. Chem. Int. Ed.* **1999**, *38*, 669; f) J. Barbera, A. Elduque, R. Gimenez, L. A. Oro, J. L. Serrano, *Angew. Chem. Int. Ed. Engl.* **1996**, *35*, 2832; g) S.-S. Sun, A. J. Lees, *J. Am. Chem. Soc.* **2000**, *122*, 8956; h) F. S. McQuillan, T. E. Berridge, H. Chen, T. A. Hamor, C. J. Jones, *Inorg. Chem.* **1998**, *37*, 4959; i) P. J. Stang, N. E. Persky, J. Manna, *J. Am. Chem. Soc.* **1997**, *119*, 4777; j) O. Mamula, A. von Zelewsky, G. Bernardinelli, *Angew. Chem. Int. Ed.* **1998**, *37*, 289; k) B. Hasenknopf, J.-M. Lehn, G. Baum, B. O. Kneisel, D. Fenske, *Angew. Chem. Int. Ed. Engl.* **1996**, *35*, 1838.
- [3] a) R. F. Carina, A. F. Williams, G. Bernardinelli, *Inorg. Chem.* **2001**, *40*, 1826; b) R.-D. Schnebeck, L. Randaccio, E. Zangrando, B. Lippert, *Angew. Chem. Int. Ed.* **1998**, *37*, 119; c) R.-D. Schnebeck, E. Freisinger, B. Lippert, *Chem. Commun.* **1999**, 675; d) R.-D. Schnebeck, E. Freisinger, F. Glahé, B. Lippert, *J. Am. Chem. Soc.* **2000**, *122*, 1381; e) S. Ghosh, D. R. Turner, S. R. Batten, P. S. Mukherjee, *Dalton Trans.* **2007**, 1869; f) A. K. Bar, R. Chakrabarty, K.-W. Chi, S. R. Batten, P. S. Mukherjee, *Dalton Trans.* **2009**, 3222; g) M. Ferrer, M. Mounir, O. Rossell, E. Ruiz, M. A. Maestro, *Inorg. Chem.* **2003**, *42*, 5890; h) M. Ferrer, A. Gutiérrez, M. Mounir, O. Rossell, E. Ruiz, A. Rang, M. Engeser, *Inorg. Chem.* **2007**, *46*, 3395; i) Z. Qin, M. C. Jennings, R. J. Puddephatt, *Chem. Commun.* **2001**, 2676; j) Z. Qin, M. C. Jennings, R. J. Puddephatt, *Inorg. Chem.* **2003**, *42*, 1956.
- [4] a) Y. Sekioka, J. Kaizaki, J. M. Mayer, T. Suzuki, *Inorg. Chem.* **2005**, *44*, 8173; b) E. Becker, K. Mereiter, R. Schmid, K. Kirchner, *Organometallics* **2004**, *23*, 2876; c) N. Begum, S. E. Kabir, G. M. G. Hossain, A. F. M. M. Rahman, E. Rosenberg, *Organometallics* **2005**, *24*, 266; d) M. Kotera, Y. Sekioka, T. Suzuki, *Inorg. Chem.* **2008**, *47*, 3498; e) K. E. Neo, H. V. Huynh, L. L. Koh, W. Henderson, T. S. A. Hor, *Dalton Trans.* **2007**, *48*, 5701; f) S. Liu, H. Wang, P.-C. Zhang, L.-H. Weng, X.-F. Hou, *Organometallics* **2008**, *27*, 713; g) P.-C. Zhang, H. Wang, S. Liu, X.-Q. Guo, X.-F. Hou, *J. Organomet. Chem.* **2008**, *693*, 2903.
- [5] a) K. E. Neo, H. V. Huynh, L. L. Koh, W. Henderson, T. S. A. Hor, *Dalton Trans.* **2007**, 5701; b) K. Nunokawa, S. Onaka, Y. Mizuno, K. Okazaki, T. Sunahara, M. Ito, M. Yaguchi, H. Imai, K. Inoue, T. Ozeki, H. Chiba, T. Yosida, *J. Organomet. Chem.* **2005**, *690*, 48; c) C. Díaz, A. Arancibia, *Polyhedron* **2000**, *19*, 2679; d) H. C. Bajaj, A. Das, R. van Eldik, *J. Chem. Soc., Dalton Trans.* **1998**, 1563; e) Y.-F. Han, Y.-J. Lin, W.-G. Jia, G.-X. Jin, *Dalton Trans.* **2009**, 2077; f) H. Wang, X.-Q. Guo, R. Zhong, Y.-J. Lin, P.-C. Zhang, X.-F. Hou, *J. Organomet. Chem.* **2009**, *694*, 3362–3368.
- [6] a) F. Würthner, C. C. You, C. R. Saha-Möller, *Chem. Soc. Rev.* **2004**, *33*, 133; b) S. B. Lee, S. G. Hwang, D. S. Chung, H. S. Yun, J. I. Hong, *Tetrahedron Lett.* **1998**, *39*, 873; c) K. M. Park, S. Y. Kim, J. Heo, D. Whang, S. Sakamoto, K. Yamaguchi, K. Kim, *J. Am. Chem. Soc.* **2002**, *124*, 2140; d) M. Schweiger, S. R. Seidel, A. M. Arif, P. J. Stang, *Inorg. Chem.* **2002**, *41*, 2556; e) M. Fujita, O. Sasaki, T. Mitsuhashi, T. Fujita, J. Yazaki, K. Yamaguchi, K. Ogura, *Chem. Commun.* **1996**, 1535.
- [7] J. L. Krinsky, J. Arnold, R. Bergman, *Organometallics* **2007**, *26*, 897.
- [8] a) B. Punji, J. T. Mague, M. S. Balakrishna, *Inorg. Chem.* **2007**, *46*, 10268; b) B. Punji, J. T. Mague, M. S. Balakrishna, *Inorg. Chem.* **2007**, *46*, 11316; c) O. Piechaczyk, M. Doux, L. Richard, P. I. Floch, *Organometallics* **2005**, *24*, 1204; d) C. H. M. Amijs, G. P. M. van Klink, M. Lutz, A. L. Spek, G. van Koten, *Organometallics* **2005**, *24*, 2944; e) S. Ogo, Y. Takebe, K. Uehara, T. Yamazaki, H. Nakai, Y. Watanabe, S. Fukuzumi, *Organometallics* **2006**, *25*, 331; f) Y. Han, H. V. Huynh, G. K. Tan, *Organometallics* **2007**, *26*, 6581; g) T. Zhang, W. Wang, X. Gu, M. Shi, *Organometallics* **2008**, *27*, 753; h) T. Chen, J. Gao, M. Shi, *Tetrahedron* **2006**, *62*, 6289; i) K. M. Dawood, *Tetrahedron* **2007**, *63*, 9642; j) A. I. Moncada, M. A. Khan, L. M. Slaught-ter, *Tetrahedron Lett.* **2005**, *46*, 1399.
- [9] C.-Y. Liao, K.-T. Chan, C.-X. Tu, Y.-W. Chang, C.-H. Hu, H.-M. Lee, *Chem. Eur. J.* **2009**, *15*, 405.
- [10] M. Noskowska, E. Śliwińska, W. Duczmal, *Transition Met. Chem.* **2003**, *28*, 756.
- [11] a) *SHELXTL 6.10*, Bruker Analytical Instrumentation, Madison, WI, USA, **2000**; b) G. M. Sheldrick, *SADABS, Software for Empirical Adsorption Correction*, University of Göttingen, Göttingen, Germany, **2000**.
- [12] A. L. Spek, *J. Appl. Crystallogr.* **2003**, *36*, 7.

Received: September 9, 2009

Published Online: November 24, 2009